

THE ZTEM PRIMER

Prologue to Rev 3

Condor initiated the *ZTEM Primer* in early 2010 so as to help our clients better understand this new technology. That edition had just over 100 pages.

This edition, the last we plan to produce, has almost 300 pages, largely due to the huge number of new case studies that are now available which discuss various aspects of the use of the technology.

This coming of age for ZTEM means that the Primer has served its purpose. Condor will of course, continue to produce what we believe to be case studies of value from time to time, both for ZTEM and the other technologies we work with. With our revamped web site; www.condorconsult.com we will typically provide the new studies as 'downloads' when produced and then add them to our 'Condor Stick' which we update several times a year.

Best regards, Ken Witherly President

THE ZTEM SYSTEM

PRINCIPLES, MODELING AND ANALYSIS TECHNIQUES

GENERAL BACKGROUND

The ZTEM system was developed over the first part of the last decade (Kuzman et al 2005) and has been flying commercially since 2006. This technical note was written so as to provide Condor's clients with a basic background on the system, how the data is processed and interpreted. Additional information on the system and data processing is included with all of Geotech's ZTEM survey reports. As the system is quite new to the exploration industry, this document will most likely be modified from time to time.

The ZTEM system operates quite differently from traditional airborne EM systems such as VTEM. For VTEM and other what are sometimes referred to as active source EM systems, EM signals are transmitted into the earth and return signals received as the system moves over the ground in a fashion analogous to a towed marine sonar 'pinger'. Unlike sonar however, the transmitted EM field interacts with the underlying conductivity in the earth and the received signal (or secondary signal) gives a response that with suitable processing and analysis can define the location and quality of conductors within the earth. The image below shows the transmit and receive modes of an active source EM system.

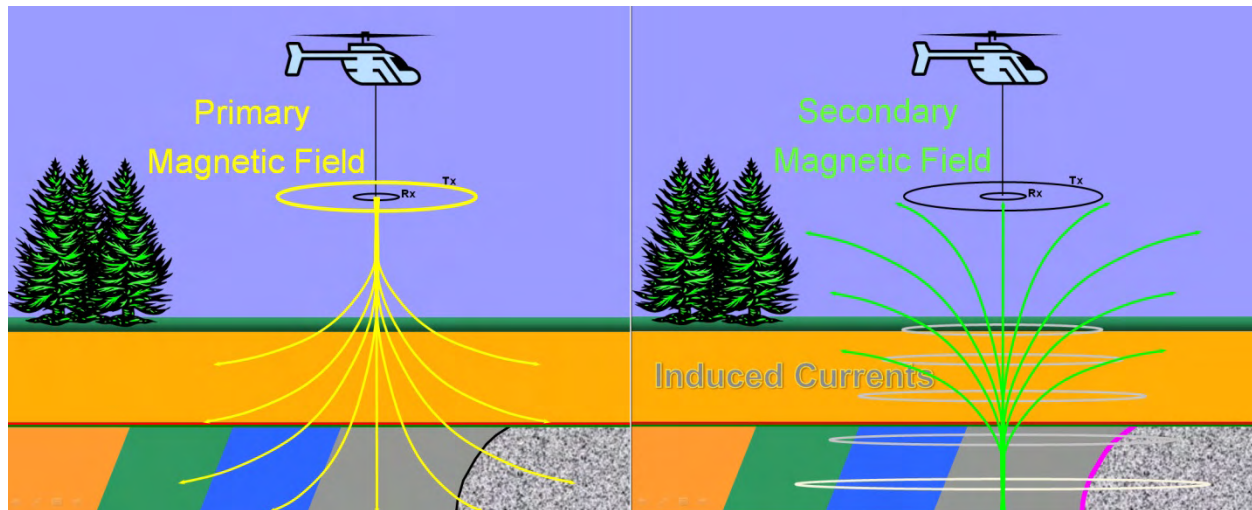


Figure 1

Rather than relying on a signal generated by the equipment on board the aircraft, ZTEM measures naturally occurring magnetic fields in the earth in a fashion similar to the Magnetotelluric (MT) technique. Fig. 2 shows the power spectrum and bandwidth of EM responses that the ZTEM operates in. ZTEM typically operates between 30-720 Hz.

Unlike conventional AEM methods which are designed to map confined conductors (targets of limited sizes) the ZTEM technique responds best to conductivity contrasts or resistivity gradients most often associated with large geological features such as shown in Fig. 3 below.

The ZTEM system measures the vertical MT field (referred to as H_z) in a loop carried below the helicopter. The other two components H_x and H_y are measured on

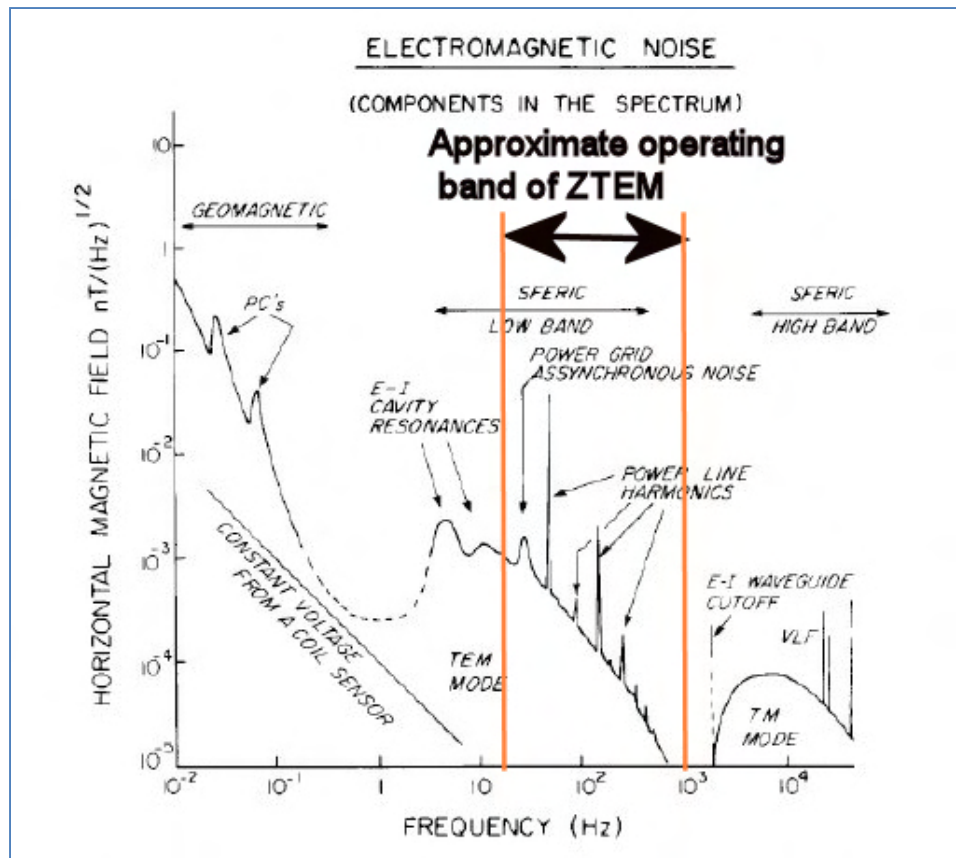


Figure 2

the ground with two fixed coils. The primary delivered data is the ratio of the H_z/H_y and H_z/H_x , commonly referred to as the tipper ratios and expressed in the form T_{zx} and T_{zy} . Geotech routinely delivers information (in-phase and quadrature data as a fraction) at the frequencies 30, 45, 90, 180, 360 and sometimes 720 Hz. As can be seen in the naturally occurring EM spectrum plot (Fig 2), the ZTEM signal strength drops as the frequency increases and the 720 Hz signal can sometimes not be obtained. Fig. 4 shows what the various parts of the ZTEM system look like.

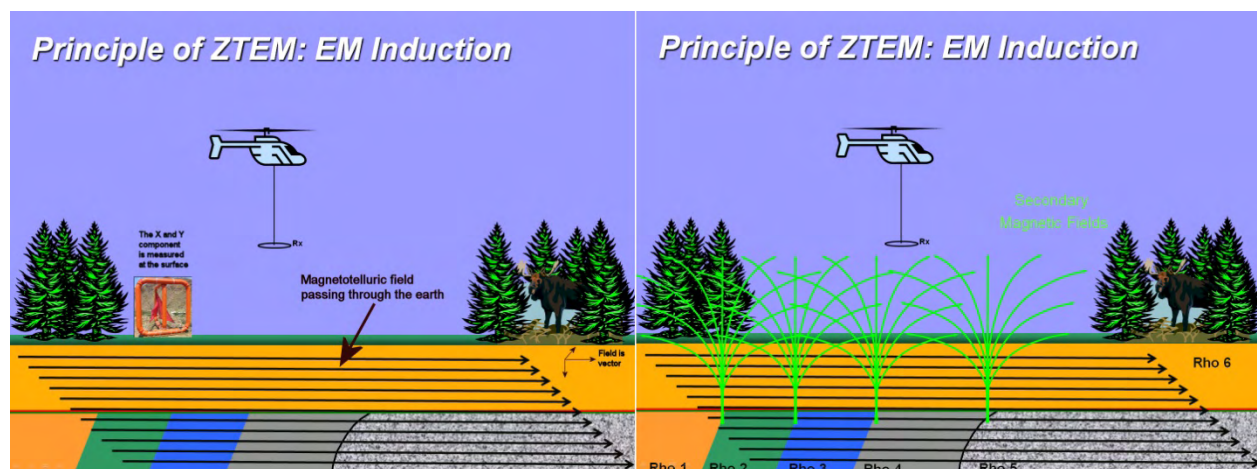


Figure 3

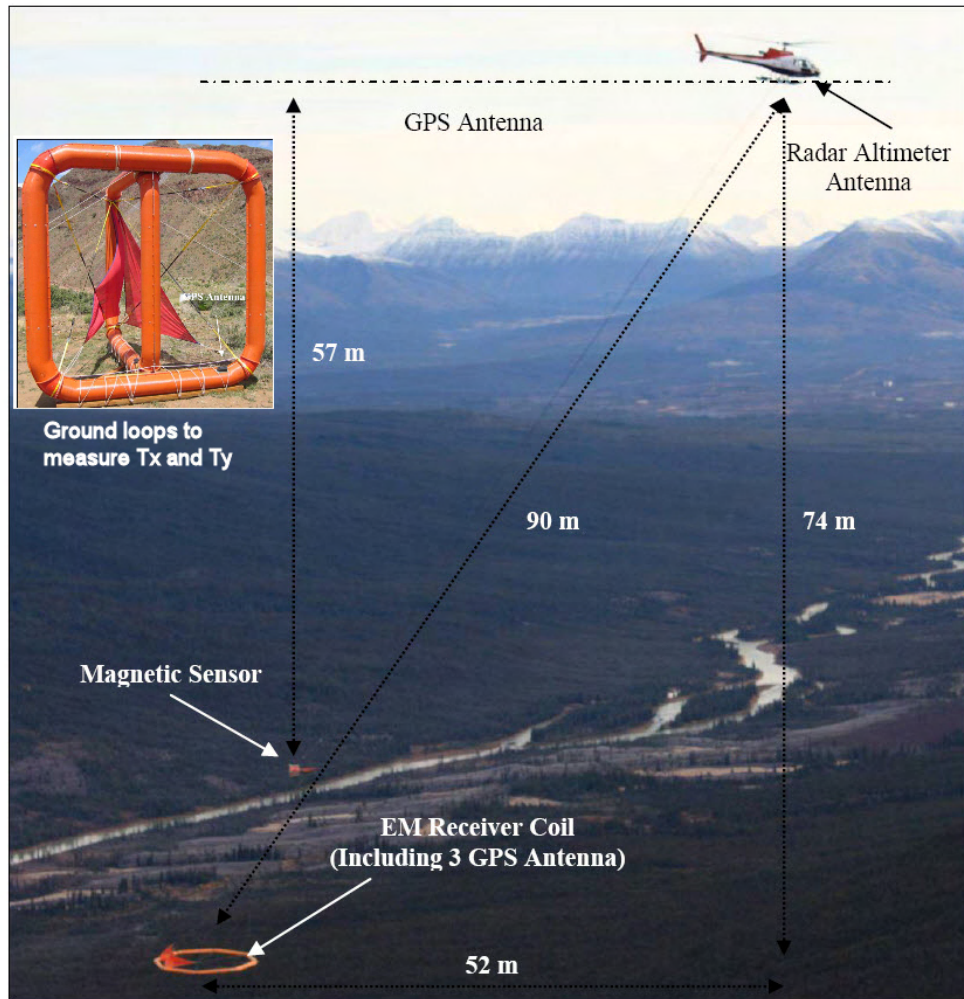


Figure 4

The Geotech standard field report discusses important issues about how the data is processed and presented to clients. A copy of a recent version is attached with this Technical Note (November 2010).

Even though ZTEM data are sensitive to lateral variations conductivity contrasts, the system can't resolve absolute earth conductivities. While calibration of the ZTEM responses using external information is theoretically possible, we have not achieved generally better outcomes of our ZTEM processing using a priori resistivity information.

The setting up of a ZTEM survey is fairly normal compared with other airborne techniques. Flight lines should be normal to the likely geological strike. As to line spacing however, due the more slowly changing primary field strength, little additional information is gained by going to line spacings closer than 200 m. For the primary processing Geotech performs to the raw ZTEM data, Geotech requires a minimum line length of 10 km to be used.

The strength of the natural EM field drops off slower with height than the primary field generated by active-source EM systems.

For this reason ZTEM can operate in more rugged terrain (flying higher) and still obtain a useful signal. Condor believes that while this aspect of ZTEM is beneficial to getting good quality data in rugged areas, the system should still be operated as close to the ground as can be safely accommodated in the specific survey conditions. There are effects from topography in the primary ZTEM results; these effects are discussed later.

ZTEM is more sensitive to power line noise than active source EM techniques and in some instances, Geotech will decline to undertake a ZTEM survey if they feel the data will be sub-standard due to excessive power line interference.

SYSTEM RESPONSES

This section shows the ZTEM response to some basic geological scenarios. These results were generated using the 2D finite element code developed by Phil Wannamaker (Wannamaker et al 1987). The first plot (Fig. 5) shows the response across a layered earth. Since H_z is zero above a 1D (layered) earth, the ZTEM T_{zx} response is also zero.

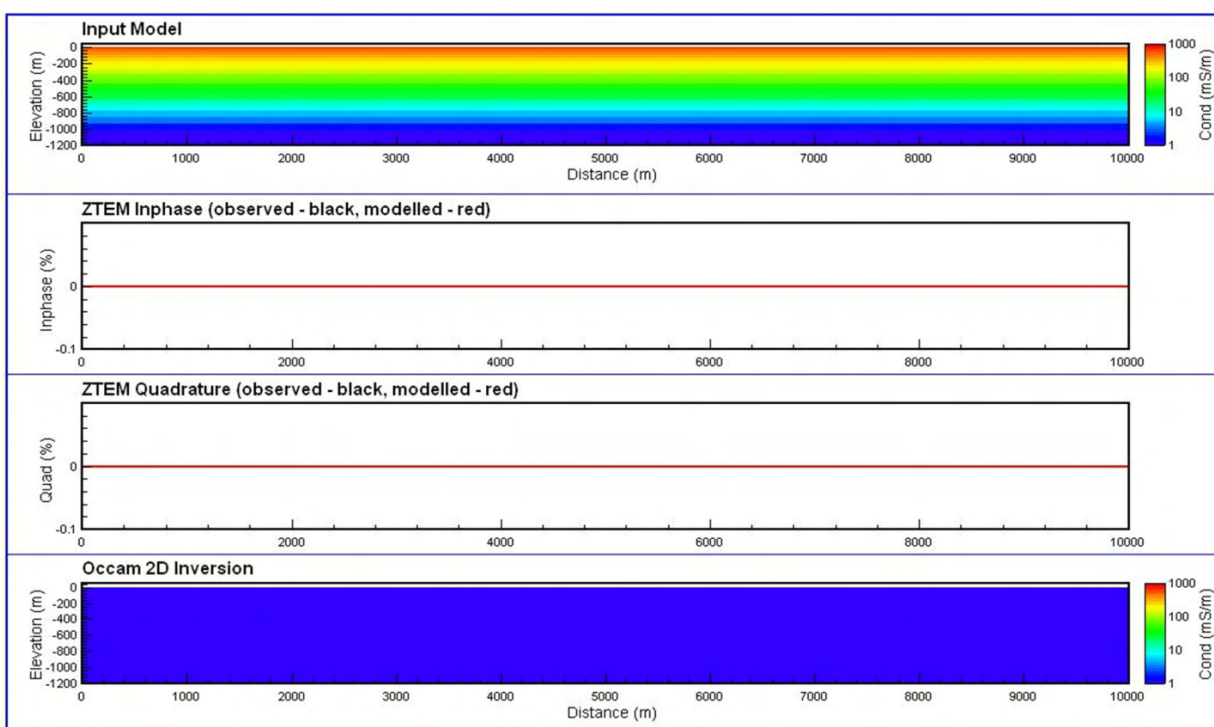


Figure 5

In the next figure (Fig. 6) the response over a contact with a fixed ratio between the two sides (1:100) but with the absolute resistivity values allowed to vary. This shows the basic shape of the ZTEM responses, a peak overtop of the contact. Note the slope of the response is steep on the conductive side and broad on the resistive side. There is also a change in amplitude with absolute value of the resistivity; higher resistivities produce slightly higher peak responses.

The next set of models (Fig. 7) shows the response for a variable contrast contact; 1:2 at the top of the figure and 1:1000 at the bottom. The higher the contrast the higher the amplitude of the response; lower contrasts also produce broader, more symmetric responses.

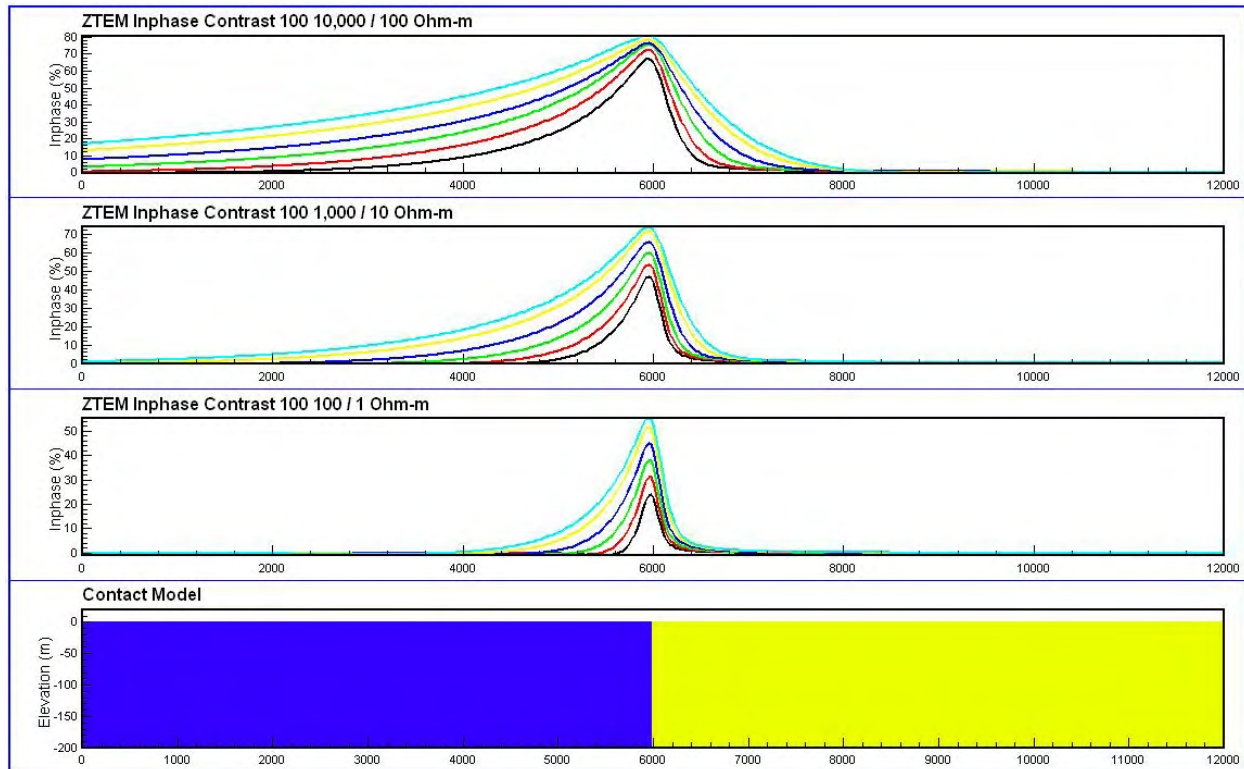


Figure 6

The next model (Fig. 8) shows the 1:100 ratio contact model that has been processed with Condor's 2D Occam code (Sattel and Witherly 2010). The observed and model fits to the data are shown in profile form and the resulting conductivity depth section at the bottom of the image. Note the resistive part of the model is well recovered but the conductive section is over-estimated in conductivity value. As well a minor contact 'artifact' appears at the contact.

A conductive body is added in the next figure (Fig. 9). In the modeling this then produces a strong conductor that is slightly shallower than the actual target depth. The resistivity of conductive unit (on right) is also better recovered in this situation.

The response over a conductive slab is shown in the next figure (Fig. 10). This highlights that ZTEM responds primarily to resistivity gradients at contacts or edges. At both edges, a strong response is observed but over the conductive slab proper, there is no response observed.

The final figure (Fig. 11) shows the response of a target under a conductive slab. Note this discrete response also allows the inversion program to achieve some definition of the surface layer as well.

In terms of anomaly shapes, over contacts (example in Figs. 6-7-8) the anomaly shapes are peaks whereas for discrete targets, the responses are more cross-over's (examples in Figs 9 & 11). This means that contact-type responses will be displaced if a phase-rotated product is used for interpretation.

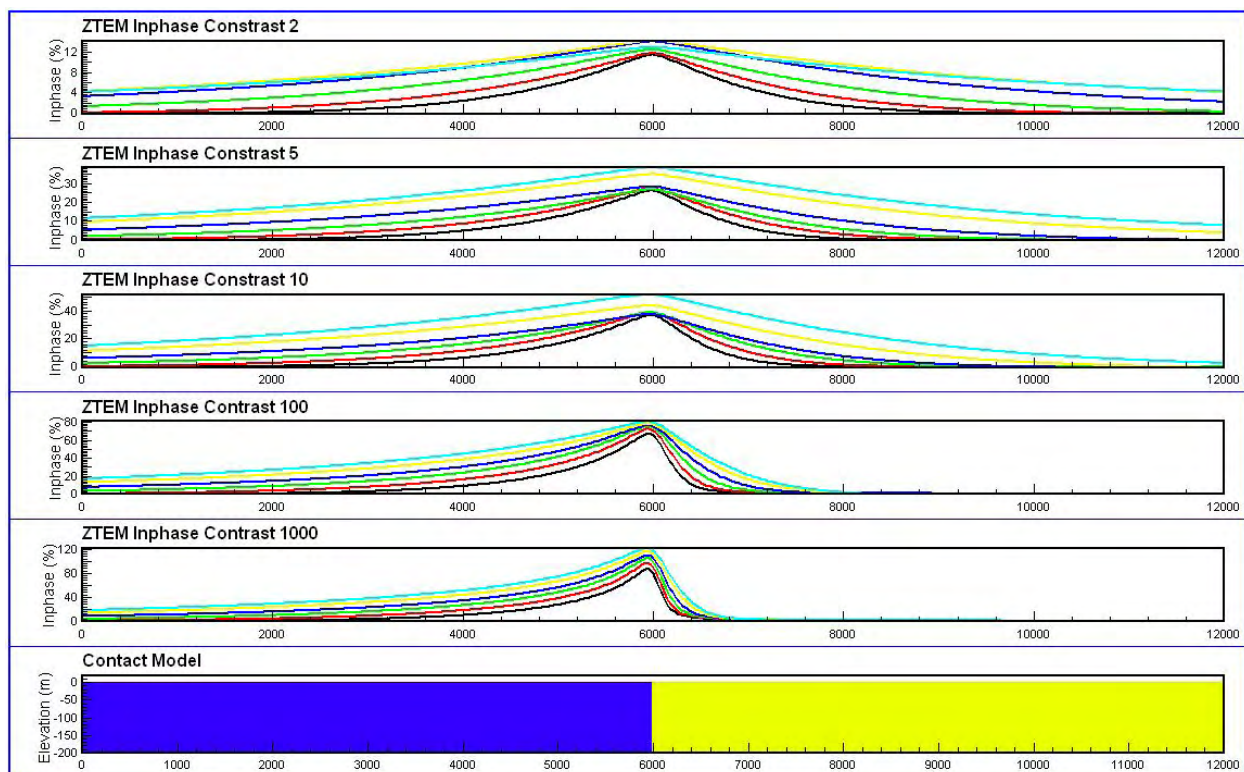


Figure 7

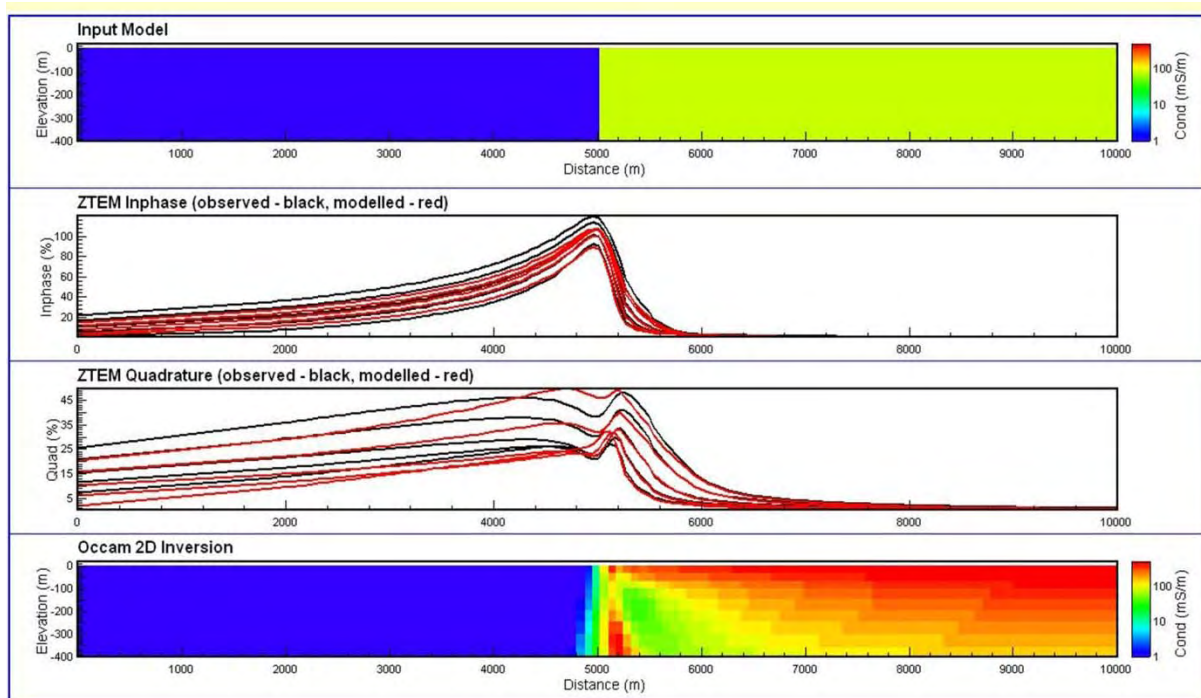


Figure 8

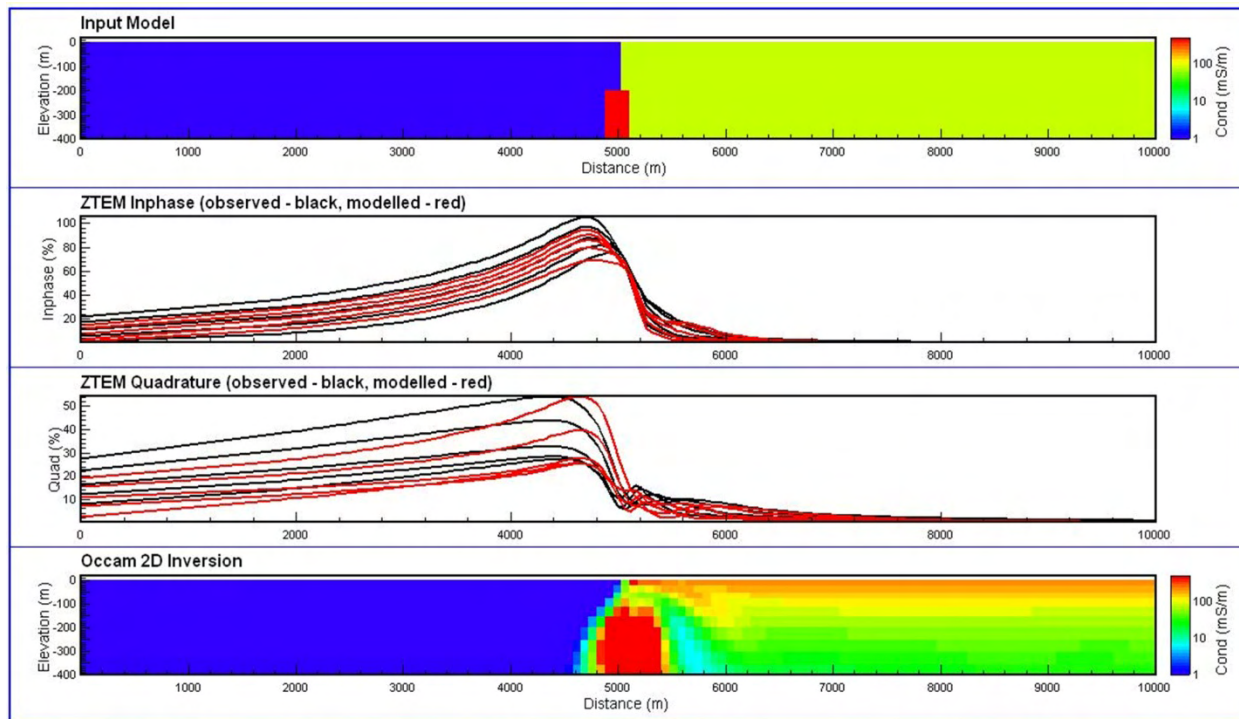


Figure 9

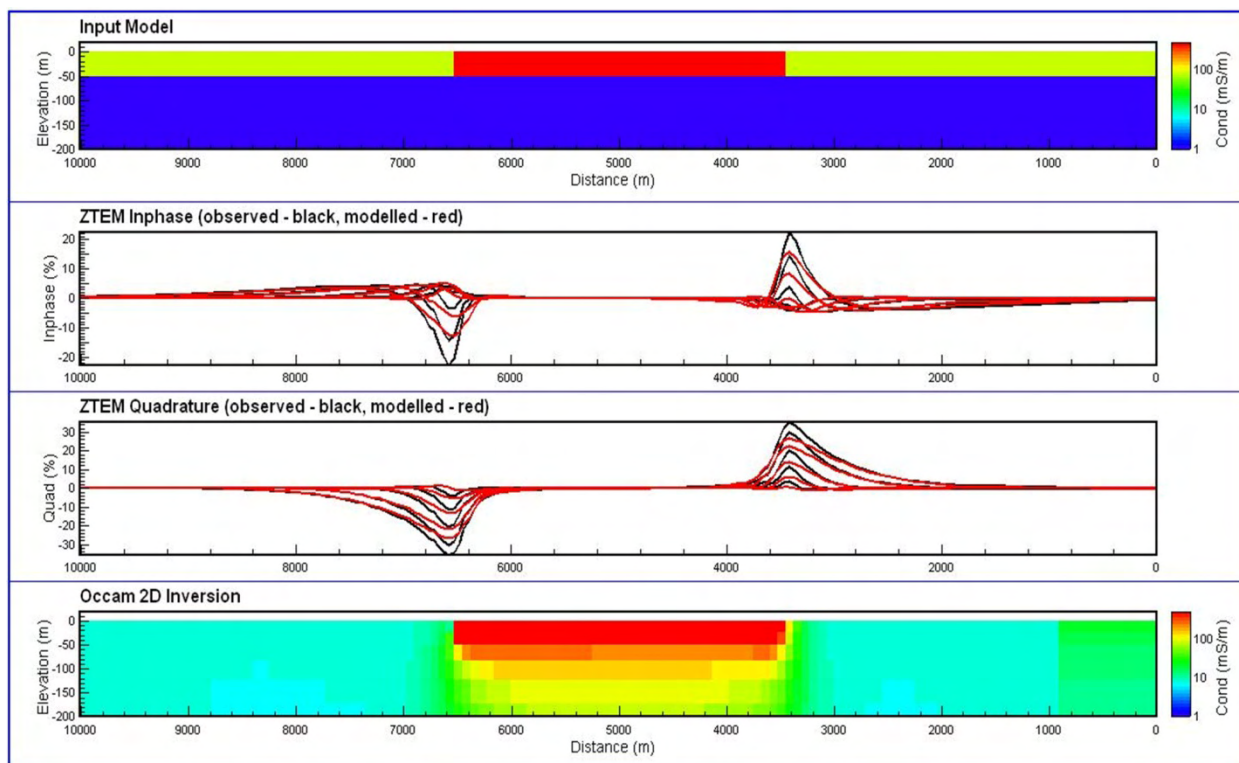


Figure 10

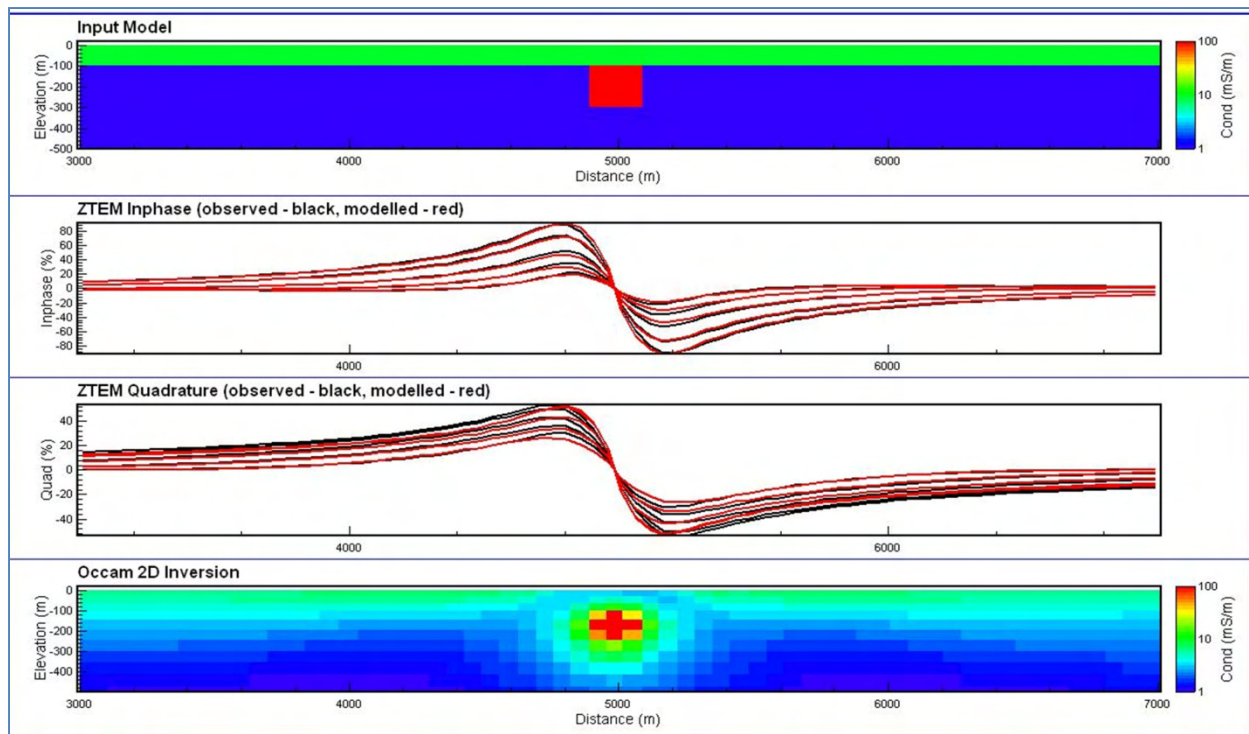


Figure 11

TOPOGRAPHY

The AFMAG fields are influenced by topography. The primary effect of topography is to induce conductive features on peaks and resistive features in troughs or valleys. Figure 12 shows this effect.

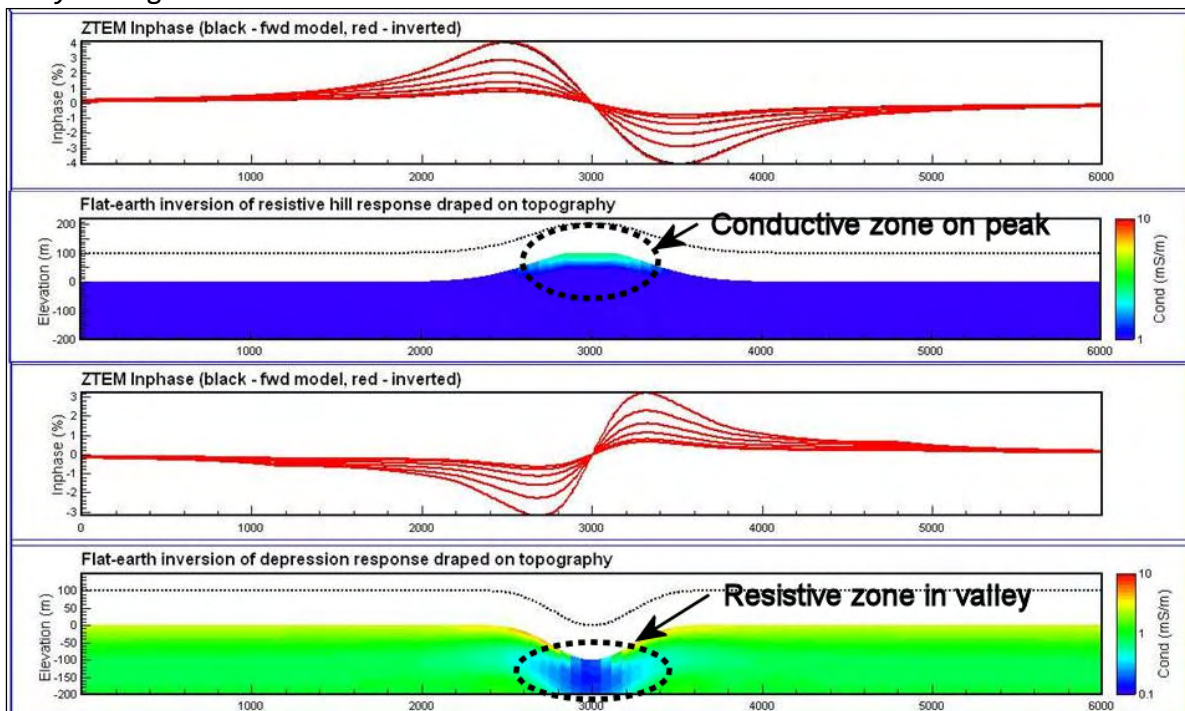


Figure 12: Theoretical modeling of topography and ZTEM responses.

With suitable processing (either 2D or 3D) the effects of topography can be largely removed.

PROCESSING & PRODUCTS

The three main forms of products that are currently generated from the ZTEM data are:

- 1) Profiles of the tipper ratios (for each of the acquired frequencies, each with an in-phase and quadrature component.
- 2) Grids of original and phase-rotated in-phase and quadrature information of the Tzx and Tzy components. The phase-rotation produces positive peaks over discrete conductive features. The same filtering over formational contacts (examples in Fig 6-7-8) will produce a slightly displaced peak since the primary anomaly shape is a positive peak (rather than a cross-over as is present over a discrete conductor (examples Fig. 9 & 11)). A further grid set is also generated from the merging of the Tzx and Tzy grids and the peaker (sum of the horizontal derivatives). The derivation of these products is discussed in more detail in the Geotech field survey report.
- 3) 2D & 3D conductivity inversions.

The application of 3D inversions has become much more common since they were first outlined by Holtham and Oldenburg (2010). A number of examples of the use of 3D inversion are provided in the Case Study section.

Profiles

Typically the in-phase and quadrature information for the various frequencies is what is commonly displayed.

Grids-Geotech

The definitions of the Geotech-derived grids are provided below. The DT and TPR grids are generated from the peaker and phase-rotated, merged Tzx and Tzy component data respectively.

DT (Total Divergence): The DT gives a clearer image of conductor's location and shape but, as a derivative, it does not preserve some of the long wavelength information and is also sensitive to noise.

TPR (Total Phase Rotation): As an alternative, a 90 degree Phase Rotation (PR) technique is also applied to the grids of each individual component (Tzx and Tzy). It transforms bipolar (cross over) anomalies into single pole anomalies with a maximum over conductors, while preserving long wavelength information (Lo et al., 2009). The two orthogonal grids are then usually added to obtain a Total Phase Rotated grid for the in-phase and quadrature.

The major purpose of various grid displays is to provide an optimal means to show the contained geological content. On a component basis, the Tzx component contains the most information about the geology normal to the survey line and the Tzy about across-line conductivity. Together (in the form of the DT or TPR products), a more 3D appreciation of the geology is conveyed.

Fig 13 shows all of the Geotech-generated grids for the Pebble 45 Hz signal. As noted above, some of the products are unique and some are the merged product of the Tzx and Tzy component data; this is indicated in the figure. There is a suite of such grids for each frequency being provided by Geotech.

Currently, there are likely more choices in grid-based products than are effective for most exploration situations; i.e. too many choices. Geotech has likely pursued this approach given the nascent state of ZTEM interpretation and a fear they might 'miss something' if they did not provide what they felt were all the products that might show useful information. At this stage, Condor has usually performed 'quick looks' using the Tx-in-phase data at one of the lower frequencies.

Condor also produces a set of products defined below. Some have similarity to what Geotech provides and some considered different. As noted above, there are likely too many derived products currently being produced for ZTEM surveys and with experience, we'll know the best suite of products to employ in most situations.

- 1) AppCon grid
- 2) 2D Occam conductivity depth model
- 3) Karous-Hjelt depth section & grids

AppCon: The apparent conductivities and phases are derived using both the Tzx and Tzy Tipper information for each frequency. This approach uses an approach first developed for VLF data by Becken and Peterson (2003) and is believed to derive a superior estimate of the conductivities being mapped.

The AppCon outcomes for Pebble are shown in Fig. 14.

2D Occam: This uses a modified version of a 2D MT inversion program developed over a number of years by Constable and Wannamaker (deGroot-Hedlin and Constable, 1990; Wannamaker et al., 1987; deLugao and Wannamaker, 1996). The primary output of the inversion is a conductivity depth section such as shown in Figs. 8-11. In addition, grids can then be created showing the conductivity at a particular depth below surface.

The result of a 2D Occam inversion for Pebble is shown in Fig. 15; the result of an inverted line of Spectrem data (active-source time domain EM system) is shown as well for comparison.

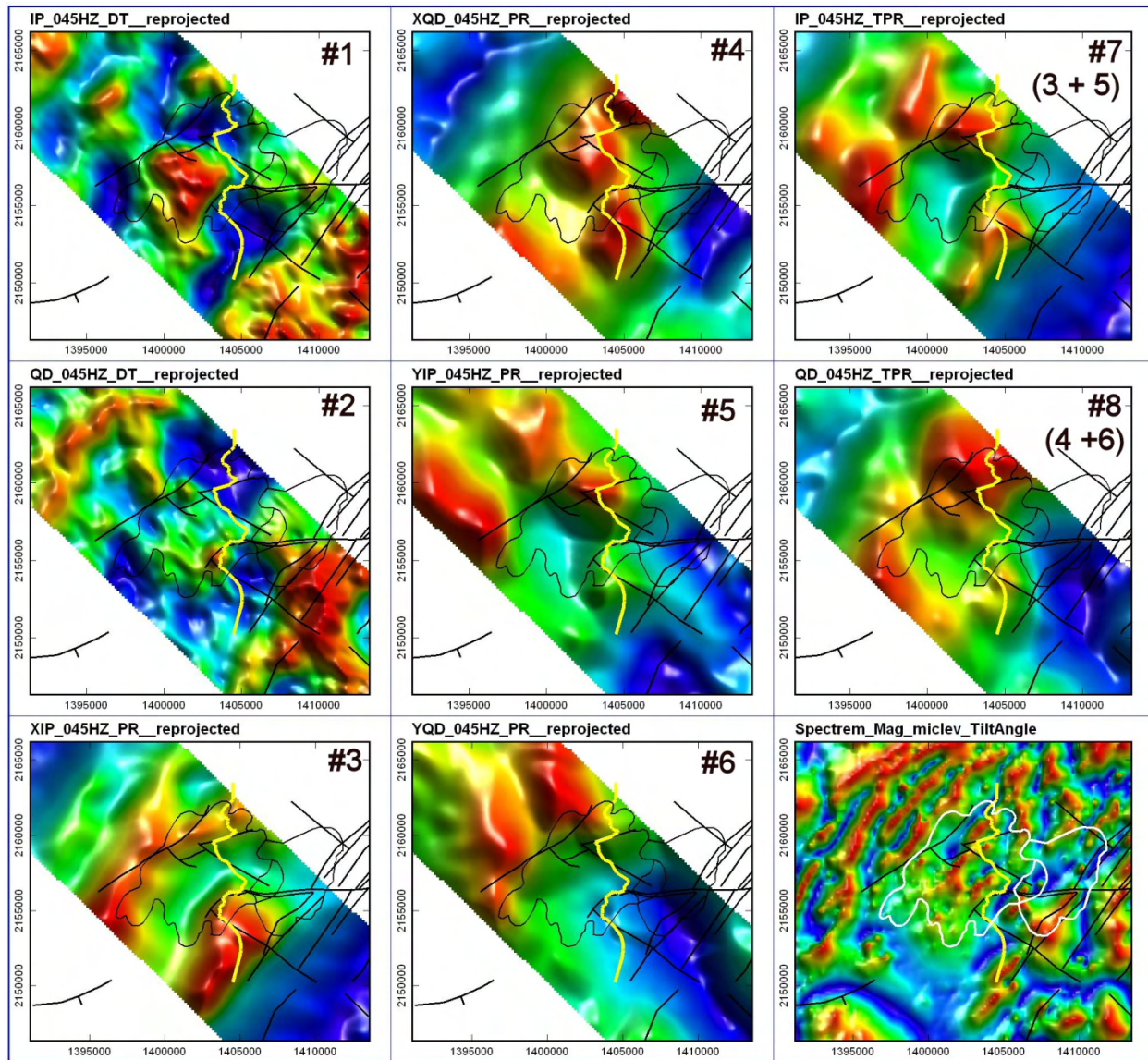


Figure 123

Fig. 16 shows a series of depth slices through a block of models derived with 2D Occam inversions from ZTEM data acquired across the Pozo Seco deposit (Witherly 2010). The depth slices from a VTEM-derived conductivity model over the same area are also shown. This example shows that the ZTEM results provide considerably more detail about the conductivity structure of the earth than the VTEM. This is considered a good example of ZTEM being more sensitive to high resistivity zones and contacts within these zones.

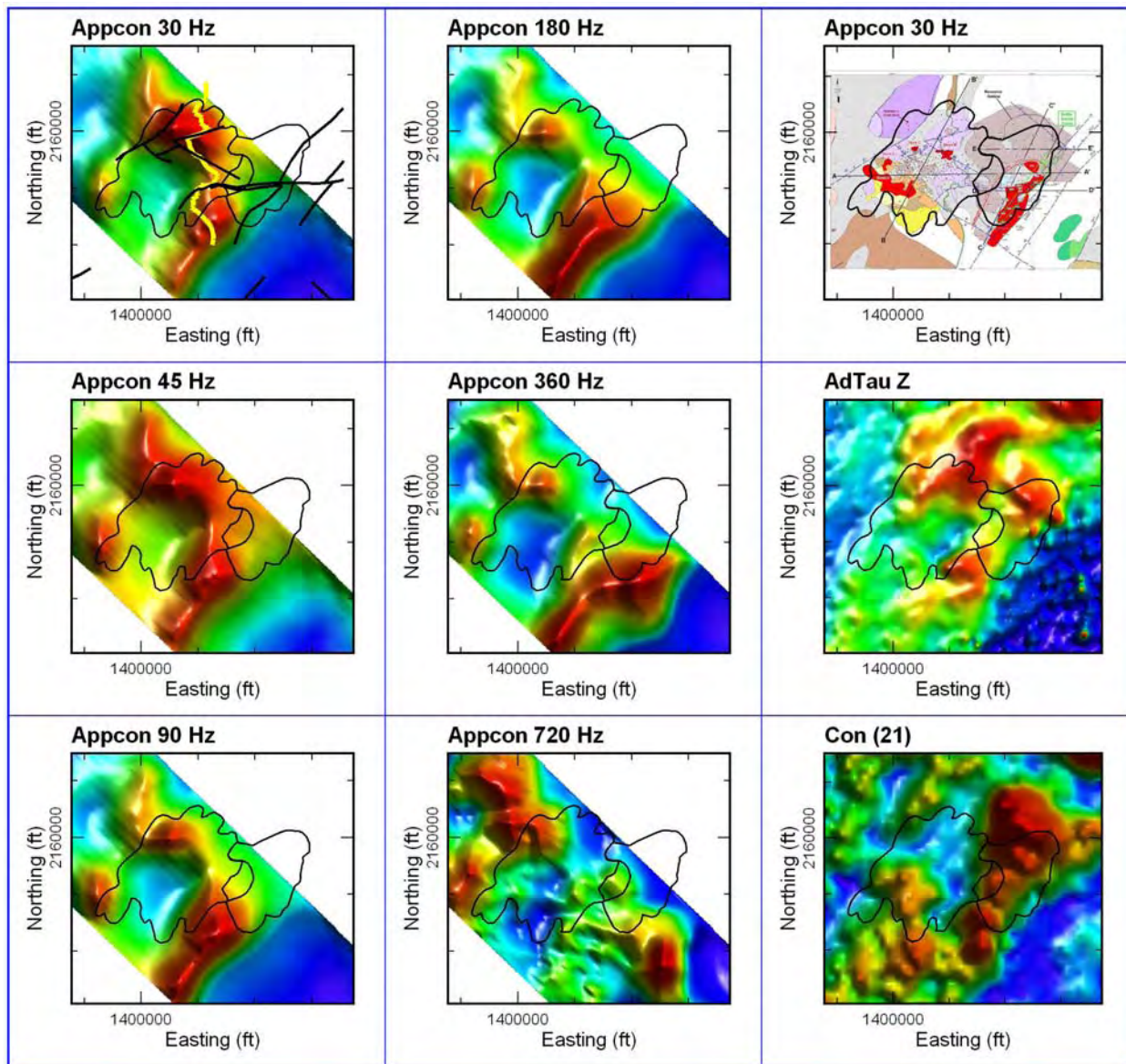


Figure 134

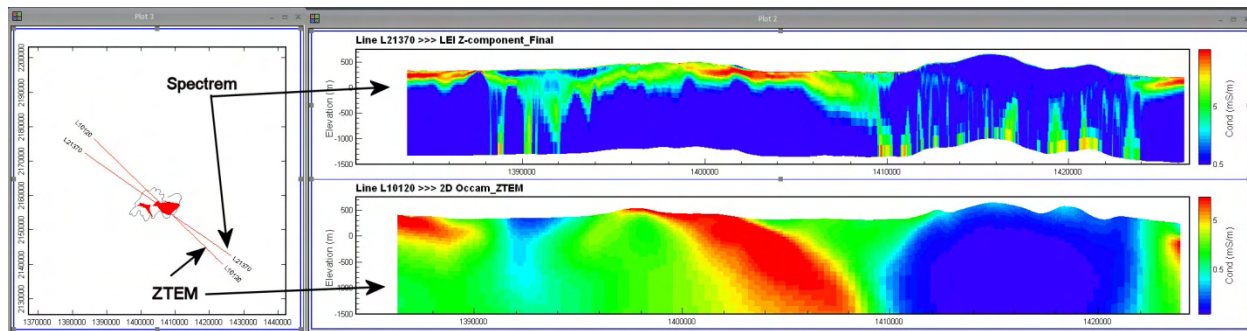


Figure 145

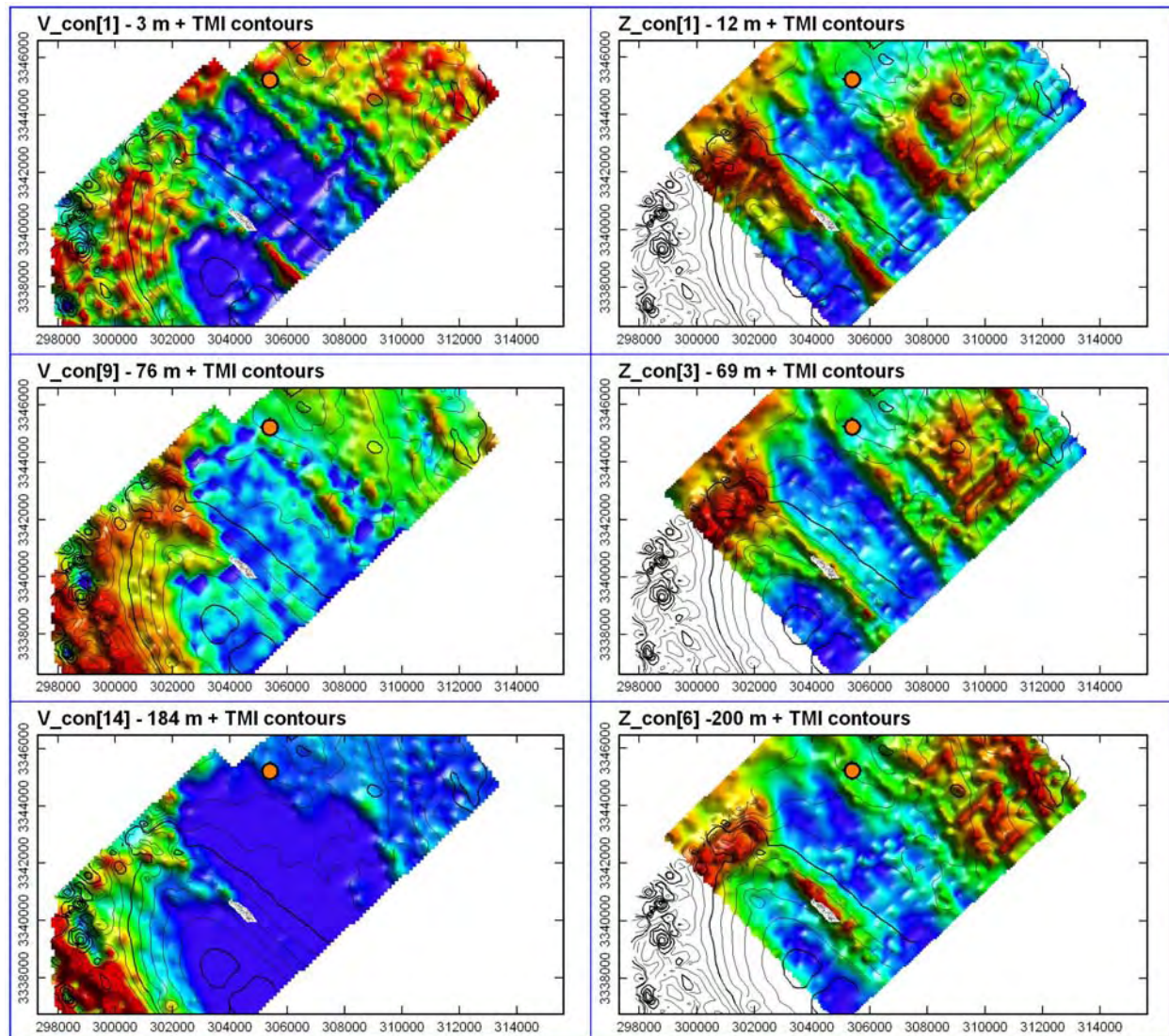


Figure 156

Karous-Hjelt depth section & grids: Pseudo-sections derived with the Karous-Hjelt filter (Karous and Hjelt, 1983) can be useful to extract subtle conductors from the ZTEM profiles. The main property of the Karous-Hjelt filter is to turn cross-over's into peaks. Grids can as well be generated from the Karous-Hjelt processing. These grids are similar to divergence grids generated by Geotech that are based on the VLF peaker derivation (Pedersen et al., 1994). The latter however, makes use of the spatial derivatives of the Tzx and Tzy tippers, whereas the Karous-Hjelt-filtered grids shown are derived from either the Tzx or Tzy data.

Fig. 17 shows the Karous-Hjelt pseudosections for a line of ZTEM over the Forrestania deposit (Sattel and Witherly 2010). Also shown is the 2D Occam inversion as well.

Depth of Investigation of ZTEM

A theoretical assessment of the ZTEM frequency group using a skin depth assumption is shown in Fig. 18 (Lo et al 2008). While this concept has merit, it

over simplifies the understanding of where the ZTEM signals are being generated. The VTEM system has a base frequency of 30 Hz (same as lowest frequency available with ZTEM) but the deepest useable signal Condor has observed is over conductors in the Athabasca Basin that have been drilled to a depth ~825 m depth. This is believed to be close to the effective depth of investigation of VTEM and is the result of both the skin depth of the primary signal as well as the signal/noise characteristics of the actual acquired data.

An examination of the modeling examples presented there and field results such as from Pebble (Fig. 15) show that the ZTEM results when modeled can produce a smeared result that is wider and deeper than the actual geological sources are most likely coming from.

CONCLUSIONS

ZTEM is one of the most exciting developments in airborne geophysics in the past decade. However, Condor advises caution when trying to interpret ZTEM outcomes as geological information whether profiles, grids or conductivity depth products are being used. More than most EM techniques, ZTEM is a somewhat paradoxical technique in that it is seen as both very sensitive to subtle changes in the earth's conductivity structure but then in some cases will only allow us to view these features as fairly unsatisfactory blurry images. In other instances, ZTEM can produce high resolution images that appear to capture very subtle geological features that no other technique is likely capable of. It is therefore deemed very important to make every effort to calibrate ZTEM outcomes with ground truth (geological or constrained geophysical results) before embracing the ZTEM results 'geo-truth'.

Condor Consulting, Inc.

December 20, 2010 Rev 1

March 25, 2011, Rev 2

March 27, 2012 Rev 3

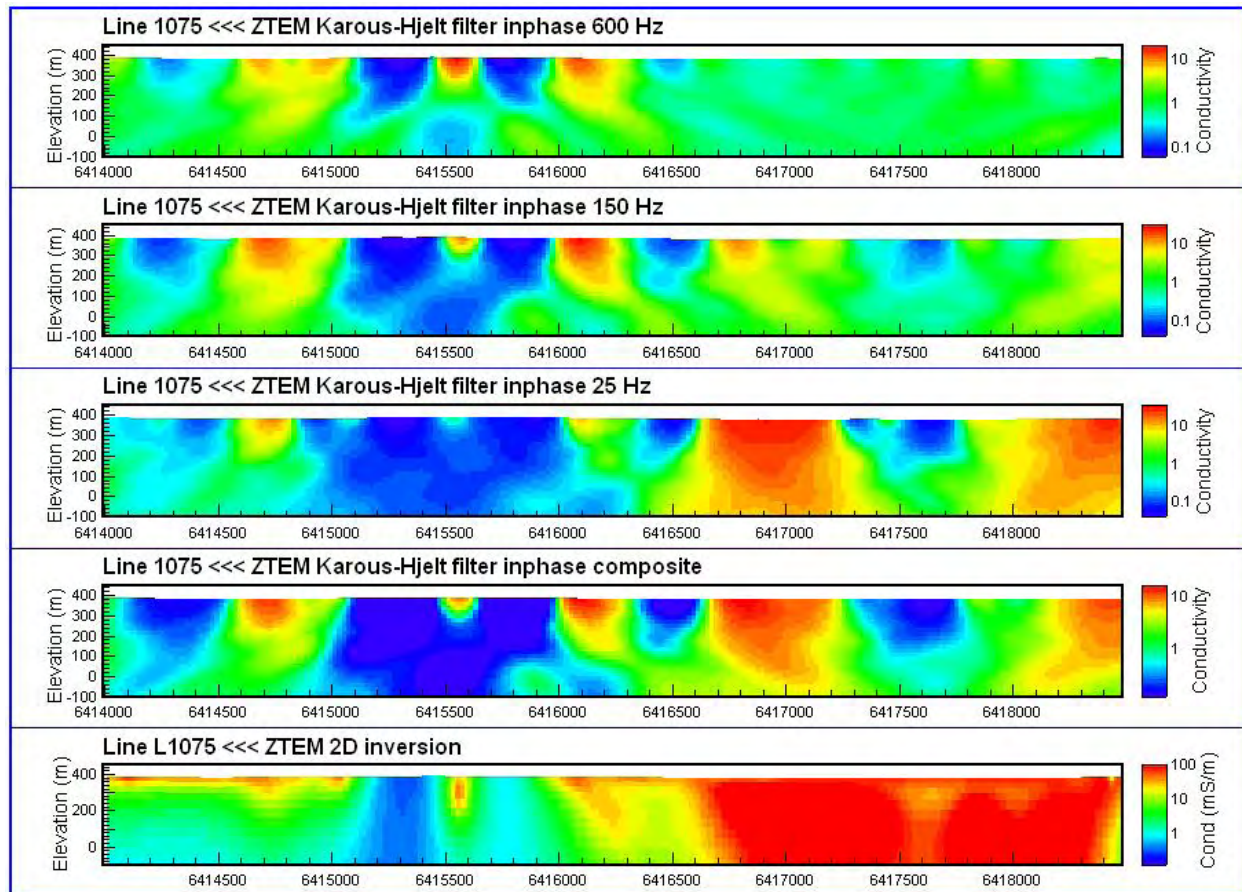


Figure 17

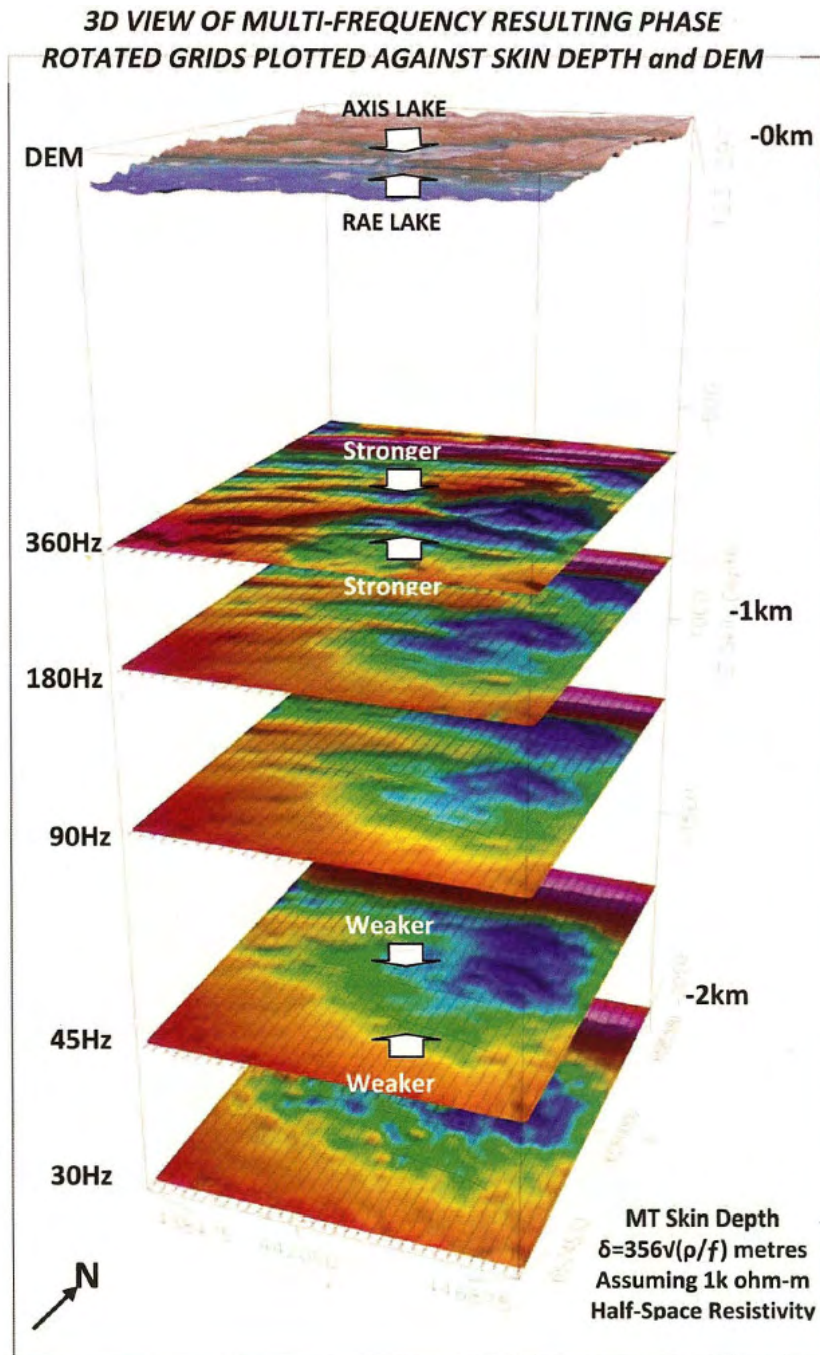


Figure 168

REFERENCES

* indicates provided with Primer Appendix B

Becken M., and Pedersen L.B., 2003, Transformation of VLF anomaly maps into apparent resistivity and phase: *Geophysics* 68, 497-505.

DeGroot-Hedlin, C. and S. Constable, 1990, Occam's inversion to generate smooth two-dimensional models from magnetotelluric data: *Geophysics* 55, 1613-1624.

De Lugao, P.P., and Wannamaker, P., 1996, Calculating the two-dimensional magnetotelluric Jacobian in finite elements using reciprocity, *Geophys. J. Int.*, 127, 806-810.

Farquharson, C.G., Oldenburg, D.W., Haber, E., and Shekhtman, R., 2002, An algorithm for the three-dimensional inversion of magnetotelluric data: 72nd International Exposition and Annual Meeting, SEG, Expanded Abstracts, 649-652.

*Holtham, E., and Oldenburg, D. W., 2010, Three-dimensional inversion of ZTEM data: *Geophysical Journal International*, 182, 168-182.

*Holtham, E. and Oldenburg, D. W. 2011, Three-dimensional inversion of MT and ZTEM data SEG Expanded Abstracts 29, 655 (2010)

*Holtham, E., and Oldenburg, D. W., 2012, Inversion of Large-scale ZTEM Data; *ASEG Extended Abstracts 2012(1)* 1 - 4

*Izarra, C., Legault, J.M., and Fontura, C., 2011, ZTEM airborne tipper AFMAG results over the Copaque Porphyry, northern Chile, SBGF Conference Expanded Abstracts, 4pp.

*Kaminski, V. F., Kuzmin, P., and Legault, J. M. 2010, AirMt - passive airborne EM system: Presented at 3rd CMOS-CGU Congress, Ottawa.

*Kaminski, V., Legault, J. M. and Kumar, H. 2010, The Drybones Kimberlite: a case study of VTEM and ZTEM airborne EM results ASEG Extended Abstracts 2010(1) 1 - 4 September 2010

*Kaminski, V. and Oldenburg, D. 2012, The geophysical study of Drybones kimberlite using 3D Time Domain EM Inversion and 3D ZTEM inversion algorithms ASEG Extended Abstracts 2012(1) 1 - 4

Karous, M., and Hjelt, S.E., 1983, Linear filtering of VLF dip angle measurements: *Geophysical Prospecting* 31, 782-794.

*Kowalczyk, P.L. and van Kooten, P.B.M 2012, ZTEM data inversion and interpretation using the UBC-GIF MTinv3D code: A case history at the Silver Queen project, British Columbia; ASEG Extended Abstracts 2012(1) 1 - 4

*Kowalczyk, P.L. and van Kooten, P.B.M 2012, Inverting ZTEM data in 3D: Process and Practice; in R. J. L. Lane (editor), *Natural Fields EM Forum 2012: Abstracts from the ASEG Natural Fields EM Forum 2012*: Published by Geoscience Australia, Geoscience Australia Record 2012/04

Kuzmin, P., Lo, B., and Morrison, E. 2005, Final Report on Modeling, interpretation methods and field trials of an existing prototype AFMAG system, Misc Data Release 167, Ontario Geol. Survey Geotech Standard ZTEM Survey Report Document covering data processing and presentation; November 2010

*Legault, J.M., Kumar, H., Milicevic, B., and Hulbert, L., 2009, ZTEM airborne tipper AFMAG test survey over a magmatic copper-nickel target at Axis Lake in northern Saskatchewan: 79th International Exposition and Annual Meeting, SEG, Expanded Abstracts, 1272-1276. (2009)

*Legault, J. M., Kumar, H., Milicevic, B., and Wannamaker, P., 2009, ZTEM tipper AFMAG and 2D inversion results over an unconformity target in northern Saskatchewan: SEG Expanded Abstracts, 28, 1277-1281 (2009)

*Legault, J.M, Orta, M., Kumar H. and Zhao S. 2011, ZTEM and VTEM airborne EM survey results over PGM-Cu-Ni targets at East Bull Lake anorthositic complex, Massey, Ontario SEG, Expanded Abstracts, 30 , no. 1, 629-634, (2011)

*Legault, J.M, Witter, J.B., Berardelli, P. and Orta M. 2010, ZTEM Airborne AFMAG EM Results over the Reese River Geothermal Test Area, central Nevada; ASEG Extended Abstracts 2010(1) 1 - 4

*Legault, J.M., Wilson, G.A., Gribenko, A.V., Zhdanov, M.Z., Zhao, S. and Fisk, K. 2012, An overview of the ZTEM and AirMT systems - A case study from the Nebo-Babel Ni-Cu-PGE deposit, West Musgrave, Western Australia, in R. J. L. Lane (editor), Natural Fields EM Forum 2012: Abstracts from the ASEG Natural Fields EM Forum 2012: Published by Geoscience Australia, Geoscience Australia Record 2012/04.

*Legault, J.M, Zhao S, and Fitch, R. 2012, ZTEM airborne AFMAG survey results over low sulphidation epithermal gold-silver vein systems at Gold Springs, south eastern Nevada; ASEG Extended Abstracts 2012(1) 1 - 4

*Lo, R. and Zang, M., 2008, Numerical modeling of Z-TEM (airborne AFMAG) responses to guide exploration strategies, SEG, Expanded Abstracts, 27 , no. 1, 1098-1102, (2008)

*Lo, R., Legault, J. M., Kuzmin, P. and Combrick, M. 2009, Z-TEM (airborne AFMAG) tests over unconformity uranium deposits; ASEG Extended Abstracts, 2009 , no. 1, 1-1, (2009)

*Pare, P., and Legault, J. M., 2010, Ground IP-resistivity and airborne SPECTREM and helicopter ZTEM survey results over Pebble copper-moly-gold porphyry deposit, Alaska: SEG Expanded Abstracts, 29, 1734-1738.

*Pare, P., Gribenko, A.V., Cox, L.H., Cuma, M., Wilson, G.A. Zhdanov, M.S., Legault, J. M., Smit J., and Polomé L. 2012, 3D inversion of SPECTREM and ZTEM data from the Pebble Cu-Au-Mo porphyry deposit, Alaska; ASEG Extended Abstracts 2012(1) 1 - 4

Pedersen L.B., Qian, W., Dynesius, L., and Zhang P., 1994, An airborne tensor VLF system. From concept to realization: Geophysical Prospecting 42, 863-883.

*Sattel, D., Witherly, K. and Becken, M. 2010, A brief analysis of ZTEM data from the Forrestania test site, WA; ASEG Extended Abstracts, Vol. 2010 No. 1 Pages 1 - 4, Published 1 September 2010

*Sattel, D., Thomas, S., and Becken, M., 2010, An analysis of ZTEM data over the Mt Milligan porphyry copper deposit, British Columbia: SEG Expanded Abstracts, 29, 1729-1733.

*Sattel, D. and Witherly, K. 2012, Extracting information from ZTEM data with 2D inversions; ASEG Extended Abstracts 2012(1) 1 - 4

*Sattel, D. and Witherly, K. 2012, An overview of ZTEM data interpretation tools; in R. J. L. Lane (editor), Natural Fields EM Forum 2012: Abstracts from the ASEG Natural Fields EM Forum 2012: Published by Geoscience Australia, Geoscience Australia Record 2012/04.

Wannamaker, P.E., Stodt, J.A., and Rijo, L., 1986, Two-dimensional topographic responses in magnetotellurics modeled using finite elements: Geophysics 51, 2131-2144.

Wannamaker, P.E., Stodt, J.A., and Rijo, L., 1987, A stable finite-element solution for two-dimensional magnetotelluric modeling: Geophysical Journal of the Royal Astronomical Society, 88, 277-296.

*Witherly, K., Sattel, D. 2012, The application of ZTEM to porphyry copper-gold exploration; ASEG Extended Abstracts 2012(1) 1 - 4

*Zhdanov, M.Z., Gribenko, A.V., Čuma, M., Wilson, G.A. 2012, 3D mega-cell inversion of land, marine, and airborne natural field EM data' in R. J. L. Lane (editor), Natural Fields EM Forum 2012: Abstracts from the ASEG Natural Fields EM Forum 2012: Published by Geoscience Australia, Geoscience Australia Record 2012/04.

Commercial Presentations

*Legault, J.M. and Milicevic, B. 2009, Summary Report on Helicopter-Borne ZTEM Tipper AFMAG Survey Results over Mt-Milligan Test Block, January 2009 Mackenzie Region, British Columbia behalf of GEOSCIENCE BC and TERRANE METALS CORP. Geotech Ltd. report

*Legault, J.M. and Kumar, H. 2009, 8222 - Preliminary Report on ZTEM Airborne Geophysical Survey, Shea Creek Test Block, northwestern Saskatchewan, for AREVA Resources Canada Ltd., April-2009.

*Legault, J.M. 2010, ZTEM Tipper AFMAG Results over the Lalor Lake VMS deposit; Geotech case study Feb 2010.

*Legault, J.M. 2010, ZTEM Tipper AFMAG Results over the Morrison Copper/Gold Porphyry deposit; Geotech case study Aug 2010.

Legault, J.M. and Berardelli, P. 2012, Ten years of passive airborne EM system development for mineral exploration; KEGS Symposium, March 2012

*Prihodko, A. 2010 Tribute Minerals VTEM and ZTEM Modeling: Geotech presentation. March 2010.

Robertson, K., 2011, The 2009 Pozo Seco molybdenum-gold discovery, presented at KEGS Symposium, March 2011

*Witherly, K. 2010, An Assessment of VTEM And ZTEM Data Over the Pozo Seco Skarn-CRD Molybdenum-Gold Deposit, Mexico; Condor Consulting, Inc. internal report, August 2010

*Witherly, K. 2011, ZTEM for Precious Metals Exploration; Extending the Envelope; Geotech PDAC Seminar March 2011

*Witherly, K. 2011, ZTEM-A New Paradigm in Airborne EM; CAMESE PDAC presentation; March 2011

*Witherly, K. 2010 An Assessment of Spectrem and ZTEM data over the Pebble Copper gold Porphyry Copper Deposit, ALASKA; Condor Consulting, Inc. internal report, December 2010

Appendix A: Geotech Field Logistics Report-November 2010

4. DATA PROCESSING AND PRESENTATION

Data compilation and processing were carried out by the application of Geosoft OASIS Montaj and programs proprietary to Geotech Ltd.

4.1 Flight Path

The flight path, recorded by the acquisition program as WGS 84 latitude/longitude, was converted into the WGS 84, UTM Zone 4 North coordinate system in Oasis Montaj.

The flight path was drawn using linear interpolation between x, y positions from the navigation system. Positions are updated every second and expressed as UTM easting's (x) and UTM northing's (y).

4.2 In-field Processing and Quality Control

In-Field data processing and quality control are done on a flight by flight basis by a qualified data processor (see Section 3.0). Processing steps and check up procedures are designed to assure the best possible final quality of ZTEM survey data. A general overview of those steps is presented in the following paragraphs.

The In-Field quality control can be separated into several phases:

- a. GPS Processing Phase: GPS Data are first examined and evaluated during the GrafMov processing.
- b. Raw data, ZTEM viewer phase:

Data can be viewed, examined for consistency, individual channel spectra examined and overall noise estimated in the viewer provided by the ZTEM proprietary software, on the raw flight data and raw base station data separately, on the merged data, and finally on the data that have undergone ZTEM processing.
- c. Field Geosoft phase:

Magnetic data, Radar altimeter data, GPS positioning data are re-examined and processed in this phase. Prior to splitting the lines EM data are examined flight by flight and the effectiveness of applying the attitude correction evaluated. After splitting the lines, a set of grids are generate for each parameter and their consistency evaluated. Data profiles are also re-evaluated on a line to line basis. A power line monitor channel is available in order to identify power line noise.

4.3 GPS Processing

Three GPS sensor (mounted on the airborne receiving loop) measurements were differentially corrected using the Waypoint GrafMovTM software in order to yield attitude corrections to recorded EM data.

4.4 ZTEM Electromagnetic Data

The ZTEM data were processed using proprietary software. Processing steps consist of the following preliminary and final processing steps:

4.4.1 Preliminary Processing

- a. Airborne EM, Mag, radar altimeter and GPS data are first merged with EM base station data into one file.
- b. Merged data are viewed and examined for consistency in an incorporated viewer
- c. In the next, processing phase, the following entities are taken into account:
 - the Base station coils orientation with respect to the Magnetic North,
 - the Local declination of the magnetic field,
 - Suggested direction of the X coordinate (North or line direction),
 - Sensitivity coefficient that compensates for the difference in geometry between the base station and airborne coils.
 - Rejection filters for the 60 Hz and helicopter generated frequencies.
- d. Six frequencies (30, 45, 90, 180 & 360Hz) are extracted from the airborne EM time-series coil response using windows of 0.4 seconds and the base station coils using windows of 1.0 seconds.
- e. The real (In-Phase) and imaginary (Quadrature) parts of the tipper transfer functions are derived from the In-line (X or Tzx) and Cross-line (Y or Tzy) components.
- f. Such processed EM data are then merged with the GPS data, magnetic base station data and exported into a Geosoft xyz file.

4.4.2 Geosoft Processing

Next stage of the preliminary data processing is done in a GeosoftTM environment, using the following steps:

- a. Import the output xyz file from the AFMAG processing, as well as the base Mag data into one database.
- b. Split lines according to the recorded line channel,
- c. GPS processing, flight path recovery (correcting, filtering, calculating Bird GPS coordinates, line splitting)
- d. Radar altimeter processing, yielding the altitude values in metres.
- e. Magnetic spike removal, filtering (applied to both airborne and base station data). Calculation of a base station corrected mag.
- f. Apply preliminary attitude corrections to EM data (In phase and Quadrature), filter and make preliminary grids and profiles of all channels.

4.4.3 Final Processing

Final data processing and quality control were undertaken by Geotech Ltd headquarters in Aurora, Ontario by qualified senior data processing personnel.

A quality control step consisted of re-examining all data in order to validate the preliminary data processing and to allow for final adjustments to the data.

Attitude corrections were re-evaluated, and re-applied, on component by component, flight by flight, and frequency by frequency bases. Any remaining line to line system noise was removed by applying a mild additional levelling correction.

4.4.4 ZTEM Profile Sign Convention

Tzx and Tzy tipper components do not exhibit maxima or minima above conductors, resistors or at contacts; in fact they produce cross-over type anomalies (Ward, 1959; Vozoff, 1972; Labson, 1985). The crossover polarity sign convention for ZTEM is according to the right hand Cartesian rule (Z positive –up) that is commonly used for multi-component transient electromagnetic methods.

For the North East to South West lines at the Block the sign convention for the Tzx in-line component crossover is positive-negative pointing South West to North East for tabular conductors perpendicular to the profile (Figure 6). The corresponding Tzy component in-phase cross-over polarity is positive-negative pointing South East to North West (90 degrees counter clockwise to Tzx) according to the right hand Cartesian rule.

Conversely, tabular resistive bodies produce In-Phase cross-over's that are opposite in sign to conductors. A brief discussion of ZTEM and AFMAG, along with selected forward model responses is presented in Appendix D.

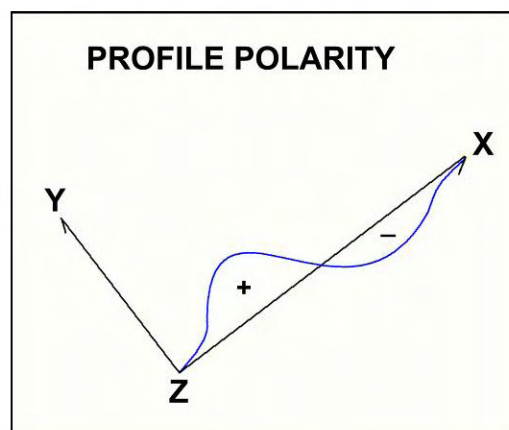


Figure 6 - ZTEM Crossover Polarity Convention for Tzx and Tzy

4.4.5 ZTEM Quadrature Sign Dependence

One important note regarding the sign of the ZTEM Quadrature, relative to the In-Phase component, particularly with regards to computer modeling and inversion.

The sign of the magnetotelluric Quadrature relative to the In-Phase tipper transfer function component pertains to the Fourier transformation of the time series to give frequency domain spectra. There are two widely used conventions for time dependence in the transformations, **$\exp(+i\omega t)$** and **$\exp(-i\omega t)$** . That which is implemented largely is a matter of personal preference and precedent. The importance of the In-Phase and Quadrature sign convention is not critical, provided that it is known and documented.

In ZTEM, the data processing code used for the Fourier transformation the time-series data to frequency domain spectra adopts a **$\exp(-i\omega t)$** time dependence (J. Dodds, Geo Equipment Manufacturing, pers. comm., Nov-2009). Whereas in the forward modeling and inversion program Zvert2d, the sign of the Quadrature relative to the In-Phase transfer function assumes an **$\exp(+i\omega t)$** dependence².

The reasons for adopting $e^{-i\omega t}$ used in ZTEM are several: a) In-phase and Quadrature profile and contour plan maps can be readily compared, since they are usually in the same-sign and quadrant (i.e. Figure 7); b) Phase-rotation and Total Divergence (DT) parameters need not be changed when comparing In-Phase versus Quadrature data.

As a result, for users interested in computer modeling and inversion of ZTEM data, the sign of the Quadrature will need to be reversed, relative to the In-Phase component, in order to provide a proper result (Figure 7). Indeed this reverse Quadrature polarity convention is assumed in all forward modeling and inversion of ZTEM data, as described in Figures 5-7 in Appendix D.

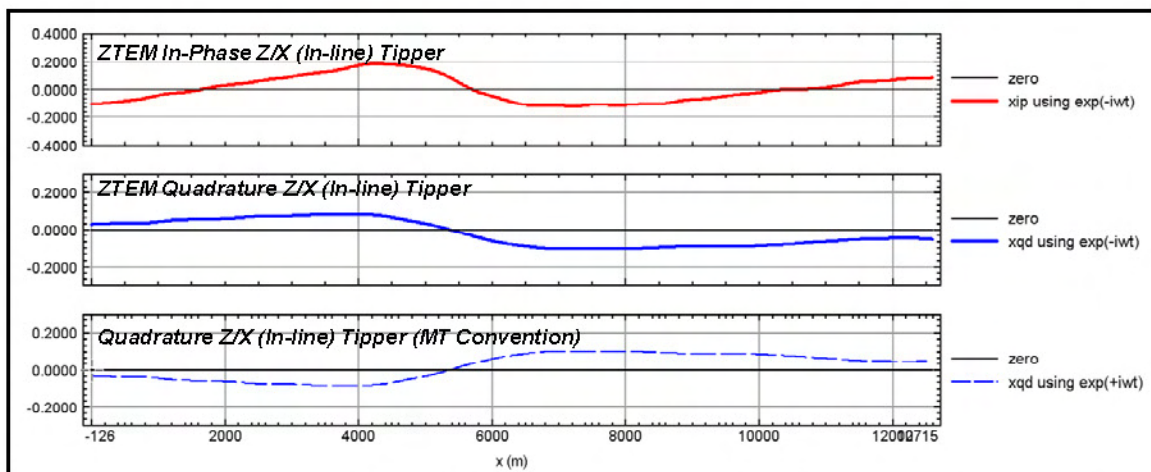


Figure 7 - Illustration of ZTEM In-Phase & Quadrature Tipper transfer function polarity convention ($e^{-i\omega t}$) relative to equivalent MT Tipper Quadrature polarity convention ($e^{+i\omega t}$) for a graphitic conductor in Athabasca Basin, SK.

² Phillip E. Wannamaker (2009): Two-dimensional Inversion of ZTEM data: Synthetic Model Study and Test Profile Images, Internal Geotech technical report by Emblem Exploration Services Inc., January 22, 2009, 32 pp.

4.4.6 Total Divergence and Phase Rotation Processing

In a final processing step DT (Total Divergence) and PR (Phase Rotation) processing are applied to the multi-frequency In-phase and Quadrature ZTEM data. This is due to the crossover nature of the Tipper Responses; these additional processing steps are applied to convert them into local maxima for easier interpretation.

To present the data from both tipper components into one image, the Total Divergence parameter, termed the DT is calculated from the horizontal derivatives of the Tzx and Tzy tippers (Lo and Zang, 2008). It is analogous to the “Peaker” parameter in VLF (Pedersen, 1998).

$$\text{Total Divergence DT:} \quad DT = DIV(T_{zx}, T_{zy}) \\ = d(T_{zx})/dx + d(T_{zy})/dy$$

This DT parameter was introduced by Petr Kuzmin (Milicevic, 2007, p. 13) and is derived for each of the In Phase and Quadrature components at individual frequencies. These in turn allow for minima over conductors and maxima over resistive zones. DT grids for each of the extracted frequencies were generated accordingly, using a reverse colour scheme with warm colours over conductors and cool colours over resistors.

The DT gives a clearer image of conductor’s location and shape but, as a derivative, it does not preserve some of the long wavelength information and is also sensitive to noise.

As an alternative, a 90 degree Phase Rotation (PR) technique is also applied to the grids of each individual component (Tzx and Tzy). It transforms bipolar (cross over) anomalies into single pole anomalies with a maximum over conductors, while preserving long wavelength information (Lo et al., 2009). The two orthogonal grids are then usually added to obtain a Total Phase Rotated grid for the In-Phase and Quadrature.

$$\text{Total Phase-Rotation:} \quad = PR(T_{zx}) + PR(T_{zy})$$

A presentation of the ZTEM test survey results over unconformity uranium deposits that illustrates DT and TPR examples, as documented by Lo et al. (2009) is provided in Appendix E.

4.4.7 2D EM Inversion

2d inversions of the ZTEM results were performed over selected lines using the Geotech Zvert2d software developed by Phil Wannamaker, U. of Utah, for Geotech Ltd. The inversion algorithm is based on the 2D inversion code with Jacobians of de Lugao and Wannamaker (1996), the 2D forward code of Wannamaker et al (1987), and the Gauss-Newton parameter step equations of Tarantola (1987). Zvert2d has been developed/modified for use with our ZTEM platform by taking into account the 75-80m air-layer between radar bird and ground surface, as well as the mobile Hz receiver and fixed Hx-Hy base stations.

The 2D code only considers the In-Line (Tzx) data and assumes that the strike lengths of bodies are infinite and orthogonal to the profile. The inversion uses a model-mesh consisting of 440 cells laterally and 62 cells vertically. Typically the ZTEM data are de-sampled to 192 pts, in order to allow the inversion to run in 10minutes or less. Typically, between 1-2% errors are added to the In-line in-phase (XIP) and Quadrature (XQD) data obtained at 30,45,90,180 & 360Hz. Errors are adjusted until numerical convergence (<1.0 rms) is attained in 8 iterations or less. All inversions are based on a predetermined homogenous starting half-space model, with 1000 ohm-m being typically used.

4.5 Magnetic Data

The processing of the total magnetic field intensity (TMI) data involved the correction for diurnal variations by using the digitally recorded ground base station magnetic values. The base station magnetometer data was edited and merged into the Geosoft GDB database on a daily basis. The aeromagnetic data was corrected for diurnal variations by subtracting the observed magnetic base station deviations.

Due to the absence of tie-lines, further tie-line or micro levelling were not applied to the magnetic data.

The corrected magnetic data was interpolated between survey lines using a random point gridding method to yield x-y grid values for a standard grid cell size of 62.5 metres. The Minimum Curvature algorithm was used to interpolate values onto a rectangular regular spaced grid.

5. DELIVERABLES

5.1 Survey Report

The survey report describes the data acquisition, processing, and final presentation of the survey results. The survey report is provided in two paper copies and digitally in PDF format.

5.2 Maps

Final maps were produced at scale of 1:50,000. The coordinate/projection system used was WGS84, UTM Zone 4 North. All maps show the flight path trace and topographic data; latitude and longitude are also noted on maps.

The preliminary and final results of the survey are presented as profile plans for the EM data that were generated for individual real (In-Phase) and imaginary parts (Quadrature) of the Tzx and Tzy components. Colour contour maps of the corresponding DT (Total Divergence) or TPR (Total Phase Rotated) grids for three of the five frequencies, (30, 45, 90, 180 and 360Hz), as well as for corresponding Phase Rotated Grids for individual components.

3D views have been constructed by plotting the either DT or TPR grids at their respective penetration depths using a 1000 ohm-m half space, using the Bostick skin depth rule (Bostick, 1977) see Appendix D.

Final maps were chosen, in consultation with the client, to represent all collected data, are listed in Section 5.3.

Sample maps of the related 3D view, Magnetic and Total Divergence are included in this report and presented in Appendix C.

5.3 Digital Data

- Two copies of the data and maps on 2 DVDs were prepared to accompany the report. Each DVD contains a digital file of the line data in GDB Geosoft Montaj.
- DVD #1 structure.
 - There are two (2) main directories;
 - Data:** contains databases, Geosoft grids & PDF maps, as described below.
 - Report:** contains a copy of the report and appendices in PDF format.
- DVD #2 structure
 - This contains the Geosoft map files

Databases in Geosoft GDB format, containing the channels listed in Table 4.

Table 4 - Geosoft GDB Data Format

Column	Description
X:	UTM Easting WGS84 Zone 4N, (Centre of the ZTEM loop) (meters)
Y:	UTM Northing WGS84 Zone 4N, (Centre of the ZTEM loop) (meters)
Longitude:	Longitude – WGS84 (Centre of the ZTEM loop) (Decimal degree)
Latitude	Latitude – WGS84 (Centre of the ZTEM loop) (Decimal degree)
Z:	Elevation- WGS84 (Centre of the ZTEM loop) (metres)
Radar:	Helicopter terrain clearance from radar altimeter (metres - AGL)
Radar_B:	Calculated ZTEM Bird terrain clearance (metres)
DEM	Digital Elevation Model (meters)
Gtime	GPS Time (seconds)
basemag	Base station mag
Mag1	Measured Total Magnetic Intensity, raw (de-spiked)
Mag2	Measured Total Magnetic Intensity, diurnal corrected
Mag3:	Levelled Total Magnetic field data
xIp_030Hz:	Tzx In-Phase 30 Hz final corrected
xIp_045Hz:	Tzx In-Phase 45 Hz final corrected
xIp_090Hz:	Tzx In-Phase 90 Hz final corrected
xIp_180Hz:	Tzx In-Phase 180 Hz final corrected
xIp_360Hz:	Tzx In-Phase 360 Hz final corrected
xQd_030Hz:	Tzx Quadrature 30 Hz final corrected
xQd_045Hz:	Tzx Quadrature 45 Hz final corrected
xQd_090Hz:	Tzx Quadrature 90 Hz final corrected
xQd_180Hz:	Tzx Quadrature 180 Hz final corrected
xQd_360Hz:	Tzx Quadrature 360 Hz final corrected
yIp_030Hz:	Tzy In-Phase 30 Hz final corrected
yIp_045Hz:	Tzy In-Phase 45 Hz final corrected
yIp_090Hz:	Tzy In-Phase 90 Hz final corrected
yIp_180Hz:	Tzy In-Phase 180 Hz final corrected
yIp_360Hz:	Tzy In-Phase 360 Hz final corrected
yQd_030Hz:	Tzy Quadrature 30 Hz final corrected
yQd_045Hz:	Tzy Quadrature 45 Hz final corrected
yQd_090Hz:	Tzy Quadrature 90 Hz final corrected
yQd_180Hz:	Tzy Quadrature 180 Hz final corrected
yQd_360Hz:	Tzy Quadrature 360 Hz final corrected
PLM:	Power Line Monitor (60Hz)

- Grids in Geosoft GRD format, as follows:

MAG:	Total Magnetic Intensity
DEM:	Digital Elevation Model
XIP_30Hz_PR:	Tzx In-Phase Component Phase Rotated grid at 30 Hz
XIP_45Hz_PR:	Tzx In-Phase Component Phase Rotated grid at 45 Hz
XIP_90Hz_PR:	Tzx In-Phase Component Phase Rotated grid at 90 Hz
XIP_180Hz_PR:	Tzx In-Phase Component Phase Rotated grid at 180 Hz
XIP_360Hz_PR:	Tzx In-Phase Component Phase Rotated grid at 360 Hz
XQd_30Hz_PR:	Tzx Quadrature component Phase Rotated grid at 30 Hz
XQd_45Hz_PR:	Tzx Quadrature component Phase Rotated grid at 45 Hz
XQd_90Hz_PR:	Tzx Quadrature component Phase Rotated grid at 90 Hz
XQd_180Hz_PR:	Tzx Quadrature component Phase Rotated grid at 180 Hz
XQd_360Hz_PR:	Tzx Quadrature component Phase Rotated grid at 360 Hz
YIP_30Hz_PR:	Tzy In-Phase Component Phase Rotated grid at 30 Hz
YIP_45Hz_PR:	Tzy In-Phase Component Phase Rotated grid at 45 Hz
YIP_90Hz_PR:	Tzy In-Phase Component Phase Rotated grid at 90 Hz
YIP_180Hz_PR:	Tzy In-Phase Component Phase Rotated grid at 180 Hz
YIP_360Hz_PR:	Tzy In-Phase Component Phase Rotated grid at 360 Hz
YQd_30Hz_PR:	Tzy Quadrature component Phase Rotated grid at 30 Hz
YQd_45Hz_PR:	Tzy Quadrature component Phase Rotated grid at 45 Hz
YQd_90Hz_PR:	Tzy Quadrature component Phase Rotated grid at 90 Hz
YQd_180Hz_PR:	Tzy Quadrature component Phase Rotated grid at 180 Hz
YQd_360Hz_PR:	Tzy Quadrature component Phase Rotated grid at 360 Hz
IP_30Hz_DT:	Total Divergence grid from In-phase components at 30 Hz
IP_45Hz_DT:	Total Divergence grid from In-phase components at 45 Hz
IP_90Hz_DT:	Total Divergence grid from In-phase components at 90 Hz
IP_180Hz_DT:	Total Divergence grid from In-phase components at 180 Hz
IP_360Hz_DT:	Total Divergence grid from In-phase components at 360 Hz
QD_30Hz_DT:	Total Divergence grid from Quadrature components at 30 Hz
QD_45Hz_DT:	Total Divergence grid from Quadrature components at 45 Hz
QD_90Hz_DT:	Total Divergence grid from Quadrature components at 90 Hz
QD_180Hz_DT:	Total Divergence grid from Quadrature components at 180 Hz
QD_360Hz_DT:	Total Divergence grid from Quadrature components at 360 Hz
IP_30Hz_TPR:	Total Phase Rotated grid from In-phase components at 30 Hz
IP_45Hz_TPR:	Total Phase Rotated grid from In-phase components at 45 Hz
IP_90Hz_TPR:	Total Phase Rotated grid from In-phase components at 90 Hz
IP_180Hz_TPR:	Total Phase Rotated grid from In-phase components at 180 Hz
IP_360Hz_TPR:	Total Phase Rotated grid from In-phase components at 360 Hz
QD_30Hz_TPR:	Total Phase Rotated grid from Quadrature components at 30 Hz
QD_45Hz_TPR:	Total Phase Rotated grid from Quadrature components at 45 Hz
QD_90Hz_TPR:	Total Phase Rotated grid from Quadrature components at 90 Hz
QD_180Hz_TPR:	Total Phase Rotated grid from Quadrature components at 180 Hz
QD_360Hz_TPR:	Total Phase Rotated grid from Quadrature components at 360 Hz

Appendix B: ZTEM Case Studies

Three-dimensional inversion of ZTEM data

Elliot Holtham and Douglas W. Oldenburg

UBC-Geophysical Inversion Facility, Department of Earth and Ocean Sciences, University of British Columbia, Vancouver, BC V6T 1Z4, Canada.

E-mail: eholtam@eos.ubc.ca

Accepted 2010 April 17. Received 2010 April 7; in original form 2009 June 1

SUMMARY

Z-Axis Tipper Electromagnetic Technique (ZTEM) data are airborne electromagnetic data which record the vertical magnetic field that results from natural sources. The data are transfer functions that relate the local vertical field to orthogonal horizontal fields measured at a reference station on the ground. The transfer functions depend on frequency and provide information about the 3-D conductivity structure of the Earth. The practical frequency range is 30–720 Hz and hence it is possible to see structures at depths of a kilometre or more if the earth is of moderate conductivity. This depth of penetration is significantly greater than that obtained with controlled source EM techniques and, when coupled with rapid spatial acquisition with an airborne system, means that ZTEM data can be used to map large-scale structures that are difficult to survey with ground based surveys. We present some fundamentals about understanding the signatures obtained with ZTEM transfer functions and then develop a Gauss–Newton algorithm to invert ZTEM data. The algorithm is applied to synthetic examples and to a field data set from the Bingham Canyon region in Utah. The field data set requires a workflow procedure to estimate appropriate noise levels in individual frequency components. These noise levels can then be used to invert multiple frequencies simultaneously. ZTEM data are insensitive to a 1-D conductivity structures and hence the background can be difficult to estimate. We provide two methods to determine appropriate background models. Interestingly, topography, which is usually a hinderance in field data interpretation, provides a first-order signal in the ZTEM data and helps with this calibration.

Key words: Inverse theory; Electromagnetic theory; Magnetotelluric.

1 INTRODUCTION

Natural source electromagnetics have an important role in understanding the electrical conductivity of upper regions of the earth. Their primary advantage, compared to controlled source methods, is the large depth of penetration that is a consequence of the plane wave excitation. The magnetotelluric (MT) method, uses ratios of electric and magnetic fields as data and it has played a significant role in crustal studies as well as in mining and hydrocarbon exploration. Its recognized importance, combined with increased computational abilities, has been the impetus for significant work in 3-D MT inversion (among others Mackie & Madden 1993; Newman & Alumbaugh 2000; Zhdanov *et al.* 2000; Farquharson *et al.* 2002; Sasaki 2004; Siripunvaraporn *et al.* 2005). A practical limitation of the MT technique and other deep probing controlled source electromagnetic methods, is that surveys are costly and time consuming because they are extremely labour intensive. It would be preferable to collect MT data in an aircraft but this goal has not yet been achieved because of the difficulty in measuring the electric fields.

In an effort to continue to use the penetration advantage of natural sources, it has long been recognized that tipper data, the ratio of the

local vertical magnetic field to the horizontal magnetic field, provide information about 3-D electrical conductivity structure. The underlying reason is that the inducing electromagnetic fields are vertically propagating plane waves and if the earth is 1-D then the vertical component of the magnetic field is zero. Non-zero values of the tipper data are thus directly related to anomalous currents. It was this understanding that prompted the development of Audio Frequency Magnetism (AFMAG) technique (Ward 1959). The original airborne AFMAG technique used the amplitude outputs from two orthogonal coils towed behind an aircraft to determine the tilt of the plane of polarization of the natural magnetic field. The tilt angle is zero over a 1-D Earth and hence the technique was particularly effective when crossing conductors. However, because the direction and strength of the inducing field varied with time, AFMAG results were not always repeatable. Limitations of the AFMAG technique were outlined in Ward *et al.* (1966).

Some of the AFMAG problems can be removed by using improved signal processing and data acquisition techniques. In particular, Labson *et al.* (1985) developed a technique that used ground based horizontal and vertical coils to measure the magnetic fields. They used MT processing techniques to show how tipper data could be obtained from the measured magnetic fields.

A further improvement to the original AFMAG technique combines improved instrumentation and MT data processing techniques. This has resulted in the Z-Axis Tipper Electromagnetic Technique (ZTEM) (Lo & Zang 2008). In ZTEM, the vertical component of the magnetic field is recorded above the entire survey area, while the horizontal fields are recorded at a ground-based reference station. MT processing techniques yield frequency domain transfer functions that relate the vertical fields over the survey area to the horizontal fields at the reference station. By taking ratios of the two fields (similar to taking ratios of the E and H fields in MT), the effect of the unknown source function is removed. Since new instrumentation exists to measure the vertical magnetic fields by helicopter, data over large survey areas can quickly be collected. The result is a cost effective procedure for collecting natural source EM data that provide information about the 3-D conductivity structure of the earth. Over the last several years industry has recognized the potential in this technique and the need to be able to invert these data.

In this paper, we present a 3-D inversion algorithm for ZTEM data. Forward modelling is fundamental to any inversion algorithm and we first show how to model the magnetic transfer functions. A simple example is used to illustrate the principles associated with ZTEM data. Next, we present our algorithm for inverting ZTEM data and apply it to a synthetic test problem. Finally, the technique is tested on a field data set from the Bingham Canyon region in Utah. We discuss practical issues of implementing the inversion and develop a workflow methodology to make the procedure more efficient.

1.1 ZTEM system and data acquisition

ZTEM instrumentation, developed by Geotech Inc, uses a helicopter to tow a coil which measures the vertical component of the magnetic field. Orthogonal coils from a single reference station measure the horizontal components of the magnetic field. The essential components of the system can be seen in Fig. 1. Time-series of the magnetic fields are recorded with a fixed sampling rate and data are binned and processed to generate transfer functions in the frequency domain. The lowest frequency of the transfer function depends upon the speed of the helicopter, and the highest depends upon the sampling rate, signal strength and noise. Although frequen-

cies up to 2800 Hz are potentially available, in practise the useable bandwidth is about 22–720 Hz. The lower frequency has a skin depth of 3300 m in a 1000 Ω m background and 330 m for a 10 Ω m background. These are depth limits that are extremely difficult to achieve with controlled source ground or airborne systems.

1.2 Magnetic transfer functions

ZTEM data are transfer functions that relate the vertical magnetic fields computed above the earth to the horizontal magnetic field at some fixed reference station. This relation is given by

$$H_z(r) = T_{zx}(r, r_0)H_x(r_0) + T_{zy}(r, r_0)H_y(r_0), \quad (1)$$

where r is the location for the vertical field, r_0 is the location of the ground based reference station and T_{zx} and T_{zy} are the vertical field transfer functions. Solving for the transfer functions requires that the vertical fields are known for two independent polarizations. The fields for each polarization are given by

$$H_z^{(1)} = T_{zx}H_x^{(1)} + T_{zy}H_y^{(1)}, \quad (2a)$$

$$H_z^{(2)} = T_{zx}H_x^{(2)} + T_{zy}H_y^{(2)}, \quad (2b)$$

or

$$\begin{pmatrix} H_z^{(1)}(r) \\ H_z^{(2)}(r) \end{pmatrix} = \begin{pmatrix} H_x^{(1)}(r_0) & H_y^{(1)}(r_0) \\ H_x^{(2)}(r_0) & H_y^{(2)}(r_0) \end{pmatrix} \begin{pmatrix} T_{zx} \\ T_{zy} \end{pmatrix}, \quad (3)$$

where the superscripts (1) and (2) refer to the source field polarization in the x and y directions, respectively. Solving eq. (3) yields the following expressions for the transfer functions,

$$T_{zx} = \frac{H_y^{(2)}H_z^{(1)} - H_y^{(1)}H_z^{(2)}}{H_x^{(1)}H_y^{(2)} - H_x^{(2)}H_y^{(1)}}, \quad (4a)$$

$$T_{zy} = \frac{-H_x^{(2)}H_z^{(1)} + H_x^{(1)}H_z^{(2)}}{H_x^{(1)}H_y^{(2)} - H_x^{(2)}H_y^{(1)}}. \quad (4b)$$

To forward model the transfer functions, one must have the capability to solve the natural source field problem for different polarizations of the source field. A procedure to do this is presented next.

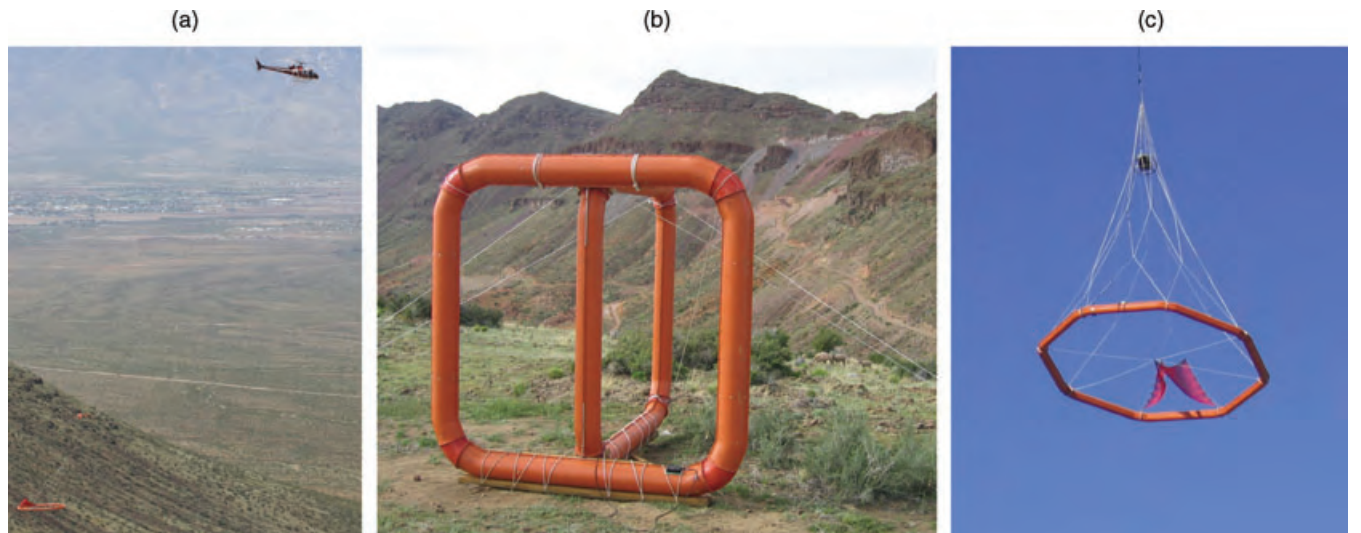


Figure 1. (a) Helicopter flying a coil to measure the vertical magnetic field. (b) Ground based reference station. (c) Coil used to measure the vertical fields.

1.3 Forward modelling

Our forward modelling procedure is essentially that outlined in Farquharson *et al.* (2002), where the solution of Maxwell's equations is that of Haber *et al.* (2000). In brief, Maxwell's equations in the quasi-static regime, when combined with the constitutive relations of charge conservation and Ohm's law, form the necessary equations for ZTEM modelling. These equations read,

$$\nabla \times \mathbf{E} - i\omega\mu\mathbf{H} = 0, \quad (5a)$$

$$\nabla \times \mathbf{H} - \sigma\mathbf{E} = 0, \quad (5b)$$

$$\nabla \cdot \mathbf{J} = 0, \quad (5c)$$

$$\mathbf{J} - \sigma\mathbf{E} = 0, \quad (5d)$$

where \mathbf{E} is the electric field, \mathbf{H} is the magnetic field, ω is the angular frequency, σ is the conductivity, and \mathbf{J} is the current density. We have assumed an $e^{-i\omega t}$ time-dependence and that the magnetic permeability μ is constant and equal to that of free space, μ_0 . To solve for the fields, the electric field is decomposed into vector and scalar potentials $\mathbf{E} = \mathbf{A} + \nabla\phi$ and the Coulomb gauge condition $\nabla \cdot \mathbf{A} = 0$ is imposed for uniqueness. Using the decomposition and eliminating \mathbf{H} yields the potential equations

$$\nabla^2 \mathbf{A} + i\omega\mu_0\sigma(\mathbf{A} + \nabla\phi) = 0, \quad (6)$$

$$\nabla \cdot \mathbf{J} = \nabla \cdot [\sigma(\mathbf{A} + \nabla\phi)] = 0. \quad (7)$$

For our modelling we discretize the earth into rectangular cells and, after applying a finite volume technique (Haber *et al.* 2000) to eqs (6) and (7), we obtain the system of equations to be solved. In this staggered discretization, the scalar potential is defined on the cell centres while the vector potential is defined by the normal components at the centre of the cell faces. To solve for the total fields we use a primary-secondary decomposition. The primary fields equations, which must only be solved once on the background conductivity model, are

$$\begin{pmatrix} \mathbf{L} + i\omega\mu_0\mathbf{S} & i\omega\mu_0\mathbf{SG} \\ \mathbf{DS} & \mathbf{DSG} \end{pmatrix} \begin{pmatrix} \mathbf{A}_p \\ \phi_p \end{pmatrix} = 0. \quad (8)$$

\mathbf{A}_p are the primary vector potentials on the mesh and ϕ_p are the primary scalar potentials. \mathbf{L} represents the discretization of the Laplacian operator, \mathbf{S} represents the harmonically averaged background cell conductivities, and \mathbf{G} and \mathbf{D} are the discretizations of the gradient and divergence operators. The normal component of \mathbf{J} and the tangential component of $\nabla \times \mathbf{A}$ are specified on the boundary by computing the appropriate one and 2-D boundary values. Once the background fields have been calculated, the source term is known for the secondary field calculation. The equations for the secondary field are

$$\begin{pmatrix} \mathbf{L} + i\omega\mu_0\mathbf{S} & i\omega\mu_0\mathbf{SG} \\ \mathbf{DS} & \mathbf{DSG} \end{pmatrix} \begin{pmatrix} \mathbf{A}_s \\ \phi_s \end{pmatrix} = \begin{pmatrix} -i\omega\mu_0\Delta\mathbf{S}\mathbf{E}_p \\ -\mathbf{D}\Delta\mathbf{S}\mathbf{E}_p \end{pmatrix}, \quad (9)$$

where $\Delta\mathbf{S} = \mathbf{S} - \mathbf{S}_p$ is the difference between the averaged conductivities of the actual model and those of the background, and \mathbf{E}_p is the primary electric field. For the secondary formulation the secondary potentials are assumed to vanish on the mesh boundaries. For each source polarization (one for an x -directed H-field at the top of the mesh, and the other for a y -directed H-field) the resulting H fields are computed.

1.4 Currents and transfer functions

Since a 1-D earth produces no vertical magnetic fields, it is deviations from a 1-D conductivity structure that causes a ZTEM response. With the addition of two and 3-D structure, new anomalous currents will flow in the earth. It is these anomalous currents,

$$\mathbf{J}_{\text{anomalous}} = \mathbf{J}_{\text{total}} - \mathbf{J}_{\text{primary}} \quad (10)$$

the give rise to vertical magnetic fields. We investigate the currents and associated vertical magnetic fields by considering the models in Fig. 2 of conductive and resistive prisms in a moderate conductivity host. Fig. 3 shows the anomalous current density, computed using the 3-D forward modelling code described in the previous section, for a vertical slice through the prisms. The anomalous current is fairly uniform and strongest inside the block. The magnetic field and transfer functions (Fig. 4) look like that obtained from an extended dipole current. The anomalous currents for a resistive block flow in the opposite direction compared to the conductive block. For Fig. 4, the T_{zx} transfer functions correspond to the electric field

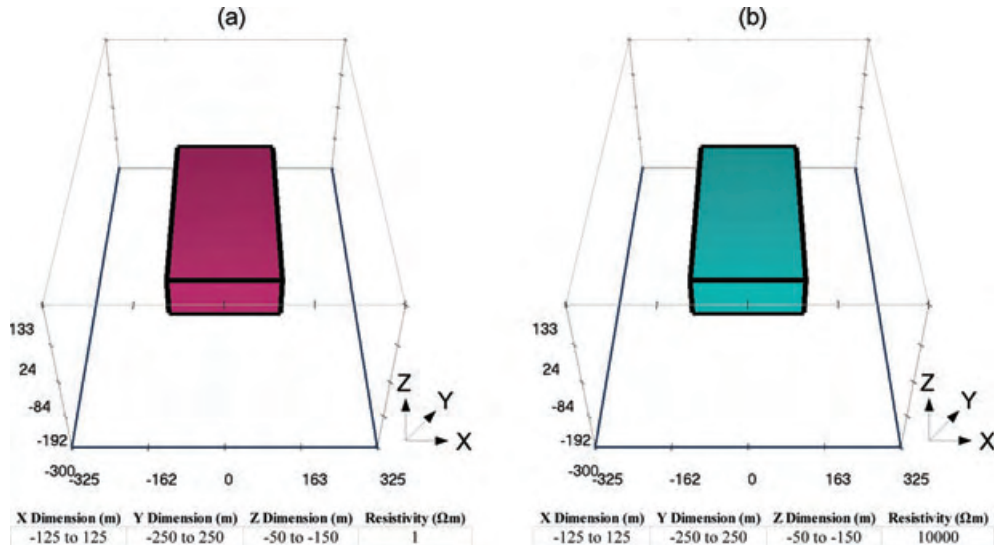


Figure 2. (a) 1 Ωm conducting block buried in a 200 Ωm background. (b) 10000 Ωm resistive block buried in a 200 Ωm background.

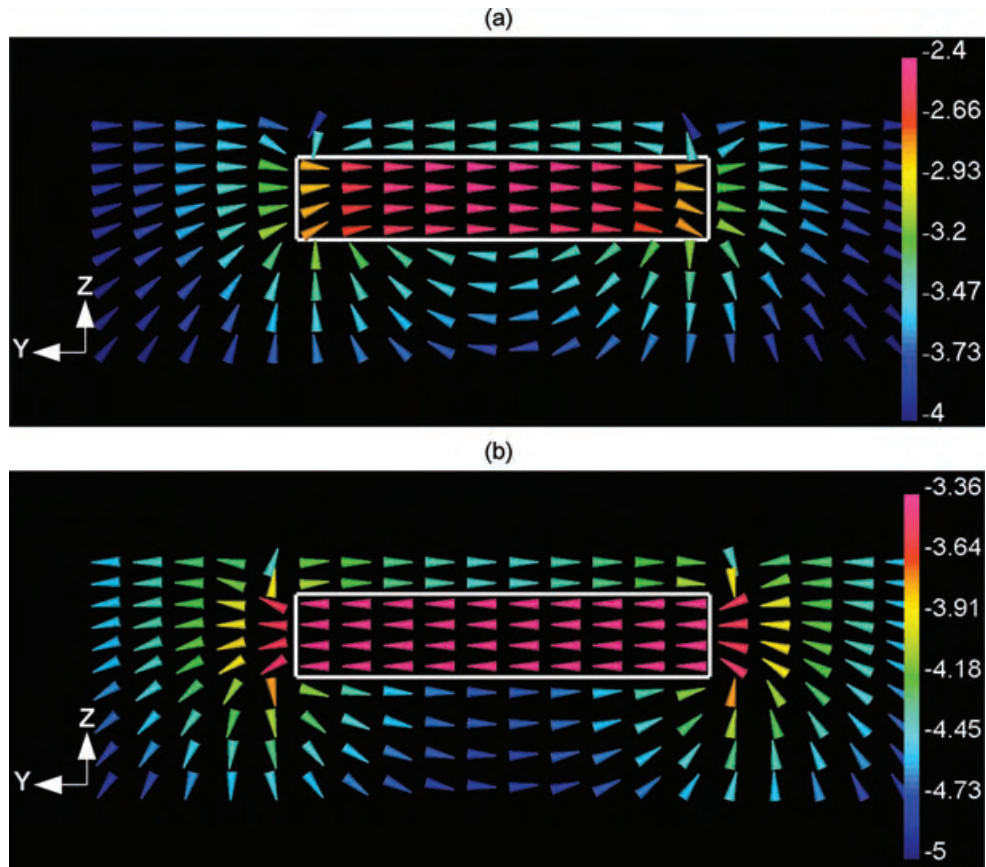


Figure 3. The real anomalous current densities [$\text{Log}_{10}(\frac{A}{m^2})$] in the z - y plane ($x = -25$ m) for a source whose electric field is polarized in the $(-\hat{y})$ direction. The white rectangles are the outlines of the original blocks. Panel (a) is the current for the conductive block, while panel (b) is the current for the resistive block. The anomalous current is mostly localized inside the block.

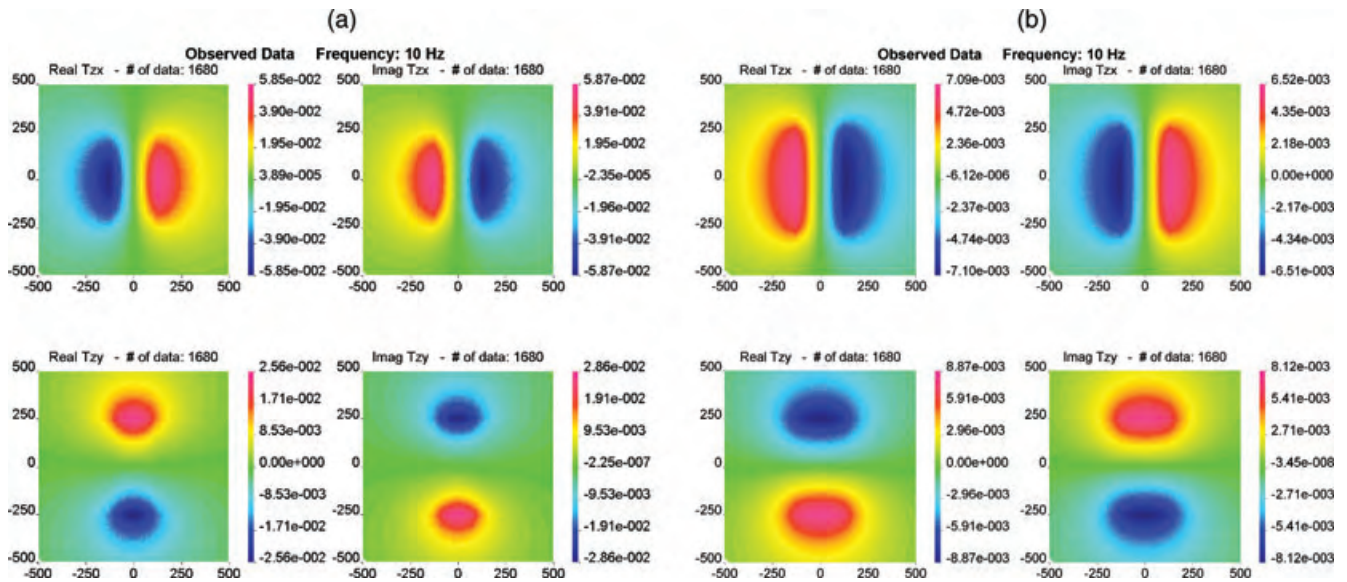


Figure 4. Resulting transfer functions for the two block example of Fig. 2. Panel (a) corresponds to a conductive block while panel (b) corresponds to a resistive block. The transfer functions closely resemble the magnetic fields due to a finite line current inside the blocks.

polarized in $-\hat{y}$, while the T_{zy} response corresponds to the orthogonal polarization where the electric field is in \hat{x} . The direction of the anomalous current determines the sign of the response while the distance between positive and negative maxima is related to the size of the block.

2 INVERSE PROBLEM

For simple geometries the concepts of anomalous currents can help interpret ZTEM data. For instance, a linear filter can be applied to the vertical magnetic field (Karous & Hjelt 1983) to generate current

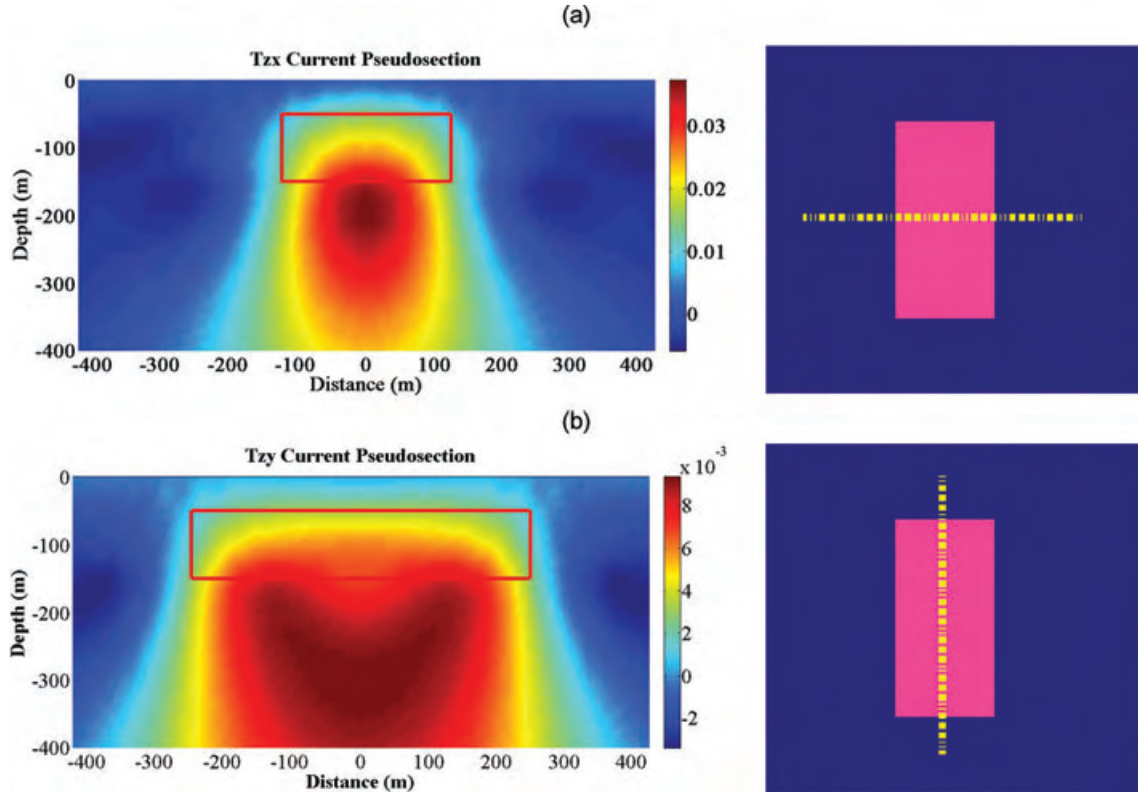


Figure 5. Current pseudo-section obtained by linear filtering the transfer functions for the model in Fig. 2. Panel (a) is the linear filtering of the T_{zx} transfer function along the cross section $y = 0$ m. Panel (b) is the filtering of the transfer function T_{zy} , along the cross section $x = 0$ m. The true outline of the conducting block is superimposed in red. For this simple example, linear filtering the two transfer functions gives an indication about the lateral boundaries of the block.

pseudo-sections. An example of filtering the real components of the transfer functions produced from the conductive model in Fig. 2 is shown in Fig. 5. These plots were generated using the Matlab code of Sundararajan *et al.* 2006. For this simple block in a half-space example, the block geometry may be adequately interpreted from the current pseudo-sections. Nonetheless, in the case of complex 3-D models, 3-D inversions are necessary.

Our inversion algorithm is based on the MT inversion code of Farquharson *et al.* (2002). By minimizing the objective function

$$\Phi = \phi_d + \beta \phi_m, \quad (11)$$

we obtain our solution to the inverse problem. ϕ_d is the data-misfit, ϕ_m is amount of structure in the model and β is the trade-off or regularization parameter. We use the sum of squares as the measure of misfit

$$\phi_d = \|\mathbf{W}_d(\mathbf{d}^{\text{obs}} - \mathbf{d}^{\text{prd}})\|_2^2, \quad (12)$$

where \mathbf{d}^{obs} is the observation vector, \mathbf{d}^{prd} is the vector of predicted data and \mathbf{W}_d is a diagonal matrix whose elements are the reciprocals of the standard deviations of the data errors. The measure of model

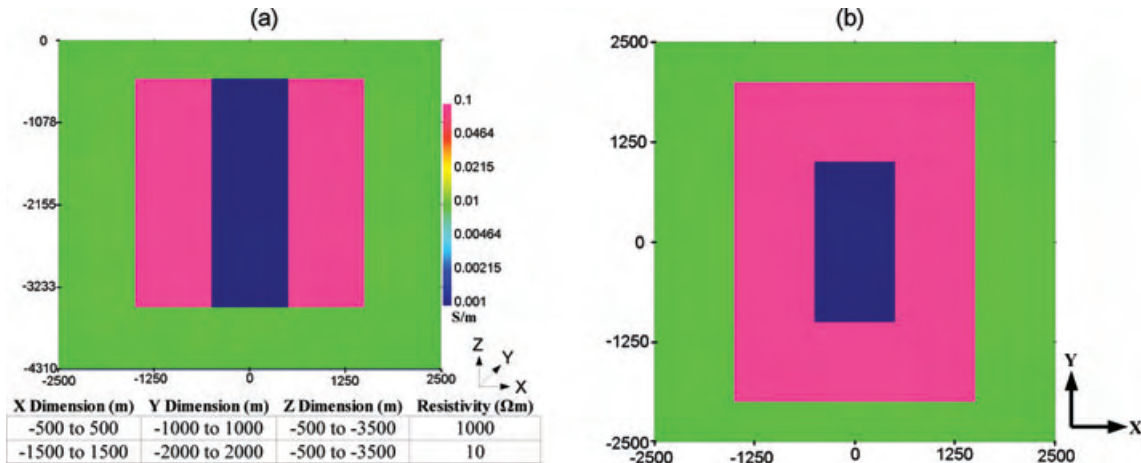


Figure 6. Conductivity model: a resistor surrounded by a conductor, all buried in a 100 Ωm background half-space. (a) Cross-section through $y = 0$ m. The bottom table summarizes the block dimensions and resistivities. (b) Depth slice at 1000 m.

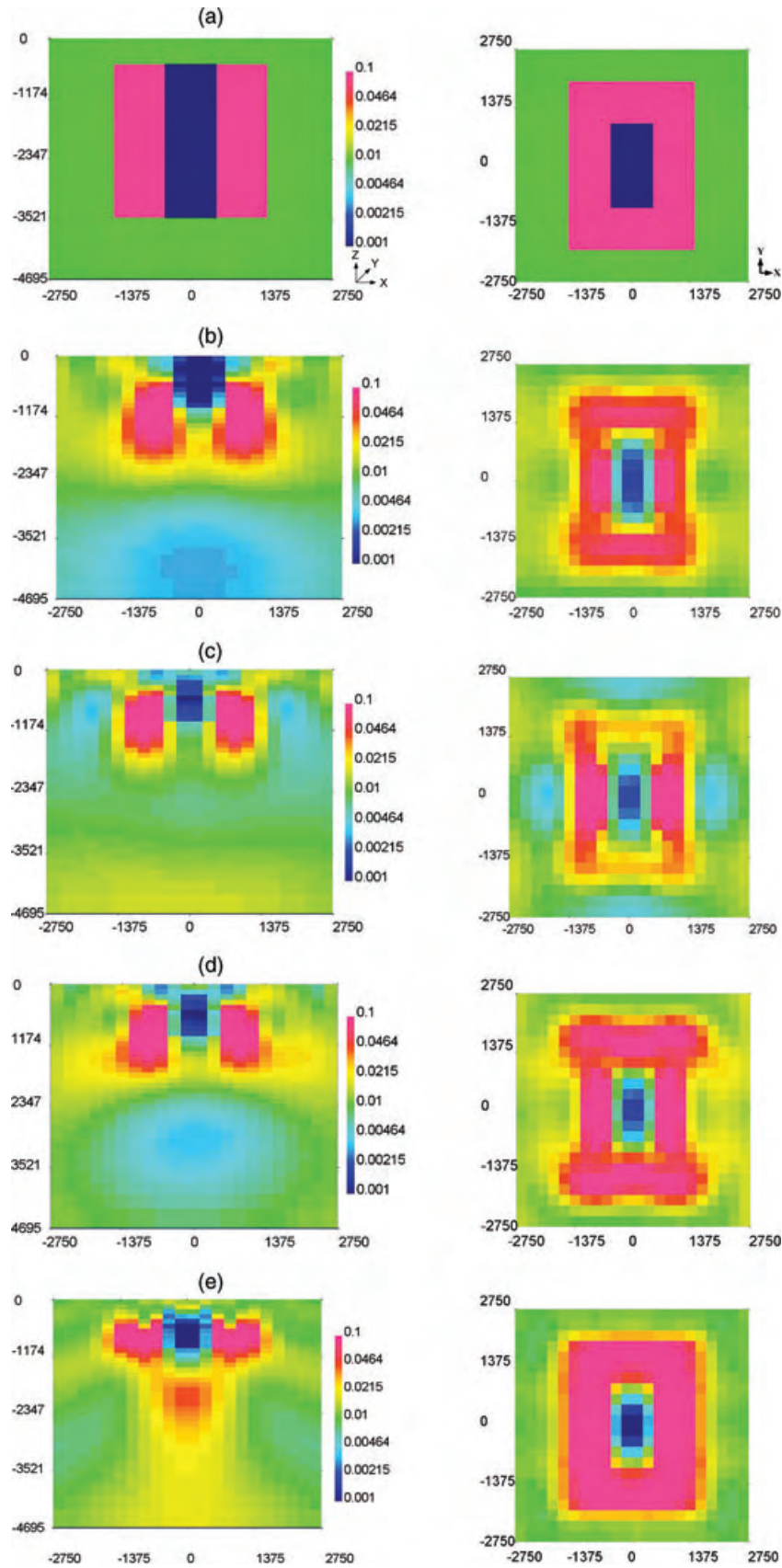


Figure 7. Conductivity model (S m^{-1}) from the inversion of the synthetic model data. Figure (a) is a cross section at the centre of the model and a plan view section at a depth of 800 m. Panels (b)–(d) are results of inverting data at 1 Hz. Panel (b) is the inversion of the real parts, panel (c) is the imaginary parts and panel (d) is the real and imaginary components. Panel (e) is the simultaneous inversion of six frequencies.

structure is

$$\phi_m = \alpha_s \|\mathbf{W}_s(\mathbf{m} - \mathbf{m}^{\text{ref}})\|_2^2 + \alpha_x \|\mathbf{W}_x(\mathbf{m} - \mathbf{m}^{\text{ref}})\|_2^2 + \alpha_y \|\mathbf{W}_y(\mathbf{m} - \mathbf{m}^{\text{ref}})\|_2^2 + \alpha_z \|\mathbf{W}_z(\mathbf{m} - \mathbf{m}^{\text{ref}})\|_2^2,$$

where \mathbf{W}_s is a diagonal matrix and \mathbf{W}_x , \mathbf{W}_y and \mathbf{W}_z are the first-order finite-difference matrices in the x , y and z directions, and \mathbf{m}^{ref} is a reference model. The α 's are adjustable parameters. α_s controls the closeness of the recovered model to the reference, while $\alpha_{x,y,z}$ determine the smoothing in the x , y and z directions. For the minimization of the objective function at the $(n + 1)$ th iteration, the Gauss–Newton method requires the solution of

$$(\mathbf{J}^T \mathbf{W}_d^T \mathbf{W}_d \mathbf{J} + \beta \mathbf{W}^T \mathbf{W}) \delta \mathbf{m} = -\mathbf{J}^T \mathbf{W}_d^T \mathbf{W}_d (\mathbf{d}^{\text{obs}} - \mathbf{d}^n) - \beta \mathbf{W}^T \mathbf{W} (\mathbf{m}^n - \mathbf{m}^{\text{ref}}), \quad (13)$$

where \mathbf{m}^n is the vector of model parameters from the previous iteration, \mathbf{J} is the Jacobian matrix of sensitivities, \mathbf{W} is such that $\mathbf{W}^T \mathbf{W} = \sum \alpha_k \mathbf{W}_k^T \mathbf{W}_k$, and $\delta \mathbf{m}$ is the model perturbation. Since

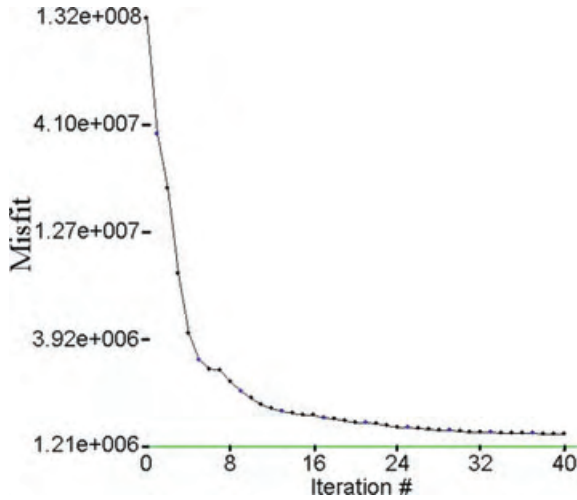


Figure 8. Convergence curve for the inversion of six frequencies for the synthetic inversion model. The algorithm reduced the misfit to 1.38×10^6 (target misfit 1.21×10^6)

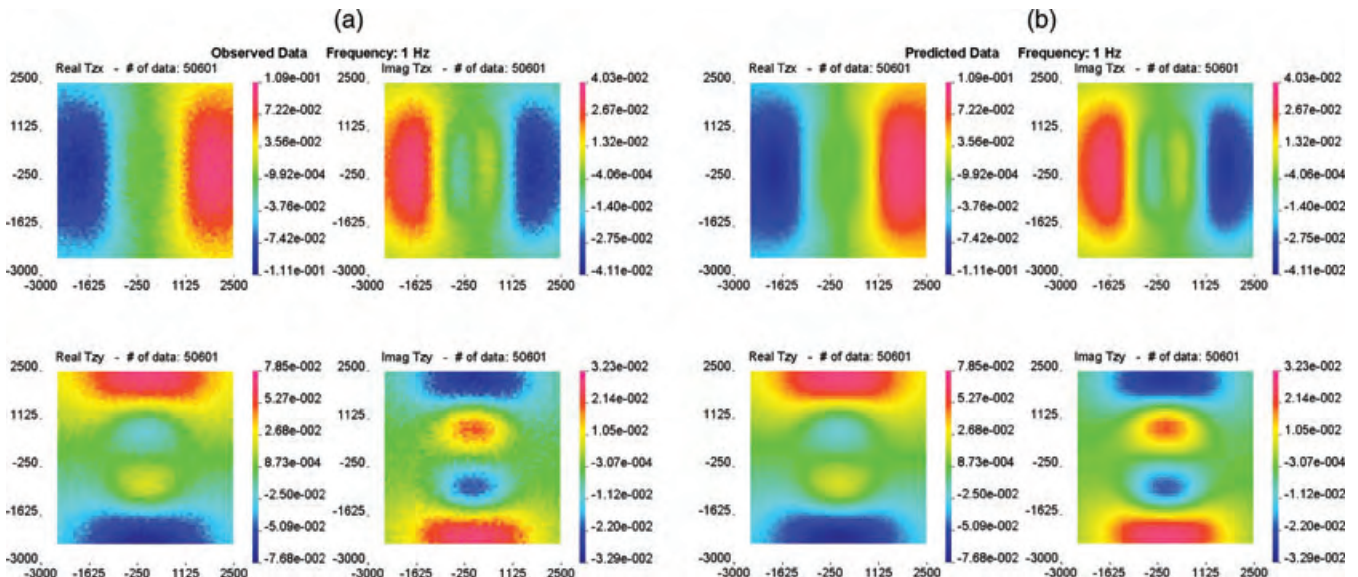


Figure 9. Panel (a) is the observed data and panel (b) is the predicted data for the synthetic model at 1 Hz. There is excellent agreement between the observed and predicted data.

ZTEM data are different than MT data, the Jacobian matrix must be modified accordingly. The implementation however follows that outlined in Farquharson *et al.* (2002). Eq. (13) is solved using an inexact preconditioned conjugate gradient (IPCG) (Saad 2003) algorithm. Typically, 5 IPCG iterations are performed to solve equation (13) for each value of β . Since \mathbf{J} is prohibitively large to compute, this solution method only requires the sparse matrix operations $\mathbf{W}^T \mathbf{W}$, \mathbf{J} , \mathbf{J}^T on a vector. β is initially chosen to be large such that $\beta \mathbf{W}^T \mathbf{W}$ dominates the approximate Hessian in eq. (13). It is then reduced in a cooling schedule such that at each subsequent iteration $\beta_{k+1} = \gamma \beta_k$, where γ is a constant. Efficient implementation of this inversion in application to field data sets requires a workflow procedure but we postpone details about that until Section 4.

3 SYNTHETIC INVERSION

We illustrate the inversion of ZTEM data using a synthetic example that was chosen to emulate a porphyry deposit. The model has a central resistive core, an outer region of high conductivity, and is buried in a moderate conductivity background. The conductivity structure is shown in Fig. 6. The Earth was discretized into a mesh containing $42 \times 42 \times 57$ cells in the x , y and z directions, respectively. The cell dimensions in the central core region were $250 \times 250 \times 100$ m in the x , y and z directions, respectively. The vertical fields at 1, 3.2, 5.6, 10, 18 and 32 Hz were computed at a fixed height of 100 m over the surface. This frequency range is shifted somewhat from the traditional ZTEM survey but this is inconsequential for the purpose of testing the code. The data were computed at 10 m intervals and 50 m line-spacing over a $5 \text{ km} \times 5 \text{ km}$ region. The horizontal field components were computed at a ground based reference station at a location r_0 of $x = -3000$ m, $y = -3000$ m. For each component of each frequency Gaussian noise, equal to 3.5 per cent of the difference between the 10th percentile and 90th percentile data, was added. The initial model and reference models were homogeneous half-spaces of $100 \Omega\text{m}$. We first inverted different subsets of the data to determine their information content. The 1 Hz data were inverted with the real and imaginary components separately and then the 1 Hz data were inverted with both the real and imaginary components. From the two sections of the model

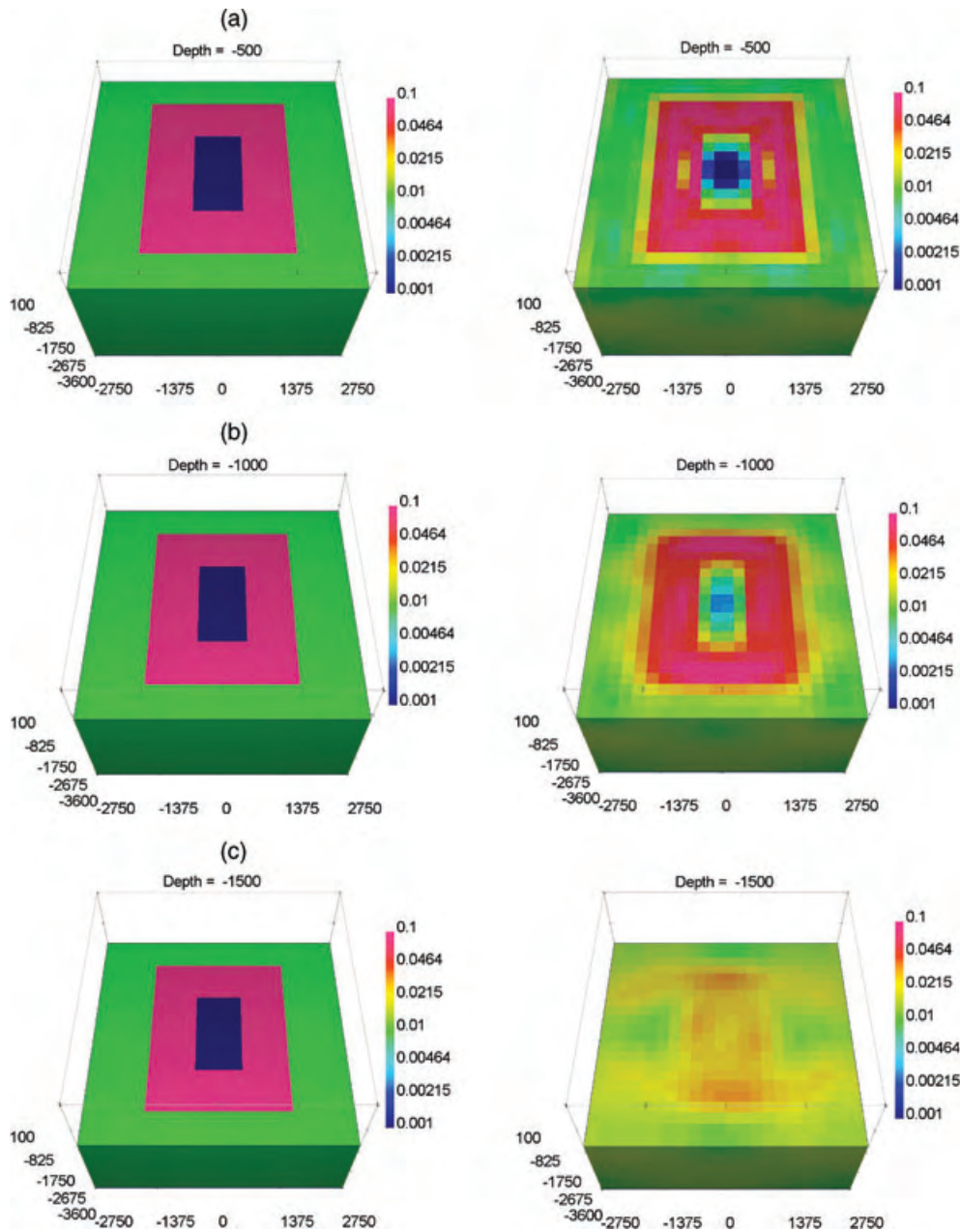


Figure 10. Conductivity model (S m^{-1}) from the inversion of the synthetic model using six frequencies. Slices of the true model (left-hand panels) and recovered model (right-hand panels) are shown at 500, 1000 and 1500 m.

inversions in Fig. 7, it is clear that both the real and imaginary components contain significant information and that both components of the data should be obtained in a ZTEM survey. Since 1 Hz is the lowest frequency used, it also resolves the deepest structure. Next all six frequencies were inverted simultaneously. The inversion was executed in parallel over 6 dual processors. The convergence curve for the inversion is shown in Fig. 8. The recovered model fits the data well and select data are shown in Fig. 9. The final model in Fig. 10 recovers both the conductivity and block dimensions in the x and y directions very well. There is significant improvement in the block resolution in the x and y directions over the single 1 Hz inversion. The inverted result shows that the top interface is well resolved, however, the base of the blocks are not. This is consistent with skin depth arguments of the lowest frequency.

3.1 Effect of the reference station

An important component of the ZTEM survey is the reference station that is used to compensate for the unknown source amplitude and polarization. The transfer functions are the ratio of the vertical fields to the horizontal field at the reference station. Ideally the fields at the reference station are those due to a 1-D conductivity structure; however this is not necessary for two reasons. First, the variation between the horizontal fields at the reference station and the observation point are generally small even if there are lateral changes in conductivity. Second, the location of the reference station is included in the modelling, and no assumptions have been made about the conductivity structure between the reference station and the observation point. To illustrate that the choice of reference

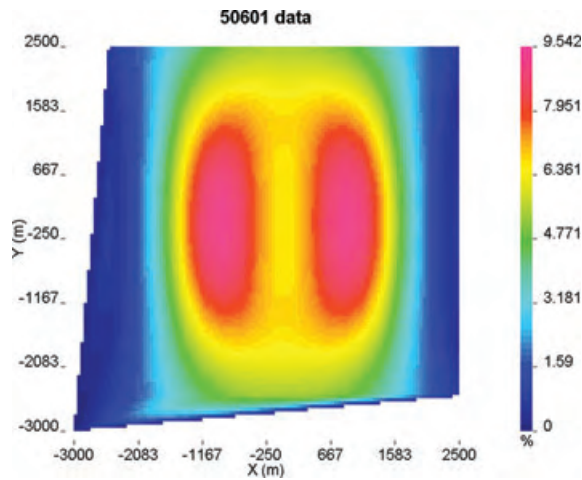


Figure 11. Per cent difference in the \hat{x} component of the magnetic field between the reference location and the measurement location (source electric field in the $-\hat{y}$ direction).

station does not drastically change the inversion result, we compute the relative difference, $\frac{||H_x(r) - H_x(r_{ref})||}{||H_x(r_{ref})||}$ for one source polarization on the synthetic inversion model using a reference station at $x = -3000$ m, $y = -3000$ m. As can be seen in Fig. 11 the variations in the horizontal fields are less than 9.5 per cent over the entire survey area.

The location of the maximum deviations of 9.5 per cent occurs at $x = -900$ m, $y = 0$ m. We now recompute the data using a new reference station located at this point of maximum deviation. We invert the new data keeping all other aspects of the inversion unchanged from the inversion using a reference station at $x = -3000$ m, $y = -3000$ m. The comparison between the two inversion results can be seen in Fig. 12. As we would expect, when the reference location is correctly modelled, the inversion result is not strongly dependent upon the location of the reference station.

A more interesting example concerns the result of working with an incorrect location of the reference station. In some surveys, the model domain can be excessively large if the remote is far away from the survey area. It would be desirable to have an artificial location for the reference station inside the modelling domain. We simulate this by computing the data using the reference location outside the survey area ($x = -3000$ m, $y = -3000$ m), and then mislocating the reference location to $x = -900$ m, $y = 0$ m during the inversion. By misplacing the reference station, we are in essence scaling the data by a factor that depends on the difference in horizontal fields between the true location and the new reference location. The results from this inversion in Fig. 12 show that even if the reference station is misplaced to the worst location, we may still recover a reasonable model.

4 3-D INVERSION OF ZTEM FIELD DATA

In the winter of 2008, field data were acquired by Exploration Syndicate Inc. over a $15 \text{ km} \times 20 \text{ km}$ area adjacent to the Bingham Canyon mine in Utah. The data were collected as time-series which were then stacked and processed into transfer functions using proprietary Geotech software. The results were filtered and attitude corrected. The terrain in the survey block is extremely rugged which makes it challenging to interpret the data. During the survey, 495.5 line kilometres of data (real and imaginary components) were acquired

at five frequencies (30, 45, 90, 180 and 360 Hz). To complicate the problem, a significant portion of the data was affected by cultural noise and needed to be removed before the data could be inverted.

The 3-D inversion of any geophysical field data set is a complex and time consuming process that requires a logical work flow in order to be completed accurately and efficiently. We present our workflow in (Fig. 13). In this section of the paper, we invert the field data and at the same time illustrate some specific parts of this workflow.

4.1 Discretizing the earth

To solve the necessary differential equations, the Earth must be discretized into a mesh and the discrete system for Maxwell's equations formed. In this discretization step a compromise must be achieved between the numerical accuracy in the forward modelling and the computational resources required. As with MT discretization problems, the usual guidelines that cell sizes must not violate skin depth rules apply. Unique to the ZTEM problem is that the reference station may be located far from the region of interest. This may increase the number of cells in the model because it is necessary to keep the cells small in order to accurately model the fields at the reference station. Also, since ZTEM data are very sensitive to topography, it is important to finely discretize the topography. These requirements, when combined with the high frequency and large geographic areas covered in ZTEM surveys, can require large meshes and significant computational overhead.

Due to large survey areas and extremely rugged topography it was challenging to obtain an efficient discretization for the Bingham Canyon survey. The topography was obtained from the United States National Elevation Database (Fig. 14). The Earth was discretized into a mesh containing $96 \times 92 \times 95$ cells in the x , y and z directions. Over a single flight path the elevation could change by over 3000 ft and over the entire model the elevation changed by 4000 ft. The central region had $78 \times 65 \times 54$ cells that were $250 \text{ m} \times 250 \text{ m} \times 50 \text{ m}$ in the x , y and z directions. This 50 m vertical cell dimension allowed for the topography to be reasonably modelled. To keep the number of cells in the mesh as small as possible, during the inversion the location of the reference station was moved closer to the ZTEM lines.

4.2 Determining a background model

In the MT problem, where electric fields are measured, the background can be chosen either using the apparent resistivities or by choosing the half-space conductivity which minimizes the data misfit between the half-space data and the true data. These methods cannot be used for ZTEM since all 1-D conductivity models produce zero data. Nevertheless, the anomalous currents and data are affected by the background conductivity for 3-D models. Our experience shows that it is important to initialize the inversion with a good estimate of the background conductivity, especially if the anomalous bodies are deeply buried. If this is not done, then the inversion may recover a reasonable estimate of the relative conductivities, but fail to adequately reproduce the data and also be a poor approximation to the true model. We illustrate these principals by starting the 1 Hz inversion of the synthetic model with an initial background of $10\,000 \text{ } \Omega\text{m}$ instead of the $100 \text{ } \Omega\text{m}$ true background. The model smallness parameter, α_s , was set to be 0 so that the reference model does not affect the inversion. From the misfit curve in Fig. 15 we see that the inversion was initially able to significantly reduce the misfit. During the first part of the inversion, some

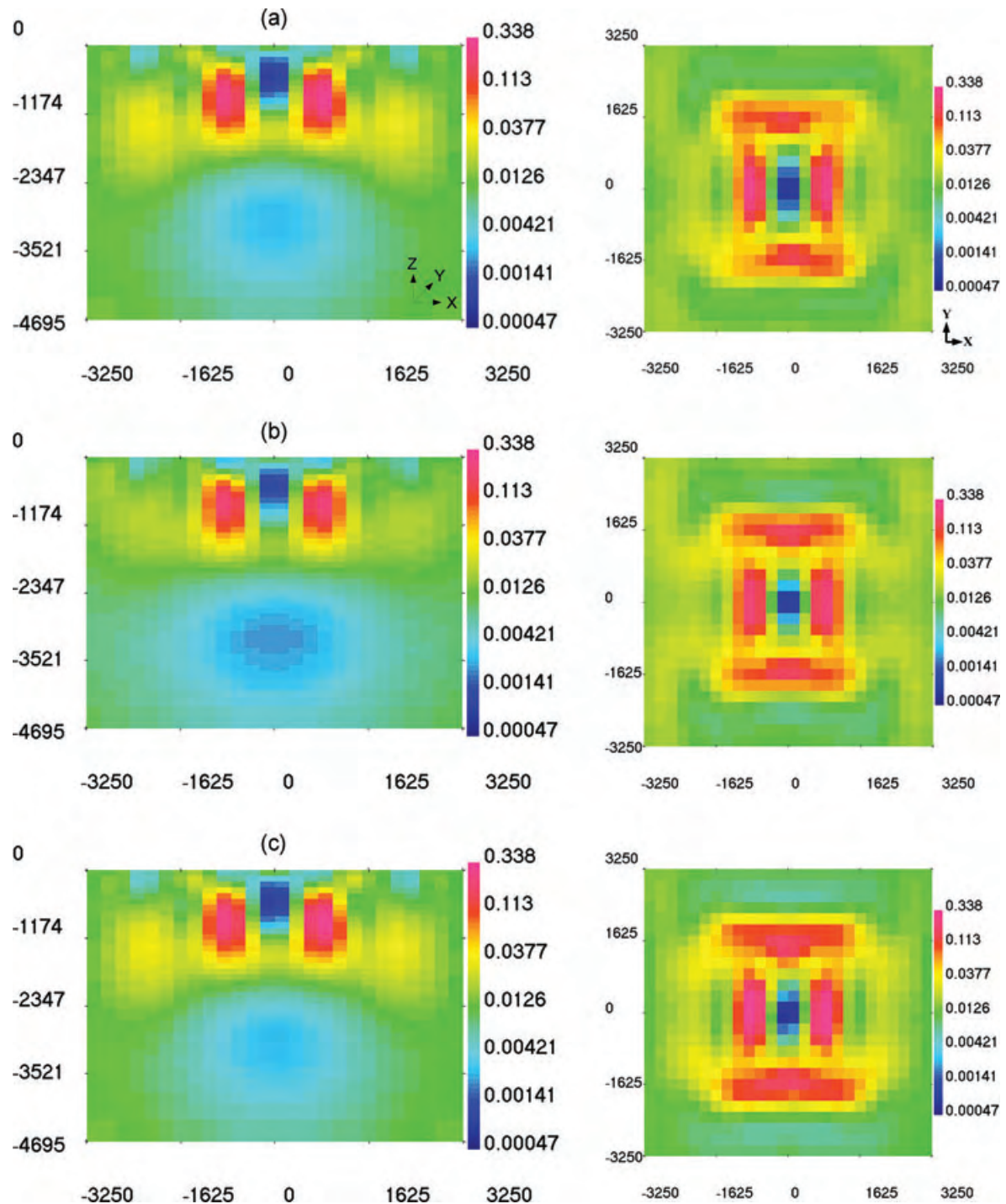


Figure 12. Conductivity model (S m^{-1}) from the inversion of the synthetic model data using different reference station locations. Figure (a) is a cross section at the centre of the model and a plan view section at a depth of 800 m that corresponds to a reference station located at $x = -900$ m, $y = 0$ m. For each inversion all of the parameters except the location of the reference station remain unchanged. Panel (a) corresponds to a reference station located at $x = -3000$ m, $y = -3000$ m. panel (b) corresponds to a reference station located at $x = -900$ m, $y = 0$ m. Panel (c) corresponds to data computed using a reference station at $x = -3000$ m, $y = -3000$ m, but during the inversion process the reference station is mislocated at $x = -900$ m, $y = 0$ m.

estimate of the relative conductivity has been established, however, it becomes increasingly difficult to fit the data since the background conductivity is drastically incorrect. Eventually, the inversion algorithm terminates with the final model in Fig. 15. Clearly, this is not a satisfactory result.

This inversion result motivated the following procedure. We used the inversion shown in Fig. 15 but selected a model just prior to the

sharp change in slope on the misfit curve. We assumed that the relative conductivities on that model were correct. That conductivity was scaled by various constants and the data from the models were computed. The misfit between the true data and data produced from the scaled models is shown in Fig. 16. The smallest data misfit occurred when the conductivity of the preliminary model was scaled by a factor of 10. The conductivity in the survey area of the scaled

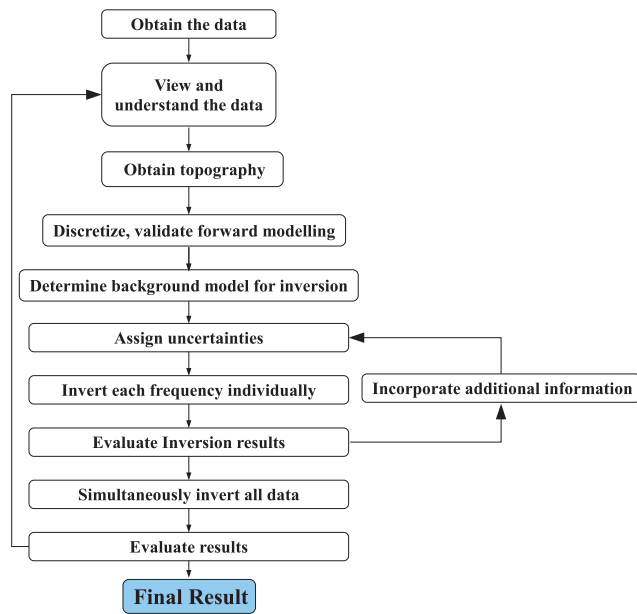


Figure 13. Work flow process summarizing the critical step in a ZTEM inversion.

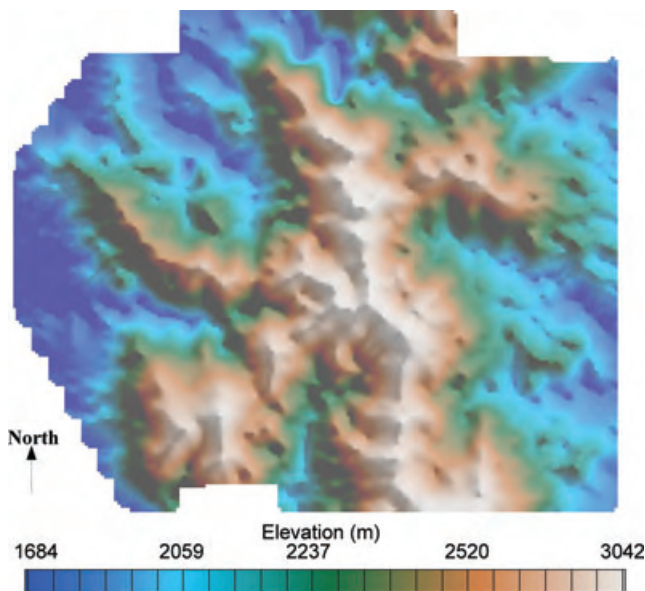


Figure 14. Topography from survey area near Bingham Canyon.

model was then averaged to obtain a background conductivity. This new conductivity was determined to be $169 \Omega\text{m}$ instead of the actual $100 \Omega\text{m}$. This procedure of determining relative conductivities, scaling, and averaging, provides a method for determining appropriate starting models even if the starting background conductivity is incorrect by a few orders of magnitude. The final inversion result using the new $169 \Omega\text{m}$ background is shown in Fig. 17. It is a significant improvement over the preliminary inversion in Fig. 15.

With significant topography, even a uniform conductivity model will generate charge build up and anomalous currents. For these geometries it is possible to find the conductivity that best fits the given data. This method is illustrated using a synthetic model of a mountain with a resistor and conductor buried underneath. This model, shown in Fig. 18, has a true background resistivity of $100 \Omega\text{m}$. Data were computed at 960 locations above the mountain. Uniform

background models (50, 75, 100, 150, 200 and $250 \Omega\text{m}$) with the correct topography, were forward modelled to obtain data at the same 960 locations. The data misfits between the background and the true models were computed and are shown in Fig. 19. The background that produces the smallest data misfit matches the true conductivity. This method thus allows background models to be created when topography exists and when little additional information is available.

4.3 Assigning uncertainties

Assigning uncertainties to data is a critical step in any geophysical inversion. Overestimating the noise will result in a loss of information which could have been extracted from the data. Similarly, underestimating the noise may create artefacts in the inverted model that are not present in the data. Assigning uncertainties for any geophysical field data set is difficult because there are many error sources, each of which is difficult, if not impossible to quantify. Survey errors such as instrument repeatability, human error, external noise, and misorientation of receivers are often thought to be the only sources of errors that need to be considered in an inversion. These sources are important, however, there are many additional sources of errors such as discretization, modelling approximations, and matrix solution errors. Ultimately, it is difficult to quantify the individual error sources, let alone their sum. Nevertheless it is essential that there is a robust and repeatable method to assign uncertainties to the data.

Unlike some electromagnetic surveys where the dynamic range of the data can vary by several orders of magnitude, ZTEM data generally have small dynamic ranges. Because of this, the standard deviations are assigned as a constant value for each data component. Nevertheless, for field inversions these levels are not known and hence we have used an iterative approach to estimate them. For individual frequencies, each datum is assigned an uncertainty which is a fraction of the dynamic range of the data. Each frequency is inverted separately and then the assigned uncertainties are scaled such that the achieved normalized misfit is unity. This balances the relative importance of each frequency when the simultaneous inversion is carried out. This iterative approach in which the errors on individual frequencies are examined first, before tackling the full inversion problem, ensures that assigning incorrect uncertainties on a few data points, or data associated with a certain frequency, does not ruin the entire inversion.

For the Bingham Canyon inversion, the quality of the data in each component of each frequency was examined. Some regions of the data were removed because they were suspect or because the data were acquired in a region of high power line noise. The dynamic range of each data component (real and imaginary components separately) was determined by sorting the absolute values of the data. The range was assigned to be the difference between the 10th percentile and 90th percentile data. For each frequency and data component, the errors were initially assigned as 12.5 per cent of the range. Inverting each frequency independently ensured the correct data weighting between each frequency. Fig. 20 shows the misfit curve for two frequency components inverted with the initial error estimates. It is clear that the two frequencies need to be scaled by different amounts.

4.4 Bingham Canyon inversion results

Both the real and imaginary components of five frequencies were inverted for the Bingham Canyon ZTEM survey. The inversion was completed without prior knowledge of the geology so no additional

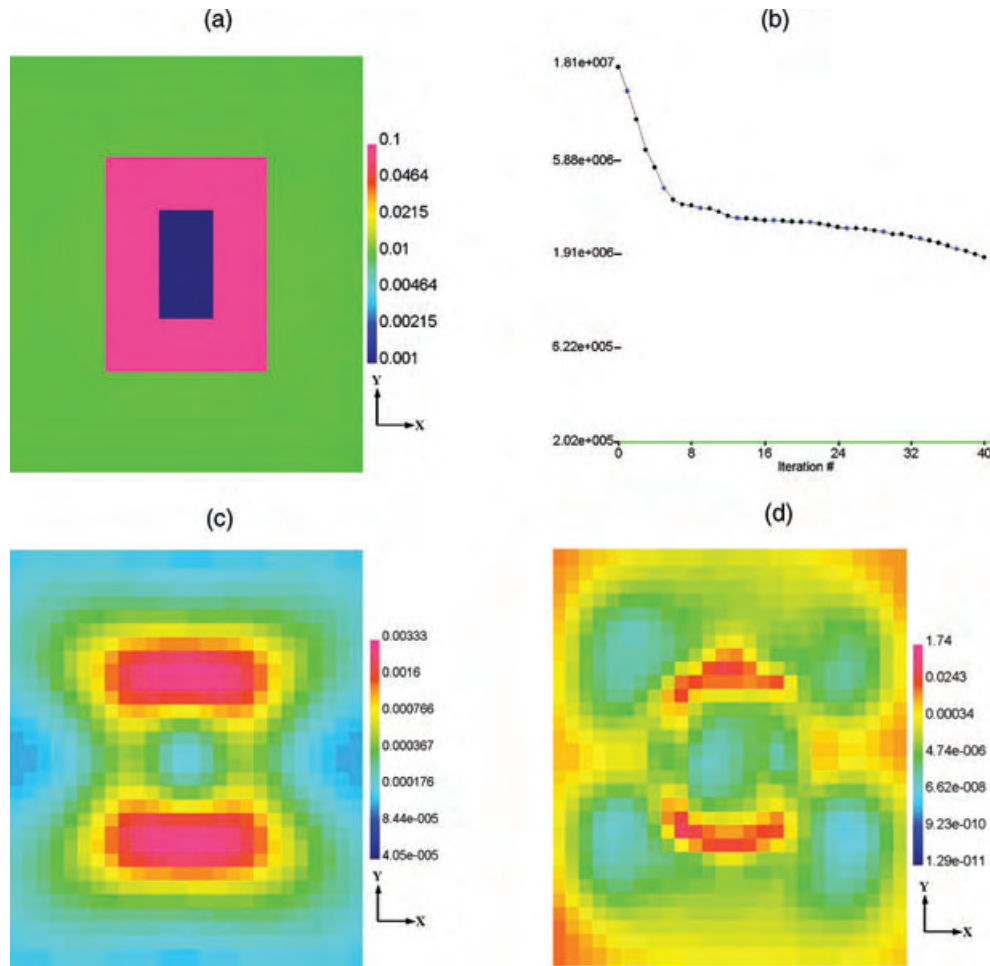


Figure 15. (a) Conductivity (S m^{-1}) of the synthetic true model at a depth of 800 m. (b) Misfit curve. (c) Inverted model at 800 m, using a 10 000 Ωm starting model, taken at the sharp change of slope on the misfit curve. (d) Final inversion model starting with a 10 000 Ωm initial model. The recovered model structure and conductivity values are not reasonable. Here $\alpha_s = 0$, $\alpha_x = \alpha_y = \alpha_z = 1$.

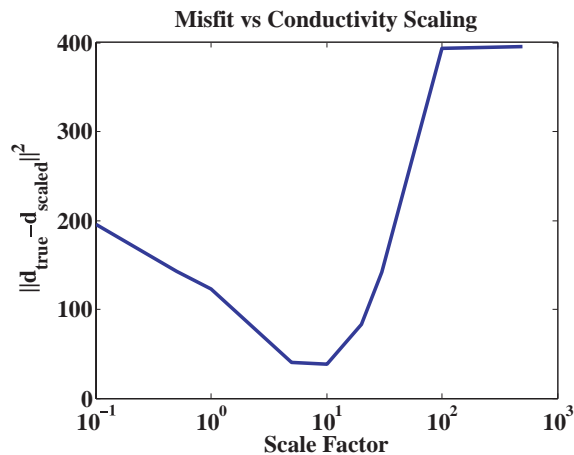


Figure 16. Data misfit for various conductivity scaling factors.

information was incorporated into the inversion. We did however impose respective upper and lower bounds of 2 S m^{-1} – $3.33 \times 10^{-5} \text{ S m}^{-1}$ on the allowed model conductivity for the inversion. The initial and reference models had a constant resistivity of 500 Ωm , and the model smallness parameter, α_s , was set to 10^{-12} . The inversion was run on 5 Intel Xeon 2.33 Ghz dual quad core processors.

It took 76 hr to decrease the misfit to 1.59×10^6 (target misfit 1.52×10^6). After the inversion was completed, a basic geological model for the survey area was obtained. Some surface features in our conductivity model seem to correspond with the local geology. In particular, a well known conducting shale region in the southeast and another conductor to the west have expressions in the inverted model (Fig. 21). Of more economic potential is a feature shown in Fig. 21(b) which coincides with a porphyry outcrop.

5 DISCUSSION AND CONCLUSIONS

The ZTEM technique is a promising method to explore for large scale targets at depth because of easy data acquisition and deep penetration of natural source fields. The data are transfer functions that relate the vertical magnetic field at the observation point to the horizontal fields at a ground based reference station. The reference station is an important component of the system and is needed to compensate for the unknown source field amplitude and polarization. The reference station would ideally be located outside the survey block in a flat region with a 1-D conductivity structure. In practice this is often not possible. However, because the horizontal fields generally have small variations over the survey area and the location of the reference station is modelled in the data, the inversion of ZTEM data is fairly robust with respect to the placement of

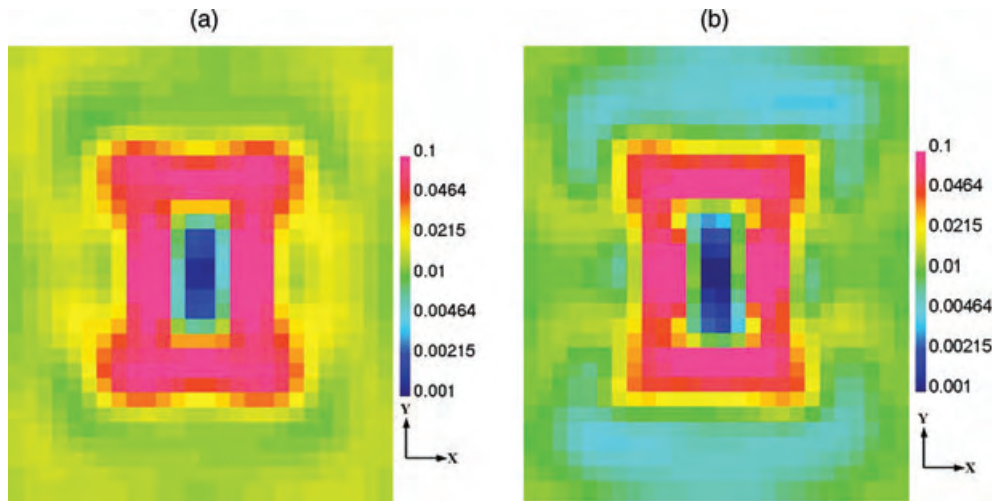


Figure 17. (a) Inverted model (S m^{-1}) at a depth of 800 m starting with the correct initial background conductivity. (b) Inverted model at a depth of 800 m using the scaling method to determine the initial conductivity.

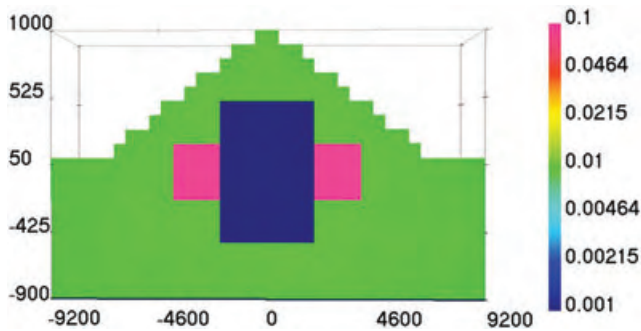


Figure 18. Synthetic test example (S m^{-1}) to show that the method of fitting a best fitting half-space to the data can be used if the model has sufficient topography. The synthetic model has a resistor and conductor buried below a 100 Ωm mountain.

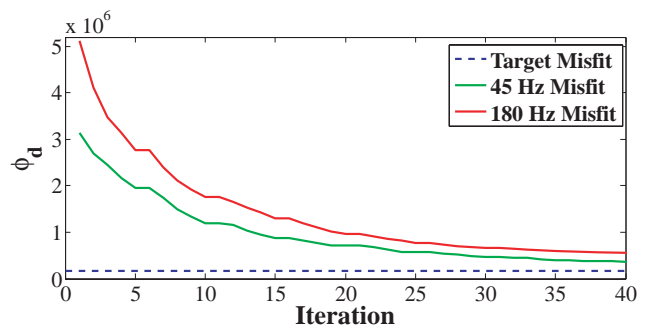


Figure 20. Misfit curve for initial error estimates at 45 and 180 Hz. Even though the same initial error estimates were applied to both frequencies, the assigned errors on the two frequencies must be scaled by different amounts so that they have equal influence in the final inversion. Here $\alpha_s = 10^{-12}$, $\alpha_x = \alpha_y = \alpha_z = 1$.

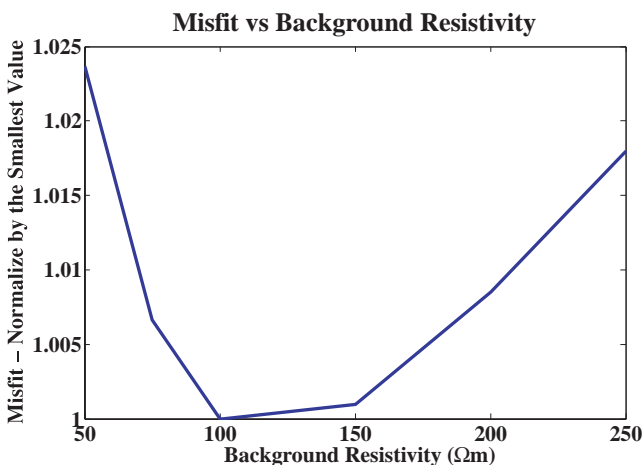


Figure 19. Misfit between the true data and the data produced from different conductivity background models. It is apparent that the 100 Ωm background model which matches the true model background conductivity produces the smallest data misfit.

the reference station. Also, we have shown here that mislocation of reference station may not be critical to a first pass interpretation.

Despite the above comments, there are possible developments with respect to the reference station that may improve ZTEM inversion results. One option would be to use multiple reference locations. A remote reference station (Goubau *et al.* 1978; Gamble *et al.* 1979a,b; Clarke *et al.* 1983) can be used to remove noise from measured magnetotelluric signals and this could be applied to further remove unwanted noise from ZTEM signals. Also, multiple reference stations could be used to obtain information about the horizontal fields in both the background region and the survey area. A natural extension of this idea would be to measure both the vertical and horizontal fields from the helicopter. In this configuration, the data would be the ratio of the vertical field and horizontal field measured at the same location. In addition, it may be possible to derive new useful data from horizontal transfer functions that relate the horizontal field recorded at the helicopter to the horizontal field at a reference station.

In summary, we have developed a 3-D inversion algorithm for ZTEM data using a Gauss–Newton approach. The inversion algorithm shows promising results on a synthetic test problem and illustrates the enhanced depth of penetration that can be obtained by using natural source fields. Because 3-D inversion of

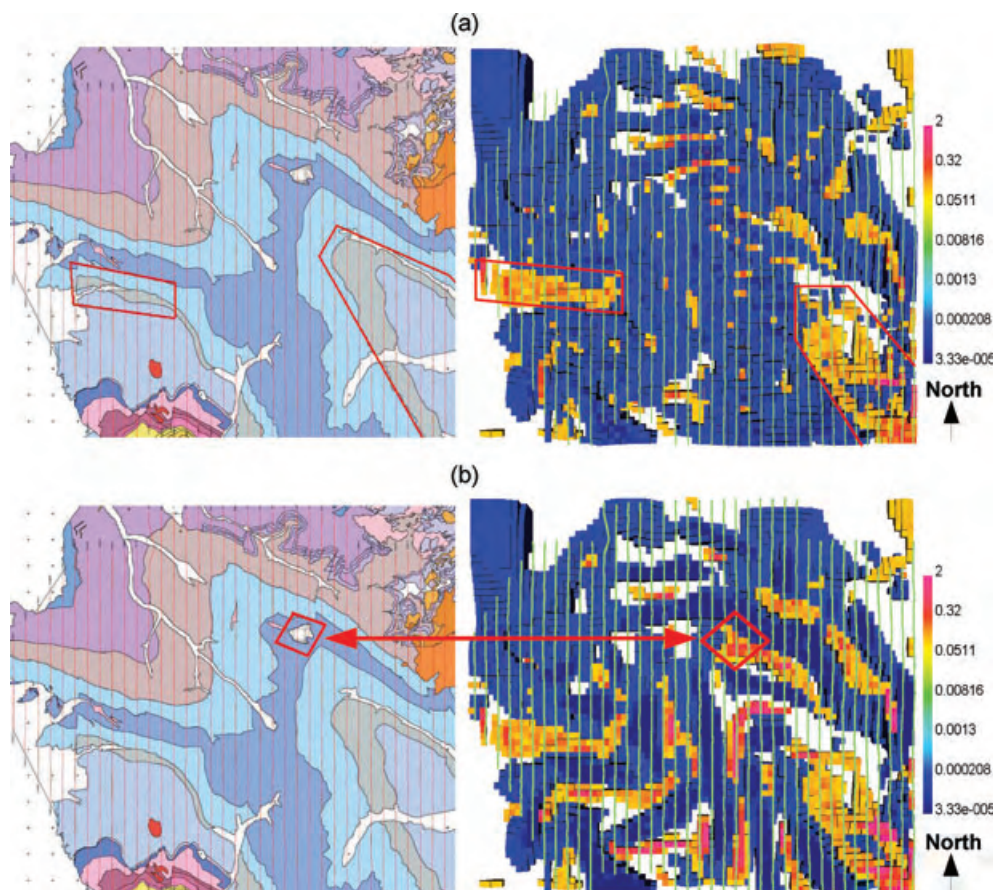


Figure 21. (a) Comparison of the known surface geology (left-hand panel) and inverted model, at the surface, (right-hand panel). There is agreement between the two large known conducting features, outlined in red. The inverted model has cut-offs to show conductors ($>0.1 \text{ S m}^{-1}$), and resistors ($<0.00025 \text{ S m}^{-1}$). (b) Comparison of a small porphyry outcropping from the geological model and the inverted model viewed at 1600 m. The inverted model has cut-offs to show conductors ($>0.1 \text{ S m}^{-1}$), and resistors ($<0.00025 \text{ S m}^{-1}$). Note that the inversion places a large conductor directly below the porphyry outcropping.

electromagnetic field data is a complex task, we present the essential inversion elements as a workflow process. Using this approach, field data were inverted from the Bingham Canyon region in Utah. The final inverted model not only fit the data but also showed correspondences with some known geological features from the area.

ACKNOWLEDGMENTS

The authors would like to acknowledge Exploration Syndicate Inc. for providing the data and a geological map of the Bingham Canyon region.

REFERENCES

- Clarke, J., Gamble, T., Goubau, W.M., Koch, R. & Miracky, R., 1983. Remote-reference magnetotellurics: equipment and procedures, *Geophys. Prospect.*, **31**(1), 149–170.
- Farquharson, C.G., Oldenburg, D.W., Haber, E. & Shekhtman, R., 2002. An algorithm for the three-dimensional inversion of magnetotelluric data, in *Proceedings of the 72nd Annual International Meeting, SEG, Expanded Abstracts*, pp. 649–652.
- Gamble, T.D., Goubau, W.M. & Clarke, J., 1979a. Magnetotellurics with a remote magnetic reference, *Geophysics*, **44**(1), 53–68.
- Gamble, T.D., Goubau, W.M. & Clarke, J., 1979b. Error analysis for remote reference magnetotellurics, *Geophysics*, **44**(5), 959–968.
- Goubau, W.M., Gamble, T. & Clarke, J., 1978. Magnetotelluric data analysis: removal of bias, *Geophysics*, **43**, 1157–1166.
- Haber, E., Ascher, U.M., Aruliah, D.A. & Oldenburg, D.W., 2000. Fast simulation of 3D electromagnetic problems using potentials, *J. Comput. Phys.*, **163**(1), 150–171.
- Karous, M. & Hjelt, S.E., 1983. Linear filtering of vlp dip-angle measurements, *Geophys. Prospect.*, **31**(5), 782–794.
- Labson, V.F., Becker, A., Morrison, H.F. & Conti, U., 1985. Geophysical exploration with audiofrequency natural magnetic fields, *Geophysics*, **50**(4), 656–664.
- Lo, B. & Zang, M., 2008. Numerical modeling of z-tem (airborne AF-MAG) responses to guide exploration strategies, *SEG Technical Program Expanded Abstracts*, **27**(1), 1098–1102.
- Mackie, R.L. & Madden, T.R., 1993. Three-dimensional magnetotelluric inversion using conjugate gradients, *Geophys. J. Int.*, **115**, 215–229.
- Newman, G.A. & Alumbaugh, D.L., 2000. Three-dimensional magnetotelluric inversion using non-linear conjugate gradients, *Geophys. J. Int.*, **140**, 410–424.
- Saad, Y., 2003. *Iterative Methods for Sparse Linear Systems*, Society for Industrial and Applied Mathematics, Philadelphia, PA, USA.
- Sasaki, Y., 2004. Three-dimensional inversion of static-shifted magnetotelluric data, *Earth Planets Space*, **56**(2), 239–248.
- Siripunvaraporn, W., Egbert, G., Lenbury, Y. & Uyeshima, M., 2005. Three-dimensional magnetotelluric inversion: data-space method, *Phys. Earth planet. Inter.*, **150**(1–3), 3–14, Electromagnetic Induction in the Earth.

- Sundararajan, N., Ramesh Babu, V., Shiva Prasad, N. & Srinivas, Y., 2006. Vlfpros—a matlab code for processing of vlf-em data, *Comput. Geosci.*, **32**, 1806–1813.
- Ward, S.H., 1959. Aftmag—airborne and ground, *Geophysics*, **24**(4), 761–787.
- Ward, S.H., O'Donnell, J., Rivera, R., Ware, G.H. & Fraser, D.C., 1966. Aftmag - applications and limitations, *Geophysics*, **31**(3), 576–605.
- Zhdanov, M.S., Fang, S. & Hursan, G., 2000. Electromagnetic inversion using quasi-linear approximation, *Geophysics*, **65**(5), 1501–1513.

Three-dimensional inversion of MT and ZTEM data

Elliot Holtham and Douglas W. Oldenburg, UBC-Geophysical Inversion Facility, University of British Columbia*

SUMMARY

ZTEM is an airborne electromagnetic survey in which the vertical magnetic field from natural sources is recorded. The data are transfer functions that relate the local vertical field to orthogonal horizontal fields measured at a reference station on the ground. The transfer functions depend on frequency and provide information about the 3D conductivity structure of the Earth. Since a 1D conductivity structure produces no vertical magnetic fields, the ZTEM technique is not very sensitive to the background conductivity. In order to increase sensitivity to the background conductivity, and greatly improve the depth of investigation, MT and ZTEM data can both be collected. The combination of sparse MT data, with the economical and rapid spatial acquisition of airborne ZTEM data, creates a cost effective exploration technique that can map large-scale structures at depths that are difficult to image with other techniques. We develop a Gauss-Newton algorithm to jointly invert ZTEM and MT data. The algorithm is applied to a synthetic model and to a field example from the Reese River geothermal property in Nevada.

INTRODUCTION

Natural source electromagnetics have an important role in understanding the electrical conductivity of upper regions of the Earth. Their primary advantage, compared to controlled source methods, is the depth of penetration that is a consequence of the plane wave excitation. The magnetotelluric (MT) method uses ratios of electric and magnetic fields as data and it has played a significant role in crustal studies as well as in mining and hydrocarbon exploration. A practical limitation of the MT technique however, is that surveys are costly and time consuming because many expensive stations must be installed to measure all of the field components at the surface of the earth. It would be preferable to collect MT data in an aircraft but this goal has not yet been achieved because of the difficulty in measuring the electric fields. In an effort to continue to use the penetration advantage of natural sources, it has long been recognized that tipper data, the ratio of the local vertical magnetic field to the horizontal magnetic field, provide information about 3D electrical conductivity structure. It was this understanding that prompted the development of AFMAG (Audio Frequency Magnetics) Ward (1959). However, because the direction and strength of the inducing field varies with time, AFMAG results were not always repeatable. Limitations of the AFMAG technique were outlined in Ward et al. (1966).

Many of the AFMAG problems can be removed by using improved signal processing and instrumentation. This has resulted in the Z-Axis Tipper Electromagnetic Technique (ZTEM) Lo and Zang (2008). In ZTEM, the vertical component of the magnetic field is recorded above the entire survey area, while

the horizontal fields are recorded at a ground-based reference station. MT processing techniques yield frequency domain transfer functions typically between 30-720 Hz that relate the vertical fields over the survey area to the horizontal fields at the reference station. By taking ratios of the two fields (similar to taking ratios of the E and H fields in MT), the effect of the unknown source function is removed. Since new instrumentation exists to measure the vertical magnetic fields by helicopter, data over large survey areas can quickly be collected. The result is a cost effective procedure for collecting natural source EM data that provide information about the 3D conductivity structure of the earth. The technique is particularly good for finding large scale targets at moderate depths. It is well known however that 1D layered structures produce zero vertical magnetic fields and thus ZTEM data cannot recover such background conductivities. If the background structure is 3D there will be an effect on the data and correspondingly ZTEM data will contain information about the conductivity. In general however, ZTEM data may have reduced sensitivity about the background conductivity and it is desirable to obtain robust conductivity information from other sources. This information could come from a priori geologic and petrophysical information or from additional geophysical data such as MT.

To counter the costly nature of large MT surveys and the insensitivity of the ZTEM technique to the background conductivity, an effective exploration survey can collect both MT and ZTEM data. A sparse MT survey grid can gather information about the background conductivity and deep structures while keeping the survey costs affordable. Higher spatial resolution at moderate depths can be obtained by flying multiple lines of ZTEM data. In this paper we show how MT and ZTEM data can be jointly inverted in three dimensions to provide cost effective exploration solutions.

ZTEM DATA

The ZTEM data relate the vertical magnetic fields computed above the Earth to the horizontal magnetic field at some fixed reference station. This relation is given by

$$H_z(r) = T_{zx}(r, r_0)H_x(r_0) + T_{zy}(r, r_0)H_y(r_0), \quad (1)$$

where r is the location for the vertical field, and r_0 is the location of the ground based reference station. Our source functions for the natural fields are random and, as with MT, we need two polarizations. The transfer functions for each polarization are given by

$$\begin{pmatrix} H_z^{(1)}(r) \\ H_z^{(2)}(r) \end{pmatrix} = \begin{pmatrix} H_x^{(1)}(r_0) & H_y^{(1)}(r_0) \\ H_x^{(2)}(r_0) & H_y^{(2)}(r_0) \end{pmatrix} \begin{pmatrix} T_{zx} \\ T_{zy} \end{pmatrix}, \quad (2)$$

where the superscripts (1) and (2) refer to the source field polarization in the x and y directions respectively.

Modelling ZTEM and MT data

INVERSION

Our MT inversion algorithm is that of Farquharson et al. (2002) and our ZTEM inversion algorithm is that of Holtham and Oldenburg (2008) and Holtham and Oldenburg (2010). Our algorithm to invert MT and ZTEM data simultaneously was obtained by modifying these codes. The solution is obtained by an iterative Gauss-Newton procedure based on Haber et al. (2000).

By minimizing the objective function

$$\Phi = \phi_d + \beta \phi_m, \quad (3)$$

we obtain our solution to the inverse problem. ϕ_d is the data-misfit, ϕ_m is amount of structure in the model, and β is the trade-off or regularization parameter. Although the forward problems for ZTEM and MT are extremely similar, when considering the data there are many differences that can have important implications for the inversion process. Firstly the surveys are often performed at different times with significant differences in the source strengths and polarizations. Furthermore, because MT data are collected on the ground while ZTEM data are collected in the air, the number of data from each survey and the data errors can be drastically different. Our data misfit is computed via,

$$\phi_d = \|\mathbf{W}_{d1}(\mathbf{d}_{ZTEM}^{obs} - \mathbf{d}_{ZTEM}^{prd})\|_2^2 + \gamma \|\mathbf{W}_{d2}(\mathbf{d}_{MT}^{obs} - \mathbf{d}_{MT}^{prd})\|_2^2, \quad (4)$$

where γ is a constant that must be determined. Although determining the optimal weights for different data types in an inversion is a difficult problem, we adopted the approach that MT and ZTEM should play approximately equal roles in the inversion. The constant was thus determined by inverting the MT and ZTEM individually before scaling each data set such that the final data misfits are equal.

SYNTHETIC EXAMPLE

We demonstrate the effectiveness of jointly working with MT and ZTEM data by examining the synthetic model in figure 1. The model has a central resistive core, an outer region of high conductivity, all intruded in a background host. The Earth was discretized into a mesh containing 56, 56, and 70 cells in the x, y, and z-directions respectively. MT data (0.04, 0.1, 0.4, 1, 3.5, 7, 30, 45, 90, 180, 360 Hz) and ZTEM data (30, 45, 90, 180, 360 Hz) were computed from the synthetic model using three different survey configurations over an approximate 10 x 10 km area. The first survey is a coarse MT survey with 72 stations in total with 1 km station spacing and 1 km line spacing. This significant station spacing will not be adequate to achieve the high resolution required for many detailed exploration projects. The second survey configuration is a finer MT survey with 1564 stations in total with 200 m station spacing and 300 m line spacing. Having over 1500 stations will be prohibitively expensive for most exploration programs considering a typical MT station can cost well in excess of \$1000. The final ZTEM survey has 10 m data spacing and 300 m line spacing. Gaussian noise was added to all the data before being inverted. In addition, to demonstrate the advantages of working with sparse MT and ZTEM, the data from the coarse MT

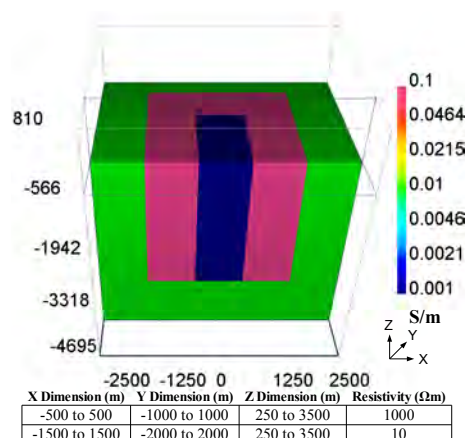


Figure 1: Synthetic conductivity structure of a resistor surrounded by a conductor except on the top and bottom. Both blocks are embedded in a 100 Ωm background halfspace. Block dimensions are summarized in the accompanying table.

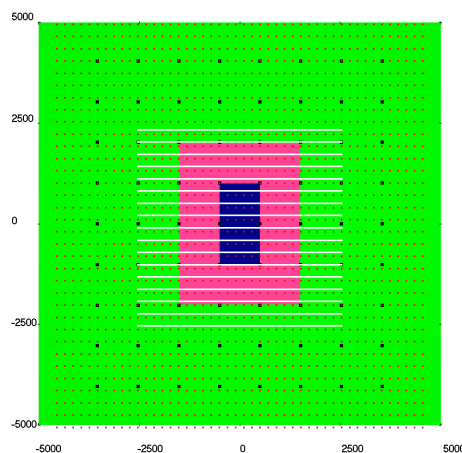


Figure 2: Survey grids for the synthetic inversions. The three grids are the coarse MT (black squares), fine MT (red squares), and ZTEM (white lines).

grid and the ZTEM grid were jointly inverted. For all the inversions, the predicted data fit the observed synthetic data very well. All of the inversions came close to achieving the target misfits. The final conductivity models can be seen in figure 3.

The coarse MT inversion result (figure 3b) recovers a crude estimate for the outline of the conductive block. Because of the limited data coverage from the 1 km x 1 km MT station spacing, the boundary of the blocks are not very well resolved. Nevertheless, the limited number of MT stations is enough to resolve the conductive block down to approximately 2500 m. By increasing the number of MT stations the boundaries of the blocks become better resolved (figure 3c). Had traditional MT tipper data been used, the additional information from the vertical fields may have improved the fine MT inversion result. The ZTEM inversion (figure 3d) shows good resolution down to almost 1000 m which is impressive for an airborne

Modelling ZTEM and MT data

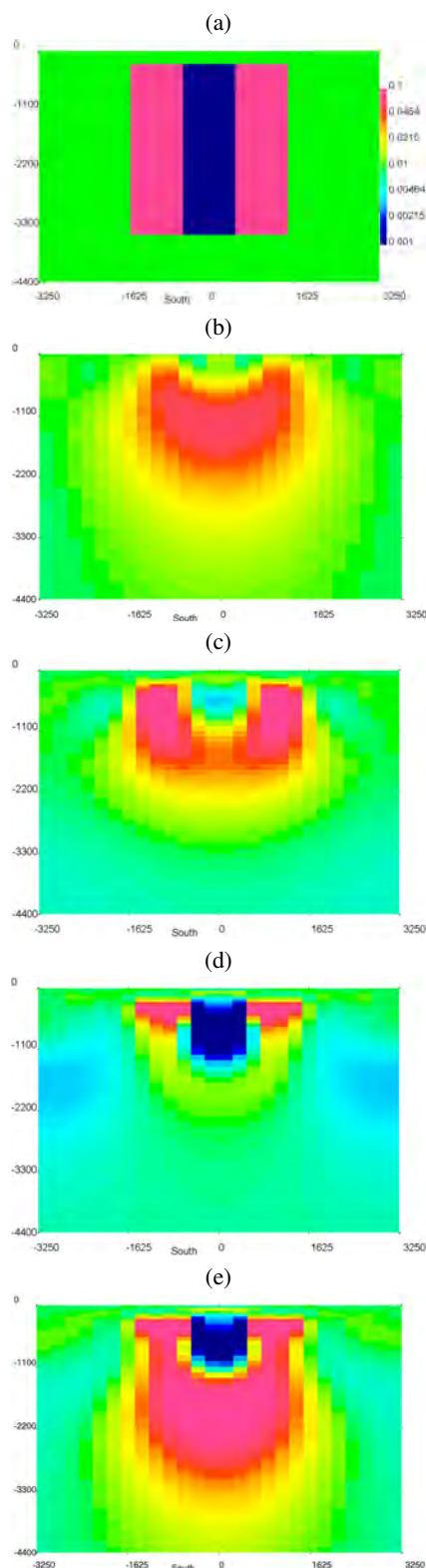


Figure 3: Inversion of the synthetic model in figure 1 all shown on the same color scale. a) True cross section of the model. Inversion results of the coarse MT grid (b), fine MT grid (c), ZTEM data (d), and joint coarse MT and ZTEM (e). Adding the ZTEM data to the coarse MT data greatly improved the inversion result.

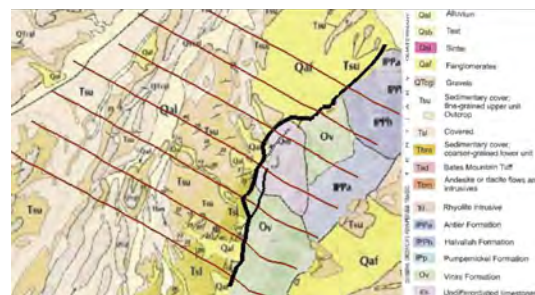


Figure 4: Reese River surface geology. The outline of the north south trending fault is shown in black. The MT lines are also shown.

technique. By jointly inverting the coarse MT grid and ZTEM grid (figure 3e), the inversion recovers both the deep structure from the low frequency MT data and fine structure from the ZTEM data. The 1 km x 1 km station spacing which was inadequate to recover the near-surface details is ideal to recover large scale features at the 2-3 km depth range. Interestingly, as one might expect, improving the model in the near-surface also improves the model at depth and resolves the model down to 3.5 km instead of the 2.5 km without the ZTEM data.

FIELD DATA

The joint inversion of MT and ZTEM data is an excellent technique to search for geothermal targets because it has the capability to penetrate the highly conductive clay cap often associated with geothermal reservoirs (Pellerin et al. (1996)). We demonstrate this by inverting overlapping MT and ZTEM data from the Reese River geothermal site in Nevada.

Reese River Geology

The Reese River property is divided by a north-south trending fault. At the near-surface, to the west of the fault is a sedimentary basin while to the east of the fault are more resistive rocks such as limestones. The surface geology and fault can be seen in figure 4.

Inversion Result

For the inversion the Earth was discretized on a mesh that contained 76, 78, and 87 cells in the x, y and z directions respectively. The cell dimensions in the central core region were 100 x 83.3 x 25 m. The MT data (0.048, 0.14, 0.44, 1.3, 3.7, 7 Hz) and the ZTEM data (30, 45, 90, 180, 360, 720 Hz) were inverted individually before being jointly inverted. The relative weights of the MT and ZTEM data in the inversion were scaled such that they had approximately equivalent contributions to the data misfit. The initial background conductivity was set to be 20 Ωm and the topography was obtained from the USGS national elevation database.

The inversion took 3 days running on 3 Intel Xeon 2.33Ghz dual quad core processors. The recovered conductivity model maps the fault very well as can be seen from the inversion re-

Modelling ZTEM and MT data

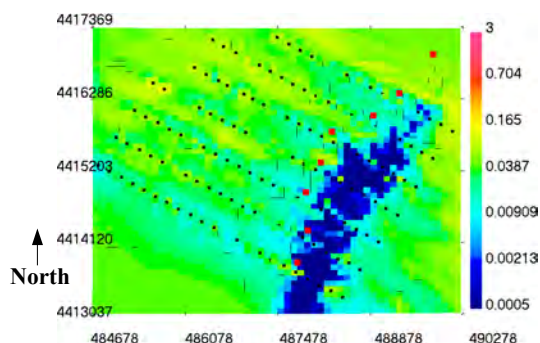


Figure 5: Conductivity model at a depth of 1800m which is the approximate average elevation of the fault boundary. The outline of the fault is shown by the red squares. The MT stations are shown in black. The conductivity model does a good job of showing the fault boundary.

The clear solution is to collect both MT and ZTEM data and exploit the strengths of each technique. The first step is to collect the minimal amount of MT data required to estimate the background conductivity and resolve the deep structure. High spatial resolution can then be achieved by flying multiple ZTEM lines over the sparse MT grid. The result is a cost effective solution that can map deep structures over large areas. We have developed a Gauss-Newton style inversion algorithm to jointly invert ZTEM and MT data. The algorithm shows promising results on both a synthetic test problem and a field example from the Reese River geothermal project.

ACKNOWLEDGEMENTS

The authors would like to thank Sierra Geothermal Power for their help on the Reese River Project

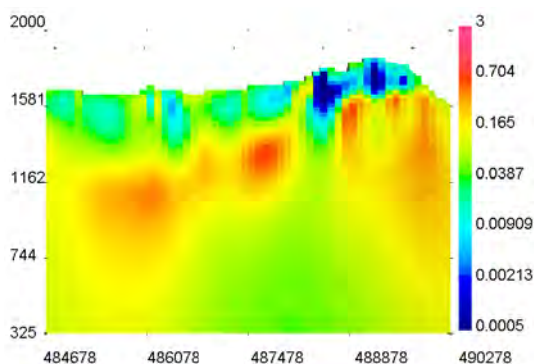


Figure 6: Cross section of the 3D conductivity model along northing 4415620.

sult in figure 5. A slice of the model along northing 4415620 can be seen in figure 6. The inversion result seems to reproduce the limited geologic information available from the area.

CONCLUSIONS

MT, the traditional natural source electromagnetic method, has the greatest depth of investigation of all electromagnetic methods. Despite this, the costly nature of each MT station makes it impractical for large surveys that require high spatial resolution. Another natural source technique, ZTEM, is a promising method to explore for large scale targets at depth because of easy data acquisition and deep penetration of natural source fields. While the depths of investigation are limited somewhat by the lowest frequency signal that can be recorded in the air, the technique can still image to depths that are difficult to image with other controlled source airborne and ground based systems. One limitation of the technique is that there is little sensitivity to the background conductivity, especially as the Earth becomes a 1D medium.

EDITED REFERENCES

Note: This reference list is a copy-edited version of the reference list submitted by the author. Reference lists for the 2010 SEG Technical Program Expanded Abstracts have been copy edited so that references provided with the online metadata for each paper will achieve a high degree of linking to cited sources that appear on the Web.

REFERENCES

- Farquharson, C. G., D. W. Oldenburg, E. Haber, and R. Shekhtman, 2002, An algorithm for the three-dimensional inversion of magnetotelluric data: 72nd Annual International Meeting, SEG, Expanded Abstracts, 649–652.
- Haber, E., U. Ascher, and D. Oldenburg 2000, On optimization techniques for solving nonlinear inverse problems: *Inverse Problems*, **16**, no. 5, 1263–1280, [doi:10.1088/0266-5611/16/5/309](https://doi.org/10.1088/0266-5611/16/5/309).
- Holtham, E., and D. Oldenburg, 2008, Three-dimensional forward modelling and inversion of Z-TEM data: 78th Annual International Meeting, SEG, Expanded Abstracts, 564–568.
- Lo, B., and M. Zang, 2008, Numerical modeling of Z-TEM (airborne AFMAG) responses to guide exploration strategies: 78th Annual International Meeting, SEG, Expanded Abstracts, 1098–1102.
- Pellerin, L., J. Johnston, and G. Hohmann, 1996, A numerical evaluation of electromagnetic methods in geothermal exploration: *Geophysics*, **61**, 121–137, [doi:10.1190/1.1443931](https://doi.org/10.1190/1.1443931).
- Ward, S., J. O'Donnell, R. Rivera, G. H. Ware, and D. C. Fraser, 1966, AFMAG - applications and limitations: *Geophysics*, **31**, 576–605, [doi:10.1190/1.1439795](https://doi.org/10.1190/1.1439795).
- Ward, S. H., 1959, AFMAG—airborne and ground: *Geophysics*, **24**, 761–787, [doi:10.1190/1.1438657](https://doi.org/10.1190/1.1438657).

Inversion of Large-scale ZTEM Data

Elliot Holtham

UBC-Geophysical Inversion Facility
Dept. of Ocean and Earth Sciences
University of British Columbia
6449 Stores Rd
Vancouver, BC V6T 1Z4, Canada
eholtham@eos.ubc.ca

Douglas W. Oldenburg

UBC-Geophysical Inversion Facility
Dept. of Ocean and Earth Sciences
University of British Columbia
6449 Stores Rd
Vancouver, BC V6T 1Z4, Canada
doug@eos.ubc.ca

SUMMARY

As the number of near surface deposits decreases, it becomes increasingly important to develop geophysical techniques to image at depth. Because of the penetration advantage of plane wave natural sources, these techniques are ideal to answer questions about the deep subsurface to the earth. A ZTEM survey is an airborne electromagnetic survey which records the vertical magnetic field that result from natural sources. The data are transfer functions that relate the local vertical field to orthogonal horizontal fields measured at a reference station on the ground. While the airborne nature of the survey means that large survey areas can be surveyed quickly and economically, the high number of cells required to discretize the entire survey area at reasonable resolution can make the computational costs of inverting the entire data set all at once prohibitively expensive. Here we present a workflow methodology that can be used to invert large natural source surveys by decomposing the large inverse problem into smaller more manageable problems before combining the tiles into a final inversion result. We use the procedure to invert synthetic ZTEM data for the Noranda mining camp as well as a field data example. Both of these data sets were far too large to solve on a single grid even with multiple processors at our disposal.

Key words: inversion, electromagnetics, airborne EM

INTRODUCTION

Since most shallow and outcropping deposits have already been discovered, many of the earth's remaining natural resources are buried deep in the subsurface and they are difficult to find. In order to satisfy the strong global resource demand, techniques to explore for these big targets at depth must be developed. Electromagnetic methods can be used to map electrical conductivity which can then be linked to geologic features of interest. When exploring for large, deeply buried targets, natural source electromagnetic methods can be advantageous over controlled source methods because of the deeper penetration of plane wave sources.

The traditional natural source method, the magnetotelluric (MT) method, has been effectively applied to both mining and hydrocarbon exploration. A practical limitation of the MT technique is that surveys are costly and time consuming because many expensive stations must be installed to measure

the needed electromagnetic field components on the earth's surface. It would be preferable to collect MT data in an aircraft but this goal has not yet been achieved because of the difficulty in measuring the electric fields. In an effort to continue to use the penetration advantage of natural sources, it has long been recognized that tipper data, the ratio of the local vertical magnetic field to the horizontal magnetic field, provide information about 3D electrical conductivity structure. It was this understanding that prompted the development of AFMAG (Audio Frequency Magnetics) (Ward, 1959). However, because the direction and strength of the inducing field varies with time, AFMAG results were not always repeatable. Limitations of the AFMAG technique were outlined in (Ward et al., 1966).

Many of the AFMAG problems can be removed by using improved signal processing and instrumentation. This has resulted in the Z-Axis Tipper Electromagnetic Technique (ZTEM) (Lo and Zang, 2008). In ZTEM, the vertical component of the magnetic field is recorded above the entire survey area, while the horizontal fields are recorded at a ground-based reference station. MT processing techniques yield frequency domain transfer functions typically between 30-720 Hz that relate the vertical fields over the survey area to the horizontal fields at the reference station. Since new instrumentation exists to measure the vertical magnetic fields by helicopter, data over large survey areas can quickly be collected. The result is a cost effective procedure for collecting natural source EM data that provide information about the 3D conductivity structure of the earth.

On the district and regional scale, particularly when the subsurface geology is hidden under cover, high quality airborne data sets are excellent exploration tools. For example large ZTEM surveys, in excess of 5000 line-km of data, have been collected. However, in order to justify spending significant money on collecting such data, interpretation methods must be capable of inverting the data in a reasonable amount of time. This requires that inversions are fairly fast, especially for field data where multiple inversions are often performed using different parameters. Unfortunately, for surveys that cover large areas and where even moderate resolution is desired, the discrete 3D Maxwell systems for solving the EM problem quickly become very large. Although computer technology continues to improve, clock speed and instruction level parallelism has started to flatten since 2003 (Shalf, 2007). This means that the majority of future improvements in the size of inverse problem that can be tackled must come from improved methodologies and increased parallelism.

One viable method to solve large inverse problems is to reduce the modelling domain by using footprint methods, where computations are simplified by only considering model cells that influence the data above some threshold criterion. These methods have been used to invert large airborne controlled source electromagnetic data sets (Cox et al., 2010) and MT data sets (Gribenko et al., 2010). Another solution is to use domain decomposition methods (DDM) and split the computational domain into smaller manageable subproblems which can then be solved quickly in parallel. In this paper we present a highly parallel and effective workflow procedure to invert large natural source surveys.

ZTEM DATA

ZTEM data are transfer functions that relate the vertical magnetic fields computed above the earth to the horizontal magnetic field at some fixed reference station. This relation is given by

$$H_z(r) = T_{zx}(r, r_0)H_x(r_0) + T_{zy}(r, r_0)H_y(r_0) \quad (1)$$

where r is the location for the vertical field, r_0 is the location of the ground based reference station and T_{zx} and T_{zy} are the vertical field transfer functions. Solving for the transfer functions requires that the vertical fields are known for two independent polarizations.

INVERSION METHODOLOGY

Our MT inversion algorithm is that of (Farquharson et al., 2002), and our ZTEM inversion algorithm is that of (Holtham and Oldenburg 2008) and (Holtham and Oldenburg, 2010). We wish to solve the inverse problem by minimizing the objective function

$$\min \phi = \|\mathbf{W}_d(F(\mathbf{m}) - \mathbf{d})\| + \beta\phi_m, \quad (2)$$

where \mathbf{W}_d is a diagonal measurement weighting matrix, ϕ_m is the model objective function, F is the forward modelling operator which acts on the model \mathbf{m} , and \mathbf{d} is the data vector. Although the goal is to solve this problem, it is difficult to tackle directly because of the size of the problem and the cost of evaluating $F(\mathbf{m})$. While the full inverse problem may be too expensive to solve, coarsely discretized models can be solved quickly and efficiently.

We first start by decomposing the model domain, \mathbf{m} , and the data set, \mathbf{d} , into smaller subdomains,

$$\begin{aligned} \mathbf{m}_j &= P_j^m \mathbf{m}, j = 1, \dots, J, \\ \mathbf{d}_j &= P_j^d \mathbf{d}, j = 1, \dots, J, \end{aligned} \quad (3)$$

where P_j^m and P_j^d are projection operators which form the model and data subdomains respectively. Here P_j^m is constructed such that the \mathbf{m}_j 's are overlapping. We would like to invert these subproblems separately and in parallel but there are interactions between subdomains that cannot be ignored. In order to mitigate this problem we determine the first order interactions between domains by performing a coarse inversion and then use the computed fields as source terms for the subdomain inversions. That is, first we obtain a coarse inversion result \mathbf{m}_c by inverting the entire data set on the

coarse mesh. The coarse model is then interpolated onto the J subdomains to create initial models. The electric fields obtained by forward modelling the coarse conductivity structure, are also interpolated onto the J domains. Although these new fields are only defined on individual subdomains, they still contain information about the full conductivity structure. These electric fields are used as the primary fields when carrying out an inversion on each subdomain. By using a primary-secondary field formulation and using primary fields computed from a global scale model, the correct large-scale physics of the problem is maintained.

Once all of the individual subdomain models, \mathbf{m}_j 's have been determined, an update to the full model \mathbf{m} is given by merging each subdomain into a final full conductivity structure. To ensure that this new result is acceptable, the predicted data from this full fine scale model is computed. If the data misfit is acceptable, then a solution to the desired inverse problem has been obtained. If the data have not been sufficiently fit, then new fields generated by this new inversion result can be used as the primary fields for another iteration of subdomain inversions. This procedure can be repeated until the data has been sufficiently fit.

SYNTHETIC EXAMPLE

In this section a synthetic model is used to examine in detail a few elements of the general methodology described in the previous section. The synthetic model is from the Noranda District in Canada, home to 20 economic volcanogenic massive sulphide deposits (VMS), 19 orogenic Au deposits, and several intrusion-hosted Cu-Mo deposits (Gibson and Galley 2007). The original model provided courtesy of the Xstrata mining group contained 12.7 million cells covering an area of almost 20 x 20 km. The 38 geologic units in the model were converted into expected conductivities, before the entire 12.7 million cell model was forward modelled at 30, 45, 90, 180, 360 and 720Hz, and then corrupted with noise to form the observed synthetic data. A depth slice at -275m of the synthetic model can be seen in figure 3.

PRELIMINARY COARSE INVERSION

The first step in attempting to find an approximate solution to the full inverse problem is to perform a coarse inversion to determine the large scale conductivity structure that will be used to compute the primary fields and starting models for subsequent finer cell size inversions. The earth is discretized into relatively large cells such that the total number of cells in the mesh is small and the inverse problem can be solved quickly. In this example the coarse mesh contained 42 x 42, 500m cells in the x and y directions. It contained 73 cells in the z direction. Working initially on a coarse mesh, which for this synthetic example can be inverted in approximately 30 minutes, allows multiple inversions to be simultaneous run with different parameters and starting models. Because of the large cell dimensions, some geologic structures such as accurate body boundaries and fine scale features may not be recovered by the discretization. Therefore it is important not to overfit the data and risk adding discretization artifacts into the inversion result. This is particularly true for higher frequency data which will have smaller skin depths and contain more information about fine scale features. In fact, because the initial goal of the coarse scale inversion is to quickly determine the large scale conductivity features, some

data, particularly the higher frequency data may be omitted to reduce the computational cost and prevent the large cell sizes of the coarse mesh from violating the shorter skin depths at the higher frequencies. In this example the 360 Hz and 720 Hz data were omitted for the coarse mesh inversion.

SETUP AND SUB-DOMAIN INVERSIONS

The coarse inversion result is used as an initial starting model and for computing the primary fields for subsequent finer discretized inversions. Once this is completed the subdomain meshes must be designed. When decomposing the computational domain and designing the subdomain meshes, the two critical elements pertain to handling the interactions between the domains and ensuring that there is continuity of conductivity structures across domain boundaries. Incorporating domain interactions is done by using primary fields in the tiled inversions which have been computed from full domain conductivity structures. Continuity of the conductivity structure across domain boundaries is accomplished by using both data and mesh overlap. Generally the meshes are chosen to overlap by slightly less than a skin depth at the lower frequencies. Here a tradeoff must be achieved between increased overlap and increased computational requirements. Another tradeoff that must be considered is the number of tiles used to decompose the domain. As the number of tiles increases, while the individual inversion time for each subproblem might decrease, the percentage of overlap cells versus total number of cells in each mesh increases and the decomposition may become less efficient. Here it is up to the user to choose a reasonable number of tiles such that each tile runs efficiently on their available computer hardware.

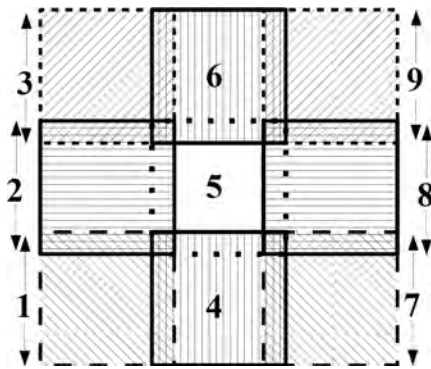


Figure 1 Mesh layouts for the example using nine overlapping domains. Each mesh contained approximately 1.4 million cells with $139 \times 140 \times 70$ cells in the x,y and z directions. Each domain overlapped by 20, 50m cells in both the x and y directions.

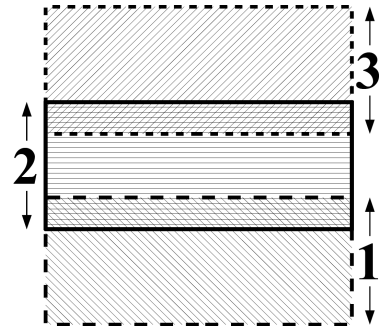


Figure 2 Mesh layouts for the example using three overlapping domains. Each subdomain mesh contained approximately 3.5 million cells with $353 \times 140 \times 70$ cells in the x,y and z directions. Each domain overlapped by twenty 50m cells

For this synthetic example, two different sets of meshes, one with three tiles and the other with nine tiles are used to demonstrate the scalability and robustness of the methodology. Both the 3 and 9 tile examples contained the same sized cells (50 x 50 m cells in the x and y directions) in the core and overlapping regions. In the vertical direction the cells dimensions started at 25m, and then expanded with depth. Both sets of meshes used 20 overlapping cells on each mesh boundary. The mesh layouts and overlaps for the three and nine tile examples can be seen in figures 1 and 2.

Once the tiled models are inverted they are stitched together using a linear distance weighted averaging scheme across the overlapping regions. The final inversion models from the 3 and 9 tile examples in figures 4 and 5 recovers the large scale geological features very well. In addition several of the larger known deposits which were not evident from the in initial coarse inversion result are imaged. Here the inversion results of the 3 and 9 tile examples, run on dual Xeon X5660 processors, are very similar. This illustrates that the inversion results are not highly dependent on the choice of subdomain meshes. During the subdomain inversions the initial beta is chosen to be the final beta from the initial coarse inversion result and the same cooling scheme is used on the tiled inversions as in the initial coarse inversion.

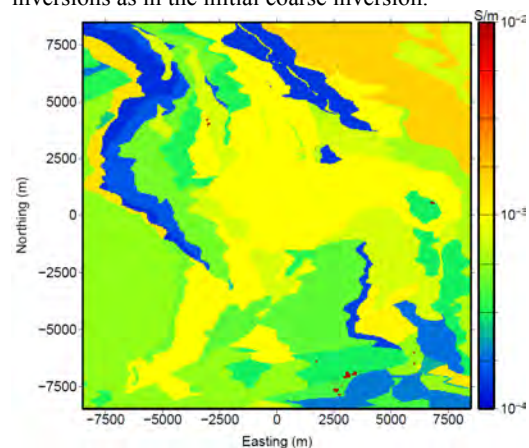


Figure 3 Depth slice at -275m of the true model. The topography for the synthetic model ranges from -25m to -250m. The conductivity of the ore was chosen to be 5 Ωm ; however, the color scale on the model has been clipped at 100 Ωm to improve the visualization of the other geologic units.

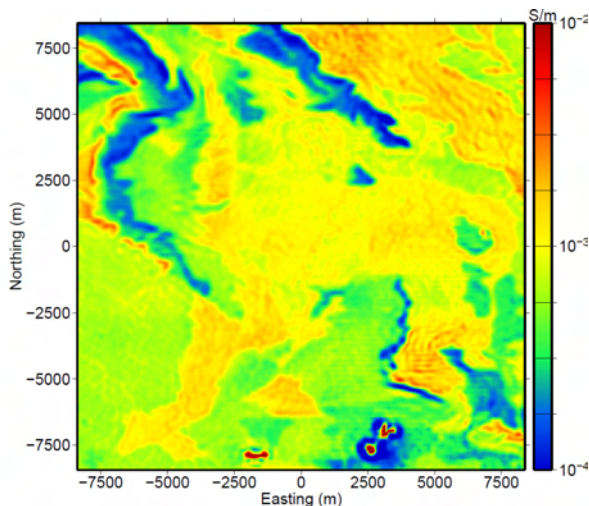


Figure 4 Depth slice at -275m of the inversion result after merging the three tiles together shown on the same color scale as the true model. The resolution in this model is greatly improved compared to the coarse result. Several of the larger known deposits have now been recovered; they were not visible from the initial coarse inversion.

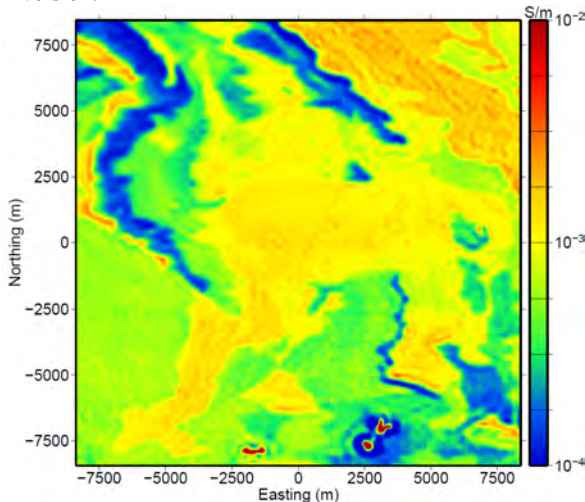


Figure 5 Depth slice at -275m of the inversion result after merging the 9 tiles together shown on the same color scale as the true model.

CONCLUSIONS

In this paper we show how large scale ZTEM survey data can be inverted by using a strategy involving coarse and fine meshes as well as a domain decomposition that splits the computational domain into smaller manageable subproblems which can be solved in parallel. We have presented a practical workflow procedure to carry this out. The methodology shows promising results on a synthetic example from the

Noranda mining camp, and on a field data example that is currently being worked on.

ACKNOWLEDGEMENTS

The authors would like to thank the Mike Allard from Xstrata Zinc, Louis Martin from Xstrata Copper and Gervais Peron from Mira Geosciences, for providing the geologic shape model for the Noranda mining camp that has formed the basis of our synthetic example.

REFERENCES

- Cox, L. H., G. A. W., and M. S. Zhdanov, 2010, 3d inversion of airborne electromagnetic data using a moving footprint: *Exploration Geophysics*, 41, 250–259.
- Farquharson, C. G., D. W. Oldenburg, E. Haber, and R. Shekhtman, 2002, An algorithm for the three-dimensional inversion of magnetotelluric data: 72nd Annual International Meeting, SEG, Expanded Abstracts, 649–652.
- Gibson, H., and A. Galley, 2007, Gibson, h., and galley, a.g, in *Mineral Deposits of Canada: A Synthesis of Major Deposit-Types, District Metallogeny, the Evolution of Geological Provinces*: Mineral Deposits Division, 5, 533–552.
- Gribenko, A., A. G. M. C. M. Z., 2010, Efficient 3d inversion of mt data using integral equations method and the receiver footprint approach: application to the large-scale inversion of the earthscope mt data: Expanded Abstracts Denver.
- Holtham, E., and D. Oldenburg, 2008, Three-dimensional forward modelling and inversion of z-tem data: SEG Extended Abstracts, Las Vegas.
- , 2010, Three-dimensional inversion of ztem data: *Geophysical Journal International*, 182, 168–182.
- Lo, B., and M. Zang, 2008, Numerical modeling of z-tem (airborne afmag) responses to guide exploration strategies: SEG Technical Program Expanded Abstracts, 27, 1098–1102.
- Shalf, J., 2007, The new landscape of parallel computer architecture: *Journal of Physics: Conference Series*, 78.
- Ward, S. H., 1959, Afmag—airborne and ground: *Geophysics*, 24, 761–787.
- Ward, S. H., J. O'Donnell, R. Rivera, G. H. Ware, and D. C. Fraser, 1966, Afmag - applications and limitations: *Geophysics*, 31, 576–605.

ZTEM airborne tipper AFMAG results over the Copaquire Porphyry, northern Chile

Carlos Izarra, Jean M. Legault*, and Ali Latrous, Geotech Ltd.

Summary

ZTEM airborne electromagnetic surveys over the Copaquire porphyry deposit, in northern Chile, were designed to map its alteration and structure due resistivity contrasts, to depth, based on successful applications of the method in north America. ZTEM is an airborne variant of the AFMAG passive EM method whose source fields are related to world-wide thunderstorm activity. The ZTEM results over Copaquire appear to map the resistive potassic alteration associated with known Marta and Cerro Moly porphyries, below the surficial secondary enrichment layer and extending to depth. These are in turn surrounded by more conductive, barren pyrite-rich phyllic and propylitic alteration. Over the other two known mineralized prospects, at Sulfato North and South, the ZTEM results are different, with more resistive rocks at surface becoming more conductive at depth – perhaps reflecting a different geologic setting. Overall, these results are consistent with ZTEM results obtained over other, similar calc-alkaline porphyry systems and also agree with the known geology.

Introduction

In December 2010, Geotech Ltd conducted a ZTEM helicopter-borne geophysical survey for International PBX Ventures Ltd (Vancouver, BC) on its Copaquire Project, in northern Chile (Figure 1). The Copaquire project hosts a porphyry system with mineralized zones enriched in copper, molybdenum and rhenium. The project is situated in one of the most productive copper belts in the world, with operating porphyry copper mines, such as Quebrada Blanca and Collahuasi, located nearby.

The objectives of the ZTEM survey over Copaquire were: a) to map the known porphyry deposits and potential prospects from surface to depth, based on resistivity contrasts, b) as a survey comparison against previous ground MT results obtained on the property (Figure 2).

ZTEM surveys have proven particularly useful in porphyry copper exploration for their ability to map resistivity contrasts associated with geologic structures and alteration that accompany these large mineral deposits – particularly between the potassic-altered core of the porphyries, which tend to be resistive, and the surrounding phyllic and/or propylitic alteration halos, which are more conductive (Lo and Zang, 2008; Paré and Legault, 2010; Sattel et al., 2010).

Property Geology

The geological setting and mineralization type of Copaquire are similar to that found at Collahuasi (5 Bt @ 0.83% Cu, 0.02% Mo) and Quebrada Blanca Mines (1 Bt



Figure 1: Copaquire Property Location in northern Chile (courtesy International PBX Ventures Ltd.).

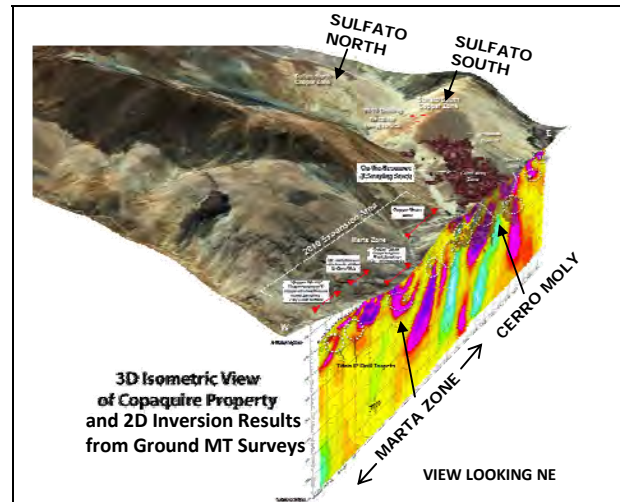


Figure 2: 3D Isometric view of Copaquire property and 2D inversion of ground MT along southern boundary of property (courtesy International PBX Ventures Ltd.).

@ 0.62% Cu oxides). The Copaquire property contains 2 large mineralized porphyry systems (Figure 2): Copaquire and Marta. The Copaquire porphyry includes three zones (Sulfato North, Sulfato South & Cerro Moly) that cover an area of roughly 7 km² and possesses the potassic, phyllic, argillic and propylitic phases of alteration typical of calc-alkaline Andean porphyry copper systems. The porphyry has a leached cap and secondary chalcocite blanket exposed

ZTEM airborne tipper AFMAG over Copaquire Porphyry, Chile

in the Sulfato Zone north of the Cerro Moly ridge. A preliminary assessment report focusing on the molybdenum rich core of the Cerro Moly zone defined a resource of 307.8 million pounds Mo and 1.2 billion pounds Cu. The Marta Porphyry is in the western area of the property. Recent exploration has revealed mineralized zones close to historic underground workings which exhibit stockwork type molybdenum mineralization similar to that developed at Cerro Moly and areas of porphyry copper and copper skarn mineralization (G. Sookchoff, personal communication, 2011).

The magnetic analytic signal map (Figure 3) obtained from the aeromagnetic data collected during the ZTEM survey, shows Marta area inside a magnetic regional high with localized bull-eye anomalies. Cerro Moly is located over a moderate magnetic high, while the Sulfato Zones are represented by a regional magnetic low. These observations provide evidence that points to potential differences in magnetic mineral content resulting from the hydrothermal alteration processes responsible for mineral accumulation at Copaquire.

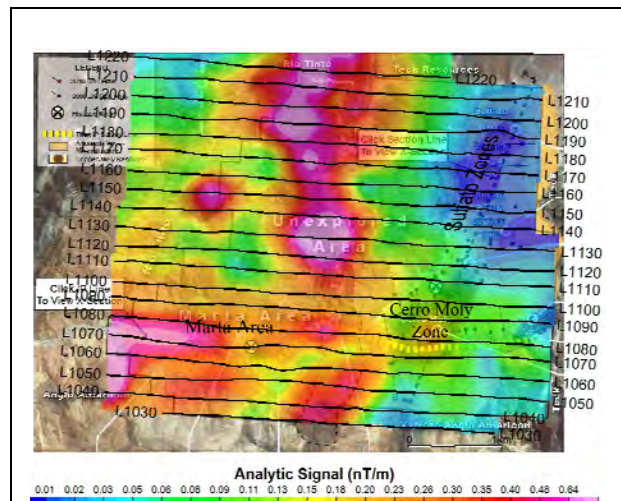


Figure 3: Analytic signal of total magnetic intensity contour plan map, showing the known mineralized zones and with flight lines clipped to the property extents.

General Theory

The ZTEM airborne AFMAG system measures the anomalous vertical secondary magnetic fields that are created by the interaction between naturally occurring, plane wave audio frequency EM fields and electrical heterogeneities in the earth. The vertical magnetic field is linearly related to the horizontal fields according to the following equation (Vozoff, 1972):

$$H_z = T_{zx}H_x + T_{zy}H_y$$

where the magnetic field vector $\mathbf{T} = (T_{zx}, T_{zy})$, known as the Tipper, is complex and a function of frequency, but has

rotationally invariant properties, such as its magnitude and direction, that are independent of the subsurface, the measurement direction and the field polarization (Labson et al., 1985).

AFMAG uses naturally occurring audio frequency magnetic fields as the source of the primary field signal, and therefore requires no transmitter (Ward, 1959). The primary fields resemble those from VLF except that they are lower frequency (tens & hundreds of Hz versus tens of kHz), are pseudo-periodic and are not as strongly directionally polarized. These EM fields used in AFMAG are derived from world wide atmospheric thunderstorm activity, have the unique characteristic of being uniform, planar and horizontal, and also propagate vertically into the earth – to great depth, up to several km, as determined by the magnetotelluric (MT) skin depth (Vozoff, 1972), which is directly proportional to the ratio of the bedrock resistivity to the frequency.

$$\delta_s = 503 * \sqrt{(\rho / f)} \text{ metres}$$

In AFMAG, the tipper is obtained by measuring the vertical Hz secondary EM field in the presence of both the horizontal Hx and Hy components, which are a mix of primary and secondary fields (Stodt et al., 1981). ZTEM is a variant of the AFMAG method whereby, as an approximation, the vertical magnetic field Hz is measured using a mobile receiver, towed from a helicopter, and the orthogonal horizontal Hx and Hy fields are obtained at a separate, fixed base station reference site. As such ZTEM is therefore analogous to the telluric-magnetotelluric adaptation (Hermance and Thayer, 1975) used by modern controlled-source AMT and also distributed array MT systems for rapid reconnaissance mapping purposes.

ZTEM Survey Results

The airborne geophysical survey consisted of a ZTEM (Z-axis Tipper Electromagnetic) System and Caesium magnetometer. A total of 503 km were flown at a nominal line-spacing of 200m over an area of 97km². The ZTEM survey receiver, towed roughly 75m below the helicopter, at a 60m nominal height clearance, is flown over the survey area in a grid pattern. Two orthogonal horizontal axis coils (3.5m dia.) are placed close to the survey site to measure the horizontal EM reference fields. Data from the three coils are used to obtain the Tzx (In-line) and Tzy (cross-line) ZTEM tippers, whose transfer functions (In-Phase & Quadrature) are derived at six frequencies in the 25 to 600 Hz band.

Figures 4-5 present the ZTEM tipper results in plan shown as Total Phase Rotated (TPR) images of the In-Phase component, with overlying flight paths above the Copaquire Project area. The TPR combines the 90-degree phase-rotations of both the Tzx and Tzy tipper cross-over responses in peaks for easier visualization in plan (Lo et al., 2009). In the TPR image, warm colours represent

ZTEM airborne tipper AFMAG over Copaquire Porphyry, Chile

conductive structures and contacts; cool colours represent more resistive units.

Cerro Moly and Marta areas appear associated with an east-west conductive trend as shown in the 600Hz frequency results (Figure 4), potentially relating to the argillic/phyllitic alteration and supergene enrichment blanket and skarns at shallow depth levels. Whereas in the deeper, lowest frequency 37Hz image (Figure 5), both Cerro Moly and Marta are better contrasted and more resistive than the surrounding rocks. This is consistent with the potassic altered core of these porphyry systems relative to the surrounding phyllic/propylitic altered rocks. In contrast, the Sulfato zones (South and North) display the opposite geoelectrical pattern: At higher frequency, they exhibit clear high resistivity contrast; whereas at greater depth they become moderately conductive and adjacent to more conductive parallel trends. This suggests that the Sulfato zones may be responding to a surficial potassic alteration zone and a surrounding pyritic phyllic-propylitic altered halo and/or geological structures at depth.

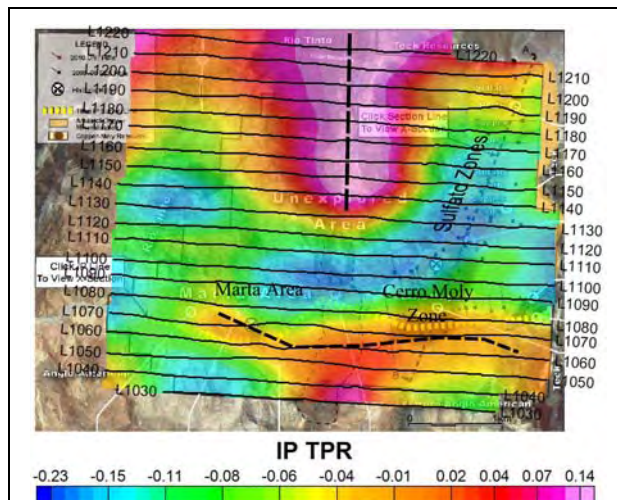


Figure 4: ZTEM high frequency (600Hz) Total Phase Rotated In-Phase tipper contour plan map, showing the known Copaquire mineralized zones and with flight lines clipped to the property extents.

Figures 6-7 present the 2D inversion results for the In-Line (Tzx) ZTEM tipper data, using the Zvert2d code, which accounts for the ZTEM mobile Hz and fixed Hx approximation and also for the air-layer below the receiver (Legault et al., 2009). Figure 6 shows the 2D resistivity cross-section obtained from the inversion of a line directly over the Cerro Moly and Marta Area, proximal to the MT survey line, presented in Figure 2. As indicated, both the known porphyry centers coincide with well defined resistivity highs that are surrounded by lower resistivity rocks, which is consistent with the known geology. The thin near-surface conductive layer that is imaged above the deposits could either represent the secondary enrichment blanket or else is possibly caused by 2D inversion artifacts

due to topography. Although less detailed than the corresponding MT 2D inversion model, the ZTEM section appears to map similar resistivity structures and trends – albeit possibly to lesser depth-extent. For example, the pinching of the Cerro Moly resistive feature below 1km depths in Figure 6 is not observed in the MT model (see Figure 2).

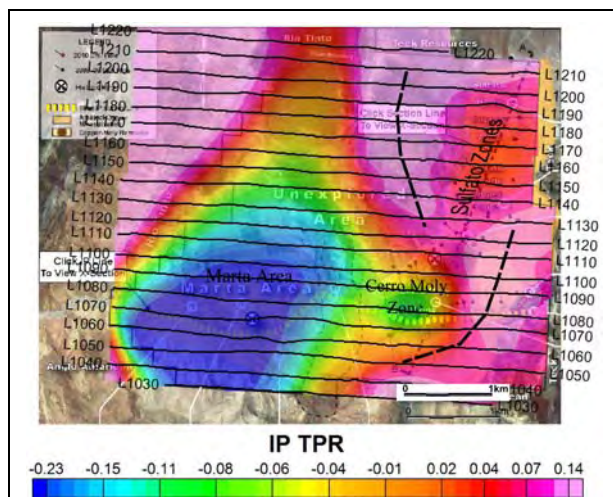


Figure 5: ZTEM low frequency (37Hz) Total Phase Rotated In-Phase tipper contour plan map, showing the known Copaquire mineralized zones and with flight lines clipped to the property extents.

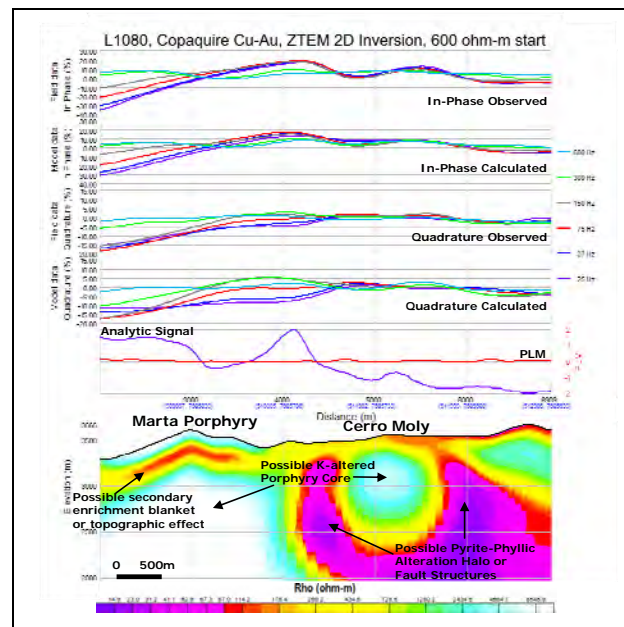


Figure 6: ZTEM low frequency (37Hz) Total Phase Rotated In-Phase tipper contour plan map, showing the known Copaquire mineralized zones and with flight lines clipped to the property extents.

ZTEM airborne tipper AFMAG over Copaquire Porphyry, Chile

Figure 7 presents a 3D Voxel representation of the 2D ZTEM inversion results showing the resistive core below Cerro Moly and conductive surficial layer above the larger Marta porphyry. Further north, the Sulfato zones are modeled as east dipping resistivity features, with the more resistive portion occurring close to surface and weakening at depth. This is interpreted to reflect either a different alteration at depth or is due to structural controls.

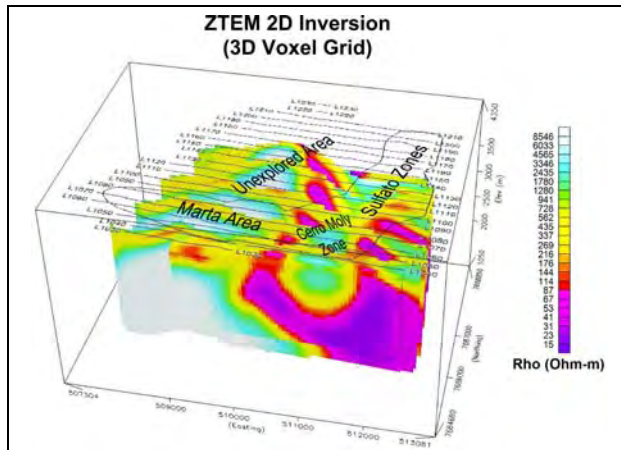


Figure 7: *3D Voxel view of 2D ZTEM inversion results for In-line Txx component (25-600Hz) at Copaquire, showing known mineralized zones and flight lines.*

Conclusions

Airborne ZTEM surveys over the Copaquire porphyry property have defined possible alteration and structural features, based on resistivity contrasts. The ZTEM results appear to map the resistivity highs relating to mineralized potassic altered cores of the Marta porphyry and the smaller Cerro Moly zone, to great depth. These porphyry centers are in turn surrounded by more conductive rocks, which is consistent with either the barren pyrite-rich phyllic and propylitic alteration or else fault structures. In addition, the ZTEM appears to map a surficial conductive layer, possibly the secondary enrichment blanket that lies above the deposits. Comparisons with MT survey results suggest that ZTEM is mapping similar geology, though less detailed and to lesser depth-extent (<2km). Over the other two known mineralized prospects, Sulfato North and South, the ZTEM results differ somewhat, with the resistive, potassic altered rocks at surface becoming more conductive at depth. Hence the results appear to indicate a different mineralization style.

These findings are consistent with ZTEM results obtained over other, similar calc-alkaline porphyry systems and also agree with the known geology. Certainly, 3D inversion of the ZTEM data (Holtham and Oldenburg, 2010) could provide further insights on the mineralized zones and controlling structures at Copaquire. The survey results obtained suggest that ZTEM airborne EM could be

successfully applied to porphyry copper exploration elsewhere in the Andes of South America

Acknowledgements

The authors wish to thank Geotech Ltd. and International PBX Ventures Ltd. for allowing us to present these results and for sponsoring this study

EDITED REFERENCES

Note: This reference list is a copy-edited version of the reference list submitted by the author. Reference lists for the 2011 SEG Technical Program Expanded Abstracts have been copy edited so that references provided with the online metadata for each paper will achieve a high degree of linking to cited sources that appear on the Web.

REFERENCES

- Hermance, J. F., and R. E. Thayer, 1975, The telluric-magnetotelluric method: *Geophysics*, **40**, 664–668, doi:10.1190/1.144055.
- Holtham, E., and D. Oldenburg, 2010, Three-dimensional inversion of ZTEM data: 80th Annual International Meeting, SEG, Expanded Abstracts, 655-659.
- Labson, V. F., A. Becker, H. F. Morrison, and U. Conti, 1985, Geophysical exploration with audiofrequency natural magnetic fields: *Geophysics*, **50**, 656–664, doi:10.1190/1.1441940.
- Legault, J. M., H. Kumar, B. Milicevic, and P. Wannamaker, 2009b, ZTEM tipper AFMAG and 2D Inversion results over an unconformity uranium target in northern Saskatchewan: 79th Annual International Meeting, SEG, Expanded Abstracts, 1277-1281.
- Lo, B., J. M. Legault, P. Kuzmin, and M. Combrinck, 2009a, Z-TEM (Airborne AFMAG) tests over unconformity uranium deposits: 20th International Geophysical Conference & Exhibition, ASEG, Extended Abstracts.
- Lo, B., and M. Zang, 2008, Numerical modeling of Z-TEM (airborne AFMAG) responses to guide exploration strategies: 78th Annual International Meeting, SEG, Expanded Abstracts, 1098-1101.
- Paré, P., and J. M. Legault, 2010, Ground IP-resistivity, airborne spectrum and helicopter ZTEM survey results over Pebble copper-moly-gold porphyry deposit, Alaska: 80th Annual International Meeting, SEG, Expanded Abstracts, 1734-1738.
- Pastana de Lugo, P., and P. E. Wannamaker, 1996, Calculating the two-dimensional magnetotelluric Jacobian infinite elements using reciprocity: *Geophysical Journal International*, **127**, 806–810, doi:10.1111/j.1365-246X.1996.tb04060.x.
- Pedersen, L. B., 1998, Tensor VLF measurements: Our first experiences: *Exploration Geophysics*, **29**, 52–57, doi:10.1071/EG998052.
- Sattel, D., S. Thomas, and M. Becken, M., 2010, An analysis of ZTEM data over the Mt. Milligan porphyry copper deposit, British Columbia: 80th Annual International Meeting, SEG, Expanded Abstracts, 1729-1733.
- Stodt, J. A., G. W. Hohmann, and S. C. Ting, 1981, The telluric-magnetotelluric method in two- and three-dimensional environments: *Geophysics*, **46**, 1137–1147, doi:10.1190/1.1441254.
- Tarantola, A., 1987, *Inverse problem theory*, Elsevier.
- Vozoff, K., 1972, The magnetotelluric method in the exploration of sedimentary basins: *Geophysics*, **37**, 98–141, doi:10.1190/1.1440255.
- Wannamaker, P. E., J. A. Stodt, and L. Rijo, 1987, A stable finite element solution for two-dimensional magnetotelluric modeling: *Geophysical Journal of the Royal Astronomical Society*, **88**, 277–296.
- Ward, S. H., 1959, AFMAG - airborne and ground: *Geophysics*, **24**, 761–787, doi:10.1190/1.1438657.



Joint CMOS-CGU Congress

"Recent development in airborne geophysics"

May 31—June 4, 2010, Ottawa, ON, Canada

The AirMt passive airborne EM system

Vlad Kaminski, Petr Kuzmin and Jean Legault – Geotech Ltd., Aurora, ON, CA

The AirMt (airborne magnetic tensor) passive EM system is the new state of the art technology developed by Geotech Ltd. (Aurora, ON, Canada) that is designed for deep electromagnetic (magneto-variational) airborne prospecting and mapping. It is the third generation of passive source airborne EM system developed by Geotech since 2005 (Kuzmin et al., 2005), following the ZTEM (Z-axis tipper electromagnetic) system (Lo and Zang, 2008), which has been successfully used for commercial mining and geothermal applications since 2007. AirMt source fields are the distant EM fields from sferic electrical storm activity, identical to those used in audio-magnetotellurics and AFMAG (Ward, 1959). Its advantage over ZTEM is the capability to measure three orthogonal components of primary and secondary magnetic field (H_x , H_y and H_z), as opposed to a single vertical component measurement. The three measured components are further converted into a rotationally-invariant total field tensor parameter " H_t ", which is sensitive to electrical properties of the geological targets and tectonic disruptions.

The major practical benefit of the total field measurement approach is the absence of H_x - H_y - H_z component separation through tilt-compensation, which significantly improves signal to noise, permits a more compact design, simplifies the data acquisition & processing and allows the system to be utilized more freely in mountainous terrains. Just as ZTEM data have been uniquely inverted for electrical properties for a 2D generalized earth model using a-priori constraints (Legault et al, 2009), a similar 2D interpretation tool will provide additional proof of concept for the method. In addition to test flights comparing the AirMt system against ZTEM and VTEM (Witherly et al., 2004), a commercial survey example flown with AirMt in Nevada showcases the system capability to differentiate between rock types in a porphyry copper environment, which makes the system suitable for mining and geothermal, and potentially oil and gas applications.

The AirMt system consists of three mutually perpendicular airborne loops and three identical base station loops which measure natural varying magnetic fields in frequency-domain. The measurements include six frequency bands (20-30 Hz, 30-60 Hz, 60-120 Hz, 120-240 Hz, 240-480 Hz and 480-960 Hz, for 60-hertz countries).

The Drybones Kimberlite: a case study of VTEM and ZTEM airborne EM results

Vlad Kaminski
Geotech Ltd.
Aurora, ON, CA
vlad@geotech.ca

Jean M. Legault
Geotech Ltd.
Aurora, ON, CA
jean@geotech.ca

Harish Kumar
Geotech Ltd.
Aurora, ON, CA
harish@geotech.ca

SUMMARY

Two airborne EM surveys were conducted over the Drybones Kimberlite by Geotech Ltd. A VTEM helicopter time domain EM survey flown in 2005 is compared to a ZTEM helicopter tipper AFMAG EM survey flown in 2009. Both surveys detect anomalous responses over the pipe, however according to conductivity-depth transforms and skin-depth estimates, supported by 3D modeling, it seems unlikely that VTEM response is representative of the actual kimberlite, buried more than 100 meters underneath the conductive sediments. It appears that the consolidated kimberlite might be too resistive to be differentiated from granodiorites using conventional TEM methods. On the other hand the ZTEM response appears to be able to differentiate between the diatreme (consolidated kimberlite) and the host rock, lying below the conductive blanket.

Key words: ZTEM, VTEM, AFMAG, electromagnetic, airborne, kimberlite.

INTRODUCTION

The Drybones Kimberlite is situated approximately 45 km SE from the town of Yellowknife, NWT, Canada (Figure 1). It was initially discovered in 1994 with a single drill hole. The kimberlite is situated in Slave Province of the Canadian Shield.



Figure 1: Geographic location of the Drybones kimberlite (Google Earth, 2009)

The bedrock geology in Drybones area consists of Archean granite, granodiorite and tonalite (Kretchmar, 1995). The kimberlite is located in Drybones Bay and lies completely underwater, at an average depth of 38 m. The kimberlite itself is further overlain by 65-75 m of lake sediments, predominantly clay, till and sand. The morphology of the pipe can be described as a spatially elongated intrusion (900 m by 400 m), consisting of three facies (diatreme, crater and pyroclastic) distinguished by physical and mineralogical properties of the rock (Figure 2). In general, the diatreme facies appears to be more consolidated and therefore more electrically resistive.

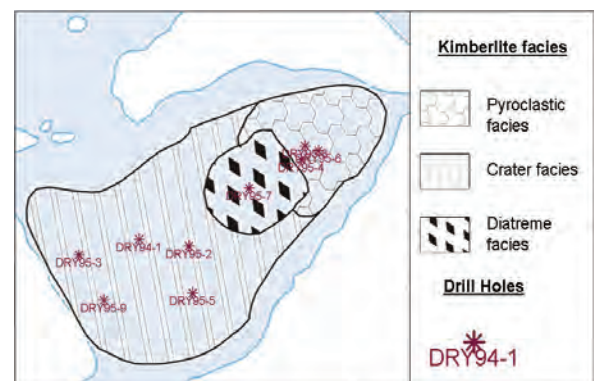


Figure 2: Surface morphology of the Drybones pipe and the locations of 1994-95 Drill Wells (Kretchmar, 1997)

EM SURVEYS OVER DRYBONES

Geotech, Ltd has conducted two airborne EM test surveys over the Drybones Kimberlite (Figure 3). A VTEM (Witherly et al, 2004) time-domain electromagnetic survey was flown over the pipe in 2005, followed by a larger ZTEM (Lo and Zang, 2008; Lo et al., 2009) tipper AFMAG (Ward, 1953) survey in 2009.

The VTEM test survey was flown at a nominal receiver height of 35m with data sampled at 3m intervals; the ZTEM test survey was flown at a nominal receiver height of 61m at 10m sampling intervals. Both surveys were flown at a 100m nominal line-spacing. The surveys were designed in a manner so the ZTEM and VTEM flight lines would overlap each other as much as possible. In particular, VTEM flight line 50 corresponds to ZTEM flight line 1190. Both EM geophysical studies were successful in identifying the anomaly over the kimberlite (Figure 4).

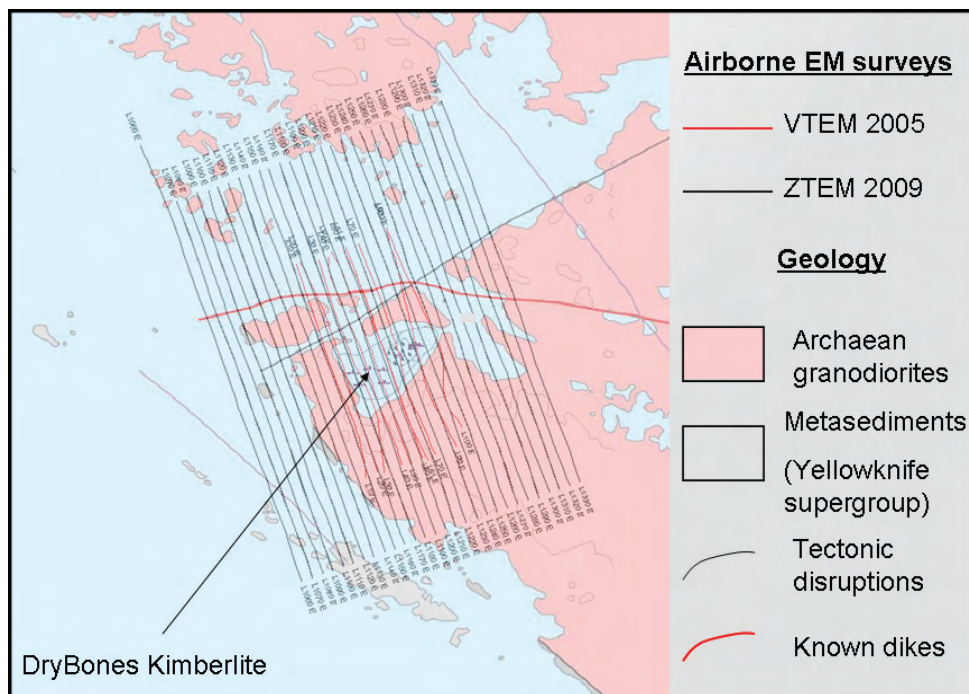


Figure 3: Airborne EM survey flight lines over the Drybones kimberlite pipe

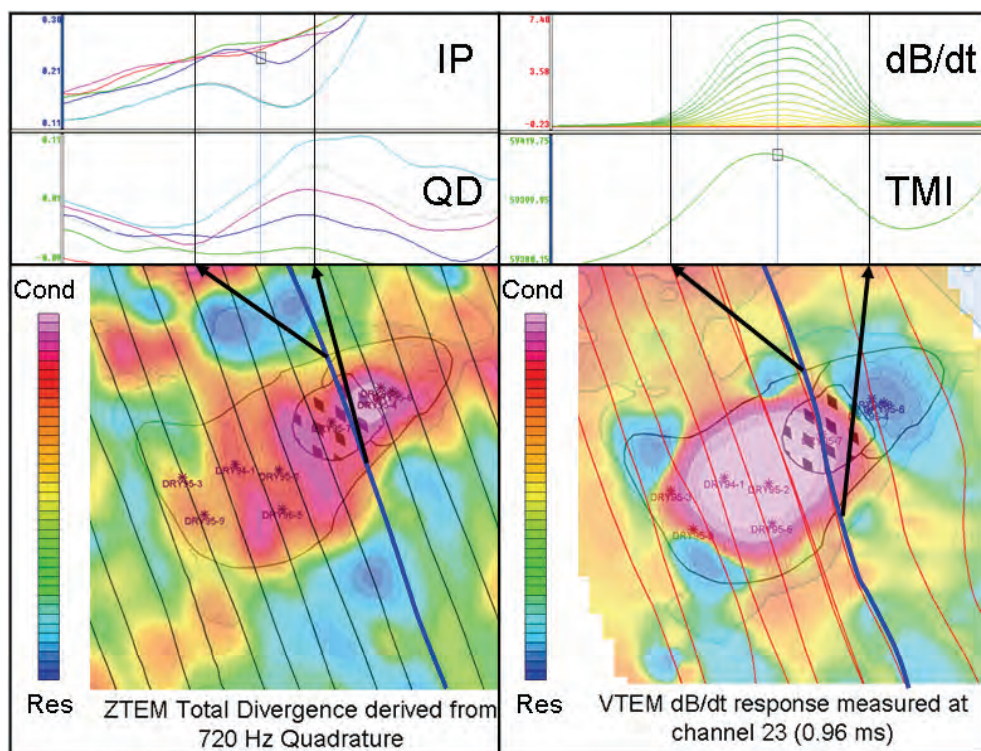


Figure 4: ZTEM and VTEM anomaly comparisons over Drybones kimberlite pipe (red color indicates more conductive response)

DISCUSSION

EM data recorded during the 2005 and 2009 studies over the Drybones Kimberlite were corroborated with the 1994-95 drilling data. In Figure 4 it seems that the anomaly maxima are displaced relative to each other with the VTEM anomaly maximum being centered over the thickest pack of lake sediments, while the ZTEM Quadrature total divergence (DT; Lo et al., 2009) anomaly seems to correlate well with the location of kimberlite diatreme facies. The Quadrature part of the ZTEM tipper is shown because it provides a more distinct response over the kimberlite than the In-Phase. This is attributed to naturally higher levels of noise noted in the measured ZTEM In-Phase data.

The EM data have been inverted using the conductivity-depth imaging transform (CDI) software for the VTEM dB/dt vertical component data (Prikhodko, 2010) and the Zvert2d inversion for ZTEM (Legault et al., 2009) of de Lugao and Wannamaker (1996), for the In-line Hz/Hx tipper data, using both In-Phase and Quadrature components from 30 - 720Hz. For the ZTEM Hz/Hx In-Phase 180Hz data, a current density-depth transform was also applied using the Karous-Hjelt filtering technique (Karous and Hjelt, 1983). Results of these procedures for a central line over the Drybones Kimberlite are presented in Figure 5.

The inversion model sections reflect the morphology of the kimberlite recovered by each survey (Figure 5). The VTEM CDI suggests that VTEM data, although they define a strong anomaly over the kimberlite (approx. 4S), might in fact be only reflecting the response from the water-saturated fine-grained sediments at the bottom of the bay, i.e., VTEM might not be resolving any deeper response due to strong EM signal attenuation in the thick pack of conductive sediments and high electrical resistivity of consolidated kimberlite. In fact this is consistent with general observations of EM survey results over kimberlites. In contrast, the ZTEM 2D inversion and Karous-Hjelt images both suggest a deeper anomalous structure that reflects the deeper geology, i.e.,

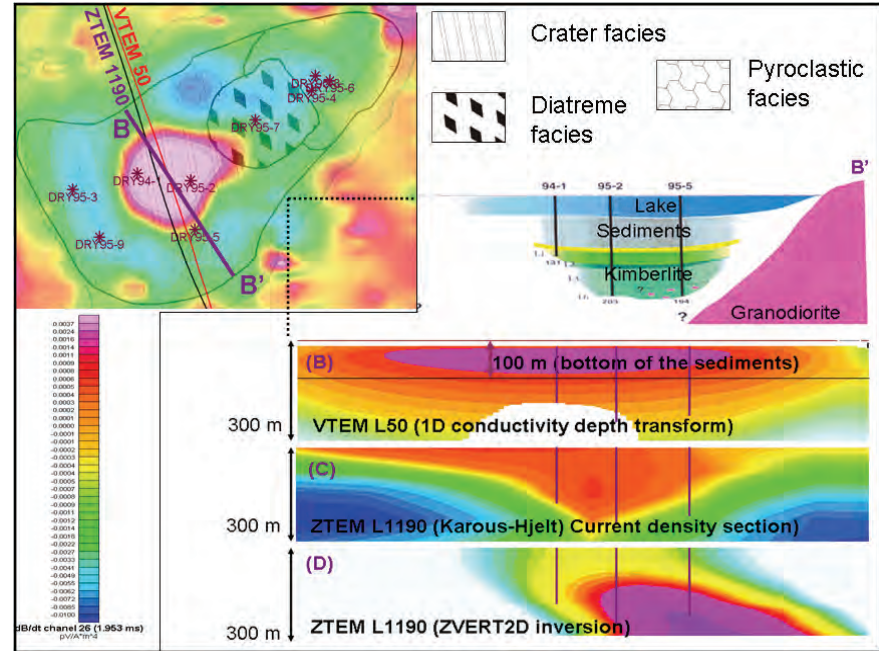


Figure 5: (A): Geologic cross-section over Drybones kimberlite pipe (Kretchmar, 1995); **(B):** Conductivity-depth transform over VTEM line 50; **(C):** Karous-Hjelt Current Density-Depth transform (derived from Hz/Hx In-Phase 180 Hz Channel) for Line 1190; **(D):** Zvert2d inversion over ZTEM line 1190.

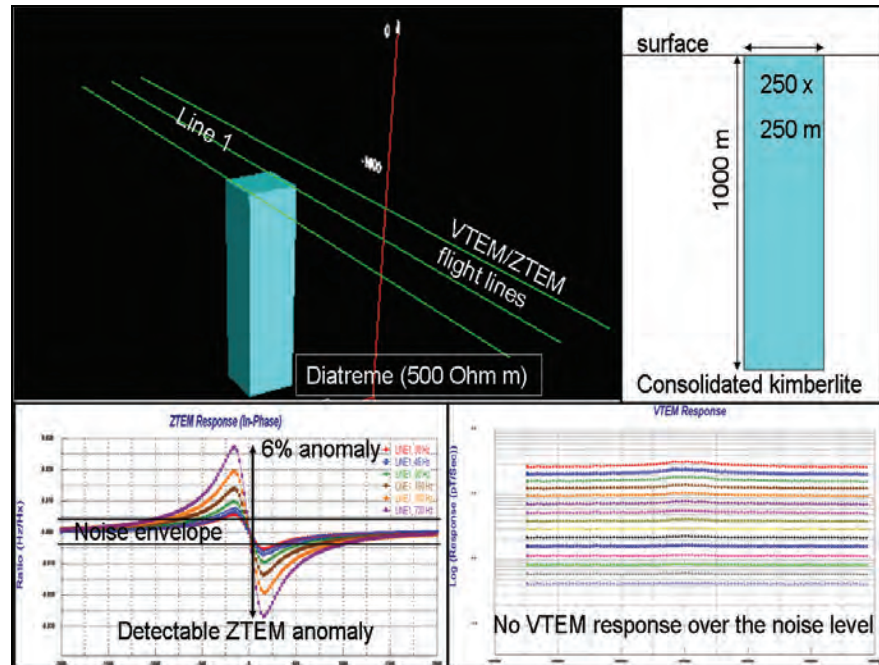


Figure 6: ZTEM forward model (Hz/Hx In-Phase) vs. VTEM forward model over 500 Ohm m target (consolidated kimberlite with no overburden) in 2000 ohm-m host rock, using Emigma 3D forward modeling software.

relatively insensitive to the shallower overburden, which is consistent with the large depths of penetration and planar horizontal primary fields for ZTEM.

These observations are further studied using 3D forward EM modeling using the Emigma (PetRos EiKon Inc., Brampton, ON, Canada). Figure 6 presents the expected ZTEM and the VTEM survey profile response over a representative kimberlite, similar to Drybones, considering no conductive overburden. The host and target resistivities were estimated from the VTEM and ZTEM inversion results, but otherwise represent reasonable physical properties. As shown in the simulation, the expected ZTEM anomaly response of 6% is above the 1% noise envelope, however, the VTEM forward model indicates the detectable signal would be barely above the expected geologic and system noise levels. These results confirm the importance of the overburden on the VTEM response relative to ZTEM.

CONCLUSIONS

Both the VTEM and ZTEM EM technologies proved to be effective in detecting an anomalous EM response over the Drybones Kimberlite. Inversion modeling and imaging of the VTEM suggests that it mainly defines the thick overburden, overlaying the kimberlite (top 100 m) and poorly resolves the deeper crater facies. In contrast, examination of the ZTEM inversion and imaging results suggest that it defines the lateral resistivity contrasts between the deeper Archean bedrock and target kimberlite.

3D forward modeling confirms that VTEM will not be easily able to differentiate between units of high electrical resistivity, associated with consolidated diatreme facies of the kimberlite and the surrounding granodiorite. Similar 3D modeling of the ZTEM, on the other hand, confirms that the kimberlite will be easily differentiated from the host rock and compare well with the observed data obtained over Drybones.

The observed differences between the two technologies are consistent with relative sensitivities between absolute and relative conductivities, relative source field orientations vs. the target host-rock geometries, as well as relative differences in depth penetration.

EM techniques, in general, are routinely used in kimberlite exploration. However it is widely accepted that they are indirect detection tools that can only assist provided the eroded kimberlites are overlain by an overburden that is sufficiently conductive to be discerned. The recent tests suggest that the newer ZTEM airborne technology should prove to be an effective for the detection and deep geologic mapping of kimberlites, due to its greater sensitivity to electrical resistivity contrasts and greater penetration, relative to other airborne EM methods.

Approximately 30% of kimberlite pipes are non-magnetic (Kaminski, 2000); many of them remain undetected, because they do not have any erosional overburden, crater or pyroclastic facies, which would allow them to be detected by conventional EM methods. Such pipes can provide sufficient electrical contrast for ZTEM airborne surveys to be effective tools. In fact Drybones remains the only kimberlite pipe detected on the

Western boundary of Slave Province of the Canadian Shield. Our results strongly suggest ZTEM technology could be more widely applied as a primary or secondary airborne method for kimberlite detection and characterization in resistive environments.

REFERENCES

- De Lugao, P. P., and Wannamaker, P. E., 1996, Calculating the two-dimensional magnetotelluric Jacobian in finite elements using reciprocity: *Geophysics Journal. International*, **127**, 806-810.
- Kaminski, V. F., 2000, Application of Airborne Geophysical methods to kimberlite exploration on the Canadian Shield: M.Sc. thesis, Moscow State University, published in Russian, 167 pp.
- Karous, M.R., and Hjelt, S. E., 1983, Linear filtering of VLF dip-angle measurements: *Geophysical Prospecting*, **31**, 782-794.
- Kretschmar, U., 1995, Drill Report on the Drybones Bay Kimberlite Property, Drybones Bay, Great Slave Lake, District of MacKenzie, Northwest Territories, for Trade Wind Resources Ltd., Vancouver, BC: submitted to NWT Dept. Indian & Northern Affairs Mining Recorder, 36 pp.
- Legault, J.M., Kumar, H., Milicevic, B., and Wannamaker, P.E., 2009, ZTEM tipper AFMAG and 2D inversion results over an unconformity uranium target in northern Saskatchewan: *SEG Expanded Abstracts*, **28**, 1277-1281.
- Lo, B., Legault, J.M., Kuzmin, P., and Combrinck, M., 2009, Z-TEM (Airborne AFMAG) tests over unconformity uranium deposits: 20TH ASEG International Geophysical Conference & Exhibition, Adelaide, AU, Extended Abstract, 6 pp.
- Lo, B., and Zang, M., 2008, Numerical modeling of Z-TEM (airborne AFMAG) responses to guide exploration strategies: *SEG Expanded Abstracts*, **27**, 1098-1101.
- Prikhodko, A., 2010, Conductivity Depth Imaging software (TEMRDI.gx): personal communication.
- Ward, S. H., 1959, AFMAG - Airborne and Ground: *Geophysics*, **24**, 761-787.
- Witherly, K., Irvine, R., and Morrison, E.B., 2004, The Geotech VTEM time domain helicopter EM system: *SEG Expanded Abstracts*, **23**, 1217-1221.

The geophysical study of Drybones kimberlite using 3D Time Domain EM Inversion and 3D ZTEM inversion algorithms

Vlad Kaminski

UBC-Geophysical Inversion Facility
6339 Stores Road,
Vancouver, BC, V6T1Z4
vkaminski@eos.ubc.ca

Douglas Oldenburg

UBC-Geophysical Inversion Facility
6339 Stores Road,
Vancouver, BC, V6T1Z4
doug@eos.ubc.ca

SUMMARY

Two airborne EM surveys were conducted over the Drybones kimberlite, NWT, Canada. A VTEM helicopter time domain EM survey was flown by Geotech in 2005, followed by a ZTEM helicopter tipper EM survey flown in 2009. The data sets collected over the kimberlite were inverted and interpreted first by Geotech, Ltd using a 1D TDEM conductivity-depth transform for VTEM data and a 2D inversion for ZTEM data. The data sets were transferred to UBC-GIF for 3D inversions and comparative analysis. Both the VTEM and ZTEM data have now been inverted in 3D and the results compared with the drill data over the kimberlite and with older results of previous geophysical interpretation. The 2D and 3D ZTEM inversions show the same general structure but the 3D inversion has greater electrical conductivity contrast and may have fewer artefacts in zones of low sensitivity. On a large scale the conductivity structure, recovered from the 3D inversion of time domain data, is comparable to that from the CDI transform, but the 3D result shows a more complicated distribution of the conductive properties. The 3D magnetic inversion had not been done previously and it shows susceptible material to depths of approximately 400 m, which is consistent with the known geometry of the kimberlite.

Keywords: 3D inversion, TDEM, ZTEM, kimberlite, airborne

GEOLOGICAL SETTING

The Drybones kimberlite is located approximately 45 km SE from the town of Yellowknife, NWT, Canada (Figure 1A). The bedrock geology in Drybones area consists of Archean granite, granodiorite and tonalite (Kretchmar, 1995). The kimberlite is located on the geological contact between granodiorites and metasediments (schists) of Yellowknife supergroup (Dunn et al., 2001). In addition there are several known tectonic faults present in direct vicinity of the kimberlite. A diabase dike propagates in the E-W direction across the area under study (Figure 1B).

Drybones kimberlite lies completely underwater, at an average depth of 38 m. It is further overlain by 65-75 m of lake sediments, predominantly clay, till and sand (Figure 1C). The

morphology of the pipe can be described as a spatially elongated intrusion (900 m by 400 m), consisting of three main facies (diatreme, crater and pyroclastic) distinguished by physical and mineralogical properties of the rock. The level of consolidation of the kimberlite varies between different facies, which is expected to be reflected in the electrical properties of the kimberlite (greater consolidation corresponds to higher electrical resistivity values).

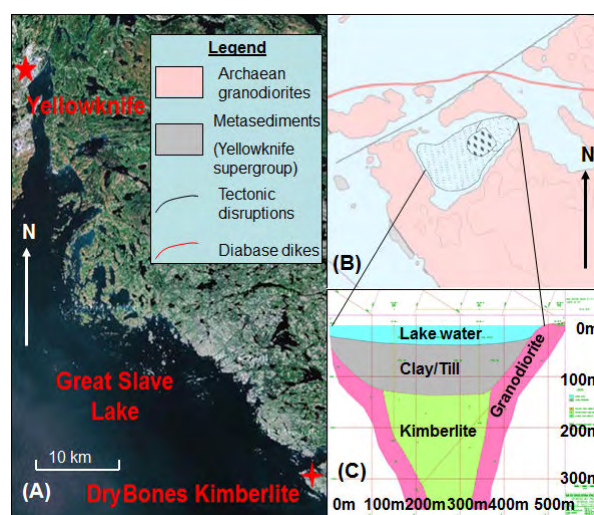


Figure 1. Location and geology of Drybones kimberlite. (a): Geographic location; (b): Contours of the kimberlite facies; (c): Drybones kimberlite in the cross-section.

The mineralogical analysis of the Drybones kimberlite samples reveals signs of alteration due to elevated contents of Cr and Nb, as well as due to low totals of TiO₂ in ilmenites (Dunn et al, 2001). The geochemical alteration may be reflective in the magnetic properties of the kimberlite.

GEOPHYSICAL SURVEYS OVER DRYBONES

Numerous geophysical studies have been performed over Drybones kimberlite since 1994, including total field magnetic surveys, gravity surveys, VTEM and ZTEM surveys (Kaminski et al, 2010). In this study we are focusing on geophysical surveys flown by Geotech, Ltd from 2005 to 2009, which include two airborne EM studies (VTEM and ZTEM) each accompanied by total magnetic intensity study. In particular, our main emphasis is on 3D inversions which

include inversion of magnetic data, ZTEM data and TDEM data.

3D INVERSION OF MAGNETIC DATA

Total magnetic intensity data were to recover magnetic susceptibility from the 2525 IGRF-corrected magnetic data, flown in tandem with the ZTEM survey. Data were collected with a cesium vapor magnetic sensor flown at the altitude of 60 meters above ground.

The 3D region used for the inversion of magnetic data has been discretized onto 620,136 cells mesh, centered around the core region inclusive of the kimberlite pipe. The core region of the mesh is composed of blocks 25x25x10 meters in size. The maximum depth of the core region reaches 660 meters. The data have been assigned standard deviations of 3nT and inverted using depth weighting (Li and Oldenburg, 1996). The inversion showed convergence to desired misfit (2525) in 4 iterations.

Figure 2 shows depth slices of the recovered magnetic susceptibility plotted over the known contours of the Kimberlite pipe. Elongated magnetic structure in the northern part corresponds to known diabase unit and the kimberlite material shows magnetic signature to depth of 300 m. Figure 3 shows geological depth sections AA' and BB' matched with recovered distribution of the susceptible material. The high susceptibility material associated with the kimberlite is observed to be well differentiated from non-magnetic sediments and this boundary seems to be consistent in all directions. It is possible that the kimberlite material is present at depths greater than 300m, and the magnetically susceptible material only marks that portion of kimberlite, subject to geochemical alteration.

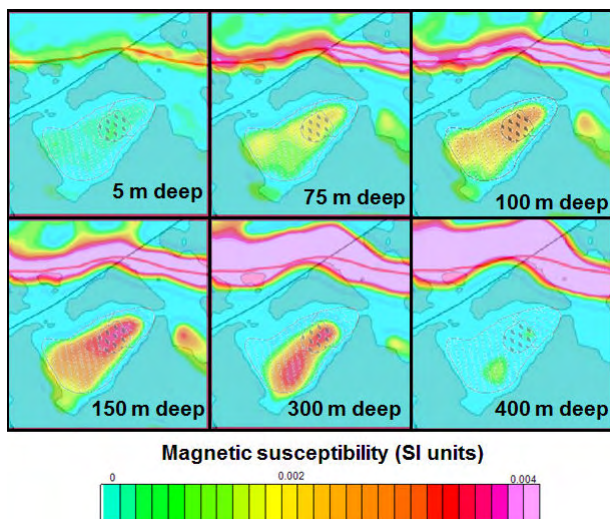


Figure 2. Recovered magnetic susceptibility over Drybones kimberlite overlain with geologic unit contours and presented as a series of depth slices at 5, 75, 100, 150, 300 and 400 m below surface.

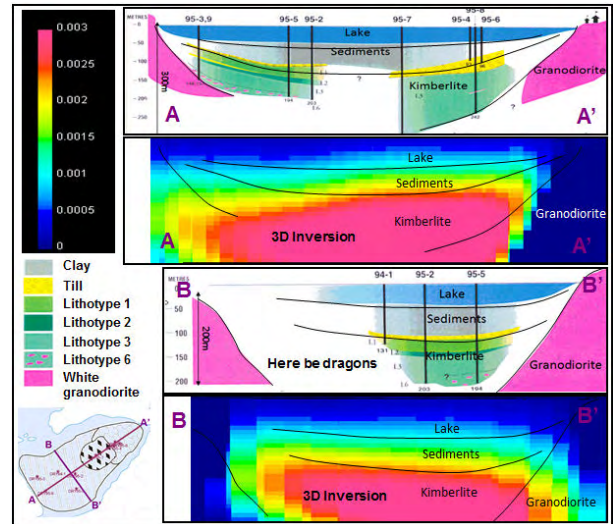


Figure 3. Geological cross-sections based on drilling compared to the magnetic susceptibility model recovered by 3D inversion. For details regarding kimberlite lithotypes refer to (Kretchmar, 1995).

3D INVERSION OF VTEM DATA

Time domain EM data were collected by a VTEM system in 2005. More detailed description of the survey can be found in (Kaminski et al, 2010). The data were inverted using UBC-GIF multi-transmitter 3D time domain inversion code H3DTD (Oldenburg, Haber and Shekhtman, 2011).

The inversion code uses a time-stepping and both the on-time and off-time portions of the waveform are discretised into time segments in which the step interval is a constant. Efficiency of the code in handling multi-transmitters is achieved by decomposing the Maxwell forward modelling matrix. One decomposition is required for each time segment. The discretised waveform is shown in figure 4 and was designed to accommodate 10 time gates, covering the interval from 190 to 1900 μ s with at least one discrete step per time gate..

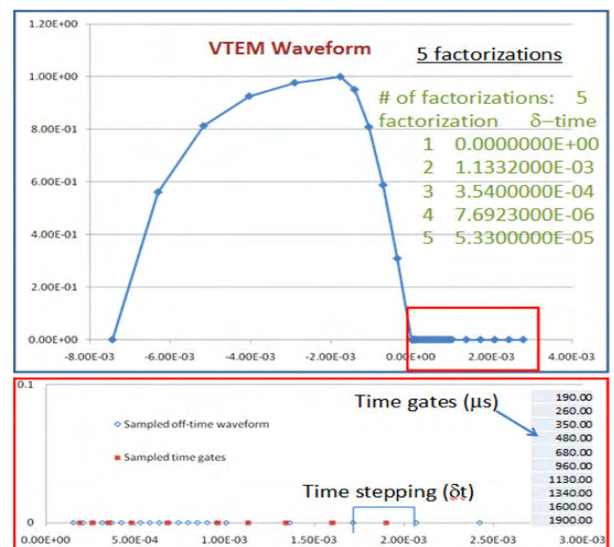


Figure 4. VTEM waveform discretised for H3DTD time-stepping computations.

An initial (coarse) inversion was done on a 156,604 cell mesh consisting of core region and an outer padding area. The smallest cell in the core region measured at 50x50x15m. The data set was sub-sampled to 76 transmitters. This was followed by another 3D TDEM inversion on a refined 252,450 cell mesh (smallest cell: 20x20x7m), centred exactly on the kimberlite, and using 176 transmitters.

The preliminary (coarse) inversion was terminated after 17 iterations and the misfit was 2.058×10^5 . A total of 43 parallelized Intel Xeon processors were employed for the inversion. The following refined inversion was performed using 52 parallelized processors and after 14 iterations achieved a final misfit of 3.82×10^4 . The total number of cells 7.3×10^5 . The data fit for selected VTEM stations and the convergence curves are shown in figure 5.

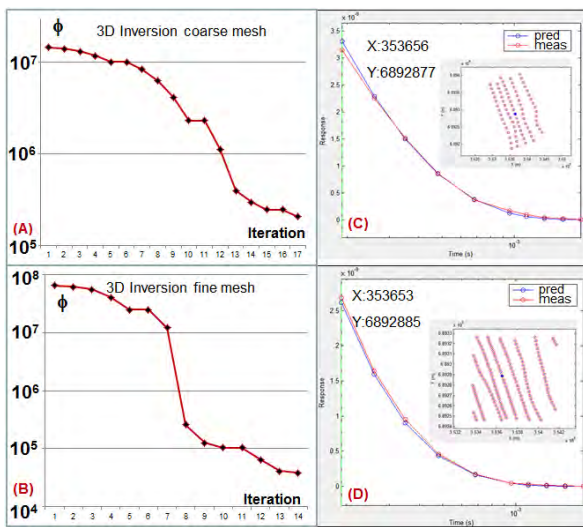


Figure 5. Convergence of two 3D VTEM inversions. (a): Convergence curve for preliminary (coarse) inversion; (b): Convergence curve for refined inversion; (c): Observed versus predicted data for 10 time gates shown at selected location for preliminary (coarse) inversion; (d): Observed versus predicted data for 10 time gates shown at same location as (c) for the refined inversion.

The conductivity models recovered from both inversions were verified against the known geology. This comparison over selected cross-section (AA') is shown in figure 6.

The recovered conductivity values range from 20 Ohm m to 10,000 Ohm m. This is consistent with the anticipated values and fits well with previously done conductivity-depth transforms (Kaminski et al, 2010). In figure 6 it is shown how the fine-meshed 3D VTEM inversion model resembles the contacts between different geological formations. These formations can be subdivided according to their electrical resistivity. The “blue” zone includes values above 500 Ohm m and marks the contact between the kimberlite and granodiorite. The “green-yellow” zone covers the interval between 500 and 50 Ohm m and is consistent with known kimberlite; finally the “red” zone combines all material of less than 50 Ohm m in resistivity and constitutes the top

conductive layer of sediments and lake water. The latter is consistent with previous studies.

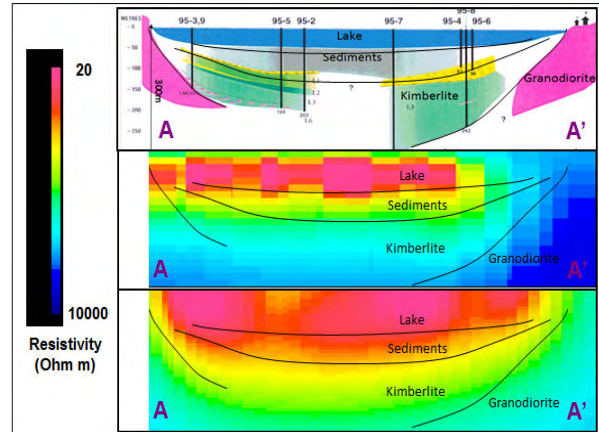


Figure 6. VTEM 3D inversion results compared to known geology. From above to below: lithological cross-section (Kretchmar, 1995); conductivities from coarse 3D VTEM inversion; conductivities from refined 3D VTEM inversion.

3D INVERSION OF ZTEM DATA

The ZTEM survey data were inverted using MTZ3D, which can invert MT, ZTEM and combined inversions over 3D structures with topography.

The 3D unconstrained ZTEM inversion was performed on a decimated data set, which accommodated 10,169 ZTEM stations, sampled at 6 frequencies (30 to 720 Hz) and recorded for 4 components (real and imaginary X-tipper and Y-tipper). Please refer to (Vozoff, 1972; Berdichevsky, 2003) for details on tipper transfer functions. The total number of data was therefore 244,056. The data were inverted on a 874,800 cell mesh with smallest cells discretized to 50x50x25 m measure. The inversion has converged to 2.29×10^6 in 20 iterations showing good overall data fit (see figure 7).

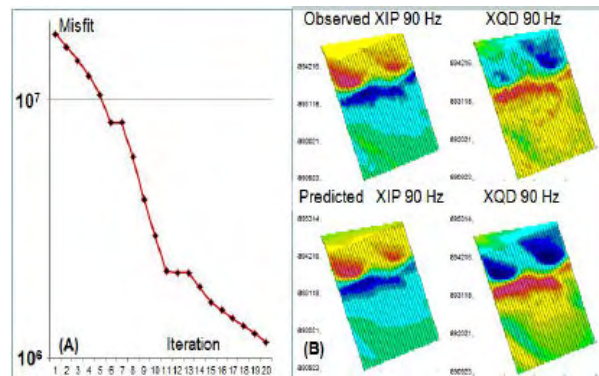


Figure 7. ZTEM 3D inversion convergence and data fit. (a): Convergence curve; (b): Observed X-tipper (real and imaginary at 90 Hz) compared to predicted equivalents. NOTE: UBC-GIF uses standard MT coordinate system and defines tipper transfer function in Weise sense (Wiese, 1965; Parkinson, 1959; Berdichevsky, 2003), which is not consistent with their tipper and coordinate convention.

The results of the ZTEM inversion were compared with the geology as well as with the conductivity models recovered using 3D VTEM inversions. Furthermore, the results were supported by previously carried out 2D inversions of ZTEM data (Kaminski and Legault, 2010) using Zvert2d, a Geotech in-house software for inverse modelling. In figure 8 a selected profile positioned directly over the kimberlite is subjected to comparative analysis showing similarities and differences in recovered geo-electrical properties to the depth of 800m.

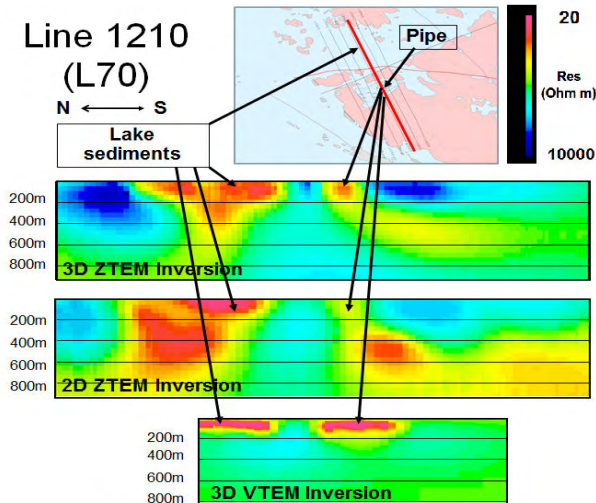


Figure 8. Comparison of three conductivity models cross-sectioned at ZTEM line 1210 (VTEM line 70). Top to bottom: 3D ZTEM inversion (UBC-GIF); 2D ZTEM inversion (Geotech); 3D VTEM inversion (UBC-GIF).

The areal coverage of ZTEM survey is greater than that of the VTEM survey, however there are clear similarities. Both show the conductive signature of known structures and electrical conductivities from the inversions are with the same numerical range.

CONCLUSIONS

The comparative analysis carried out for three independent conductivity models, acquired without a-priori constraints, shows great similarities. The conductive lake sediments are clearly delineated in all 3 inversions. The kimberlite pipe is clearly outlined and coincides with its mapped positioning. The main differences include the signatures of deep-seated structures, which can be only seen in ZTEM inversions. This can be attributed to the fact that ZTEM, as a natural plane wave source EM system, has greater penetration depth. Other differences are between the 2D and 3D ZTEM inversion models. In general, the 3D model (UBC) shows greater conductivity contrast. Another advantage of using the 3D code is the recovery of a more vertically confined sedimentary layer, which has been known to reach no more than 150m in thickness.

Figure 9 shows the 3D distribution of electrical conductivity recovered by ZTEM 3D inversion (UBC) compared to interpolated 2D results (Geotech). The geometry of the structure recovered by the 3D code is a more accurate model of the kimberlite, which shows the transition from more conductive crater facies to consolidated (less conductive) diatreme. Validity of this transition is yet to be confirmed.

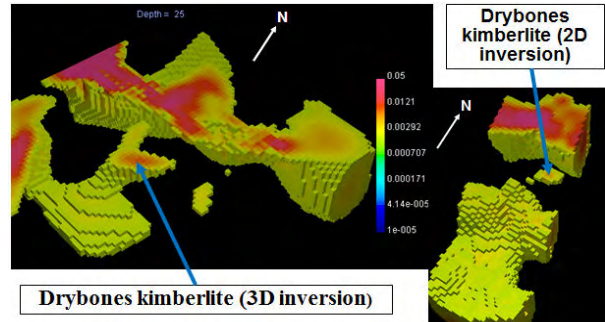


Figure 9. 3D distribution of electrical conductivity, truncated at 500 Ohm m, showing the transition from crater facies to the diatreme in case with 3D ZTEM inversion (UBC-GIF).

In conclusion, the study confirms that using airborne natural source EM surveying is an effective technology for kimberlite exploration and perhaps one of very few airborne EM techniques, which may be capable of delineating electrical property variations in resistive domain. The latter may be extremely important for exploration of non-magnetic kimberlites with weathered crater facies and mainly composed of consolidated material. Such targets are extremely challenging for conventional EM/Mag combination and in some estimates may number up to 25% of total kimberlites occurring within the Canadian Shield (Kaminski et al, 2010).

REFERENCES

- Berdichevsky, M. N., Dmitriev, V., Golubtsova, N., Mershchikova, N., Pushkarev, P., 2003, Magnetovariational Soundings: New Possibilities., *Physics of Solid Earth*, 3, 3-30.
- Dunn, C.E., Smith, D., Kerr, D.E., 2001, Biogeochemical survey of the Drybones Bay area, NWT using outer bark of black spruce. Geological Survey of Canada, Open File 3919.
- Kaminski, V., Legault, J.M., Kumar, H. (2010) The Drybones kimberlite: a cast study of VTEM and ZTEM airborne EM results, 21ST ASEG International Geophysical Conference and Exhibition, Extended Abstract. Sydney, Australia, 22-25 August 2010, 4 pp.
- Kretschmar, U., 1995, Drill Report on the Drybones Bay Kimberlite Property, Drybones Bay, Great Slave Lake, District of MacKenzie, Northwest Territories, Canada.
- Li Y., Oldenburg D. W., 1996, 3-D inversion of magnetic data. *Geophysics* 61, 394-408.
- Oldenburg, D. W., Haber, E., Shekhtman, R., 2011, Three dimensional inversion of multi-source time domain electromagnetic data, Submitted to *Geophysics*, May 2011, 41p.
- Parkinson, W.D., 1959, Direction of rapid geomagnetic fluctuations, *Geophys. J. R. Astron. Soc.*, 2, 1-14.
- Vozoff, K., 1972, The Magnetotelluric Method in the Exploration of Sedimentary Basins, *Geophysics*, 37, 1, 98-141.
- Wiese, H., 1962, Geomagnetische Tiefentellurik XI Die streichrichtung der untergrundstrukturen des elektrischen widerstandes, entschlossen aus geomagnetischen variationen, *Geofis. Pura.*, 52, 45, 303 (published in German).

ZTEM data inversion and interpretation using the UBC-GIF MTinv3D code: A case history at the Silver Queen project, British Columbia

Peter L. Kowalczyk

Mira Geoscience Ltd.

*Advanced Geophysical Interpretation Centre
Vancouver, British Columbia, Canada*

peterk@mirageoscience.com

Patrick B. M. van Kooten

Mira Geoscience Ltd.

*Advanced Geophysical Interpretation Centre
Vancouver, British Columbia, Canada*

patrickv@mirageoscience.com

SUMMARY

Z-axis Tipper Electromagnetic (ZTEM) surveys are rapidly becoming an integral part of geophysical exploration. This airborne AFMAG EM system measures the tipper of natural magnetotelluric fields at frequencies typically from 30Hz to 720Hz.

The ZTEM system responds primarily to current channelling and operates at lower frequencies than active-source EM systems. As such, it maps bulk conductivity of the ground to lower values and greater depths than active-source airborne EM systems. ZTEM is particularly suited to mapping large regional structures, sulfide vein systems and intrusives that characterize porphyry copper deposits. The 3D resistivity model produced by inversion of ZTEM data using the UBC-GIF MT3Dinv code proves very useful for focussing exploration into the most prospective zones of a project area.

The Silver Queen polymetallic vein system is a high grade past producer south of Houston, British Columbia. Current exploration around the old Silver Queen mine by New Nadina Explorations Ltd is conceptually based targeting of a blind, buried bulk tonnage deposit near the old mine and deeper in the mineralized system. Inversion of the ZTEM data and the magnetic data acquired over and surrounding the old mine, has identified a favourable setting close to an interpreted nearby intrusive body and within a large regional structure that flexes around it. Exploration is now focussed in this area, with a deeply penetrating induced polarization, electrical resistivity, and magnetotelluric ground survey completed over the target areas to direct drilling. The ZTEM processing and the inversion results from the ZTEM and magnetic data are presented.

Key words: ZTEM, AFMAG, airborne electromagnetics, 3D EM inversion modelling, natural source EM

INTRODUCTION

The Z-axis Tipper EM (ZTEM) system, developed by Geotech Ltd (Legault et al., 2009), measures the tipper of the MT field in both the along-line (X) and cross-line (Y) polarizations.

The tipper (Vozoff, 1972) is the ratio of the vertical magnetic field, as measured with a large horizontal loop receiver towed beneath the survey aircraft, and the horizontal magnetic field as measured at a reference base station located in a non-anomalous area within or near the survey area. The real and imaginary components of the tipper are recorded for both the X and Y polarizations of the MT field. Measurements are typically made from 30Hz to 720Hz, with 3 or 4 frequencies per decade. The low frequency limits of the system are determined by the speed of the aircraft since a certain number of cycles need to be measured to acquire a reading, and the high frequency limits are determined by the strength of the MT signal, which falls off at higher frequencies. Thus, four measurements are made at each frequency, comprising of the real and imaginary components of the X and Y polarizations. Thus, if measurements are made at 6 frequencies then 24 separate readings would be recorded at each receiver location along the line.

Conductive anomaly trends produce cross-over anomalies in the polarization which crosses their strike. These are straightforward to recognize yet difficult to interpret in a quantitative way. When 6 frequencies are being measured, the 24 separate maps produced are confusing and the imaginary-component response maps are non-intuitive, even to an experienced geophysicist. Cross-over anomalies can also be produced by topographic effects, the strength of the anomaly being a function of the ground conductivity, the amount of topographic variation, the polarization direction and the frequency being measured. The combined inversion of this data to produce one consistent model of ground conductivity provides a unified interpretation of the whole dataset.

ZTEM INVERSION

The UBC-GIF MT3D inversion codes (Farquharson et al., 2002, 2003) produce robust 3D conductivity models. However, careful preparation of the data is critical before one can achieve a good result. The most important aspects of this preparation are the assignment of relative errors to the data and the removal of bad data, which is usually spatially associated with power lines. We have found that visual inspection of the each component of the data is essential. Bad data can usually be recognized visually and are subsequently removed prior to attempting a trial inversion of the remaining data. As the topography contributes to the response, and the topographic effect needs to be accounted for by the inversion, it is necessary to have a good topographic model. The

geodetic datum and horizontal datum of the GPS and Digital Elevation Model (DEM) need to be checked carefully to ensure they are as expected. This is normally done by comparison with a reference DEM in a known datum, for example the SRTM data which is available worldwide in the WGS84 datum, within which elevations are quoted with respect to mean sea level.

After careful review and acceptance of the ZTEM data, it is necessary to design a discretised mesh for the project area, taking cognizance of the size of the area, the flight line spacing and the topographic relief. If the area is being inverted in multiple meshes and being merged together afterwards, then sufficient overlap needs to be assigned in the design of the meshes to allow the results to be merged together successfully.

Given the design of an appropriate inversion mesh, and comfort with the data quality, then the next step is to do some trial inversions of the data using one frequency at a time. These trials are done in order to check data quality and to assign appropriate errors to each data point. If the inversion process converges at each frequency to an acceptable level of detail, then the data at that frequency can be put aside for use in the final combined frequency inversion. The errors assigned to each frequency can be balanced to assign appropriate weights to each frequency at the single frequency inversion stage. Once the data at frequency is tested using a single frequency inversion, then all the data can be combined together to do a multi-frequency inversion.

The multi-frequency data is often first inverted at a reduced resolution, using a coarser mesh discretization. The result from this may be used as a starting model for the final inversion at the highest resolution and the largest mesh that can be run using the computational resources available. The limits of resolution are principally determined by the errors assigned to the data. The size of the inversion mesh is primarily controlled by the amount of memory and compute time available on the computer being used. In a parallelized computing environment, each frequency requires four processors, so a six frequency inversion would require a 24 processor cluster. The current version (V.201001) of the MT3Dinv code normally takes one or two days per iteration, which can add up to a week or ten days to achieve a solution using a good high end computing cluster. Actual compute times vary considerably depending on individual hardware configurations, available system resources and increase non-linearly with increasing mesh size.

MAGNETIC INVERSION

The magnetic data acquired during a ZTEM survey can be inverted separately to generate a 3D magnetic susceptibility model that provides additional and corroborating geological information about the survey area. The code normally used to invert the magnetic data is the UBC-GIF MAG3D inversion package, which operates in a similar way to the UBC-GIF MT3D program package. The design of meshes as well as the optimization of the input data for this program are well understood in the geophysical industry and are thus not discussed in detail here.

SILVER QUEEN ZTEM DATA

In June 2011, a ZTEM survey was flown over the Silver Queen project area of New Nadina Explorations Ltd. The project area is south of the town of Houston, British Columbia and not far from the Huckleberry mine, which is a producing copper, molybdenum porphyry deposit. The Silver Queen mine is a vein type polymetallic deposit and past producer. The target sought by New Nadina Explorations Ltd is a large, bulk tonnage type deposit close to and below the Silver Queen vein system. There are abundant small veins and showings around the old mine, but no clear indications of where the mineralizing source fluids for the mine came from, nor where one should look for a blind, bulk tonnage deposit that might be associated with the mineralized vein system. The mine sits in a metavolcanic and metasedimentary sequence, and the presence of an intrusive close by was inferred from an anomaly in an old airborne magnetic survey, but the survey did not cover a large enough area to allow the geometry of any magnetic stock present to be interpreted.

The ZTEM and magnetic inversion results were reviewed to identify areas close to the Silver Queen Vein system, near or within an intrusive stock, and within a regional structure that could control the emplacement of a disseminated, bulk type mineral deposit. Figures 1 and 2 show the results of these inversions. A favourable area next to an inferred intrusive, close to the south end of the Silver Queen Vein system, and within a jog in a large NE-SW trending regional fault system has been identified. Ground follow-up using a deeply penetrating induced polarization, resistivity and magnetotelluric system has been done and deep drilling is scheduled to commence in September and October 2011. The combination of geophysical and drilling programs, applied sequentially but using information from one in designing the other has allowed a rapid, focussed, and cost effective exploration program.

CONCLUSIONS

The ZTEM and magnetic inversion results have provided direction to a ground geophysical and drilling program looking for a buried disseminated bulk tonnage deposit close to and below the known Silver Queen vein system. Exploration has been focussed into a particular area in a cost effective and rapid manner, providing targets for a deep drilling program while reducing the risk and cost of the program. The ZTEM survey has identified the Silver Queen Vein system as an electrically resistive trend; it has identified a potential intrusive below the vein system that may be genetically related, and it has identified a flexure in a regional structure passing by this intrusive that is a favourable setting for a blind bulk tonnage deposit. Inversion of the magnetic data provides independent corroboration that the electrically resistive body is likely an intrusive, as the resulting magnetic model shows a coincident stock-like magnetic body. Follow-up ground geophysical surveys have identified several prospective induced polarization targets and these are currently being drilled.

ACKNOWLEDGMENTS

The authors wish to thank New Nadina Explorations Ltd for granting permission to show the ZTEM and magnetic data results from their Silver Queen project.

REFERENCES

Farquharson, C. G., Oldenburg, D. W., Haber, E., 2002, An algorithm for the three-dimensional inversion of magnetotelluric data: 72nd Annual International Meeting, SEG, 649-652.

Farquharson, C., Haber, E., Shekhtman, R., Oldenburg, D., 2003, Theoretical Background for the Magnetotelluric Inversion Program MT3Dinv. Technical Report, University of British Columbia.

Legault, J.M., Kumar, H., Milicevic, B., and Hulbert, L., 2009, ZTEM airborne tipper AFMAG test survey over a magmatic copper-nickel target at Axis Lake in northern Saskatchewan: 79th International Exposition and Annual Meeting, SEG, Expanded Abstracts, 1272-1276.

Vozoff, K., 1972, The magnetotelluric method in the exploration of sedimentary basins, *Geophysics* 37, 98-141.

FIGURES

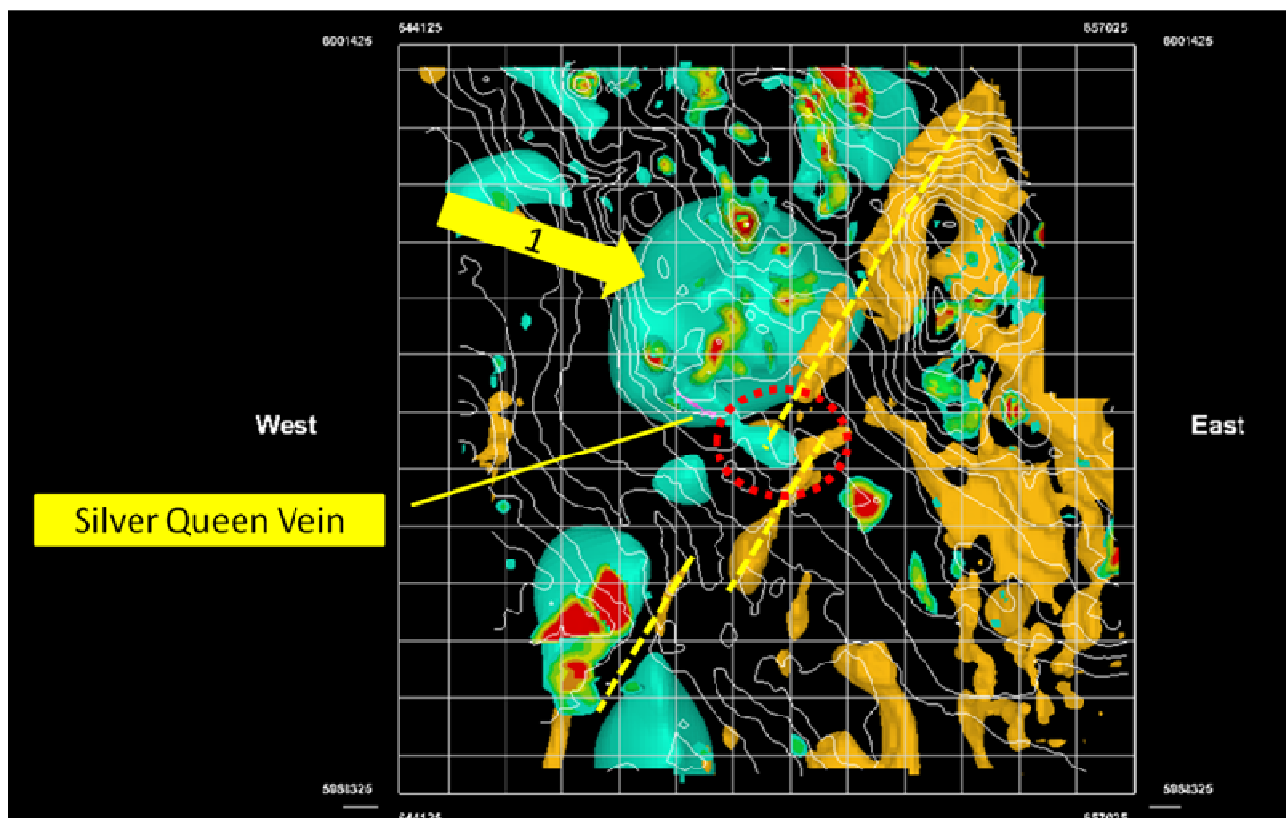


Figure 1. ZTEM INVERSION RESULTS: The 500 ohm.m and 12.5 ohm.m isosurfaces derived from the ZTEM inversion model are shown in light blue and light brown respectively. The Silver Queen Vein system is shown as a small purple body striking NW. The large balloon shaped light blue resistive isosurface immediately below and to the north of the Silver Queen Vein system is interpreted to be an intrusive. The interpreted NE-SW regional structure is shown as a yellow dashed line. The red ellipse identifies the favourable region where a zone of structural accommodation for the NE-SW fault system is present close to the intrusive.

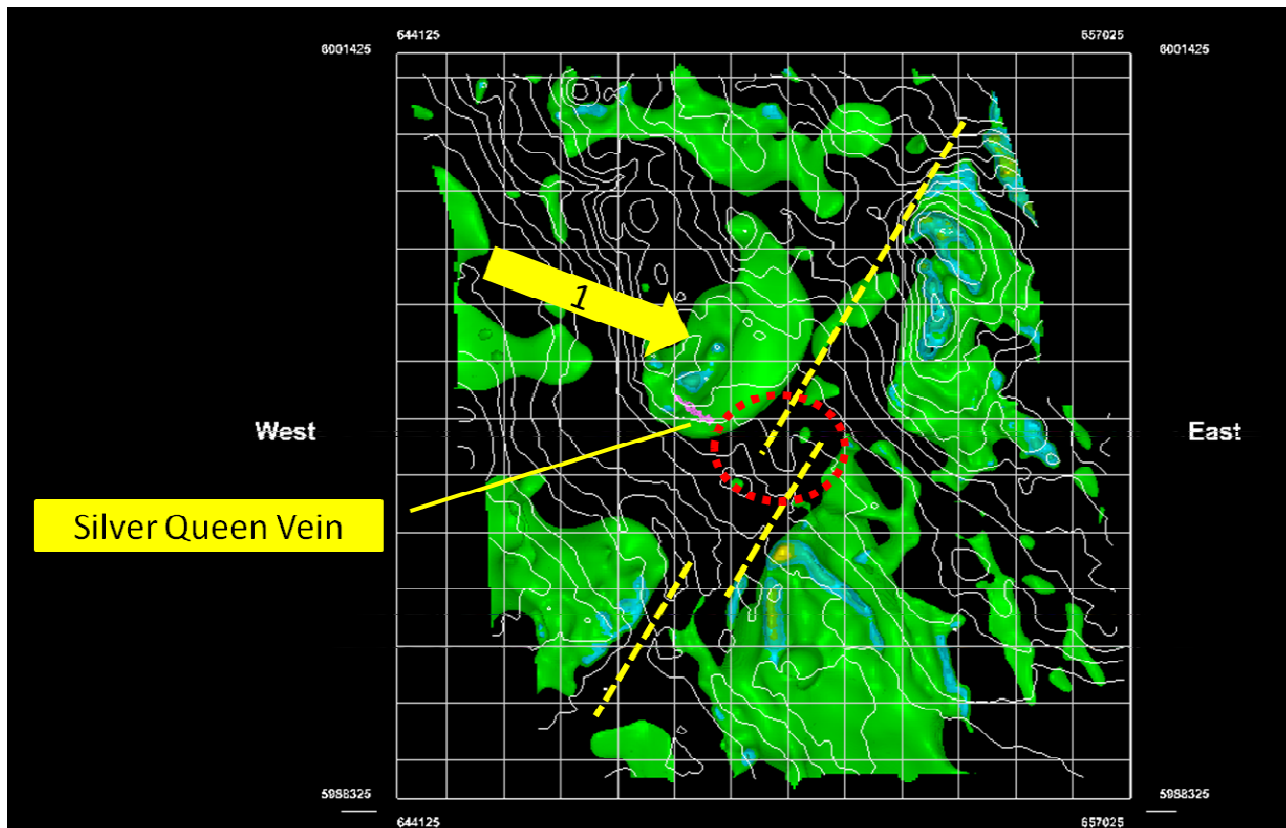


Figure 2. MAGNETIC INVERSION RESULTS: The 0.002 SI isosurface derived from the magnetic susceptibility model produced by the 3D inversion using the UBC-GIF MAG3Dinv code is shown in green. Note that the intrusive interpreted from the ZTEM resistivity model below the Silver Queen Vein system corresponds with a volume of increased magnetic susceptibility. The NE-SW structural trend corresponds with a magnetic low.

Inverting ZTEM data in 3D: Process and Practice

Peter L. Kowalczyk ¹ and Patrick B. M. Van Kooten ²

¹ *Mira Geoscience Ltd., Advanced Geophysical Interpretation Centre, Vancouver, British Columbia, Canada (peterk@mirageoscience.com)*

² *Mira Geoscience Ltd., Advanced Geophysical Interpretation Centre, Vancouver, British Columbia, Canada (patrickv@mirageoscience.com)*

Summary

The Z-axis Tipper Electromagnetic system (ZTEM) is an airborne EM system that measures the tipper of natural magnetotelluric (MT) fields at frequencies from 30 Hz to 720 Hz (Legault et al., 2009). It is a passive system that measures both the along-line (X) and cross-line (Y) polarizations of the EM tipper. As such, the survey data are insensitive to flight-line direction.

The principal ZTEM response is from channelling of magnetotelluric (MT) currents through more conductive regions of the survey area (Vozoff, 1972). The system is well suited to mapping regional structures, large breccias and other features of moderate to low-conductivity which would otherwise be poorly mapped by active EM systems.

A plan map of the ZTEM Tipper measurement at a single frequency is intuitively straightforward to understand in that conductive features produce tilt-angle crossovers above the conductive axis of the feature. However, interpretation of these maps for multiple frequencies is less intuitive, since the real and quadrature components for two polarizations of each tipper will produce four maps for each frequency. Nonetheless, this problem is well suited to inversion since this process incorporates a consideration of all of the data acquired by the ZTEM system and will produce a modelled conductivity volume that is immediately useful for interpretation and for targeting drill holes.

We present an example of a ZTEM inversion in conjunction with the integrated interpretation of ZTEM, magnetic and ground-based Titan24 electrical data which has led to the discovery a new buried molybdenum porphyry prospect at the Silver Queen project of New Nadina Exploration Limited.

Introduction

ZTEM data acquired at the Silver Queen Project in northern British Columbia have been inverted to produce a 3D conductivity model. During the acquisition phase of the ZTEM survey, a magnetic data set was also acquired, and this was subsequently inverted to produce a magnetic susceptibility model. The resulting conductivity and susceptibility models were combined with a 3D model of the known vein type mineralization and previous drilling. Integrated interpretation of these results was then used to direct an exploration program comprising a Titan24 electrical survey followed by drilling. The electrical survey targeted blind mineralization in a structurally favourable, yet undrilled location proximal to the known mineralization. This exploration program has led to the discovery of a significant zone of porphyry-style molybdenum mineralization.

Processing of ZTEM data is straightforward. Our practice is to interpolate ZTEM data as delivered to a grid format and then to inspect for regions of poor data. After deleting noisy or corrupted data, the data are prepared for inversion. We invert ZTEM data using the UBC-GIF group's MT3Dinv code package. This is an MT specific version of the more general UBC EH3Dinv code, with provision made for the plane wave MT source field assumption. We normally invert each frequency by itself and then use one of the results from a single frequency inversion as a starting model for a multi-frequency inversion considering all the data simultaneously.

In the following sections, we describe the process in more detail then illustrate this process applied in practice to aid exploration at a minerals prospect.

Data preparation and inversion

Prior to inversion, the data need to be reviewed, coordinate systems checked, bad data removed, a mesh designed, and errors assigned to the data. Then the data can be inverted, first using single frequency inversions to assess the quality of the data as well as the appropriate errors to assign, and then as a combined multi-frequency inversion done with all frequencies, or a selected subset thereof (Figure 1).

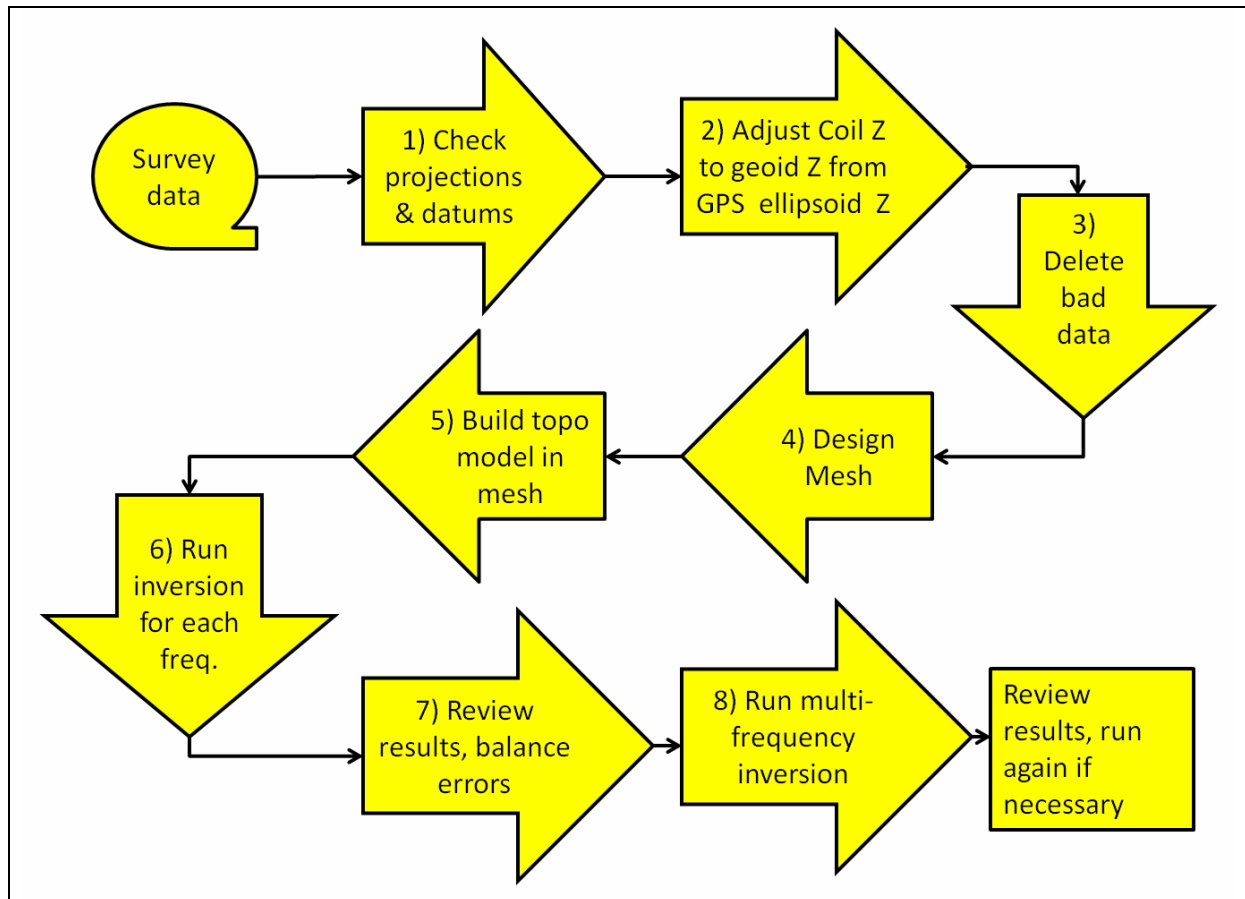


Figure 1. Chart illustrating the process workflow for a ZTEM inversion project. Note that both the single frequency and multi-frequency inversion may be run several times until a satisfactory result is achieved.

Datums and coordinate systems are an ongoing source of trouble. Generally the data are received in WGS84 UTM, with latitude and longitude in the database, and x, y, and z for the ZTEM receiver in the WGS84 UTM projection. However, the data can have the latitude, longitude, and elevation referenced to the WGS84 ellipsoid, and the XY coordinate in another projection (e.g., NAD27). As there are many possible variations, the user must exercise considerable caution. Another source of confusion is elevations. The coil Z is generally referenced to the ellipsoid, while topographic elevations are given with reference to the geoid (mean sea level). Differences in excess of 100 m can exist between elevations referenced to the ellipsoid and those referenced to the geoid. When building a digital elevation model from the GPS record of the aircraft position and the recorded laser/radar altimeter data, the user must ensure that the aircraft position used is an elevation referenced to the geoid. This is very important when building the topographic surface for use in an inversion project as the aircraft GPS position and laser/radar altimeter are often the best data or only data available for this task. When constructing the quantized topographic model, the effect of using large blocks to approximate the topography in steep terrain can result in a topographic model that is not optimum. Considerable differences may exist between the actual ground surface elevation and the top of the model used by the inversion algorithm. This effect is illustrated in Figure 2 and Figure 3.

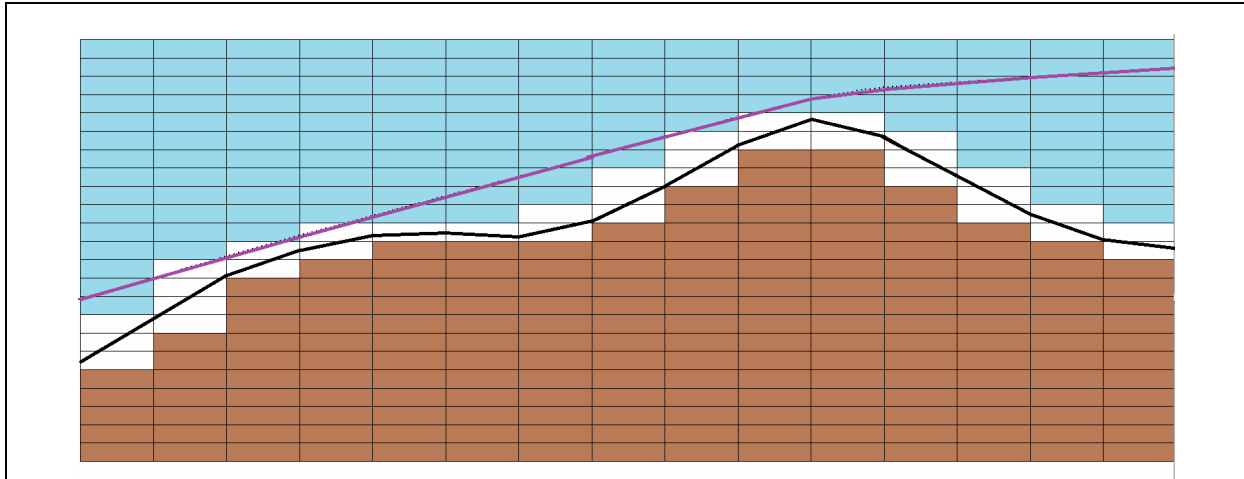


Figure 2. Shown is an example of a real flight (purple) and topographic surface (black) and a topographic model with 200m x 200m x 50m mesh cells. The MT3Dinv code will truncate the surface so no cell extends above the topographic data points supplied as input to the algorithm. Cells fully below the topographic surface are brown, mixed air/ground blocks assigned as air in MT3Dinv are white, and air only blocks are blue. Note that the average flight height off the ground is effectively increased in the inversion block model created by the programme.

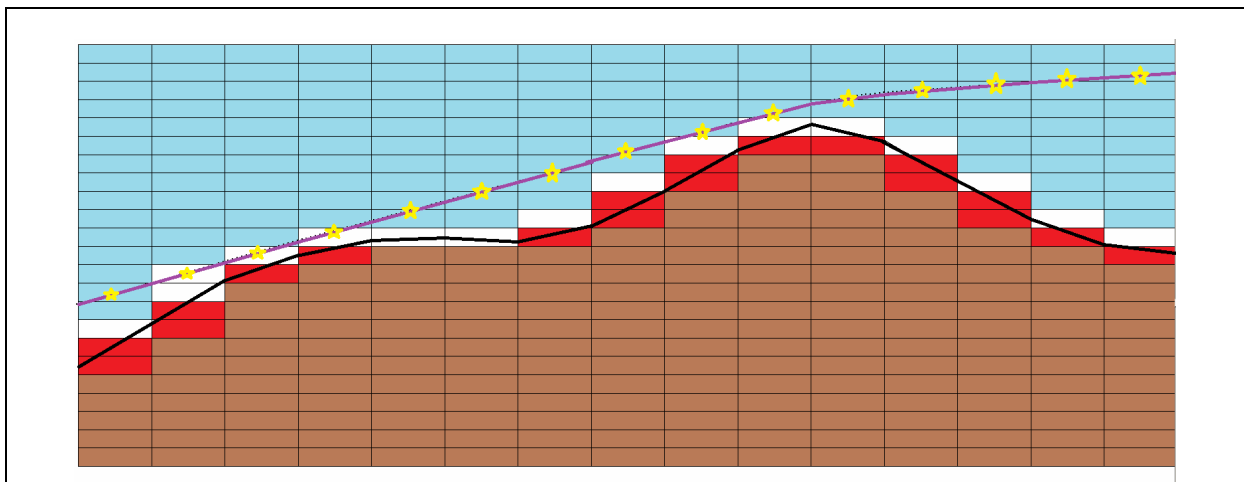


Figure 3. The effect of truncating topography can be reduced if data and topography are only located over the centre of mesh cells and the topography value is rounded up or down to an elevation corresponding to the top of a mesh cell. Red cells shown are added to the inversion model if this process is followed. The resulting cell based model is a better representation of the real topography.

It is essential to review the ZTEM data at all frequencies and both polarizations and to mark or remove bad data. The method we use is to grid the data and then to inspect the power-line monitor maps along with maps of each data field to identify data that are geologically unreasonable. Generally, these are high amplitude short spotty anomalies or anomalies that are correlated with the high values of the power-line monitor and that break up the trends of the map. This is somewhat arbitrary, but has produced the best results for us. If bad data are left in the data sets, they can also be identified later in the workflow if the inversion routine was yet unable to fit these well. This methodology requires an understanding of what tilt-angle anomalies look like and how they are generated by geological features at the frequencies used by the ZTEM system. Comfort with the historical interpretation of tilt-angle anomalies measured with VLF EM receivers such as an EM 16 is very useful. A review of the well-established literature describing VLF EM theory and interpretation is strongly recommended by anybody planning to invert ZTEM data (e.g., Wright, 1988; McNeil and Labson, 1992). The typical form of a tilt angle EM anomaly is shown in Figure 4, whilst data from a ZTEM survey prior to and after the removal of bad data is shown in Figure 5.

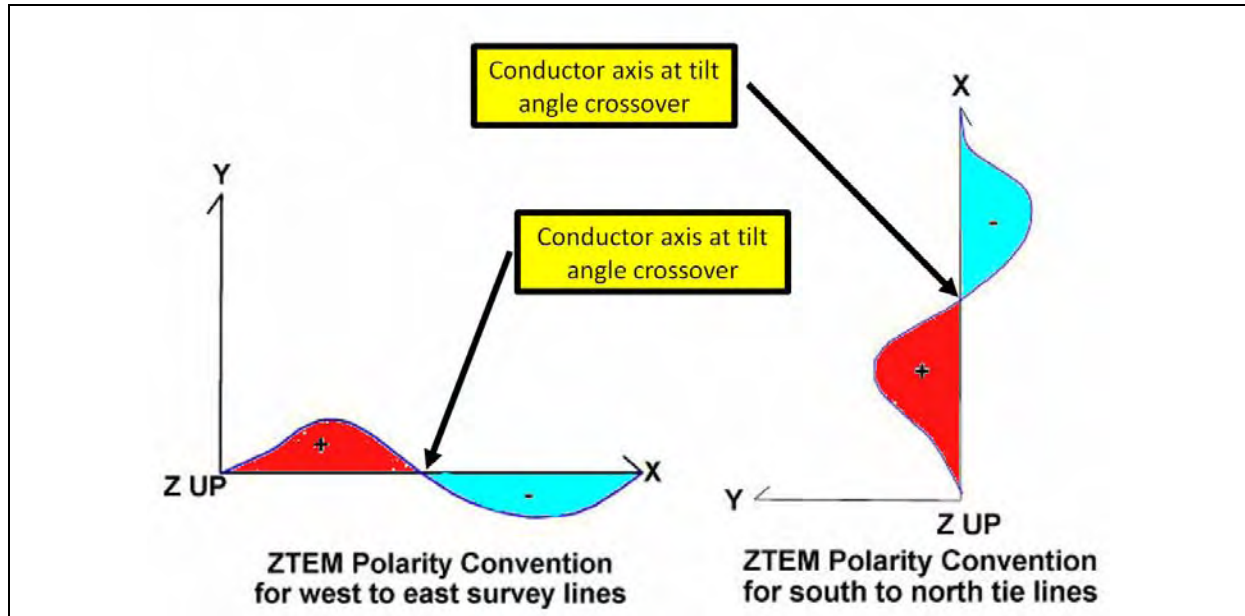


Figure 4. Tilt angle anomaly polarities for a north-south conductive anomaly axis on an east west traverse line, and an east-west anomaly axis on a north-south traverse line using the Geotech ZTEM polarity conventions. This is the typical sign convention used in VLF EM data but is not the EM sign convention used in the MT3Dinv program. ZTEM data needs to be transformed to the MT3Dinv EM sign and polarity conventions prior to use in an inversion.

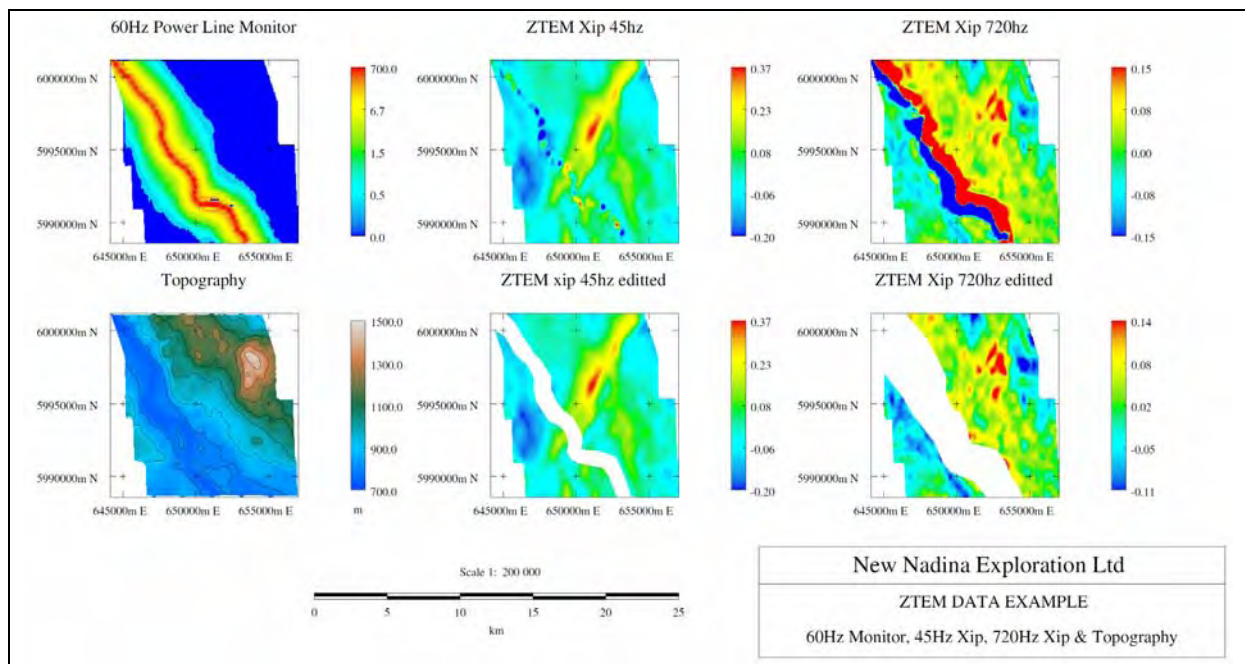


Figure 5. Sample plots illustrating the method used to identify and remove bad ZTEM data. The power line monitor map and project area topography are included for reference. Visual inspection of the gridded data field, in this case the X polarization 45 Hz in-phase and the X polarization 720 Hz in-phase data, shows regions of bad data coinciding with the region of increased power line noise response. The areas of noisy data were identified by inspection and then digitized and flagged as bad. Generally, noisy data are associated with elevated power line response, but it is difficult to remove the bad data using an algorithm. Note the region of bad data at 720 Hz (right side of figure) is considerably larger than the region of bad data removed from the 45 Hz data (centre). Deletion of bad data needs to be done separately for all four parameters of each frequency for best results.

The MT3Dinv program is well documented and a GUI is available to manage inversion runs (Farquharson et al., 2002; Farquharson et al., 2003). We use a Linux 12 core computer (dual Xeon 5660 2.8 GHz) with 48 MB RAM as a computational resource for running the inversions. Typically, a single run might take 3 to 5 days for a model with 6 frequencies and about 1.2 million cells.

Silver Queen project example

A ZTEM survey was flown over the Silver Queen project of New Nadina Exploration Limited. The project area has recorded production of copper, lead, zinc and gold from a past producing underground mine. Considerable drilling has been done around the old mine, including a number of deep holes. The property was recognized to have potential for buried porphyry style mineralization, but no porphyry style mineralization had been encountered in the exploration drill holes.

The magnetic data as well as the ZTEM data were inverted and visualized in 3D to identify the location of an intrusive stock below the Silver Queen mine, and to map large regional structures and the geological domains in the mine area (Figure 6 and Figure 7). Interpretation of these data identified a favourable structural setting for porphyry style mineralization and a Titan24 ground based IP and MT electrical survey was commissioned to find targets for drilling.

The criteria used to identify the favourable area for detailed ground based geophysics are shown in Table 1. These are not complex, but served to focus attention on the area subsequently covered with a ground-based Titan24 electrical survey. The Titan24 induced polarization and resistivity data were inverted and drill targets identified. Thirteen holes were drilled. The first drill hole encountered quartz vein stock-work alteration with copper and molybdenum mineralization (Figure 8). Hole 11-S_13 ended in good porphyry style molybdenum mineralization at 777 m. The ZTEM, Titan24 work and drilling were all done in one short northern Canadian field season.

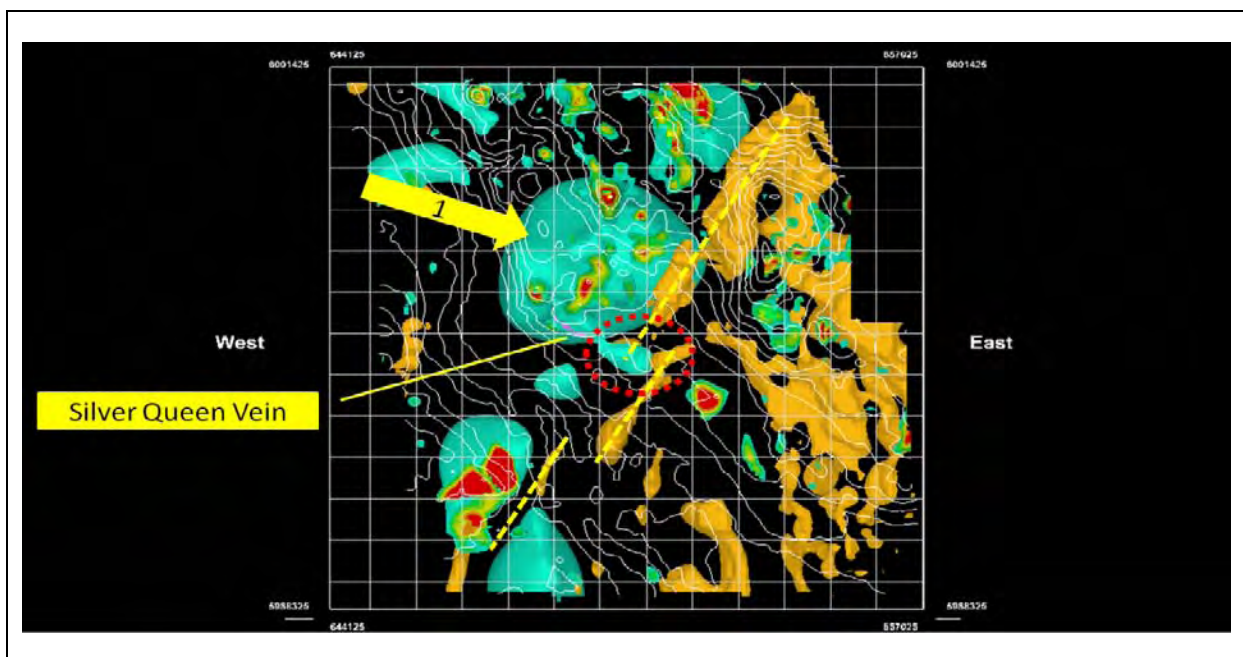


Figure 6. ZTEM inversion results. The 500 ohm-m isosurface (blue) and the 12.5 ohm-m isosurface (brown) from the ZTEM inversion are shown. The Silver Queen Vein system is shown as a small purple body striking NW. The large balloon shaped blue resistive isosurface (marked 1 by the yellow arrow) immediately below and to the north of the Silver Queen Vein system is interpreted to be an intrusive. A yellow dashed line delineates an interpreted NE-SW regional structure. This has been identified based upon the conductive linear feature shown by the brown coloured isosurface. The red ellipse identifies the favourable region close to the intrusive boundary where a zone of structural accommodation exists as movement transfers from the main structure going NE to a parallel arm of the NE-SW fault system that carries on to the SW. A small zone of increased conductivity that may be a breccia is seen below the blue linear resistive feature extending east south-east from the Silver Queen vein system and in the centre of the red ellipse.

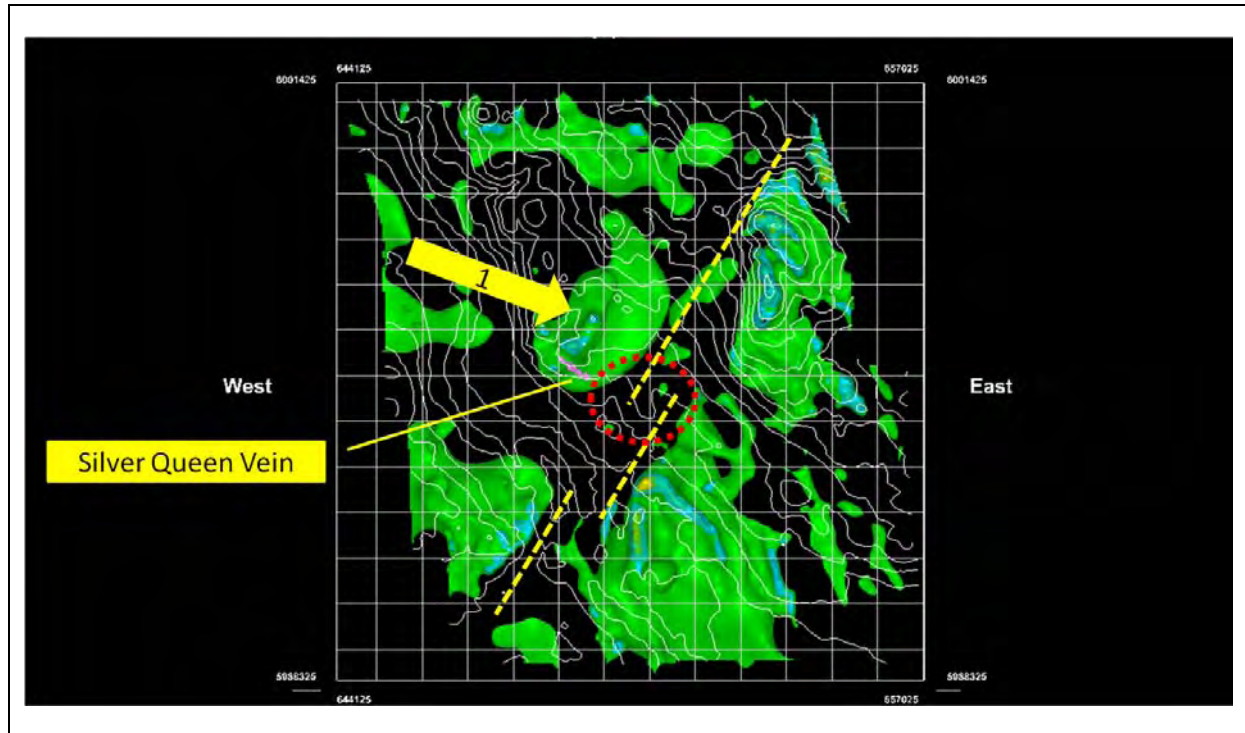


Figure 7. Susceptibility isosurfaces from the magnetic inversion model. The green isosurface is the 0.002 SI surface. This identifies a stock-like body interpreted as a magnetic phase of the intrusive below the Silver Queen vein system. This interpreted intrusive body is marked with the yellow arrow (1). The differing shapes of the inferred intrusives from the ZTEM inversion and the magnetic inversion suggest multiple phases, with magnetic and non-magnetic intrusive phases both being present. The NE-SW structural trend corresponds with a magnetic low. In the SE corner of the project area, magnetic and conductive units exist (green in Figure 7 and brown in Figure 6). This is a region of basalts. The different magnetic and electrical character of this region can be recognized in the ZTEM and magnetic inverted models.

Table 1. Criteria used to identify an area for detailed ground based follow-up using the ZTEM and Magnetic survey inversion results.

Criteria	Source of data
Close to known mineralization.	Old mine workings plotted in 3D, with a corroborating resistive feature seen near surface in the ZTEM inversion.
Close to or in the boundary of intrusive body.	Intrusive boundaries were interpreted using ZTEM inversion conductivity isosurfaces and MAG3DINV susceptibility isosurfaces.
In a regional structure at a thickening of the structure, a kink, or a dilational zone of accommodation transferring movement between parallel structures.	Linear zones of lowered conductivity in ZTEM inversion associated with linear features and magnetic lows in airborne magnetic data were interpreted as zones of brecciation mapping regional structures.
In a zone of increased brecciation.	Interpreted from local zones of increased conductivity indicated by ZTEM inversion.

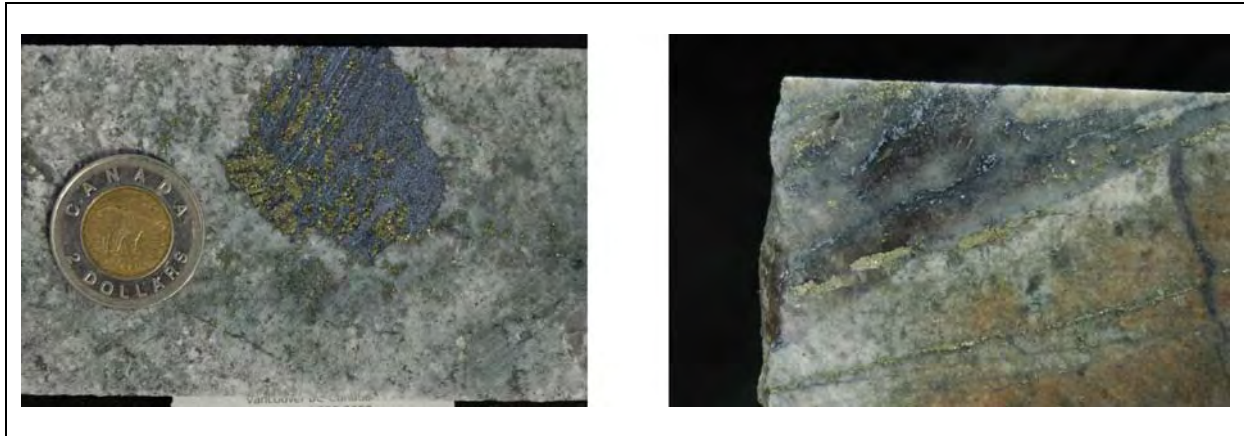


Figure 8. Core photographs showing molybdenum mineralization and stock-work veining. This mineralization evidenced itself as a zone of moderate to lower resistivity and high chargeability in the induced polarization and resistivity inversion results, respectively. The near-surface zone of increased resistivity seen in [Figure 6](#) as extending into the area of interest in the ZTEM inversion was identified in the 3D resistivity inversion as a near-surface resistive zone.

Conclusions

We have successfully inverted ZTEM data at the Silver Queen project of New Nadina Exploration Ltd. using the UBC-GIF MT3Dinv inversion code package. The inversion model result was interpreted to identify a favourable area for porphyry style mineralization. Ground follow-up work with a Titan24 electrical survey found targets subsequently validated by drilling. The work done has resulted in the discovery of a significant new porphyry molybdenum prospect. The combination of ZTEM and magnetic data, inverted for 3D conductivity and a magnetic susceptibility models, respectively, and then combined with a 3D geological model provided guidance to locate a detailed deep penetrating Titan24 electrical survey on the ground. Follow-up drilling of the induced polarization anomalies identified from the Titan24 survey data intersected a significant and previously unknown mineralized zone. Using the ZTEM data in this process was cost effective as it directed the follow up ground exploration to a smaller area of increased prospectivity and shortened the time necessary to explore the project area.

Acknowledgments

We gratefully acknowledge permission from New Nadina Exploration Ltd., and in particular Ms. Ellen Clements, President, to show these results from the ongoing exploration program at the Silver Queen project.

References

- Farquharson, C. G., Oldenburg, D. W., and Haber, E., 2002, An algorithm for the three-dimensional inversion of magnetotelluric data: SEG Expanded Abstracts, 21, 649-652.
- Farquharson, C., Haber, E., Shekhtman, R., and Oldenburg, D., 2003, Theoretical Background for the Magnetotelluric Inversion Program MT3Dinv: Unpublished Technical Report, University of British Columbia – Geophysical Inversion Facility.
- Legault, J. M., Kumar, H., Milicevic, B., and Hulbert, L., 2009, ZTEM airborne tipper AFMAG test survey over a magmatic copper-nickel target at Axis Lake in northern Saskatchewan: SEG Expanded Abstracts, 28, 1272-1276.

McNeill, J. D., and Labson, V. F., 1992, Geological mapping using VLF radio fields: In *Electromagnetic Methods in Applied Geophysics* (ed. Misac Nabighian), Vol.2, Society of Exploration Geophysicists, Tulsa, OK, 521-640.

Vozoff, K., 1972, The magnetotelluric method in the exploration of sedimentary basins: *Geophysics* 37, 98-141.

Wright, J. L., 1988, VLF interpretation manual: EDA Instruments (now Scintrex), Toronto.

ZTEM airborne tipper AFMAG test survey over a magmatic copper-nickel target at Axis Lake in northern Saskatchewan

Jean M. Legault*, Harish Kumar and Biljana Milicevic, Geotech Ltd., Larry Hulbert, Pure Nickel Inc.

Summary

An airborne AFMAG demonstration test survey was conducted using the ZTEM tipper electromagnetic prospecting system over a known magmatic copper-nickel occurrence in northern Saskatchewan, Canada. These tests were conducted in early 2008 and were flown to test the system's capability to detect the conductive but relatively weakly mineralized sulphide deposits and to define potential extensions at depth. The AFMAG method utilizes naturally occurring audio telluric fields from worldwide sferic activity as its primary field source and is capable of large penetration depths – in the order of hundreds of metres to km. The AFMAG field tests corroborate previously airborne transient electromagnetic, magnetic and ground follow-up EM surveys. 2D forward modelling results agree with the >300m vertical depth extent as defined in subsequent diamond drill testing.

Introduction

Airborne tipper AFMAG (audio frequency electromagnetics) surveys were conducted over the Axis Lake property that is situated in the Fond du Lac region of northern Saskatchewan (Figure 1) in May, 2008 (Milicevic et al., 2009). The survey consisted of Tipper AFMAG measurements using the ZTEM system (Lo and Zang, 2008), shown in Figure 2, as well as aeromagnetics using a caesium magnetometer. The survey was comprised of thirty four (34) approximately 10.5 km long, North-South oriented flight lines, totalling 358.7 line-km, that were obtained at nominal 250m line spacing over an approximately 8 x 10km area (Figure 3). The property hosts known copper-nickel sulphide showings (Axis Lake East & West, Rae Lake and Currie Lake), has been previously surveyed using the VTEM (Witherly et al., 2004) helicopter EM system, with ground follow-up using UTEM (West et al., 1984) surveys, and has subsequently been drilled (Vivian and Lo, 2007). The property was chosen to test the ZTEM capability to identify and define potential along strike and deep extensions of the known Cu-Ni mineralization to below 500m.

The measurements of the vertical (Z) tipper data were obtained using an air coil system (Figure 2), suspended at approximately 100m elevation above ground level. The vertical component data (Hz) were then ratioed to fixed horizontal field measurements (Hx-Hy) obtained using identical reference coils, that were oriented in the in-line (X) and cross-line (Y) directions, in order to obtain the tipper functions Z/X and Z/Y. The In-Phase and Quadrature components tipper ratio data were then extracted from the time-series, using Fourier-based, digital signal processing analyses, at 5 frequencies, between 30Hz and 360Hz.

AXIS LAKE PROPERTY LOCATION

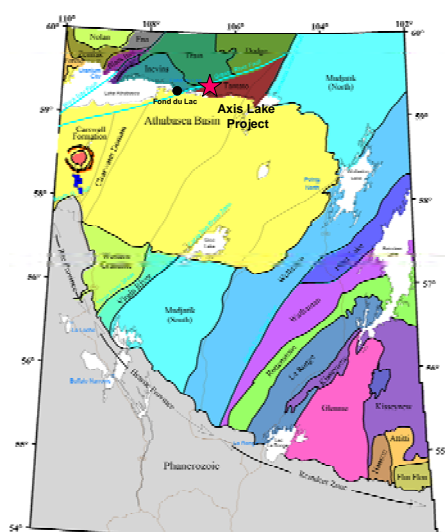


Figure 1: Axis Lake property location and regional geology in northern Saskatchewan, Canada.

General Theory

The ZTEM system uses naturally occurring AFMAG magnetotelluric fields as the source of the primary fields, and therefore requires no transmitter (Ward, 1959). The fields resemble those from VLF except that they are lower frequency (tens & hundreds of Hz versus tens of kHz) and are not strongly directionally polarized (Labson et al., 1985). These AFMAG EM fields, derived from world wide atmospheric thunderstorm activity, have the unique characteristic of being uniform, planar and horizontal, and also propagate vertically into the earth – to great depth, up to several km, as determined by the magnetotelluric (MT) skin depth (Vozoff, 1972), which is directly proportional to the ratio of the bedrock resistivity to the frequency. At the frequencies used for ZTEM, the MT skin depths likely range between approx. 600m to 2km in this region, according to the following equation for the Bostick skin depth (Murakami, 1985):

$$\delta_s = 356 * \sqrt{(\rho_A / f)} \text{ metres}$$

The other unique aspect of AFMAG fields is that they react to relative contrasts in the resistivity, and therefore do not depend on the absolute conductance, as measured using inductive EM systems, such as VTEM – hence poorly conductive targets, such as alteration zones and fault zones, can be mapped, as well as higher conductance features, like graphitic units. Conversely, resistive targets can also be

ZTEM airborne tipper AFMAG results over a copper-nickel target in northern Saskatchewan

mapped using AFMAG— provided they are of a sufficient size and contrast to produce a vertical field anomaly. Indeed resistors produce reversed anomalies relative to conductive features. Still, copper-nickel mineralization is consistent with moderate to strongly conductive bodies.



Figure 2: ZTEM AFMAG Hz Receiver Coil (foreground) and Hx-Hy Reference Coils (background)

Geological setting

The Axis Lake property is located in the Tantato domain, Fond du Lac area, north-northeast of Lake Athabasca. The Tantato domain is defined as a triangular area underlain by granulite to upper amphibolite facies metamorphosed sediments, volcanics, and granitoids (Figure 3). Mineralization on the Axis Lake property is associated with magmatic nickel-copper sulphides. Mineralization has been transported along a prominent fault conduit formed in an extensional rift environment. Norite magmas containing sulphide droplets settle out of the magma in areas where differentiation of the magma occurs. (Vivian and Lo, 2007).

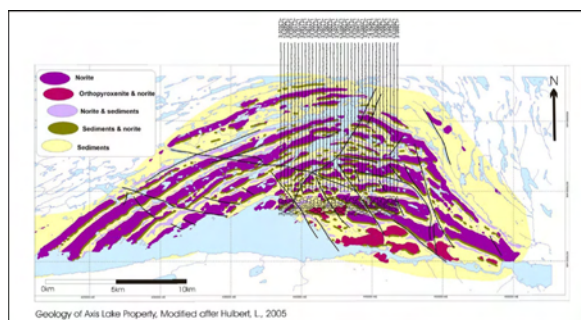


Figure 3: Axis Lake general geology and AFMAG flight lines (after Vivian and Lo, 2007).

The rocks at Axis Lake consist mainly of diatexite, which is a highly metamorphosed sediment, and mafic noritic granulites, which are metamorphic plutonic rocks. Geologic mapping has been assisted with the aid of the property-

wide Total Field Magnetic survey and further delineated the diatexite and mafic granulite units as shown in Figure 3. Diatexite sediments occupy areas of low magnetic response while the metanorite is coincident with the high magnetic signatures.



Figure 4: Slide showing texture of sulphides in Axis Lake diamond drill core (after Vivian and Lo, 2007).

Pyrrhotite dominates the sulphide mineralogy at the Axis, Rae and Currie Lake Zones (Figure 4). There are three styles of mineralization: 1) fine to coarsely disseminated, from 1-5% and up to 10% sulphides; 2) network to net-textured mineralization of up to 15% sulphide, trending to 30%; and 3) massive sulphide horizons comprising up to 50% mineralization but occurring only locally in zones less than 0.5 m thick. Sulphide mineralogy is dominated by pyrrhotite (up to 90%) with accessory compositions of chalcopyrite (up to 5%) and pyrite (usually less than 5%). The nickel-bearing sulphide is pentlandite and it is also common to see the nickel to copper ratios approximately 2:1 to 3:1 (Vivian and Lo, 2007).

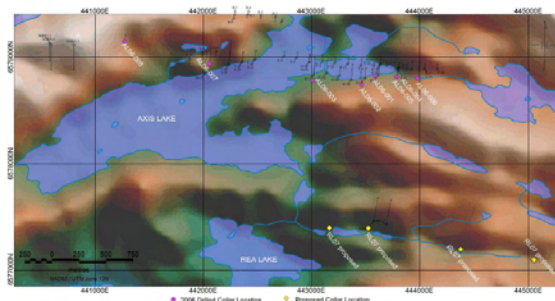


Figure 5: Existing Diamond Drill-holes, 2006 Holes and Proposed drill-holes over DEM model (Vivian and Lo, 2007)

ZTEM airborne tipper AFMAG results over a copper-nickel target in northern Saskatchewan

Seven diamond drill holes, totaling 2260 metres were completed in Spring 2006 that were located based on the 2005 VTEM and 2006 UTEM results and to infill Cu-Ni mineralization intersected previously (Figure 5). All holes intersected Cu-Ni sulphides. The results showed that the sulphide mineralization in the East and West zones ranges from fine to coarsely disseminated, to semi-massive network textures to massive, with nickel and copper values in the range of 1-2% and 0.4-0.6% respectively. Rae Lake remains untested (Vivian and Lo, 2007).

Previous geophysical survey results

VTEM and aeromagnetic surveys were undertaken in March, 2005 at 150-250m line-spacings and totaling 1503 line-km (Orta et al., 2005). Over 40 conductive responses were identified in the VTEM data and the results show that the Axis Lake zone EM response is quite varied and less extensive than the known mineralization (Figure 6). The East Zone dips south and reveals better amplitudes due to better connectivity than the West Zone. The Rae Lake zone also dips south, is more continuous but is slightly less conductive than Axis Lake. The Currie Lake zone dips north but is indicated to be of limited size. Additional areas for ground follow-up were also defined elsewhere on the property (Vivian and Lo, 2007).

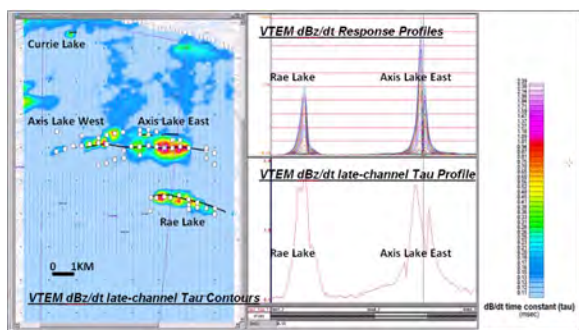


Figure 6: VTEM EM Time-Constant, UTEM anomalies and Known Mineralized Zones at Axis Lake.

The UTEM survey outlined numerous conductive responses on the Axis Lake property, including 4 significant areas at Axis Lake East & West, Rae Lake and Currie Lake. In particular, modeling suggests that mineralization at Axis and Rae Lakes extends to 400+ metres. South dips are indicated at Axis and Rae Lakes, and steep dips at Currie Lake. The 5-10 siemens conductivities obtained suggest that the Cu-Ni sulphide mineralization is weak, likely semi-massive, particularly at Currie Lake (Vivian and Lo, 2007).

AFMAG survey results

There are distinctive differences observed between the Z/X (In-Line) component profile results (Figure 7A), which are most sensitive to structures orientated perpendicular to the In-Line direction - notably the 2 prominent, thin EW lineaments that are centered directly over the known Axis

Lake East & West and Rae Lake mineralized zones; as well as 2 major EW conductive zones located south and north of Currie Lake – the latter of which appears correspond to the Tantato Domain contact, and might represent a major regional fault structure. A other unexplained EW conductive lineament represents a New Target, that is along strike with a VTEM anomaly defined southwest of Currie Lake. This image contrasts the Z/Y (Cross-line) component profiles (Figure 7B), which are sensitive to structures oriented oblique/parallel to the In-Line flight direction. Indeed the Z/Y images are less well defined except for a SW-NE lineament extending across Axis Lake zone, potentially relating to a fault structure; and the Tantato Domain boundary to the north which is equally as prominent as in the Z/X results, presumably because it is NE-SW oriented.

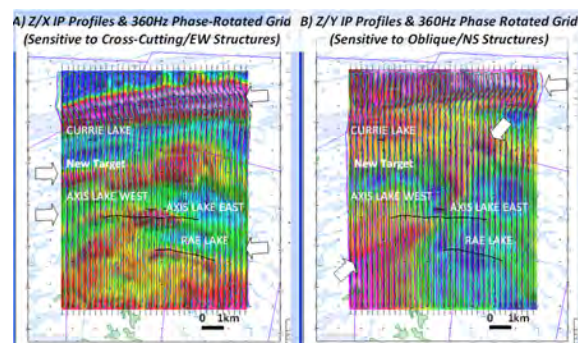


Figure 7: Axis Lake ZTEM Test Block: In-Phase Z/X Component Profiles over 360Hz Phase-Rotated (PR) Grid (left) versus Corresponding In-Phase Z/Y Profiles & 360Hz PR Grid (right).

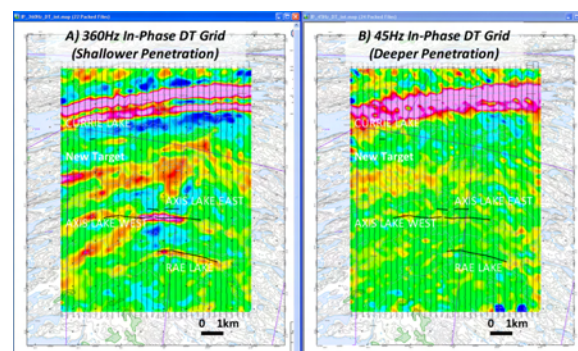


Figure 8: Axis Lake Block: 360Hz In-Phase Total Divergence (DT) Grid (left) versus Corresponding 45Hz In-Phase DT Grid (right) and Mineralized Zones.

When the 2 Tippers are combined, using the DT (Kuzmin et al., 2005) grid method (Figure 8) that is analogous to the VLF Peaker (Pedersen, 1998), the imaging of geoelectric structures becomes omni-directional, with all structures being highlighted. The DT (total divergence) images at 360Hz and 90Hz shown below each also demonstrate the notable differences in the frequency-dependence of the responses, that imply resolved differences in the vertical

ZTEM airborne tipper AFMAG results over a copper-nickel target in northern Saskatchewan

depth of the defined structures – including: a) the main Axis Lake and the Rae Lake Zone responses, that rapidly weaken from high to low frequency, and b) similarly for the New Target and the Currie Lake zone, barely visible. This suggests that they relate more to the near-surface geology and may not extend to significant depths. These behaviours contrast the main Tantato Domain contact zone response, furthest north, which is equally strong from 45 Hz to 360Hz in both the Resulting PR and DT images. This suggests that it represents a major crustal fault feature, with great depth extent.

Two-dimensional MT Tipper forward modeling

2D synthetic data were obtained that simulate and compare the expected Tipper responses for the Axis Lake geologic model using the PW2d 2D forward MT modeling code of Wannamaker et al. (1987).

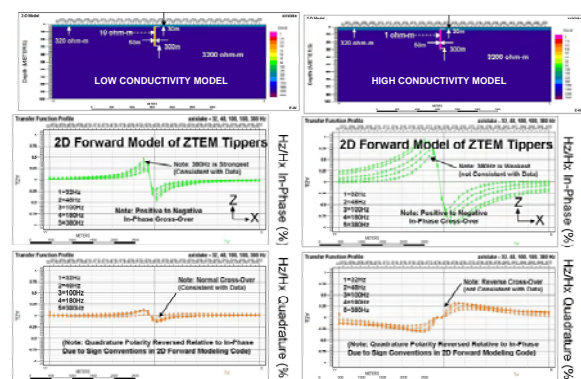


Figure 9: Axis Lake 2D Resistivity Models and 2D Forward Model Z/X profiles for low conductivity model (left) and high conductivity model (right), extending to 300m depths

Figure 9 presents the 2D synthetic forward model responses of the In-line (Z/X) In-Phase and Quadrature for 2 similar geologic models, whose only dissimilarity is the target conductivity, which is 10x less for the low conductivity model (10 ohm-m=5 siemens), shown on the left, versus the high conductivity model (1 ohm-m = 50 siemens), shown on the right. The notable similarities that the low conductivity model have with the measured data are: a) In-Phase (IP) responses that diminish in amplitude at lower frequencies, and b) Quadrature phase (QP) responses that follow the same polarity as the In-phase (note the reversed sign for QP relative to our measured results is due to polarity convention in MT 2d code utilized), and c) model amplitudes for the IP and QP for the low conductivity model closely match the observed data (i.e., +/- 40% IP and +/- 10% QP – Figure 10) and are significantly weaker than for the high conductivity model. Hence the 2D forward modeling results suggest that the Axis Lake mineralized zones are only moderately conductive (~5 siemens) and may not extend to significant depth (~300-500m) – both of which agree with the VTEM and UTEM survey results and the known geology.

Conclusion

The ZTEM results appear to correlate very well with the known geology, in particular the presence of a Cu-Ni mineralized conductive horizons, at Axis Lake and Rae Lake, which are known to occur at surface and are followed along several kilometers along strike. In particular, the ZTEM results provide indications of the longer strike continuity of the known mineralized horizons, as compared to the VTEM results, that likely relate to more weakly mineralized, lower conductivity extensions of the zones (Figure 10). This also agrees with the ground UTEM anomaly trends that extend beyond the known mineralized zones. In fact, an unexplained ZTEM anomaly northwest of the known Cu-Ni showings and south of Currie Lake correlate well with the east-extension of VTEM conductor and therefore represents a new target for follow-up (Figure 10). Other ZTEM lineaments also correlate well with similar areomagnetic trends and structures, which highlight its ability to provide complementary information. In addition to mapping lithology and structure, the ZTEM results appear to corroborate both the moderate conductance (~5 siemens) and the relatively limited vertical depth-extent (~300-500m) of the defined mineralized zones and therefore agree with the previous geophysical and drill-tested geologic findings. These results over a Cu-Ni target add to the variety of successful applications of the ZTEM technique, notably for sedimentary-exhalative and porphyry copper type deposits (Lo and Zang, 2005), as well as unconformity uranium targets (Lo et al., 2009).

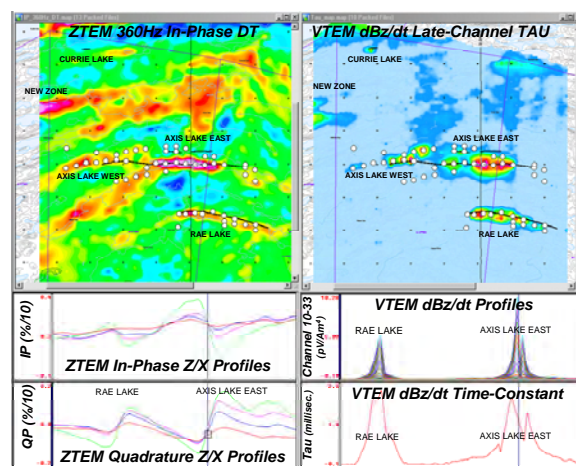


Figure 10: Axis Lake ZTEM 360Hz In-Phase Total Divergence (left), VTEM Late-Channel Tau (right) Results, and related Profile Data, along with Known Mineralized Zones and Ground UTEM Anomalies (circles)

Acknowledgements

The authors would like to thank Geotech Ltd., as well as Pure Nickel Mines Inc. for graciously allowing us to present these data and for providing the geologic and historical geophysical data.

EDITED REFERENCES

Note: This reference list is a copy-edited version of the reference list submitted by the author. Reference lists for the 2009 SEG Technical Program Expanded Abstracts have been copy edited so that references provided with the online metadata for each paper will achieve a high degree of linking to cited sources that appear on the Web.

REFERENCES

- Kuzmin, P., B. Lo, and E. Morrison, 2005, Final report on modeling, interpretation methods and field trials of an existing prototype AFMAG system: Miscellaneous Data Release, 167, Ontario Geological Survey.
- Labson, V. F., A. Becker, H. F. Morrison, and U. Conti, 1985, Geophysical exploration with audio-frequency natural magnetic fields: *Geophysics*, **50**, 656–664.
- Lo, B., J. M. Legault, P. Kuzmin, and M. Combrinck, 2009, Z-TEM (Airborne AFMAG) tests over unconformity uranium deposits: 20th ASEG International Geophysical Conference and Exhibition, Australian Society of Exploration Geophysicists, Extended Abstracts.
- Lo, B., and M. Zang, 2008, Numerical modeling of Z-TEM (airborne AFMAG) responses to guide exploration strategies: 78th Annual International Meeting, SEG, Expanded Abstracts, 1098–1101.
- Milicevic, B., E. Steffler, and J. M. Legault, 2009, Report on helicopter-borne Z-axis tipper electromagnetic (ZTEM) and aeromagnetic geophysical survey, Axis Lake test block, northern Saskatchewan: Pure Nickel Inc., internal report by Geotech Ltd.
- Murakami, Y., 1985, Two representations of the magnetotelluric sounding survey: *Geophysics*, **50**, 161–164.
- Orta, M., J. Zhu, and R. Barlow, 2005, Report on helicopter-borne time-domain electromagnetic geophysical survey, Stony Rapids project, northern Saskatchewan: Hull Consulting Services Ltd., internal report by Geotech Ltd.
- Pedersen, L. B., 1998, Tensor VLF measurements: Our first experiences: *Exploration Geophysics*, **29**, 52–57.
- Vivian, G., and B. Lo, 2007, Technical report—Organic soil sampling, airborne and ground geophysics and diamond drilling, Fond du Lac property, northern Saskatchewan: Pure Nickel Inc., 43-101 report.
- Vozoff, K., 1972, The magnetotelluric method in the exploration of sedimentary basins: *Geophysics*, **37**, 98–141.
- Wannamaker, P. E., J. A. Stodt, and L. Rijo, 1987, A stable finite element solution for two-dimensional magnetotelluric modeling: *Geophysical Journal of the Royal Astronomical Society*, **88**, 277–296.
- Ward, S. H., 1959, AFMAG —Airborne and ground: *Geophysics*, **24**, 761–787.
- West, G. F., J. C. Macnae, and Y. Lamontagne, 1984, A time-domain EM system measuring the step response of the ground: *Geophysics*, **49**, 1010–1026.
- Witherly, K., R. Irvine, and E. B. Morrison, 2004, The Geotech VTEM time domain EM system: 74th Annual International Meeting, SEG, Expanded Abstracts, 1217–1221.

ZTEM tipper AFMAG and 2D inversion results over an unconformity uranium target in northern Saskatchewan

Jean M. Legault*, Harish Kumar and Biljana Milicevic, Geotech Ltd., Philip Wannamaker, consultant.

Summary

An airborne AFMAG demonstration test survey was conducted using the ZTEM tipper electromagnetic prospecting system over an unconformity uranium occurrence in northern Saskatchewan, Canada. These tests were conducted in early 2008 and were flown to test the system's capability to penetrate and define the basement geology below a thick sequence of Athabasca sandstones, as well as defining resistivity structure relating to possible fault-controlled alteration zones. The AFMAG method utilizes naturally occurring audio telluric fields from worldwide sferic activity as its primary field source and is capable of large penetration depths – in the order of hundreds of metres to km. The AFMAG field tests corroborate previously airborne transient electromagnetic, magnetic and ground follow-up EM surveys. A 2D inversion algorithm has been modified to account for the air layer required for the ZTEM tipper data. The results agree with the known geology to below >500m.

Introduction

As part of a larger series of demonstration tests for the ZTEM (Z-Axis Tipper Electromagnetic) airborne AFMAG system (Lo and Zang, 2008; Lo et al., 2009), a survey was conducted over a test block situated in the North Athabasca Basin of northern Saskatchewan (Figure 1) in May, 2008. The test area was chosen because it hosts known uranium occurrences and hosts significant thicknesses of Athabasca sandstone (500-750+ metres) cover above a known basement graphitic conductor. It had been partially flown using VTEM (Witherly et al., 2004) and, due to the significant depth of cover, had proven challenging for ground and airborne geophysical methods (Lo et al., 2009). The current study presents the results of the survey and the 2-dimensional inversion solution for the quantitative interpretation of ZTEM airborne results.

General Theory

The ZTEM airborne AFMAG system measures the anomalous vertical secondary magnetic fields that are created by the interaction between naturally occurring, plane wave audio frequency EM fields and electrical heterogeneities in the earth. The vertical magnetic field is linearly related to the horizontal fields according to the following (Vozoff, 1972):

$$H_z = T_x H_x + T_y H_y$$

where the magnetic field vector $T = (T_x, T_y)$, known as the tipper, is complex and a function of frequency, but has rotationally invariant properties, such as its magnitude and direction, that are independent of the subsurface, the meas-

urement direction and the field polarization (Labson et al., 1985).

ATHABASCA BASIN, NORTHERN SASKATCHEWAN

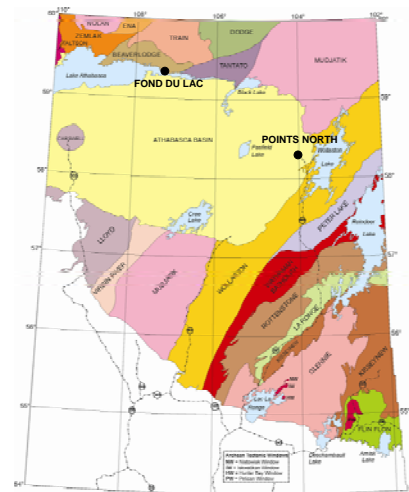


Figure 1: Athabasca Basin and regional geology in northern Saskatchewan, Canada (courtesy of Ministry of Energy and Resources, Saskatchewan).

AFMAG uses naturally occurring audio frequency magnetic fields as the source of the primary field signal, and therefore requires no transmitter (Ward, 1959). The primary fields resemble those from VLF except that they are lower frequency (tens & hundreds of Hz versus tens of kHz) and are not strongly directionally polarized (Labson et al., 1985). These EM fields used in AFMAG are derived from world wide atmospheric thunderstorm activity, have the unique characteristic of being uniform, planar and horizontal, and also propagate vertically into the earth – to great depth, up to several km, as determined by the magnetotelluric (MT) skin depth (Vozoff, 1972), which is directly proportional to the ratio of the bedrock resistivity to the frequency.

At the frequencies used for ZTEM, the investigation depths likely range between approx. 600m to 2km in this region (approx. 1k ohm-m avg. resistivity assumed), according to the following equation for the Bostick skin depth (Murakami, 1985):

$$\delta_s = 356 * \sqrt{(\rho / f)} \text{ metres}$$

The other unique aspect of AFMAG fields is that they react to relative contrasts in the resistivity, and therefore do not depend on the absolute conductance, as measured using inductive EM systems, such as VTEM – hence poorly, conductive targets, such as alteration zones and fault zones

ZTEM tipper AFMAG and 2D inversion results over an unconformity uranium target in northern Saskatchewan

can be mapped, as well as higher conductance features, like graphitic units. Conversely, resistive targets can also be detected using AFMAG— provided they are of a sufficient size and contrast to produce a vertical field anomaly. Indeed resistors produce reversed anomalies relative to conductive features. Hence AFMAG can be effective as an all-round resistivity mapping tool, making it unique among airborne EM methods.

The tipper from a single site contains information on the dimensionality of the subsurface (Pedersen, 1998), for example, in a horizontally stratified or 1D earth, $T=0$ and as such H_z is absent. For a 2D earth with the y-axis along strike, $T_y=0$ and $H_z = T_x \cdot H_x$. In 3D earths, both T_x and T_y will be non-zero. H_z is therefore only present, as a secondary field, due to a lateral resistivity contrast, whereas the horizontal H_x and H_y fields are a mixture of secondary and primary fields (Stodt et al., 1981). But, as an approximation, as in the telluric-magnetotelluric method (T-MT; Hermance and Thayer, 1975) used by distributed MT acquisition systems (Legault et al., 2008), the horizontal fields are assumed to be practically uniform, which is particularly useful for rapid reconnaissance mapping purposes. By measuring the vertical magnetic field H_x , using a mobile receiver (Figure 2), and the orthogonal horizontal H_x and H_y fields at a fixed base station reference site, ZTEM is a direct adaptation of this technique for airborne AFMAG surveying.

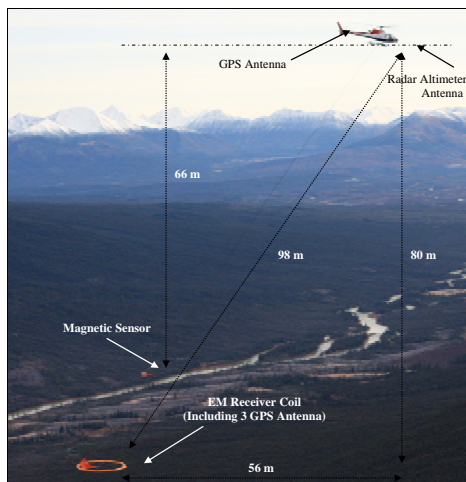


Figure 2: The ZTEM helicopter receiver system

Geophysical background and General Geology

Uranium deposits within the Athabasca Basin are associated with the unconformity between the flat-lying Proterozoic Athabasca Group sandstones and the underlying Archean-Paleoproterozoic metamorphic and igneous basement rocks. They occur along basement faults and fracture zones above graphitic pelites. Since the uranium deposits themselves are relatively small and without significant physical property contrasts, except their density and radio-

activity, geophysical exploration for unconformity type uranium targets below the sandstone focuses on the search for the conductive graphitic basement fault structures, using EM and magnetic methods (Mathews et al., 1997). More recently the focus has also been on the larger alteration halos of clay or silica enrichment around the deposits that produce either weak resistivity low or high signatures above the deposits (Powell et al., 2007) – making them difficult targets for inductive airborne EM (Lo et al., 2009).

The test area lies along the northern rim of the Athabasca Basin and entirely underlain by Manitou Falls sandstones with more conductive Wolverine Point mudstones outcropping further the south. Within the survey area, the Athabasca sandstone thickens from approx. 550m to the north and dips to >700m depths towards the center of the survey area. At depth, below the Manitou Falls sandstones, the Archean basement geology hosts at least one major SW-NE graphitic EM conductor that is structurally controlled. This graphitic fault zone, that is a focus for uranium exploration, extends from the north into the center of the survey block, but eventually becomes too deep for ground or airborne EM detection but whose presence is inferred from regional magnetics.

The ZTEM survey objectives were to penetrate the thick sandstone cover to help define the deep basement geology, using the graphitic markers, as well as detecting possible alteration zones in the overlying sandstone.

AFMAG survey results

The ZTEM survey comprises airborne tipper AFMAG as well as aeromagnetics using a caesium magnetometer (Figure 2). The vertical (Z) component data were obtained using the Geotech ZTEM aircoil receiver system (Figure 2), suspended at approximately 85m elevation above ground level. The vertical component data (H_z) were then ratioed to fixed horizontal field measurements (H_x - H_y) obtained using identical reference coils, that were oriented in the in-line (X) and cross-line (Y) directions, in order to obtain the scalar tipper functions Z/X and Z/Y . The In-Phase and Quadrature components ZTEM field ratio data were obtained, using Fourier-based, digital signal processing analyses, at 5 frequencies, between 30Hz and 360Hz. The magnetometer was towed at approximately 100m above ground level (Figure 2).

The survey consisted of fifty-four (54) 11.5km long, NW-SE oriented flight lines, totalling 620 line-km, that were obtained at nominal 400m line spacings over an approximately 30 x 60km area. The North Athabasca test area ZTEM results, in particular, display a relatively high data quality, in terms of low signal/noise and well defined anomaly resolution. Particularly given the fact that a) the data were obtained in early May, and therefore not at the peak season of sferic activity – hence at best moderate natural field levels expected; b) the data were obtained using aircraft flying at ~80km/hr, approximately 80m

ZTEM tipper AFMAG and 2D inversion results over an unconformity uranium target in northern Saskatchewan

above ground level – hence without significant stacking or additional processing applied, and c) the strength of response obtained from geologic targets at >500-700+ metre depths, below the sandstone cover.

The 90 Hz In-Phase Tipper (Z/X = In-line – Z/Y = Cross-line) profile data with corresponding 90-degree phase-rotated (PR) grids are presented in Figures 3. The phase rotations, designed to convert the typical cross-overs over tabular conductors to peak responses, are obtained using a simple magnetic pole-reduction grid manipulation (Lo and Zang, 2008). The 2ND vertical derivative of the airborne total magnetic intensity results are also compared to the ZTEM DT (total divergence) grid results in Figure 4. The DT (Kuzmin et al., 2005), that is analogous to Peaker parameter of Pedersen (1998), sums the horizontal derivatives of Z/X and Z/Y to obtain peak responses over conductors (and resistors) and is rotationally invariant.

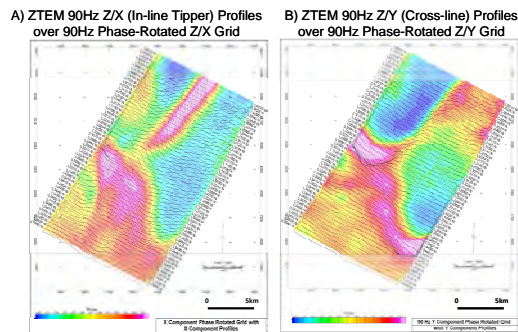


Figure 3: North Athabasca ZTEM test block: 90Hz In-Phase Z/X (in-line tipper) component profiles and phase-rotated (PR) grid contour (left) versus corresponding In-Phase Z/Y (cross-line) profiles PR grid (right).

There are distinctive differences observed between the Z/X (In-Line) component profile results (Figure 3a), which are most sensitive to structures orientated perpendicular to the In-Line direction, versus the Z/Y (Cross-line) component profiles (Figure 3b), which are sensitive to structures oriented oblique/parallel to the In-Line flight direction. When the 2 Tippers are combined, using either the PR or DT grid methods, as shown, the imaging of geoelectric structures becomes omni-directional, with all orientations being highlighted.

In this North Athabasca test area, the DT results (Figure 4a) highlight a well-defined conductor associated with the known main NE-SW orientated graphitic fault zone, extending from the north whose depth increases from 500 to >750m depths; whereas they also define other oblique-to-flight-line NW-SE oriented features – notably: a) the inference of a synformal fold structure in the central survey area, and b) a possibly NNW-SSE oblique shear zone-hosted, alteration zone, in the south-central survey area, where the numerous radioactive indicators are found and the geology is inferred to exceed 700-900m. These features are not as well defined in the magnetic results (Figure 4b).

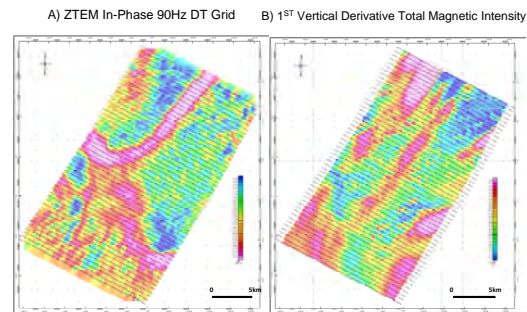


Figure 4: North Athabasca ZTEM test block: 90Hz In-Phase total divergence (DT) Grid (left) versus 1ST vertical derivative of total magnetic intensity (right).

2-dimensional forward and inverse problem

The performance of a two-dimensional (2-D) inversion of ZTEM data profiles using a prototype algorithm developed from MT was tested using a synthetic structure and example data profiles from the ZTEM system. The ZVERT2D algorithm makes use of the finite element forward problem and inversion parameter sensitivities using reciprocity of Wannamaker et al. (1987) and de Lugao and Wannamaker (1996), together with the regularized Gauss-Newton non-linear parameter step estimate described by Tarantola (1987). The regularization is simple damping of the spatial slope of the model variation across the section. All models were run on a desktop Pentium with 3 GHz processor, most required ~5500 parameters to define the 2-D section, and took ~20 minutes to execute. Airborne receiver positions were simulated by imposing an ‘overburden’ layer with air properties (10^{18} ohm-m) of equal thickness to flight height and constraining the inversion mesh to lie below this layer.

To gauge the utility of inversion of ZTEM data, the response of a known structure is computed and an image formed by Zvert2d. The body is a 5 ohm-m brick 360 m deep in a 1000 ohm-m half-space host (Figure 5a). The brick is 600 m wide and 420 m thick. MT tipper responses (Figure 5c) were calculated at the 5 frequencies of the ZTEM system for 91 sites at 100 m intervals centred over the body and assigned uncertainty intervals of 0.02 (2%) (dimensionless). Because this is a prototype examination, the algorithm was not modified to consider fixed ground coil locations, but rather used H-fields local to the H_z receiver as in traditional MT. This is not considered a major variation for the purposes of this study. The 2d inversion considers that the host resistivity is known (1000 ohm-m). Nevertheless, the formed inversion images overall are quite promising. In Figure 5b, we see that the inversion image is accurately located when the profile is positioned 300 m above the surface. The image is of somewhat lower contrast and more spread out as expected, but is still well centered.

The In-line (Z/X) data for a line profile, taken from the north end of North Athabasca Lake test block, were used to create the 2D inversion image presented in Figure 6a. The

ZTEM tipper AFMAG and 2D inversion results over an unconformity uranium target in northern Saskatchewan

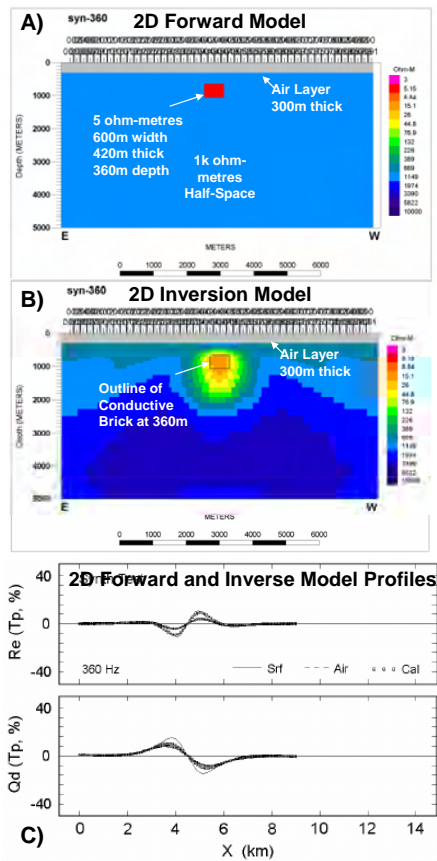


Figure 5: a) Calculated 2D forward and b) inverse model responses for In-Line (Z/X) IP and QP components over buried conductor in resistive half space. The gray region is a 300 m thick air layer. c) Synthetic data and inversion model responses at 360Hz for Z/X response profile at surface (solid curves) and 300 m in the air (dashed curves). Small open squares are the inversion fits.

input data utilized both the In-Phase and Quadrature Phase data from all five measured frequencies. Due to the impractical nature of the >1000 data points from the ZTEM profile, these were under sampled to 90 points in order to perform the calculation and proved effective. An error of 2% was assigned to the data for inversion. A host of 1000 ohm-metres was assumed for the model. Despite non-ideality of the data error, a value of nRMS of close to unity (1.0) was achieved in 4-6 iterations with starting nRMS values of 5-6.

Figure 6 presents the 2D resistivity cross-section obtained from the Zvert2d inversion and the corresponding In-Phase and Quadrature profiles showing the measured vs. 2D forward model data fits at 360Hz. As shown, although the anomaly appears at first like a simple but strong cross-over response, the inversion image is surprisingly detailed and appears to accurately describe the inferred geology. The host to conductive anomaly has moved during the inversion to be considerably higher than 1000 ohm-m. This is believed to have helped deepen the vertical extent of the anomaly to lower frequencies by increasing contrast. The

top of the conductor occurs at 500m, which is geologically accurate. The bedrock conductor is mildly arcuate downward with some asymmetry and dips to the east. The conductive near-surface layer's 400-500m thickness is also consistent with the known geology.

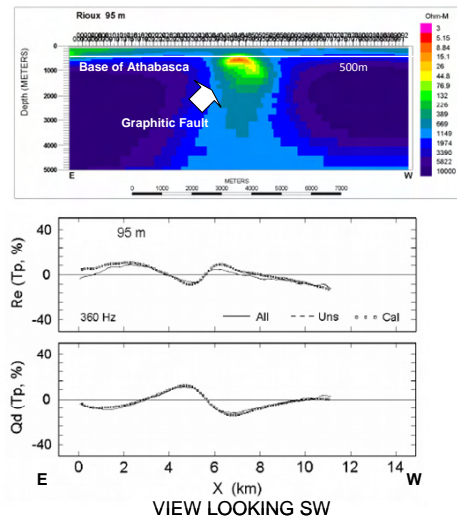


Figure 6: Above: 2D inversion image for ZTEM flight line 95m above the ground; below: Observed (solid curves) and computed 2D inversion model responses (open squares) for 95m ZTEM line.

Conclusion

The ZTEM test results performed over an unconformity-type uranium target appear to correlate very well with the known geology, in particular the presence of a graphitic conductor that is known to occur at depths exceeding 500-750m. In addition, the ZTEM results appear to explain/corroborate changes in the geologic strike in the deeper, more thickly sandstone-covered portions of the survey area. In particular, the ZTEM results point to the presence of a synformal conductive structure, that relates to the graphitic fault zone, in the central survey area, as well as a weak NNW-SSE oriented low resistivity zone inferred to occur in the shallower sandstone cover rocks, which correlates with geochemical anomalies and potentially relates to a shear-hosted alteration zone.

The 2D inversion using the Zvert2d algorithm appears to have been able to compute accurate ZTEM responses in the air and to invert them for reasonable earth resistivity cross section in this region of the North Athabasca Basin. Provided approximate constraints on the host resistivity are available, inversion anomaly positions are more accurate. With poor constraints, trials with a variety of host resistivities are required to judge their dependency.

Acknowledgements

The authors would like to thank Geotech and the mining company involved for allowing us to present these results, as well as Bill Doerner for his involvement in the 2d study.

EDITED REFERENCES

Note: This reference list is a copy-edited version of the reference list submitted by the author. Reference lists for the 2009 SEG Technical Program Expanded Abstracts have been copy edited so that references provided with the online metadata for each paper will achieve a high degree of linking to cited sources that appear on the Web.

REFERENCES

- De Lugao, P. P., and P. E. Wannamaker, 1996, Calculating the two-dimensional magnetotelluric Jacobian in finite elements using reciprocity: *Geophysical Journal International*, **127**, 806–810.
- Hernance, J. F., and R. E. Thayer, 1975, The telluric-magnetotelluric method: *Geophysics*, **37**, 349–364.
- Kuzmin, P., B. Lo, and E. Morrison, 2005, Final report on modeling, interpretation methods and field trials of an existing prototype AFMAG system: Miscellaneous Data Release, **167**, Ontario Geological Survey.
- Labson, V. F., A. Becker, H. F. Morrison, and U. Conti, 1985, Geophysical exploration with audio-frequency natural magnetic fields: *Geophysics*, **50**, 656–664.
- Legault, J. M., D. Carriere, and L. Petrie, 2008, Synthetic model testing and distributed acquisition dc resistivity results over an unconformity uranium target from the Athabasca Basin, northern Saskatchewan: *The Leading Edge*, **27**, 46–51.
- Lo, B., J. M. Legault, and P. Kuzmin, 2009, personal communication.
- Lo, B., and M. Zang, 2008, Numerical modeling of Z-TEM (airborne AFMAG) responses to guide exploration strategies: 78th Annual International Meeting, SEG, Expanded Abstracts, 1098–1101.
- Matthews, R., R. Koch, and M. Leppin, 1997, Advances in integrated exploration for unconformity uranium deposits in western Canada, in A. Gubins, ed., *The proceedings of exploration 97: Prospectors and Developers Association of Canada*, 993–1024.
- Murakami, Y., 1985, Short note: Two representations of the magnetotelluric sounding survey: *Geophysics*, **50**, 161–164.
- Pedersen, L. B., 1998, Tensor VLF measurements: Our first experiences: *Exploration Geophysics*, **29**, 52–57.
- Powell, B., G. Wood, and L. Bzdel, 2007, Advances in geophysical exploration for uranium deposits in the Athabasca Basin, in *Proceedings of Exploration 07: Fifth Decennial International Conference on Mineral Exploration*.
- Stodt, J.A., G. W. Hohmann, and S. C. Ting, 1981, The telluric-magnetotelluric method in two- and three-dimensional environments: *Geophysics*, **46**, 1137–1147.
- Tarantola, A., 1987, *Inverse problem theory*: Elsevier.
- Vozoff, K., 1972, The magnetotelluric method in the exploration of sedimentary basins: *Geophysics*, **37**, 98–141.
- Wannamaker, P. E., J. A. Stodt, and L. Rijo, 1987, A stable finite element solution for two-dimensional magnetotelluric modeling: *Geophysics Journal of Royal Astronomical Society*, **88**, 277–296.
- Ward, S. H., 1959, AFMAG: Airborne and ground: *Geophysics*, **24**, 761–787.
- Witherly, K., R. Irvine, and E. B. Morrison, 2004, The Geotech VTEM time domain helicopter EM system: 74th Annual International Meeting, SEG, Expanded Abstracts, 1217–1221.

ZTEM and VTEM airborne EM survey results over PGM-Cu-Ni targets at East Bull Lake anorthositic complex, Massey, Ontario

Jean M. Legault*, Marta Orta, Harish Kumar, and Shengkai Zhao, Geotech Ltd.

Summary

Heliborne VTEM and ZTEM surveys were flown over East Bull Lake Intrusive Complex near Massey ON. The VTEM results show good correlation with known occurrences and identify new areas for follow-up. The ZTEM survey results correlate well with known geology and provide indications of deep structure that agree with previous scalar and tensor AMT survey results. Comparisons between these data sets and the East Bull Lake geology and structure are showcased using 1D-2D-3D inversion modeling.

Introduction

In September 2010, Mustang Minerals Corp. (Toronto, ON) contracted Geotech to fly heliborne ZTEM survey over East Bull Lake property (Figure 1). The survey followed a previously successful VTEM survey in May-June, 2007. The East Bull Lake Intrusion (EBLI) is a 20km long gabbro-anorthosite intrusive complex located 80km west of Sudbury, Ontario. It consists of two separate zoned intrusions joined by a 5km long feeder dyke (Figure 2). The EBLI is also crosscut by two major structures: the Folsom Lake (FLFZ) and Parisien Lake (PLFZ) fault zones; Figure. 2). The property is considered to have excellent potential to host a significant nickel-copper, PGM (platinum group metal) deposit but is, as yet, not developed for mining.

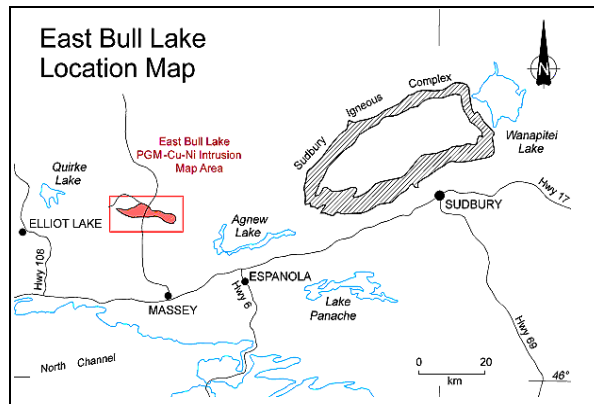


Figure 1: East Bull Lake property location (courtesy Mustang Minerals Corp.; <http://www.mustangminerals.com>).

Property History

The East Bull Lake area had seen limited mineral exploration activity take place between 1950 and 1962 involving a number of mining and exploration companies that were exploring a portion of the property for gold, copper and nickel deposits. The potential for PGM deposits on the property was not considered until the late 1980's (Brisbin et al., 2001).

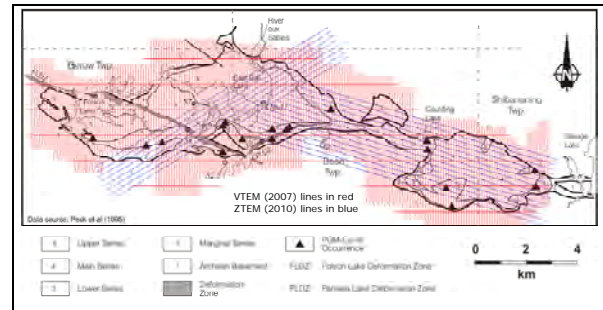


Figure 2: East Bull Lake Intrusion geology, PGM occurrences and VTEM-ZTEM survey lines (modified after Brisbin et al., 2001).

In the early 1980's, EBLI was also one of a small number of Precambrian crystalline intrusions selected by Atomic Energy of Canada Ltd. to test the capability of geotechnical methods for defining fault structures within bedrock and also for the purpose of evaluation for long-term storage of nuclear waste. At that time, in addition to ground VLF EM, magnetic, gravity surveys, both scalar and tensor audio magnetotelluric (AMT-MT) survey measurements were obtained on the site by the GSC (Kurtz et al., 1986; Fig. 3).

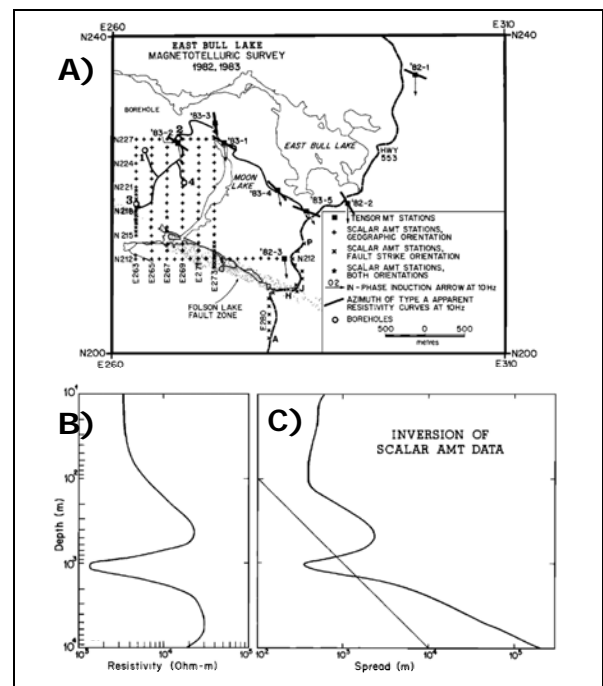


Figure 3: a) Location of scalar AMT and tensor MT sites obtained at East Bull Lake in 1982 and 1983; b-c) 1D inversion of scalar AMT data over EBLI, showing well resolved conductor at depth below 800m (after Kurtz et al., 1986).

ZTEM and VTEM airborne EM results over PGM-Cu-Ni targets at East Bull Lake anorthositic complex

In addition to identifying the ESE-WNW trending Folsom Lake fault zone (FLFZ) as a major regional conductive structure (Figure 2-3a), on the basis of the AMT-MT results, a well resolved conductor was found at a depth below 800m (Fig. 3b) and was later drill-tested by AECL to reveal a faulted, troctolitic later marking the base of the East Bull Lake intrusive, which was also PGM-mineralized (R. Dunbar, Mustang Minerals, pers. comm., Sept-2010).

In 1990, the Ontario Ministry of Northern Development, Laurentian University and Ontario Geological Survey completed an extensive study of EBLI that concluded that the "potential exists for extremely large tonnages of sulphide mineralization, perhaps even massive sulphides (along the floor of the intrusion), which have platinum-group element-enrichment levels equating to reef environments" (www.mustangminerals.com).

Following the 2007 VTEM survey over East Bull Lake, prospective EM anomalies were identified in areas where mineralization was previously unknown and which were later proven to be associated with highly anomalous nickel-copper-PGM values in surface samples and drilling.

In early 2008 initial drilling of a VTEM target at Parisien Lake yielded intersections that included 1.1m of 9.3% copper and 12/5 g/t PGM from 89m down hole depth and 10m of 0.4% nickel at shallow depth. Historical drilling at East Bull Lake prior to Mustang's involvement intersected 0.5m of 3.9 % nickel in the central part of the intrusion (www.mustangminerals.com). The ZTEM survey objectives were to define potential deep extensions or structures potentially associated with the VTEM mineralized conductive features.

VTEM Survey Results

The 2007 VTEM (versatile time-domain electromagnetic) system (Witherly et al., 2004, Witherly and Irvine, 2006, Prihodko et al., 2010) survey (Orta and Bagrianski, 2007) consisted on 867 line-km flown along 100m spaced NS lines and 1km spaced EW tie-lines, with EM and magnetic sensors at 40m and 65m avg. elevations, respectively. The VTEM and magnetic results at EBLI are presented in Figures 4-5. The late-channel (off-time) EM Time Constant (Tau) image in Figure 4a was obtained from the Z-coil, dB/dt response.

For potential conductive mineralized targets, the eddy current decays more slowly with of time, giving larger values of Tau, relative to poor conductors. Medium-to-large values of Tau, with responses extending into late times, are an indication of potential mineralization for base-metal and PGM exploration. VTEM anomalies are generally not expected over disseminated sulphides, unless secondary enrichment is present.

At EBLI, small-to-medium values of Tau in the range of 0.21 to 3.3 milliseconds are generated from the dB_Z/dt

response (Figure 4a and Figure 5b); with a similar range obtained from the B_Z-field response. Anomalies (A-N – Fig. 4) occur as either small isolated groups or as short lineaments.

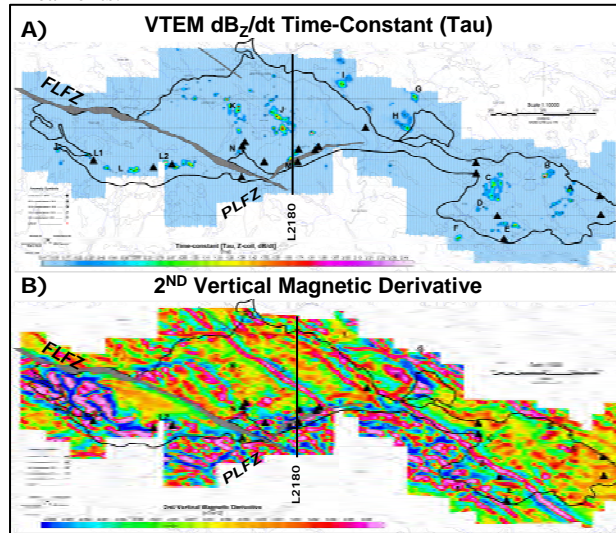


Figure 4: East Bull Lake VTEM survey results: a) dB_Z/dt time-constant (Tau) and b) 2ND vertical magnetic derivative of TMI, with EM anomaly picks, anomalous zones (A-N), known mineral occurrences (triangles) and EBLI outline.

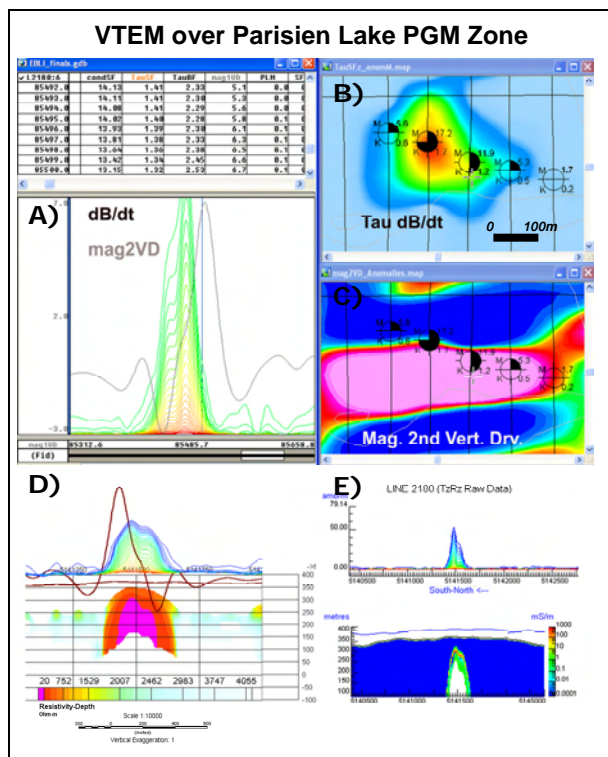


Figure 5: VTEM survey results over Parisien Lake PGM-sulphide occurrence (Anomaly M): a) dB_Z/dt late-channel decay and magnetic 2VD profiles; b-c) plan views dB_Z/dt Tau and magnetic 2VD of TMI with picked EM anomalies; d) RDI effective resistivity and e) EMflow CDI cross-sections.

ZTEM and VTEM airborne EM results over PGM-Cu-Ni targets at East Bull Lake anorthositic complex

In order to discriminate between near surface and deepest sources, the second vertical magnetic derivative was calculated (Figure 4b). Magnetic lineaments related to late dikes and secondary faults are observed with north-west to south-east trends. Stronger magnetic signatures along the southern margin of EBLI, where the mineral occurrences are concentrated, relate to the lower and marginal series phases that feature higher magnetite and are also PGM sulphide enriched (Brisbin et al., 2001). Most VTEM anomalies have a strong magnetic correlation, while others (C, K, I) are only weakly magnetic.

A VTEM anomaly (M) located in the lower margin suite of rocks of the EBLI was drill-tested at Parisien Lake and intersected two mineralized zones: notably, a 10m thick disseminated Ni-sulphide zone at surface and a deeper 1.1m thick massive sulphide PGM-Cu zone at 89m down hole depth (www.mustangminerals.com).

Figure 5c presents the RDI resistivity-depth image (Meju, 1998) over L2180 from Parisien Lake (see Fig. 4) that shows the strongest conductive anomaly at 93 metres of depth (just 4 metres below actual); but with an exaggerated depth extent of 90 metres. The Emflow™ conductivity-depth image (CDI; Fig. 5d) misplaces the top of the target at a shallower depth of 69-72 metres (20 metres above); but is more realistic in terms of its depth extent of just a few metres. From both these results, we conclude that the VTEM response is accurately mapping the massive Cu-PGM sulphide occurrence intersected at 89m down hole. Maxwell™ 3D EM plate models corroborate these results.

ZTEM Survey Results

The 2010 ZTEM (z-axis tipper electromagnetic) system (Lo and Zang, 2008, Lo et al., 2009, Legault et al., 2009ab, Pare and Legault, 2010) survey consisted on 228 line-km flown along 200m spaced over two survey blocks, East and West, that centred on each EBLI lobe (Venter et al., 2010). East block was flown in a SE-NW ($N-107^{\circ}$) direction and West block with NE-SW ($N-059^{\circ}$) lines. The EM and magnetic sensors were at 85m and 100m avg. elevations, respectively. The ZTEM survey results at EBLI are presented in Figures 6-8.

ZTEM is an airborne variant of the AFMAG natural field EM technique (Ward, 1959, Labson et al., 1985) where a single vertical-dipole air-core receiver coil is flown over the survey area in a grid pattern, similar to regional airborne EM surveys. Two orthogonal, air-core horizontal axis coils are placed close to the survey site to measure the horizontal EM reference fields. Data from the three coils are used to obtain the Tzx and Tzy Tipper (Vozoff, 1972) components at five frequencies in the 30 to 720 Hz band.

Figure 6 presents the ZTEM tipper results in plan shown as Total Divergence (DT) images (Lo et al., 2009) that are analogous to the VLF Peaker parameter of Pedersen (1998). DT's convert the tipper cross-overs into peaks for

easier interpretation/visualization in plan view. Shown are the high (360Hz) and Low (30Hz) frequency DT's of the In-Phase component, for depth-comparison purposes, with the EBLI outline overlain. Several prominent linear conductive trends are identified (ZW1-ZE2), including the Folsom Lake FLFZ and the northern contact of EBLI. The similarity of 360Hz high and 30Hz low frequency results suggests that these major structures subcrop and also have considerable vertical extent in this skin depth range. However, there seems to be little correlation with ZTEM and the VTEM anomalies or the known PGM occurrences – this may relate to their limited size and depth extent. It seems that ZTEM is defining regional geologic structures.

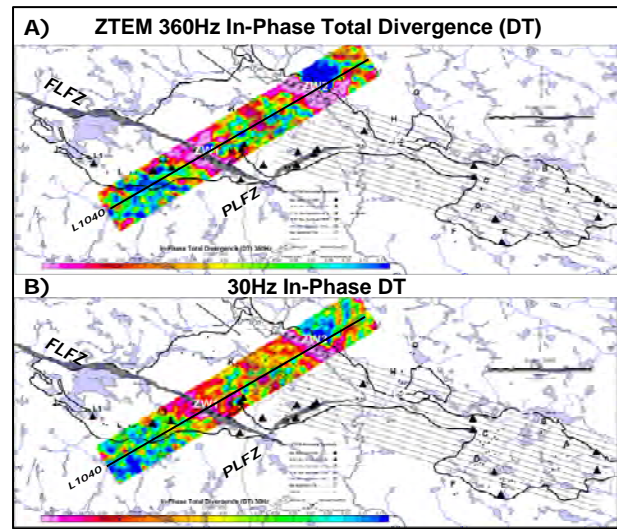
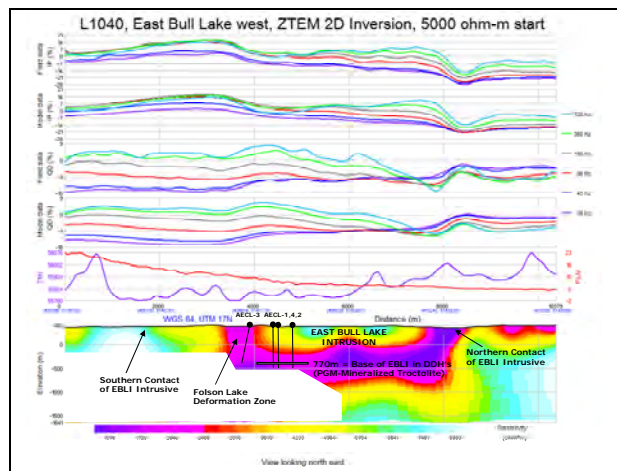


Figure 6: ZTEM Total Divergence (DT) of In-Phase Tipper at: a) 360Hz and b) 30Hz, with EM anomaly picks, anomalous zones (ZW1-ZE3), known mineral occurrences (triangles) and EBLI outline. ZTEM results from East Block are masked by request.



ZTEM and VTEM airborne EM results over PGM-Cu-Ni targets at East Bull Lake anorthositic complex

Figure 7 present the 2D cross-sectional resistivity results obtained from the Zvert2D inversion (Legault et al., 2009b) based on the 2D MT codes/methods of Wannamaker et al. (1987), Tarantola (1987) and de Lugao and Wannamaker (1996). Zvert2d utilizes the In-Line (Tzx) ZTEM tipper data, an apriori model (in this case, 5k Ω -m half-space) and imposes an “air layer”, below the receiver, in order to obtain a 2D resistivity distribution. L1040 directly over the EBLI intrusive indicates that it is a shallower, more resistive body surrounded by lower resistivity rocks at depth and further west, which is consistent with the location of the Folsom Lake FLFZ and the northern EBLI contact, which is a known fault-fracture zone. Significantly, the ZTEM inversion defines a deep conductive layer at 0.5-1km depth which coincides with the known base of EBLI and agrees with the AMT-MT findings of Kurtz et al. (1986). Figure 8 presents the 3D Voxel of the combined 2D inversions for all West Block lines which highlights the good correlation between ZTEM and the known geology.

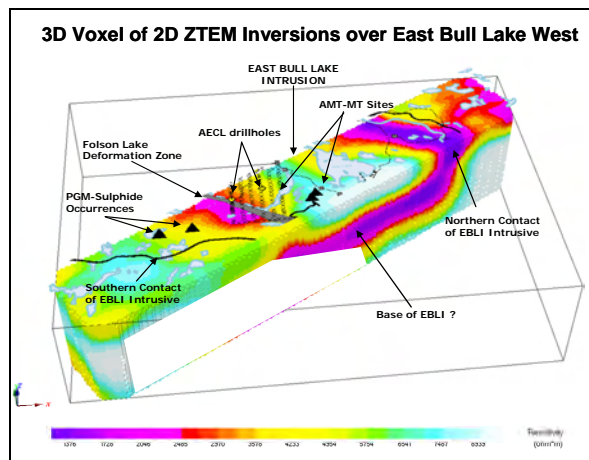


Figure 8: 3D Voxel view of ZTEM 2D inversion over East Bull Lake West block, with location of AECL drillholes & AECL-GSC AMT-MT sites, PGM occurrences and EBLI outline. Results in lower left hand corner have been masked by request.

Conclusions

Helicopter-borne VTEM survey results over the East Bull Lake Intrusive Complex have identified weak to moderate conductance anomalies associated with previously unmapped, highly anomalous PGM-sulphide occurrences, many of which have been successfully drill-tested. ZTEM AFMAG surveys have defined major structures surrounding the EBLI that strikingly agree with previous AMT-MT findings, as well as drilling, including the fractured PGM-mineralized base of the complex, at 800m depths.

The relative success of the VTEM and ZTEM surveys at East Bull Lake is in marked contrast to the apparently poor correlation between VTEM and ZTEM anomalies. This is logically explained by the differences in depth resolution-penetration and relative size-conductivity of the targets

each system is most sensitive to. VTEM is best suited for high resolution mapping of higher-conductance massive to semi-massive sulphide targets in the 0-500m range – with depth-detectability sensitivity proportional to target size. On the other hand, ZTEM is best suited for larger scale and deeper resistivity structures, associated with regional geology and sometimes extending to great depth (1-2km), that depend only on lateral resistivity contrasts. It seems that both technologies complement each other as mapping tools of targets of different scale & style as applied to PGM-sulphide exploration.

Certainly, 3D inversion of ZTEM and VTEM data could provide valuable insight and further explanation of the relationship between the mineralized zones and controlling structures at East Bull Lake.

Acknowledgements

The authors wish to thank Mustang Minerals Corp., joint-venture partner Western Areas NL and Geotech Ltd. for allowing us to show these results and for sponsoring the study. We also thank Nick Venter and Biljana Milicevic for their involvement in this geophysical data processing at East Bull Lake.

References

- Brisbin, D., Wood, P., Kleinboeck, J., and Lapierre, K., 2001, Geology of the East Bull Lake Intrusion and its contact-type PGE-Cu-Ni mineralization, Field Trip Guidebook, Laurentian University SEG Student Chapter 2ND Annual Workshop in Mineral Exploration, 25 pp.
- De Lugao, P.P., and Wannamaker P., 1996, Calculating the two-dimensional magnetotelluric Jacobian in finite elements using reciprocity, *Geophysical Journal International*, **127**, 806-810.
- Kurtz, R.D., Ostrowski, J.A., and Niblett, 1986, A magnetotelluric survey over the East Bull Lake Gabbro-Anorthosite Complex, *Journal of Geophysical Research*, **91**, 7403-7416.
- Labson, V. F., Becker A., Morrison, H. F., and Conti, U. , 1985, Geophysical exploration with audio frequency natural magnetic fields, *Geophysics*, **50**, 656-664.
- Legault, J.M., H. Kumar, B. Milicevic, and L. Hulbert, 2009, ZTEM airborne tipper AFMAG test survey over a magmatic copper-nickel target at Axis Lake in northern Saskatchewan, *SEG Expanded Abstracts*, **28**, 1272-1276.
- Legault, J.M., H. Kumar, B. Milicevic, and P. Wannamaker, 2009, ZTEM tipper AFMAG and 2D Inversion results over an unconformity uranium target in northern Saskatchewan, *SEG Expanded Abstracts*, **28**, 1277-1281.

ZTEM and VTEM airborne EM results over PGM-Cu-Ni targets at East Bull Lake anorthositic complex

Lo, B., Legault, J.M., Kuzmin, P., and Combrinck, M., 2009, Z-TEM (Airborne AFMAG) tests over unconformity uranium deposits, 20TH ASEG International Geophysical Conference & Exhibition, Adelaide, AU, Extended Abstracts, 5 pp.

Lo, B., and Zang, M., 2008. Numerical modeling of Z-TEM (airborne AFMAG) responses to guide exploration strategies, SEG Expanded Abstracts, **27**, 1098-1101.

Meju, M.A., 1998, Short Note: A simple method of transient electromagnetic data analysis, *Geophysics*, **63**, 405–410.

Orta, M., and Bagrianski, A., 2007, Report on a helicopter-borne versatile time domain electromagnetic (VTEM) geophysical survey, East Bull Lake property, for Mustang Minerals Corp., internal report by Geotech Ltd., 28 pp.

Paré, P., and Legault, J.M., 2010, Ground IP-Resistivity, airborne Spectrem and helicopter ZTEM survey results over Pebble copper-moly-gold porphyry deposit, Alaska, SEG Expanded Abstracts, **29**, 1734-1738.

Pedersen, L.B., 1998, Tensor VLF measurements: Our first experiences, *Exploration Geophysics*, **29**, 52-57.

Prikhodko, A., Morrison, E., Bagrianski, A., Kuzmin, P., Tishin, P., and Legault, J.M., 2010, Evolution of VTEM – technical solutions for effective penetration, 21ST ASEG International Geophysical Conference & Exhibition, Sidney, AU, Extended Abstracts, 5 pp.

Tarantola, A., 1987, *Inverse Problem Theory*, Elsevier, New York, 613 pp.

Venter, N., Legault, J.M., Zhao, S., and Kumar, H., 2010, Report on a helicopter-borne z-axis tipper electromagnetic (ZTEM) and aeromagnetic geophysical survey, East Bull Lake east and west blocks, for Mustang Minerals Corp., internal report by Geotech Ltd., 58 pp.

Vozoff, K., 1972, The magnetotelluric method in the exploration of sedimentary basins: *Geophysics*, **37**, 98–141.

Wannamaker, P. E., Stodt, J. A., and Rijo, L., 1987, A stable finite element solution for two-dimensional magnetotelluric modeling: *Geophysical Journal of Royal Astronomical Society*, **88**, 277-296.

Ward, S. H., 1959, AFMAG - Airborne and Ground: *Geophysics*, **24**, 761-787.

Witherly, K., and R. Irvine, 2006, The VTEM airborne electromagnetic system – benchmarking continuous improvement via repeat surveys over time, SEG Expanded Abstracts, **25**, 1273-1277.

Witherly, K., Irvine, R., and Morrison, E.B., 2004, The Geotech VTEM time domain helicopter EM system: SEG Expanded Abstracts, **23**, 1217-1221.

Fig 4a

VTEM dB_Z/dt Time-Constant (Tau)

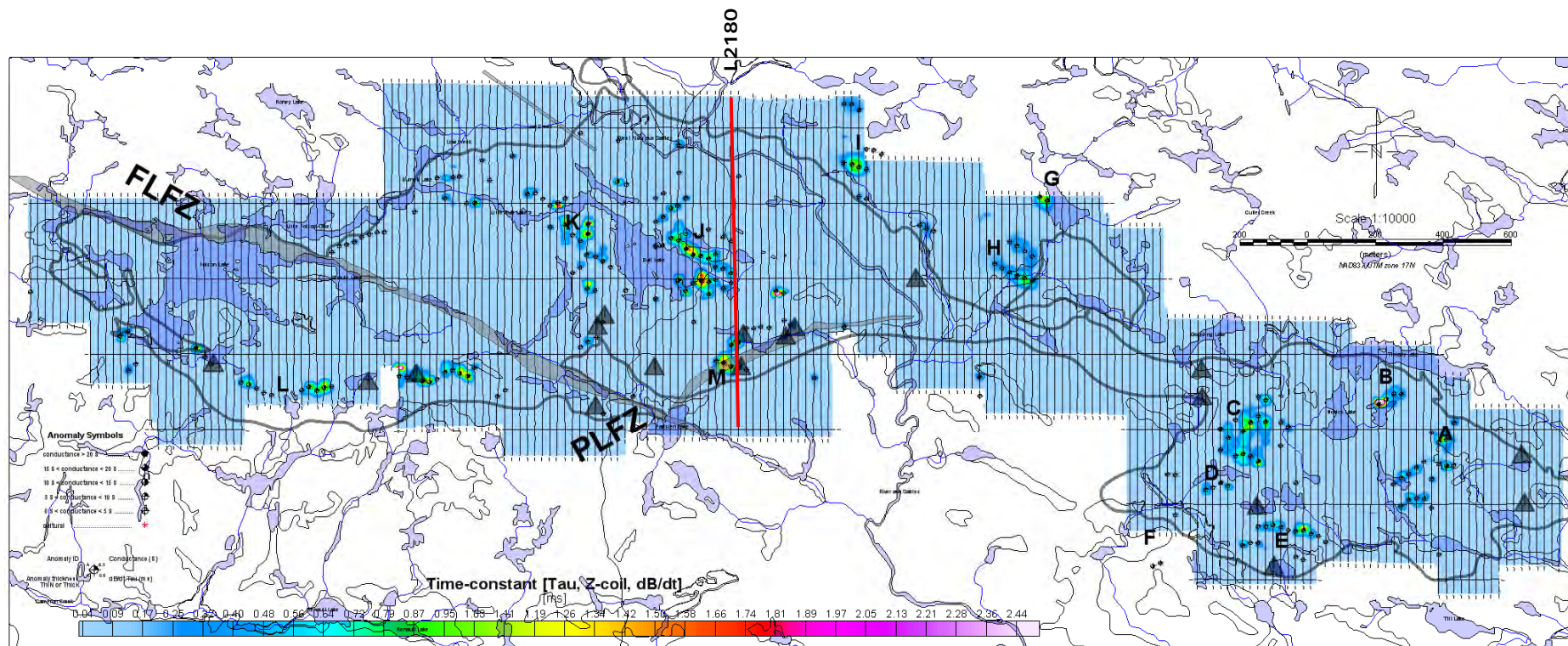


Fig 4b

2ND Vertical Magnetic Derivative

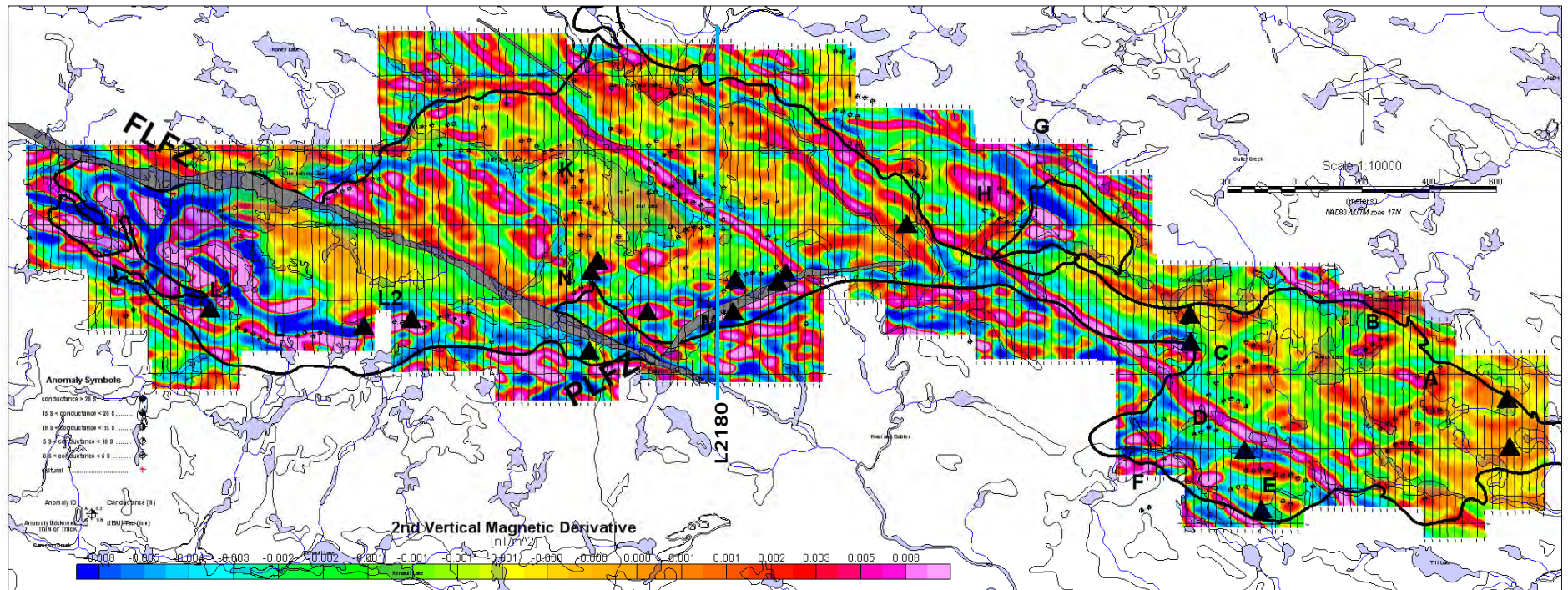


Fig 6a

ZTEM 360Hz In-Phase Total Divergence (DT)

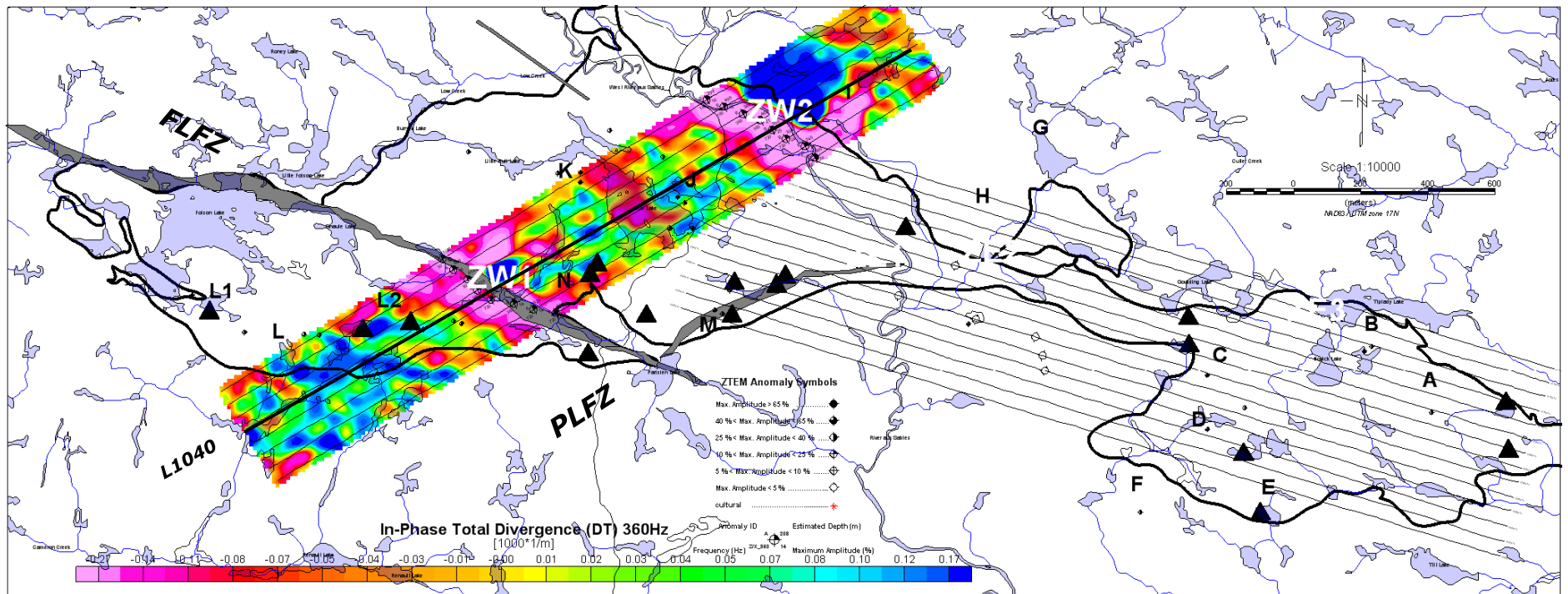


Fig 6b

30Hz In-Phase DT

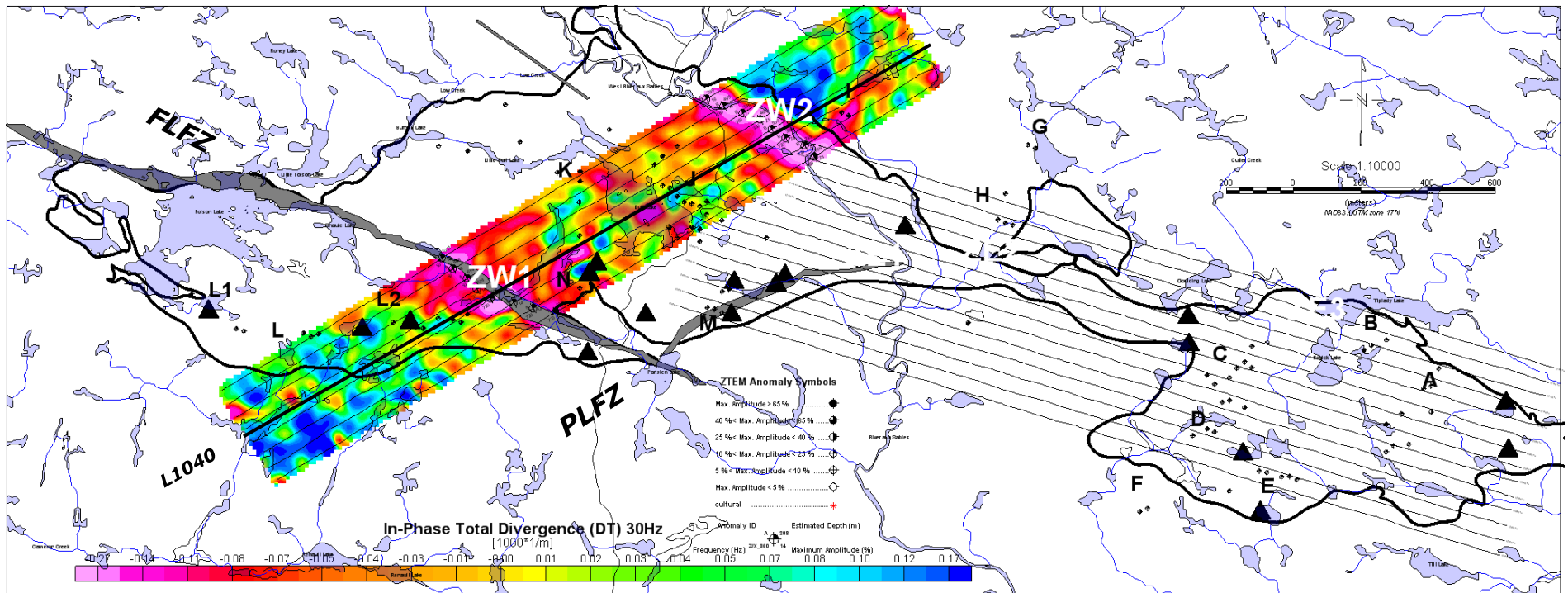


Fig 7

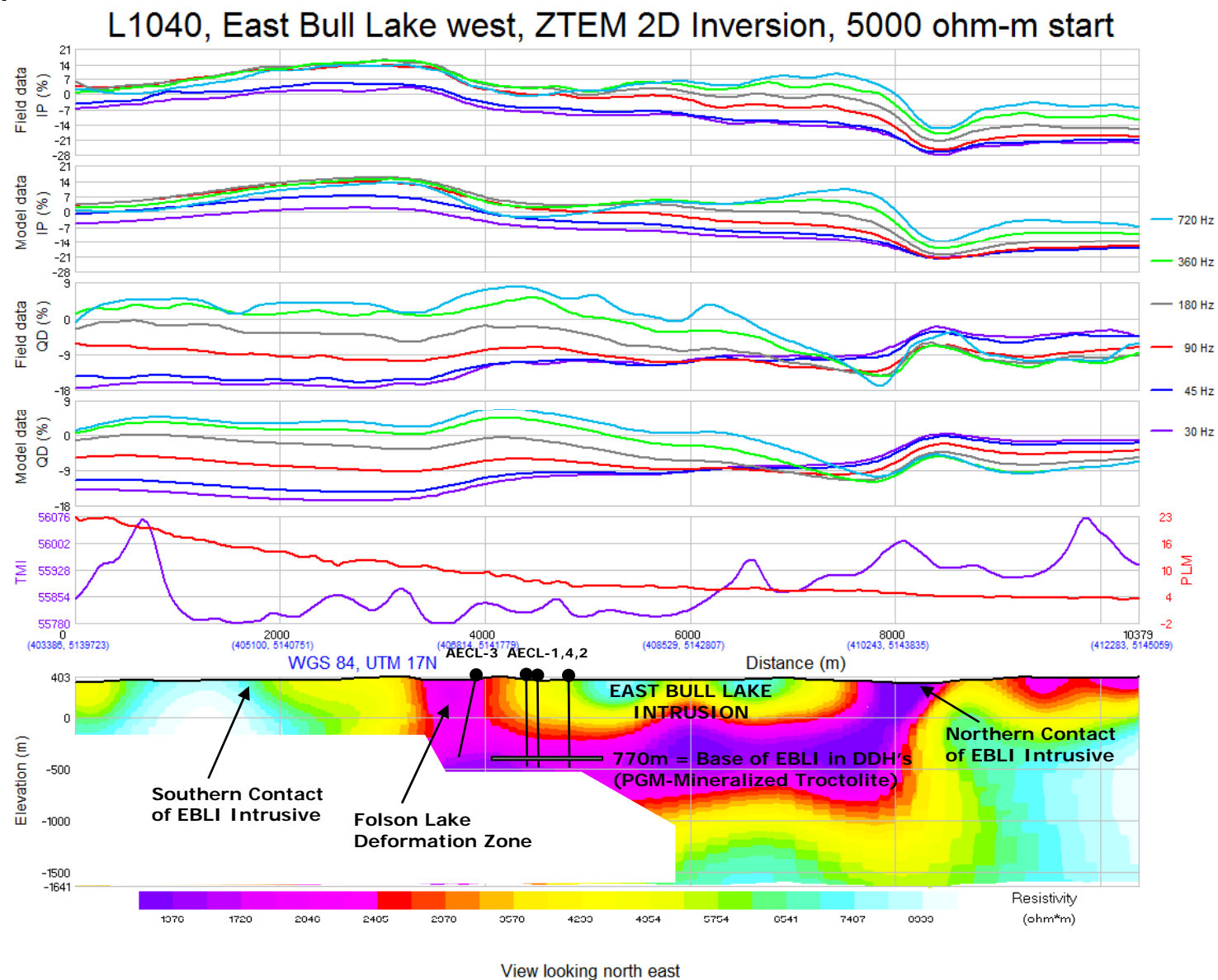
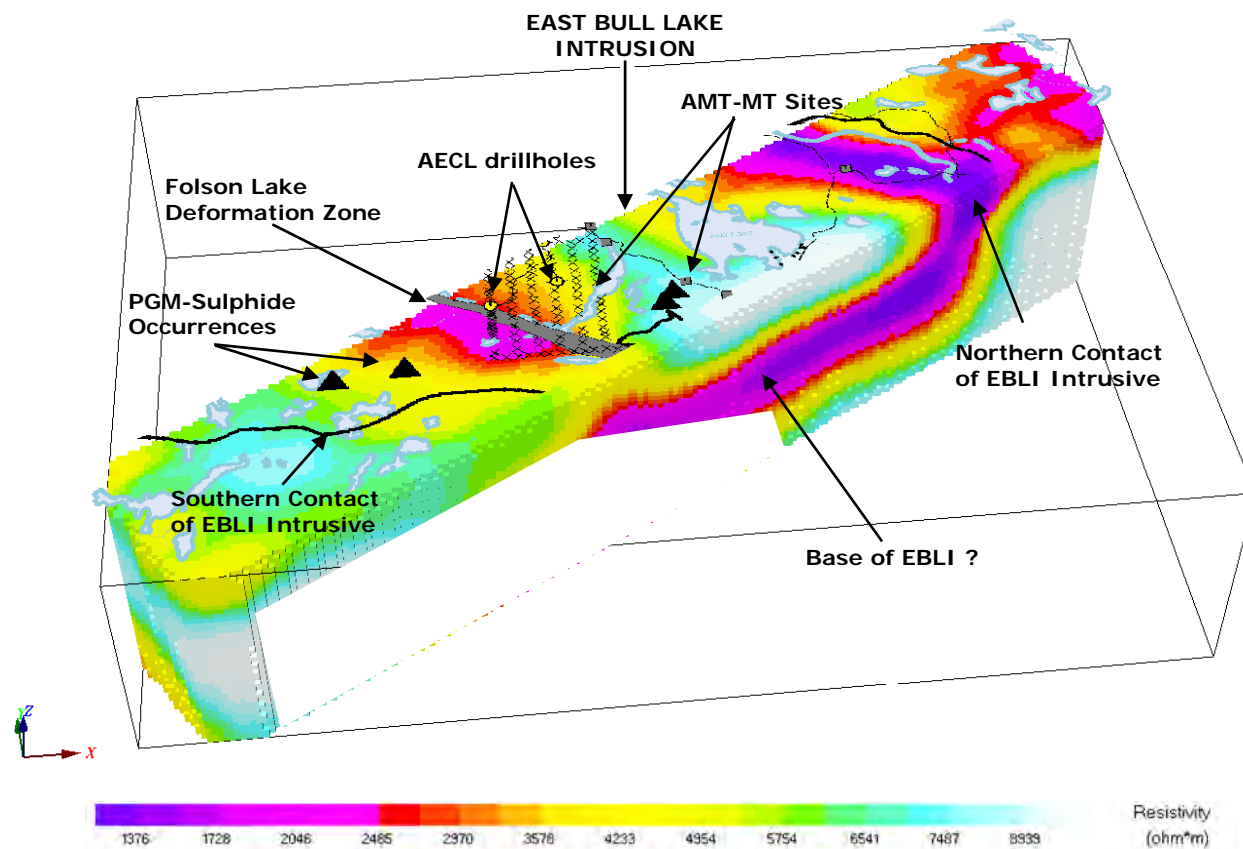


Fig 8

3D Voxel of 2D ZTEM Inversions over East Bull Lake West



ZTEM Airborne AFMAG EM Results over the Reese River Geothermal Test Area, central Nevada

Jean M. Legault
Geotech Ltd.
Aurora, ON, CA
jean@geotech.ca

Jeffrey B. Witter
Sierra Geothermal Power
Corp., Vancouver, BC, CA
jwitter@sierrageopower.com

Paolo Berardelli
Geotech Ltd.
Aurora, ON, CA
paolo@geotech.ca

Marta Orta
Geotech Ltd.
Aurora, ON, CA
marta@geotech.ca

SUMMARY

A ZTEM (Z-Tipper Axis Electromagnetic) airborne AFMAG survey was conducted over the Reese River Test Block, situated in central Nevada in August, 2009. The Reese River prospect is a “blind” geothermal resource that lacks surface characteristics such as hot springs. A number of geophysical surveys have been conducted at the prospect, including seismic, gravity, magnetotelluric (MT) and radiometric surveys. Resistivity methods, such as MT, are typically used to map structure, lithology and alteration, particularly the smectite-zeolite zones which form a low resistivity cap over the outer margins of the higher resistive reservoir at depth. The ZTEM survey at Reese River has overflown lines previously surveyed using MT for comparison purposes.

The ZTEM results appear to correlate very well with previous magnetotelluric results and the known geology, in particular the presence of both major and secondary fault structures and geologic contacts. 2D inversions of the airborne ZTEM appear to agree very well with the inversions obtained from ground MT, except in areas of pronounced 3D behaviour, where the 2D assumption is no longer valid.

Key words: Airborne, electromagnetic, AFMAG, magnetotelluric, resistivity, inversion, geothermal.

INTRODUCTION

Geophysics, in particular EM methods, have been used for geothermal exploration for decades. Historically, DC-Resistivity and TEM sounding methods have been used to map the electric properties of the geology at depth. More recently ground MT has become the preferred electrical method, providing good depths of investigation and resolution but at a very high cost. ZTEM represents a new airborne technology capable of providing cost-effective mapping of large areas whilst detailing the electrical properties of the geological structures at depths.

A ZTEM (Z-Tipper Axis Electromagnetic; Lo and Zang., 2008; Lo et al., 2009) survey was conducted over the Reese River Test Block (Figure 2), belonging to Sierra Geothermal Power Corp. (Vancouver, BC) and situated in Lander County, central Nevada. The survey comprised airborne Tipper AFMAG (Ward, 1959; Labson et al., 1985) measurements using the ZTEM system (Figure 1), as well as aeromagnetics

using a caesium magnetometer. The survey consisted of seven (7) approximately 10 km long, Northwest-Southeast oriented flight lines, totalling 70 line-km, that were obtained at nominal 500m line spacing over an approximately 3 x 10km area (yellow lines in Figure 3).

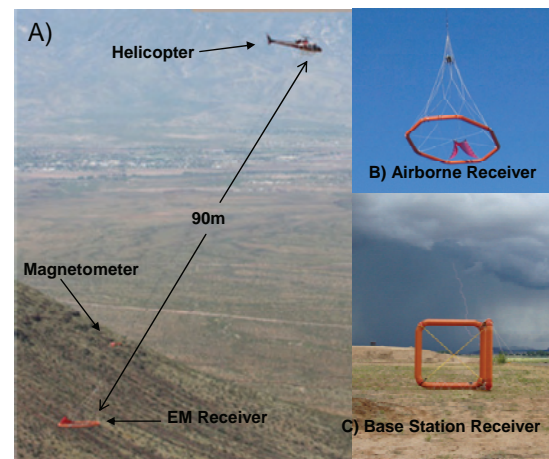


Figure 1: a) ZTEM helicopter EM system in flight, showing Hz receiver Coil and magnetic sensor; b) Hz receiver coil, c) Hx-Hy base station coils located at a remote site adjacent to survey area.

The Z-axis tipper measurements of the vertical (Z) component were obtained using Geotech's patented ZTEM induction aircoil system (Figure 1), suspended at approximately 100m elevation above ground level. The vertical component data (Hz) were then ratioed to fixed horizontal field measurements (Hx-Hy) obtained using identical reference coils, that were oriented in the in-line (X) and cross-line (Y) directions, in order to obtain the tipper functions Z/X and Z/Y. The In-Phase and Quadrature components ZTEM field ratio data were obtained, using Fourier-based, digital signal processing analyses, at 6 frequencies, between 30Hz and 720Hz. The magnetometer was a Geometrics optically pumped caesium vapour magnetic field sensor, towed at approximately 120m above ground level.

Geologic Setting

The Reese River property is located in central Nevada, 45 km north of Austin and 300 km east of Reno, Nevada (Figure 2). The property is geologically located within a basinal formation west of the Shoshone Mountain Range, within a region of NE trending faults known as the Humboldt structural zone and also in an area of elevated heat flow known as the Battle Mountain High (Witter et al, 2009).



Figure 2: General location of Reese River geothermal site.

The region contains several other geothermal areas (i.e., Dixie Valley and Beowawe) but the Reese River prospect is a “blind” geothermal resource that lacks the typical geothermal surface characteristics, such as hot springs or hydrothermal deposits. It lies completely buried and was discovered by chance as a result of hot water being encountered in exploration drill holes for Uranium. Shallow drilling from the 1970’s to 1980’s has mapped a 10x3km wide geothermal anomaly. More recent deep drilling has confirmed commercial grade temperatures reaching ~150°C (Witter et al., 2009).

Previous Geophysics

The Reese River Geothermal play has been host to a number of geophysical surveys, including seismic, gravity, magneto-telluric and radiometric surveys. The seismic survey was less effective than anticipated in identifying subsurface geologic structure. The gravity survey has provided preliminary information regarding depth-to-bedrock and subsurface structures at the Reese River prospect. Temperature data identified a large thermal anomaly located in the south central part of the survey area (Figure 3).

A small ground MT survey, consisting of 7 lines for a total of 30 line km, was conducted in 2008. The lines are oriented North-West to South-East (red Lines in Figure 3) roughly perpendicular to the known geology. Dipole spacing was 200m in the x-direction and 100m in the y-direction. The operating frequency bandwidth of the MT survey was 0.001 to 1000 Hz giving a depth of investigation of 1.5 to 2.0 km.

The ground MT survey covered the main areas of interest over the site. The purpose for running the MT lines was to map the smectite-zeolite zone which forms a low resistivity cap over the outer margins of the reservoir while observing higher resistivity below.

The MT data at Reese River indicate the presence of a widespread, shallow, low-resistivity zone that may be a clay-cap overlying a warm (~70 °C) tabular geothermal aquifer at ~150 m depth. The MT data also resolve deeper low-resistivity zones that likely correspond to argillic (clay) alteration. Zones of high resistivity at depth are thought to

correspond to limestone units that also outcrop at the surface. Overall, observation of the 2D resistivity profiles suggests that the resistivity variations at Reese River have a 3 dimensional aspect to them which is difficult to resolve with 2D profiles (Witter et al., 2009).

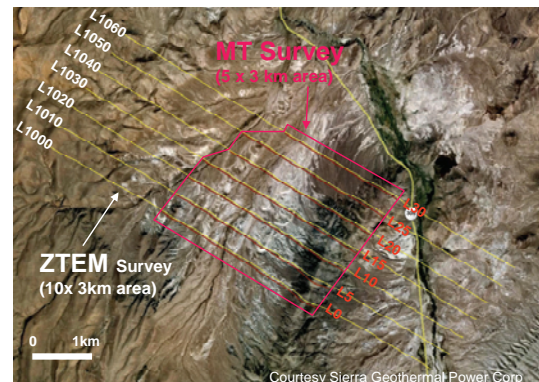


Figure 3: Reese River ZTEM Flight lines (Yellow Lines) over the Ground MT Lines (Red Lines).

Synthesis of Exploration Data

Figure 4 shows an MT resistivity profile with the subsurface structure (estimated from gravity, borehole and geologic data) overlain. Subsurface temperature distributions, constrained by temperature gradient well measurements, have also been added. The subsurface distribution of rock types has been constrained near drillholes based on geological well log data and inferred from regional stratigraphy in areas far from drillholes. Inferred fluid pathways are also indicated.

One plausible assumption regarding the resistivity distribution shown in Figure 4 is that areas of low resistivity (<5 ohm-m) are altered and smectite-rich and thus have low permeability. A corollary to this assumption is that the areas of high resistivity (>50 ohm-m) are smectite-poor and may be permeable (Witter et al., 2009).

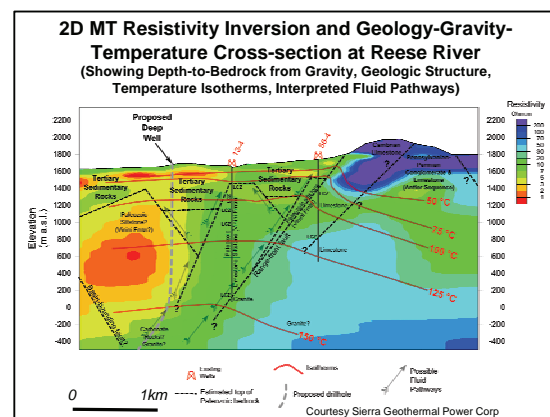


Figure 4: Cross-section through the Reese River prospect showing 2D MT resistivity inversion, depth to bedrock (estimated from gravity, geology and borehole data), temperature isotherms from boreholes, subsurface geology, existing wells and possible fluid pathways (revised after Witter et al., 2009)

As shown in Figure 4, a proposed deep well located to the west of 13-4 would be expected to hit the Paleozoic siltstone bedrock at ~500 m depth. At deeper levels, carbonate rocks or granite basement are likely to be encountered. Drilled directionally, this deep drillhole would extend underneath a large, low resistivity zone that may act as a clay cap on top of a deeper geothermal system (Witter et al., 2009).

RESULTS AND DISCUSSION

The two In-Phase Tipper profile data ($Z/X = \text{In-line} - Z/Y = \text{Cross-line}$), with corresponding 90Hz 90-degree Phase-Rotated (PR) grids (Lo et al., 2009; used to convert Tipper cross-over to peaks) are presented in Figures 5-6 and compare the relative orthogonal and oblique geoelectric structures, respectively. In these images, warm colours represent conductive zones, whereas cool colours (blues) represent resistive zones. The Z/X results (Figure 5) highlight long linear NE-SW regional fault zones, whereas the Z/Y results (Figure 6) define more localized resistivity anomalies located in the more mountainous central survey area that features more 3D behaviour.

ZTEM In-Phase Profiles over 90Hz Phase Rotated IP Grid
In-line (Z/X) In-Phase Component

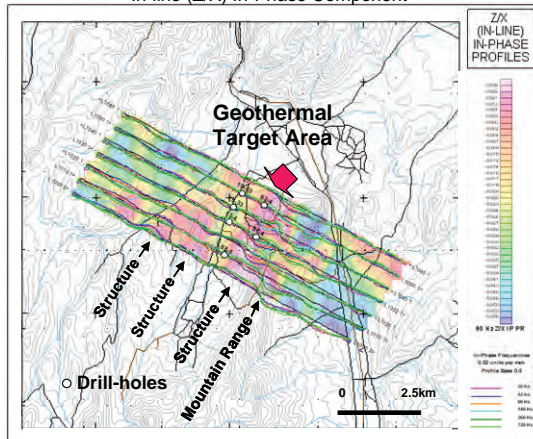


Figure 5: ZTEM In-phase Z/X (In-line) tipper profiles over 90Hz Phase Rotated XIP Grid.

The In-Phase Total Divergence (DT; Lo et al., 2009) results at 30Hz, shown in Figure 7, are a different representation of the ZTEM tipper data that allow the orthogonal Z/X and Z/Y components to be combined. Analogous to the Peaker parameter, used in VLF (Pedersen, 1998), the DT grid imaging of geoelectric structures is omni-directional, with all orientations being highlighted. The 30Hz DT images the deep tipper data - with the deeper results highlighting both the conductive NE-SW structures previously defined in Figure 5 and the prominent deep circular high resistivity feature (blue) from Figure 6 that lies in the geothermal target area and likely contributes to the 3D resistivity behaviour observed locally.

MT and ZTEM 2D Inversion Results

The ZTEM survey tipper results can be converted to their equivalent resistivity-depth source model using 2D inversion. The Zvert2d algorithm (Legault et al., 2009) has been adapted for ZTEM by accounting for the air layer as well as the mobile

Hz and fixed Hx base station. Zvert2d uses the finite element

ZTEM In-Phase Profiles over 90Hz Phase Rotated IP Grid
Cross-line (Z/Y) In-Phase Component

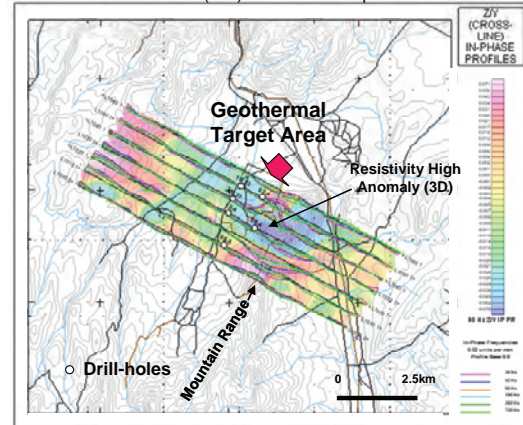


Figure 6: ZTEM In-phase Z/Y (Cross-line) tipper profiles over 90Hz Phase Rotated YIP Grid.

ZTEM 30Hz In-Phase Total Divergence (DT) Grid
(Deeper Penetration)

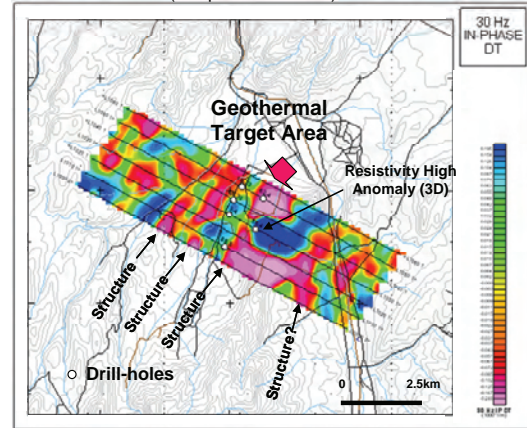


Figure 7: ZTEM 30 Hz In-phase Total Divergence (DT).

forward problem and inversion parameter sensitivities using reciprocity of Wannamaker et al. (1987) and de Lugao and Wannamaker (1996), with the regularized Gauss-Newton non-linear parameter step estimate of Tarantola (1987).

The input data for the ZTEM 2D inversions were the In-line (Z/X) In-Phase and Quadrature Phase data from all six measured frequencies (30-720Hz). Due to the impractical nature of the >1000 data points from the ZTEM profile, these were re-sampled to <200 points in order to perform the calculation and proved effective. An error of 1-2% was assigned to the data for inversion. A host of 100 ohm-metres was assumed for the starting model. Despite non-ideality of the data error, a value of nRMS of close to unity (1.0) was achieved in 4-6 iterations.

Below, we show examples comparing corresponding lines of 2D MT inversion against the 2D inverted ZTEM data from the southern and central survey area (see Figures 8 and 9). The close correlation between the MT and ZTEM images for southernmost L0/L1000 shown in Figure 8 is clear, including the relative depth and location of resistivity highs and lows that relate to structure, lithology and alteration.

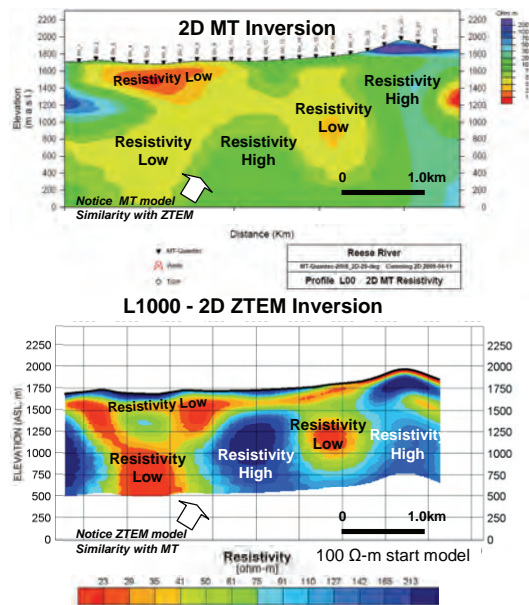


Figure 8: 2D Inversion of Ground MT Line L0 (above) and ZTEM Line 1000 (below). Notice MT similarity to ZTEM.

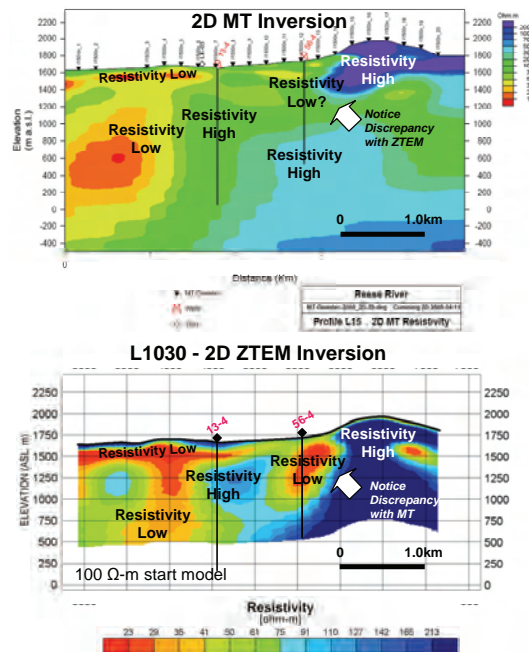


Figure 9: 2D Inversion of MT Line L15 (above) and ZTEM Line 1030 (below). Notice discrepancy below well 56-4.

In marked contrast, the slightly contradictory images of the geoelectric MT and ZTEM responses illustrated in Figure 9, from L015/L1030 in the central survey area, are particularly noticeable below well 56-4. Interestingly, this area also coincides with the region of visible 3D behaviour, described previously. This suggests that the MT and ZTEM inversions are affected by 3D behaviour in the geothermal target area and may not produce geologically accurate images locally.

CONCLUSIONS

The ZTEM results appear to correlate well with the magnetotelluric results and the known geology, in particular the presence of both major and secondary fault structures and geologic contacts. In addition, the ZTEM results appear to indicate differences in the relative source depth and vertical depth-extent of the defined geothermal features that are geologically plausible. In particular, the ZTEM results point to the presence of major NE-SW-trending conductive range front faults. In addition, the known geothermal area is marked by a prominent deep circular resistivity high feature, that is surrounded and capped by lower resistivity, and possibly relates to the higher geothermal alteration zone and surrounding lower temperature smectite-zeolite alteration.

The ZTEM and previous ground MT results were compared using 2D inversions. The Zvert2d inversion is a finite element 2D MT code specifically adapted for airborne ZTEM. Overall, the 2D inversions of the airborne ZTEM appear to agree very well with the inversions obtained from ground MT, except in areas of pronounced 3D behaviour, where 2D is invalidated.

REFERENCES

- De Lugao, P.P., and Wannamaker P., 1996, Calculating the two-dimensional magnetotelluric Jacobian in finite elements using reciprocity, *Geophysical Journal International*, **127**, 806-810.
- Labson, V. F., Becker A., Morrison, H. F., and Conti, U. , 1985, Geophysical exploration with audio frequency natural magnetic fields, *Geophysics*, **50**, 656-664.
- Legault, J.M., Kumar H., Milicevic B., and Wannamaker P., 2009, ZTEM tipper AFMAG and 2D Inversion results over an unconformity uranium target in northern Saskatchewan, *SEG Expanded Abstracts*, **28**, 1277-1281.
- Lo, B., and Zang, M., 2008. Numerical modeling of Z-TEM (airborne AFMAG) responses to guide exploration strategies, *SEG Expanded Abstracts*, **27**, 1098-1101.
- Lo, B., Legault, J.M., Kuzmin, P., and Combrinck, M., 2009, Z-TEM (Airborne AFMAG) tests over unconformity uranium deposits, 20TH ASEG International Geophysical Conference & Exhibition, Adelaide, AU, Extended Abstracts, 5 pp.
- Pedersen, L.B., 1998, Tensor VLF measurements: Our first experiences, *Exploration Geophysics*, **29**, 52-57.
- Tarantola, A., 1987, *Inverse Problem Theory*, Elsevier, New York, 613 pp.
- Wannamaker, P. E., Stodt, J. A., and Rijo, L., 1987, A stable finite element solution for two-dimensional magnetotelluric modeling: *Geophysical Journal of Royal Astronomical Society*, **88**, 277-296.
- Ward, S. H., 1959, AFMAG - Airborne and Ground: *Geophysics*, **24**, 761-787.
- Witter J.B., Ronne J.A. and Thompson G.R., 2009, Exploration at the Reese River Geothermal Prospect in Nevada, *Geothermal Research Council 33RD Annual Meeting*, San Francisco, CA, Extended Abstract, 8pp.

An overview of the ZTEM and AirMt systems – A case study from the Nebo-Babel Ni-Cu-PGE deposit, West Musgrave, Western Australia

Jean Legault ¹, Glenn A. Wilson ², Alexander V. Gribenko ³, Michael S. Zhdanov ⁴,
Shengkai Zhao ⁵ and Keith Fisk ⁶

¹ Geotech (jean@geotech.ca)

² Technolmaging (glenn@technolmaging.com)

³ University of Utah & Technolmaging (alex@technolmaging.com)

⁴ University of Utah & Technolmaging (mzhdanov@technolmaging.com)

⁵ Geotech (shengkai@geotech.ca)

⁶ Geotech Airborne (keith@geotechairborne.com)

Introduction

Over the last decade, airborne electromagnetic (AEM) acquisition systems have evolved, many adopting higher moments to achieve greater depth penetration, whilst sensor calibration and post-acquisition processing technologies have also improved data quality significantly. As an alternative to conventional AEM, the Z-axis Tipper Electromagnetic (ZTEM) and Airborne Magnetic Tensor (AirMt) systems were developed to measure the transfer functions of audio-frequency natural electromagnetic sources from airborne platforms. The ZTEM system measures tipper transfer functions, and the AirMt system measures the rotational invariant of the transfer functions. Ancillary data measured by both systems include radar altimeter, receiver coil altitude, GPS elevation, and total magnetic intensity. For both ZTEM and AirMt, data are typically measured from 25-30 Hz to 600-720 Hz, giving detection depths to 1 km or more, depending on the terrain conductivity. This makes it practical for these systems to be used for mapping large-scale geological structures.

The first commercial surveys for ZTEM were commissioned in 2006, and the first commercial surveys for AirMt were commissioned in 2009. Development of both systems has been aided by Geotech's logistical and technical experience with active-source AEM systems. Presently, eight ZTEM systems and one AirMt system are in operation around the world. ZTEM and AirMt surveys have been flown in Australia, Indonesia, North America, South America, Africa and the Middle East for Sedex, VMS, IOCG, Ni-Cu-PGE, porphyry, uranium and precious metal mineralization systems for numerous major and junior exploration companies. In this paper, we present a case study for the 3D interpretation ZTEM and AirMt surveys flown over the Nebo-Babel Ni-Cu-PGE deposit in Western Australia.

Background

Since the 1950s, magnetotelluric (MT) surveys have been carried out, measuring horizontal electric and magnetic fields induced from ambient (natural) sources, generally assuming that these can be treated as plane electromagnetic waves. The amplitude and phase of the primary field are unknown. By processing the electric and magnetic fields to a complex impedance tensor, the unknown source terms are removed and the transfer functions are dependent only upon frequency and the Earth's conductivity. Magnetovariational (MV) methods are an extension of the MT concept, whereby the transfer functions between the horizontal and vertical magnetic fields:

$$H_z(\mathbf{r}) = W_{zx}(\mathbf{r})H_x(\mathbf{r}) + W_{zy}(\mathbf{r})H_y(\mathbf{r}) \quad (1)$$

form a complex vector often called the Weiss-Parkinson vector, induction vector, or tipper. Similar to the impedance tensor for MT data, the tipper effectively removes otherwise unknown source terms. Since the vertical magnetic field is zero for plane waves vertically propagating into a 1D Earth model, non-zero vertical magnetic fields are directly related to 2D or 3D structures.

This served as the basis for the original development of the audio-frequency magnetic (AFMAG) method (Ward, 1959) whereby two orthogonal coils were towed behind an airborne platform to determine the tilt angle of the plane of polarization of ambient (natural) magnetic fields in the 1 Hz to 20 kHz band. The natural magnetic fields of interest originate from atmospheric thunderstorm activity and propagate over large distances with little attenuation in the Earth-ionosphere waveguide. Given that the tilt angle is zero over a 1D Earth, the AFMAG method produced a non-zero response when crossing conductors. However, the direction and amplitude of the natural magnetic fields randomly varies with time and periodically with season, meaning AFMAG data were not repeatable (Ward et al., 1966). By using MT processing techniques for ground-based orthogonal horizontal magnetic field measurements, Labson et al. (1985) demonstrated that repeatable tipper data could be recovered from measured magnetic fields.

The AFMAG method of Labson et al. (1985) remained largely undeveloped until the recent commercialization of ZTEM (e.g., Legault et al., 2009; Pare and Legault, 2010) (Figure 1) and subsequently, AirMt (e.g., Kaminski et al., 2010) (Figure 2) systems. ZTEM measures the tipper components as the transfer function of a vertical magnetic field measured from an airborne receiver coil to the horizontal components measured at a ground-based reference receiver coil array:

$$H_z(\mathbf{r}) = W_{zx}(\mathbf{r}, \mathbf{r}_0)H_x(\mathbf{r}_0) + W_{zy}(\mathbf{r}, \mathbf{r}_0)H_y(\mathbf{r}_0) \quad (2)$$

AirMt directly measures the rotational invariant of the transfer function for the three magnetic fields measured from an airborne receiver coil array to the three magnetic fields measured at a ground-based (reference) location. Generalizing the Weiss-Parkinson relationship, the three components of a magnetic field measured at a receiver coil array are linearly related to the magnetic fields measured at a ground-based reference receiver coil array:

$$\begin{bmatrix} H_x(\mathbf{r}) \\ H_y(\mathbf{r}) \\ H_z(\mathbf{r}) \end{bmatrix} = \begin{bmatrix} W_{xx}(\mathbf{r}, \mathbf{r}_0) & W_{xy}(\mathbf{r}, \mathbf{r}_0) & 0 \\ W_{yx}(\mathbf{r}, \mathbf{r}_0) & W_{yy}(\mathbf{r}, \mathbf{r}_0) & 0 \\ W_{zx}(\mathbf{r}, \mathbf{r}_0) & W_{zy}(\mathbf{r}, \mathbf{r}_0) & 0 \end{bmatrix} \begin{bmatrix} H_x(\mathbf{r}_0) \\ H_y(\mathbf{r}_0) \\ H_z(\mathbf{r}_0) \end{bmatrix} \quad (3)$$

If we write \mathbf{W}_1 and \mathbf{W}_2 as the first and second columns of the transfer function, then we can introduce the variable:

$$\mathbf{K} = \mathbf{W}_1 \times \mathbf{W}_2 \quad (4)$$

and obtain the complex scalar:

$$K = \mathbf{K} \cdot \frac{\text{Re}(\mathbf{K})}{|\text{Re}(\mathbf{K})|} \quad (5)$$

called the amplification parameter (AP), which can be shown to be rotationally invariant (Kuzmin et al., 2010; Dodds, 2010, pers. comms.; Wannamaker, 2010, pers. comms.). Since the amplification parameter does not depend on the orientation of the sensor, it negates the post-acquisition need to correct for the sensor orientation with the AirMt system.

For both ZTEM and AirMt systems, the time series of the magnetic fields are recorded at fixed sampling rates, and the data are binned and processed to generate in-phase and quadrature transfer functions in the frequency-domain (i.e., tippers for ZTEM, amplification parameter for AirMt). The lowest frequency of the transfer functions depend upon the speed of the airborne platform, and the highest frequency depends on the sampling rate. For helicopter-borne or fixed-wing ZTEM and helicopter AirMt systems, transfer functions are typically obtained at five or six frequencies from 25 Hz to 600 Hz, giving skin depths ranging between 600 m and 2000 m for typical terrain conductivities.

Instrumentation

For helicopter surveys, the ZTEM and AirMt systems are carried as an external sling load, and are independent of the helicopter (Figure 1 and Figure 2). The ZTEM receiver coil is a 7.4 m diameter air-core loop sensor that measures the vertical magnetic field. The AirMt receiver coil array measures

three components of the magnetic field using three mutually perpendicular, 3.04 m diameter air-core loops. ZTEM and AirMt receiver coils use a patented suspension system mounted inside a fibreglass shell to attenuate the majority of vibrations. The receiver coil arrays are nominally towed from the helicopter by a 90 m long cable, and are flown with a nominal ground clearance of 80 m. Altitude positioning of the receiver coil array is enabled by GPS antennas mounted on the frame in combination with GPS and radar onboard the helicopter. For both ZTEM and AirMt, the magnetic field time-series are measured with a 2 kHz sampling frequency.

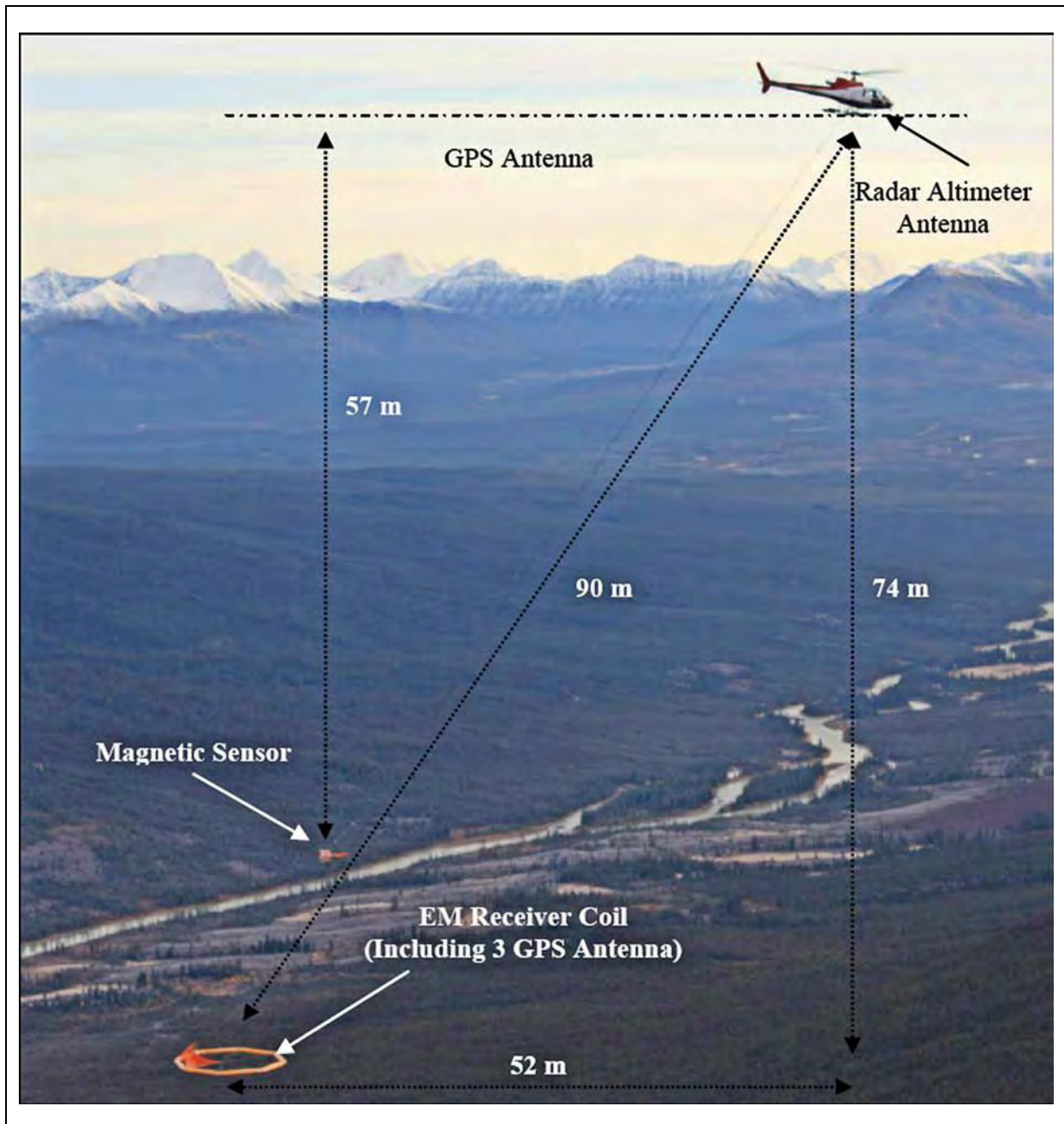


Figure 1. ZTEM (Z-Axis Tipper ElectroMagnetic) system configuration.

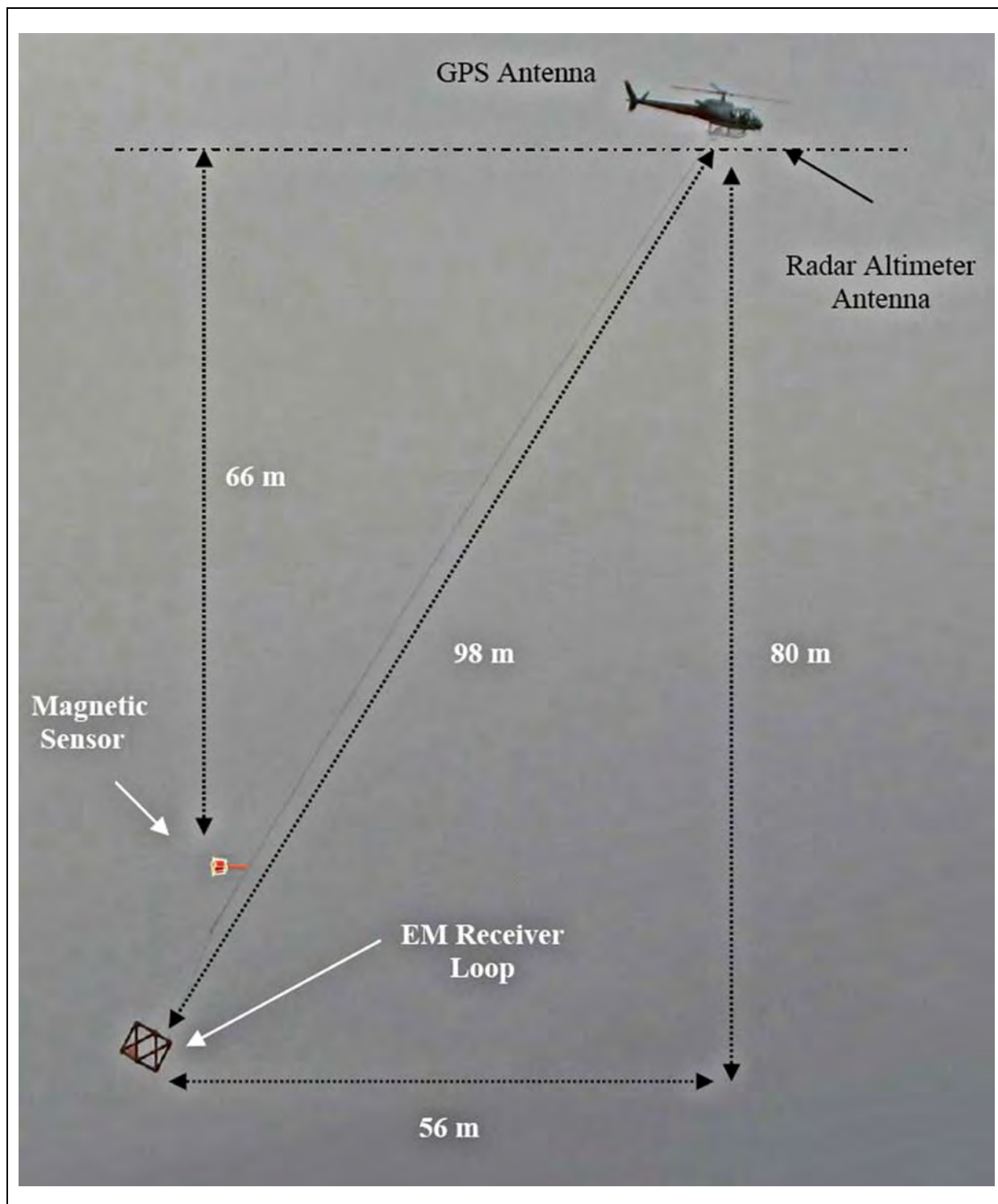


Figure 2. AirMt (Airborne Magnetic Tensor) system configuration.

The base station for these systems is typically the AirMt sensor, consisting of three mutually perpendicular, 3.04 m diameter air-core loops, as shown in Figure 3. The base station provides a reference field which when processed with the airborne receiver coil data, produces the appropriate transfer functions which are output at 2.5 Hz, or approximately 10 m sample intervals.



Figure 3. ZTEM and AirMt base station sensor.

Interpretation

Given the use of the same assumption of plane wave source terms, modelling and inversion for ZTEM and AirMt data is similar to that of MT. However, unlike MT surveys, ZTEM and AirMt surveys typically contain hundreds to thousands of line kilometres of data with measurement locations every few metres, covering areas thousands of square kilometres in size. Geotech's standard products for ZTEM and AirMt include total divergence and phase rotation grids, and 2D Gauss-Newton inversion based upon modifications to algorithms by Wannamaker et al. (1987), de Lugao and Wannamaker (1996), and Tarantola (1987). Third parties provide additional products such as 2D pseudo-sections by Karous-Hjelt filtering (e.g., Sattel et al., 2010) or 2D Occam inversions based on their own modifications of algorithms by Wannamaker et al. (1987) and Constable et al. (1987). Holtham and Oldenburg (2010) introduced 3D ZTEM inversion based on modifications of the 3D MT inversion by Farquharson et al. (2002). In the subsequent case study for both ZTEM and AirMt, our 3D MT inversion analog is that of Zhdanov et al. (2011).

Case study – Nebo-Babel, West Musgrave, Western Australia

Geology

Most world-class deposits of nickel and platinum-group elements (PGE) are found in mafic igneous rocks of Proterozoic age that are part of exceptional large igneous provinces (LIPs). The West Musgrave Block, located in central Australia, is one such example, but one where the most of the prospective ground lies beneath regolith. Access for explorers has been limited in line with the wishes of the traditional landholders. However, access has become more widespread in recent years. One example of early success in the area was WMC's (now BHP Billiton) surface geochemistry-led discovery of the Nebo-Babel Ni-Cu-PGE deposit in 2000 (Groves et al., 2007). The discovery of other large deposits in the West Musgrave region requires the identification, below cover, of the crustal-scale feeder systems of the most voluminous mafic-ultramafic magmatic events. This directly feeds back to the aforementioned need for airborne geophysical techniques capable of deep penetration beneath conductive cover, and 3D imaging of the large-scale data sets acquired.

For Nebo-Babel, drill intersections include 106.5 m at 2.4% Ni, 2.7% Cu, and 0.2g/t PGE; and a resource of about 1 million tonnes contained Ni and 1 million tonnes contained Cu+Co has been released. The Nebo-Babel deposit is hosted within a concentrically-zoned, tube-like gabbro-norite intrusion (1078 Ma) that has a 5 km east-west extent, a 1 x 0.5 km plan view cross section, and a shallow WSW-plunge (Figure 4). The gabbro-norite has intruded felsic orthogneissic country rocks of

amphibolite to granulite facies metamorphic grade and is offset along the north-south Jameson Fault, which separates the Babel and Nebo deposits that are of similar morphology. Babel is a large, generally EW to SW striking, mainly low-grade disseminated deposit that subcrops through thin sand cover to the east but plunges under more than 400 m of country rock and remains open to a depth of 600 m (Figure 4b). Nebo, 2 km to the northeast, is buried under a few metres of aeolian dune sand and is smaller than Babel, but contains a number of high grade massive sulphide pods that are mainly found in the upper part of the intrusion. It extends at least 1.8 km east-west, but its eastern limit and lower intrusive contact (inferred at >600 m – Figure 4b) have not yet been drill-defined. The deposits were discovered using deflation lag sampling on a 1 km x 0.5 km grid drill pattern. However, strong magnetic, electromagnetic, and gravity anomalies highlight the massive and disseminated mineralization in the deposit. Nebo-Babel has a number of features in common with other Ni-Cu-PGE deposits hosted in dynamic magma conduits (e.g., Voisey's Bay, Canada), such as multiple magma pulses and sulphide entrainment from depth, rather than in-situ sulphide segregation (Seat et al., 2007, 2009).

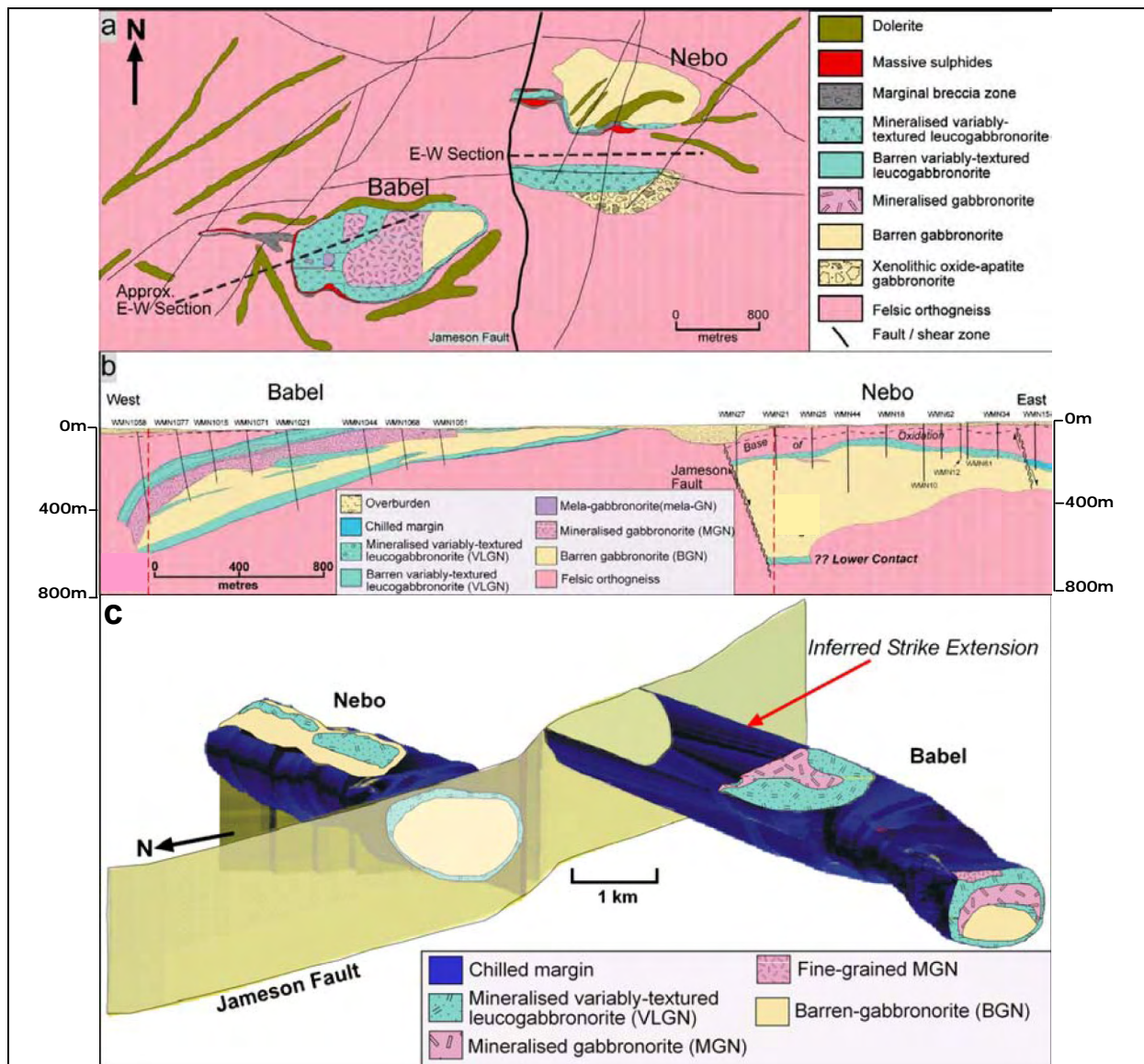


Figure 4. a) Surface projection of the gabbro-norite rock units, mineralized domains, and major structural elements at West Musgrave. b) Longitudinal east-west section through the Nebo-Babel intrusion. c) South-east facing three-dimensional geological model showing spatial and morphological relationships between the Nebo and Babel parts of the intrusion (after Seat et al., 2007).

ZTEM and AirMt Results

Under agreement between Geotech and BHP Billiton, both ZTEM and AirMt surveys were flown over the Nebo-Babel deposit area of West Musgrave (Figure 5 and Figure 6). Previous airborne systems flown over the deposits have included GEOTEM airborne electromagnetics and FALCON airborne gravity gradiometry. A total of 541 line km of ZTEM data and 574 line km of AirMt data were acquired along both east-west and north-south flight lines (Figure 6). The survey area has minimal topographic relief, varying from 460 to 494 m above sea level. The ZTEM receiver coil was flown with a nominal ground clearance of 78 m. ZTEM data were acquired at six frequencies; 25 Hz, 37 Hz, 75 Hz, 150 Hz, 300 Hz, and 600 Hz. The AirMt receiver coil array was flown with a nominal ground clearance of 78 m. AirMt data were acquired at six frequencies; 24 Hz, 38 Hz, 75 Hz, 150 Hz, 300 Hz, and 600 Hz. Total magnetic intensity (TMI) data were also acquired using a caesium magnetometer for both surveys. Figure 7 shows the reduced-to-pole (RTP) magnetic response, which highlights a number of features, including a) a linear NS magnetic low over the Jameson fault, possibly due to alteration or overburden fill, b) NE-trending magnetic lineaments, which mostly correlate with late mafic dolerite dykes (Figure 7), c) a partial ring-like magnetic high centred on a magnetic low over the Babel deposit, that is likely responding to the increased sulphides on the outer perimeter of the intrusive, and d) a broad magnetic high that is largely centred with the Nebo intrusive that likely indicates increased magnetite content in the gabbro-norite body.

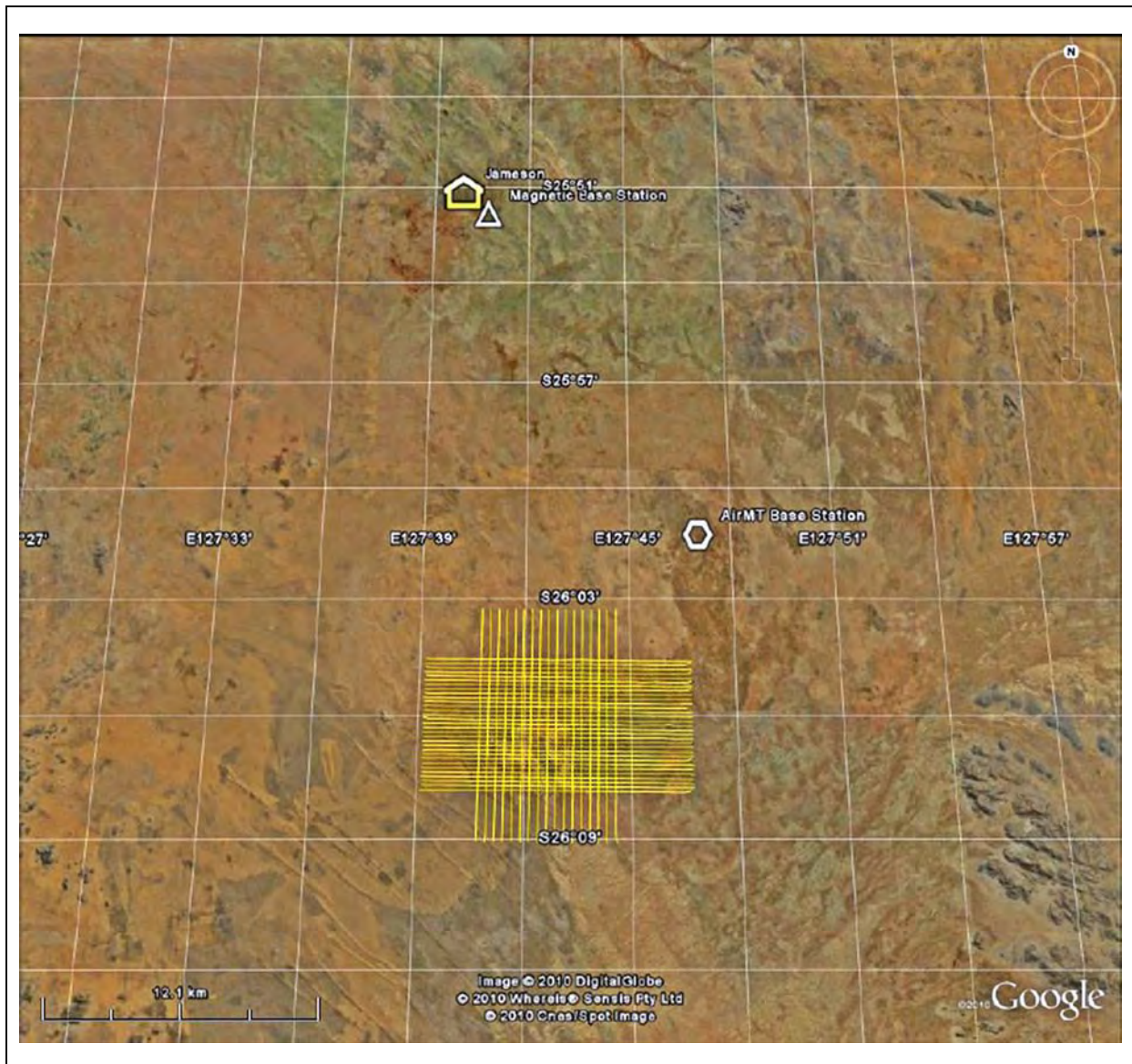


Figure 5. ZTEM and AirMt survey flight lines and base station locations over Nebo-Babel.

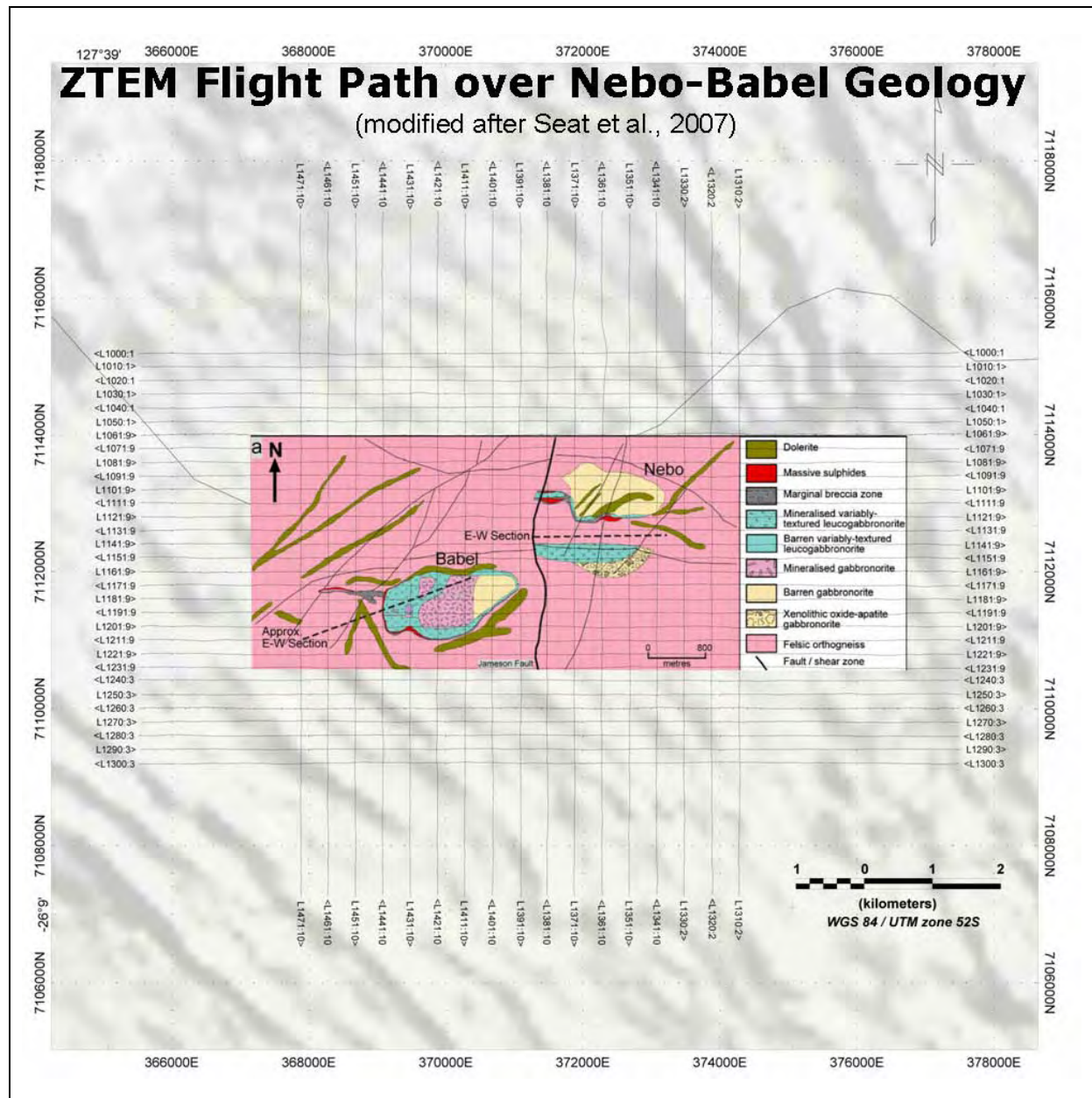


Figure 6. ZTEM and AirMt flight lines over Nebo-Babel geology (modified after Seat et al., 2007).

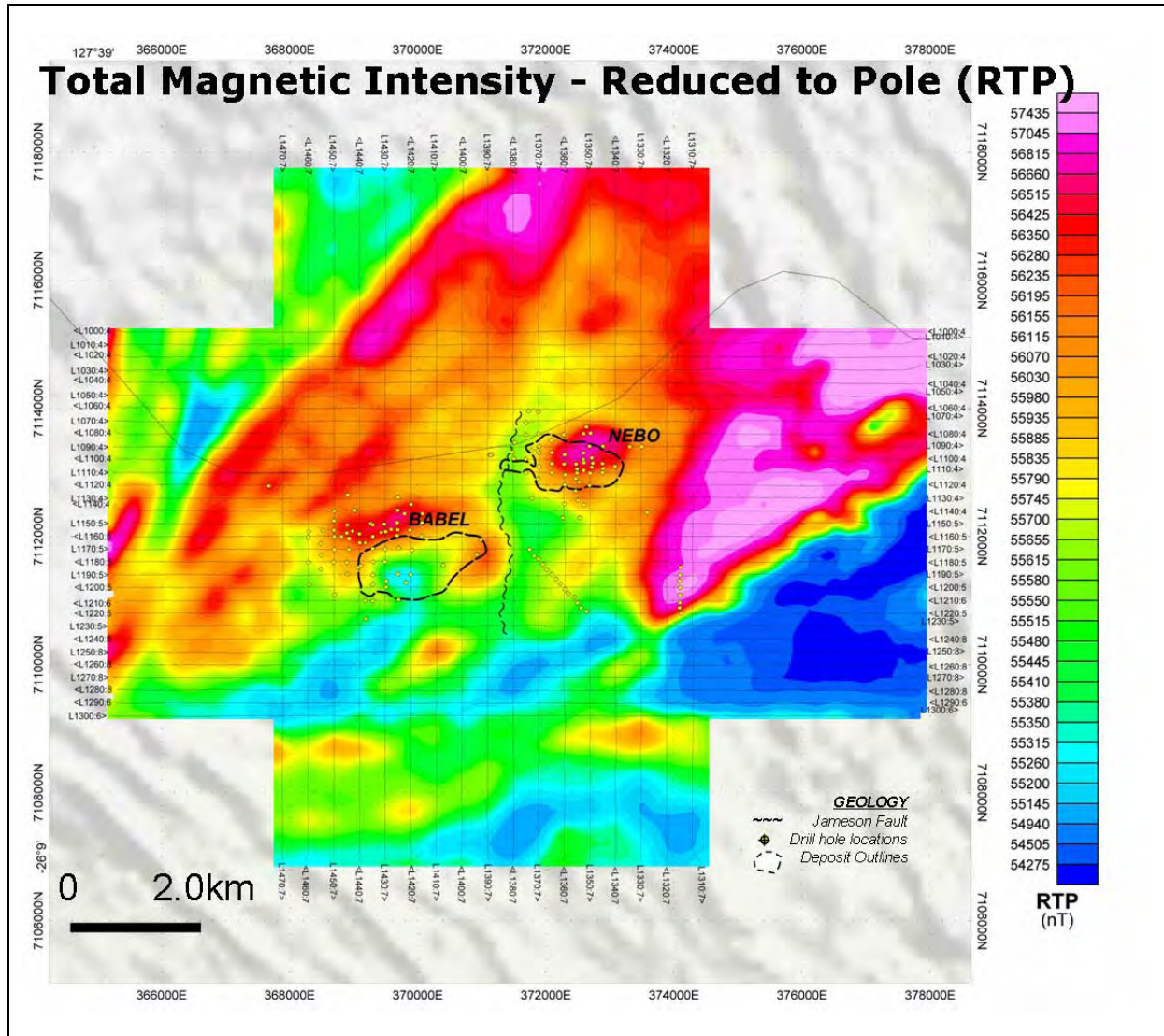


Figure 7. Total magnetic intensity (TMI) – reduced to pole (RTP).

Examples of the 75 Hz ZTEM and AirMt data are shown in plan in Figure 8, Figure 9 and Figure 10. Multi-frequency profiles of the ZTEM and AirMt data are also presented in Figure 11, for a representative north-south flight line (L1430) across the Babel deposit.

To present data from both tipper components in one image, and to compensate for the cross-over nature of ZTEM data (e.g., Figure 11 a and b), the total divergence (DT) is introduced as the horizontal derivatives of the tipper components:

$$DT = \frac{\partial T_{zx}}{\partial x} + \frac{\partial T_{zy}}{\partial y}, \quad (6)$$

and is derived for each of the in-phase and quadrature components at individual frequencies. These in turn allow for minima-over-conductors and maxima-over-resistive zones. DT grids for each of the extracted frequencies were generated accordingly, using a reverse colour scheme with warm colours over conductors and cool colours over resistors (e.g., Figure 8).

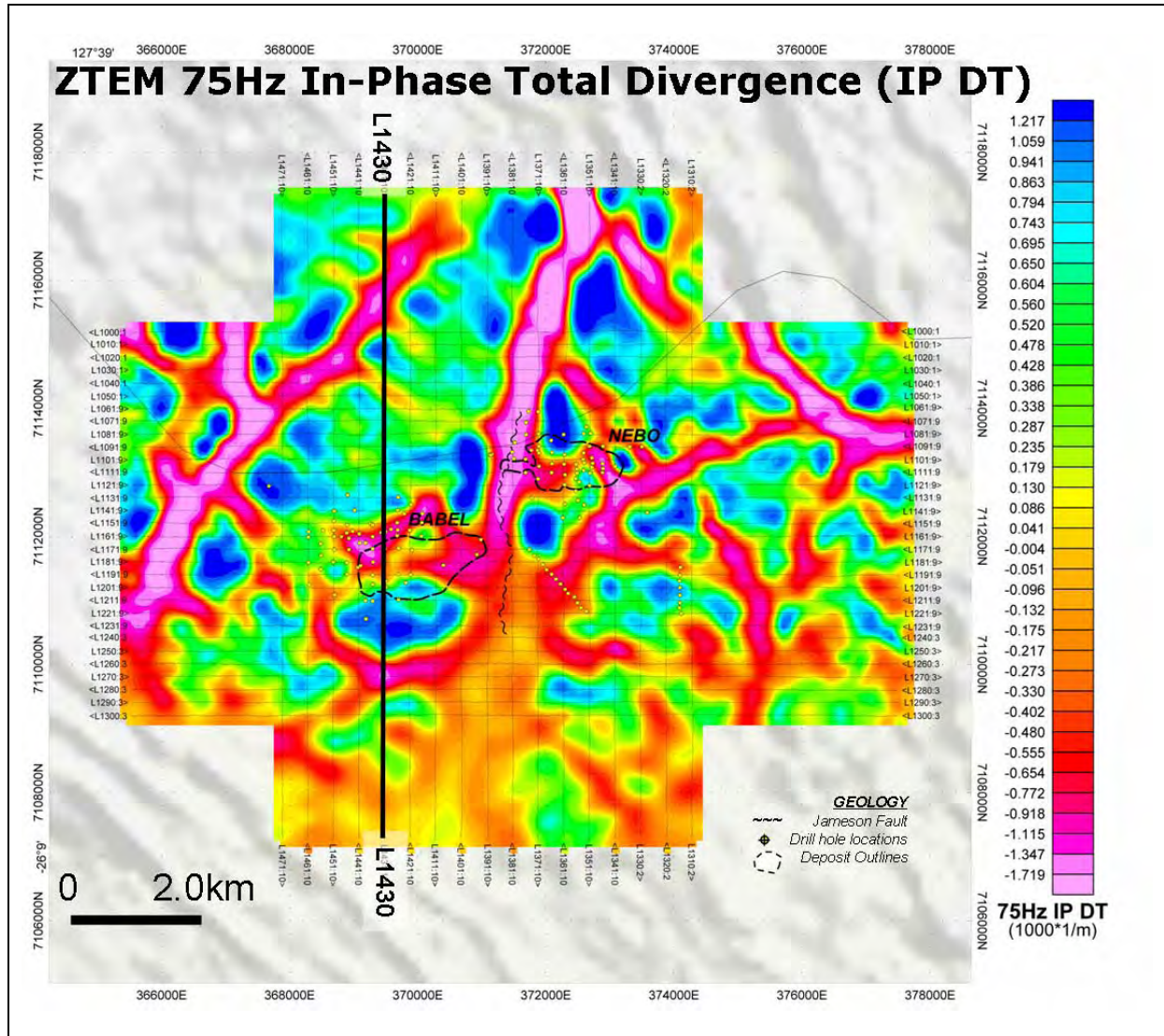


Figure 8. ZTEM 75Hz In-Phase Total Divergence (DT).

Alternatively, a 90 degree phase rotation (PR) can be applied to the grids of each tipper component. This transforms bipolar (i.e., cross-over) anomalies into single pole anomalies with a maximum over conductors, while preserving long wavelength information. The two orthogonal grids are then added together:

$$TPR = PR(T_{zx}) + PR(T_{zy}) \quad (7)$$

to obtain a total phase rotated (TPR) grid for each of the in-phase and quadrature components (e.g., Figure 9).

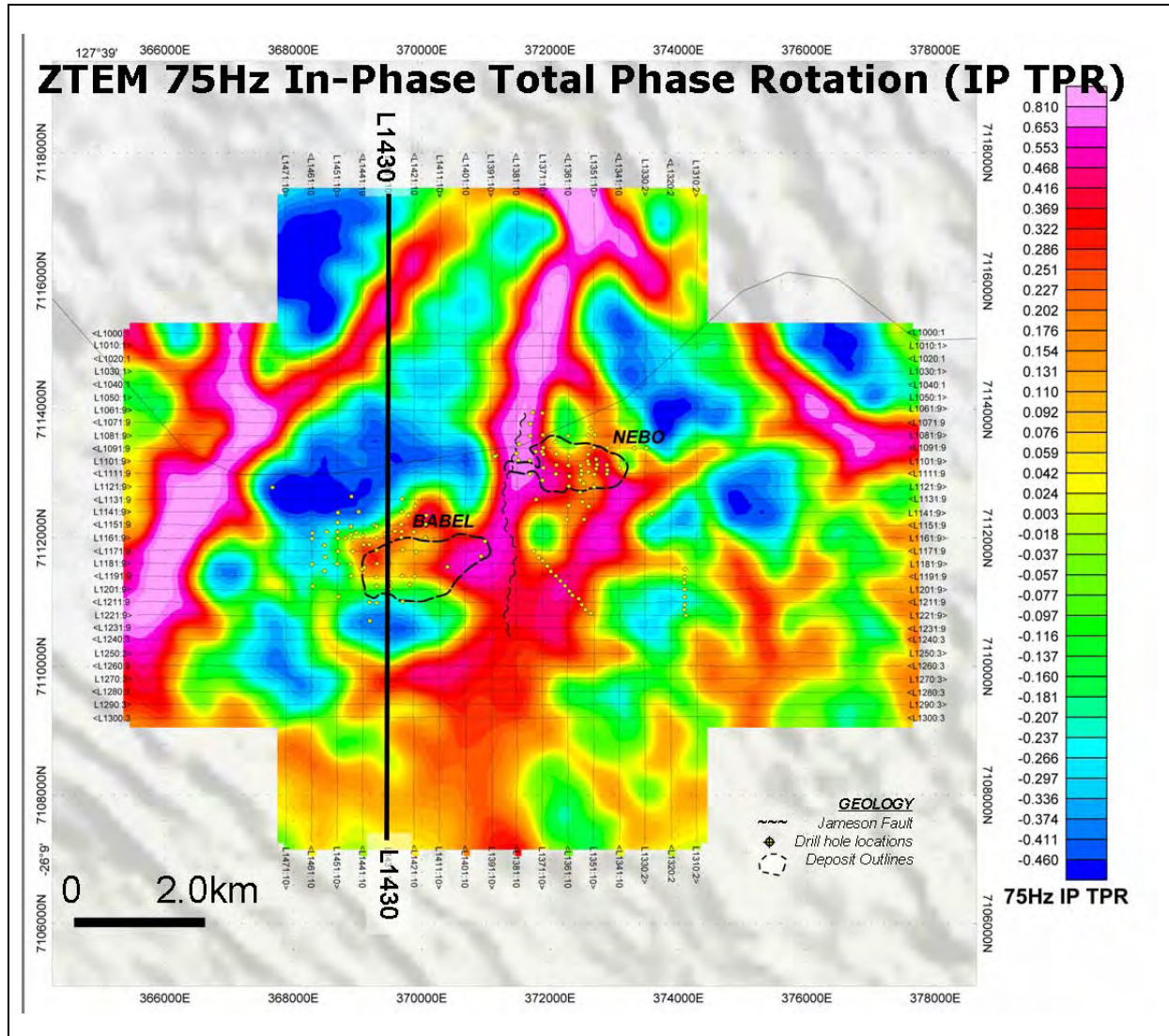


Figure 9. ZTEM 75Hz In-Phase Total Phase Rotation (TPR).

In contrast to the cross-over behaviour demonstrated by ZTEM tipper data, the AirMt amplitude parameter displays peak maxima and minima across conductive and resistive zones, respectively. Hence, no further processing of the AirMt data are required for plan-view presentation, as shown in the 75 Hz AP image in [Figure 10](#).

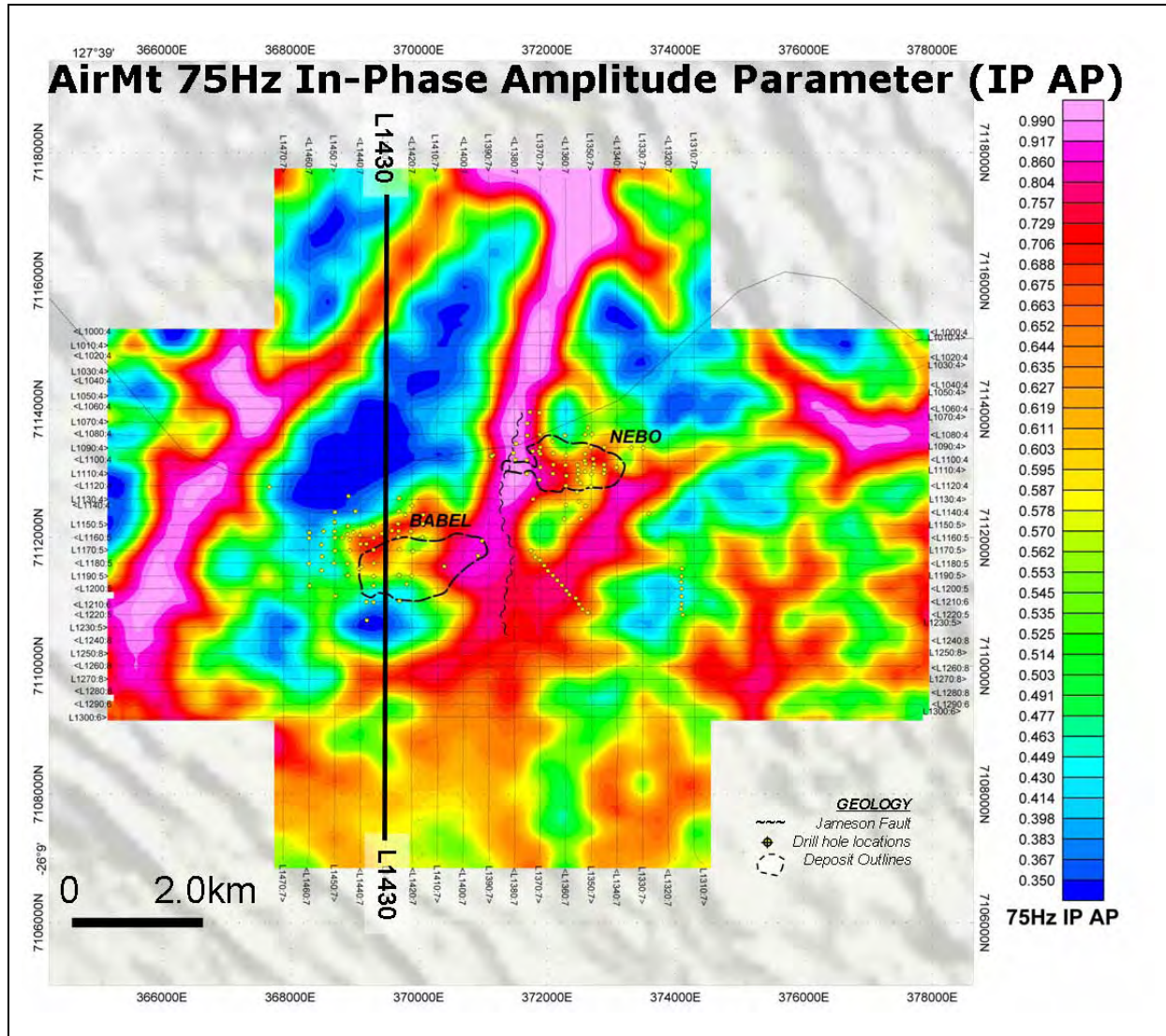


Figure 10. AirMt 75Hz In-Phase Amplitude Parameter (AP).

Comparing the three images in Figure 8, Figure 9, and Figure 10, the ZTEM DT, TPR and AirMt AP results are remarkably consistent and highlight similar geologic features defined in the magnetic results, such as a) the conductive Jameson fault that extends north and south of the survey area, b) a ring-like conductive anomaly that partially coincides with the Babel deposit and, c) a smaller conductive anomaly over Nebo deposit that appears to coincide with the known massive sulphide lenses. Other ZTEM-AirMt conductive lineaments that are defined, in part, appear to correlate with either magnetic lineaments (e.g., Figure 7) or else mapped faults (Figure 6), and may therefore indicate increased porosity or clay in the faults or possible near-surface paleochannel or overburden relief structures (Greg Walker, 2011, pers. comm.).

What seems clear from these results is that the cross-cutting behaviour in the ZTEM and AirMt clearly points to a 3-dimensional environment at Nebo-Babel. While the DT, TPR and AP grids can be used for qualitative analysis, neither they nor the raw data profiles themselves (Figure 11) are able to easily provide any quantitative information about these 3D structures. For this, inversion modelling is required.

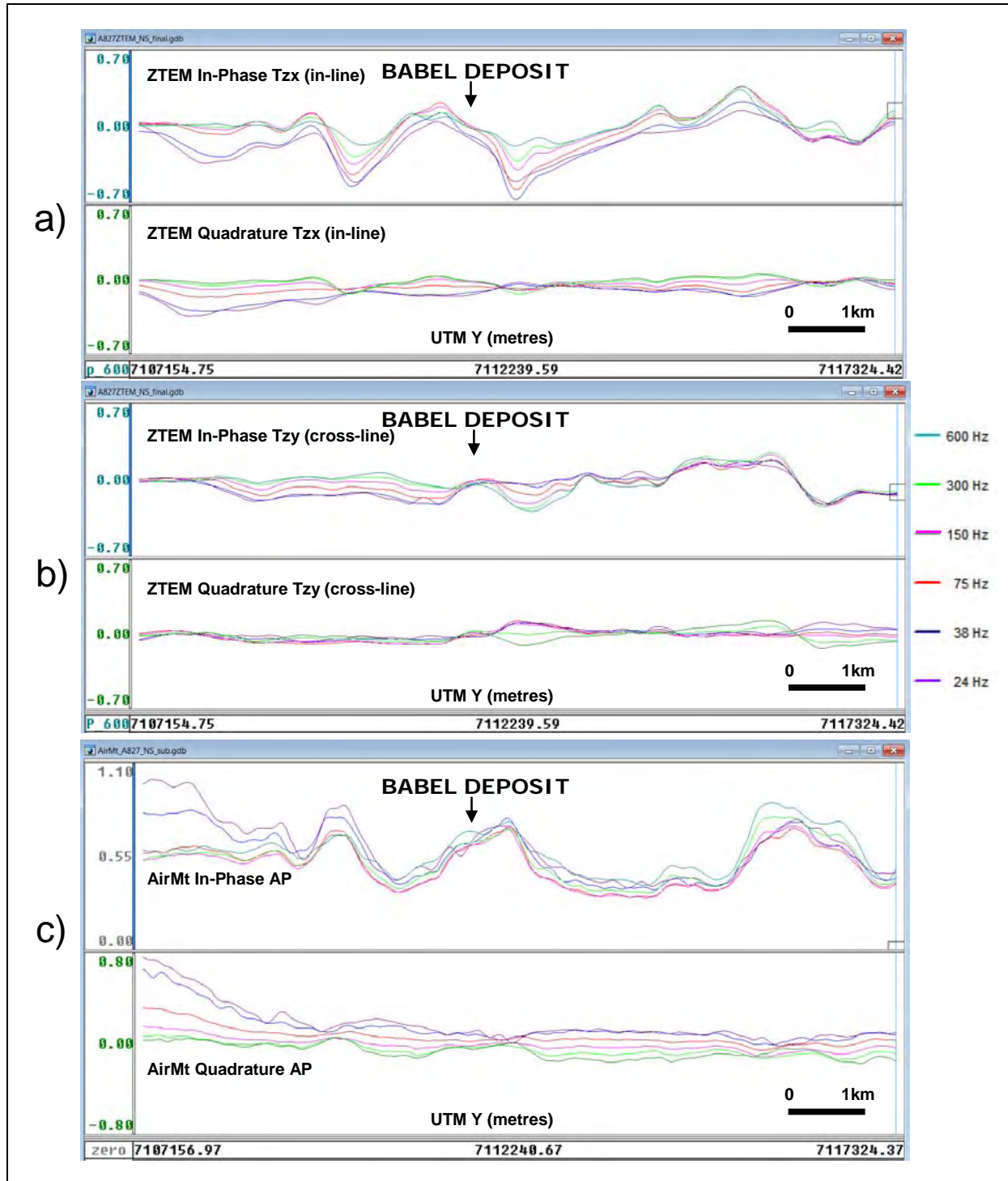


Figure 11. Multi-frequency (24-600Hz) In-Phase and Quadrature data profiles for L1430 a) ZTEM In-line (Tzx) component (XIP & XQD), b) ZTEM Cross-line (Tzy) component (YIP & YQD), and c) AirMt Amplitude Parameter (AIP & AQD).

Geotech's 2D inversion is based on modifications to the MT modelling algorithm of Wannamaker et al. (1987), with sensitivities by de Lugao and Wannamaker (1996) in an iterative Gauss-Newton method (Tarantola, 1987). The algorithm is programmed to operate in serial fashion and runs on desktop computers. Each line is inverted independently. For 2D ZTEM inversion, this software only inverts the inline tipper data and assumes orthogonal and infinite strike length of all targets. For 2D AirMt inversion, the software inverts the amplification parameter assuming orthogonal and infinite strike length of all targets. This approximation is reasonable if the geological structures have strike lengths

orthogonal to the flight line direction in the order of a skin depth; i.e., greater than the footprint or sensitivity of the ZTEM or AirMt systems. In both cases, the 2D ground topography and the air-layer thickness below the receiver coil array are accounted for. The inversions require *a priori* starting models that are reasonably close to the true half-space resistivity. At Nebo-Babel, 300 ohm-m was chosen for the starting half-space resistivity based on available ground AMT survey results provided by BHP Billiton.

For the Nebo-Babel 2D inversions, model convergence RMS fits of 1.0 or less were achieved in 4 to 5 iterations, with data errors of 0.03 to 0.05 for ZTEM whereas considerably higher data errors of 0.1 to 0.22 were required for AirMt data fitting. This relative inability to properly fit the data in 2D is interpreted to reflect the greater sensitivity of AirMt AP measurement to 3D distortion, relative to the ZTEM in-line component data, but also an indication the 3-dimensionality of the Nebo-Babel geologic environment. Similarly, 2D inversions of data along north-south lines appear to best highlight the Nebo and Babel deposit responses, due to their dominant EW strike, with the ZTEM models seemingly more successful than AirMt. On the other hand, neither of the technologies' 2D inversions along east-west lines (not shown) appears to have successfully resolved either deposit, possibly due to the dominance of the Jameson Fault signature. Panels a and b of [Figure 12](#) presents 2D inversions of ZTEM and AirMt data, respectively, along the north-south L1430 profile which crosses the Babel deposit. The approximate outline of the intrusion is also shown.

Technolmaging's 3D modelling is based on the 3D integral equation method (Hursán and Zhdanov, 2002), and the inversion itself uses a regularized re-weighted conjugate gradient (RRCG) method with focusing stabilizers (Zhdanov, 2002). Unlike smooth regularization, focusing enables the recovery of 3D models with higher contrasts and sharper boundaries. This is an analog of the 3D MT inversion described by Zhdanov et al. (2011). The software is fully parallelized for running on cluster computers, meaning that it can be scaled to invert very large survey areas. Panels d and e of [Figure 12](#) show vertical cross-sections from the 3D inversions of ZTEM and AirMt data, respectively, along the L1430 north-south profile across the Babel deposit.

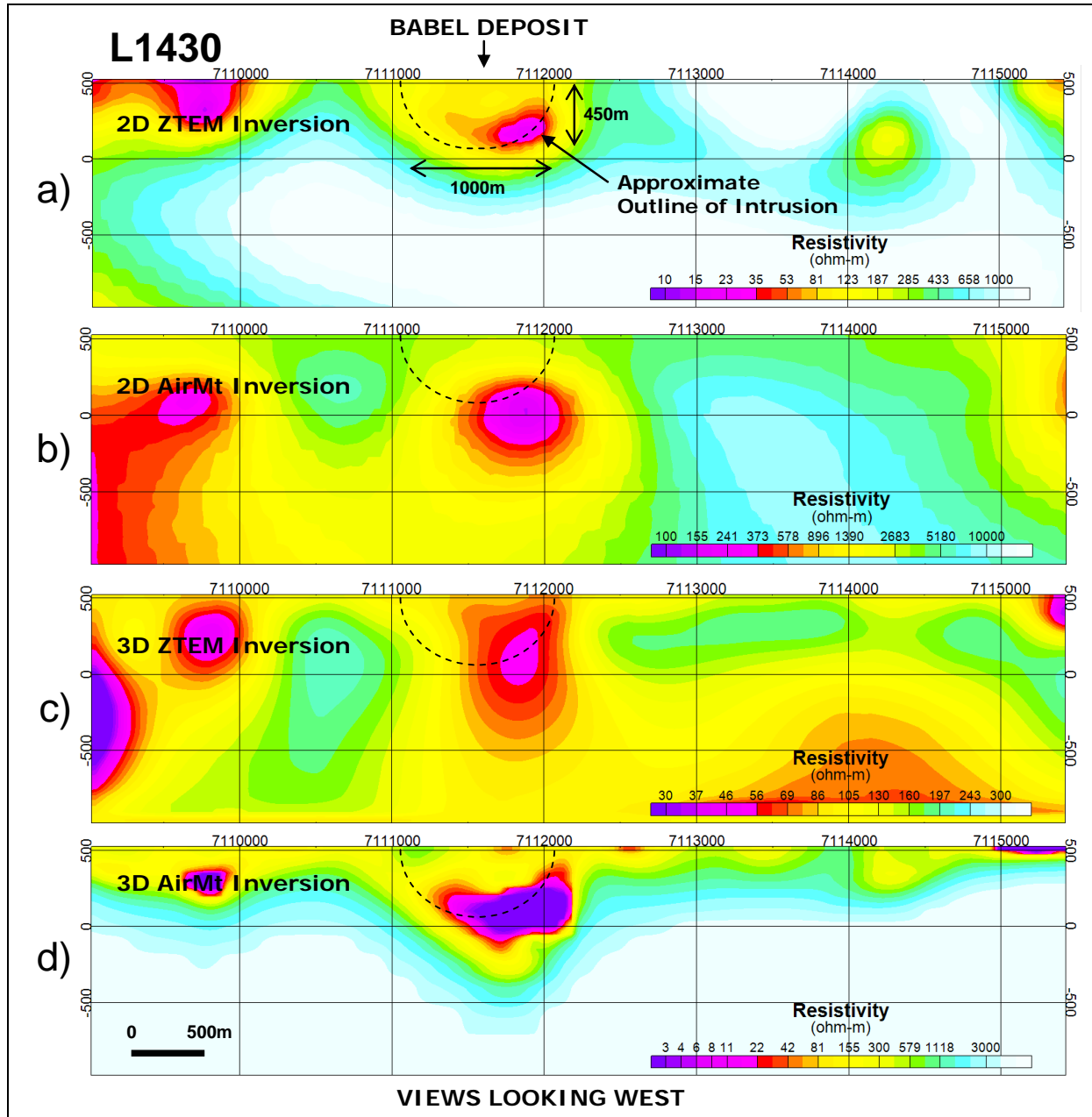


Figure 12. Resistivity cross-sections for L1430 obtained from: a) ZTEM 2D Inversion, b) AirMt 2D Inversion, c) ZTEM 3D Inversion, and d) AirMt 3D Inversion.

Discussion of Results

Comparing the 3D and 2D inversion cross-sections in Figure 12, at first glance, all four appear to show a reasonably well defined anomalous conductive response over the Babel deposit, with the maximum conductivity generally offset towards the north edge and base of the intrusive. Interestingly, this increased conductivity at depth is not easily supported geologically yet is a consistent feature in all 4 models. However, the overall shape and size/extent of the semi-concentric intrusive appear to be better resolved in the 2D ZTEM, and particularly, in the 3D ZTEM and AirMt model images, the lattermost which features the best resolved and most contrasted conductivity anomaly of the four. The generally lower resistivity values found in the gabbro-norite are also consistent with ground AMT results (Greg Walker, 2011, pers. comm.). In contrast, the 2D AirMt model appears to overestimate the target depth, relative to the remaining three inversions, but this may also reflect the poorer quality model-misfits. The increased near-surface conductivity observed in all four model sections that extends south of Babel is consistent with thicker, higher conductance overburden cover that was also observed in ground AMT results.

Figure 13, Figure 14, Figure 15, and Figure 16 provide representative resistivity depth-slices from the 2D and 3D ZTEM and AirMt inversion models for north-south lines over Nebo Babel. Unlike the cross-sectional views, these plan maps clearly highlight the improved imaging of the 3D inversion results as compared to the 2D – in particular: A) Although 2D ZTEM resistivity slice in Figure 13 shows anomalous conductivity over both deposits, across Babel, in particular, the east-west strike length appears to be over-exaggerated, likely due to effects of footprint side-scanning in the 2D inversion; more importantly, the Jameson Fault is not defined, due to fact that it is parallel to the north-south line orientation chosen for the 2D inversions;. B) Although the 2D AirMt resistivity slice in Figure 14 arguably better defines the NNE-SSW Jameson Fault, relative to ZTEM 2D, neither the Babel nor the Nebo deposits are particularly well defined or highlighted in plan; on the other hand, the strike extension of Babel to the southwest is consistent with the geologic plunge of the deposit. C) Of the four images shown, the 3D ZTEM inversion resistivity slice in Figure 15 shows anomalous conductivity that is not only more focused, with shorter strike-lengths indicated, and better centred directly over both Nebo and Babel, but also readily images the Jameson Fault, a result that had been absent in previous 2D inversion results; D) The 3D AirMt inversion resistivity depth-slice in Figure 16 is somewhat coarser than the other 3 inversion images, but nonetheless displays the best contrasted anomalous conductivities over Nebo, Babel and the Jameson Fault; it also appears to be the least impacted of the 3 inversions by the thickening conductive overburden blanket in the south survey area.

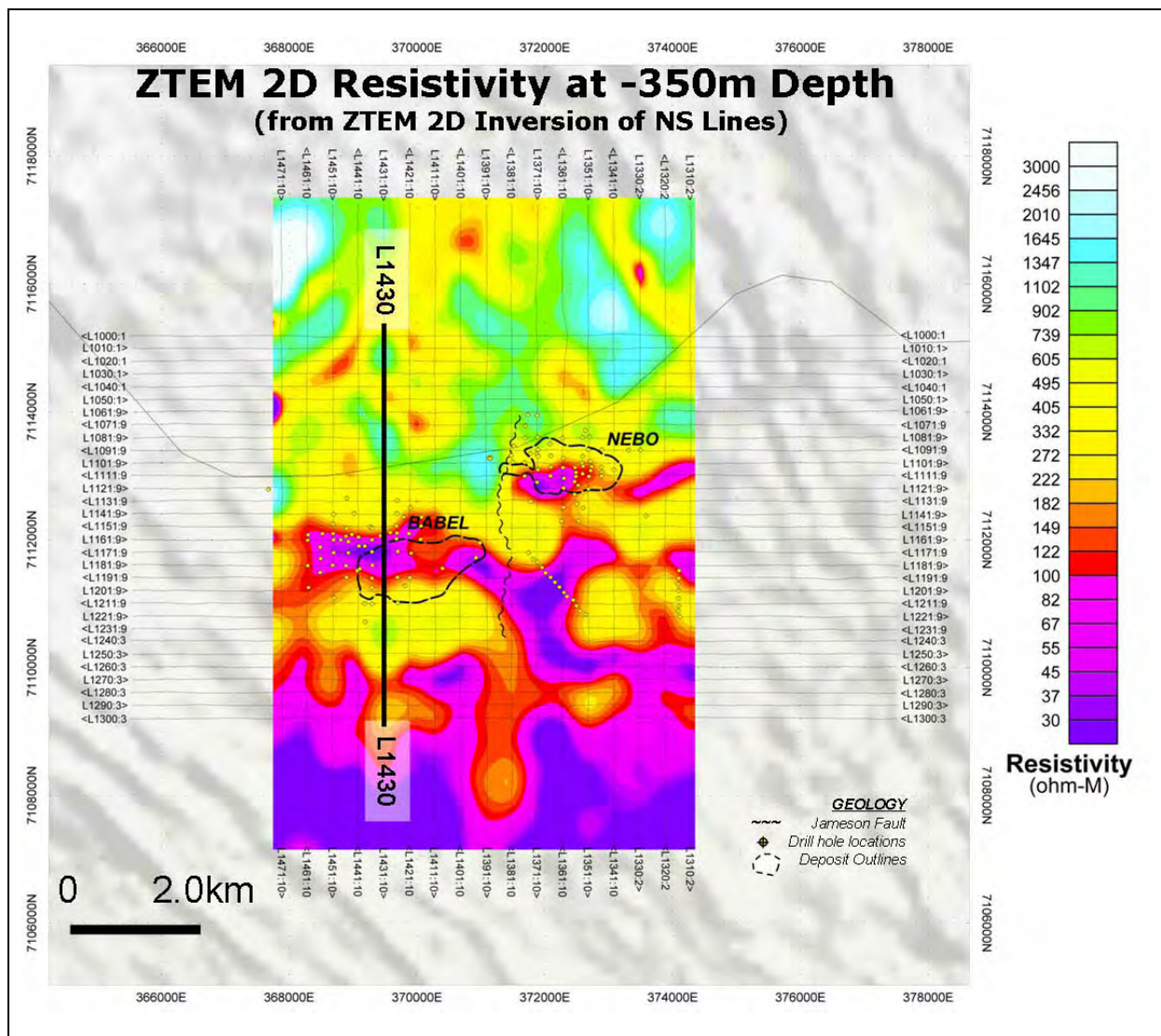


Figure 13. Resistivity depth-slice at -350 m from 2D ZTEM inversions.

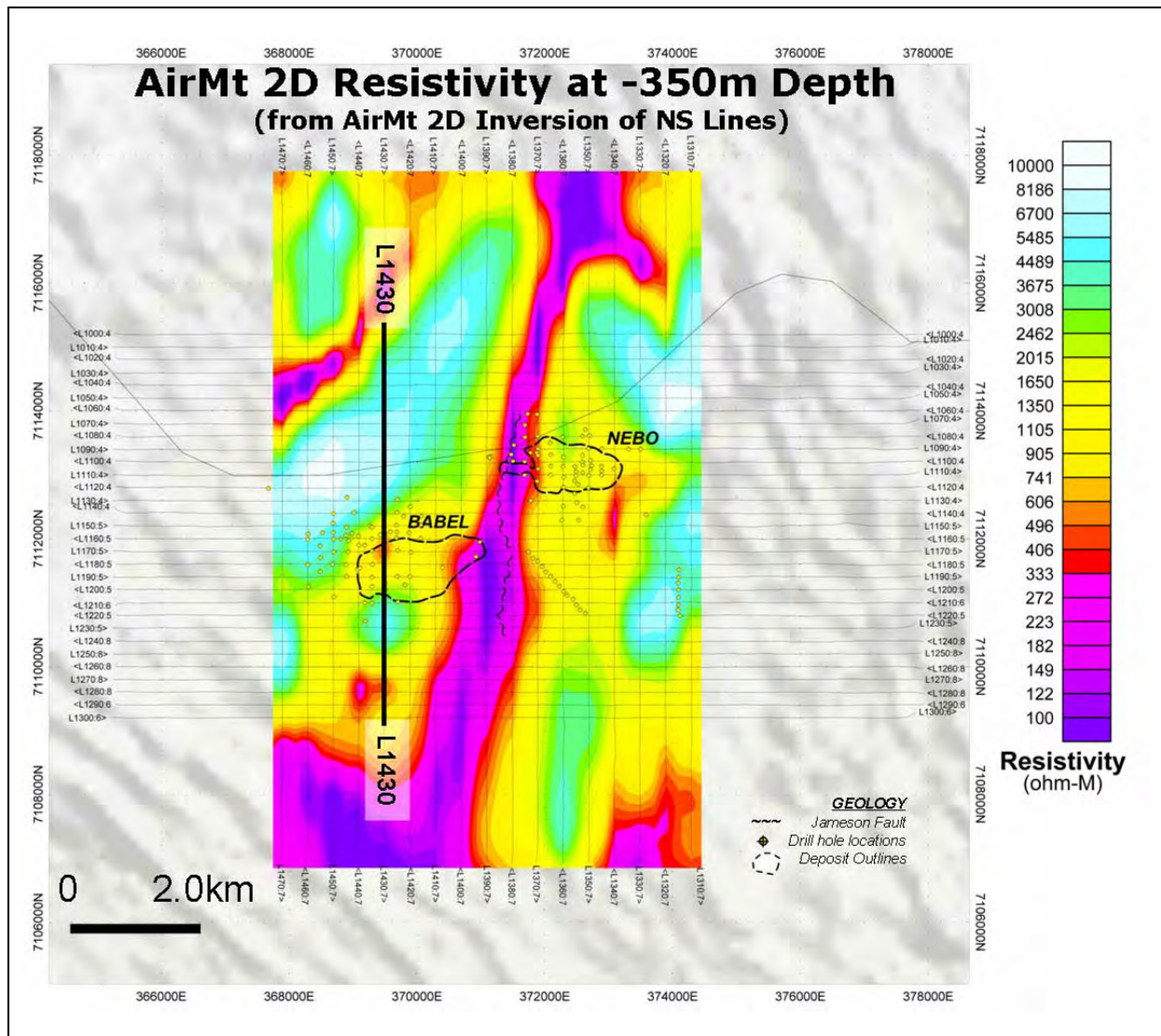


Figure 14. Resistivity depth-slice at -350 m from 2D AirMt inversions.

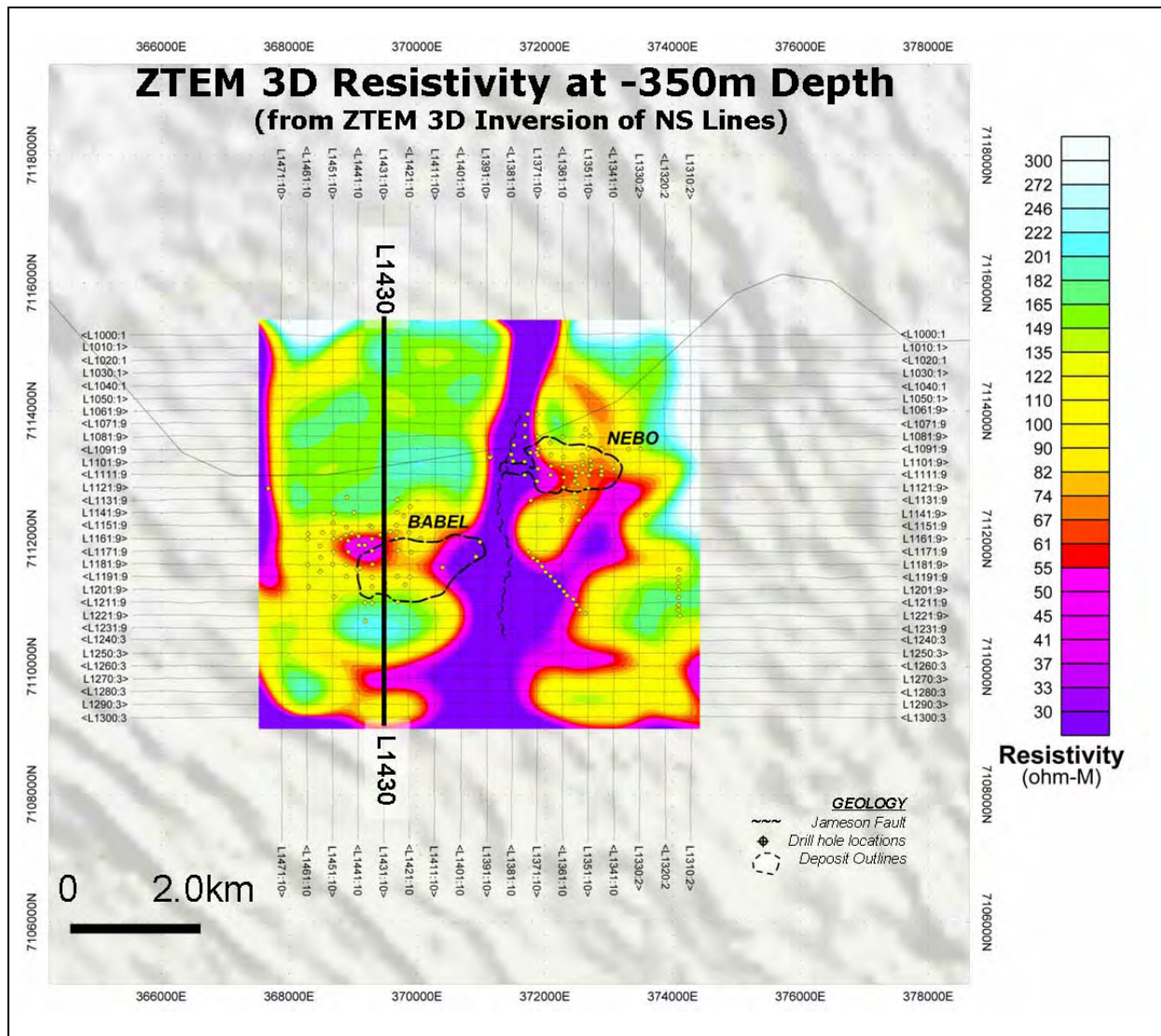


Figure 15. Resistivity depth-slice at -350 m from 3D ZTEM inversion.

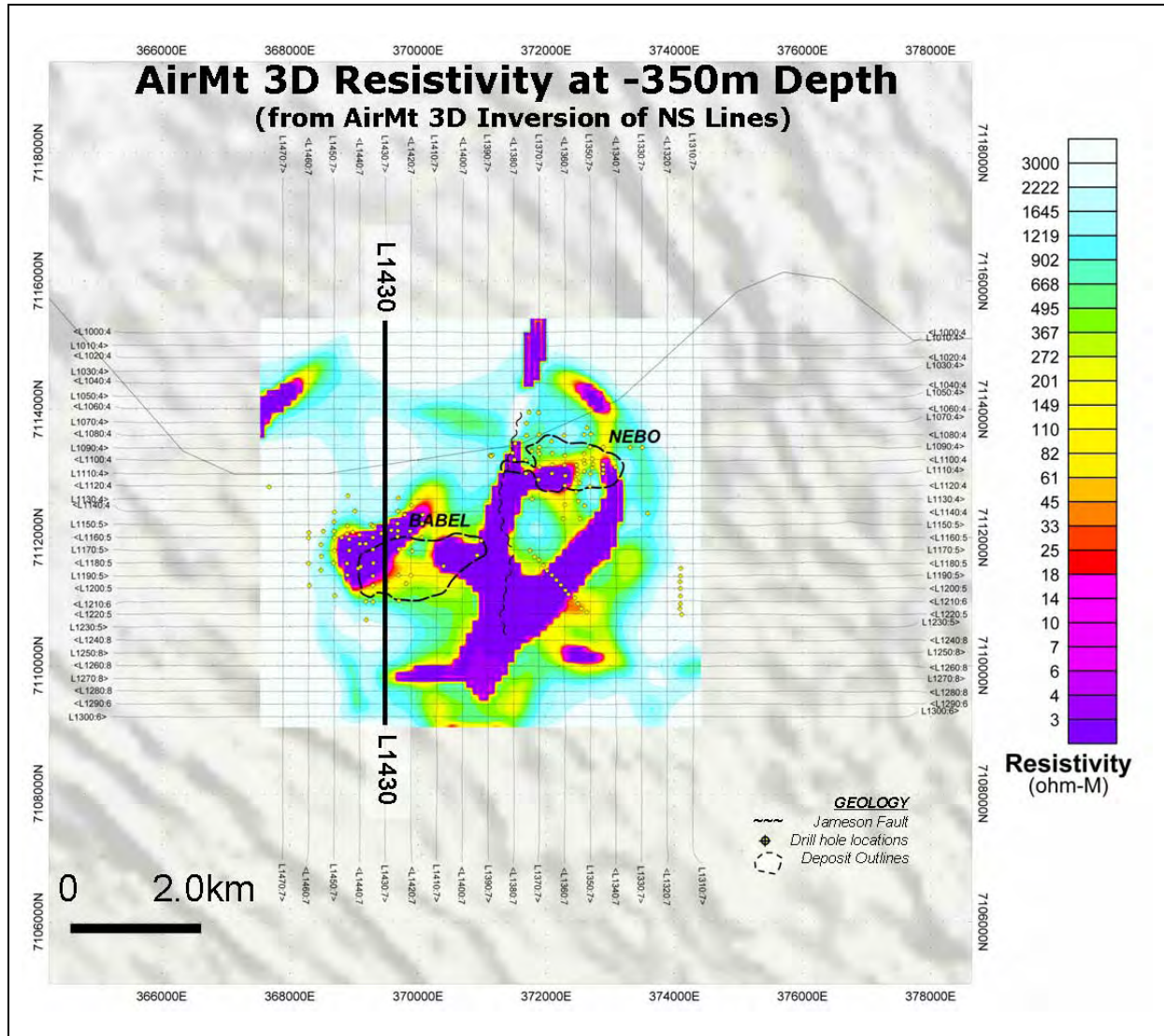


Figure 16. Resistivity depth-slice at -350 m from 3D AirMt inversion.

Conclusions

Given global industry trends towards deeper exploration under cover, ZTEM and AirMt represent practical airborne electromagnetic methods for mapping conductivity to depths in excess of 1 km in terrain of suitable conductivity. As ambient (natural) source electromagnetic methods, allowing a plane wave source to be reasonably assumed in most instances, ZTEM and AirMt data are derived from robust data processing techniques that enable 3D quantitative interpretation. Interpretation of both ZTEM and AirMt data is analogous to magnetovariational (MV) data, and in principle, similar to magnetotelluric (MT) data. We have demonstrated this with a case study involving the interpretation of over 500 line km of both ZTEM and AirMt data from BHP Billiton's Nebo-Babel Ni-Cu-PGE deposit in Western Australia's West Musgrave district.

The analyses of the ZTEM and AirMt survey results and their interpretation using 2D and 3D inversion have shown that both passive EM technologies map the subsurface geology and structure, based on lateral resistivity contrasts, seemingly equally well. Comparisons between ZTEM DT and TPR data images against the AirMt AP data image show strong similarities between both technologies, which is perhaps to be expected. On the other hand, although both ZTEM and AirMt display anomalous responses over the Nebo and Babel deposits, neither appears to resolve or differentiate the increased conductivity associated with the massive sulphides contained in them from more weakly conductive features in the surrounding geology, notably fault-structures and lithological features. This can possibly

be seen as an advantage by some in terms of geologic mapping of mineral deposit environments, or as a disadvantage by others in terms of the direct detection of mineral deposits themselves.

In contrast with visualizing the data on their own, the process of inversion appears to significantly improve the resolution and differentiation of the Nebo and Babel mineral deposits, particularly in cross-section, where the known deposit locations feature well defined conductive anomalies in the 2D and 3D inversion models for both ZTEM and AirMt. The airborne resistivity images also generally agree with those from ground resistivity surveys.

In plan, however, the weaknesses of the 2D inversions are highlighted, notably: a) the directional sensitivity of line orientation to geologic strike that affects the 2D ZTEM inversions to the greatest extent (i.e., Nebo-Babel is only properly imaged in NS lines and the Jameson Fault is only imaged in EW lines); and b) the more weakly contrasted 2D AirMt image that is due, in part, to its inherently smooth behaviour, but also because of lower model-data misfits that are, presumably, a reflection of greater sensitivity of the AirMt AP data measurement to 3D behaviour. In marked comparison to these 2D models, the 3D inversion images in plan appear to more clearly define distinctive anomalies over Nebo and Babel that can also be more easily differentiated from the NS and NE structures that are present. And in the case of ZTEM, the conductive anomalies over Nebo and Babel are better defined in the 3D inversion model; whereas for AirMt, the 3D inversion appears to produce the most contrasted anomalies over the deposits and fault zones, relative to 2D.

The ZTEM and AirMt case-study and inversion comparison at Nebo-Babel has not only served to introduce two new airborne EM survey applications but has also presented field results over a well known ore deposit in a typical Australian regolith environment. It has enabled the current interpretation methodologies to be clearly described and illustrated, including initial plan view data processing, 2D inversion and culminating in the more advanced 3D inversion approaches. This should be of great value to those contemplating similar surveys or those faced with interpretation of acquired data.

Acknowledgements

The authors acknowledge Geotech, TechnoImaging, and BHP Billiton for permission to publish. Gribenko and Zhdanov acknowledge support of the University of Utah's Consortium for Electromagnetic Modeling and Inversion (CEMI).

References

- Constable, S. C., Parker, R. L., and Constable, C.G., 1987, Occam's inversion: A practical algorithm for generating smooth models from electromagnetic sounding data: *Geophysics*, 52, 289-300.
- de Lugao, P. P., and Wannamaker, P.E., 1996, Calculating the two-dimensional magnetotelluric Jacobian in finite elements using reciprocity: *Geophysical Journal International*, 127, 806-810.
- Farquharson, C. G., Oldenburg, D. W., Haber, E., and Shekhtman, R., 2002, An algorithm for the three-dimensional inversion of magnetotelluric data: *SEG Expanded Abstracts*, 21, 649-652.
- Groves, D. I., Groves, I. M., Gardoll, S., Maier, W., and Bierlein, F. P., 2007, The West Musgrave – a potential world-class Ni-Cu-PGE sulphide and iron oxide Cu-Au province? Presented at AIG Conference, Perth.
- Holtham, E., and Oldenburg, D. W., 2010, Three-dimensional inversion of ZTEM data: *Geophysical Journal International*, 182, 168-182.
- Hursán, G., and Zhdanov, M. S., 2002, Contraction integral equation method in three-dimensional electromagnetic modeling: *Radio Science*, 37, doi: 10.1029/2001RS002513.
- Kaminski, V. F., Kuzmin, P., and Legault, J. M. 2010, AirMt – passive airborne EM system: Presented at 3rd CMOS-CGU Congress, Ottawa.

- Kuzmin, P. V., Borel, G., Morrison, E. B., and Dodds, J., 2010, Geophysical prospecting using rotationally invariant parameters of natural electromagnetic fields: WIPO International Patent Application No. PCT/CA2009/001865.
- Labson, V. F., Becker, A., Morrison, H. F., and Conti, U., 1985, Geophysical exploration with audiofrequency natural magnetic fields: *Geophysics*, 50, 656-664.
- Legault, J. M., Kumar, H., Milicevic, B., and Hulbert, L., 2009, ZTEM airborne tipper AFMAG test survey over a magmatic copper-nickel target at Axis Lake in northern Saskatchewan: *SEG Expanded Abstracts*, 28, 1272-1276.
- Pare, P., and Legault, J. M., 2010, Ground IP-resistivity and airborne SPECTREM and helicopter ZTEM survey results over Pebble copper-moly-gold porphyry deposit, Alaska: *SEG Expanded Abstracts*, 29, 1734-1738.
- Sattel, D., Thomas, S., and Becken, M., 2010, An analysis of ZTEM data over the Mt Milligan porphyry copper deposit, British Columbia: *SEG Expanded Abstracts*, 29, 1729-1733.
- Seat, Z., Beresford, S. W., Grguric, B. A., Waugh, R. S., Hronsky, J. M. A., Gee, M. A. M., Groves, D. I., and Mathison, C. I., 2007, Architecture and emplacement of the Nebo-Babel gabbro-norite-hosted magmatic Ni-Cu-PGE sulphide deposit, West Musgrave, Western Australia: *Mineralium Deposita*, 42, 551–581.
- Seat, Z., Beresford, S. W., Grguric, B. A., Mary Gree, M. A., and Grassineau, N. V., 2009, Re-evaluation of the role of external sulfur addition in the genesis of Ni-Cu-PGE deposits – evidence from the Nebo-Babel Ni-Cu-PGE deposit, West Musgrave, Western Australia: *Economic Geology*, 104, 521-538.
- Tarantola, A., 1987, *Inverse problem theory*: Elsevier, Amsterdam.
- Wannamaker, P. E., Stodt, J. A., and Rijo, L., 1987, A stable finite element solution for two-dimensional magnetotelluric modeling: *Geophysical Journal of the Royal Astronomical Society*, 88, 277-296.
- Ward, S., 1959, AFMAG – airborne and ground: *Geophysics*, 24, 761-787.
- Ward, S. H., O'Donnell, J., Rivera, R., Ware, G. H., and Fraser, D. C., 1966, AFMAG – applications and limitations: *Geophysics*, 31, 576-605.
- Zhdanov, M. S., 2002, *Geophysical inverse theory and regularization problems*: Elsevier, Amsterdam.
- Zhdanov, M. S., Smith, R. B., Gribenko, A., Čuma, M., and Green, A. M., 2011, Three-dimensional inversion of large-scale EarthScope magnetotelluric data based on the integral equation method – geoelectrical imaging of the Yellowstone conductive mantle plume: *Geophysical Research Letters*, 37, doi:10.1029/2011GL046953.

ZTEM airborne AFMAG survey results over low sulphidation epithermal gold-silver vein systems at Gold Springs, south eastern Nevada

Jean M. Legault
Geotech Ltd.
Aurora, ON, CAN
jean@geotech.ca

Shengkai Zhao
Geotech Ltd.
Aurora, ON, CAN
shengkai@geotech.ca

Ralph Fitch
High Desert Gold Corp.
Denver, CO, USA
ralphfitch@yahoo.com

SUMMARY

A ZTEM (Z-Tipper Axis Electromagnetic) helicopter AFMAG test survey was conducted in April, 2011, over the Gold Springs Project, in south eastern Nevada, for low sulphide epithermal gold exploration. Previous ground CSAMT surveys at Gold Springs revealed a positive correlation between the known epithermal gold systems and buried, subvertically-dipping resistivity high features that extend to depth. Synthetic forward modeling showed that ZTEM could also be successful, provided topographic effects were accounted for.

The ZTEM test results performed over the known epithermal gold prospect in southeastern Nevada appear to correlate very well with the CSAMT results and the known geology, in particular the presence of all the known epithermal centers over resistivity highs. Similar anomalies have been identified in previously unexplored areas of thicker overburden cover. 2D inversions of the airborne ZTEM, using a newly developed Avert2d code that accounts for bird clearance and 2d topography, appear to agree very well with the inversions obtained from ground CSAMT. These results provide encouragement for the application of ZTEM for epithermal gold deposits elsewhere in the district.

Key words: ZTEM, AFMAG, airborne, electromagnetic, epithermal, gold, resistivity.

INTRODUCTION

Exploring for epithermal vein gold deposits has long posed significant challenges for airborne electromagnetic methods, due to the disseminated nature of the sulphides that makes them virtually undetectable using EM, particularly when buried below overburden cover. This is easily the case for low sulphidation epithermal gold-silver vein systems, whose minor sulphide content (<2%) within the silica-rich stockworks, breccias and veins often make them difficult to detect even with ground induced polarization. Indeed, in addition to magnetics, and gravity, electrical methods have been successfully applied in epithermal gold exploration (Williams, 1997), including controlled-source audio-magnetotelluric (CSAMT) surveys (Zonge and Hughes, 1991). Frequency domain airborne EM methods have long been known to be able to successfully map geology based on resistivity contrasts (Palacky and West, 1988; Holladay and Lo, 1997) but are

limited by their shallow depth of penetration. More recently, ZTEM (z-axis tipper electromagnetics; Lo and Zang, 2008) airborne AFMAG (Ward, 1959; Thomson et al., 2007) have proven effective in mapping alteration and structure to great depth related to porphyry copper deposits (Lo and Zang, 2008; Paré and Legault 2010; Izarra et al., 2011) and smaller carbonate replacement deposits (CRD) and skarns (Roberston, 2011) as well as shear-hosted gold deposits (Witherly, 2011). ZTEM has therefore been proposed as possible alternative to ground CSAMT for regional exploration for vein-type epithermal gold deposits in Nevada.

A ZTEM helicopter EM survey was conducted in April, 2011 over the Gold Springs Project, located in eastern Lincoln County, Nevada and Western Iron County, Utah, on behalf of High Desert Gold Corporation (Denver, CO). The survey consisted of 41 east-west lines flown at a line spacing of 200 m and 6 north-south tie lines (Figure 1), totalling 470 line-km. The survey included ZTEM helicopter Tipper AFMAG (audio frequency electromagnetics) measurements, as well as aeromagnetics using a caesium magnetometer.

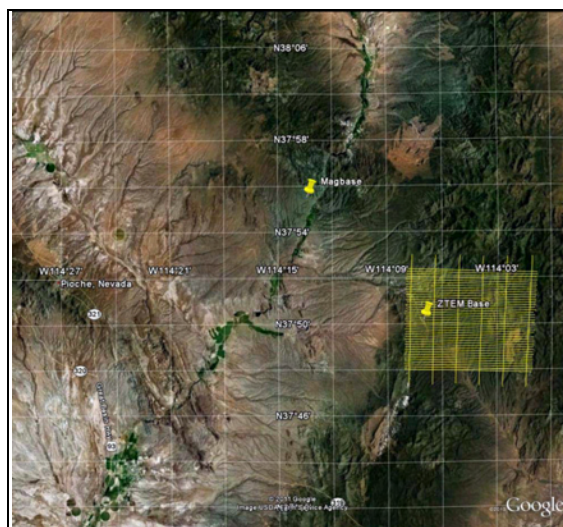


Figure 1. Google Earth image showing property location for Gold Springs Project and ZTEM flight lines.

The Gold Springs district hosted numerous high grade gold-silver mine workings that were discovered in the late 1890's and where mining continued until the early 1950's. Gold mineralization is hosted by complex sheeted veins, breccias and stockwork veins which consist of quartz, adularia, and

bladed calcite with minor sulphides (<2%) representing low sulphidation, epithermal gold-silver vein systems. At least fourteen discrete gold-silver bearing targets have been identified and are described as large, wide, structural zones, often extending for kilometres along strike. Previous ground CSAMT surveys revealed a positive correlation between the known epithermal gold systems and buried, subvertically-dipping resistivity high features that extend to depth.

The objectives of these ZTEM and magnetic surveys are the following: (1) Define bedrock resistivity structure from ZTEM data. (2) Define bedrock magnetic structure from magnetic data. (3) Identify other similar epithermal gold deposit signatures from both ZTEM and magnetic data.

Geological and Geophysical Model

Epithermal gold deposits form at shallow depths and are near-surface portions of fossil geothermal systems, which contrasts them to porphyry deposits which are formed at greater depth (Williams, 1997). Low sulphidation (LS) epithermal deposits differ from high sulphidation (HS) deposits in the low pH acidity of their hydrothermal fluids. As a general rule, hydrothermal systems lower the bulk resistivity in country rocks, by adding clay minerals and increasing the porosity, permeability and pore salinity. But within the LS system, more intense silicification increases the apparent resistivity, accompanied by magnetite destruction and increased density.

Typically, the LS alteration systems are also mushroom shaped, with significant widening in the near-surface (Figure 3). Whereas HS epithermal zones tend to be more subvertical, are typically vuggy and brecciated within the silica core, with the argillic to propylitic zoned alteration extending outward, and are more strongly mineralized with disseminated sulphides, primarily pyrite. The relative absence of sulphides in LS epithermal systems, explains why resistivity methods, like CSAMT, are usually the preferred tools used in their exploration.

General Theory

The ZTEM airborne AFMAG system measures the anomalous vertical secondary magnetic fields that are created by the interaction between naturally occurring, plane wave audio-frequency EM fields and electrical heterogeneities in the earth.

The vertical magnetic field is linearly related to the horizontal fields according to the following (Vozoff, 1972; Labson et al., 1985):

$$H_z = T_{zx}H_x + T_{zy}H_y$$

where the magnetic field vector $T = (T_{zx}, T_{zy})$, known as the tipper, is complex and a function of frequency, but has rotationally invariant properties, such as its magnitude and direction, that are independent of the subsurface, the measurement direction and the field polarization (Labson et al., 1985).

AFMAG uses naturally occurring audio frequency magnetic fields from worldwide atmospheric thunderstorm activity as the source of the primary field signal, and therefore requires no transmitter. The primary fields resemble those from VLF except that they are not man-made, are at lower frequency

(tens & hundreds of Hz versus tens of kHz), are pseudo-random, rather than periodic, and are usually not as strongly

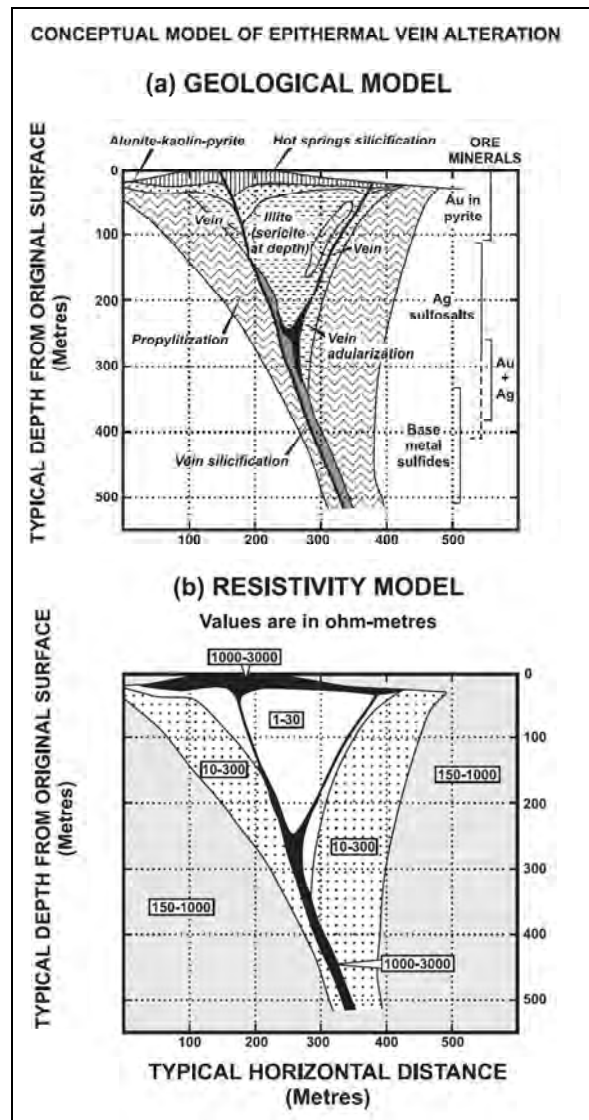


Figure 3. Schematic illustration of cross-sections of (a) a low sulphidation epithermal gold deposit (b) electrical resistivity associated with the different alteration types (modified after Williams, 1997).

directionally polarized. These EM fields used in AFMAG have the unique characteristic of being uniform, planar and horizontal, and also propagate vertically into the earth – to great depth, up to several km, as determined by the magnetotelluric (MT) skin depth (Vozoff, 1972):

$$\delta_s = 503 * \sqrt{(\rho / f)} \text{ metres}$$

which is the depth where the amplitudes of the EM fields are reduced to 1/e (37%) of their surface values and is directly proportional to the ratio of the bedrock resistivity to the frequency.

ZTEM is an airborne variant of the AFMAG technique where the vertical dipole axis air-core magnetic receiver towed by the helicopter (Figure 1) is coupled with a fixed ground base

station that measures the horizontal primary fields using similar dipole axis magnetic sensors (Thomson et al, 2007; Lo and Zang, 2008).

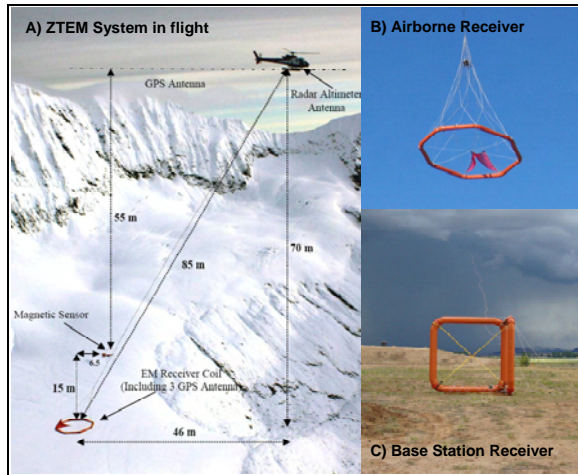


Figure 4. a) ZTEM helicopter EM system in flight, showing Hz receiver Coil and magnetic sensor; b) Hz receiver coil, c) Hx-Hy base station coils located at a remote site adjacent to survey area.

Synthetic Modeling

Using 2D inversion results of previous CSAMT survey data obtained at Gold Springs over one of the many historical gold deposits, as a guide (Figure 5), prior to the survey, 2D synthetic forward modeling was performed to simulate the expected airborne tipper AFMAG responses for a low-sulphidation epithermal geologic model using the 2D forward MT modeling code of Wannamaker et al. (1987).

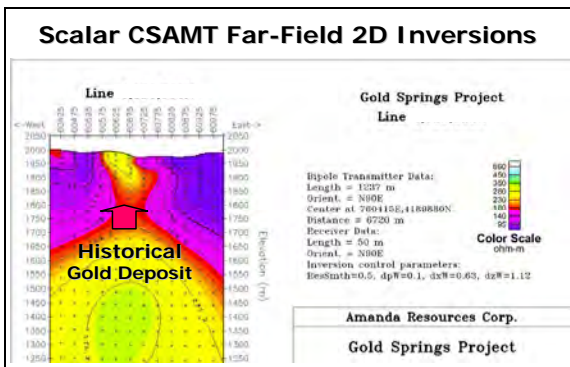


Figure 5. 2D Inversion of scalar CSAMT data obtained over a historical gold det at Gold Springs (by Zonge Engineering; courtesy High Desert Gold Corporation).

Figure 6 presents the 2D synthetic forward model responses of the In-line (Tzx) In-Phase and Quadrature over a mushroom shaped LS epithermal target that resembles the schematic model in Figure 3 and having similar physical properties and dimensions as the 2D CSAMT model in Figure 5, including a topographic high. The results suggest that ZTEM airborne AFMAG could be successful for mapping similar epithermal gold systems as those identified using CSAMT – provided the appropriate topographic corrections are applied during the inversion.

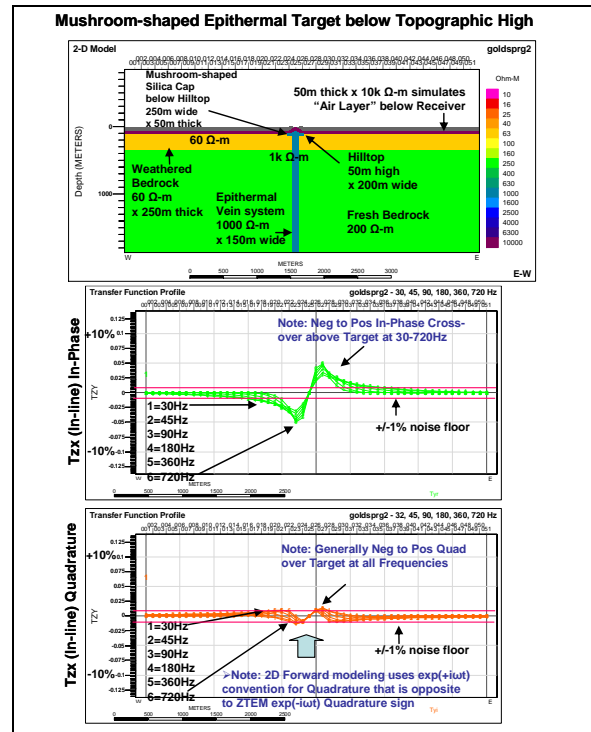


Figure 6. 2D resistivity model of Gold Springs epithermal gold target and related 2D forward modelled airborne In-line tipper profile results.

RESULTS AND DISCUSSION

ZTEM Results

DT (Total Divergence) imaging, analogous to the VLF Peaker parameter of Pedersen (1998), converts the ZTEM tipper cross-over data into peak-responses which assists their interpretation in plan. Figure 7 presents the mid-frequency (90Hz) In-Phase DT map along with EM anomaly picks and the location of known gold deposits. Red colours indicate DT low (conductive) areas and the blue colours indicate DT high (resistive) areas. As indicated in the previous ground CSAMT geophysical surveys over the property, the focus for the low-sulphidation epithermal gold targets are in relatively resistive areas. The cluster of resistive areas indicated in the In-Phase DT maps clearly show a good correlation with the known gold deposits, suggesting separate epithermal cells within a volcanic center, which fits the geologic model.

2d Inversion Results

ZTEM tipper results can be readily converted to an equivalent resistivity-depth section using computer 2D or 3D inversion. In this case a new version of the Zvert2d program, described in Legault et al. (2009) and based on the 2D code of de Lugao and Wannamaker (1996), called Av2dtopo, was implemented that accounts topography and bird altitude. The 2D inversions were performed on the Tzx (in-line) component data along the west-east flight direction using all 6 available frequencies (30, 45, 90, 180, 360 and 720 Hz). Using the previous CSAMT 1D and 2D inversion results as a guide, a 300 ohm-m uniform half-space starting model was used throughout. Figure 8 presents the 2D ZTEM inversion results of Line

1200. As shown, the known gold occurrences are all located in resistivity high features.

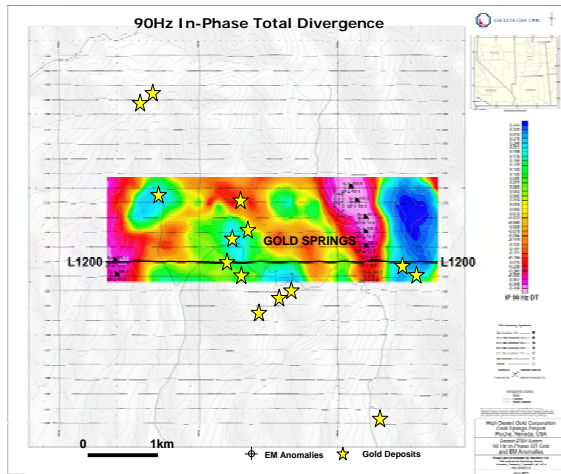


Figure 7. 90Hz In-Phase DT results, EM anomaly picks and historical gold prospects over Gold Springs project (windowed at client's request).

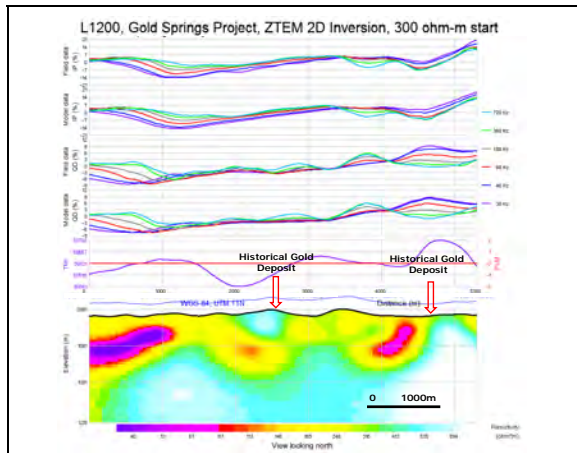


Figure 8. ZTEM 2D inversion results for L1200. Known gold occurrences/workings are indicated.

CONCLUSIONS

ZTEM inversion results indicate that most of the known gold workings/occurrences are located in a region featuring localized zones of high resistivity and high magnetic susceptibility areas, mainly found in the central part of the survey area. The clustering of these resistivity highs suggests they were formed in a volcanic center, which is consistent with the formation of LS epithermal deposits. The survey results also indicate that a number of other similar resistive and magnetic anomalies occur further south and west, in areas of overburden cover, which represent promising areas for follow-up. As predicted in the earlier forward modeling analysis, the ZTEM inversion results agree with those obtained from previous CSAMT survey and have extended the mineral potential over a much larger survey area.

ACKNOWLEDGMENTS

The authors wish to thank High Desert Gold Corporation and Geotech Ltd. for allowing us to present these results. We also

thank Phil Wannamaker for the topographic-correction development to the ZTEM 2D inversion code.

REFERENCES

- De Lugao, P.P., and Wannamaker P., 1996, Calculating the two-dimensional magnetotelluric Jacobian in finite elements using reciprocity, *Geophysical Journal International*, **127**, 806-810.
- Izarra, C., Legault, J.M., and Fontura, C., 2011, ZTEM airborne tipper AFMAG results over the Copaque Porphyry, northern Chile, SBGF Conference Expanded Abstracts, 4pp.
- Labson, V. F., Becker A., Morrison, H. F., and Conti, U. , 1985, Geophysical exploration with audio frequency natural magnetic fields, *Geophysics*, **50**, 656-664.
- Legault, J.M., Kumar H., Milicevic B., and Wannamaker P., 2009, ZTEM tipper AFMAG and 2D Inversion results over an unconformity uranium target in northern Saskatchewan, SEG Expanded Abstracts, **28**, 1277-1281.
- Lo, B., and Zang, M., 2008. Numerical modeling of Z-TEM (airborne AFMAG) responses to guide exploration strategies, SEG Expanded Abstracts, **27**, 1098-1101.
- Palacky, G.J., and West, G.F., 1988, Airborne electromagnetic methods, in "Electromagnetic Methods in Applied Geophysics, V. 2. Application", edited by M.N. Nabighian, 811-879.
- Paré, P., and J. M. Legault, 2010, Ground IP-resistivity and airborne SPECTREM and helicopter ZTEM survey results over Pebble copper-moly-gold porphyry deposit, Alaska, SEG Expanded Abstracts, 1734-1738.
- Robertson, K., 2011, The 2009 Pozo Seco molybdenum-gold discovery, presented at KEGS Symposium, Toronto, CAN.
- Thomson, S., Fountain, D., and Watts, T., 2007, Airborne geophysics – evolution and revolution, in "Proceedings of Exploration 07: Fifth Decennial International Conference on Mineral Exploration", edited by B. Milkereit, 19-37
- Wannamaker, P. E., Stodt, J. A., and Rijo, L., 1987, A stable finite element solution for two-dimensional magnetotelluric modeling: *Geophysical Journal of Royal Astronomical Society*, **88**, 277-296.
- Ward, S. H., 1959, AFMAG - Airborne and Ground: *Geophysics*, **24**, 761-787.
- Williams, P.K., 1997, Towards a multidisciplinary integrated exploration process for gold discovery, In "Proceedings of Exploration 97: Fourth Decennial International Conference on Mineral Exploration" edited by A.G. Gubins, 1015-1028.
- Witherly, K., 2011, ZTEM for precious metals exploration: Extending the envelope, presented at PDAC-CAMESE Exhibitors Innovation Forum, Toronto, CAN.
- Zonge, K.L., and Hughes, L.J., 1988, Controlled source audio-frequency magnetotellurics, in "Electromagnetic Methods in Applied Geophysics, V. 2. Application", edited by M.N. Nabighian, 713-807

Numerical modeling of Z-TEM (airborne AFMAG) responses to guide exploration strategies

Bob Lo*, Geotech Ltd., Michael Zang, Exploration Syndicate Inc.

Summary

Mineral exploration using the Z-TEM or Z-Axis Tipper Electromagnetics, an airborne AFMAG system, has been guided by numerical modeling of the target types. Numerical modeling is used to plan the survey in terms of survey line spacing, survey height, and expected signatures of the targets. Knowing the Z-TEM response of a deposit of the type that is being explored for, aids in the interpretation of the results. Numerical modeling has demonstrated that the Z-TEM system is ideally suited for large, deep deposits of low to high resistivity contrasts such as porphyry copper and SEDEX deposits.

Introduction

Z-TEM, has been flown commercially since mid-2007. Exploration Syndicate and Geotech. have flown a number of demonstration and large commercial surveys following an exploration strategy of selecting the best area to explore based on geological models and an assessment of the suitability of the Z-TEM for the particular target type.

Z-TEM uses the natural or passive fields of the Earth as the source of transmitted energy. These natural fields are planar and due to the manner in which they propagate, are horizontal. Any vertical EM field is caused by conductivity contrasts in the Earth. The Z-TEM system measures the vertical EM field in the air along the survey lines and makes use of a base station to measure the horizontal fields. The assumption is that the horizontal fields are relatively homogenous over the survey area and the base station location. The vertical EM field is remotely referenced to the horizontal EM fields.

Numerical modeling of the Z-TEM response over deposits or representative deposits is done to gain an understanding of the expected signature from these deposits to aid in the interpretation of the data. The data is also used to help determine the acquisition parameters such as line spacing, extracted frequencies, surveying height, etc. To this end, a number of world class deposits such as the Spence porphyry copper deposit, and the Red Dog SEDEX massive sulphide deposit were selected for numerical simulation.

Z-TEM Background

Instrumentation

As the Z-TEM instrumentation is relatively new, a brief description of the system and its data processing stream will be given.

Z-TEM instrumentation consists of a 7.4 metre diameter single axis air-cored airborne coil measuring the vertical component of the EM field. The airborne coil is deployed from a helicopter using a 90 metre long cable to separate the coil as much as possible from the helicopter EM noise, while still maintaining a structure that can be controlled by a skilled pilot.

The horizontal reference field is measured by a base station consisting of two, four metre square air-core coils placed orthogonal to each other. The horizontal field can be decomposed into the two orientations of the survey flight.



Figure 1 - picture of the airborne coil with the base station in the background.

The airborne coil is designed to fly horizontally at a constant speed. A minor amount of tilt is introduced when the aircraft speeds up or slows down. We assume that the vertical field measurements are not unduly affected. However, the cross coupling between the horizontal and vertical EM field caused by the coil tilt must be removed. Three GPS receivers are placed on the Z-TEM airborne coil to measure the attitude. From the attitude information, the amount of horizontal field detected by the airborne is removed.

Data Processing and Presentation

The raw data are recorded as time series, digitized at 2,000 Hz using a 24 bit ADC. Time synchronization between the airborne data and the base stations uses the 1 pps pulse from the GPS receiver. Figure 2 shows an example of the merged datasets and of the filtering that is performed. The top two traces are the base station coils. The third trace is of the airborne coil. Note that the motion noise is evident as a low frequency variation in the airborne coil. This is filtered away prior to the calculation of the two tippers. The direction of the event is shown in the circle.

Numerical modeling of Z-TEM (airborne AFMAG) responses to guide exploration strategies

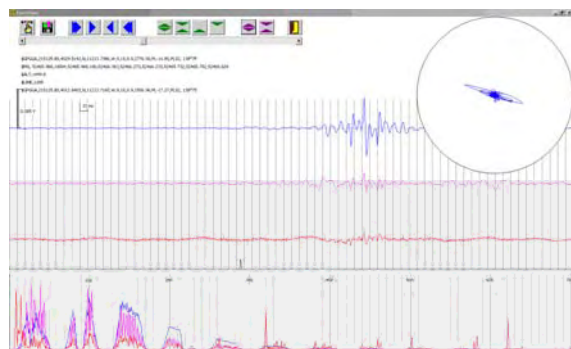


Figure 2 – an example of the merged dataset. The bottom panel show the power spectrum after digital filtering of powerline and other cultural noise.

The relationship between the vertical fields and the two horizontal fields is the tipper. The tipper is a cross-over type of anomaly over a steeply dipping body. We wish to combine the two components into one single one which is centred over the conductive anomaly – i.e. not a cross-over anomaly. In order to combine the two components and to transform the cross-overs into peaks, the data is presented in terms of the DT. The DT is defined as the divergence of tipper relations $DT = \text{div} (Z/X, Z/Y) = d(Z/X)/dx + d(Z/Y)/dy$. The DT has a local minima over a conductive body, so we use an inverted colour bar when presenting the DT.

The divergence being a derivative, does not preserve some of the long wavelength, and thus might not convey all information about the conductor's depth and extent. Phase rotated grids (by 90 degrees) exhibit maxima over conductors and are sometimes used. They preserve longer wavelength, but have the disadvantage of favouring one direction (X or Y) only.

Numerical Simulation

Z-TEM should be suited for large deposits at depth, with or without a large resistivity contrast. Porphyries and SEDEX are the obvious target types.

Numerical modeling of simple shapes representing, say, the conductive alteration surrounding the intrusive core of a porphyry were conducted. Porphyry copper deposits are a well recognized type of large, low grade copper-gold mineral deposit. Porphyry copper deposits originate with the intrusion of porphyritic rock. The hydrothermal fluid circulation caused by the hot magma modifies the minerals in the rocks they pass through in a process called hydrothermal alteration. The metallic minerals that the intrusion and the host rocks contain can be concentrated and precipitated at various zones. The hydrothermal alteration accompanying these deposits causes changes in

the physical property of the rocks. Hydrothermal alteration and sulphide deposition causes change in the resistivity of the rock. Pervasive clay minerals associated with argillic-propylitic alteration zones generate low resistivities in the 10 to 30 ohm-metre range. (Allis, 1990). The low grade core, with lower sulphide content, would have a higher resistivity as should the host rock.

Initially, the higher resistivity low grade core was not modeled. A cylinder, 2,000 m in diameter and 1,000 km tall, capped with a dome of 500 metres height of 50 ohm-m is used to represent the conductive alteration package. There is 10 metres of 10 ohm-m overburden over a conductive host of 200 ohm-m. The results from the Emigma software package are shown below.

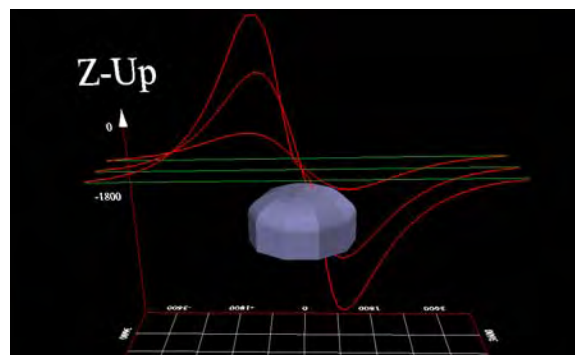


Figure 3 – perspective view of the inphase Tx Tipplers over a "porphyry" feature.

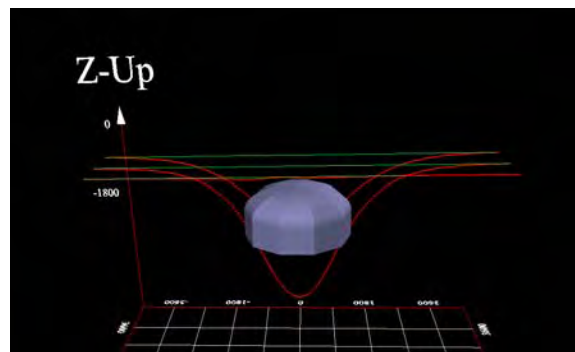


Figure 4 – perspective view of the inphase Ty Tipplers over a "porphyry" feature.

The top of the dome is 100 metres below the surface. The source polarization for the model is from 0° azimuth and the peak-to-peak value of the Tx ratio is 0.16 (0.08 for Ty) which above the noise floor of the instrumentation.

The results of the modeling showed that Z-TEM responded sufficiently well to relatively poorly conductive targets.

Numerical modeling of Z-TEM (airborne AFMAG) responses to guide exploration strategies

This is thought to be due to the uniform excitation of the large geological structures by the natural fields.

Demonstration Survey

Encouraged by the results of the simulation results, a demonstration survey was conducted over two known porphyries in southwestern USA. The flight lines over simplified geology is shown in Figure 5.

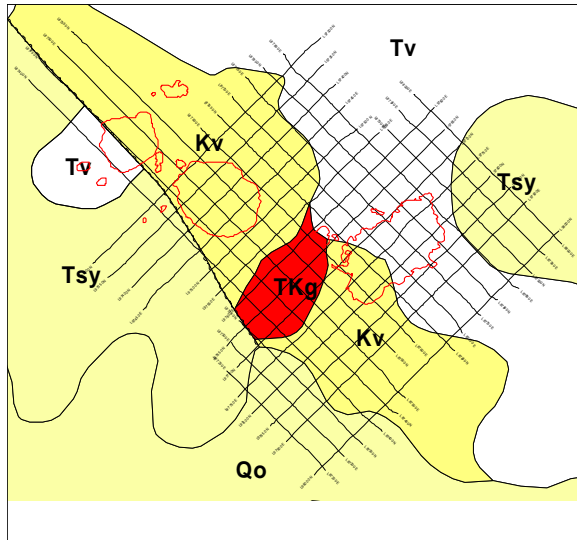


Figure 5 – simplified geology over the demonstration survey. Qo = Surficial Deposits (Holocene to mid Pleistocene), Tsy = Sedimentary Rocks (Pliocene to mid Miocene), Tv=Volcanic Rocks (Mid Miocene to Oligocene), TKg = Granitoid Rocks (Early Tertiary to Late Cretaceous), Kv = Volcanic Rocks (Late Cretaceous to early Tertiary).

Also shown in Figure 5 is the outline of the two porphyries covered by the survey.

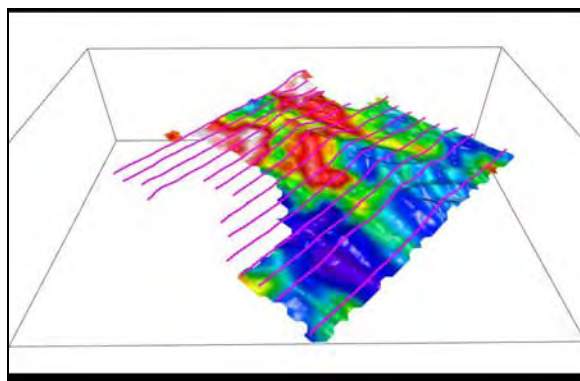


Figure 6 – perspective view of the phase rotated inphase in-line Tippers.

Figure 6 shows a perspective view of the phase rotated, in-line, 109 Hz real component of the tipper. Note that the data from the area to the southwest was contaminated by powerlines and was not useable. Only the northeast line data is presented. Note the half circular feature in the southwestern portion of the survey and the almost circular feature in the approximate middle of the survey.

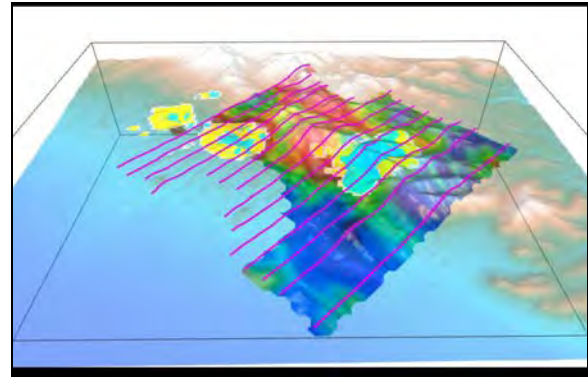


Figure 7 – perspective view of the phase rotated inphase in-line Tippers superimposed on topography and with the outlines of the porphyry mineralization and alteration (yellow) and intrusion (blue) superimposed.

Figure 7 has the outline of the alteration and mineralization of the porphyries shown in yellow, superimposed on the data. The visual correlation between the phase rotated Z-TEM highs, due to conductive features, and the outline of the alteration and mineralization is very compelling. Note that the survey results did not readily match with model results presented early. This is perhaps due to a lower erosional level of the porphyry system. Depending on the level of erosion, different alteration packages are exposed. A level or plan cut to the level below the low grade core will yield an alteration pattern in plan, that consists of annuli of different alteration. The resistivity response in this case would be an annulus of low resistivity surrounding a core of higher resistivity as more or less seen in the data.

Additional Numerical Simulation

Building on the knowledge gained, models were generated of various known world class deposits to determine the signature of these deposits so that similar targets can be recognized, to guide the exploration efforts, and to reduce the risk in exploration. Results from the Spence Deposit are shown.

Numerical modeling of Z-TEM (airborne AFMAG) responses to guide exploration strategies

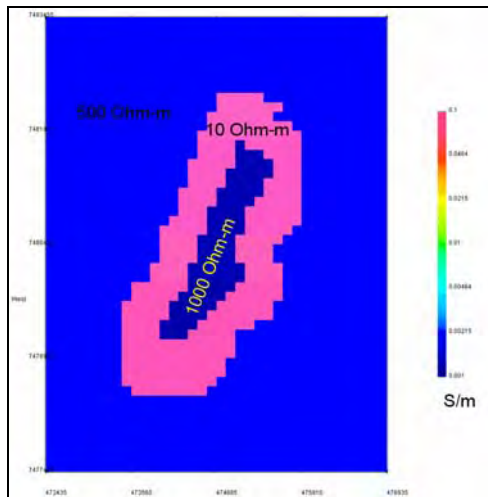


Figure 8 – plan view of the block model used for the Spence deposit.

Figure 8 shows the plan view of the block model and the resistivities used for the forward modeling. Initially, the topography was assumed to be flat and the barren core was at the surface.

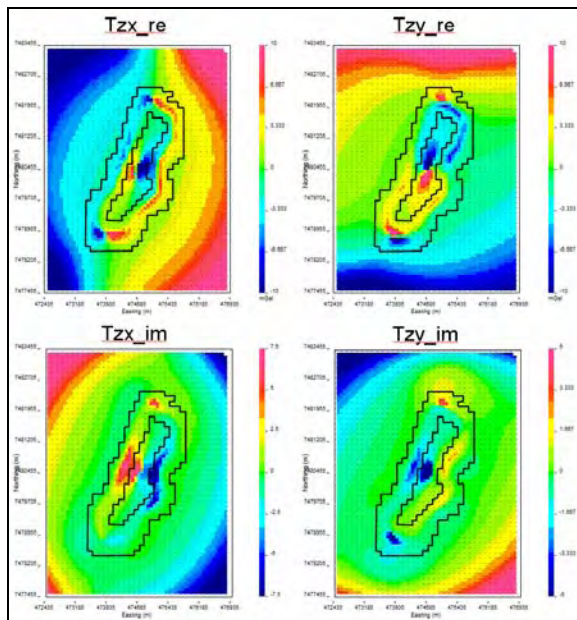


Figure 9 – plan view of the responses from the Spence deposit at 32 Hz.

The Spence model can be made more complex with the addition of topography and burying the intrusive core. A conductive response surrounding the intrusive core is seen in the model results, as expected.

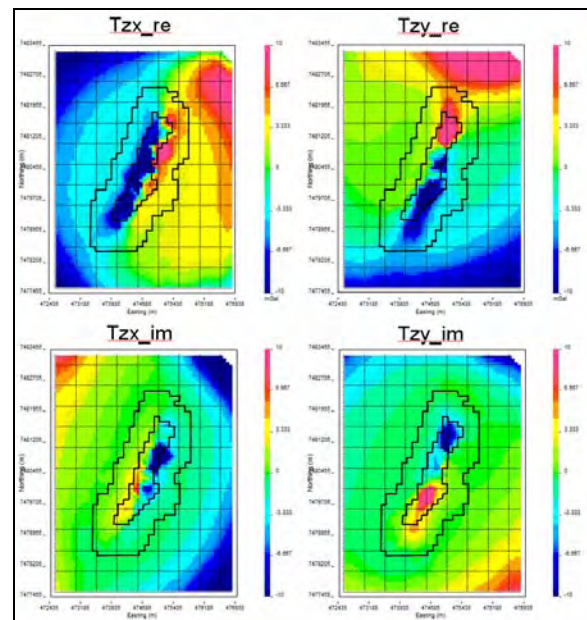


Figure 10 – plan view of the response from the Spence model incorporating topography, overburden and burying the intrusive core.

Conclusions

The ZTEM system has unambiguously detected a robust anomaly coincident with part of the large blind porphyry Cu deposit. By inference big deposits should produce big anomalies.

The optimal presentation of the data is dependant upon the interpretation purpose with geological input being critical.

Numerical modeling of Z-TEM results greatly aids the exploration process and reduces risk in geophysical exploration.

Acknowledgements

The authors thank Geotech Ltd. and Exploration Syndicate Inc. for allowing the authors to work on this paper and for the release of data and reports for this paper.

Nigel Phillips, Doug Oldenburg, and Peter Kowalczyk of the Advanced Geophysical Interpretation Center and Ross Groom of Petros Eikon are also thanked for their contributions.

EDITED REFERENCES

Note: This reference list is a copy-edited version of the reference list submitted by the author. Reference lists for the 2008 SEG Technical Program Expanded Abstracts have been copy edited so that references provided with the online metadata for each paper will achieve a high degree of linking to cited sources that appear on the Web.

REFERENCES

- Allis, R. G., 1990, Geophysical anomalies over epithermal systems: *Journal of Geochemistry Exploration*, 36.
- Anav, A., S. Cantarano, P. Cerruli-Irelli, and G. V. Pallotino, 1976, A correlation method for measurement of variable magnetic fields: *Geoscience of Electricity*, GE14, 106–114.
- Kuzmin, P., B. Lo, and E. Morrison, 2005, Final report on modeling, interpretation methods and field trials of an existing prototype AFMAG system: *Miscellaneous Data Release*, 167, Ontario Geological Survey.
- Labson, V. F., A. Becker, H. F. Morrison, and U. Conti, 1985, Geophysical exploration with audio-frequency natural magnetic fields: *Geophysics*, **50**, 656–664.
- Strangway, D. W., C. M. Swift Jr., and R. C. Holmer, 1973, The application of audio-frequency magnetotellurics (AMT) to mineral exploration: *Geophysics*, **38**, 1159–1175.
- Vozoff, K., 1972, The magnetotelluric method in the exploration of sedimentary basins: *Geophysics*, **37**, 98–141.
- 1991. The magnetotelluric method: SEG.
- Ward, S. H., 1959, AFMAG—Airborne and ground: *Geophysics*, **24**, 761–787.

Z-TEM (AIRBORNE AFMAG) TESTS OVER UNCONFORMITY URANIUM DEPOSITS

*Bob Lo¹, Jean Legault², Petr Kuzmin³, Magdel Combrinck⁴
Exploration Syndicate, Inc., bob.lo@expsyn.com¹, Geotech Ltd., jean@geotech.ca²,
Geo Equipment Manufacturing Ltd., petr@geotech.ca³,
Geotech Ltd, magdel@geotechairborne.com⁴*

Key Words: Z-TEM, AFMAG, electromagnetic, airborne, uranium, Athabasca.

INTRODUCTION

A series of demonstration tests were conducted using the Z-TEM, airborne AFMAG system over deep targets in the Athabasca Basin of Saskatchewan, Canada. These tests were conducted in mid-2008 and were flown to test Z-TEM's ability to detect large conductive targets at depth; deeper than conventional airborne EM methods. Data are presented over areas where the conductors are located 800 metres beneath the surface. As well, a case of Z-TEM following the plunge of a conductor to over 800 metres depth is shown.

BACKGROUND

The Z-TEM system is the latest implementation of an airborne AFMAG system first commercialized in late 2006. Z-TEM uses a large, 8 metre diameter airborne air core coil, slung from a helicopter, to measure the vertical component of the AFMAG signal. Two 4 metre square coils are deployed on the ground to measure the horizontal field. The Z-TEM system has flown successful demonstration surveys over porphyry copper deposits in the southwest USA (Zang et al., 2008).

Z-TEM was tested in the Athabasca Basin in Canada in May of 2008 to determine its depth of investigation and to determine its suitability for mapping deep conductors in the crystalline basement. Over 30% of the world's U₃O₈ is mined in the Athabasca Basin from unconformity uranium deposits. Unconformity uranium deposits of the Athabasca Basin are often associated with conductors located in the crystalline basement. The search for economic uranium deposits is moving to areas of the basin which are deeper and beyond the detection limits of modern airborne instrumentation. This creates the requirement for a system which can detect conductivity past the detection limits of modern traditional EM systems. This was the motivation behind the field trials of the Z-TEM system in the Athabasca Basin. Several areas where known deep conductors (800m+) were located were flown. Also, a test survey block in the northern part of the basin was able to trace a deep and plunging conductor to depths that no other airborne EM system has been able to achieve.

ATHABASCA BASIN GEOLOGY

The high-grade uranium deposits within the Athabasca Basin are associated with the unconformity between the essentially flat-lying Proterozoic Athabasca Group sandstones and the underlying Archean-Paleoproterozoic metamorphic and igneous basement rocks. The deposits occupy a range of positions from wholly basement-hosted to wholly sediment-hosted, at structurally favourable sites in the interface between the deeply weathered basement and overlying sediments of the Athabasca Basin (Ruzicka, 1997). The locations of these deposits are lithologically and structurally controlled by the sub-Athabasca

unconformity and basement faults and fracture zones, which are localized in graphitic pelitic gneisses that may flank structurally competent Archean granitoid domes (Quirt, 1989).

In general, most of the known important deposits tend to occur within a few tens to a few hundred metres of the unconformity and within 500 m of the current ground surface. This may be more of a limitation of exploration techniques. There is no reason to believe that the distribution of the deposits is dependent on the modern day depth of burial.

Empirically, the geophysical exploration for unconformity type uranium targets have been to search for large basement structures which post date the sandstone deposition of the basement (Matthews et. al, 1997). All the deposits located so far are associated with fault structures associated with a graphitic conductive basement. An alteration zone of clay silicification and enrichment around the deposits probably leads to magnetite destruction causing the magnetic low observed around the deposits. The clay alteration should give rise to a resistivity low signature about the deposits. The low conductivity of the clay alteration makes it a difficult target for airborne EM if it is buried at significant depth.

Z-TEM INSTRUMENTATION AND PRESENTATION

Z-TEM is an airborne AFMAG system introduced by Geotech Ltd. of Canada in early 2007 (Lo et al., 2008). In a Z-TEM survey, a single vertical dipole air-core coil is flown over the survey area in a grid pattern similar to other airborne electromagnetic surveys. Two orthogonal, air-core, horizontal axis coils placed close to the survey site measures the horizontal EM fields for reference. A GPS array on the airborne coil monitors its attitude for post-flight corrections.

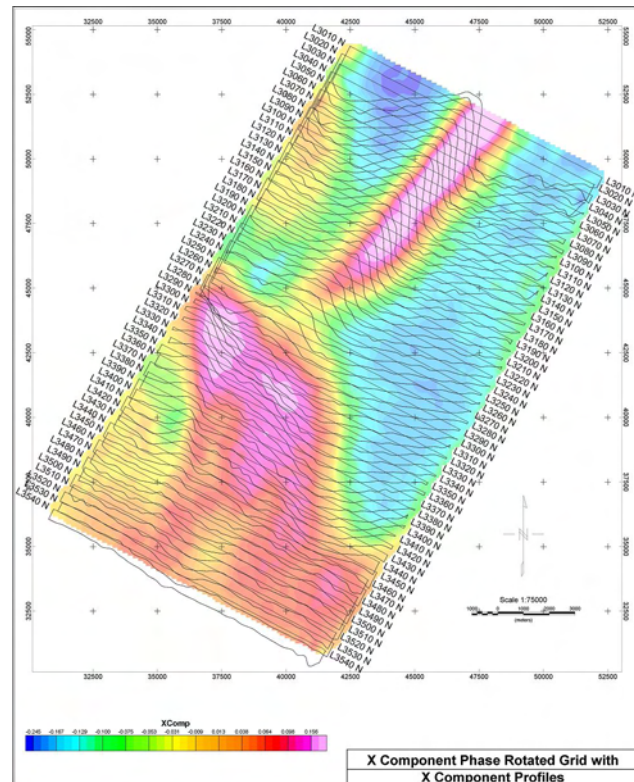


Figure 1 – Stacked profiles of the x-component Tipper over the gridded values of the phase rotated x-component data. Note that the cross-overs in the profiles are now peaks on the image.

As the source field is assumed to be far away, the excitation of the ground is more or less uniform. For large structures, the signal fall-off will be much slower than from a dipole source, such as those energised by traditional airborne systems. With the Z-TEM system being less susceptible to terrain clearance, the planned ground clearance height is higher and the terrain drape is looser as compared to standard helicopter EM surveys.

The two Tippers obtained from the relationship between the vertical airborne coil and the two ground coils have a cross-over over a steeply dipping, plate-like body. The cross-overs can be made into local maxima via a 90 degree phase rotation which allows for easier interpretation of the gridded values. Figure 1 is an example of this transformation.

To present the data of both Tippers as one image, we calculate a parameter termed the DT which is the horizontal divergence of the two Tippers, much in the same manner as the “peaker” parameter in VLF (Pedersen, 1998). The DT is typically plotted with an inverted colour bar as it is negative over a steeply dipping thin body.

Z-TEM RESULTS – NORTHERN ATHABASCA BASIN

Figure 2 shows gridded values from a number of Z-TEM lines over an area where the sedimentary cover is approximately 800 metres thick. A number of traditional EM systems have also been flown over this block. While they were able to detect conductors, the resolution of the conductive features is not nearly as detailed as the information provided by Z-TEM.

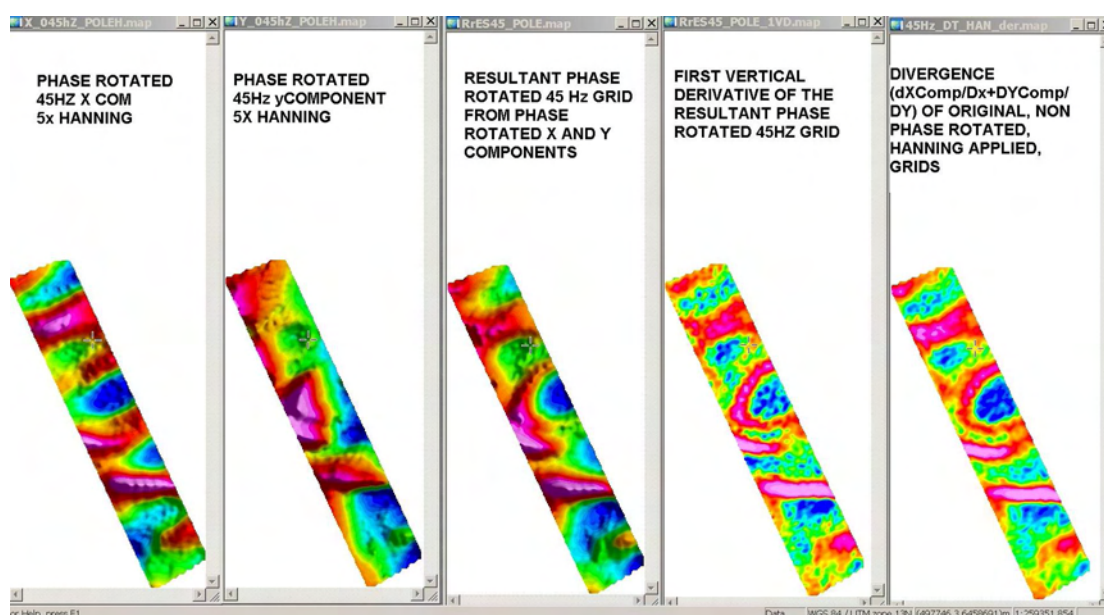


Figure 2 – Z-TEM results over an area of 800 metre thick sedimentary cover.

Figure 3, from another area, shows the data from one of the larger blocks that was flown. It is a 3D composite image of the DT at various frequencies plotted at the equivalent skin depth assuming a 1,000 ohm-m average resistivity.

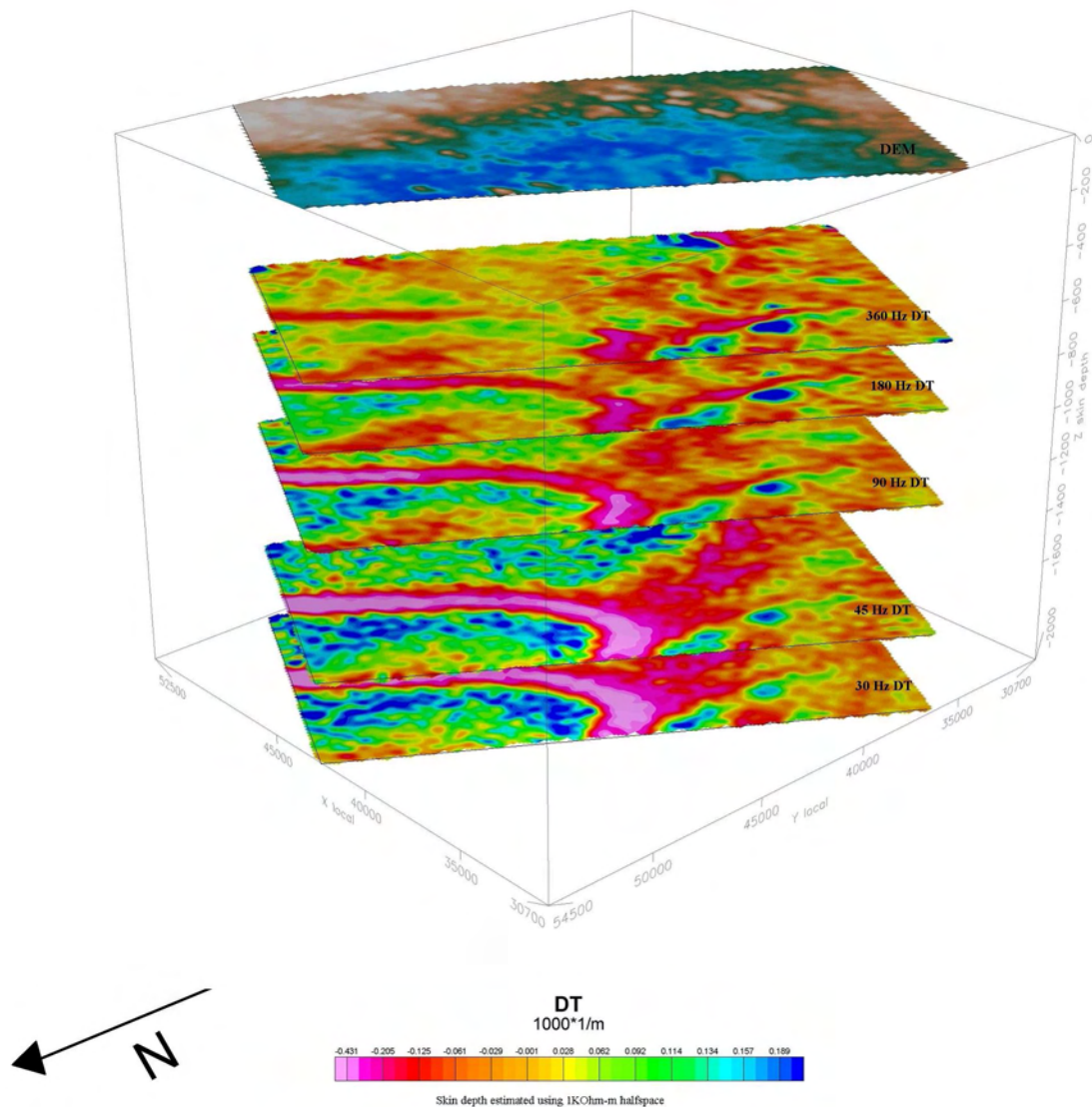


Figure 3 - Perspective view of DT's of different frequencies plotted at the skin depth (using a 1,000 ohm-m Earth).

The data in Figure 3 come from a survey over the north rim of the Athabasca Basin. The sandstone cover is about 500m on the left hand side of the image, and progressively getting deeper to the right. It is about 700m in the middle part of the image and over 800 metres thick on the right middle portion where exploration drilling is concentrated. Starting in the middle left and trending to the right of the image, there is a known graphitic shear.

In the uppermost (600m) “depth slice”, Figure 3 shows a linear conductive feature that progressively weakens as one moves to the right until it is no longer seen. This is interpreted to be due to the graphitic shear conductor plunging deeper past the depth of investigation of the 360 Hz data. The lower frequencies penetrate more into the sedimentary cover that is deeper towards the right. DT's of decreasing frequency show the linear conductive feature extending more and more to the right. The feature also strengthens/sharpens into a synformal shape with lower frequencies. This fits with what the known geology of a plunging conductor at depth is doing.

At the nose of the fold, in the right third of the images, we also see another, broader anomalous zone that trends towards the back of the image. At this location, two radioactive

springs are situated. These spring waters which are anomalously high in uranium and radon may reflect the upward migration of deep waters along faults, suggesting structural targets in areas where basal waters may have tapped a radioactive source. This broad DT trend might be the plunge of the fold axis that is aligned away from the front of the image. An anomaly along this trend, at the highest frequency, that steadily grows with each decreasing frequency can be seen. This might represent an alteration zone in the sandstone that is detected at the shallowest depth. By about the 90Hz DT depth slice or so, we are possibly in the deeper basement and into a basement graphitic unit.

CONCLUSIONS

A number of successful Z-TEM tests were conducted over the Athabasca Basin. The tests demonstrated that Z-TEM can easily detect conductivity to 800 metres beneath relatively resistive sedimentary cover. Assuming a 1,000 ohm-metre resistivity, the skin depth of the 30 Hz data is approximately 2,000 metres. The 30 Hz data presented have good signal to noise ratios indicating a deep depth of exploration. The observation that Z-TEM may be detecting the clay alteration above the crystalline basement is a significant advantage for exploration of unconformity uranium deposits.

More demonstration surveys are planned in the Athabasca Basin later this year. And more target types for testing are also planned.

ACKNOWLEDGEMENTS

The authors thank Geotech Ltd. for allowing them to publish this work and for providing the support required to write this abstract and to present this paper.

REFERENCES

- Labson, V. F., Becker A., Morrison, H. F., and Conti, U., 1985, Geophysical exploration with audiofrequency natural magnetic fields, *Geophysics*, Vol. 50, pp. 656-664.
- Lo, B., Zang, M., Kuzmin, P., 2008, Geotech's Z-TEM (Airborne AFMAG) Instrumentation, a paper presented at KEGS PDAC 2008 Symposium, Toronto.
- Matthews, R., Koch, R. and Leppin, M., 1997, Advances in Integrated Exploration for Unconformity Uranium Deposits in Western Canada; in *Proceeding of Exploration 97*, edited by Arnis Gubins, Prospectors and Developers Association of Canada, Toronto.
- McMullan, S.R., Matthews, R.B, and Robertshaw, P., 1990, Exploration geophysics for Athabasca Uranium Deposits, in: *Proceedings of Exploration 87*, Ontario Geological Survey.
- Pedersen, L.B, Qian, W., Dynesius, L., Zhang, P., 1994, An airborne tensor VLF system. From concept to realization, *Geophysical Prospecting*, Vol. 42.

Ruzicka, V.R., 1997, Metallogenic features of the uranium-polymetallic mineralization of the Athabasca Basin, Alberta, and a comparison with other parts of the basin; in R.W. Macqueen, ed., Geological Survey of Canada, Bulletin 500, 31-79.

Wheatley, K., Murphy, J., Leppin, M., and Climie, J.A., 1996, Advances in the Genetic Model and Exploration Techniques for Unconformity-type Uranium Deposits in the Athabasca Basin; in Ashton, K.E., Harper, C.T., eds., MinExpo '96 Symposium – Advances in Saskatchewan Geology and Mineral Exploration: Saskatchewan Geological Society, Special Publication No 14, p. 126-136.

Quirt, D., 1989, Host rock alteration at Eagle Point South: Sask. Research Council, Publication no. R-855-1-E- 89, 95p.

Ward, S. H., 1959, AFMAG - Airborne and Ground: Geophysics, Vol. 24, pp. 761-787.

Zang, M., Lo, B., 2008, The Application of Airborne Natural Field Electromagnetics (Z-TEM): Some Examples from the Southwestern United States, a paper presented at the 2008 PDAC, Toronto.

Ground IP-Resistivity, and airborne Spectrem and helicopter ZTEM survey results over Pebble copper-moly-gold porphyry deposit, Alaska

Pascal Paré, Anglo-American Exploration (Canada) Ltd and Jean M. Legault*, Geotech Ltd.

Summary

Survey results from ground IP-Resistivity, Spectrem airborne electromagnetics and magnetics, and ZTEM tipper AFMAG helicopter electromagnetics are compared over the Pebble porphyry copper deposit, in southwest Alaska. The IP data display higher amplitudes associated with the increased sulphides over the Pebble alteration halo that vector towards the deposit. Lower resistivities are associated with the chargeable alteration halo and slightly higher resistivities occur in the less chargeable core at Pebble West. The deeper Pebble East was not detected in IP due to insufficient penetration. The airborne EM surveys, Spectrem and ZTEM, appear to map the resistivity contrast with more resolution than the ground IP resistivity survey, due to higher sampling and better depth of investigation. Spectrem conductors coincide with the rich pyrite mineralization, sulphide veins and alteration, but the depth of investigation is at the detection limit of Pebble East. The ZTEM tipper AFMAG survey appears more sensitive to weak resistivity contrast especially at depth. Both Pebble West and East are well detected in the ZTEM results.

Introduction

The Pebble deposit that is managed by the Pebble Partnership, a joint venture between Northern Dynasty Mines and Anglo American plc, is a calc-alkalic copper-gold-molybdenum porphyry located in the Bristol Bay region of southwest Alaska, 320 km southwest of Anchorage and 27 km west-northwest of the village of Iliamna. Pebble is reputed to be the 1ST largest gold and 6TH largest copper deposit in the world. This study compares the ground IP-Resistivity results, Spectrem airborne electromagnetic (Macnae et al., 1991; Legatt et al., 2000), and ZTEM tipper electromagnetic (Lo and Zang, 2008; Lo et al., 2009; Legault et al., 2009ab) results over the Pebble porphyry.

General geophysics

Geological, geochemical, and geophysical surveys have been conducted in the Pebble project area since 1985. Induced polarization (IP) and resistivity surveys in 1988-2001 defined a chargeability anomaly within Cretaceous rocks about 91 km² in extent that measured approximately 21 km north-south by up to 10 km east-west. It contained 11 distinct centres reflected by stronger chargeability anomalies, many of which were later demonstrated to be coincident with extensive copper, gold and molybdenum soil geochemical anomalies. All known zones of minerali-

zation of Cretaceous age in the Pebble district occur within the broad IP anomaly (Rebagliati et al., 2009).



Figure 1: Pebble property location in southwest Alaska

From 1988-2001, IP-Resistivity surveys utilized both the dipole-dipole and pole-dipole configurations, with separations of $n=1$ to 5, 7 or 8, a-spacings of 500ft, and line-separations of 300m-1km. Both time-domain and Phase IP were employed. In 2009, a Zonge time-domain IP survey utilized a larger, more deeply penetrating array with 400m a-spacing, with $n=1$ to 7, 8 to infill at a minimum of 500m line-spacing (Paré, 2010).

From 8-30 July, 2009, Spectrem Air Limited conducted an airborne electromagnetic, magnetic and radiometric survey over the Pebble project in Alaska. A total of 3,840 line kilometres were surveyed. The survey was done in two stages; a regional survey at 1500m flight-line spacing, covering an area of approximately 30 x 12 km, and a more detailed survey at 250m flight-line spacing along strike of the current deposit. A base frequency of 45Hz was used. The transmitter (Tx) height was 107m above ground and the transmitter-receiver (Tx-Rx) vertical and horizontal separations were 37.1m and 122.2m. (Klinkert et al, 2009).

On Sept. 4TH, 2009, a Geotech helicopter-borne geophysical survey was carried out over the Pebble Property. Principal geophysical sensors were a Z-Axis Tipper electromagnetic (ZTEM) AFMAG system, and a caesium magnetometer. A total of 250 line-kilometres were flown at a flight-line spacing of 200m and covered 60 square kilometres. During the survey the helicopter was maintained at mean height of 163m above the ground, allowing for a nominal EM sensor terrain clearance of 89m (Acorn et al, 2009).

Ground IP-Resistivity, airborne Spectrem and helicopter ZTEM survey results over Pebble porphyry Deposit

General geology

The Pebble property is underlain by Jura-Cretaceous to Eocene igneous and sedimentary rocks. The Pebble deposit is a calc-alkalic copper-gold-molybdenum porphyry deposit which formed in association with granodiorite intrusions emplaced at roughly 90 Ma. The deposit comprises the contiguous Pebble West and Pebble East Zones (Figure 2), discovered in 1986 and in 2005, respectively. Mineralization at Pebble West occurs around small granodioritic stocks that intrude the country rocks. The Pebble East mineralization occurs within a granodioritic stock and in sills that cut the country rocks. Pebble West extends to surface and Pebble East is entirely overlain by east-thickening, younger volcano-sedimentary cover, up to 600m thick. Pebble is bounded to the SE by the major ZG1 dip-slip fault, east of which the deeper Far East Zone (Figure 2) has been recently identified at >1.5km depths.

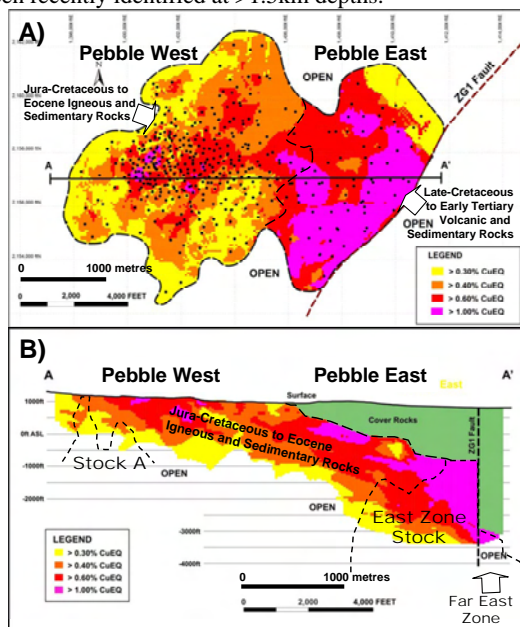


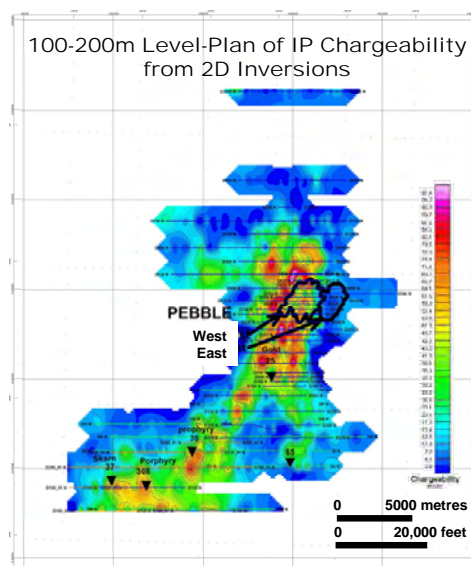
Figure 2: A) Plan view and B) Cross Section of Pebble Deposit showing general geology and grade distribution across Pebble West and Pebble East zones (modified after Rebagliati et al, 2009).

The deposit hosts K-silicate alteration and associated quartz-sulphide veins, overprinted by phyllo-silicate alteration. Sulphides mainly consist of hypogene pyrite, chalcopyrite, molybdenite and bornite; supergene and thin oxide zones also occur at Pebble West. High grade mineralization at Pebble East is associated with advanced argillic alteration. The Cu-Au-Mo mineralization, as it is currently known, extends over an east-elongated area of 4.9 by 3.3 km, and to a depth of 610m at Pebble West and at least 1525m at Pebble East. The deposit is open to the east, south, NW and SE; a larger zone of strong alteration and low grade mineralization extends to the north, south and

west. The Pebble Deposit mineral resource, at a 0.30% copper equivalent cut-off, consist of 5.94 billion tonnes of measured and indicated resources grading 0.42% Cu, 0.35 g/t Au and 250 ppm Mo (Rebagliati et al., 2009).

IP-Resistivity survey results

The IP signature over the Pebble property shows a large scale anomaly (Figure 3) of roughly 100 km-sq that extends 4km from south up to north of Pebble deposit. There is a severe north-south break in the IP response just to the east of Pebble West representing a drastic drop in the chargeability value. It appears to be explained by the thicker post mineral cover and a major structure. The strongest response is observed in the vicinity of Pebble West surrounding the north, west and south part, with chargeability values ranging from 70-100msec (Paré, 2010).



Ground IP-Resistivity, airborne Spectrem and helicopter ZTEM survey results over Pebble porphyry Deposit

are a vector leading toward the economic mineralized zone. The Pebble West deposit is surrounded by a strong response related to Py enrichment and alteration halo. The core of the deposit is characterized by a lower chargeability response. The same tendency is observed with the resistivity data set; low resistivity associated with strong chargeability and slightly more resistive and less chargeable in the core. The Pebble East ore body has not been detected by the existing IP-Resistivity surveys, which were performed before the discovery of Pebble East and thus the geometry of their configurations were not designed to see at this depth.

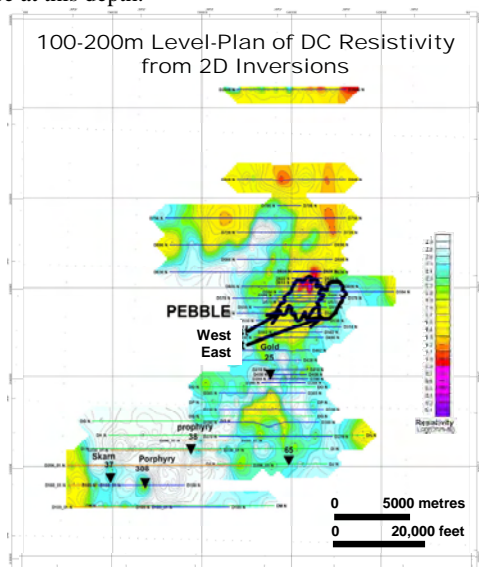


Figure 4: Level plan (100-200m elevation) of the resistivity over Pebble Deposit from 2D inversion.

Spectrem survey results

The Spectrem Air electromagnetic survey in combination with the magnetics over the Pebble area were to assist in identifying and delineating major structures that control the deposit location and high grade mineralization (i.e., ZG1 and ZE faults, etc.), as well as understanding the alteration zones and their distribution. Lastly the Spectrem EM survey was expected to help define possible sulphide enrichment zones, to 500-600m depths.

The Spectrem electromagnetic survey (Figures 8-9) has returned some interesting results regarding its capability to map resistivity contrasts. The time constant map (TAU) in Figure 8 shows an indication of the conductive pattern of the property mapped regardless to the depth and the size of the conductors. Generally the TAU map presents an excellent match with the ground resistivity survey results.

In Figure 8, the anomaly picking of the EM profiles has detected a number of conductors mostly located just north

of Pebble West and in the northern portion of Pebble East that coincide with the rich pyrite mineralization, sulphide veins and alteration. The conductors appear to be from an inductive source and have a very well defined shape in the profile. A circular conductive feature of moderate to good conductor has been picked up at the exact location where a flat lying magnetic body is interpreted. This conductive feature is also mapped in the resistivity survey.

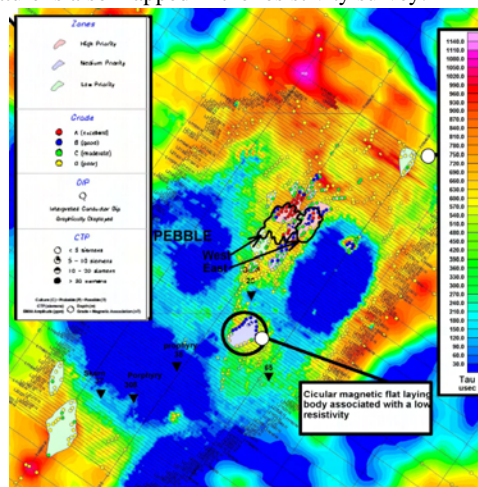


Figure 8: Spectrem time-constant (Tau) map, with picked EM anomalies

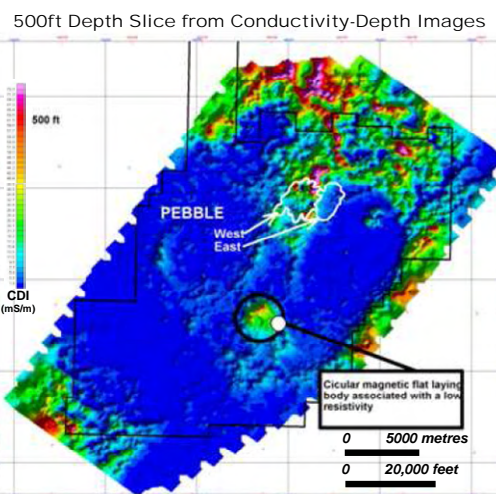


Figure 9: Spectrem depth slice at 500ft from CDI imaging.

Figure 9 shows the conductivity depth image (CDI) at 500 ft depth below surface. At depths greater than 1000ft the limit of the investigation of the survey drops drastically in conductive areas. The depth slice indicates stronger conductivity in the north and southwest property and north of Pebble. Pebble East has no signature in the 500ft CDI slice but starts appearing at 1000ft. The Pebble East low resistivity response is probably due to its alteration. Based on the EM conductivity response and the ground IP survey, the

Ground IP-Resistivity, airborne Spectrem and helicopter ZTEM survey results over Pebble porphyry Deposit

Spectrem survey appears to be generally unable to map the disseminated sulphides (as expected) but has better sensitivity to resistivity contrast associated with alteration.

ZTEM survey results

The main objectives of the ZTEM (AFMAG; Ward, 1959; Labson et al., 1985) over Pebble were to test its ability to map the porphyry deposit from surface to depth, based on resistivity contrasts and to establish a comparison study with previous geophysical surveys (Spectrem and IP).

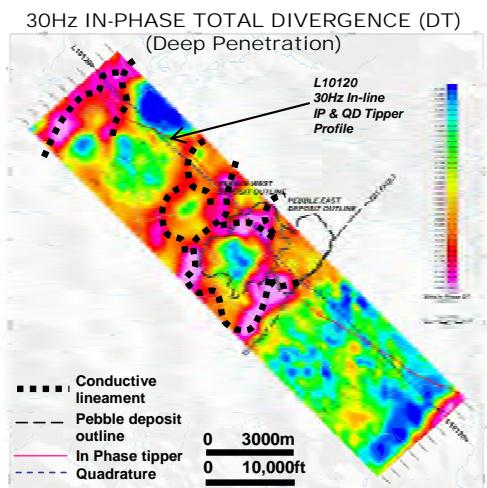


Figure 10: ZTEM Total Divergence of In-Phase tipper at 30Hz.

Figure 10 presents the ZTEM tipper results in plan shown as a Total Divergence (DT) image (Lo et al., 2009; analogous to Peaker parameter of Pedersen (1998) that converts the tipper cross-overs into peaks) of the In-Phase component with the outline of the Pebble East and West Zones overlain. The Pebble deposit is nearly invisible in the 360Hz high frequency data likely due to its limited penetration and poor relative contrasts in this skin depth range; However in the deeper, lower frequency 30Hz image, the Pebble deposit is better contrasted with the surrounding rocks. The 30Hz DT image indicates more resistive rocks in the center that correlates with the mineralized potassic-altered core; and the lower resistivities outside the deposit coincide with the surrounding clay-altered pyrite halo.

Figure 11 present the 2D cross-sectional resistivity results obtained from the Zvert2D inversion (Legault et al., 2009b) of the In-Line (Z/X) ZTEM tipper data for L10120 directly over the Pebble West and Pebble East deposits, from surface to 1.5km depths. Pebble West is defined as a shallower, more resistive body surrounded by lower resistivity rocks at depth and further west, which is consistent with the K-silicate alteration and surrounding lower grade pyritic clay-altered halo. Pebble East is defined as a deeper resistivity low that is consistent with its stronger argillization, which lies below more resistive metasedimentary cap-

rocks. East Zone appears to extend below 1km.

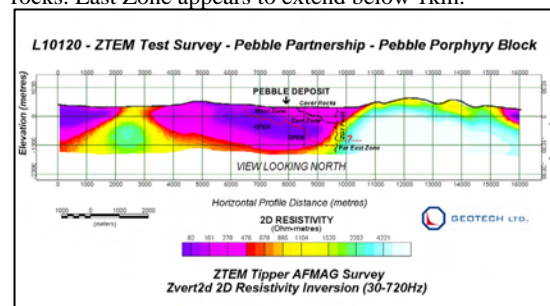


Figure 11: ZTEM L10120 2D resistivity inversion over Pebble.

Conclusion

All surveys performed over the Pebble property brought significant amount of information that improved the understanding of the geology, alteration and mineralization of the system. The IP survey remains an important tool in the exploration program over Pebble. Without IP, disseminated sulphides will not be contrasted if the country rock has a similar resistivity as the mineralized rock. Pebble East was not detected by IP due to lack of penetration of the survey configurations previously utilized.

The airborne surveys, Spectrem and ZTEM, have mapped the resistivity contrasts with more resolution than the ground resistivity survey. Their higher density sampling and better depth of investigation improved on the ground IP work (pre-2009). Spectrem conductors coincide with the rich pyrite mineralization, sulphide veins and alteration. However, as expected, Spectrem was unable to detect the disseminated mineralization in the system compared to the chargeability measurement or to properly estimate the thickness of the tertiary cover, due to the lack of physical property contrasts. The Spectrem survey depth of investigation is at the limit of detection of Pebble East.

The AFMAG (ZTEM) survey over Pebble deposit area correlates with the Spectrem data in defining geological features and structures based on lateral resistivity contrasts. The frequency bandwidth range of the ZTEM maps the near surface while the lower frequency allows for greater depth of investigation. The ZTEM AFMAG tipper is more sensitive to weak resistivity contrast than those observed on the Spectrem survey especially at depth. Both the Pebble West Zone and East Zone are detected in the ZTEM results based on resistivity contrasts due to alteration, lithology and structure. Physical properties measurements are key in the improvement of the inversion of the AFMAG data.

Acknowledgements

The authors thank Anglo American Exploration (Canada) Ltd., Northern Dynasty Mines Ltd., and Geotech Ltd. for generously allowing us to present these results.

EDITED REFERENCES

Note: This reference list is a copy-edited version of the reference list submitted by the author. Reference lists for the 2010 SEG Technical Program Expanded Abstracts have been copy edited so that references provided with the online metadata for each paper will achieve a high degree of linking to cited sources that appear on the Web.

REFERENCES

- Acorn, W., R. Coyoli, H. Kumar, and J. M. Legault, 2009, Report on helicopter-borne Z-axis tipper electromagnetic (ZTEM) and aeromagnetic geophysical survey, Pebble Property, Lliamna, Alaska, for Pebble Partnership: internal report by Geotech Ltd., 56 pp.
- Klinkert, P. S., S. Letts, J. Smit, and L. Polome, 2009, Spectrem survey of the Pebble area (Alaska), for Pebble Limited Partnership, internal report by Spectrem Air Ltd., 75 pp.
- Labson, V. F., A. Becker, H. F. Morrison, and U. Conti, 1985, Geophysical exploration with audio-frequency natural magnetic fields: *Geophysics*, **50**, 656–664, [doi:10.1190/1.1441940](https://doi.org/10.1190/1.1441940).
- Leggatt, P. B., P. S. Klinkert, and T. B. Hage, 2000, The Spectrem airborne electromagnetic system—Further developments: *Geophysics*, **65**, 1976–1982, [doi:10.1190/1.1444881](https://doi.org/10.1190/1.1444881).
- Legault, J.M., H. Kumar, B. Milicevic, and L. Hulbert, ZTEM airborne tipper AFMAG test survey over a magmatic copper-nickel target at Axis Lake in northern Saskatchewan, *SEG Expanded Abstracts*, **28**, 1272–1276.
- Legault, J. M., H. Kumar, B. Milicevic, and P. Wannamaker, 2009, ZTEM tipper AFMAG and 2D Inversion results over an unconformity uranium target in northern Saskatchewan: *SEG Expanded Abstracts*, **28**, 1277–1281.
- Lo, B., and M. Zang, 2008, Numerical modeling of Z-TEM (airborne AFMAG) responses to guide exploration strategies: *SEG Expanded Abstracts*, **27**, no. 1, 1098–1101, [doi:10.1190/1.3059115](https://doi.org/10.1190/1.3059115).
- Lo, B., J. M. Legault, and P. Kuzmin, P., and M. Combrinck, 2009, Z-TEM (Airborne AFMAG) tests over unconformity uranium deposits, *ASEG Extended abstracts*, 6 pp.
- Macnae, J. C., R. Smith, B. D. Polzer, Y. Lamontagne, and P. S. Klinkert, 1991, Conductivity-depth imaging of airborne electromagnetic step-response data: *Geophysics*, **56**, 102–114, [doi:10.1190/1.1442945](https://doi.org/10.1190/1.1442945).
- Pare, P., 2010, Pebble Project - Report on a compilation\interpretation of the IP-Resistivity, Spectrem and ZTEM Surveys, internal report by Anglo American Exploration (Canada) Ltd., 61 pp.
- Pedersen, L. B., 1998, Tensor VLF measurements: Our first experiences: *Exploration Geophysics*, **29**, no. 2, 52–57, [doi:10.1071/EG998052](https://doi.org/10.1071/EG998052).
- Rebagliati, C. M., J. Lang, E. Titley, D. Rennie, L. Melis, D. Barratt, and S. Hodgson, 2008, Technical report on the 2008 program and update on mineral resources and metallurgy, Pebble copper-gold-molybdenum project, Iliamna Lake area, southwestern Alaska, USA, for Northern Dynasty Minerals Ltd., NI-43 101 report, 170 pp.
- Ward, S. H., 1959, AFMAG—Airborne and ground: *Geophysics*, **24**, 761–787, [doi:10.1190/1.1438657](https://doi.org/10.1190/1.1438657).

3D inversion of SPECTREM and ZTEM data from the Pebble Cu-Au-Mo porphyry deposit, Alaska

Pascal Pare*

Anglo American Exploration (Canada)
Vancouver, Canada
ppare@angloamerican.ca

Alexander V. Gribenko

TechnoImaging & University of Utah
Salt Lake City, USA
alex@technoimaging.com

Leif H. Cox

TechnoImaging
Salt Lake City, USA
leif@technoimaging.com

Martin Čuma

TechnoImaging & University of Utah
Salt Lake City, USA
martin@technoimaging.com

Glenn A. Wilson

TechnoImaging
Salt Lake City, USA
glenn@technoimaging.com

Michael S. Zhdanov

TechnoImaging & University of Utah
Salt Lake City, USA
mzhdanov@technoimaging.com

Jean Legault

Geotech
Aurora, Canada
jean@geotech.ca

Jaco Smit

Anglo American
Johannesburg, South Africa
jpsmit@angloamerican.co.za

Louis Polomé

Spectrem Air
Lanseria, South Africa
louis@spectrem.co.za

SUMMARY

This case study compares 3D inversion results from Spectrem Air's SPECTREM 2000 fixed-wing time-domain airborne electromagnetic (AEM) system, and Geotech's Z-axis Tipper Electromagnetic (ZTEM) airborne audio-frequency magnetics (AFMAG) system flown over the Pebble Cu-Au-Mo deposit in Alaska. Within the commonality of their physics, 3D inversions of both SPECTREM and ZTEM recover conductivity models consistent with each other and with the known geology. Both 3D inversions recover conductors coincident with alteration associated with both Pebble East and Pebble West. The 3D interpretation of both surveys has yielded improved understanding of the geology, alteration and mineralization of the Pebble system. There are distinct practical advantages to the use of both SPECTREM and ZTEM, so we draw no recommendation on one system over the other. We do conclude however, that 3D inversions of AEM and ZTEM surveys add significant value to exploration.

Key words: 3D, inversion, AEM, AFMAG, SPECTREM, ZTEM, Pebble.

INTRODUCTION

Pebble is a calc-alkalic Cu-Au-Mo porphyry deposit located in the Bristol Bay region of southwest Alaska, approximately 320 km southwest of Anchorage and 27 km west-northwest of the village of Iliamna (Figure 1). Development of the Pebble deposit is managed by Pebble Limited Partnership (PLP), a joint venture between Northern Dynasty Mines Ltd (50%) and Anglo American plc (50%). Since discovery in 1988, over 886,177 feet of drilling in 1,085 holes have been completed, making Pebble one of the most intensively studied, undeveloped mineral systems in the world. At a 0.30% Cu equivalent cut-off, the latest Pebble resource estimate includes 5.942 billion tonnes in the measured and indicated category containing 25.0 million tonnes of copper, 66.9 million ounces of gold and 1.5 million tonnes molybdenum; and 4.835 billion

tonnes in the inferred category, containing 11.6 million tonnes of copper, 40.4 million ounces of gold and 1.0 million tonnes of molybdenum. This resource base makes Pebble the largest gold and sixth largest copper deposit in the world.



Figure 1. Pebble location in southwest Alaska.

In 2009, a 3,840 line km SPECTREM AEM, magnetic and radiometric survey was flown over the Pebble district. The survey was done in two stages; a regional survey at 1500 m flight-line spacing, covering an area of approximately 30 km x 12 km, and a more detailed survey at 250 m flight-line spacing along strike of the Pebble deposit. Also in 2009, a 250 line km helicopter ZTEM AFMAG and magnetic survey was flown at 200 m line spacing over the Pebble deposit. Previous analyses (e.g., Pare and Legault, 2010) utilized 1D conductivity depth images, time constants and anomaly picking for interpretation of the SPECTREM data, and 2D inversion of one tipper component for interpretation of the ZTEM data. With the availability of 3D inversion for both SPECTREM and ZTEM, we have reinterpreted both surveys independently, and are now able to make a more quantitative assessment of the merits for both airborne electromagnetic methods for the exploration of porphyry systems such as Pebble.

EXPLORATION HISTORY

The Pebble deposit is underlain by Jura-Cretaceous to Eocene igneous and sedimentary rocks. The Pebble deposit is a calc-alkalic Cu-Au-Mo porphyry deposit which formed in association with granodiorite intrusions emplaced at roughly

90 Ma. The deposit comprises of the contiguous Pebble West and Pebble East Zones (Figure 2), discovered in 1986 and in 2005, respectively. Mineralization at Pebble West occurs around small granodioritic stocks that intrude the country rocks. The Pebble East mineralization occurs within a granodioritic stock and in sills that cut the country rocks. Pebble West extends to surface and Pebble East is entirely overlain by east-thickening, younger volcano-sedimentary cover, up to 600 m thick. Pebble is bounded to the southeast by the major ZG1 dip-slip fault, east of which the deeper Far East Zone has been discovered in 2006 with a deep hole (DDH6438), drilled east of ZG1 fault identified at > 1.5 km depths (Figure 3).

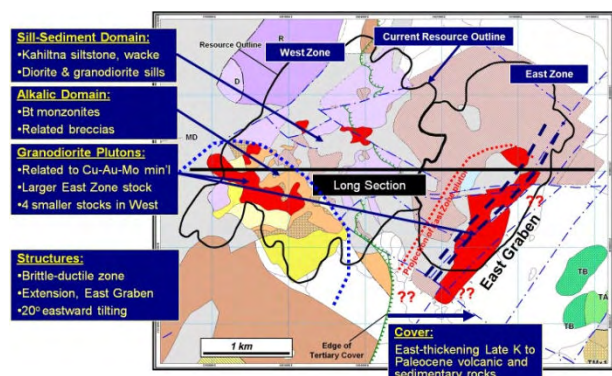


Figure 2. Geology of the Pebble deposit.

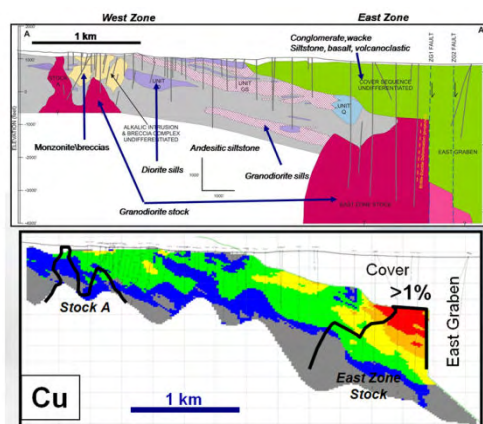


Figure 3. East-west oriented vertical cross section of the geology (upper panel) and mineralization (lower panel) of the Pebble West and Pebble East zones.

The deposit hosts K-silicate alteration and associated quartz-sulphide veins, overprinted by phyllo-silicate alteration. Sulphides mainly consist of hypogene pyrite, chalcopyrite, molybdenite and bornite; supergene and thin oxide zones also occur at Pebble West. High grade mineralization at Pebble East is associated with advanced argillic alteration. The Cu-Au-Mo mineralization, as it is currently known, extends over an east-elongated area of 4.9 by 3.3 km, and to a depth of 610 m at Pebble West, and at least 1525 m at Pebble East. The deposit is open to the east, south, northwest and southeast; a larger zone of strong alteration and low grade mineralization extends to the north, south and west. The Pebble deposit mineral resource, at a 0.30% Cu equivalent cut-off, consist of 5.942 billion tonnes of measured and indicated resources grading 0.42% Cu, 0.35 g/t Au, and 250 ppm Mo.

From 1988 to 2001, induced polarization (IP) and resistivity surveys utilized both time-domain and phase IP in both dipole-dipole and pole-dipole configurations. These surveys defined a chargeability anomaly within the Cretaceous rocks that was about 91 km² in extent, measuring approximately 21 km north-south and nearly 10 km east-west. This contained 11 distinct centers reflected by stronger chargeability anomalies, many of which were later demonstrated to be coincident with extensive Cu, Au and Mo soil geochemical anomalies. All known zones of Cretaceous age mineralization occur within this broad IP anomaly. In 2009, a time-domain IP survey utilized a larger, deeper penetrating array. Analysis of that data is beyond the intended scope of this paper.

In 2009, Spectrem Air Ltd conducted a SPECTREM AEM, magnetic and radiometric survey over the Pebble district. A total of 3,840 line kilometres were flown. The survey was done in two stages; a regional survey at 1500 m flight-line spacing, covering an area of approximately 30 km x 12 km, and a more detailed survey at 250 m flight-line spacing along strike of the Pebble deposit. The SPECTREM system is a 100% duty cycle square wave of 45 Hz base frequency measuring inline and vertical B-fields (Leggatt et al., 2000). At Pebble, the transmitter was flown with a nominal ground clearance of 107 m, with the receiver towed 37.1 m below and 122.2 m behind.

Also in 2009, Geotech Ltd conducted a helicopter ZTEM AFMAG and magnetic survey over the Pebble deposit. A total of 250 line km were flown with a flight line spacing of 200 m covering approximately 60 km². ZTEM is an audio-frequency magnetic (AFMAG) system that measured both Z/X and Z/Y tipper components at five frequencies; 30 Hz, 45 Hz, 90 Hz, 180 Hz, and 360 Hz. At Pebble, the receiver was flown with a nominal ground clearance of 89 m.

3D INVERSION METHODOLOGY

Our 3D frequency-domain modeling of fields and their sensitivities is based on an implementation of the contraction integral equation method that exploits the Toeplitz structure of large, dense matrix systems in order to solve multiple source vectors on the right-hand side using an iterative method with fast matrix-vector multiplications provided by a 2D FFT convolution (Hursán and Zhdanov, 2002). Once the Green's tensors have been pre-computed, they are stored and re-used, further reducing run time. Once computed, the magnetic fields and their sensitivities can be transformed to the AEM system response (for AEM) (e.g., Raiche, 1998) or tipper components (for ZTEM) (e.g., Holtham and Oldenburg, 2010).

Both our 3D AEM and ZTEM inversions are based on the re-weighted regularized conjugate gradient (RRCG) method. Data and model weights which reweigh the inverse problem in logarithmic space are introduced in order to reduce the dynamic range of both the data and the conductivity. Traditional regularized inversion methods recover smooth solutions, and thus have difficulties recovering sharp boundaries between different geological formations without having a priori information about those boundaries enforced. Our use of focusing regularization makes it possible to recover subsurface models with sharper resistivity contrasts and boundaries than can be obtained with smooth stabilizers, and do not require those boundaries to be enforced a priori (Zhdanov, 2002, 2009).

For 3D AEM inversion, Cox et al. (2010) introduced a practical inversion methodology which exploited the AEM system's limited footprint. The footprint of each transmitter-receiver pair is a sub-domain of the 3D earth model, and this sub-domain is used for 3D modelling of fields and sensitivities. As the footprints of all the transmitter-receiver pairs superimpose themselves over the 3D earth model, the sensitivity matrix for the 3D earth model is constructed. This sensitivity matrix is used for updating the model parameters for the 3D earth model so as to minimise the misfit between the observed and predicted data. This strategy makes it practical to invert tens of thousands of stations of time- or frequency-domain AEM data to models with millions of cells within just hours on multi-processor workstations.

3D ZTEM inversion is an analogue of 3D magnetotelluric (MT) inversion. For example Holtham and Oldenburg (2010) introduced their 3D ZTEM inversion based on modifications of the 3D MT inversion by Farquharson et al. (2002). Similarly, our 3D ZTEM inversion is an analogue of the 3D MT inversion by Zhdanov et al. (2011). One key difference between our 3D ZTEM inversion and that of Holtham and Oldenburg (2010) is that we also employ a footprint approach for each receiver. Unlike the footprint for AEM, the footprint for ZTEM is only applied to the computation of the sensitivities and not the modelling. This permits us to efficiently compute, store and manipulate the sensitivities for very large surveys.

INTERPRETATION

The depth of investigation for SPECTREM was about 750 m below the surface, and for ZTEM was about 1500 m below the surface. Both 3D SPECTREM and ZTEM inversions recovered Pebble's main alteration pattern and the known structures ZF, ZC, ZE and ZG1 (Figures 6 and 7). Generally speaking, the 3D SPECTREM inversion recovered the geological features and structures with better accuracy than the 1D inversion and CDIs. As expected, the 3D inversion produced better lateral model continuity from line to line than the non-3D inversions (e.g., Figure 4). Also, the 3D ZTEM inversion recovered the geological features and structures with better accuracy than the 2D inversions of the same data (e.g., Figure 5). As expected, the 3D inversion with focusing regularization produced sharper contrasts and better lateral model continuity from line to line than the 2D inversions with smooth regularization.

Further analysing the 3D SPECTREM and ZTEM inversions, we can make the following correlations between conductivity and known geology:

- The highly conductive zones to the known illite-pyrite and advanced argillic alteration parts of the system;
- The weak conductive zone and resistive high beneath the Pebble West and East zones are characterized by sodic-potassic, K-silicate and deep sodic-calcic domains;
- The high conductive zone on line L21370 above the Pebble East zone and confined between the ZE and ZG1 faults is associated with the advanced argillic alteration that overprints the highest grades;
- The moderately conductive layer near the surface above the Pebble East zone and to the east appears to be related with the tertiary cover;
- The main known structures (ZF, ZC, ZE and ZG1) are well resolved, and correlate with the breaking pattern of the 3D conductivity models; especially the ZG1 fault to the east of Pebble East.

The geometry of the 3D SPECTREM and ZTEM inversions follow the general trend of the alteration and ore geometry. However the correlation between conductivities and mineralization is not as directly coincident as with the alteration pattern. This suggests that the sulphide content is not a major factor in either the SPECTREM or ZTEM responses. The high grade CuEq 0.6% is not consistently following the high conductive trend. The conductive zones contrasts are mostly coincident with alteration change.

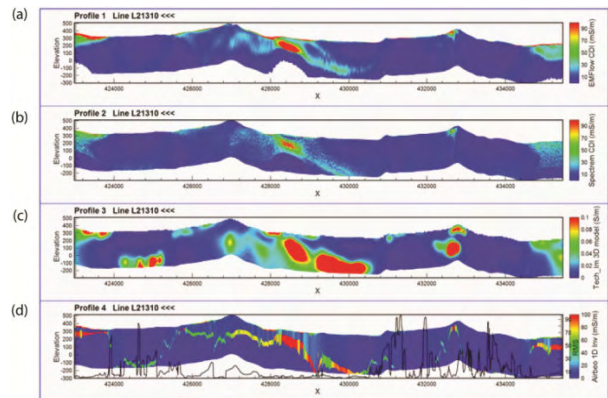


Figure 4. Comparison of (a) EMFlow CDI, (b) SPECTREM CDI, (c) 3D inversion, and (d) AirGeo 1D inversion for SPECTREM line L21310.

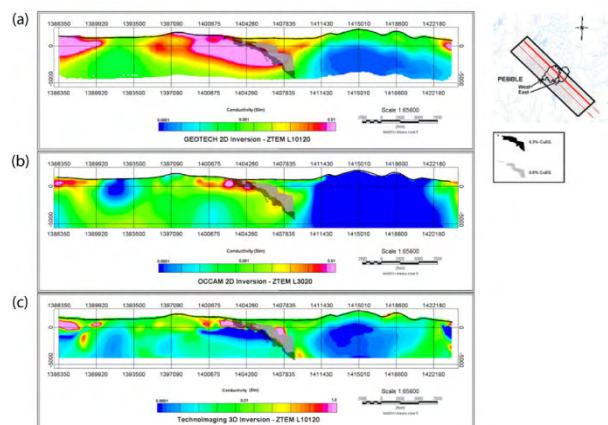


Figure 5. Comparison of (a) 2D inversion (by Geotech), (b) 2D inversion (by Condor Consulting) and (c) 3D inversion for ZTEM line L10120. The CuEq 0.3% and CuEq 0.6% ore shells are superimposed on each model.

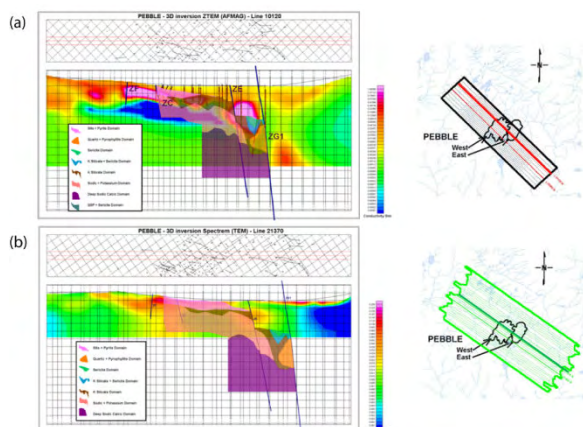


Figure 6. Comparison of (a) 3D ZTEM inversion for ZTEM line L10120 and (b) 3D SPECTREM inversion for SPECTREM line L21370, with alteration patterns superimposed.

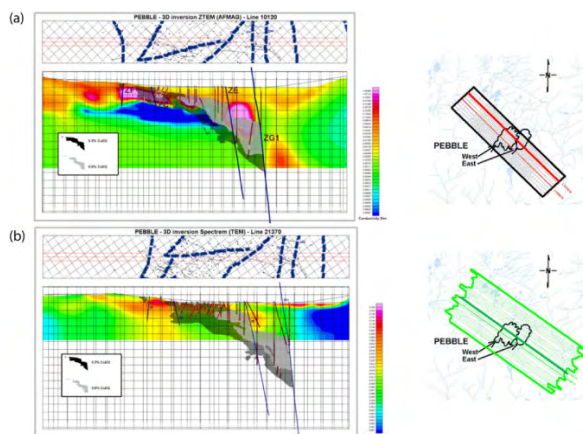


Figure 7. Comparison of (a) 3D ZTEM inversion for ZTEM line L10120 and (b) 3D SPECTREM inversion for SPECTREM line L21370, with CuEq 0.3% and CuEq 0.6% mineralization shells superimposed.

CONCLUSIONS

3D inversions of SPECTREM and ZTEM surveys over the Pebble deposit have been examined. For SPECTREM, we compared our 3D inversion results with conductivity depth images and 1D inversion results. For ZTEM, we compared our 3D inversion results with 2D inversion results. Both of our 3D inversions recovered models more consistent with the known geology than those obtained from non-3D methods. Moreover, both SPECTREM and ZTEM inversions recovered 3D models that were consistent within the commonality of their physics, and which corresponded well with the known geology. As in any exploration project, interpretation of both surveys has yielded improved the understanding of the geology, alteration and mineralization of the Pebble system. There are distinct practical advantages to the use of both SPECTREM and ZTEM, so we draw no recommendation on either system. We can conclude however, that 3D inversion of AEM and ZTEM surveys adds significant value to exploration.

ACKNOWLEDGMENTS

The authors thank Pebble Partnership Ltd, Anglo American Exploration (Canada) Ltd, Northern Dynasty Mines Ltd, Spectrem Air Ltd, Geotech Ltd, and TechnoImaging LLC for permission to publish. Gribenko, Čuma and Zhdanov acknowledge support from the University of Utah's Consortium for Electromagnetic Modeling and Inversion (CEMI) and Center for High Performance Computing (CHPC).

REFERENCES

- Cox, L. H., Wilson, G. A. and Zhdanov, M. S., 2010, 3D inversion of airborne electromagnetic data using a moving footprint: *Exploration Geophysics*, **41**, 250-259.
- Farquharson, C. G., Oldenburg, D. W., Haber, E. and Shekhtman, R., 2002, An algorithm for the three-dimensional inversion of magnetotelluric data: 72nd Annual International Meeting, SEG, Expanded Abstracts, 649-652.
- Holtham, E. and Oldenburg, D. W., 2010, Three-dimensional inversion of ZTEM data: *Geophysical Journal International*, **182**, 168-182.
- Hursán, G. and Zhdanov, M. S., 2002, Contraction integral equation method in three-dimensional electromagnetic modelling: *Radio Science*, **37**, doi: 10.1029/2001RS002513.
- Leggatt, P. B., Klinkert, P. S. and Hage, T. B., 2000, The Spectrem airborne electromagnetic system – further developments: *Geophysics*, **65**, 1976-1982.
- Pare, P. and Legault, J. M., 2010, Ground IP-resistivity and airborne SPECTREM and helicopter ZTEM survey results over Pebble copper-moly-gold porphyry deposit, Alaska: 80th Annual International Meeting, SEG, Expanded Abstracts, 1734-1738.
- Raiche, A., 1998, Modelling the time-domain response of AEM systems: *Exploration Geophysics*, **29**, 103-106.
- Zhdanov, M. S., 2002, *Geophysical Inverse Theory and Regularization Problems*, Elsevier.
- Zhdanov, M.S., 2009, *Geophysical Electromagnetic Theory and Methods*. Elsevier.
- Zhdanov, M. S., Smith, R. B., Gribenko, A., Čuma, M. and Green, A. M., 2011, Three-dimensional inversion of large-scale EarthScope magnetotelluric data based on the integral equation method – geoelectrical imaging of the Yellowstone conductive mantle plume: *Geophysical Research Letters*, **38**, L08307, doi:10.1029/2011GL046953.

A brief analysis of ZTEM data from the Forrestania test site, WA

Daniel Sattel*
EM Solutions, USA
dsattel@earthlink.net

Ken Witherly
Condor Consulting, Inc., USA
ken@condorconsult.com

Michael Becken
GFZ Potsdam, Germany
becken@gfz-potsdam.de

SUMMARY

ZTEM is a helicopter-borne AFMAG system that measures the magnetic-field response in the frequency range 25-600 Hz of naturally occurring currents in the subsurface. The resolution of this system is analyzed by forward modeling and inverting synthetic ZTEM data using a 2D algorithm for a range of conductivity scenarios.

ZTEM data acquired at the Forrestania test site are compared with overlapping VTEM data. Conductivity-depth sections derived from both data sets show broad agreement, but indicate better spatial resolution for the VTEM data. The response due to bedrock conductor IR2 is strong for the VTEM system and subtle on the ZTEM profiles, which appear to be dominated by responses to larger, elongated structures. Products derived from the ZTEM data, including apparent conductivity, phase and Karous-Hjelt filtered grids appear to map geologic structure, complementing the information gathered from the VTEM data.

Key words: AFMAG, airborne electromagnetics, EM data modeling, inversion, natural-field EM.

INTRODUCTION

The ZTEM system was developed by Geotech Ltd to measure the AFMAG responses of naturally occurring subsurface currents, induced by far-away lightning discharges (Legault et al., 2009). The vertical component is measured from a moving helicopter platform, while the horizontal components are recorded on the ground at a base station. By comparison, the VTEM system measures the magnetic-field response due to currents induced in the subsurface by the transmitter the system is carrying (Witherly and Irvine, 2007).

Geotech has flown the VTEM and ZTEM system across two bedrock conductors at Forrestania, W.A., located approximately 350 km east of Perth. The overlap of data from both surveys allow for a direct comparison of the spatial resolution and depth penetration of the two systems. Before analysing the survey data, synthetic modelling of the ZTEM data is presented, to illustrate the strengths and limitations of that system.

SYNTHETIC ZTEM DATA

Synthetic ZTEM profiles were forward modeled and inverted using a 2D MT algorithm, developed by Constable and Wannamaker (deGroot-Hedlin and Constable, 1990; Wannamaker et al., 1987; deLugao and Wannamaker, 1996).

Synthetic modeling results are shown in Figures 1-3. A flying height of 80 m was modeled. Since the vertical magnetic field, due to plane-wave excitation (magnetotelluric Hz response) is zero above a 1D earth, the ZTEM system tipper-functions T_{zx} and T_{zy} , that are determined from the magnetic field observations by statistical analysis of the relationship

$$H_z = \begin{bmatrix} T_{zx} & T_{zy} \end{bmatrix} \begin{bmatrix} H_x \\ H_y \end{bmatrix} \quad (1)$$

show no response above a layered-earth. Hence, the ZTEM system is insensitive to one-dimensional or layered conductivity structures. In Equation (1), the vertical magnetic field is measured in the air, and the horizontal components are recorded with a fixed ground station. For the computation of synthetic across-strike profiles using a 2D modeling code, Equation (1) simplifies to

$$H_z = T_{zx} H_x \quad (2)$$

The sensitivity of ZTEM data to two-dimensional conductivity structures is demonstrated with the salt lake, regolith and tabular conductor models in Figures 1-3. The inversion fitted the data to a RMS error of 1.3, which has been determined as a representative target RMS for the modeling of survey data. Since these are synthetic data, the inversion would be able to achieve a better data fit, but this exercise is meant to demonstrate the resolution of actual ZTEM field data.

In Figure 1, the ZTEM system shows a strong Tzx response at the salt-lake edges and the 2D inversion resolves the conductivity of the salt lake very well, but doesn't indicate the presence of the regolith.

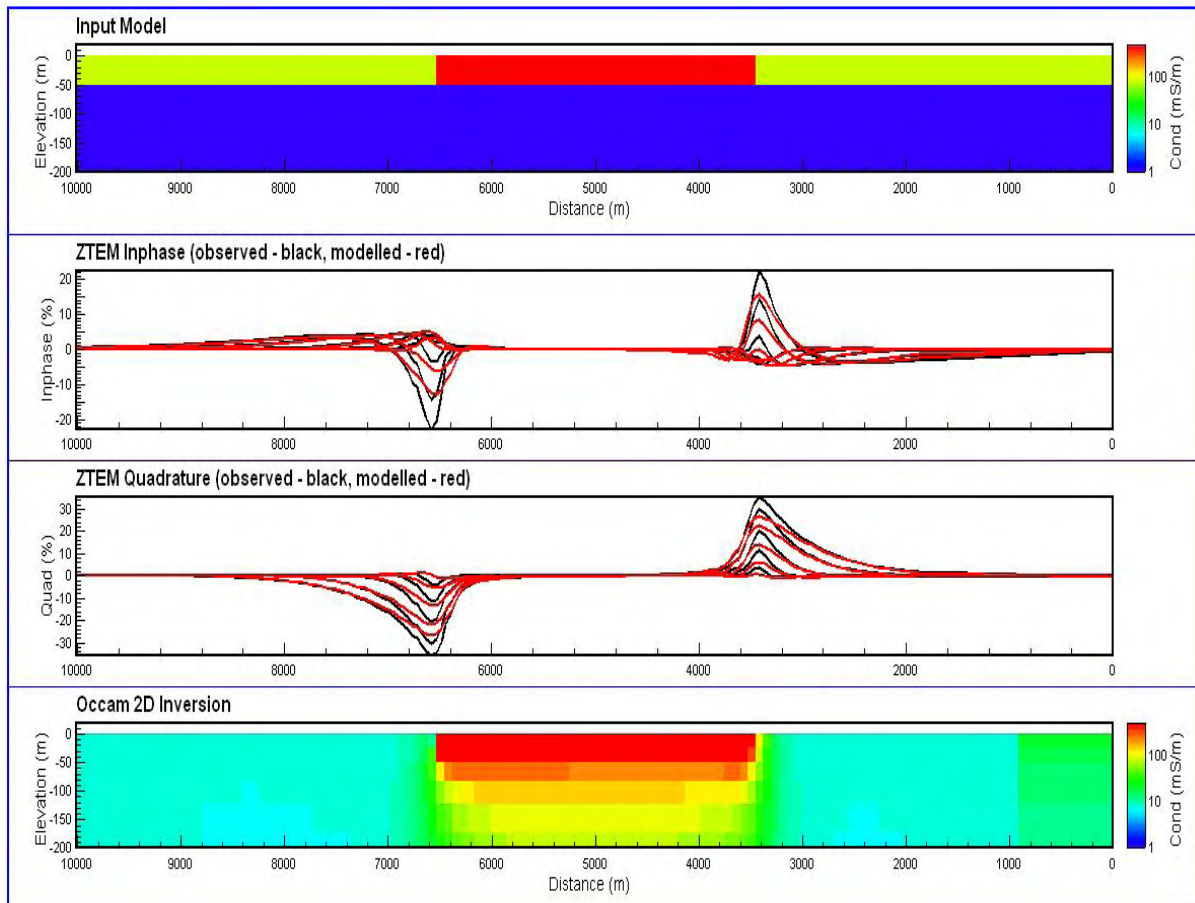


Figure 1. Observed and modelled ZTEM responses above a salt lake (50 m of 5 S/m), surrounded by regolith (50 m of 0.1 S/m) on a resistive half-space (0.0001 S/m).

Figure 2 shows that a regolith of laterally varying conductivity can show a moderate ZTEM response. The inversion recovers well the lateral conductivity gradient from the synthetic data. However, the modelled noise level does not allow for a good vertical resolution, which results in the blurred recovery of the true conductivity structure.

The ZTEM response across a tabular conductor under 100 m of overburden is shown in Figure 3. The ZTEM system shows a strong Tzx response above the conductor and the 2D inversion gives a good indication of the conductor's presence.

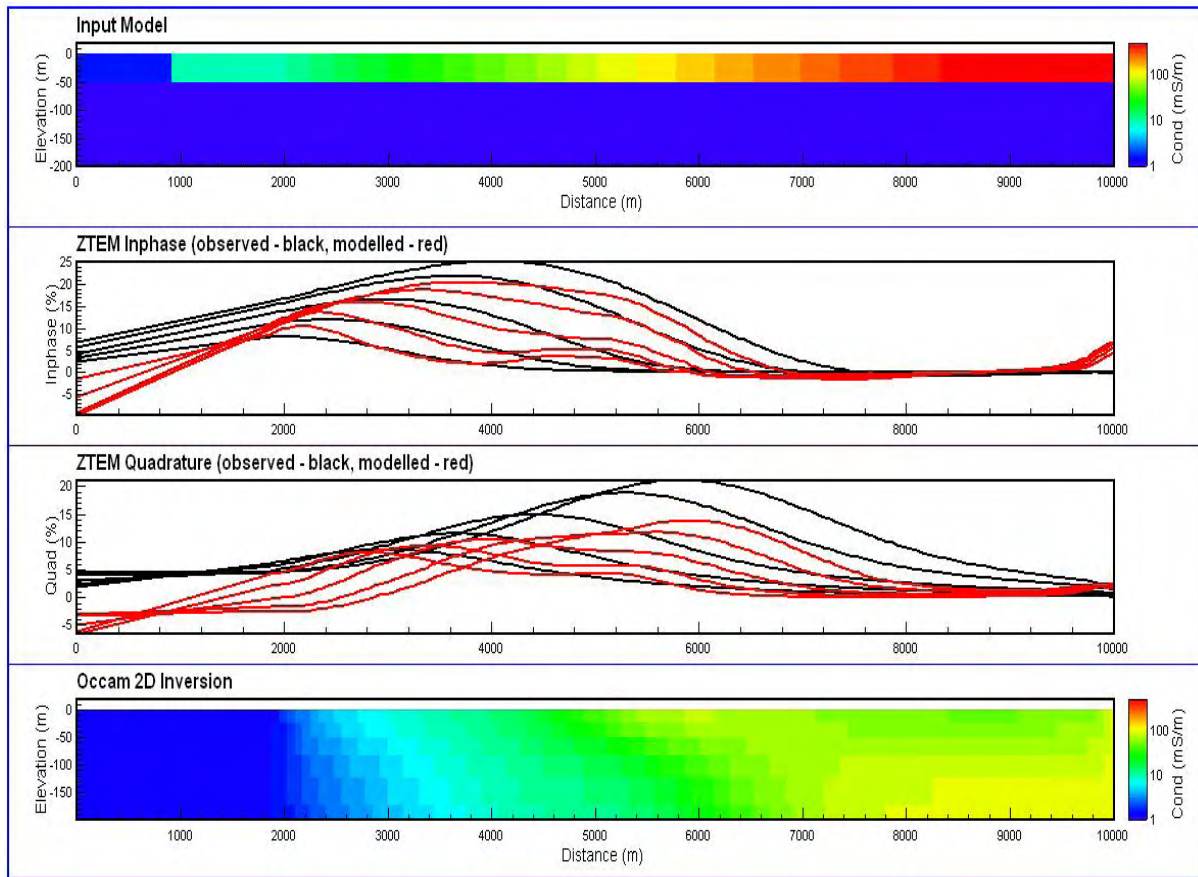


Figure 2. Observed and modelled ZTEM responses above regolith of laterally varying conductivity (50 m of 0.0015 – 0.1 S/m) on resistive half-space (0.001 S/m).

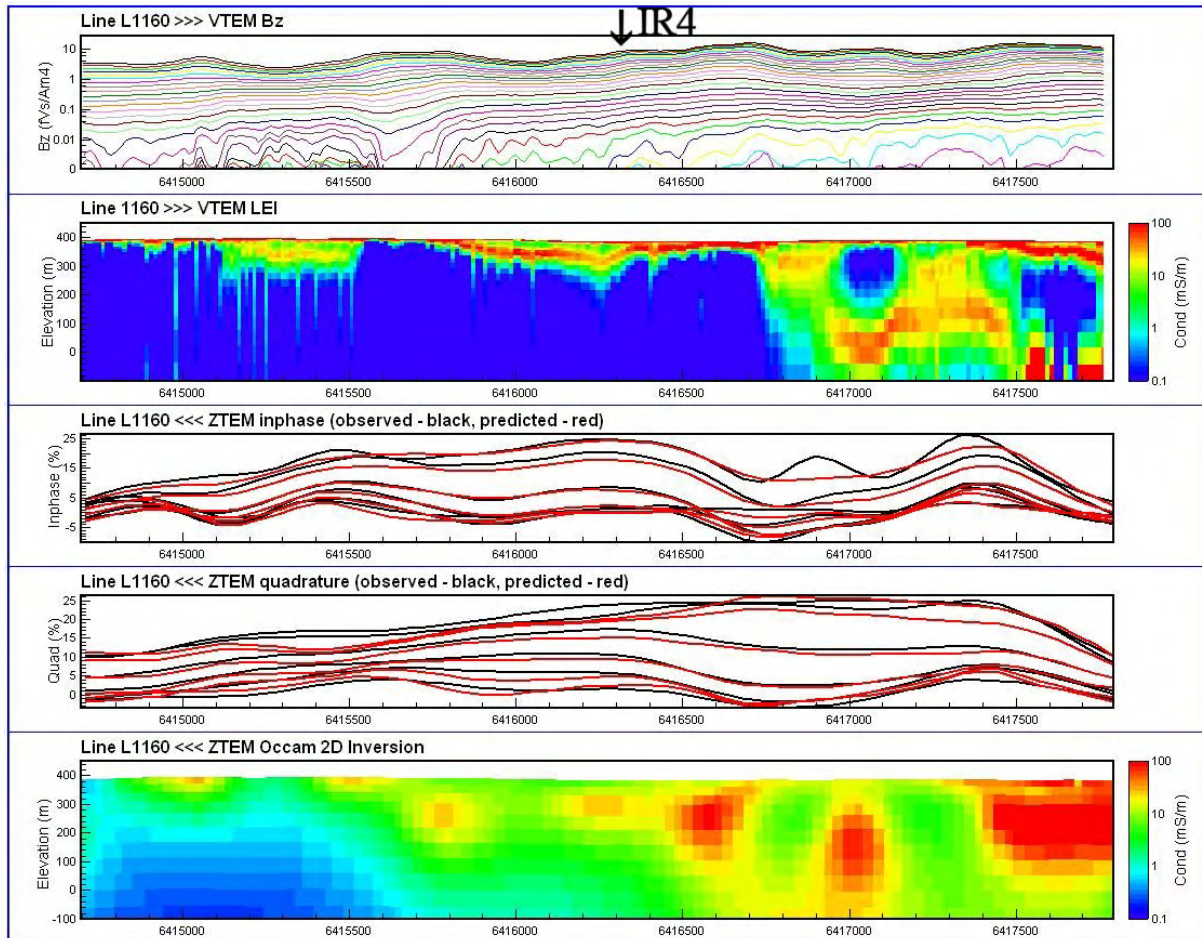
FORRESTANIA SURVEY

The Forrestania EM test range is described on the website of Southern Geoscience Consultants (www.sgc.com.au). The ground covered by the VTEM and ZTEM surveys include two drilled, barren, semi-massive to massive sulphides (IR2 and IR4), hosted in highly resistive bedrock under a conductive overburden (10-20 S). Conductor IR2 is described as shallow (<100 m), highly conductive (>7,000 S), small (<75x75 m) and dipping 30-40 degrees to the north. It is well defined by surface, downhole and some airborne EM systems. The EM anomaly at the centre of VTEM profile 1075 (see Figure 4) clearly indicates the location of IR2. Conductor IR4 is described as deep (> 300 m), highly conductive (5,000-10,000 S), extensive in strike and plunge extent (> 500 m), limited in depth extent (100-150 m) and dipping 30-40 degrees to the north. Due to its depth, IR4 is difficult to detect with airborne EM systems. The VTEM profile of line 1160 shown in Figure 6 shows no indication for the presence of IR4.

The ZTEM survey was flown in late 2009 with a line spacing of 100 m. Survey lines were acquired north-south and east-west. Results from the north-south data set are included in the following discussion.

Modelling results from data across conductor IR2 are summarized in Figures 4 and 5. The conductivity-depth section shown in Figure 4 was derived from the VTEM data by layered-earth inversion. IR2 has been clearly mapped, albeit at greater depth than expected. The shown conductivity-structure was forward modelled to predict the expected ZTEM response using the 2D MT algorithm and taking into account the system elevation. The observed and predicted ZTEM data are shown in Figure 4, showing overall good agreement.

Next, the ZTEM data were modelled using the 2D inversion algorithm by Constable and Wannamaker. The inversion result of the ZTEM data from Figure 4 is shown in Figure 5. The ZTEM-derived conductivity structure bears little resemblance with the VTEM-derived model. However, the conductor IR2 has been detected and modelled by the ZTEM data at the correct depth range and with the correct dip direction. Extensive conductive material is mapped at.



the northern end, consistently over most lines of this survey block. The discrepancy between conductivity-depth sections derived from VTEM and ZTEM data can be explained by ZTEM data being more sensitive to conductivity contrasts rather than elevated absolute conductivities, and current channelling being the major current excitation mode rather than induced vortex currents. The apparent conductivity profile shown in Figure 5, and explained below, shows a subtle peak at the location of IR2, which is overshadowed by a bigger and broader peak to the north, possibly corresponding to a shear zone.

VTEM and ZTEM profiles across IR4 with corresponding conductivity-depth sections are shown in Figure 6. Neither data set gives any indication for the presence of IR4. This is less surprising for the VTEM data, due to the depth of the conductor. It was hoped that, due the extensive strike length, the ZTEM data might be able to detect the conductor. As with the survey lines across IR2, the conductivity-depth sections derived from the two systems differ significantly, with the VTEM section indicating better spatial resolution.

Conductivity-depth grids have been derived from the inversion results of all VTEM and ZTEM lines. Figure 7 shows the conductivity at different depths. Even though the two surveys had the same line spacing, the VTEM data provide superior spatial detail, especially at shallow depths. Extensive resistive material at intermediate depths was mapped by both systems in the southwestern quadrant. Conductive detritic patterns mapped by the VTEM system agree well with similar patterns indicated by the ZTEM data, albeit at greater depth. There is good indication for conductor IR2 at shallow depths on the ZTEM-derived grids and at greater depths on the VTEM-derived grids.

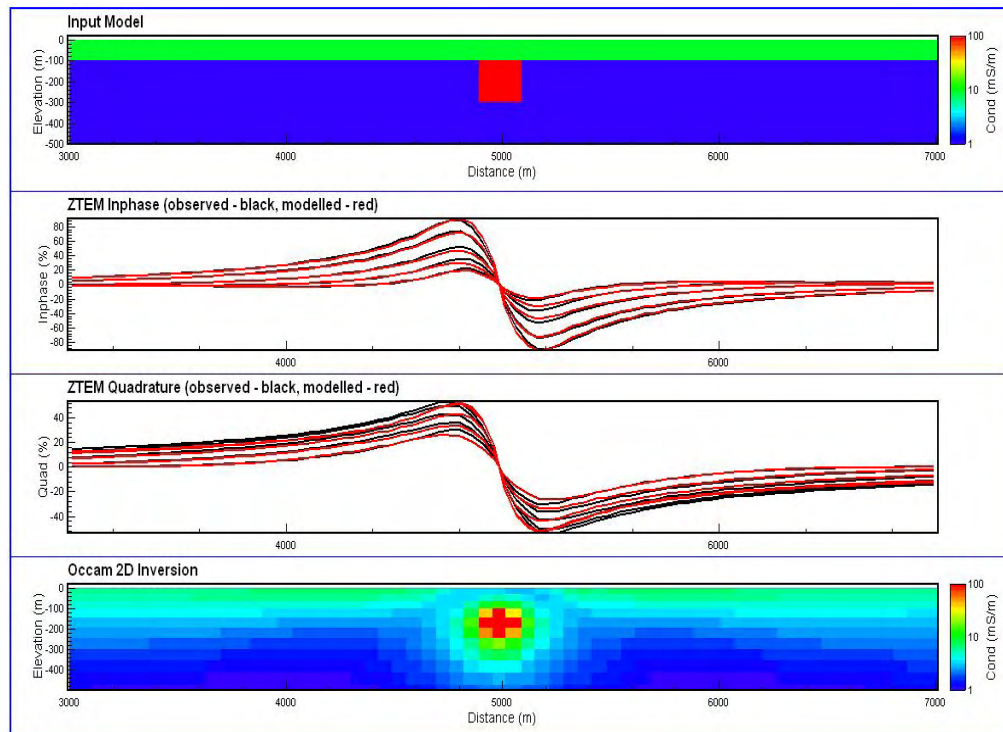


Figure 3. Observed and modelled ZTEM responses above prism (200 m x 200 m of 1 S/m) under overburden (100 m of 0.01 S/m) on resistive half-space (0.001 S/m).

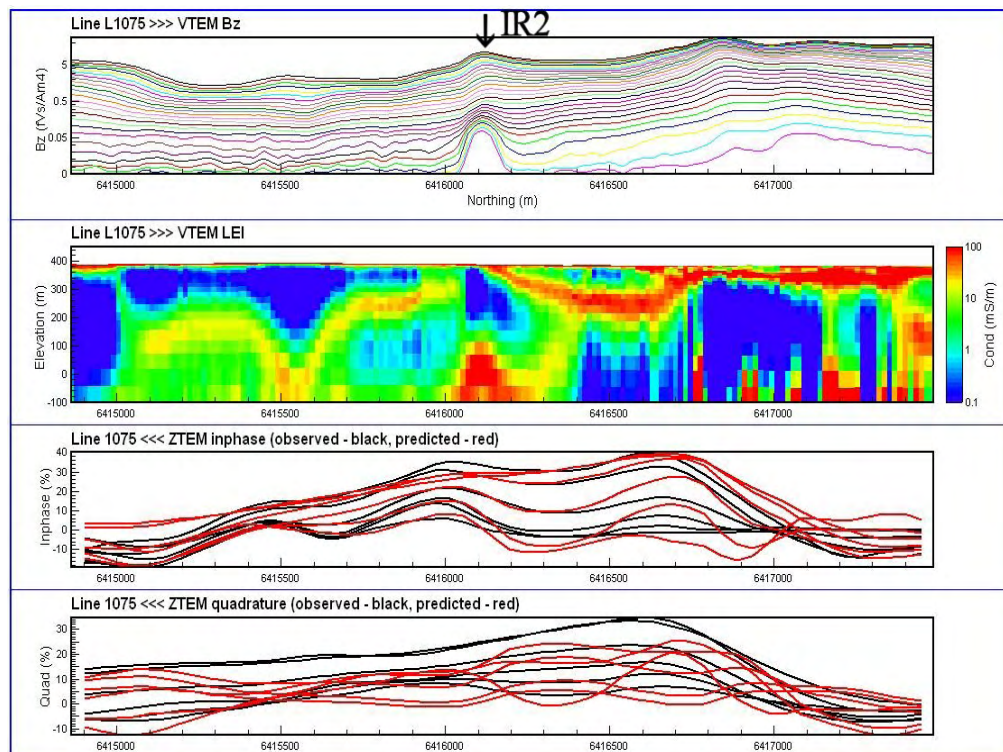


Figure 4. VTEM profile 1075 with derived conductivity-depth section (top), and observed and predicted ZTEM inphase and quadrature profiles (bottom). The ZTEM data were predicted from the VTEM-derived layered-earth section. The location of the bedrock conductor IR2 is indicated by an arrow.

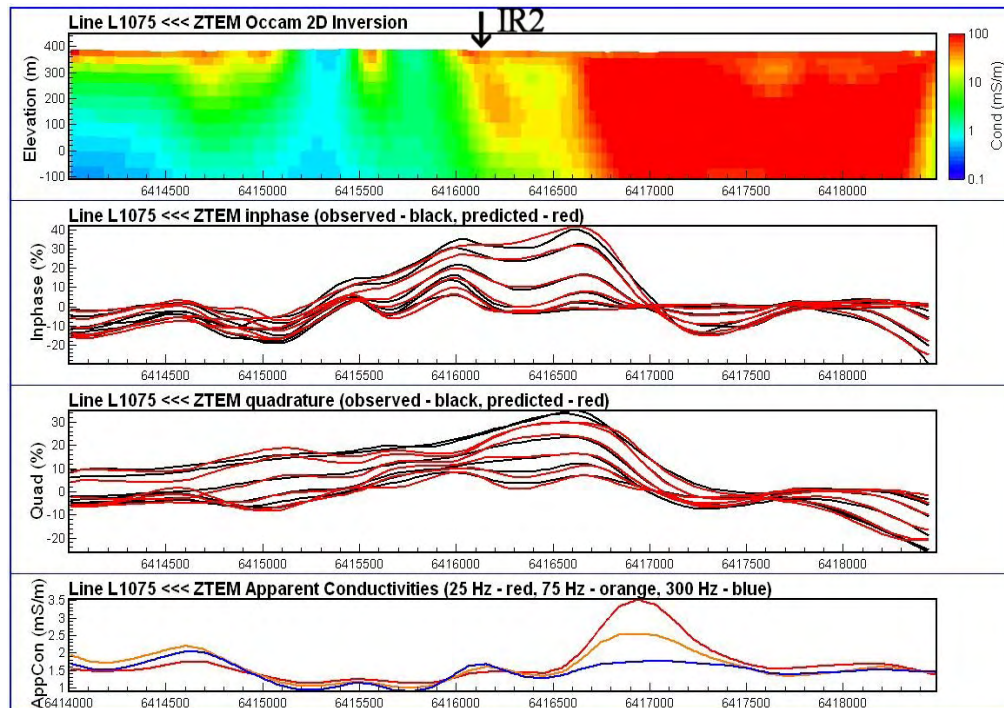


Figure 5. Line 1075, observed and modelled ZTEM responses with derived conductivity-depth section and apparent conductivity profile. The location of the conductor IR2 is indicated by an arrow.

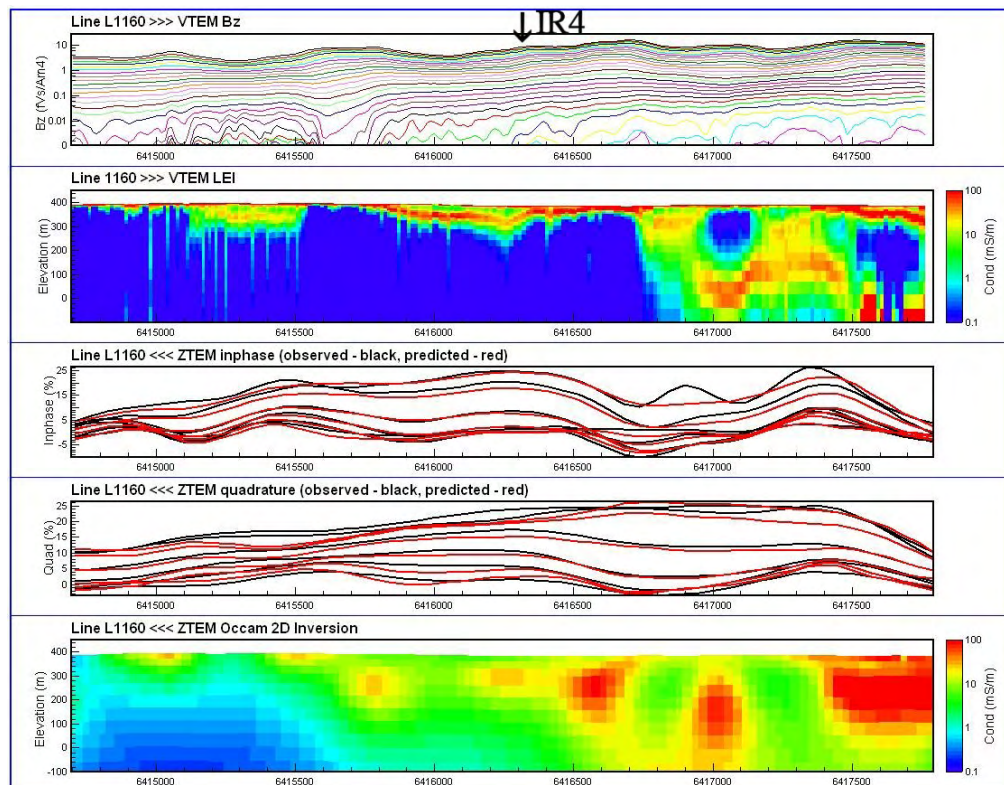


Figure 6: Line 1160, VTEM profile with derived conductivity-depth section (top) and ZTEM inphase and quadrature profiles with derived conductivity-depth section (bottom). The location of conductor IR4 is indicated by an arrow.

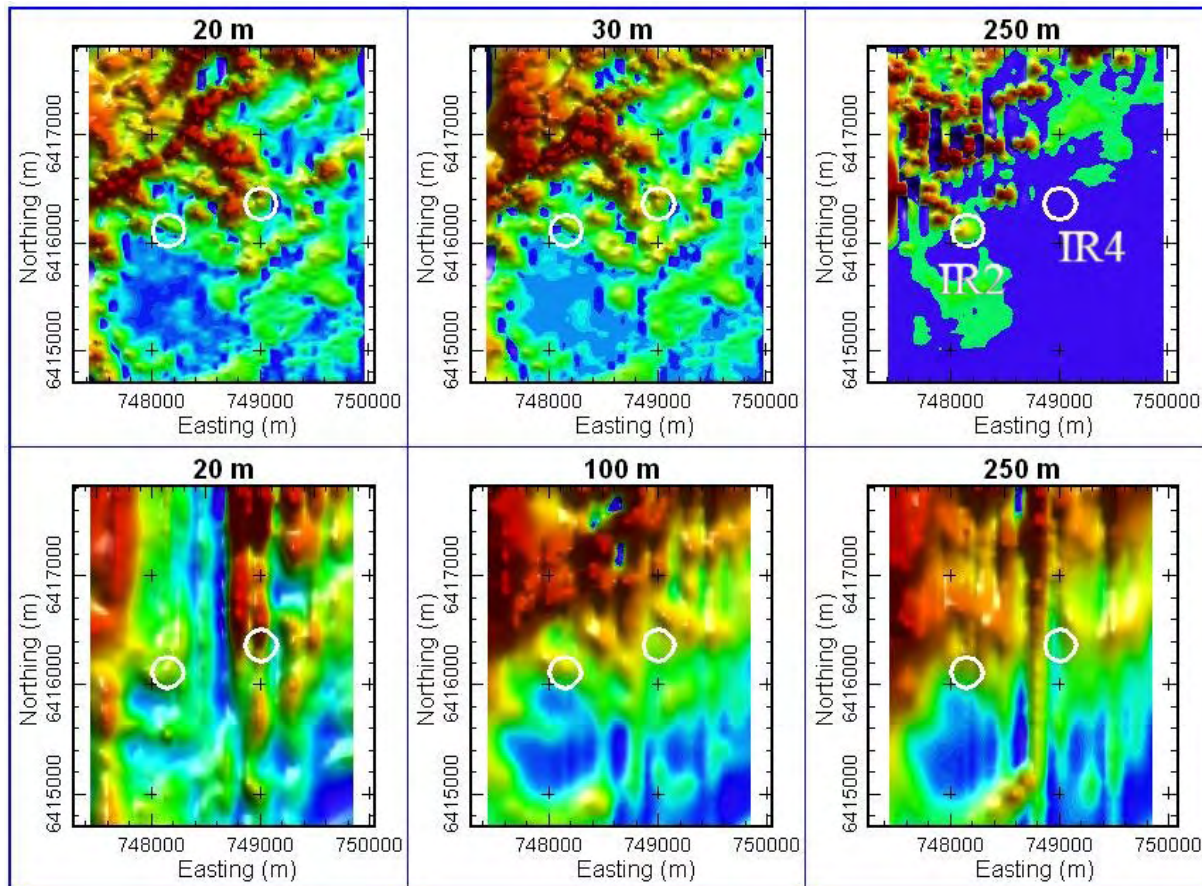


Figure 7: Top panel: conductivity-depth grids derived from VTEM inversions at depths 20 m, 30 m and 250 m. Bottom panel: conductivity-depth grids derived from ZTEM inversions at depths 20 m, 100 m and 250 m. The location of the known conductors is indicated by white circles, with IR2 being west of IR4.

Karous-Hjelt filter

Pseudo-sections derived with the Karous-Hjelt filter (Karous and Hjelt, 1983) can be useful to extract subtle conductors from the ZTEM profiles. The main property of the Karous-Hjelt filter is to turn cross-overs into peaks. Figure 8 shows pseudo-sections derived from the inphase profile of each frequency for line 1075. Even though the derivation of Karous-Hjelt sections is far less sophisticated than running 2D inversions, these sections agree overall with the 2D inversion result of Figure 5, mapping near-surface conductors, including IR2 and an extended pocket of conductive material to the east.

Near-surface grids of the Karous-Hjelt filtered ZTEM data are shown in Figure 9. These grids are similar to divergence grids generated by Geotech that are based on the VLF peaker derivation (Pedersen et al., 1994). The latter however makes use of the spatial derivatives of the Tzx and Tzy tippers, whereas the Karous-Hjelt-filtered grids shown were derived only from the Tzx data.

Apparent conductivity and phase

The derivation of apparent conductivity and phase from VLF data is discussed by Becken and Pedersen (2003). The method has been applied to the Forresteria ZTEM data, making joint use of the Tzx and Tzy tippers. The derived apparent conductivities and phases are shown in Figure 10. These images appear to indicate geological structures, such as SW-NE trending shears. A close-up of the area around the location of conductors IR2 and IR4 is shown in Figure 11. The apparent conductivities show elevated values at the location of IR2, especially for the higher ZTEM frequencies. The time-constants derived from the VTEM dB/dt and B-field data are also shown for comparison. There is strong indication for conductor IR2 on the time-constant images.

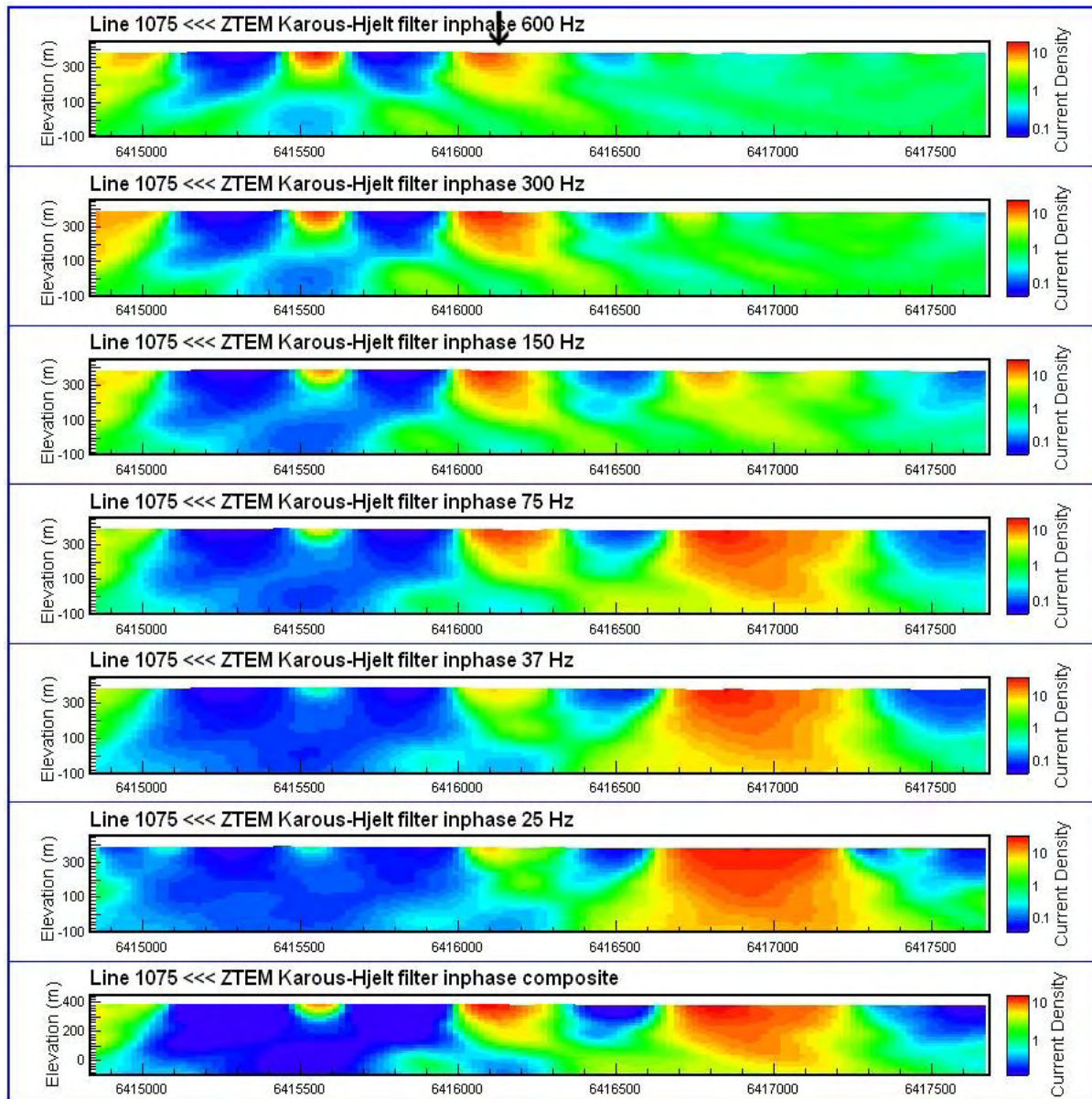


Figure 8: Line 1075, Karous-Hjelt sections derived from inphase ZTEM profiles with decreasing frequency from top to bottom and a composite section of all frequencies at the very bottom. The location of conductor IR2 is indicated by an arrow.

CONCLUSIONS

The analysis of VTEM and ZTEM data at Forrestania, WA, appears to indicate that the VTEM system offers better spatial resolution than ZTEM. In addition, the VTEM data show a strong response across a known sulphide body, whereas the corresponding ZTEM response is quite subtle. Some of the products derived from ZTEM data, including apparent conductivity grids, appear to map geological structure and, hence, complement the information gained from a VTEM survey.

ACKNOWLEDGMENTS

We are thankful to Geotech Airborne Pty Ltd for releasing the shown data for publication.

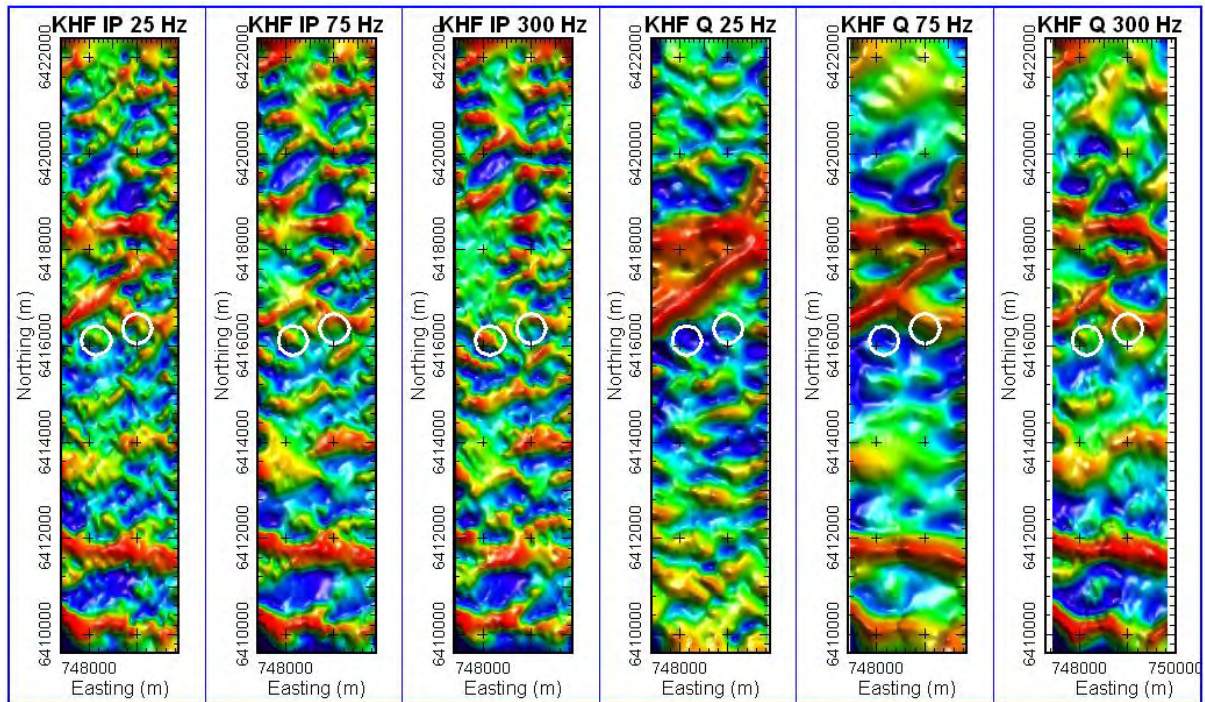


Figure 9: Karous-Hjelt near-surface grids, derived from the ZTEM inphase (left panels) and quadrature (right panels) responses. The location of the known conductors is indicated by white circles.

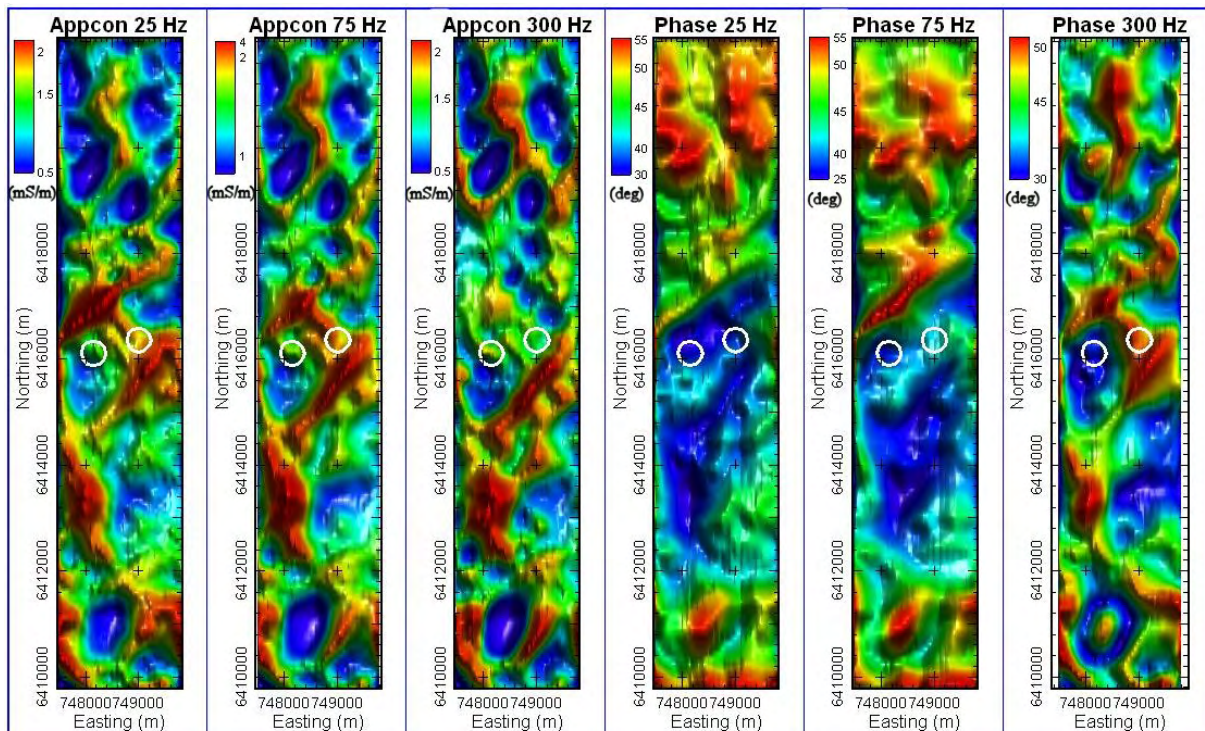


Figure 10: Apparent conductivities (left panels) and phases (right panels) derived jointly from ZTEM T_{zx} and T_{zy} responses 25-300 Hz. The location of the known conductors is indicated by white circles.

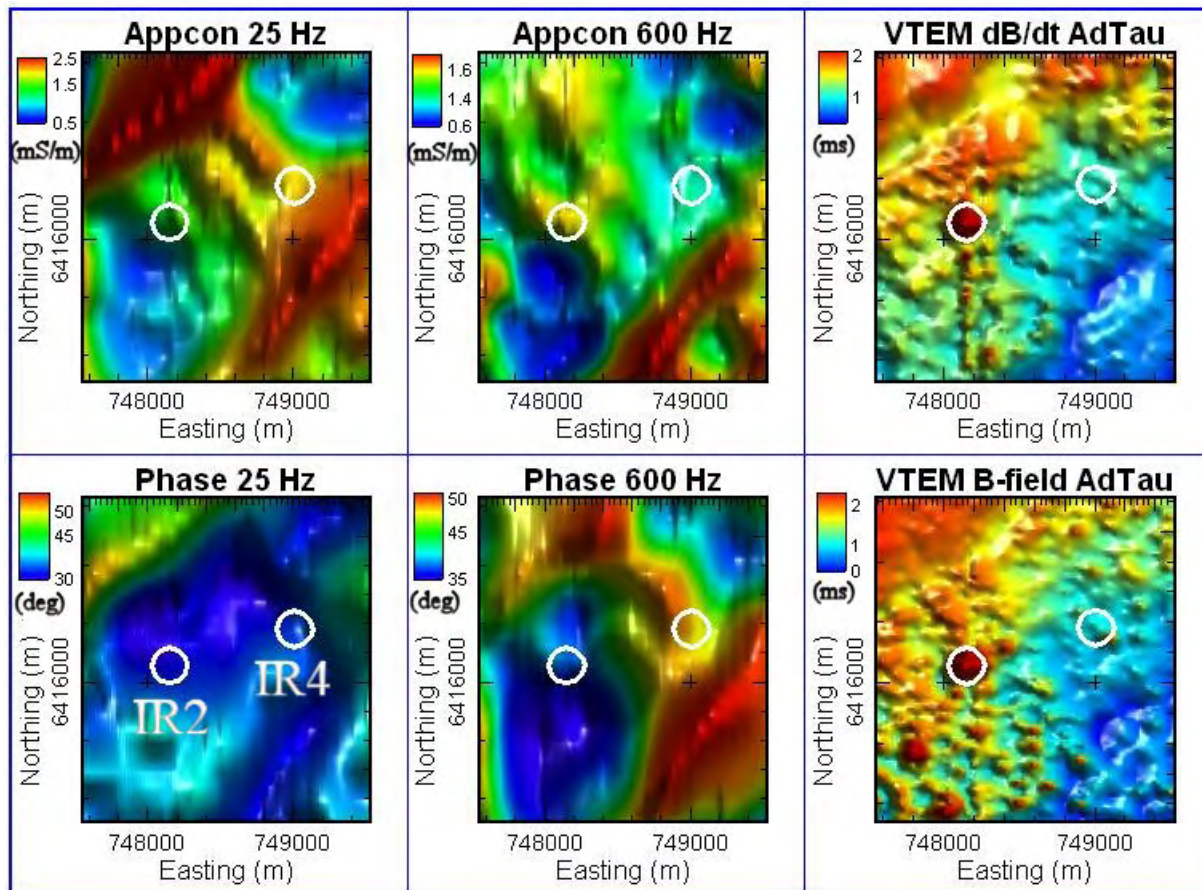


Figure 11: Close-up of some apparent conductivities and phases from Figure 9 and time-constants derived from VTEM dB/dt and B-field data. The location of the known conductors is indicated by white circles.

REFERENCES

- Becken M., and Pedersen L.B., 2003, Transformation of VLF anomaly maps into apparent resistivity and phase: *Geophysics* 68, 497-505.
- DeGroot-Hedlin, C. and S. Constable, 1990, Occam's inversion to generate smooth two-dimensional models from magnetotelluric data: *Geophysics* 55, 1613-1624.
- De Lugao, P.P., and Wannamaker, P., 1996, Calculating the two-dimensional magnetotelluric Jacobian in finite elements using reciprocity, *Geophys. J. Int.*, 127, 806-810.
- Karous, M., and Hjelt, S.E., 1983, Linear filtering of VLF dip-angle measurements: *Geophysical Prospecting* 31, 782-794.
- Legault, J.M., Kumar, H., Milicevic, B., and Hulbert, L., 2009, ZTEM airborne tipper AFMAG test survey over a magmatic copper-nickel target at Axis Lake in northern Saskatchewan: 79th International Exposition and Annual Meeting, SEG, Expanded Abstracts, 1272-1276.
- Pedersen L.B., Qian, W., Dynesius, L., and Zhang P., 1994, An airborne tensor VLF system. From concept to realization: *Geophysical Prospecting* 42, 863-883.
- Wannamaker, P.E., Stodt, J.A., and Rijo, L., 1987, A stable finite-element solution for two-dimensional magnetotelluric modeling: *Geophysical Journal of the Royal Astronomical Society*, 88, 277-296.
- Witherly, K., and Irvine, R., 2007, Mapping targets of high conductance with the VTEM airborne EM system: 19th International Geophysical Conference and Exhibition, ASEG, Extended Abstracts.

An analysis of ZTEM data over the Mt Milligan Porphyry Copper Deposit, British Columbia

Daniel Sattel*, EM Solutions LLC, Scott Thomas, Condor Consulting, Inc. and Michael Becken, GFZ Potsdam

Summary

ZTEM is a passive helicopter-borne system that measures the magnetic field response in the frequency range 30-720 Hz of naturally occurring currents in the subsurface. The resolution of this system is analyzed by forward modeling and inverting synthetic ZTEM data using a 2D algorithm for a range of conductivity scenarios.

ZTEM data acquired across the Mt Milligan Cu-Au porphyry system are compared with overlapping VTEM data. Conductivity-depth sections derived from both data sets show broad agreement, but indicate better spatial resolution for the VTEM data. Neither data set appears to show a significant response from the Cu-Au mineralization. Products derived from the ZTEM data, including apparent conductivity, phase and Karous-Hjelt filtered grids appear to map geologic structure.

Introduction

The ZTEM system has been available for commercial surveys for only a couple of years and reported case studies are therefore limited (Legault et al., 2009a, 2009b). It measures the magnetic-field response of naturally occurring subsurface currents, induced by far-away lightning discharges. By comparison, the VTEM system measures the magnetic-field response due to currents induced in the subsurface by the transmitter the system is carrying and many case studies have been reported in the literature (e.g. Witherly and Irvine, 2007).

As part of Geoscience BC's QUEST project, both the Geotech VTEM and ZTEM systems have been flown over Mount Milligan, an alkalic Cu-Au porphyry system located in British Columbia, 155 km northwest of Prince George. It should be noted that this type of mineralization is expected to be a difficult target for an electromagnetic system due to generally being associated with relatively low conductivities. However, by being sensitive to conductivity contrasts, the ZTEM system might have an advantage in resistive terrain. The overlap of data from both surveys allow for a direct comparison of the spatial resolution and depth penetration of the two systems.

The survey flight paths overlain on the Mt Milligan geology are shown in Figure 1. The VTEM data were acquired in 2007 at a line spacing of 200 m; the ZTEM survey was flown in 2008 with a line spacing of 250 m.

Before analyzing the survey data, synthetic modelling of the ZTEM data is presented, to illustrate the strengths and limitations of that system.

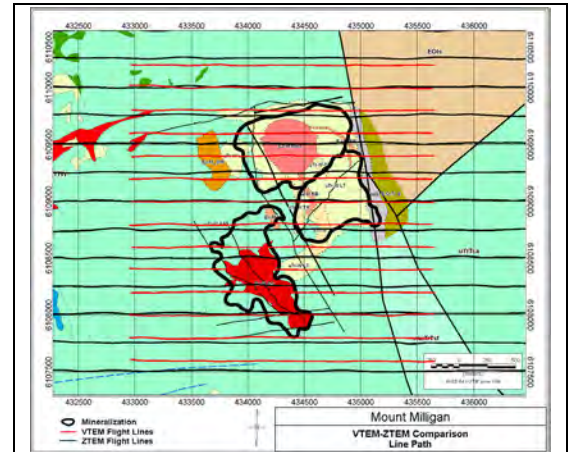


Figure 1: Flight path of VTEM and ZTEM surveys overlain on the geology of the Mt Milligan porphyry system.

Synthetic ZTEM data

Synthetic ZTEM profiles were forward modeled and inverted using a 2D MT algorithm, developed by Constable and Wannamaker (deGroot-Hedlin and Constable, 1990; Wannamaker et al., 1987; deGroot-Hedlin and Wannamaker, 1996). The inversion fitted the data to a RMS error of 1.3, which has been determined as a representative target RMS for the modeling of survey data.

Synthetic modeling results are shown in Figures 2-4. A flying height of 80 m was modeled. The insensitivity of the ZTEM system to one-dimensional or layered conductivity structures is illustrated in Figure 2. Since the vertical magnetic field, due to plane-wave excitation (magnetotelluric Hz response) is zero above a 1D earth, the ZTEM system tipper-functions T_{zx} and T_{zy} , that are determined from the magnetic field observations by statistical analysis of the relationship

$$H_z = \begin{bmatrix} T_{zx} & T_{zy} \end{bmatrix} \begin{bmatrix} H_x \\ H_y \end{bmatrix} \quad (1)$$

show no response above a layered-earth. However, the 2D inversion will still derive a resistive half-space since that

Analysis of ZTEM data at Mt Milligan

model is used to initialize the inversion. In Equation (1), the vertical magnetic field is measured in the air, and the horizontal components are recorded with a fixed ground station.

The sensitivity to two-dimensional conductivity structures is demonstrated with the quarter-space model in Figure 3.

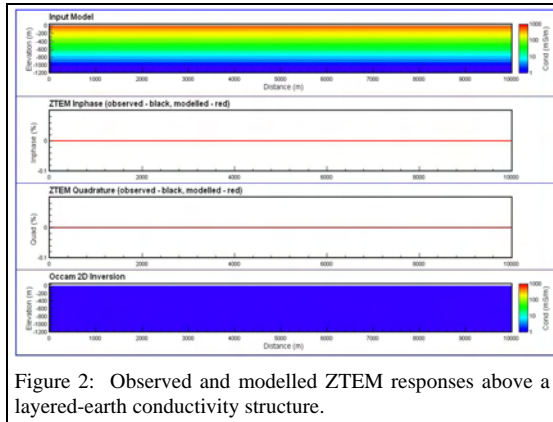


Figure 2: Observed and modelled ZTEM responses above a layered-earth conductivity structure.

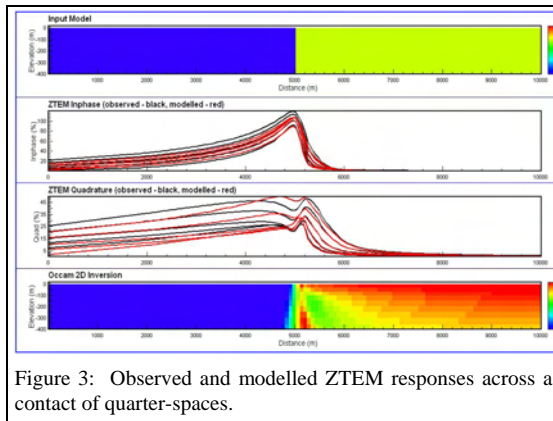


Figure 3: Observed and modelled ZTEM responses across a contact of quarter-spaces.

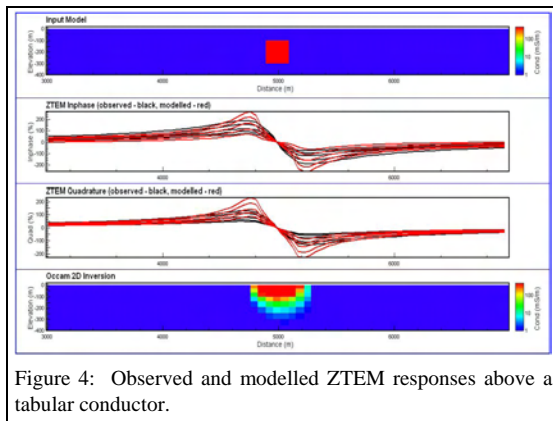


Figure 4: Observed and modelled ZTEM responses above a tabular conductor.

The ZTEM system shows a strong Tzx response at the contact of the two quarter-spaces and the 2D inversion resolves the conductivity contrast well. However, the modeled conductivity structure at the contact could be mistaken for a discrete conductor.

The ZTEM response across a tabular conductor is shown in Figure 4. The ZTEM system shows a strong Tzx response above the conductor and the 2D inversion gives a good indication of the conductor's presence, albeit at a depth range that is shallower than the actual depth of the conductor.

Mt Milligan Survey

Comparison VTEM – ZTEM

A conductivity-depth section derived from VTEM data by layered-earth inversion is shown in Figure 5. The line shown crosses the Cu-Au mineralization, for which there is no indication on the conductivity-depth section.

The derived conductivity-structure of that line was forward modelled to predict the expected ZTEM response using the 2D MT algorithm, taking into account the system elevation. Since the ZTEM line coincident with the VTEM data is longer, the conductivity structure was extrapolated at both ends. A comparison between observed and predicted ZTEM data is shown in Figure 5. There is overall agreement in the profile shape, but some difference in amplitudes. The observed ZTEM quadrature profile displays strong signal modulation most likely caused by bird swing.

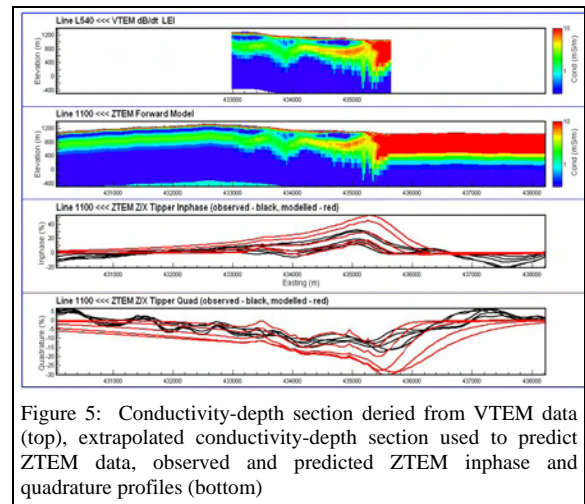


Figure 5: Conductivity-depth section derived from VTEM data (top), extrapolated conductivity-depth section used to predict ZTEM data, observed and predicted ZTEM inphase and quadrature profiles (bottom)

Next, the ZTEM data were modelled using the 2D inversion algorithm by Constable and Wannamaker. The

Analysis of ZTEM data at Mt Milligan

inversion result of the ZTEM data from Figure 5 is shown in Figure 6.

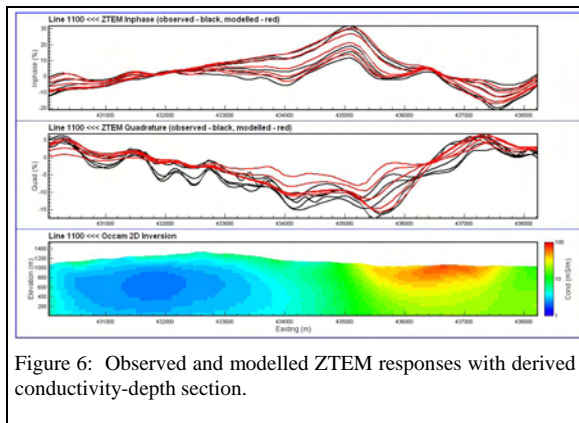


Figure 6: Observed and modelled ZTEM responses with derived conductivity-depth section.

The derived conductivity structure agrees with the VTEM results, ie conductive material is mapped to the east, while the western half is moderately resistive. However, the ZTEM-derived conductivity-depth section lacks spatial resolution compared to the VTEM section.

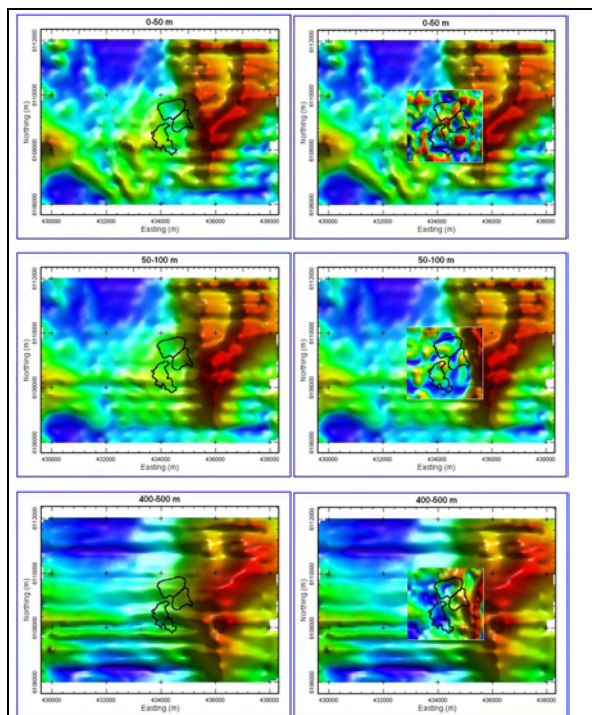


Figure 7: Left panel: conductivity-depth grids derived from ZTEM 2D inversions at depth ranges 0-50 m, 50-100 m and 400-500 m (top to bottom). Right panel: same as left panel with VTEM conductivity-grids overlain on ZTEM grids. Known mineralizations are outlined in black. The resistors seen in the VTEM are the resistive stocks.

Conductivity-depth grids have been derived from the conductivity-depth sections of all ZTEM lines. Figure 7 shows the conductivity at shallow and intermediate depths. Conductivity-depth grids derived from VTEM inversions are inserted on the spatially more extensive ZTEM grids. The two data sets agree on mapping the western edge of the conductive unit associated with the Great Eastern Fault Zone.

Karous-Hjelt Filter

Pseudo-sections derived with the Karous-Hjelt filter (Karous and Hjelt, 1983) can be useful to extract subtle conductors from the ZTEM profiles. The main property of the Karous-Hjelt filter is to turn cross-overs into peaks. Figure 8 shows pseudo-sections derived from the inphase profile of each frequency. Even though the derivation of Karous-Hjelt sections is far less sophisticated than running 2D inversions, these sections agree overall with the 2D inversion result, mapping near-surface conductors to the east and resistive material to the west.

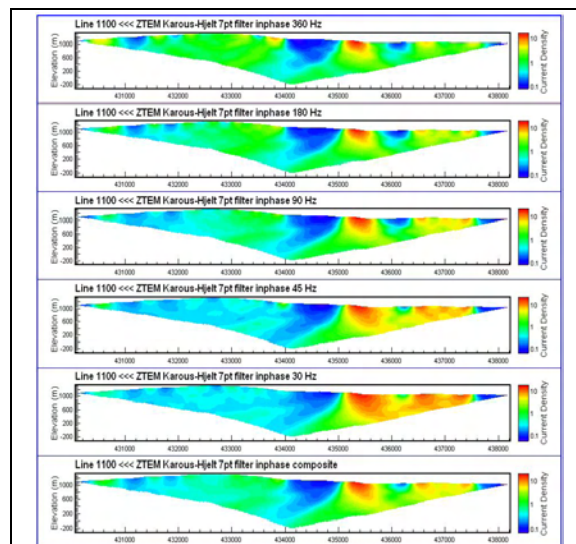


Figure 8: Karous-Hjelt sections derived from inphase ZTEM profiles with decreasing frequency from top to bottom and a composite section of all frequencies at the very bottom.

Near-surface grids of the Karous-Hjelt filtered ZTEM data are shown in Figure 9. These grids are similar to divergence grids generated by Geotech that are based on the VLF peaker derivation (Pedersen et al., 1994). The latter however makes use of the spatial derivatives of the Tzx and Tzy Tippers, whereas the Karous-Hjelt filter is derived only from the Tzx Tipper data. These grids indicate geologic structures striking NNW-SSE, including the Great Eastern Fault Zone.

Analysis of ZTEM data at Mt Milligan

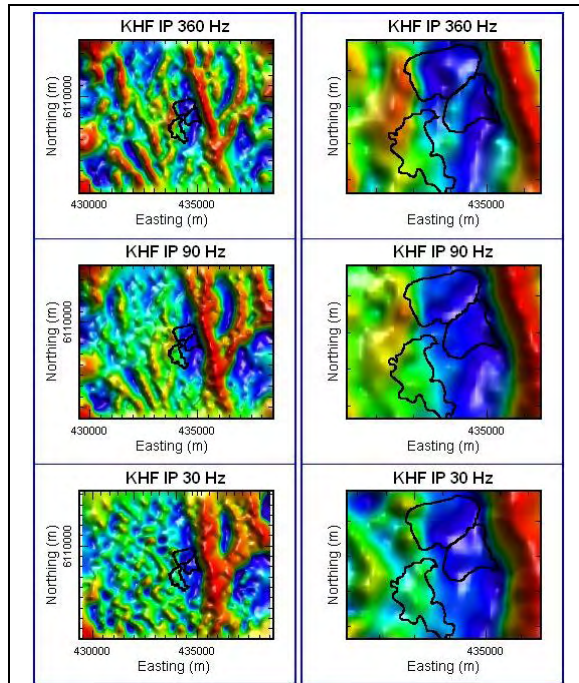


Figure 9: Karous-Hjelt near-surface grids. The entire survey is shown in the left panels, a close-up in the right panels, with known mineralizations outlined in black.

Apparent Conductivity and Phase

The derivation of apparent conductivity and phase from VLF data is discussed by Becken and Pedersen (2003). The method has been applied to the Mt Milligan ZTEM data, making joint use of the Tzx and Tzy tippers. The derived apparent conductivities and phases are shown in Figures 10 and 11. These images indicate geological structures, such as the Great Eastern Fault Zone, and a conductive zone west of the known mineralization.

Conclusions

The analysis of VTEM and ZTEM data at Mt Milligan has indicated that conductivity-sections and conductivity-depth grids derived from ZTEM data via 2D inversion show less spatial resolution than corresponding VTEM products. However, some of the products derived from ZTEM data, including apparent conductivity grids, complement the information gained from a VTEM survey.

Although the resistive stock is discernable, the ZTEM data and derived products do not appear to indicate the known mineralization at the Mt Milligan porphyry copper deposit, a difficult exploration target for electromagnetic surveys due to its expected low conductivity.

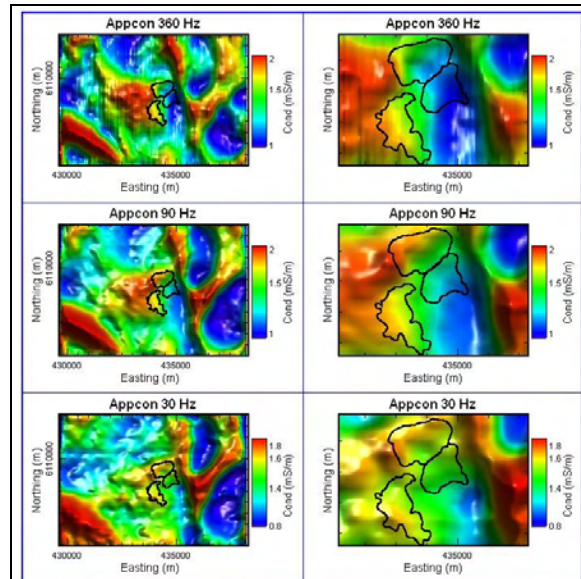


Figure 10: Apparent conductivities derived jointly from ZTEM Tzx and Tzy responses 30-360 Hz. The entire survey is shown in the left panels, a close-up in the right panels, with known mineralizations outlined in black.

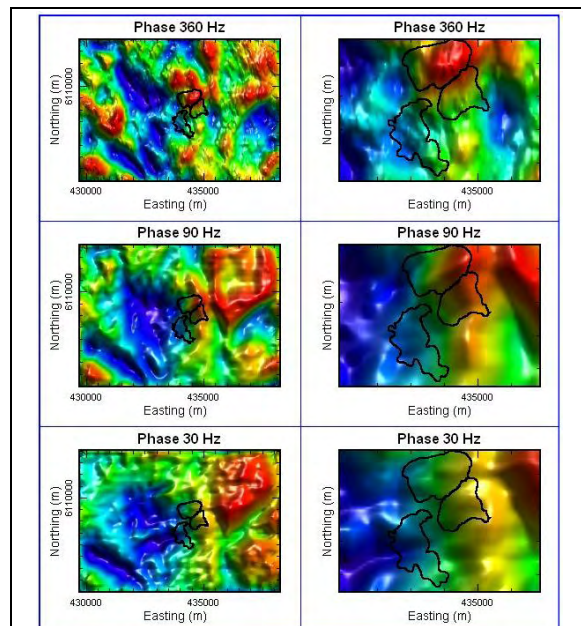


Figure 11: Phases derived jointly from ZTEM Tzx and Tzy responses 30-360 Hz.

Extracting information from ZTEM data with 2D inversions

Daniel Sattel*
EM Solutions LLC
Golden, CO, USA
dsattel@earthlink.net

Ken Witherly
Condor Consulting, Inc.
Lakewood, CO, USA
ken@condorconsult.com

SUMMARY

A 2D Occam inversion algorithm for modeling ZTEM data is described that takes into account topography and EM receiver terrain clearance. The responses of hills and depressions are shown for synthetic models. These results show that hills and depressions produce responses that could be confused with the responses of conductors and resistors, respectively.

The analysis of ZTEM data acquired at different flight-line directions at the Forrestania test site, WA, shows great consistency and repeatability of the ZTEM data. 2D inversion results indicate that the derivation of pseudo tipper profiles, perpendicular to the survey flight-line direction, from across-line data contain valuable information, especially where the local strike is not perpendicular to the flight-line direction.

Key words: AFMAG, airborne electromagnetics, EM data modelling, inversion, terrain effects.

INTRODUCTION

The ZTEM system (built and operated by Geotech Ltd.) measures the AFMAG responses of naturally occurring subsurface currents, induced by far-away lightning discharges (Legault et al., 2009). The vertical component is measured from a moving helicopter platform, while the horizontal components are recorded on the ground at a base station. The ZTEM response is extracted from the recorded dB/dt time series at discrete frequencies in the range 25-600 Hz or 30-720 Hz for survey areas with 50 and 60 Hz electric power grids, respectively. Various methods used for the modelling and interpretation of ZTEM data, including 2D inversion, Karous-Hjelt filters (Karous and Hjelt, 1983) and the derivation of apparent conductivity (Becken and Pedersen, 2003) have been discussed by Sattel et al. (2010).

After a brief discussion of a 2D algorithm used for the forward modelling and inversion of ZTEM data, ZTEM responses are shown for synthetic models to demonstrate the effect of topography and receiver terrain clearance.

For the interpretation of survey data, the in-line tipper (Tzx) profiles are generally modelled with a 2D inversion. A 3D inversion (Holtham and Oldenburg, 2010) would make use of the across-line (Tzy) data, but the 3D inversion of entire survey data sets is only now being attempted and is hence considered still experimental. In areas where the geology is not two-dimensional and/or the flight-line direction is not perpendicular to strike, useful information may be extracted from tipper profiles derived for a direction that is different

from the survey line-direction. The value of this approach is demonstrated on a data set acquired at Forrestania, Western Australia.

MODEL ALGORITHM

The 2D algorithm is based on a 2D MT algorithm developed by Constable and Wannamaker (deGroot-Hedlin and Constable, 1990; Wannamaker et al., 1987; deLugao and Wannamaker, 1996). The algorithm derives the in-line (Tzx) tipper profiles from the computed transverse electric (TE) response. The finite-element algorithm models the effect of topography (Wannamaker et al., 1986) and takes into account the terrain clearance of the airborne platform along the flight line. An example of the model mesh is illustrated in Figure 1.

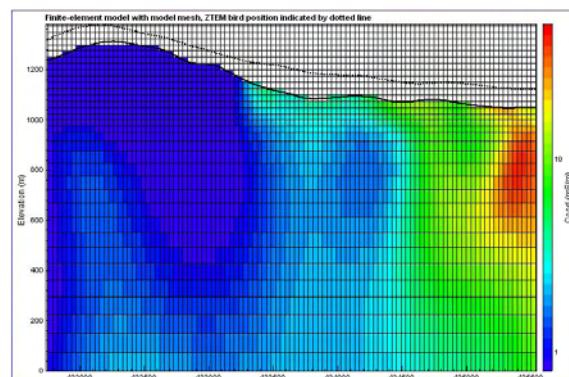


Figure 1. Illustration of model mesh for 2D inversion. Since the algorithm takes into account the topography and ZTEM bird terrain clearance along each line, air cells are an integral part of the finite-element model.

SYNTHETIC ZTEM DATA

Topography and Receiver Terrain Clearance

The effect of topography on the ZTEM response is demonstrated in Figure 2. The top panel shows a right-to-left crossover in the inphase response above the hill. When inverting these data with an algorithm assuming a flat earth, the data can be fit very well, but recovered conductivities will be distorted. The derived conductivity-depth model (draped on the true topography) indicates more conductive material at the top of the hill and more resistive material elsewhere. A left-to-right crossover in the inphase response is recorded across a depression. Inverting these data with a flat-earth model results in more resistive material being mapped at the center of the depression and more conductive material along the surface.

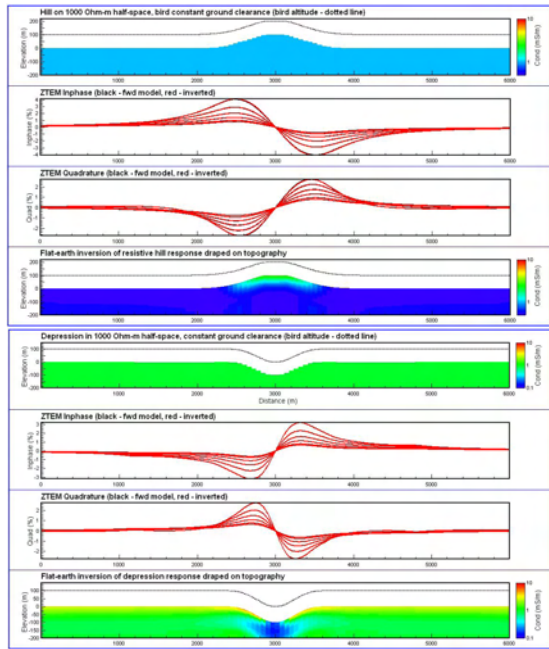


Figure 2. The ZTEM response of a hill (top panel) and depression (bottom panel). A constant EM receiver terrain clearance of 100 m was modelled. Each panel shows the input model of constant conductivity (top), the corresponding inphase and quadrature responses (centre) and the inverted section (draped on topography) assuming a flat-earth model (bottom).

The ZTEM response of a resistive hill flanked by conductive overburden is shown in Figure 3. The receiver was modelled for a constant terrain clearance of 100 m. Despite the presence of the hill, the gap in the overburden results in a left-to-right crossover in the inphase response. The quadrature response changes polarity between 25 and 600 Hz. The response of the same model for a receiver elevation of 200 m is shown at the same vertical scale in Figure 4. A comparison with Figure 3 indicates that, even though amplitudes are smaller, the response fall-off with receiver elevation is much less severe than for active-source EM systems.

Across a layered-earth, a change in the sensor terrain clearance alone does not result in a tipper response. Since the tipper response across a 1-D earth is zero, the profile with variable sensor terrain clearance is also zero (see Figure 5).

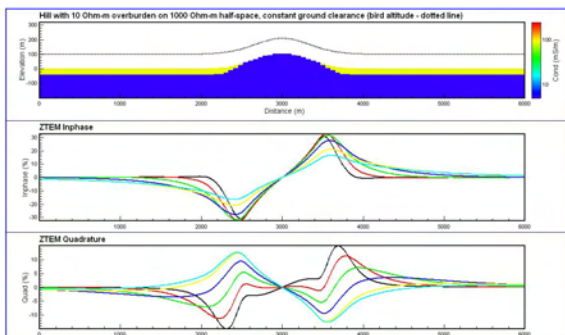


Figure 3. The ZTEM response of a resistive hill (1000 Ohm-m) flanked by conductive overburden (10 Ohm-m) for a receiver terrain clearance of 100 m.

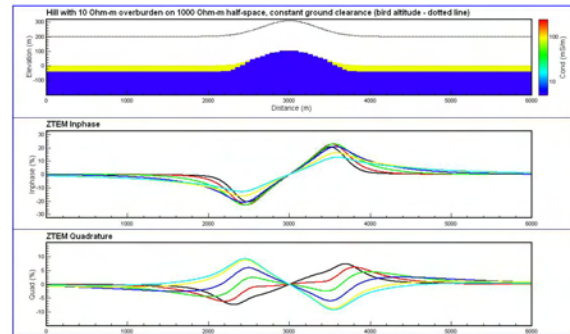


Figure 4. The ZTEM response of a resistive hill (1000 Ohm-m) flanked by conductive overburden (10 Ohm-m) for a receiver terrain clearance of 200 m.

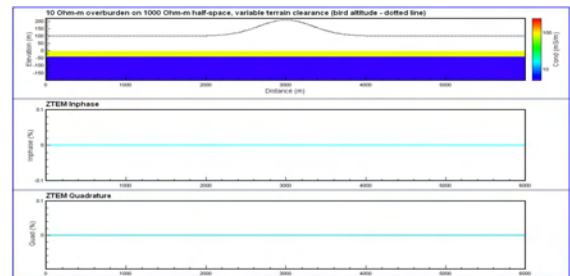


Figure 5. The ZTEM response across a layered-earth (50 m of 10 Ohm-m on 1000 Ohm-m half-space) for variable sensor terrain clearance.

2D INVERSION OF TZY DATA

A ZTEM survey data set contains in- and across-line tipper data T_{zx} and T_{zy} . Generally, the in-line T_{zx} data are modeled with a 2D inversion, because the flight-line direction is normally chosen to be perpendicular to the geological strike and the data sampling is densest along line. However, most ZTEM surveys are flown at a line spacing that allows for the derivation of in-line tipper profiles for any flight-line direction by projecting the nearest points onto that pseudo-line and by combining the T_{zx} and T_{zy} data into in-line tipper values. If the pseudo-line is perpendicular to the flight-line direction, the derived in-line tipper profile is made up of T_{zy} data, picked from the measurement points closest to the pseudo-line. The derived tipper profile can be modeled with a 2D inversion, which can provide useful results, where the geological structure is not two-dimensional and/or where the local strike is not perpendicular to the flight-line direction. The usefulness of T_{zy} data inversion is demonstrated with ZTEM data acquired at Forrestania, WA.

FORRESTANIA SURVEY

Figure 6 shows the flight lines of a survey flown at the Forrestania, WA EM test range, which is described on the website of Southern Geoscience Consultants (www.sgc.com.au). The ground covered by the ZTEM survey includes two drilled, barren, semi-massive to massive sulphides (IR2 and IR4), hosted in highly resistive bedrock under a conductive overburden (10-20 S). Previous analysis has indicated that there is no indication for sulphide IR4 in the ZTEM data set, but that a conductor has been mapped from the ZTEM data at the location of sulphide IR2 (Sattel et al., 2010). IR2 is described as shallow (<100 m), highly

conductive ($>7,000$ S), small ($<75 \times 75$ m) and dipping 30-40 degrees to the north. East-west and north-south lines have overflown IR2, which allows checking for repeatability and consistency between the two data sets.

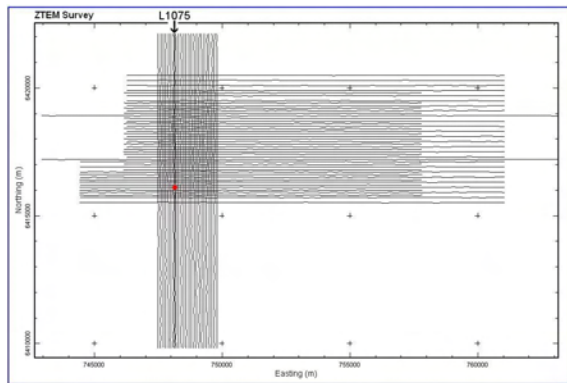


Figure 6. Flight lines of ZTEM survey at Forrestania, WA. The location of sulphide IR2 is indicated by a red dot.

The 2D inversion of the north-south line shown in Figure 7 indicates a conductive structure at the location of the sulphide body. Due to the small strike length of the sulphide a strong response was not expected. It should be noted that the response might be due to a geological structure with long strike length that hosts the sulphide. The 2D inversion result of the east-west line (not shown) does not give any indication of the presence of the conductor.

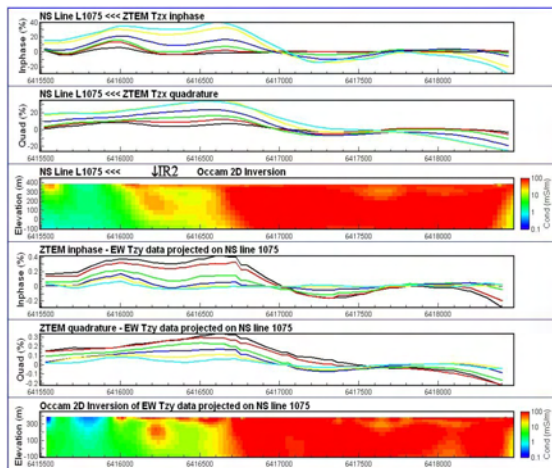


Figure 7. Forrestania ZTEM profiles across sulphide IR2, indicated by arrow, with corresponding inversion results. A portion of Tzx profiles of north-south line 1075 are shown in the top panels; the profiles derived from the Tzy data of the east-west lines are shown in the bottom panels.

For a more appropriate comparison between the east-west and north-south data sets, Tzy data from the east-west data set were extracted to derive a profile of in-line tipper values directed north-south. For this step, each east-west line contributes one point to the pseudo north-south line, and the data spacing on the pseudo profile is determined by the line spacing of the east-west data set. Due to the small flight-line spacing of the Forrestania survey (mostly 100 m) the anomaly shapes are expected to be recovered well. A comparison of

the original north-south Tzx profile (line 1075) and the pseudo profile derived from Tzy data of the east-west survey is shown in Figure 7. The corresponding inversion results are also shown. Despite the rougher appearance of the derived profile, the comparison shows excellent agreement between the two data sets and their inverted conductivity-depth sections. This indicates excellent consistency and repeatability between the two data sets flown at different flight line directions and acquired at different times.

These results also suggest that for 2D inversions to extract the maximum information of some structures, survey data might have to be projected and rotated into profiles with more appropriate flight-line directions. Since Tzx and Tzy are available for the entire survey, any angle can be chosen for reprojecting the data.

With the existence of two data sets for the Forrestania survey, each containing Tzx and Tzy data, 2D inversions were performed on 4 different sets of tipper profiles: original E-W and N-S Tzx profiles as well as pseudo N-S and E-W profiles derived from Tzy data of E-W and N-S surveys, respectively. Results are presented as conductivity-elevation slices at 120 m ASL in Figures 8 and 9. Apparent conductivity images of the 75 Hz data are shown for comparison. The derivation of the latter makes joint use of the Tzx and Tzy tipper data.

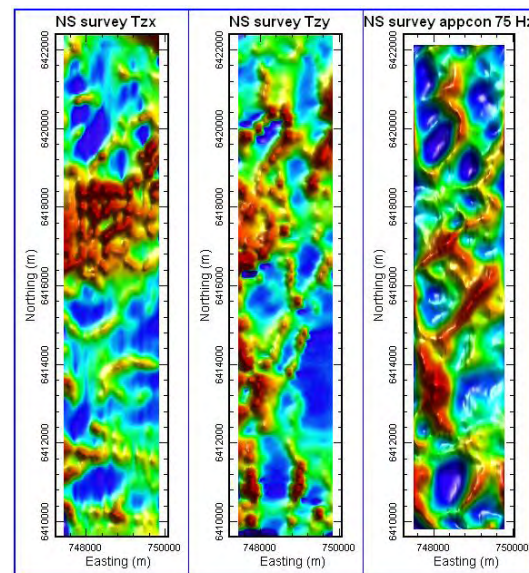


Figure 8: North-south survey data. Conductivity structure at an elevation of 120 m ASL, derived from 2D inversion of Tzx (left) and Tzy (center) data, and 75 Hz apparent conductivity (right).

As expected, the results between Tzx and Tzy inversions are quite different, since the tipper inversions indicate structures as a function of coupling between sensor orientation and subsurface current flow. For the N-S survey area, most structures appear to run SW-NE and are mapped in a comparable fashion by both tipper orientations. For the E-W data set, some prominent structures run N-S, coupling better with the Tzx data than with the Tzy data. Nevertheless, the inversion of the Tzy data indicate some subtle structures in the western third of the survey area, that are much less obvious in the corresponding Tzx conductivity-elevation slice. For both survey areas, the inversion results complement each other.

Figure 10 shows the overlapping portion of the conductivity-elevation slices shown in Figures 8 and 9. The results in the left panels are expected to agree with the results in the right panels, since the direction of the tipper data used is the same in both panels. As a function of the tipper data orientation, the conductivity structure in the top and center panel should indicate mostly E-W and N-S striking structures, respectively. The above expectations are largely met, except for the results of the Tzx E-W survey data, which don't appear to map any N-S structures and don't agree too well with the results of the Tzy N-S survey data. We assume that the tipper profiles of the Tzx E-W survey data are dominated by the stronger anomalies in the center and eastern half of the survey area, which resulted in a suboptimal data fit of subtler anomalies. The comparison of the apparent conductivity images derived from the N-S and E-W data also indicate that there are some differences in the data and data specifications (eg spatial sampling) between the two data sets.

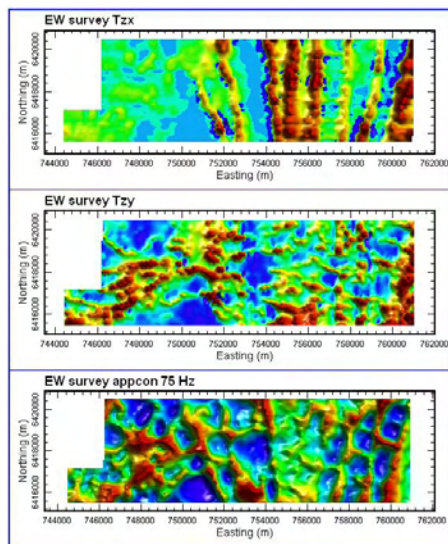


Figure 9: East-west survey data. Conductivity structure at an elevation of 120 m ASL, derived from 2D inversion of Tzx (top) and Tzy (center) data, and 75 Hz apparent conductivity (bottom).

CONCLUSIONS

The results from synthetic models indicate that taking into account of terrain topography during 2D inversions is important to derive reliable conductivity-depth sections.

The analysis of ZTEM data at Forrestania, WA has shown excellent consistency and repeatability between two data sets flown at different flight line directions and acquired at different times. The derivation of ZTEM profiles along pseudo-lines allows for the 2D inversion of structures not perpendicular to the survey flight-line direction.

ACKNOWLEDGMENTS

We are thankful to Geotech Airborne Pty Ltd for releasing the shown data for publication.

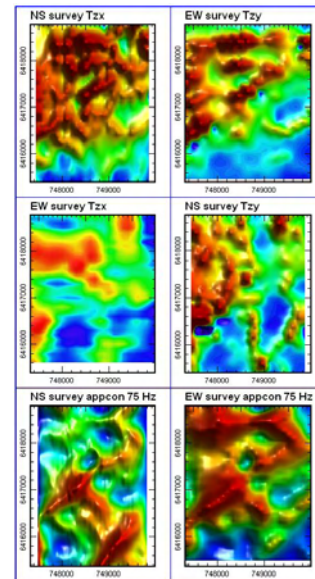


Figure 10: Close-up from Figures 8 and 9 of the overlapping area.

REFERENCES

- Becken M., and Pedersen L.B., 2003, Transformation of VLF anomaly maps into apparent resistivity and phase: *Geophysics* 68, 497-505.
- DeGroot-Hedlin, C. and S. Constable, 1990, Occam's inversion to generate smooth two-dimensional models from magnetotelluric data: *Geophysics* 55, 1613-1624.
- De Lugao, P.P., and Wannamaker, P., 1996, Calculating the two-dimensional magnetotelluric Jacobian in finite elements using reciprocity, *Geophys. J. Int.*, 127, 806-810.
- Holtham, E., and Oldenburg, D.W., 2010, Three-dimensional inversion of ZTEM data: *Geophys. J. Int.* 182, 168-182.
- Karous, M., and Hjelt, S.E., 1983, Linear filtering of VLF dip-angle measurements: *Geophysical Prospecting* 31, 782-794.
- Legault, J.M., Kumar, H., Milicevic, B., and Hulbert, L., 2009, ZTEM airborne tipper AFMAG test survey over a magmatic copper-nickel target at Axis Lake in northern Saskatchewan: 79th International Exposition and Annual Meeting, SEG, Expanded Abstracts, 1272-1276.
- Lo, B., and Zang, M., 2008, Numerical modeling of Z-TEM (airborne AFMAG) responses to guide exploration strategies: 78th International Exposition and Annual Meeting, SEG, Expanded Abstracts, 1098-1102.
- Pedersen L.B., Qian, W., Dynesius, L., and Zhang P., 1994, An airborne tensor VLF system. From concept to realization: *Geophysical Prospecting* 42, 863-883.
- Sattel, D., Witherly, K., and Becken M., 2010, A brief analysis of ZTEM data from the Forrestania test site, WA: 21st International Geophysical Conference and Exhibition, ASEG, Extended Abstracts.
- Wannamaker, P.E., Stodt, J.A., and Rijo, L., 1986, Two-dimensional topographic responses in magnetotellurics modeled using finite elements: *Geophysics* 51, 2131-2144.
- Wannamaker, P.E., Stodt, J.A., and Rijo, L., 1987, A stable finite-element solution for two-dimensional magnetotelluric modeling: *Geophysical Journal of the Royal Astronomical Society*, 88, 277-296.

An overview of ZTEM data interpretation tools

Daniel Sattel ¹ and Ken Witherly ²

¹ *EM Solutions, USA (dsattel@earthlink.net)*

² *Condor Consulting, Inc., USA (ken@condorconsult.com)*

Abstract

The airborne AFMAG-style data acquired with the ZTEM system can be modelled and interpreted with software originally developed for the interpretation of VLF and MT data. With most surveys covering large areas, image products, including apparent conductivity, phase-rotated response and the VLF peaker allow for a rapid initial assessment of the data to be carried out. Pseudo-sections can be derived with the Karous-Hjelt filter, which offer some indication for the distribution of conductivity with depth. More reliable conductivity-depth sections are derived with 2D and 3D inversion algorithms.

The latter are also used for the computation of synthetic data. ZTEM response values across contacts and fault zones were computed with a 2D algorithm. The results across these features were different, but it can be very difficult to correctly identify the differences when viewed as grid products.

For the modelling and interpretation of ZTEM data in mountainous terrain, it is crucial to take into account the topography of the survey area. It is shown that the ZTEM data acquired across a section of rugged terrain primarily reflects the topographic character of the terrain.

ZTEM data acquired at the Forrestania test site in Western Australia were modelled with 2D and 3D inversion algorithms. Since the survey was flown in two different flight line directions, we were able to evaluate the repeatability of the survey data, which turned out to be excellent. Separate inversion results for the two data sets are very consistent for the 3D algorithm and somewhat consistent for the 2D algorithm.

Introduction

The ZTEM system, built and operated by Geotech Ltd., measures the AFMAG-style magnetic field response (Ward, 1959) of naturally occurring subsurface currents, predominantly those induced by distant lightning discharges (Legault et al., 2009). The vertical component of the time rate of change of the magnetic field is measured with a receiver loop slung below a moving helicopter platform, while the horizontal components of the time rate of change of the magnetic field are recorded on the ground at a base station. The ZTEM tipper responses are extracted from the recorded dB/dt time series at discrete frequencies in the range 25-600 Hz or 30-720 Hz for survey areas with 50 and 60 Hz electric power grids, respectively.

Products originally developed for the interpretation of VLF and MT data have been adapted for application with ZTEM data. These include image products such as phase-rotated response, the VLF peaker (Pedersen et al., 1994) and apparent conductivity and phase (Becken and Pedersen, 2003). Karous-Hjelt pseudo-sections (Karous and Hjelt, 1983) can be derived to obtain some vague conductivity-depth information from ZTEM data. More reliable conductivity-depth sections are derived with 2D and 3D inversions (Holtham and Oldenburg, 2010; Legault et al., 2009; Sattel et al., 2010). In scenarios where current channelling can be ignored, the response of discrete conductors energized by vortex currents can be modelled with MAXWELL (Duncan, 1987).

2D and 3D algorithms can be used to produce forward model synthetic ZTEM profiles across conductivity scenarios of interest, and can be used to evaluate the effect of topography and survey elevation on ZTEM response.

After a brief discussion of the 2D and 3D algorithms used, ZTEM response profiles and derived image products are shown for contact and fault zone models as an interpretation aid to help distinguish these

two conductivity scenarios. The effect of topography is then demonstrated for a ZTEM data set acquired across rugged terrain.

Finally, image and section products derived from a ZTEM data set from Forrestania, Western Australia (WA) are shown. These products demonstrate the contribution of each product to the interpretation of the survey data. The acquisition of data in different flight directions allowed for a consistency check of the inversion algorithms and the survey data to be performed.

Model algorithms

The 2D algorithm used for forward modelling and inverting ZTEM data is based on a 2D MT algorithm developed by Constable and Wannamaker (deGroot-Hedlin and Constable, 1990; Wannamaker et al., 1987; deLugao and Wannamaker, 1996). The algorithm derives the in-line (Tzx) tipper profiles from the computed transverse electric (TE) response. The finite-element algorithm models the effect of topography (Wannamaker et al., 1986) and takes into account the terrain clearance of the airborne platform along the flight line. An example of the model mesh is illustrated in Figure 1.

The 3D inversion algorithm applied to the Forrestania survey data has been developed by Holtham and Oldenburg (2010), and is based on earlier work by Farquharson et al. (2002). Rather than invert individual Tzx profiles, the 3D inversion simultaneously inverts the in-line Tzx and across-line Tzy data of multiple flight lines using a Gauss-Newton approach.

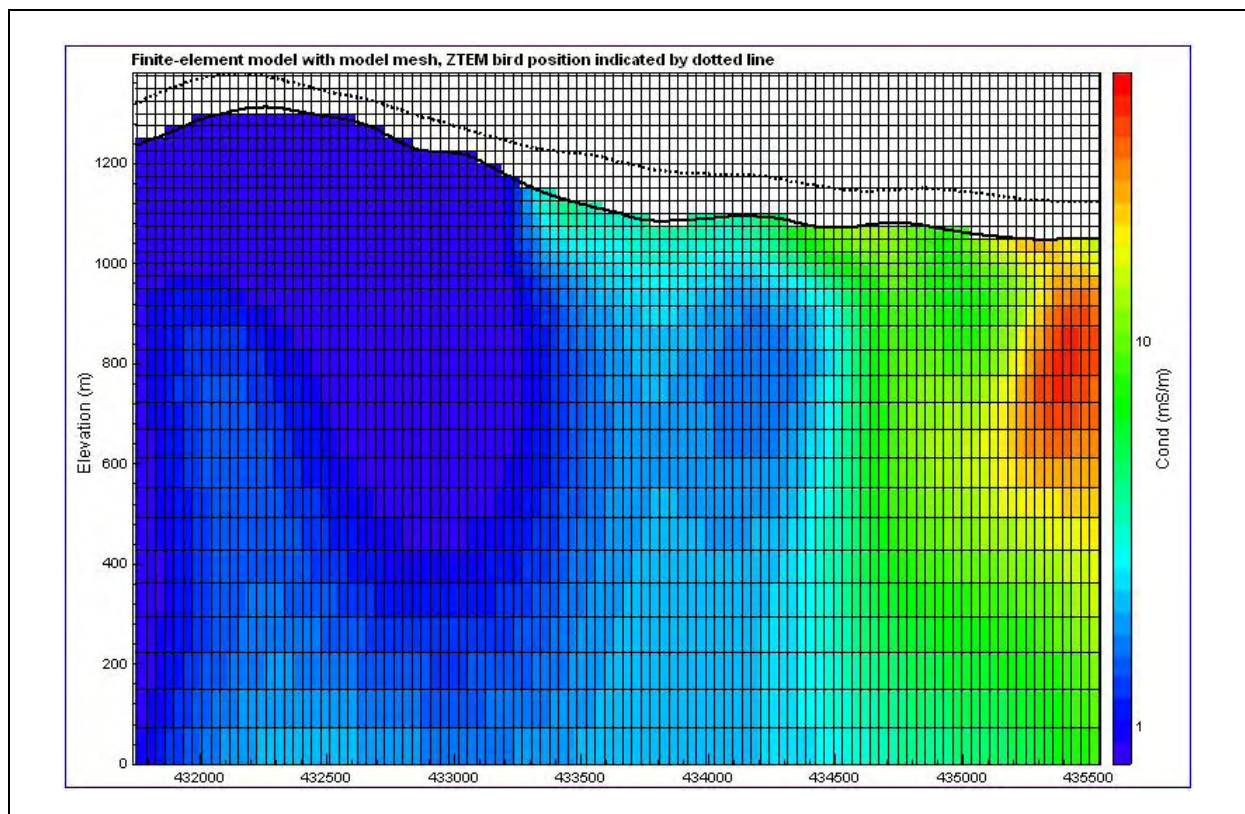


Figure 1. Illustration of a model mesh used for 2D inversion. Since the algorithm takes into account the topography and ZTEM bird terrain clearance along each line, air cells are an integral part of the finite-element model.

Synthetic ZTEM data

Contact model

The inphase response across a vertical contact is shown in Figure 2. Also shown are phase-rotated profiles obtained by reduction-to-pole (RTP) filtering and Hilbert transformation. Profiles of the horizontal derivative and apparent conductivity (Becken and Pedersen, 2003) are also shown.

For the 2D case, the horizontal derivative is equivalent to the Peaker (Pedersen et al., 1994) and the total divergence (Lo and Zang, 2008). Grids of the phase-rotated data and the total divergence are standard products supplied by Geotech with ZTEM survey data. The phase-rotated profiles of Figure 2 indicate little difference between the RTP-filtered and the Hilbert-transformed profiles.

Assuming a 2D conductivity structure, the north-south oriented profiles of Figure 2 were replicated in east and west directions to produce the images shown in Figure 3. The results of Figure 2 and Figure 3 indicate that for the contact model, all observed and derived data show a peak or a crossover at the contact. The width of the response is a function of the conductivity contrast across the contact. Unless the appropriate colour stretch is used, it can be difficult to distinguish a crossover from a peak.

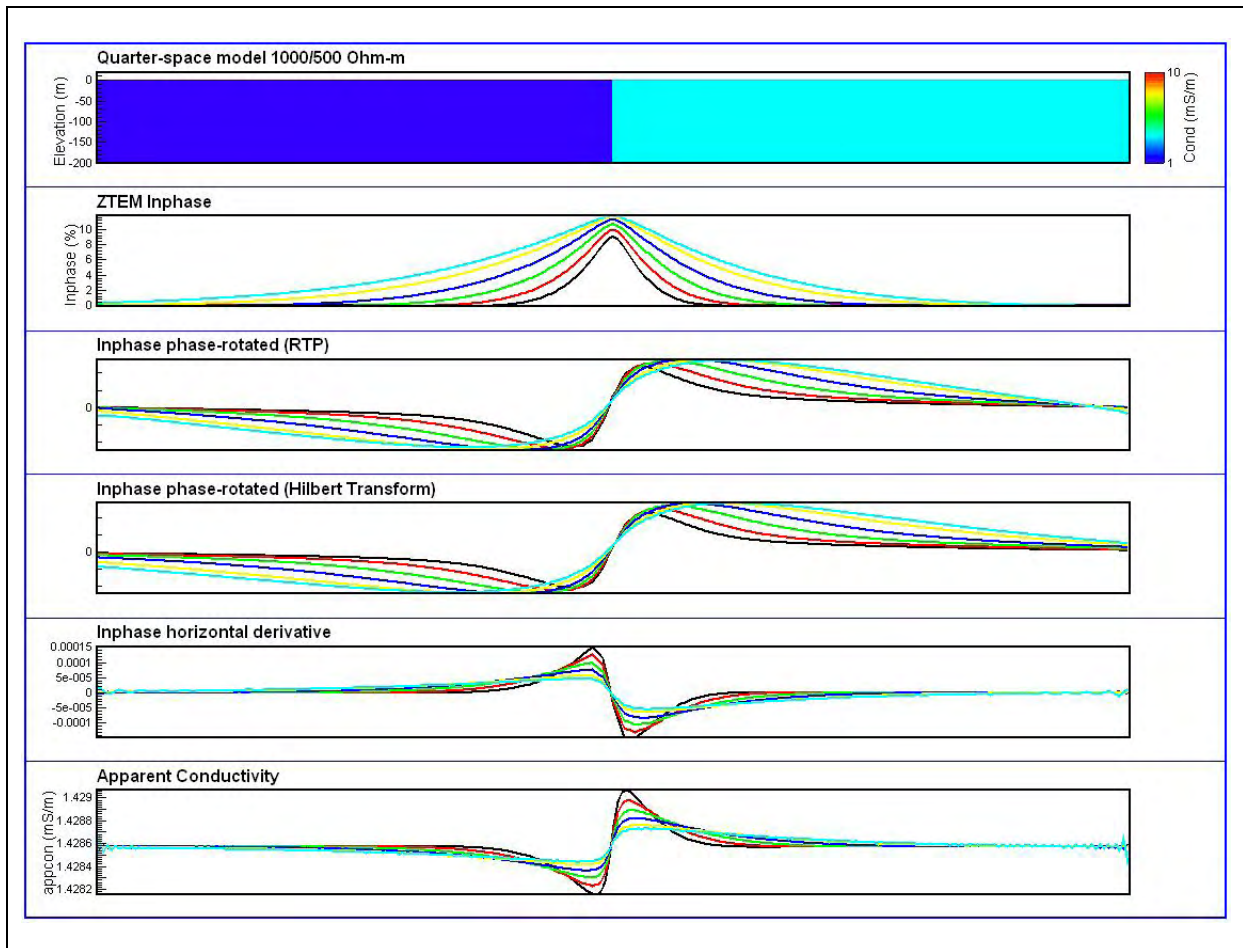


Figure 2. The ZTEM response and derived profiles across a contact, juxtaposing quarter-spaces of 1,000 and 500 ohm-m, respectively. The conductivity model, the inphase response, the phase-rotated inphase response derived by RTP filtering and Hilbert transformation, respectively, the horizontal derivative of the inphase profile and the apparent conductivity profile are shown.

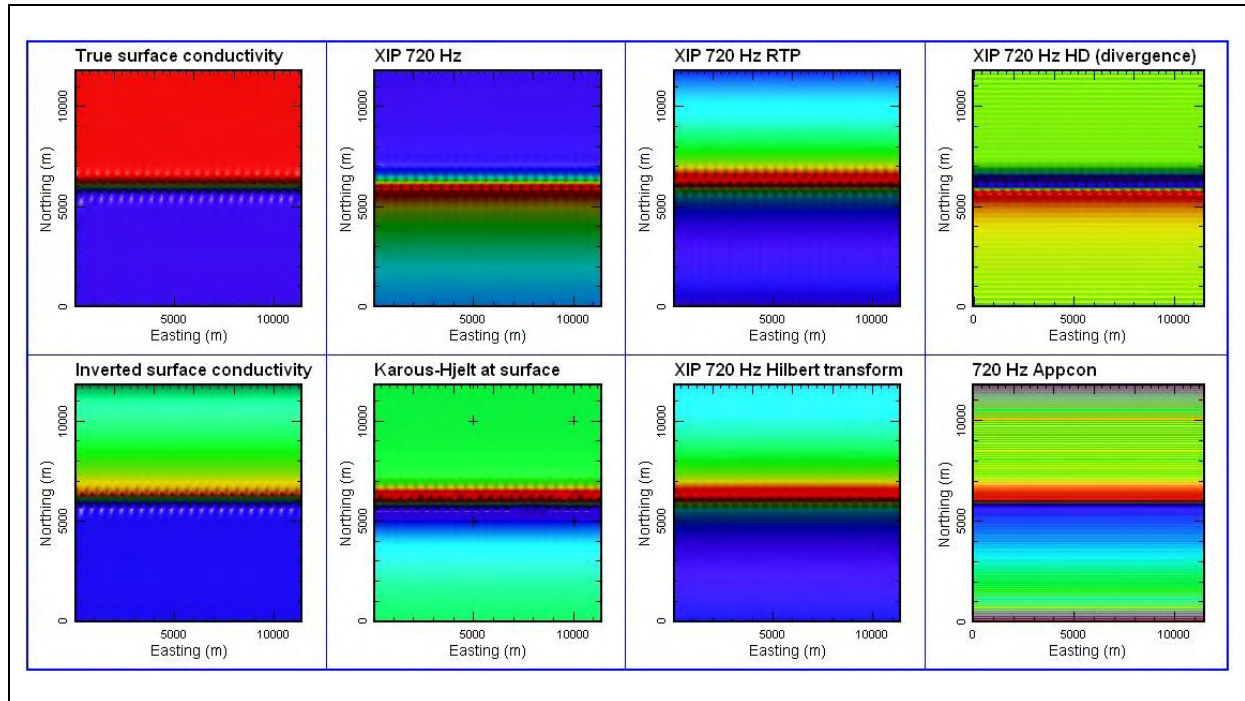


Figure 3. Grids derived from the data shown in Figure 2. Shown in the top row: the true conductivity model, the 720 Hz inphase response, the phase-rotated 720 Hz inphase response (RTP), the horizontal derivative of the 720 Hz inphase response (total divergence grid), and in the bottom row: the conductivity model recovered by 2D inversion, the near-surface Karous-Hjelt filter result of the 720 Hz inphase response, the phase-rotated 720 Hz inphase response (Hilbert transform) and the 720 Hz apparent conductivity grid.

Fault zone model

The inphase response across a conductive fault zone is shown in Figure 4. Also shown are phase-rotated profiles, horizontal derivative and apparent conductivity profiles. The corresponding grid products are shown in Figure 5. The results indicate that for the fault zone model, all observed and derived data show a peak or a crossover at the fault zone. The amplitude of the response is a function of the conductivity contrast between the host material and the fault zone, and the fault zone width.

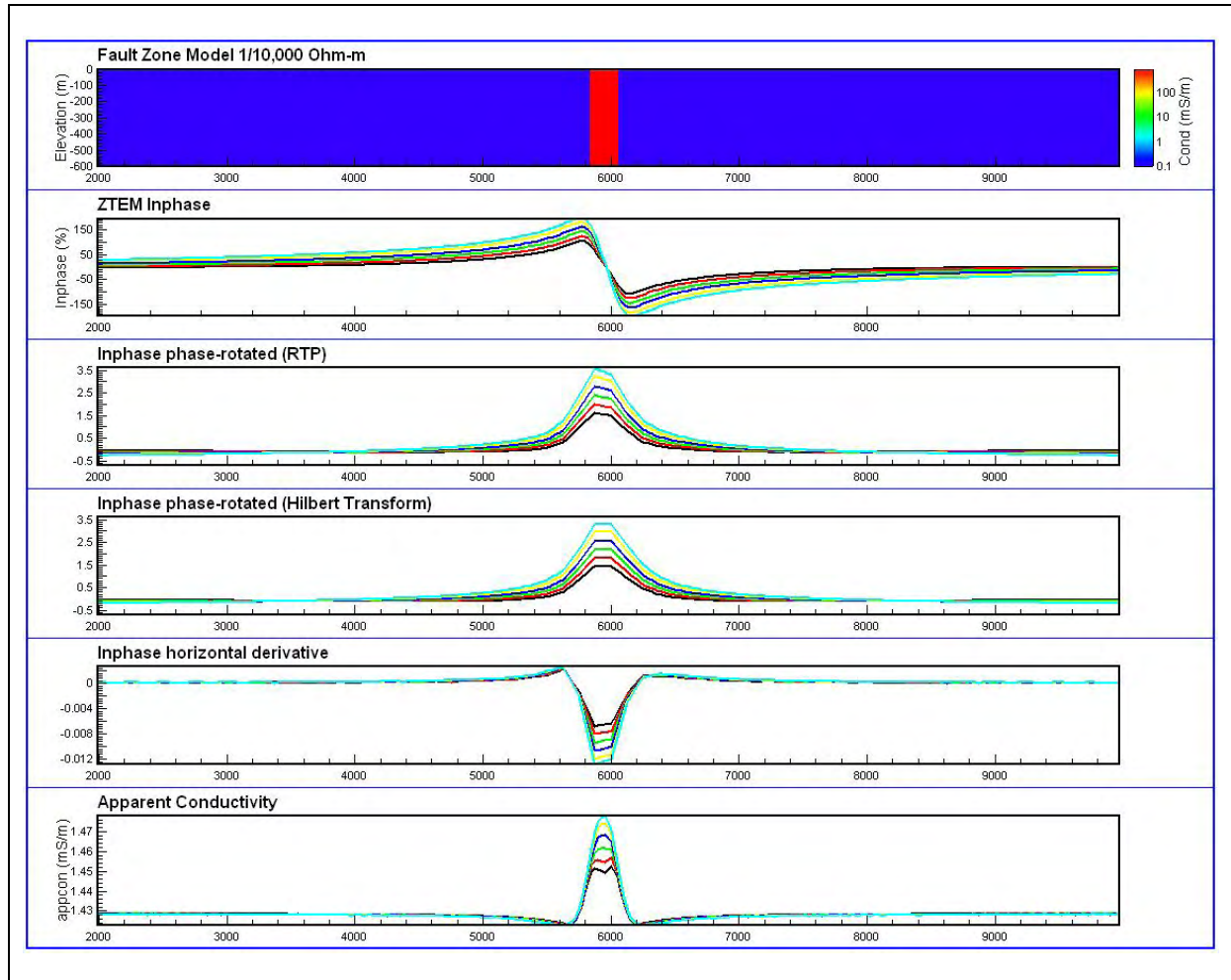


Figure 4. The ZTEM response and derived profiles across a 1 ohm-m fault zone in a 10,000 ohm-m host. The conductivity model, the inphase response, the phase-rotated inphase response derived by RTP filtering and Hilbert transformation, respectively, the horizontal derivative and the apparent conductivity profile are shown.

Even though the profiles of Figure 2 and Figure 4 are very different (i.e., where a crossover anomaly form is present for one model, a peak or trough anomaly form is present for the other model), the responses are much harder to distinguish on the grids. In both cases, a strong change in response occurs in a restricted region in close lateral proximity to the contact or conductor.

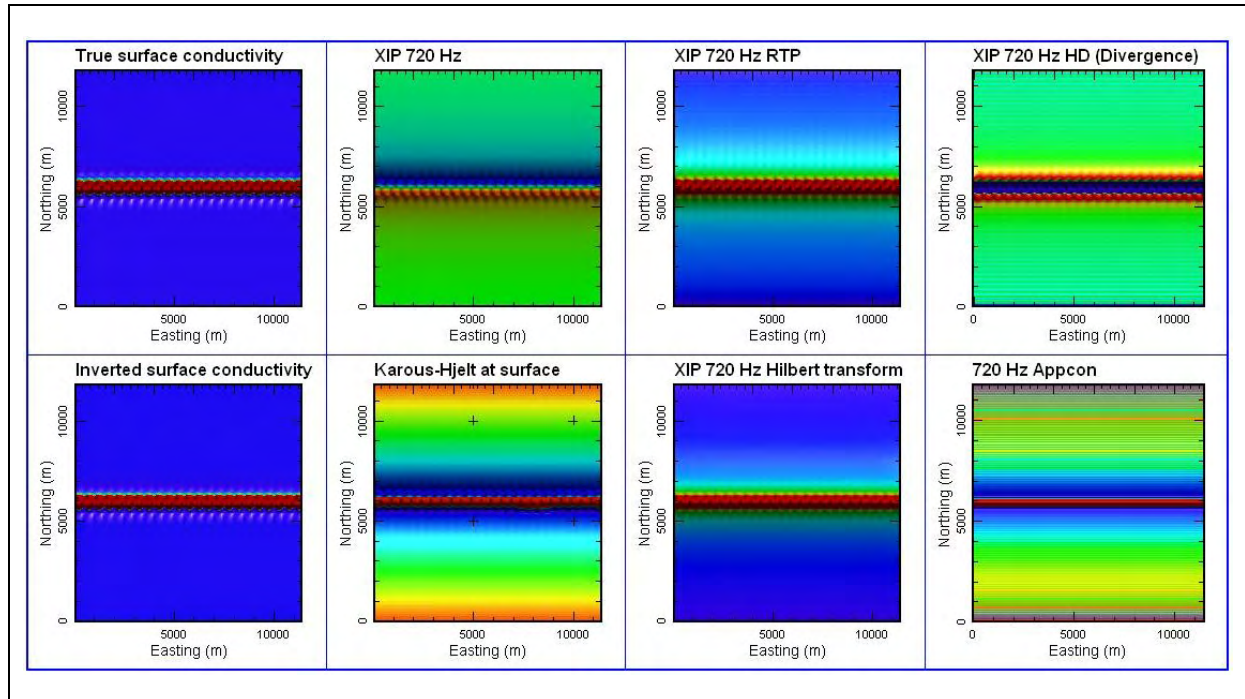


Figure 5. Grids derived from the data shown in Figure 4. Shown in the top row: the true conductivity model, the 720 Hz inphase response, the phase-rotated 720 Hz inphase response (RTP), the horizontal derivative of the 720 Hz inphase response (total divergence grid), and in the bottom row: the conductivity model recovered by 2D inversion, the near-surface Karous-Hjelt filter result of the 720 Hz inphase response, the phase-rotated 720 Hz inphase response (Hilbert Transform) and the 720 apparent conductivity grid.

The effect of topography

Although survey data can be corrected for the effect of varying receiver elevation by analytic continuation (Watts, 1975), application of a topographic correction, as discussed for VLF and MT data by Eppelbaum (1991) and Schwalenberg and Edwards (2004) appears less reliable. Correcting the data for terrain effects and the sensor elevation would allow for a less ambiguous interpretation of the various filtered image products. However, such a correction is unnecessary for the inversions, since the survey topography and the receiver elevation are taken into account by the algorithms, as illustrated in Figure 1.

Sattel and Witherly (2012) show synthetic ZTEM profiles across a hill and a depression. Their results indicate that the ZTEM response of hills and depressions can be confused with the responses of conductors and resistors, respectively, if the topography is not taken into account during a qualitative interpretation of various products or when the data are subjected to quantitative processing such as inverse modelling. Figure 6 shows images of the topography and acquired Tzx data for a ZTEM survey across mountainous terrain. The vertical relief in the survey area is approximately 2 km. Using the observed topography, Tzx responses were predicted for 100 and 1,000 ohm-m half-spaces, respectively, and are shown in Figure 6. The observed and predicted data have been phase-rotated to align peaks with conductors and troughs with resistors. A comparison of the images shows strong agreement between the observed and predicted data; this confirms that it is essential to take into account topography for the interpretation of ZTEM data in mountainous terrain.

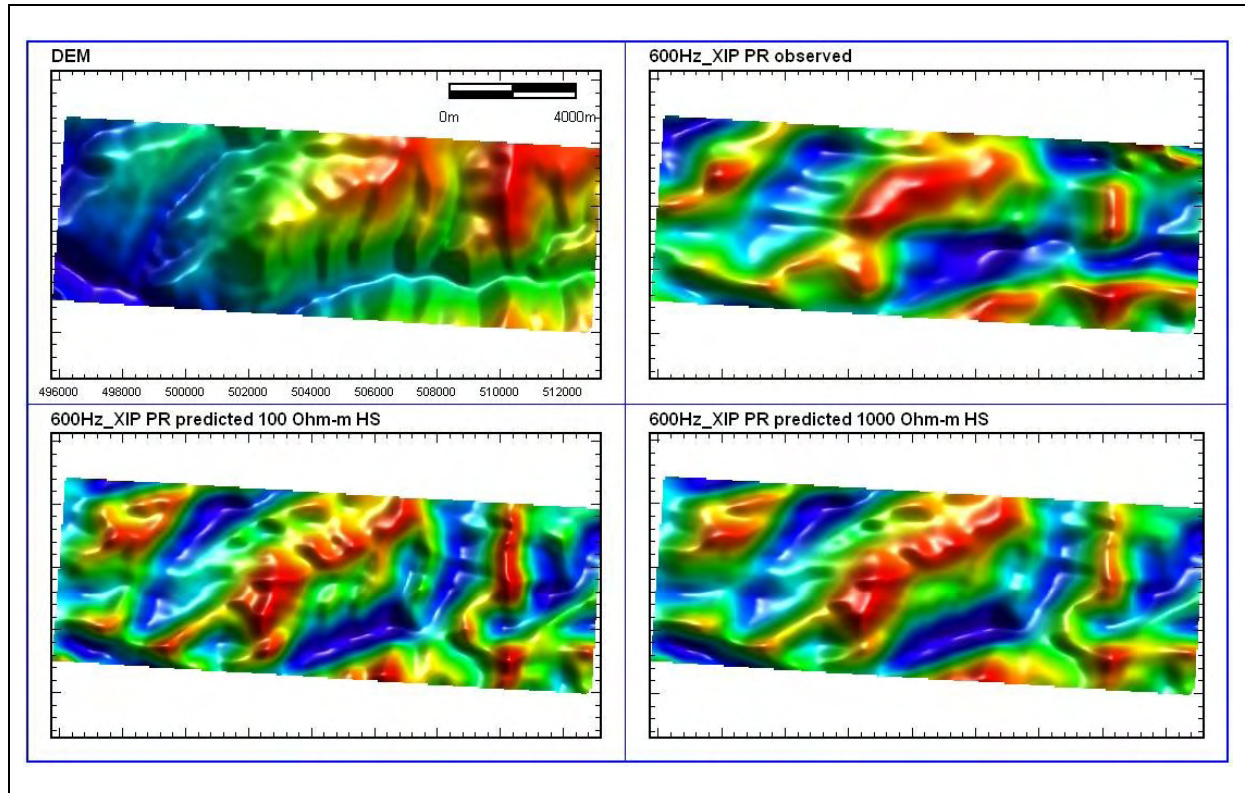


Figure 6. ZTEM response in mountainous terrain. Shown clockwise from the upper left: the survey topography, the observed 600 Hz phase-rotated Tzx inphase data, and the same data predicted for 1,000 and 100 ohm-m half-spaces, respectively. The high degree of agreement between observed and predicted data show that the response is dominated by the topographic response of the survey area.

Forresteria Survey

Figure 7 shows the flight lines of a survey flown at the Forresteria, WA, EM test range, which is described on the website of Southern Geoscience Consultants (www.sgc.com.au). The ground covered by the ZTEM survey includes two drilled, barren, semi-massive to massive sulphides (IR2 and IR4), hosted in highly resistive bedrock under a conductive overburden (10-20 S). IR2 is described as shallow (<100 m), highly conductive (>7,000 S), small (<75x75 m) and dipping 30-40 degrees to the north. It is well defined by surface, downhole and some airborne EM systems. Conductor IR4 is described as deep (>300 m), highly conductive (5,000-10,000 S), extensive in strike and plunge extent (>500 m), limited in depth extent (100-150 m) and dipping 30-40 degrees to the north. East-west and north-south lines were flown over the IR2 and IR4 bodies which allowed repeatability and consistency between the two data sets to be assessed. The terrain is flat with less than 60 m of vertical relief across the survey area, and it was thought that ZTEM response variations related to the topography would be very unlikely.

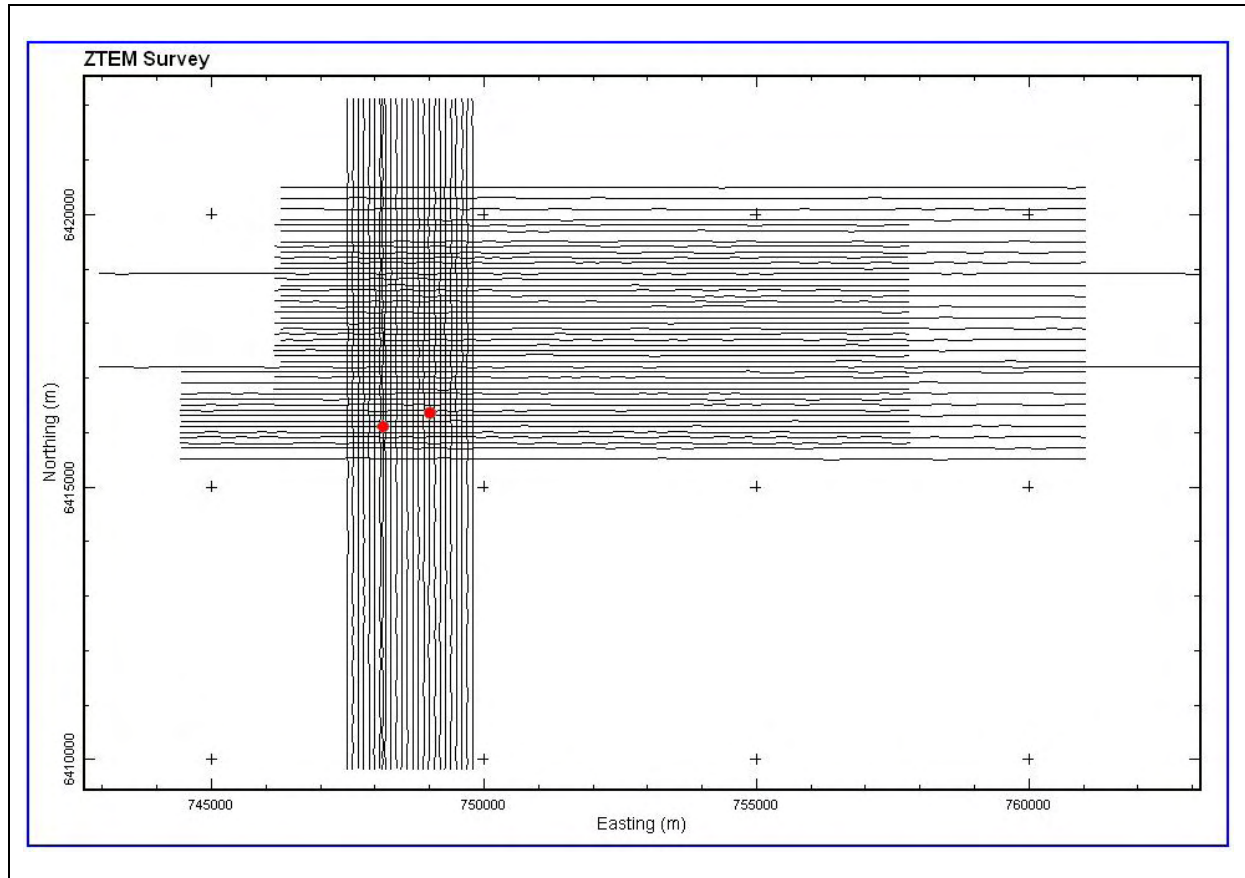


Figure 7. Flight lines from the ZTEM survey at Forrestania, WA. The locations of sulphides IR2 and IR4 are indicated by red dots.

Image products of data from the north-south lines are shown in Figure 8 to Figure 12. The Tzx and Tzy inphase data shown in Figure 8 indicate the sensitivity of the data to cross-striking structures. The corresponding phase-rotated grids of these responses are shown in Figure 9. These Tzx and Tzy inphase grids were then combined to form the total phase-rotated inphase grids shown in Figure 10. These grids show high values over cross-striking conductors and show structures striking in many directions. Total divergence grids are also shown in Figure 10. Since these are a product of the spatial derivatives, they highlight the spatial variation of the data. The apparent conductivity grids shown in Figure 11 are derived from the Tzx and Tzy data and show a close resemblance to the total phase-rotated grids in Figure 10. The corresponding phase grids are more difficult to interpret. According to Becken and Pedersen (2003), lower and higher values indicate conductivity to be decreasing and increasing, respectively, with depth.

Karous-Hjelt near-surface grids as shown in Figure 12 are another way to apply a phase rotation to the data, while also attempting to extract some depth information.

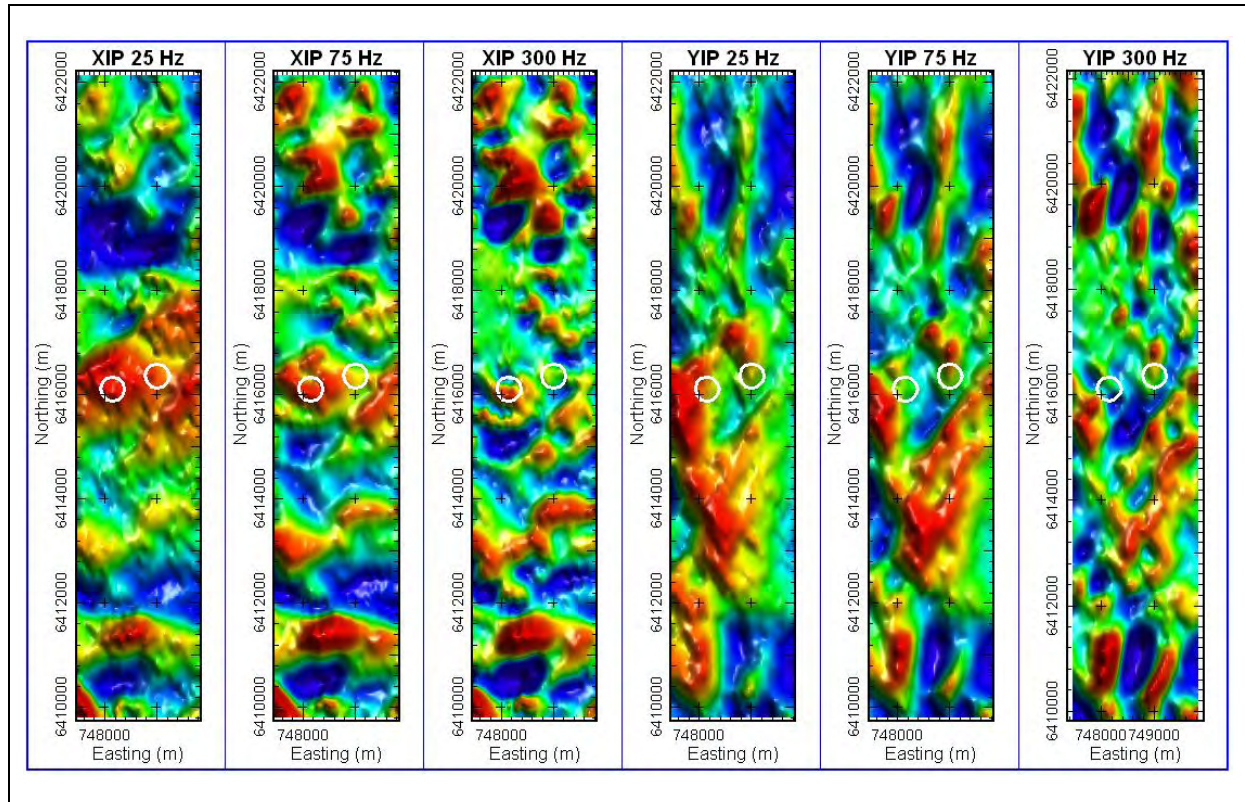


Figure 8. Grids of selected frequencies of T_{zx} (left panels) and T_{zy} (right panels) data from north-south survey lines provided by Geotech. The locations of the known sulphides IR2 and IR4 are indicated by white circles.

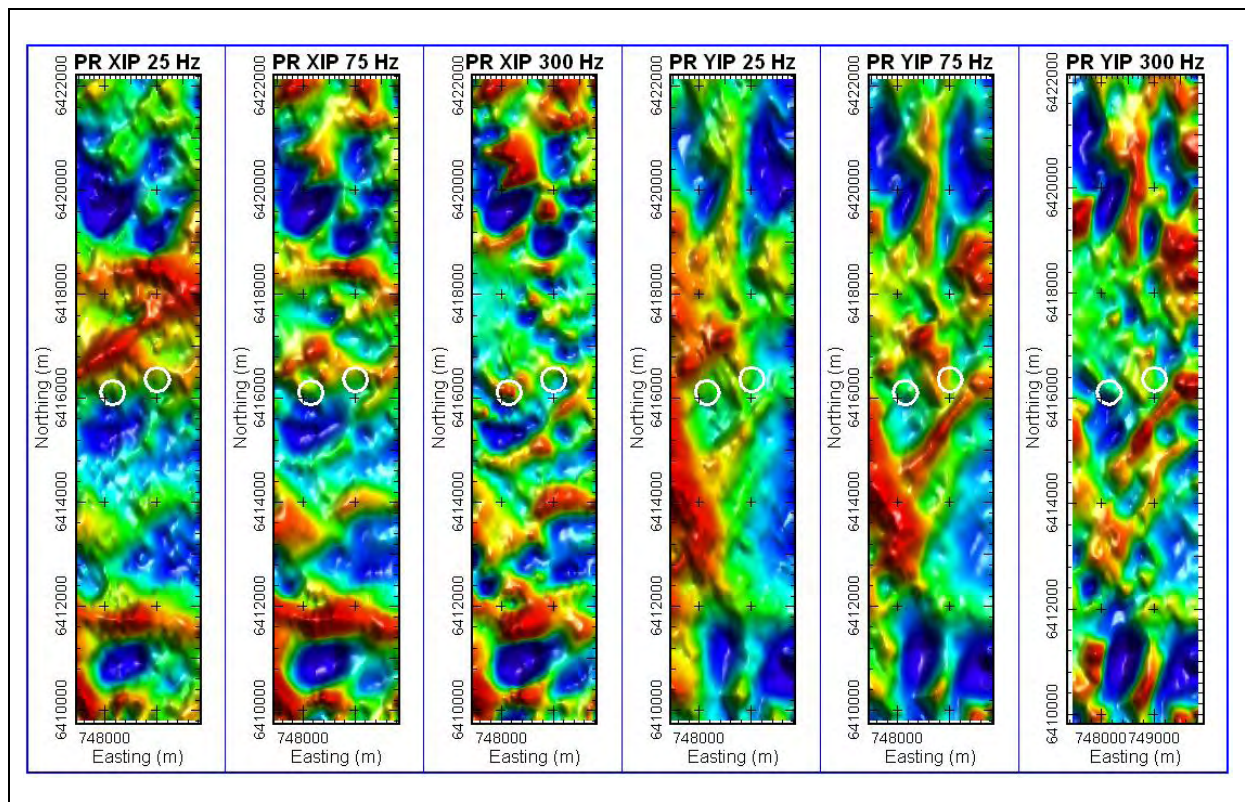


Figure 9. Phase rotated grids for the data shown in Figure 8 provided by Geotech.

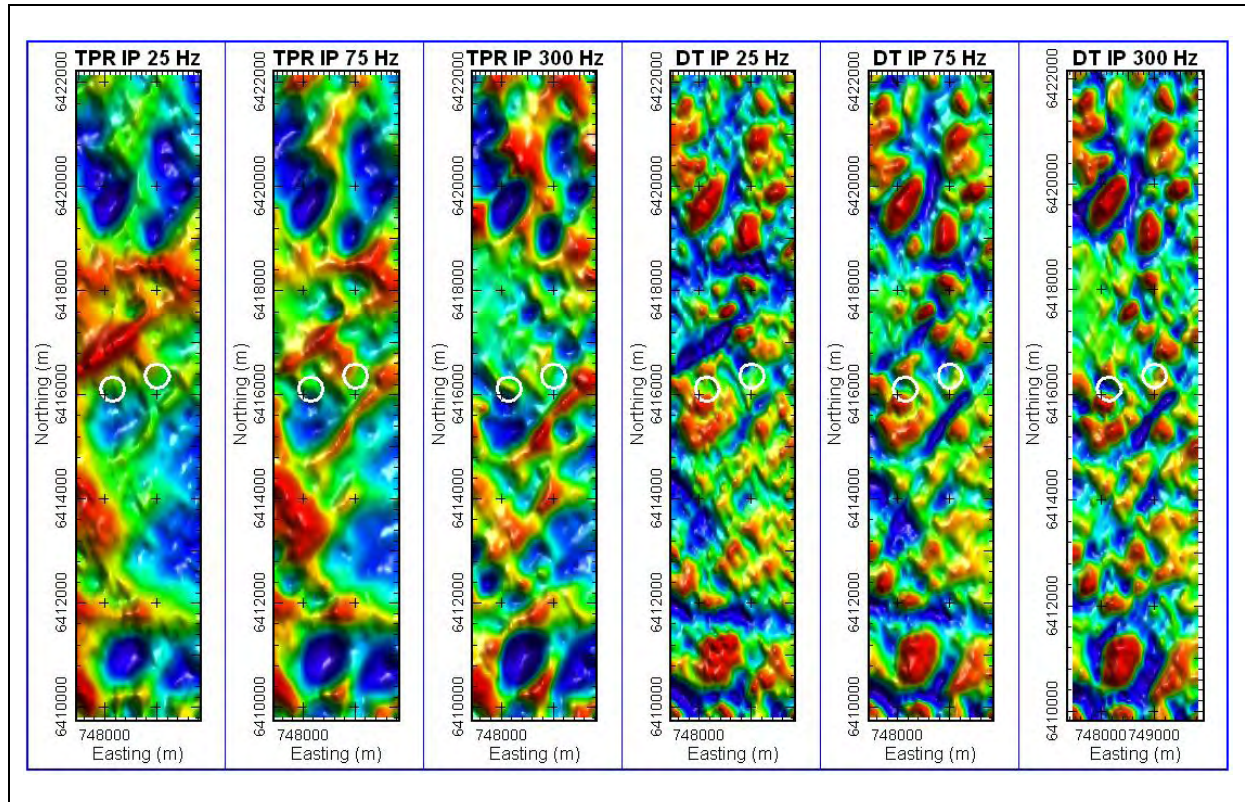


Figure 10. Total phase rotated grids (left panels) and total divergence grids (right panels) provided by Geotech.

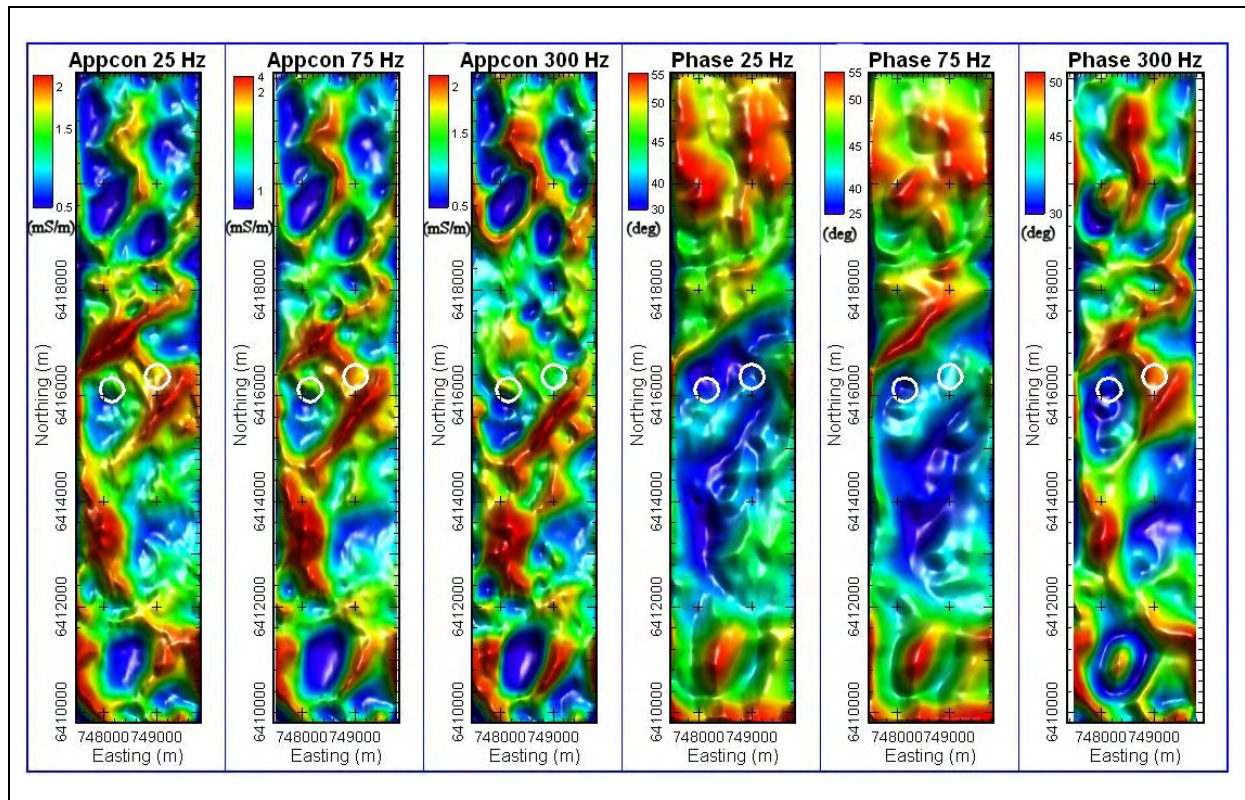


Figure 11. Apparent conductivity (left panels) and phase (right panels) grids.

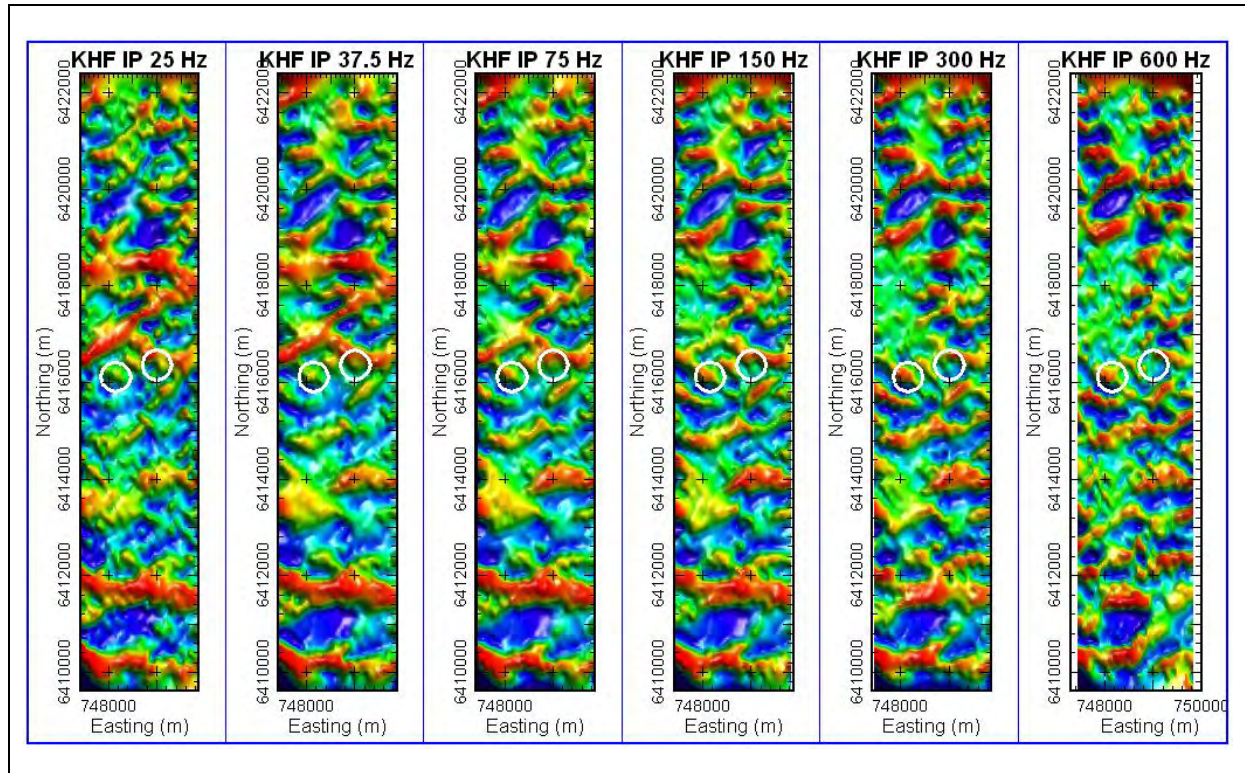


Figure 12. Karous-Hjelt near-surface grids derived from the Tzx in-phase (left panels) and quadrature (right panels) data.

Karous-Hjelt pseudo-sections derived from the Tzx in-phase data acquired across conductor IR2 are shown in Figure 13. A different section is derived for each frequency and a composite model is generated from the averaged sections of all frequencies. The location of sulphide IR2 is indicated by elevated current density values at the surface. Even though the depth information is not reliable, these pseudo-sections give some indication of the spatial distribution of the most prominent conductors and resistors. Hence, these sections can help to interpret conductors mapped on 2D or 3D inversion conductivity-depth sections that might be related to data over-fitting.

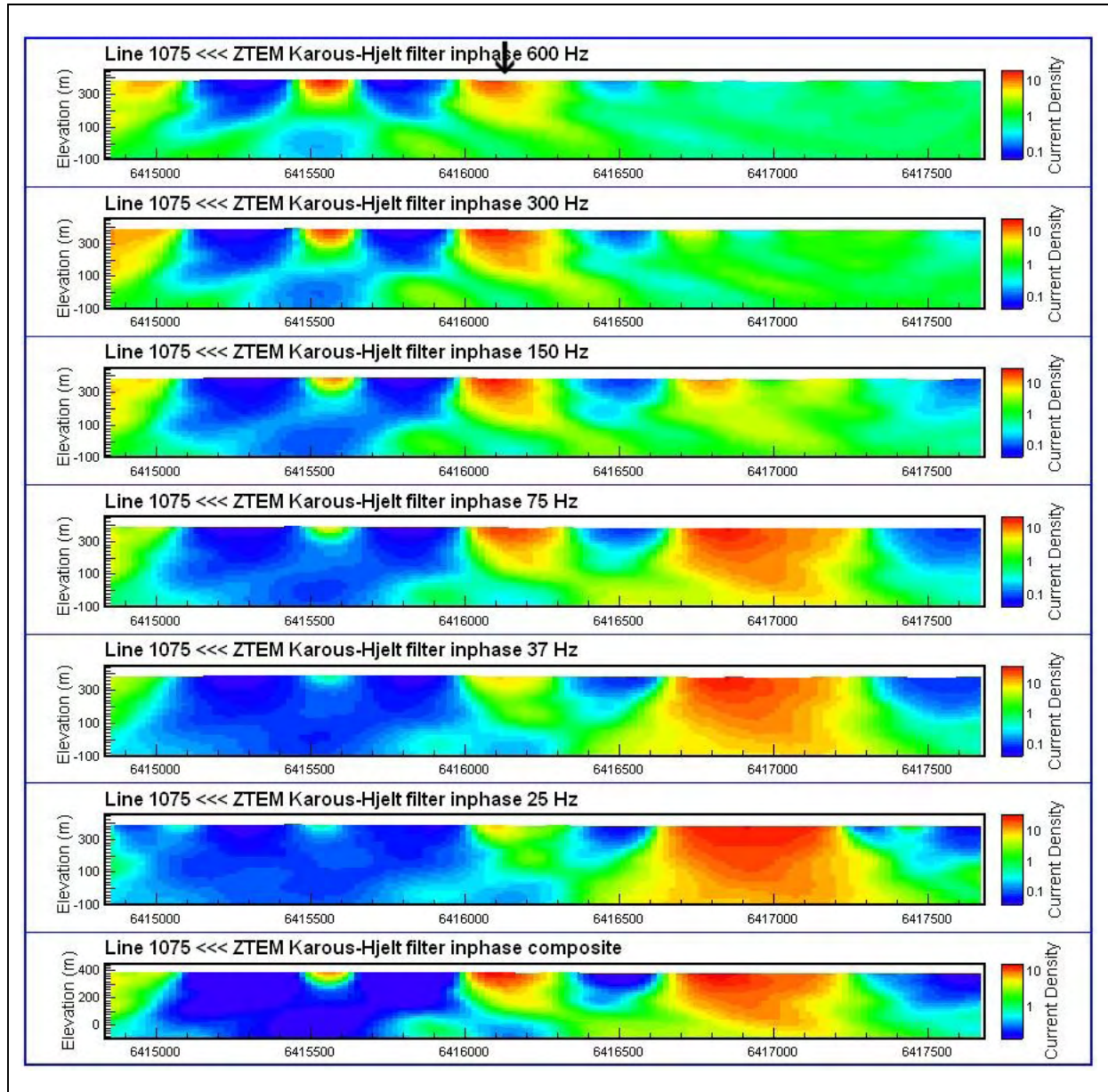


Figure 13. Sections for north-south line 1075. Karous-Hjelt sections derived from inphase ZTEM profiles with decreasing frequency from top to bottom and a composite section of all frequencies at the very bottom. The location of conductor IR2 is indicated by an arrow.

The 2D inversion result of the same line shown in Figure 14 indicates a conductive structure at the location of IR2. Due to the limited strike length of the sulphide zone, a strong response was not expected. It should be noted that the response might be due to a geological structure with long strike length that hosts the sulphide.

The 2D inversion result of the east-west line across IR2 (not shown) does not give any indication of the presence of the conductor. For a more appropriate comparison between the east-west and north-south data sets, Tzy data from the east-west data set were extracted to derive a profile of in-line tipper values directed north-south. For this step, each east-west line contributes one point to the pseudo north-south line, and the data spacing on the pseudo profile is determined by the line spacing of the east-west data set. Due to the close flight-line spacing of the Forrestania survey (mostly 100 m) the anomaly shape is recovered well and the derived conductivity structure agrees very well with the result from the north-south data. This indicates great consistency and repeatability between the two data sets flown at different flight line directions and acquired at different times.

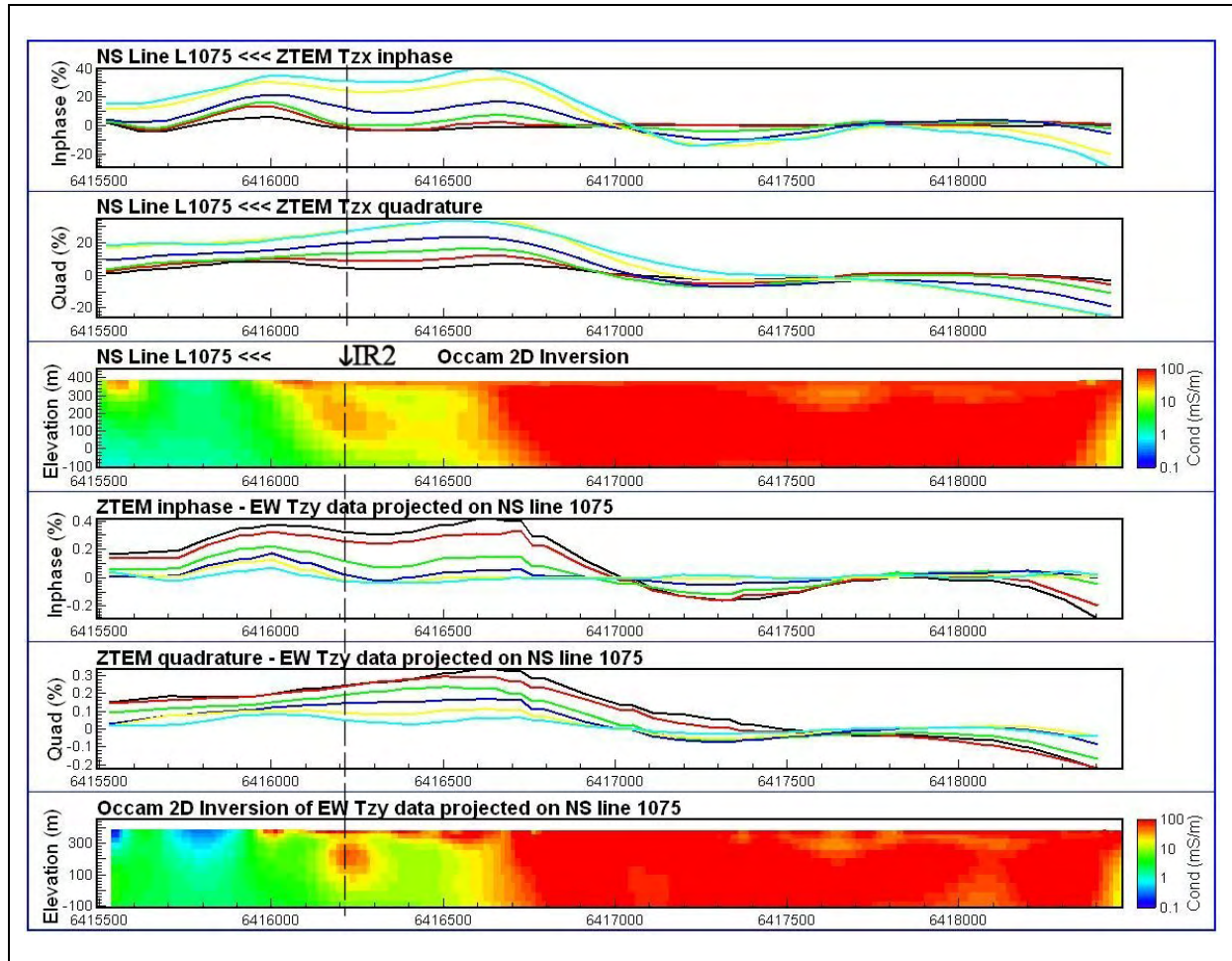


Figure 14. ZTEM profiles across sulphide IR2, indicated by a dashed line, with corresponding inversion results. A portion of Tzx profiles of north-south line 1075 are shown in the top panels; the profiles derived from the Tzy data of the east-west lines are shown in the bottom panels.

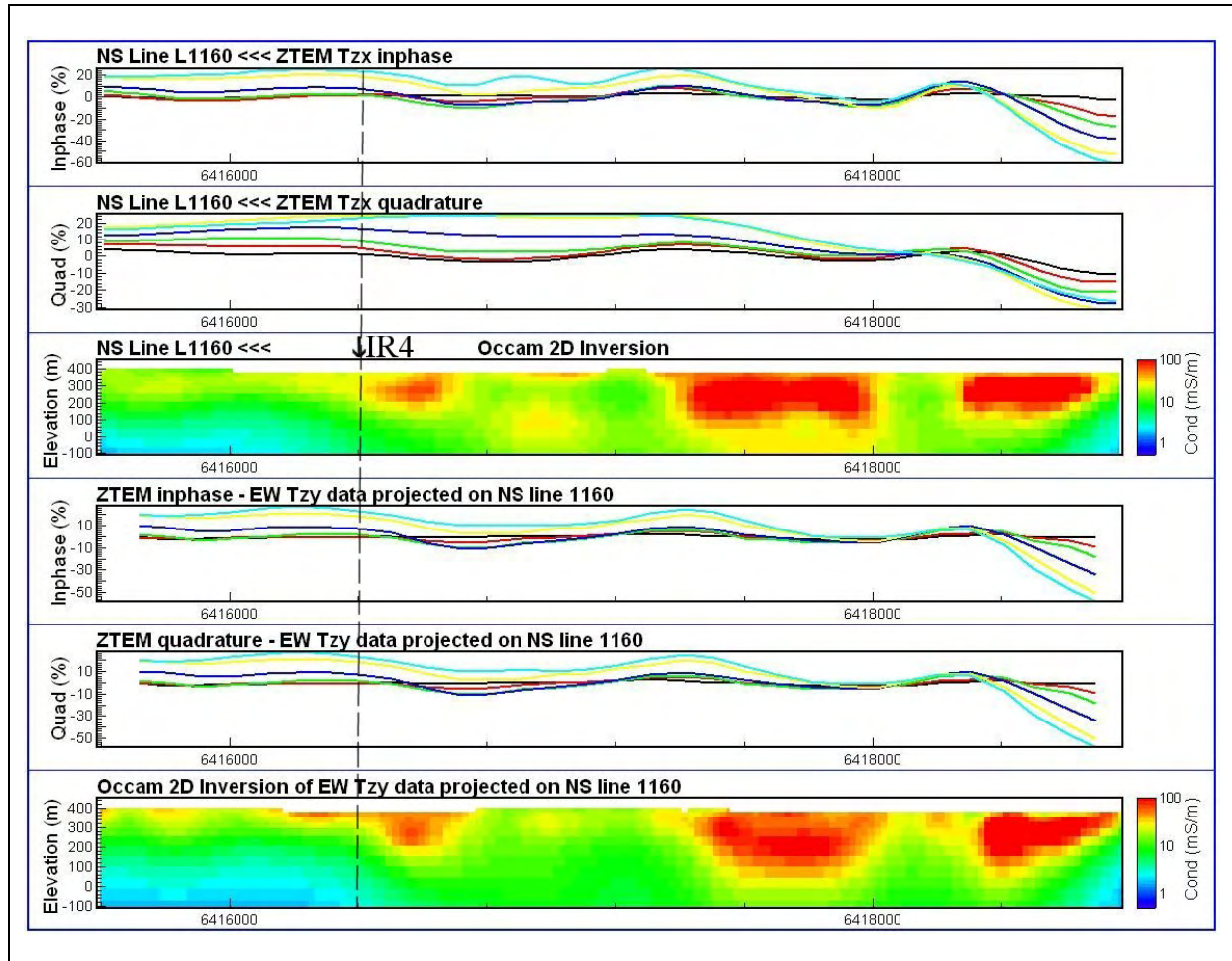


Figure 15. ZTEM profiles across the location of sulphide IR4, indicated by a dashed line, with corresponding inversion results. A portion of Tzx profiles of north-south line 1160 are shown in the top panels; the profiles derived from the Tzy data of the east-west lines are shown in the bottom panels.

The 2D inversion results of data acquired across IR4 are shown in Figure 15. The original north-south data are shown along with projected data from the east-west survey. The two data sets show excellent agreement again. The conductivity-depth sections indicate a near-surface conductor near IR4, but probably too shallow to correspond to the target sulphide body.

These results also suggest that for 2D inversions to extract the maximum information of some structures, survey data might have to be projected and rotated into profiles with more appropriate flight-line directions. Since Tzx and Tzy are available for the entire survey, any angle can be chosen for reprojecting the data. However, in complex terrain such as Forrestania, a 3D inversion is expected to give more reliable results than 2D inversions. For the 3D inversion, the entire NS survey area was inverted using horizontal cell sizes of 100x100 m, and the sub-area, corresponding to the region of overlap of the east-west and north-south surveys, was inverted with 50x50 m cells.

The north-south and east-west survey data of the sub-area were independently modelled by the 3D-inversion. The conductivity values recovered from both data sets across IR2 and IR4 are shown in Figure 16 and Figure 17. These sections are quite similar to the 2D inversion results from Figure 14 and Figure 15. The inversion results mostly agree that a shallow conductor at the location of IR2 is dipping north, agreeing with the known geometry of IR2. Near the location of IR4, the 3D inversions indicate a broad conductor with significant depth extent, whereas the 2D inversions indicate near-surface conductive material only. Since IR4 is known to be 300 m below surface and dipping north, the modelled conductive material might not correspond to the sulphide body. The profiles of predicted response for the 3D model match the observed data quite well. A better fit would have been

achievable, but at the expense of the models' smoothness which was not considered to be justified in this instance.

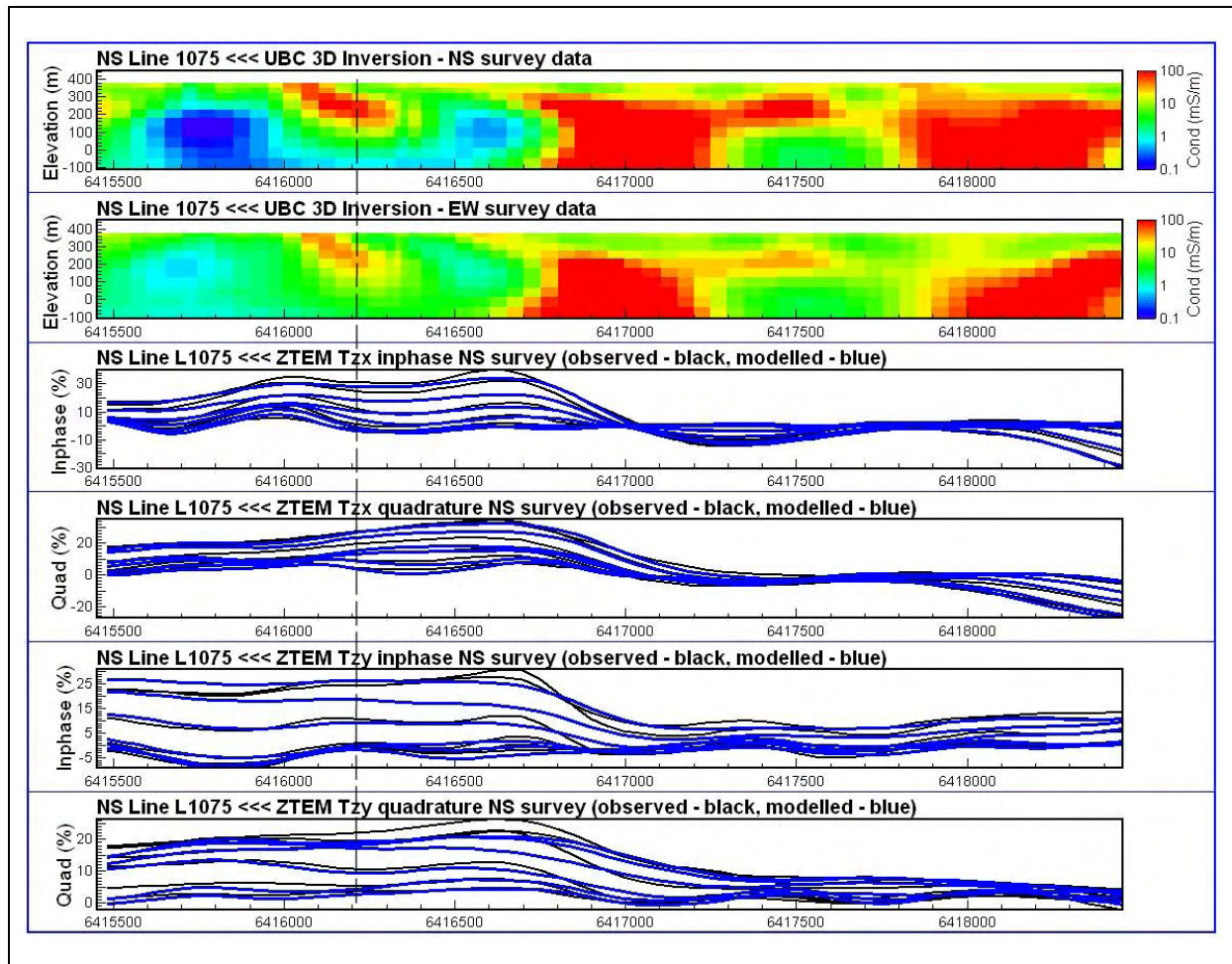


Figure 16. 3D inversion results across sulphide IR2, indicated by a dashed line. Shown are the conductivity-depth sections derived from the north-south and east-west data, respectively, and a comparison of the observed and modelled Tzx and Tzy profiles for the north-south data. Compare to 2D inversion results of Figure 14.

A comparison of conductivity slices derived from the 2D and 3D inversions for the north-south survey data is shown in Figure 18. The generation of east-west pseudo-lines allowed for the 2D inversion of the Tzy data. To capture the results of both 2D inversions, the conductivity grids of the Tzx and Tzy data were merged. As shown in Figure 18, the results of the merged grids look reasonable, and appear to have successfully combined the information of the individual results.

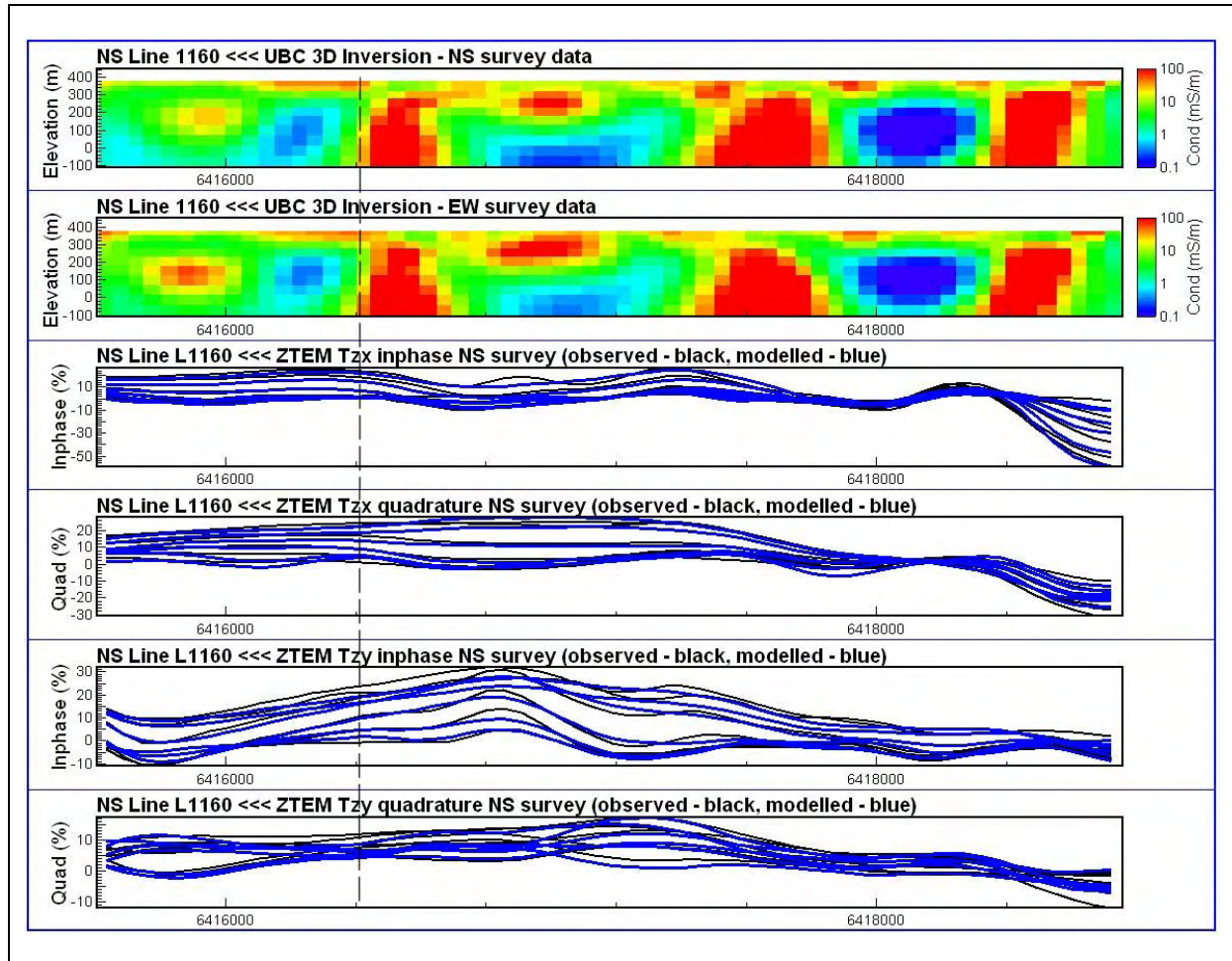


Figure 17. 3D inversion results across the location of sulphide IR4, indicated by a dashed line. Shown are the conductivity-depth sections derived from the north-south and east-west data, respectively, and a comparison of the observed and modelled Tzx and Tzy profiles for the north-south data. Compare to 2D inversion results of Figure 15.

The 3D inversion results shown in Figure 18 confirm the complexity of the conductivity structure and indicate that the strike direction is quite variable across the survey area, the latter indicating that the results from 2D inversions are likely to be less reliable. Nevertheless, the 2D and 3D results are fairly similar. The conductivity slices derived from the 2D inversion actually have better spatial resolution due to a much smaller horizontal cell size (10 m) having been used. However, it is unclear if some of the structures, shown on the 2D conductivity grids but absent on the corresponding 3D grids, are real or an artefact of the 2D processing.

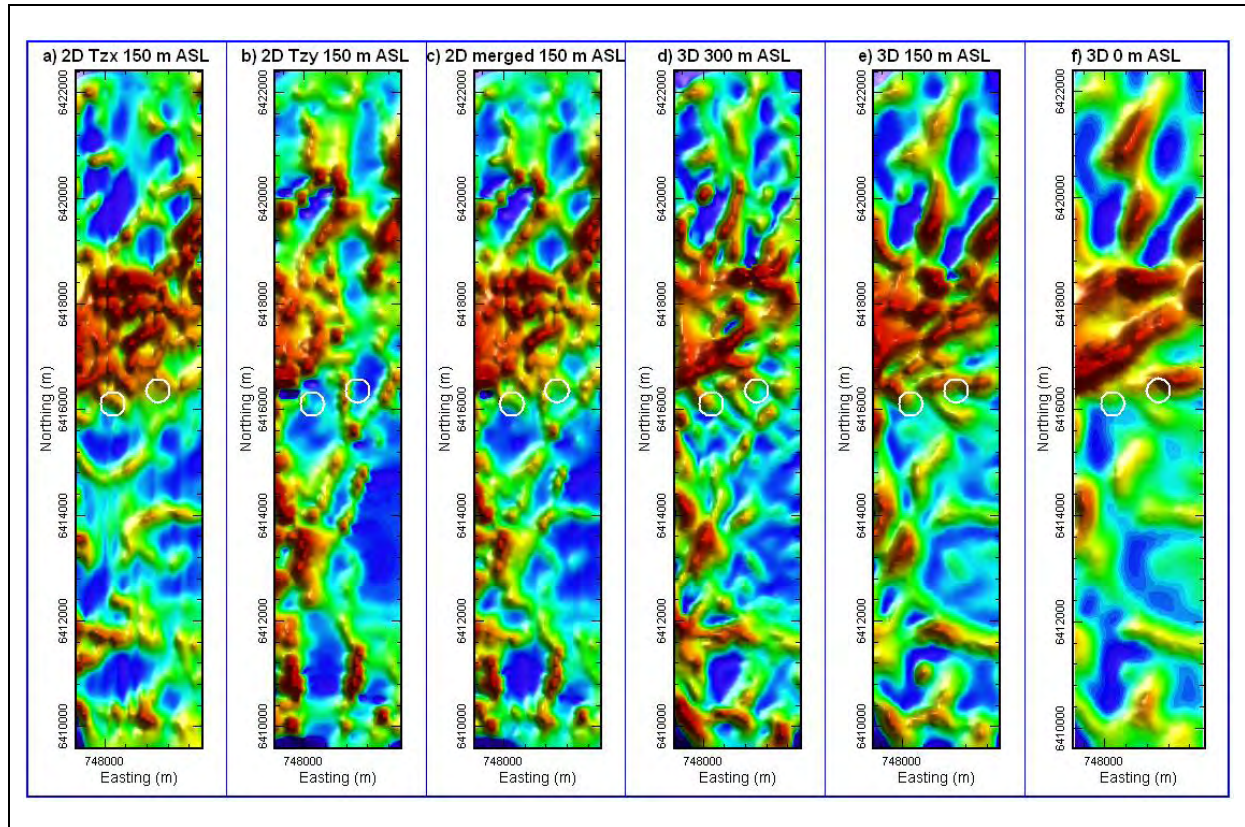


Figure 18. Conductivity-elevation slices derived from the Forrestania north-south survey data, from left to right: a) 2D inversion result of Tzx data at 150 m ASL, b) 2D inversion result of Tzy data at 150 m ASL, c) merge of a) and b), d-f) 3D inversion results at 300, 150 and 0 m ASL, respectively.

A summary of the modelling results across the two known sulphide bodies is shown in Figure 19. Since this is the area of overlap between the north-south and east-west surveys, results are shown for both data sets. The results of the total phase-rotated 150 Hz responses are quite similar between the two data sets, indicating excellent data repeatability. The former as well as the 150 Hz apparent conductivity values indicate the sulphides IR2 and IR4 to be located along northwest-southeast trending, conductive lineaments. The conductivity slices derived from the 2D inversions show great similarity where expected: 1) between the slices derived from the north-south Tzx and the east-west pseudo-line Tzy data (both being sensitive to structures striking east-west) and 2) between the slices derived from the east-west Tzx and the north-south pseudo-line Tzy data (both being sensitive to structures striking north-south). The conductivity slices derived from the 3D inversion of the two data sets show excellent agreement and map the locations of the sulphides near conductive lineaments. The conductor mapped at the location of sulphide IR2, as shown in Figure 14 and Figure 16, not being mapped as a discrete conductor in any of the images of Figure 19 suggests that IR2 is likely connected to a more extended structure, as suggested by the 3D result. Being connected to an extended structure increases current channelling into the sulphide, boosting its EM response and enabling its detection by an AFMAG method.

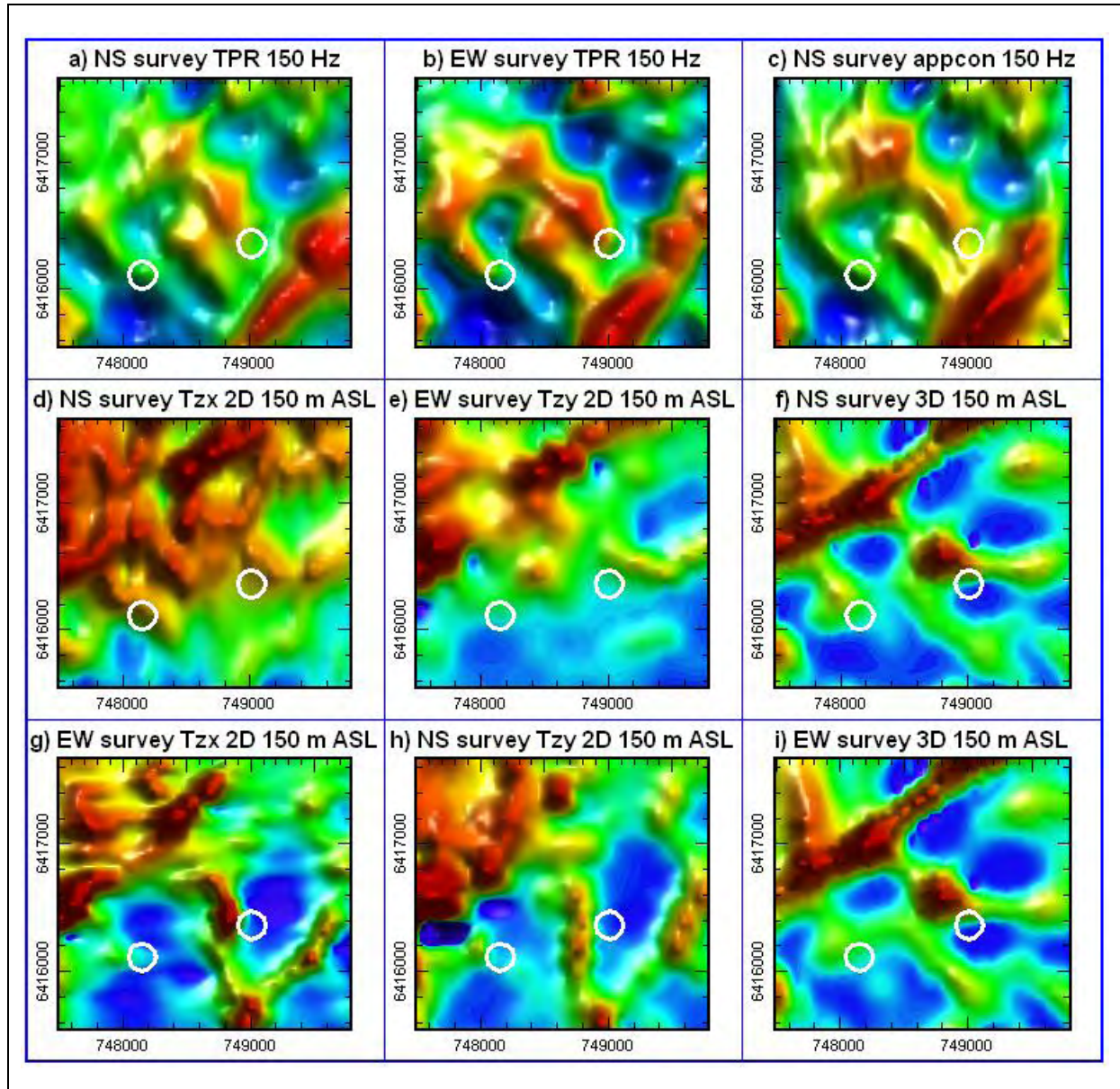


Figure 19. Summary of processing and modelling results of both surveys in the area of overlap around sulphides IR2 and IR4. In the top row: a) 150 Hz total phase-rotated inphase response for north-south lines, b) same as a) for east-west line data, c) apparent conductivity values derived from the 150 Hz north-south line data; in the center and bottom row: conductivity slices at 150 m ASL derived from d) 2D inversion of north-south Tzx data, e) 2D inversion of east-west Tzy data, f) 3D inversion of north-south data, g) 2D inversion of east-west Tzx data, h) 2D inversion of north-south Tzy data, i) 3D inversion of east-west data. Note the similarities between d) and e), g) and h), and f) and i).

Conclusions

Products originally developed for the interpretation of VLF data, such as phase-rotated response, apparent conductivity, the VLF peaker and Karous-Hjelt filtering can be applied to ZTEM data for rapid initial data assessment. For more reliable results, 2D and 3D inversion algorithms can be used. The latter can also be used to forward model conductivity scenarios and predict the response due to the topography of a survey area.

The results from synthetic models indicate that even though contacts and fault zone models produce quite different ZTEM profiles, it is difficult to distinguish them using grid products.

A brief analysis of ZTEM data acquired across rugged terrain indicates that it is essential to take into account topography for the inversion of ZTEM data in such an environment.

The analysis of ZTEM data at Forrestania, WA, has shown excellent repeatability between two data sets flown in different flight line directions and acquired at different times. The derivation of ZTEM profiles along pseudo-lines allowed suitably oriented 2D inversions to be produced for structures that were oriented in directions other than perpendicular to the survey flight-line direction. However, in terrain of complex geology and conductivity structure such as at Forrestania, 3D inversions are necessary to derive reliable conductivity-depth information from the data.

Acknowledgments

We would like to thank Doug Oldenburg and Elliot Holtham for use of their 3D inversion algorithm ZTEM_MT3Dinv, and Geotech Airborne Pty Ltd for releasing the Forrestania data shown in this publication.

References

- Becken M., and Pedersen, L. B., 2003, Transformation of VLF anomaly maps into apparent resistivity and phase: *Geophysics*, 68, 497-505.
- DeGroot-Hedlin, C. and Constable, S., 1990, Occam's inversion to generate smooth two-dimensional models from magnetotelluric data: *Geophysics*, 55, 1613-1624.
- De Lugao, P. P., and Wannamaker, P., 1996, Calculating the two-dimensional magnetotelluric Jacobian in finite elements using reciprocity: *Geophysical Journal International*, 127, 806-810.
- Duncan, A. C., 1987, Interpretation of down-hole transient EM data using current filaments: *Exploration Geophysics*, 18, 36-39.
- Eppelbaum, L. V., 1991, Examples of Terrain Corrections in the VLF-method in the Caucasian Region, USSR: *Geoexploration*, 28, 67-75.
- Farquharson, C. G., Oldenburg, D. W., Haber, E., and Shekhtman, R., 2002, An algorithm for the three-dimensional inversion of magnetotelluric data: *SEG Expanded Abstracts*, 21, 649-652.
- Holtham, E., and Oldenburg, D. W., 2010, Three-dimensional inversion of ZTEM data: *Geophysical Journal International*, 182, 168-182.
- Karous, M., and Hjelt, S. E., 1983, Linear filtering of VLF dip-angle measurements: *Geophysical Prospecting*, 31, 782-794.
- Legault, J. M., Kumar, H., Milicevic, B., and Wannamaker, P., 2009, ZTEM tipper AFMAG and 2D inversion results over an unconformity target in northern Saskatchewan: *SEG Expanded Abstracts*, 28, 1277-1281.
- Lo, B., and Zang, M., 2008, Numerical modelling of Z-TEM (airborne AFMAG) responses to guide exploration strategies: *SEG Expanded Abstracts*, 27, 1098-1102.
- Pedersen L. B., Qian, W., Dynesius, L., and Zhang, P., 1994, An airborne tensor VLF system. From concept to realization: *Geophysical Prospecting*, 42, 863-883.

- Sattel, D., Witherly, K., and Becken M., 2010, A brief analysis of ZTEM data from the Forrestania test site, WA: 21st International Geophysical Conference and Exhibition, ASEG, Extended Abstracts.
- Sattel, D., and Witherly, K., 2012, Extracting information from ZTEM data with 2D inversions: 22nd International Geophysical Conference and Exhibition, ASEG, Extended Abstracts.
- Schwalenberg, K., and Edwards, R. N., 2004, The effect of seafloor topography on magnetotelluric fields: an analytical formulation confirmed with numerical results: *Geophysical Journal International*, 159, 607-621.
- Wannamaker, P. E., Stodt, J. A., and Rijo, L., 1986, Two-dimensional topographic responses in magnetotellurics modelled using finite elements: *Geophysics*, 51, 2131-2144.
- Wannamaker, P. E., Stodt, J. A., and Rijo, L., 1987, A stable finite-element solution for two-dimensional magnetotelluric modelling: *Geophysical Journal of the Royal Astronomical Society*, 88, 277-296.
- Ward, S., 1959, AFMAG - Airborne and Ground: *Geophysics*, 24, 761-787.
- Watts, R. D., 1975, A Fortran IV program for analytic continuation of VLF electromagnetic data: U.S. Geological Survey Open-File Report 75-159, 28 p.

The application of ZTEM to porphyry copper-gold exploration

Ken Witherly*
Condor Consulting, Inc., USA
ken@condorconsult.com

Daniel Sattel
EM Solutions, USA
dsattel@earthlink.net

SUMMARY

The ZTEM airborne EM system was introduced into commercial service by Geotech Ltd. in late 2007. ZTEM is unlike any other commercial EM system in that it relies on the measurement of natural occurring EM fields in the Afmag frequency range of 25-720 Hz.

As a result of using natural EM fields that pass through the earth as plane waves, the ZTEM system response shares similarities and important differences to traditional inductive source EM systems such as VTEM or MegaTEM, used extensively by the minerals industry to explore for targets of high conductance. While ZTEM can detect discrete conductors like inductive systems, it also responds to bulk changes in resistivity and conductivity gradients that often characterize geological contacts or structures.

One important deposit style that typically lacks a discrete conductivity response are porphyry copper-gold deposits, such as commonly found in many locations around the circum Pacific region. The present study will examine the ZTEM responses for several porphyry deposits in light of other exploration data including drilling, mapped geology and other forms of airborne and ground geophysics.

Key words: Afmag, airborne EM, ZTEM, porphyry copper.

INTRODUCTION

The ZTEM system (built and operated by Geotech Ltd.) measures the Afmag responses of naturally occurring subsurface currents, induced by distant lightning discharges. The vertical component is measured from a helicopter platform, while the horizontal components are recorded on the ground at a base station; data are typically acquired over a frequency range of 30-720 Hz. Various methods are used for the modeling and interpretation of ZTEM data, including 2D inversion, Karous-Hjelt filters and the derivation of apparent conductivity; these are discussed in Sattel et al. (2010).

The 2D algorithm used for the forward modeling and inverting ZTEM data is based on a 2D MT algorithm developed by Constable and Wannamaker. The algorithm derives the in-line (Tzx) tipper profiles from the computed transverse electric (TE) response. The finite-element algorithm models the effect of topography and takes into account the terrain clearance of the airborne platform along the flight line. An example of the model mesh is illustrated in Figure 1. This application is

discussed further in Sattel and Witherly (2012). For the interpretation of survey data, the Tzx. Geotech provides a suite of grids from the primary Tzx and Tzy outcomes along with filtered versions of the primary results intended to facilitate the interpretation of outcomes. Table 1 summaries the products typically delivered by Geotech and Condor.

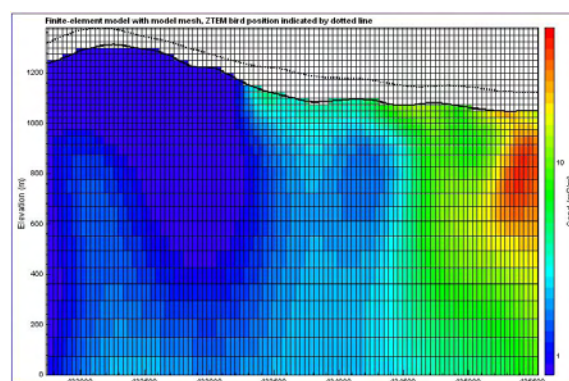


Figure 1: Illustration of model mesh for 2D inversion. Since the algorithm takes into account the topography and ZTEM bird terrain clearance along each line, air cells are an integral part of the finite-element model.

FIELD RESULTS

Pebble, Alaska: The Pebble deposit is a major copper-gold porphyry system in southern Alaska. ZTEM results over the deposit have been presented earlier by Paré and Legault (2010). The geology (plan and section) are shown in Figure 2. In addition to the ZTEM, Spectrem was flown over the deposit and surrounding area. These results have proven useful to compare with the ZTEM results. Figure 3 shows the ZTEM DT results for the three lower frequencies along with the TMI-Tilt, Spectrem tau and conductivity depth slice at 100 m. The ZTEM results show a resistive core to the shallower Pebble West deposit, with an irregular distribution of conductive trends surrounding the Pebble West. One roughly N-S linear along the eastern side of Pebble West correlates very closely to the Tertiary contact (marked as yellow line). The other ZTEM features to the north and west of the deposit are of unknown geological origin. The TMI-tilt was produced to see if the magnetic results correlated with the ZTEM trends in and around the deposit. There appeared to be no significant correlation between the magnetic and ZTEM outcomes. The Spectrem tau and a conductivity depth slice at 100 m show conductivity along the eastern side of Pebble West and across the northern edge of the deposit. The 100 m depth slice shows a strong N-S trending linear high that correlates with the mapped Tertiary contact and which is also picked up in the ZTEM results. Both the 100 m depth slice and ZTEM DT show an isolated high just off the western edge of Pebble

Table 1

Product	Source	Comments
D = primary data G = grid f(l) frequency low f(h) frequency high		
X-In-phase & Quad f(l) - f(h) D	Geotech	Primary data provided for all obtained frequencies
Y In-phase & Quad f(l) - f(h) D	Geotech	Primary data provided for all obtained frequencies
DT (Total derivative) f(l) - f(h) G	Geotech	DT is calculated from the horizontal derivatives of the Tzx and Tzy tippers; it is analogous to the "Peaker" parameter in VLF(Sattel and Witherly 2010). Long wave length information can be lost.
TPR (Total phase rotated) f(l) - f(h) G	Geotech	Transforms bipolar (cross over) anomalies into single pole anomalies with a maximum over conductors, while preserving long wavelength information
AppCon f(l) - f(h) D	Condor	Provides a better measure of conductivity changes within the data set.

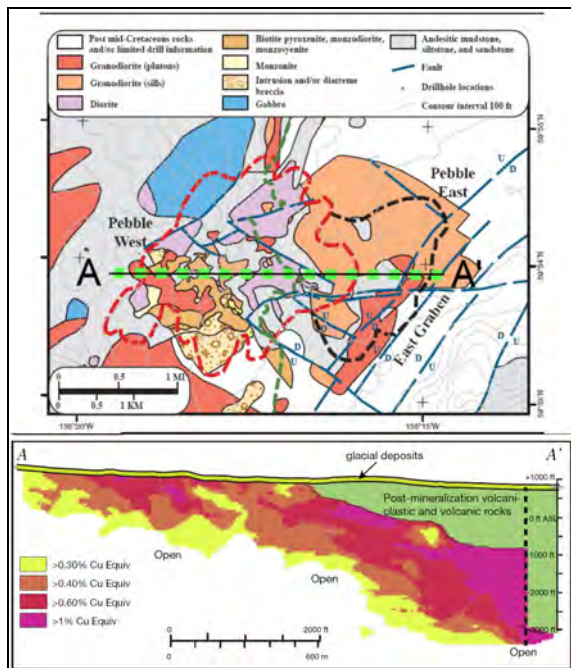


Figure 2: Geological map and section over Pebble deposit.

West; this feature is circled as a white dash on both images. Other aspects of the Spectrem and ZTEM results as well show a general agreement, while differing in detail. Figure 4 shows depth conductivity sections for the Spectrem and ZTEM results. The Spectrem data were processed with an Occam style layered earth inversion code whereas the ZTEM were processed with a 2D Occam inversion code discussed earlier in this abstract. The location of the two lines is shown in the upper left panel of Figure 3. Note, the lines were not flown using the same flight bearing but do cross over the deposit. These results show there is an extensive zone of shallow conductivity associated with Pebble West (defined by 0.3% Cu equ. zone). On both surveys however, the conductive zone extends well west of the actual deposit.

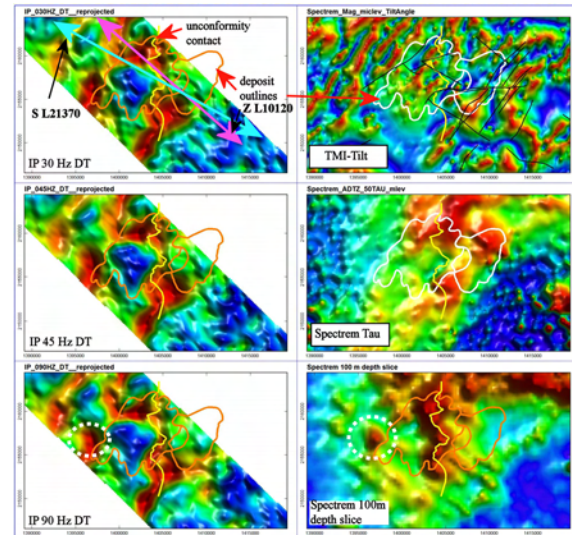


Figure 3: Pebble DT grids for 30, 45 and 90 Hz (left side); TMI-tilt (upper right), Spectrem tau and 100 m conductivity depth slice.

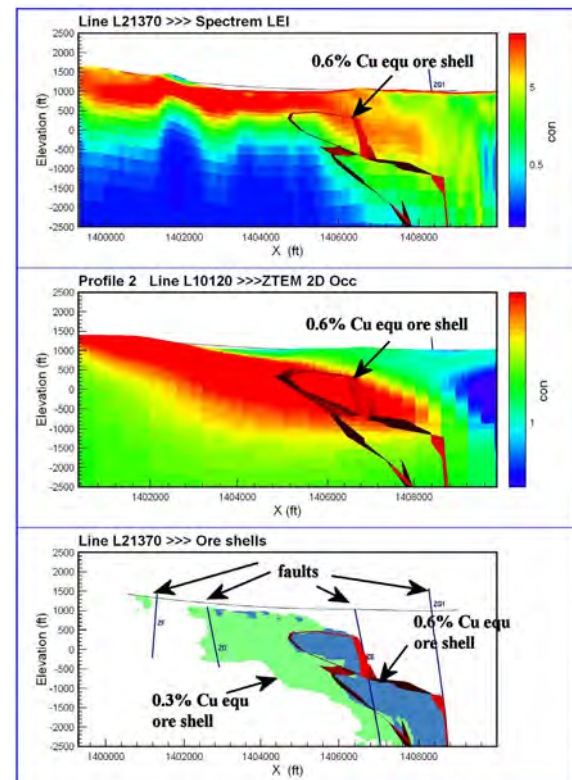


Figure 4: Conductivity depth sections from Spectrem and ZTEM along with 0.3% and 0.6% Cu equ. ore shells.

Both results as well appear to capture the faulted (down-dropped) aspect of the mineralized zone going to the east with the ZTEM appearing to capture this slightly better than the Spectrem results. The extent of the conductivity is considered unusual for this style of deposit and there is currently no petrophysical or borehole data to define a specific source. Based on geological descriptions however, a late stage alteration termed the quartz-sericite-pyrite event could be the causing much of the conductivity response not attributed to other sources such as the Tertiary contact discussed earlier.

Planned borehole physical property logging should help to establish with greater certainty what geological sources are causing the observed conductivity.

Babine Lake, British Columbia: The Babine property consists of two intrusive systems; the Nak and the Dorothy. These are shown in Figure 5. Prior to the ZTEM survey, an IP-resistivity survey and extensive drilling were carried out on the property. While the IP-resistivity survey covered both the Nak and Dorothy, the drilling was localized around the Nak.

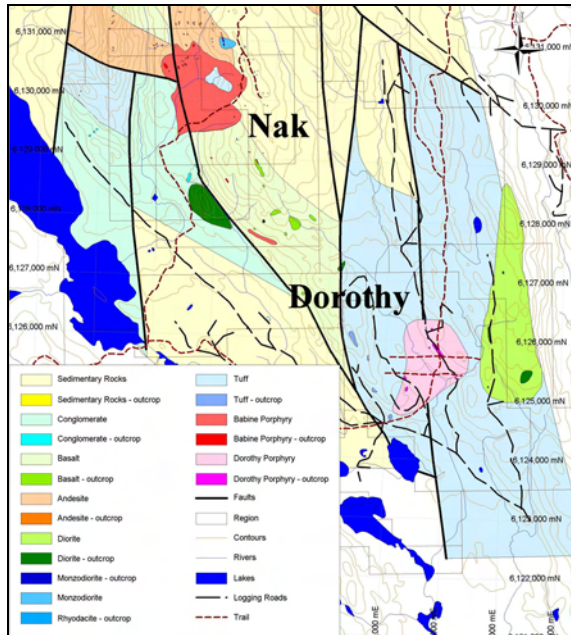


Figure 5: Geology over the Nak and Dorothy intrusives.

Figure 6 shows the TMI and ZTEM 30 Hz In-Phase TPR. The Nak and Dorothy intrusive systems are outlined. The Nak porphyry shows a direct magnetic high with dimensions similar to the mapped porphyry system. As well, the Nak outline overlaps with a discrete 30 Hz In-Phase TPR low. The Dorothy intrusive lies on the flank of the elongate magnetic high. A discrete 30 Hz In-Phase TPR low is noted just west of the intrusive. Figure 7 shows a depth slice at 100 m from the resistivity survey and the 30 Hz In-Phase TPR data. A strong linear low resistivity (colored blue) is apparent in the data and this has been traced out on both figures. In the 30 Hz In-Phase TPR response, this line corresponds very closely to a ridge of high. In Figure 8, this linear is traced over the geology map with the TMI result repeated as well.

Morrison, British Columbia: The Morrison property lies SW of the Babine Lake property discussed above. Morrison is a large tonnage, low copper-gold grade resource defined by extensive drilling. A second intrusive center called the Hearne Hill that is not significantly mineralized is also covered by the ZTEM survey. Geology and the results of an AeroTEM EM (Rudd and Sterritt 2010) and magnetic survey covering part of the property are available to help assess the ZTEM results. Figure 9 shows the outline of the ZTEM and AeroTEM surveys and the local geology with the Morrison and Hearne Hill intrusives as well as highlighting the major faults. The magnetic results show the two intrusives to be situated in different settings; Morrison is located along a narrow arcuate

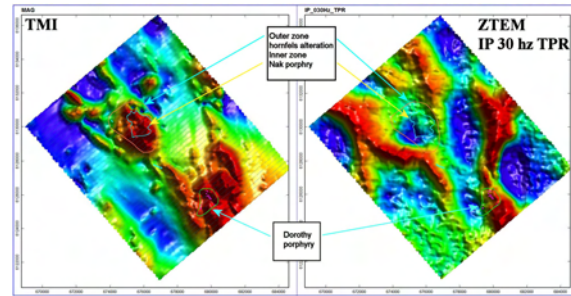


Figure 6: TMI (left) and 30 Hz In-Phase TPR (right) over Babine property.

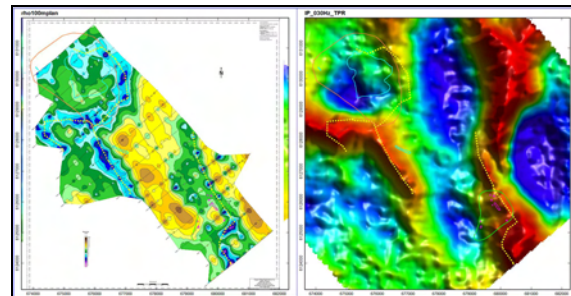


Figure 7: Resistivity 100 m depth slice (left) and 30 Hz In-Phase TPR; axis of resistivity low is highlighted in both images. Note, for the resistivity results, low resistivity values are assigned cooler colors.

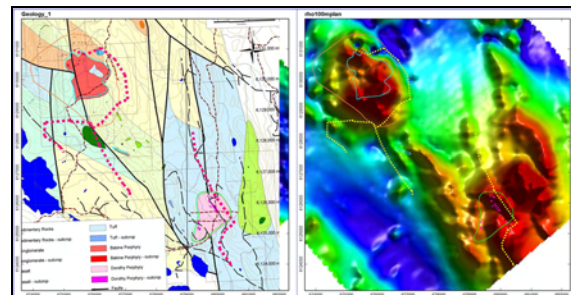


Figure 8: Geology with resistivity linear (left) and TMI showing the resistivity linear.

moderate high whereas Hearne Hill is situated within a much larger magnetic high. The mapped faults are not well expressed in the magnetic results. Figure 10 shows a zoom-in on the area with the intrusives, showing the ZTEM 90 Hz In-Phase TPR result. This result shows that the Morrison intrusive lies centered over a zone of high resistivity (blue area). The Hearne Hill intrusive however, lies over a zone of elevated ZTEM response. This zone also corresponds to a mapped NE-SW trending fault so the ZTEM response is interpreted to be that of a fault system. The geology shows a second shorter fault orientated orthogonally to the NE trending feature directly over the intrusive. The ZTEM does not appear to reflect this structure. The two major structures that trend NW and enclose the Morrison intrusive are not well represented in the ZTEM results. Figure 11 shows the zoomed-in view for 90 Hz for both the TPR and DT results. Figure 12 shows the same components at 360 Hz. This shows that the DT results at both frequencies provides more detail than observed in the TPR outcomes. Some of the DT response looks somewhat 'noisy' but the two linear highs that enclose

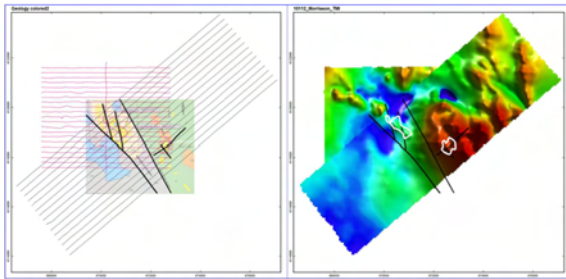


Figure 9: Geology map of Morrison and Hearne Hill intrusives with ZTEM and AeroTEM flight path (left) and merged magnetic image of two airborne surveys (right).

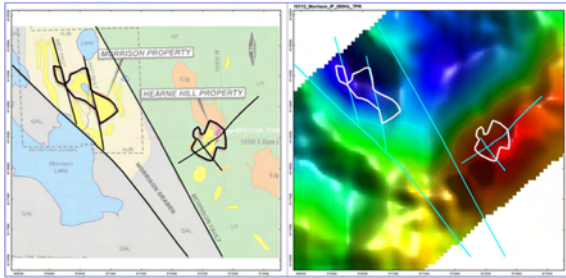


Figure 10: Geology map showing the Morrison and Hearne Hill intrusives (left) with ZTEM 90 Hz In-Phase TPR result (right).

the Morrison intrusive are better defined in the DT results and the feature that the Hearne Hill intrusive is associated with shows the Hearne to be situated within an apparent 'notch' or hole in a circular shaped DT response, whereas the TPR response lacks such detail. Figure 13 shows the AeroTEM Zoff Ch. 1 response and the ZTEM 360 Hz DT. The results show a strong degree of similarity. As with the ZTEM, the AeroTEM results show the Morrison intrusive to be of low response, bracketed by the two NW trending faults. The response of the faults is also similar but the southern-most fault in the AeroTEM appears to define a geological edge as there is an elevated response to the south of the fault whereas the ZTEM seems to show more of the edge itself. The Hearne Hill intrusive appears as being located within a ring-like high in both surveys that also appears to be open on the north side in both cases as well.

CONCLUSIONS

ZTEM results over three known porphyry copper-gold systems have been examined. In each case, the ZTEM results were showing areas of low and high conductivity as well as contacts that were identified independently via geological mapping, drilling or other geophysical surveys. At Pebble, the ZTEM showed good agreement with an overlapping Spectrem survey. While the Spectrem appeared to resolve the shallow conductivity better than ZTEM, the ZTEM appeared to show better correlation with the mineralization at depth. At Babine Lake, the main zone of mineralization termed the Nak intrusive, appears in the ZTEM as discrete resistivity high with similar dimensions to the known intrusive body. A series of linear resistivity lows defined by a resistivity survey correlate with mapped faults and show as well as clear linear highs in the ZTEM outcomes. At the Morrison property, the ZTEM showed the main Morrison intrusive as a resistivity high bounded by two faults. The near-by Herne Hill mineralization showed a quite different character with the

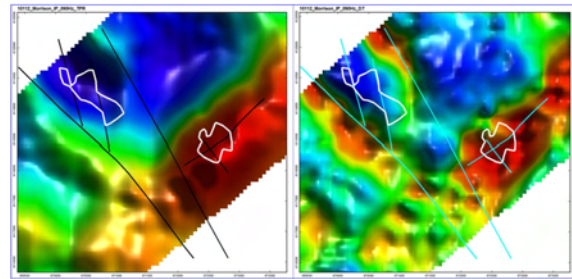


Figure 11: Zoom-in showing 90 Hz TRP (left) and DT (left) outcomes.

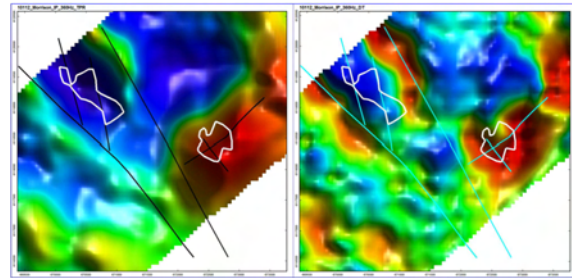


Figure 12: Zoom-in showing 360 Hz TRP (left) and DT (right) outcomes.

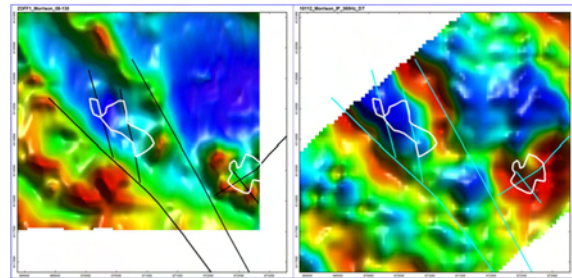


Figure 13: AeroTEM Zoff Ch. 1 (left) and ZTEM 360 Hz DT (right).

intrusive core being encircled by a ring of elevated ZTEM response. The results of an AeroTEM survey were available for part of the ZTEM block and showed quite similar character to the ZTEM outcomes.

ACKNOWLEDGMENTS

We thank Anglo American Exploration Canada, Pebble Limited Partnership, Red Tail Metals and Geotech Ltd. for providing data shown in this study.

REFERENCES

- Paré, P., and J. M. Legault, 2010, Ground IP-resistivity, airborne spectrum and helicopter ZTEM survey results over Pebble copper-moly-gold porphyry deposit, Alaska: 80th Annual International Meeting, SEG, Expanded Abstracts, 1734-1738.
- Rudd, J and Sterritt, V. Report on a Helicopter-Borne Magnetic and Electromagnetic Survey, Quest West, BC, by Aeroquest Surveys, January 2009 produced for Geoscience BC. Quest-West Project 2009.
- Sattel, D., Witherly, K., and Becken M., 2010, A brief analysis of ZTEM data from the Forrestania test site, WA: 21st International Geophysical Conference and Exhibition, ASEG, Extended Abstracts.
- Sattel, D. and Witherly, K., 2012 Extracting information from ZTEM data with 2D inversions; submitted for inclusion in 22nd International Geophysical Conference and Exhibition, ASEG, Extended Abstracts.

3D mega-cell inversion of land, marine, and airborne natural field EM data

Michael S. Zhdanov ¹, Alexander V. Gribenko ², Martin Čuma ³ and Glenn A. Wilson ⁴

¹ *University of Utah & TechnoImaging (mzhdanov@mines.utah.edu)*

² *University of Utah & TechnoImaging (alex@technoimaging.com)*

³ *University of Utah & TechnoImaging (martin@technoimaging.com)*

⁴ *TechnoImaging (glenn@technoimaging.com)*

Introduction

Natural field electromagnetic (EM) methods use plane wave EM fields that diffuse into the Earth, generating predominantly horizontal current flow. These methods came into use during the 1960's, following the theoretical basis proposed by Andrei N. Tikhonov (1950) in the USSR, Louis Cagniard (1953) in France, and Tsuneji Rikitake (1950) in Japan. Yet, knowledge of telluric currents is far from recent. As early as 1868, Sir George Biddell Airy made the first coordinated study of telluric currents and their relationship to magnetic variations (Airy, 1868). In 1862, one of the first experiments to measure telluric currents was carried out by Lamont (1862) in the Alps. Terada (1917) appears to have been the first to measure the dependence of the magnetic field relationships on the conductivity of the ground. The Schlumberger brothers also documented observing telluric currents during their experiments with DC measurements. They were the first to suggest that telluric currents could be used for oil and gas exploration. However, practical measurements showed significant variations and instability in telluric current behaviour, which made it difficult to develop any reasonable interpretation methods. The main sources of this instability were associated with complex processes in the ionosphere and magnetosphere, which were unknown at the time.

The primary discovery made independently by Tikhonov and Cagniard was that the effect of ionospheric and magnetospheric processes could be cancelled if the electric and magnetic field components of the telluric currents were normalized as a surface impedance. At the time, this was a revolutionary idea because it enabled geophysicists to transform measured data into estimates of the Earth's resistivity. As early as 1934, Hirayama found the explicit form for the surface impedance of a plane wave (Hirayama, 1934), and Hatakeyama (1938) even used tensor conductivities to explain differences in principle impedances. However, Tikhonov and Cagniard should be credited with creating the solid geophysical foundation upon which the magnetotelluric (MT) method was later developed for imaging the Earth's conductivity over the past 60 years. In the former Soviet Union, MT methods were the primary methods used for oil and gas exploration during the 1960's and 1970's, and can be attributed with the discovery of many of the giant Siberian oil and gas fields that remain in production to this day. Originally, the MT data were interpreted using a catalogue of 1D Earth models. This made it easy to provide MT sounding curves as plots of apparent resistivity versus the period or the square root of the period (which is proportional to skin depth). Since the world is 3D, distortions in the MT soundings were later falsely interpreted for oil and gas reservoirs. The development of 2D and 3D modelling in the 1980's and 1990's, and 2D and 3D inversion in the 1990's and 2000's has expanded the opportunities for MT and other natural field EM methods in exploration. We are now able to invert various forms of natural field EM data for mega-cell 3D Earth models, and this paper will review recent examples by the authors for land, marine and airborne surveys.

Magnetotellurics

In the following example, we review a classic application of MT methods for continental-scale imaging, and how 3D inversion of MT and magnetovariational (MV) data has revised thinking toward some Earth processes. First, we need to introduce EarthScope, which is a US National Science Foundation program intended to explore the structure and evolution of the North American continent, and to further understand the processes controlling earthquakes and volcanoes. A major part of the EarthScope project is the USArray of seismic, MT, and geodetic instruments that are being deployed over the current decade across the entire continental US. This transportable array of geophysical

instruments provides an unparalleled means to study the crust and mantle geology of the US through seismology and MT data. EMScope is the MT component of the USArray program, and is managed by Oregon State University on behalf of Incorporated Research Institutions for Seismology (IRIS). EMScope comprises long-period MT measurements at hundreds of sites, in addition to a number of long-period backbone MT stations. By mid-2011, MT data had been collected throughout Washington, Oregon, Idaho, Wyoming, Montana, and northern California, Nevada, Utah and Colorado.

In the example we present here (Figure 1), we focus our attention on the MT data acquired in Montana, Idaho, and Wyoming. The unique geological setting of the western US, including plate boundary transform faulting, subduction, intraplate extension of the Basin Range, and the active Yellowstone hotspot, is very important, both for its geodynamic history, and for understanding the physical processes of earthquakes and volcanoes. It is a tectonically active region, with the subducting Juan de Fuca plate and volcanically important from the effects of the Juan de Fuca and Gorda plates moving over a mantle plume currently located beneath Yellowstone National Park (YNP). For such a complex region, definitive structural interpretations based purely on seismological observations are not complete. Conductivity has a significant role in determining tectonic activities, primarily because it is sensitive to temperature, the presence of interstitial fluids, melts, volatiles, and bulk composition.

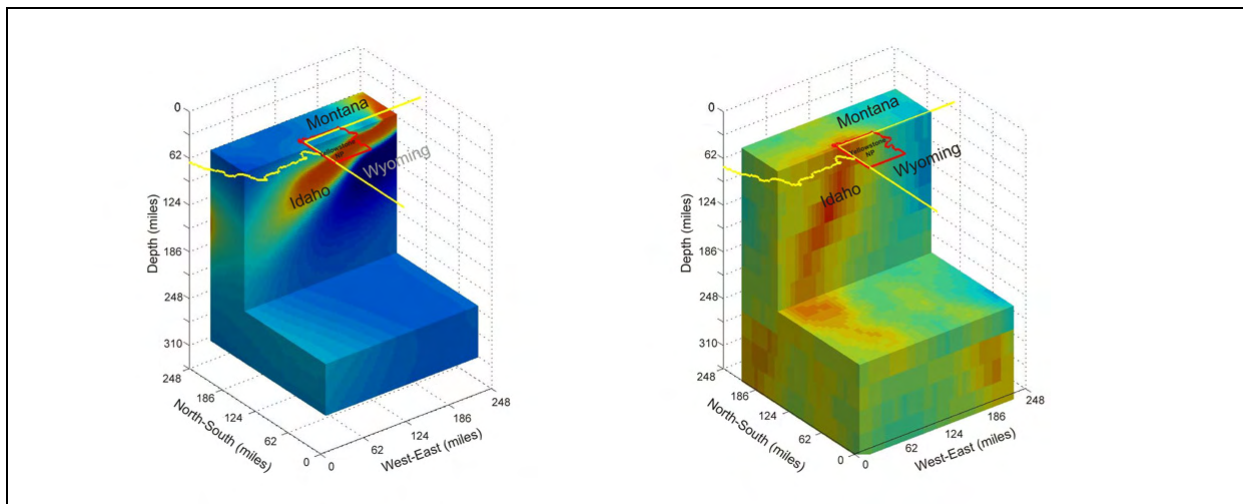


Figure 1. (left) 3D conductivity model obtained from 3D MT inversion over the Yellowstone hotspot area. (right) P-wave velocity model obtained from seismic tomography, presenting a rising column of partly molten rock originating in the mantle transition zone.

We refer the reader to Zhdanov et al. (2011a) for further details of the 3D MT inversion and a detailed discussion of its interpretation. The 3D Earth model itself was discretized to more 1.9 million cells. Here, we present a comparison of the 3D MT inversion over Yellowstone National Park (YNP) with a 3D p-wave velocity model (Figure 1). One can observe remarkable similarity between the images of the Yellowstone plume that were independently produced by seismic tomography and 3D MT inversion. The conductive body identified in the conductivity image is west dipping in a similar way to the low velocity body shown in the p-wave velocity image. Taking into account the different physical properties, one should not expect these images would coincide completely. Recent seismic studies have suggested relatively high attenuation in mantle, and this has been interpreted as a partially molten plume in which water is partitioned into the melt, and surrounded by a cooler and wetter mantle. The attenuation decrease at 200-250 km is considered as evidence that the plume is melting above this depth, and this corresponds well to the area of high conductivity in Figure 1.

Marine Magnetotellurics

In offshore hydrocarbon exploration, seismic reflection can provide detailed images of the top of salt, sedimentary layers, and basement formations. Yet, even with the introduction of wide azimuth towed streamer (WATS) and extra wide azimuth towed streamer (XWATS) seismic, common problems associated with subsalt seismic imaging include multiple reflections and mode conversions, loss of reflected energy from steeply dipping salt surfaces, and the lack of coherent features beneath salt structures. As discussed by Constable (2010), marine MT was experimented with in the 1990's for

deepwater and subsalt exploration, particularly in the Gulf of Mexico, where high costs of drilling justified the expenditure. During the 2000's, interest in marine MT was displaced by marine controlled-source EM (CSEM), even though the same receiver instruments were/are used.

In the example we present here, we focus our attention on marine MT data acquired over the Gemini prospect in the Gulf of Mexico. Located in 1 km of water approximately 200 km southeast of New Orleans, Gemini contains a salt body associated with a roho system that forced out salt both basinward and laterally, resulting in a complex 3D salt geometry. 3D seismic reflection data indicated that the salt resides between 1 and 5 km beneath the seafloor, although the deepest portions of the salt are not well resolved due to lower fidelity of the seismic data with depth. Ambiguity exists whether the Gemini salt body is still rooted to the deeper Louann salt layer, or merely bottoms out at a depth of 5 to 6 km. MT surveys were conducted in several cruises during 1997, 1998, 2001, and 2003, resulting in a grid of 42 marine MT sites (e.g., Constable et al., 1998; Key et al., 2006).

We refer the reader to Zhdanov et al. (2011b) for further details of the 3D MT inversion and a detailed discussion of its interpretation. The 3D Earth model itself was discretized into more than 1.6 million cells. Here, we present a comparison of 2D and 3D MT inversion from line H (Figure 2). The white contour in Figure 2 indicates the position of the salt dome estimated on the basis of seismic reflection data. We note, however, that the seismic outline of the salt dome shown in Figure 2 can be used only for a qualitative comparison because it depends on a selection of the seismic velocity model which could not be done objectively in this area. We observe also that the resistivity of salt recovered by 3D inversion is about 10 Ωm . Similar results were obtained by Hoversten et al. (2000), who justified this result because the “MT response saturates as the resistivity of a body becomes greater than 10–20 times that of the background. In the GOM [Gulf of Mexico], bulk salt resistivity values are more than 20 times the background sediment resistivity values and, for the skin depths of interest, the MT response is totally governed by the distortion of electric currents in the sediments around the resistive salt.” The saturation of the MT response for resistive layers is well known by MT practitioners. It is easy to demonstrate, for example, that for a 1 km thick resistive layer buried 1 km deep in 1 Ωm sediments (somewhat similar to the Gemini salt), the difference between 10 and 100 Ωm resistivity values for the layer yields no appreciable differences in the MT response; hence the response has become saturated. The difficulty to resolve thin salt at a 4 km depth logically follows from this as well.

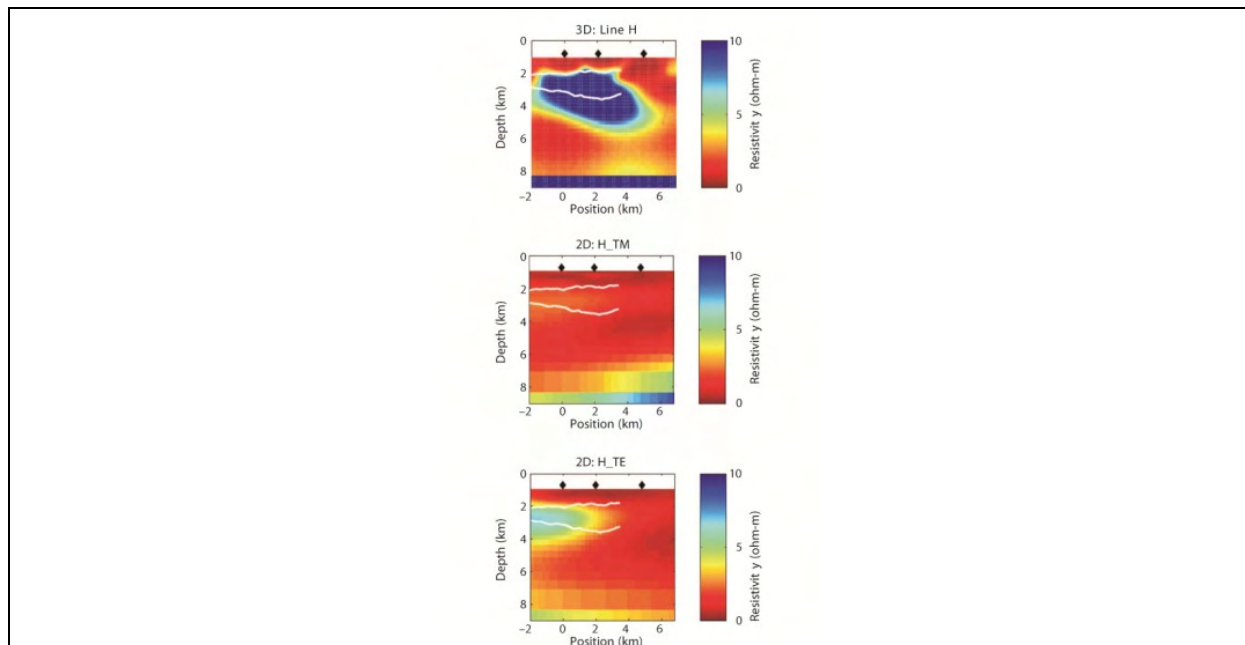


Figure 2. A comparison along line H from the marine MT survey of the Gemini prospect with the results obtained from 2D and 3D inversions. The top part shows the results of full 3D inversion, the middle part presents the result of 2D inversion of the TM-mode data, and the bottom part shows a similar result of 2D inversion of the TE-mode data obtained by Key et al. (2006). The white contour indicates the position of the salt dome estimated on the basis of seismic reflection data.

Audio-frequency magnetics (AFMAG)

It has long been recognized that magnetovariational (MV) data, being the ratio of the localized vertical magnetic field to the orthogonal horizontal magnetic fields, can provide information about the 3D conductivity distribution in the Earth (e.g., Berdichevsky and Zhdanov, 1984). The basic reasoning is that the vertical magnetic field is zero for plane waves vertically propagating into a 1D Earth. Non-zero vertical magnetic fields are thus directly related to 2D or 3D structures. This served as the basis for the original development of the audio-frequency magnetic (AFMAG) method (Ward, 1959) whereby two orthogonal coils were towed behind an airborne platform to determine the tilt angle of the plane of polarization of natural magnetic fields. The natural magnetic fields of interest originate from atmospheric thunderstorm activity and propagate over large distances with little attenuation in the Earth-ionosphere waveguide. These fields propagate vertically into the Earth as per MT fields. The tilt angle is zero over a 1D Earth, and hence the AFMAG method was effective when crossing conductors. However, the direction and amplitude of the natural magnetic fields randomly varies with time, meaning AFMAG data were not repeatable (Ward et al., 1966). By using MT processing techniques for ground-based orthogonal horizontal magnetic field measurement, Labson et al. (1985) demonstrated that repeatable tipper data could be recovered from measured magnetic fields.

The AFMAG method remained largely undeveloped until the commercialization of the Z-axis Tipper Electromagnetic (ZTEM) airborne system by Geotech. ZTEM measures the tipper components as the ratio of a vertical magnetic field measured from an airborne receiver to the horizontal components measured at a ground-based (reference) location. Similar to the ratio of electric to magnetic fields in MT data, the ratio of the magnetic fields effectively removes otherwise unknown source terms. The receiver coil is currently flown via helicopter or fixed-wing platform, meaning data can be rapidly acquired over large survey areas for relatively low cost compared to equivalent ground surveys. The time series of the magnetic fields are recorded at fixed sampling rates and the data are binned and processed to generate in-phase and quadrature transfer functions (i.e., tippers) in the frequency-domain as per Labson et al. (1985). The lowest frequency of the tipper depends on the speed of the aircraft, and the highest frequency depends on the sampling rate. Tippers are typically obtained at five frequencies from 30 Hz to 360 Hz, giving skin depths ranging between 600 m and 2000 m for terrain conductivities typically encountered in ZTEM surveys. Holtham and Oldenburg (2010) introduced 3D ZTEM inversion based on modifications of the 3D MT inversion of Farquharson et al. (2002). Similarly, our 3D ZTEM inversion is an analogue of the 3D MT inversion by Zhdanov et al. (2011a). One key difference between our 3D ZTEM inversion and that of Holtham and Oldenburg (2010) is that we employ a footprint approach for each receiver (e.g., Cox et al., 2010). This permits us to efficiently compute, store and manipulate the sensitivities for very large surveys. We also utilize focusing regularization (Zhdanov, 2002) which enables us to recover higher contrasts and sharper conductivity boundaries than with smooth regularization.

In the following example, we review a case study from the Pebble porphyry deposit where we compared 3D inversions of both ZTEM and SPECTREM airborne electromagnetic data (Pare et al., 2012). By way of introduction, Pebble is a calc-alkalic Cu-Au-Mo porphyry deposit located in the Bristol Bay region of southwest Alaska, approximately 320 km southwest of Anchorage and 27 km west-northwest of the village of Iliamna. Development of the Pebble Cu-Au-Mo mine is managed by Pebble Limited Partnership (PLP), a joint venture between Northern Dynasty Mines Ltd (50%) and Anglo American plc (50%). Since discovery in 1988, over 886,177 feet of drilling in 1,085 holes have been completed, making Pebble one of the most intensively studied, undeveloped mineral systems in the world. At a 0.30% Cu equivalent cut-off, the latest Pebble resource estimate includes 5.942 billion tonnes in the measured and indicated category containing 25.0 million tonnes of copper, 66.9 million ounces of gold and 1.5 million tonnes molybdenum; and 4.835 billion tonnes in the inferred category, containing 11.6 million tonnes of copper, 40.4 million ounces of gold and 1.0 million tonnes of molybdenum. This resource base makes Pebble the largest gold and sixth largest copper deposit in the world.

We inverted 250 line km of ZTEM data acquired at 200 m flight-line spacing along strike of the Pebble deposit. This corresponded to 5,472 stations with both Z/X (inline) and Z/Y (transverse) tipper components at five frequencies; 30 Hz, 45 Hz, 90 Hz, 180 Hz, and 360 Hz. The 3D Earth model was discretized into approximately 570,000 cells of 50 m inline by 50 m transverse discretization, where the vertical cell size varied from 10 m near the surface to 100 m at 2,000 m depth. The 3D inversion settings and constraints were assigned their default values (i.e., no specific geological constraints nor *a priori* geological information were provided). The depth of investigation for ZTEM was about

1,500 m below the surface. The 3D ZTEM inversion has recovered Pebble's main alteration pattern and the known structures ZF, ZC, ZE and ZG1. Generally speaking, the 3D ZTEM inversion recovered the geological features and structures with better accuracy than the 2D inversions of the same data. As expected, the 3D inversion with focusing regularization produced sharper contrasts and better lateral model continuity from line to line than the 2D inversions with smooth regularization.

Studying the 3D ZTEM inversion for lines L10060 highlights the following correlations (which we note are very similar to those observed in the 3D SPECTREM inversion):

- The highly conductive zones to the known illite-pyrite and advanced argillic alteration parts of the system (Figure 3);
- The weak conductive zone and resistive high beneath the Pebble West and East zones are characterized by sodic-potassic, K-silicate and deep sodic-calcic domains;
- The high conductive zone on line L10120 above the Pebble East zone and confined between the ZE and ZG1 faults is associated with the advanced argillic alteration that overprints the highest grades (Figure 3);
- The moderately conductive layer near the surface above the Pebble East zone and to the east appears to be related with the Tertiary cover;
- The main known structures (ZF, ZC, ZE and ZG1) are well resolved, and correlate with the breaking pattern of the 3D conductivity model; especially the ZG1 fault to the east of Pebble East.

It is interesting that a conductive zone is present at depth to the east of the ZG1 fault on line L10120. This feature is being investigated further and if real, could potentially be a deep extension of Pebble East. The geometry of the 3D ZTEM inversion also follows the general trend of the alteration and ore geometry. Similar to 3D SPECTREM inversion, the mineralization is not in direct correlation with the conductive zones resolved by the 3D inversions. The conductive zones are mostly coincident with alteration change. The high grade copper equivalent (CuEq) 0.6% is not consistently following the high conductive trend. As per the 3D SPECTREM inversion, this suggests that the sulphide content is not a major factor in the ZTEM response.

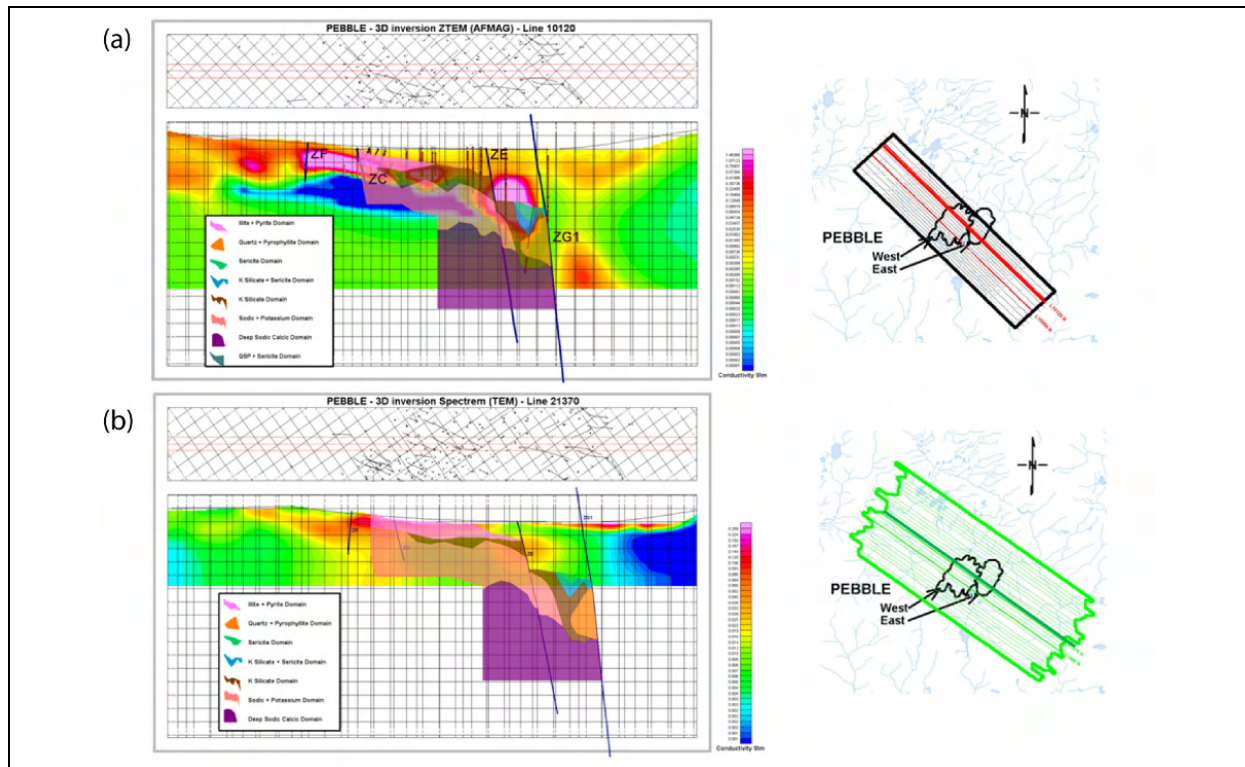


Figure 3. Comparison of (a) 3D ZTEM inversion for ZTEM line L10120 and (b) 3D SPECTREM inversion for SPECTREM line L21370, with alteration patterns superimposed.

Conclusions

Over the past decade, 3D modelling and inversion of natural source EM data has evolved so that we are now able to invert various forms of natural source EM data from land, marine and airborne systems for 3D Earth models from deposit to regional scales that can have millions of cells (i.e., mega-cell 3D models). We have provided examples from EarthScope MT data in the western US for understanding continental-scale structures, marine MT data in the Gulf of Mexico for subsalt oil and gas exploration, and ZTEM data over the Pebble Cu-Au-Mo porphyry deposit in Alaska. These examples demonstrate the variety of natural field EM methods, and 3D inversion thereof. However, given the inherent low resolution of natural field EM data, it lends itself to joint inversion with other geophysical data (e.g., gravity, gravity gradiometry, magnetics, and reflection seismic) and this is a subject of our on-going research.

Acknowledgements

The authors acknowledge TechnoImaging for support of this research and permission to publish.

Zhdanov, Gribenko, and Cuma acknowledge support of the University of Utah's Consortium for Electromagnetic Modeling and Inversion (CEMI) and Center for High Performance Computing (CHPC).

We acknowledge Professor Bob Smith at the University of Utah for his involvement in the analysis of the Yellowstone MT and seismic Earth models.

The Gemini MT results are included with permission and thanks to the Scripps Institute of Oceanography's Marine EM Laboratory. Particularly, we acknowledge Dr. Kerry Key and Professor Steve Constable for their involvement in the work presented.

The Pebble ZTEM results are included with permission and thanks to Pebble Partnership Ltd, Anglo American Exploration (Canada) Ltd, Northern Dynasty Mines Ltd, Spectrem Air Ltd, Geotech Ltd, and TechnoImaging LLC. Particularly, we acknowledge Pascal Pare, Jean Legault, Jaco Smit and Louis Polomé for their involvement in the work presented.

References

- Airy, G. B., 1868, Comparison of magnetic disturbances recorded by the self-registering magnetometers at the Royal Observatory, Greenwich, with magnetic disturbances deduced from the corresponding terrestrial galvanic currents recorded by the self-registering galvanometers of the Royal Observatory: *Philosophical Transactions of the Royal Society of London*, 158, 465-472.
- Berdichevsky, M. N., and Zhdanov, M. S., 1984, *Advanced Theory of Deep Geomagnetic Sounding*: Elsevier, Amsterdam.
- Cagniard, L., 1953, Basic theory of the magneto-telluric method of geophysical prospecting: *Geophysics*, 18, 605-635.
- Constable, S., 2010, Ten years of marine CSEM for hydrocarbon exploration: *Geophysics*, 75, 75A67-75A81.
- Constable, S. C., Orange, A. S., Hoversten, G. M., and Morrison, H. F., 1998, Marine magnetotellurics for petroleum exploration: Part 1—A sea-floor equipment system: *Geophysics*, 63, 816–825.
- Cox, L. H., Wilson, G. A., and Zhdanov, M. S., 2010, 3D inversion of airborne electromagnetic data using a moving footprint: *Exploration Geophysics*, 41, 250-259.

SUMMARY REPORT ON HELICOPTER-BORNE
ZTEM TIPPER AFMAG SURVEY RESULTS

over
MT-MILLIGAN TEST BLOCK, January 2009
Mackenzie Region, British Columbia
on behalf of
GEOSCIENCE BC and TERRANE METALS CORP.

1 Introduction

ZTEM (Z-Tipper Axis Electromagnetic) surveys were conducted over the Mt-Milligan Test Block, belonging to Terrane Metals Corp. (Vancouver, BC) and situated in the Mackenzie region of central British-Columbia, from October 15TH to 22ND, 2008, on behalf of Geoscience BC. The ZTEM survey comprised airborne Tipper AFMAG (audio frequency electromagnetics) measurements, as well as aeromagnetics using a caesium magnetometer. The survey consisted of twenty five (25) approx. 8.0 km long, EW oriented flight lines, totaling 200 line-km, that were obtained at nominal 250m line spacings over an approximately 6 x 8 km area (Figure 1). The area was chosen because it hosts the Mt Milligan copper-gold porphyry deposit, containing a Measured and Indicated Mineral Resource of 590.8 Mt at 0.193% Cu and 0.352 g/t Au, totaling 2.52 billion lb copper and 6.70 million oz gold (Terrane Metals Corp. 2008), that is not yet in production, and also because area's geology is well known and available in the public domain - making it an ideal case-history example.



Figure 1: ZTEM Hz Receiver Coil (foreground) and Hx-Hy Reference Coils (background)

The Z-axis tipper measurements of the vertical (Z) component were obtained using Geotech's patented ZTEM induction aircoil system (Figure 2), suspended at approximately 110m elevation above ground level. The vertical component data (Hz) were then ratioed to fixed horizontal field measurements (Hx-Hy) obtained using identical reference coils, that were oriented in the in-line (X) and cross-line (Y) directions, in order to obtain the tipper functions Z/X and Z/Y. The In-Phase

and Quadrature components ZTEM field ratio data were obtained, using Fourier-based, digital signal processing analyses, at 5 frequencies, between 30Hz and 360Hz. The magnetometer was a Geometrics proton-precession model towed at 130m above ground level.

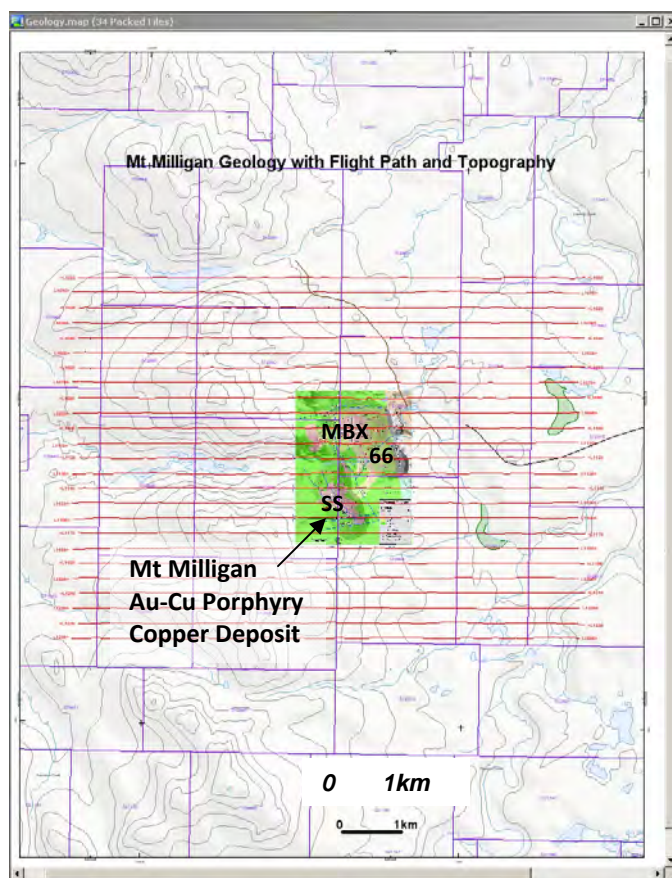


Figure 2: Mt Milligan Test Block ZTEM Flight Lines and Deposit Geology (after Terrane Metals, 2008)

1.1 General Theory

The ZTEM system uses naturally occurring Afmag magnetotelluric fields as the source of the primary fields, and therefore requires no transmitter (Ward, 1959). The fields resemble those from VLF except that they are lower frequency (tens & hundreds of Hz versus tens of kHz) and are not strongly directionally polarized (Labson et al., 1985). These AFMAG EM fields, derived from world wide atmospheric thunderstorm activity, have the unique characteristic of being uniform, planar and horizontal, and also propagate vertically into the earth – to great depth, up to several km, as determined by the magnetotelluric (MT) skin depth, which is directly proportional to the ratio of the bedrock resistivity to the frequency. At the frequencies used for ZTEM, the MT skin depths range between 600m to 2km, assuming a background resistivity of 1k ohm-metres in this region, according to the following equation for skin depth (Vozoff, 1972):

$$\delta_s = 356 * \sqrt{\rho_A / f} \text{ metres}$$

if $\rho_A = 1\text{k ohm-m}$, $\delta_s \approx 600\text{m}$ at 360Hz and $\sim 2.0\text{km}$ at 30Hz

The other unique aspect of AFMAG fields is that they react to relative contrasts in the resistivity, and therefore do not depend on the absolute conductance, as measured using inductive EM systems, such as VTEM – hence poorly conductive targets, such as alteration zones and fault zones, can be mapped, as well as higher conductance features, like graphitic units. Conversely, resistive targets can also be mapped using AFMAG– provided they are of a sufficient size and contrast to produce a vertical field anomaly. Indeed resistors produce reversed anomalies relative to conductive features. An example of a ZTEM 2D forward model profile response over a conductive body is given in Figure 3.

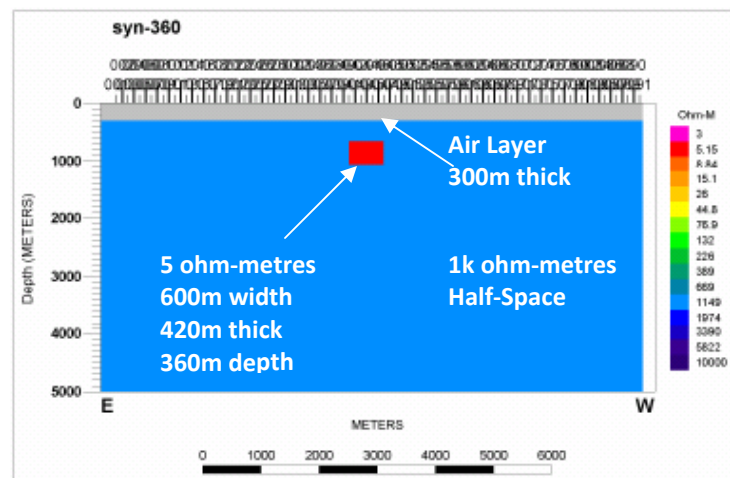


Figure 1. Above: Conductive brick used in test inversion for ZTEM data using ZVERT2D. The gray region is a 300 m thick air layer. Below: Synthetic data and inversion model responses at five frequencies for Z/X response profile along the ground (solid curves) and 300 m in the air (dashed curves). Small open squares are the inversion fits.

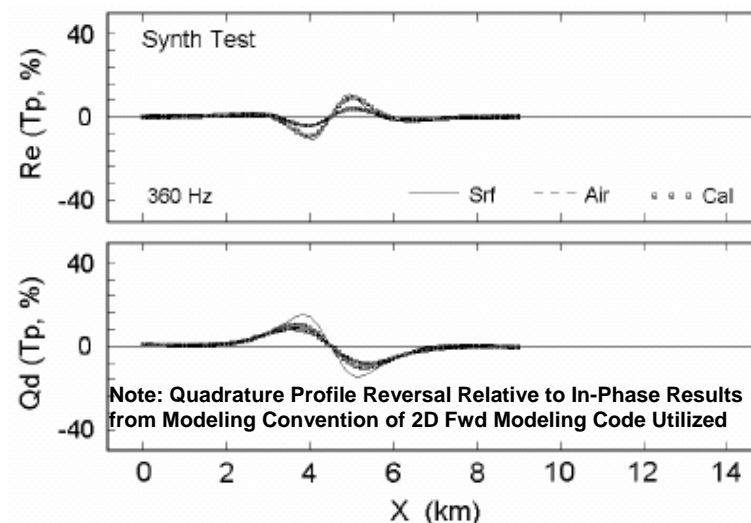


Figure 3: Calculated 2D Forward Model Response for In-Line (Z/X) In-Phase and QP Components over Buried Conductor in Resistive Half Space at 300m Elevation (Ref. Wannamaker, 2008).

1.2 General Geology

The Mt. Milligan project is within the Quesnel Terrane, a Late Triassic to Early Jurassic magmatic arc complex (Terrane Minerals Corp., 2008). The Quesnellia rocks consist of Triassic to Lower Jurassic volcanic and minor sedimentary rocks of Takla Group. The Takla Group in the Mt. Milligan area is mainly comprised of an upper, predominantly volcanoclastic Witch Lake Succession with hosts the Mt. Milligan deposits. The Witch Lake rocks are characterized by volcanoclastic and basaltic andesites that are intruded by coeval Takla Group and younger intrusions. Coeval intrusions comprise most of the Mt. Milligan intrusive complex, which consists dominantly of monzonitic rocks – including the MBX, Southern Star, Goldmark and North Slope stocks, all which host mineralization at Mt. Milligan (see Figure 4).

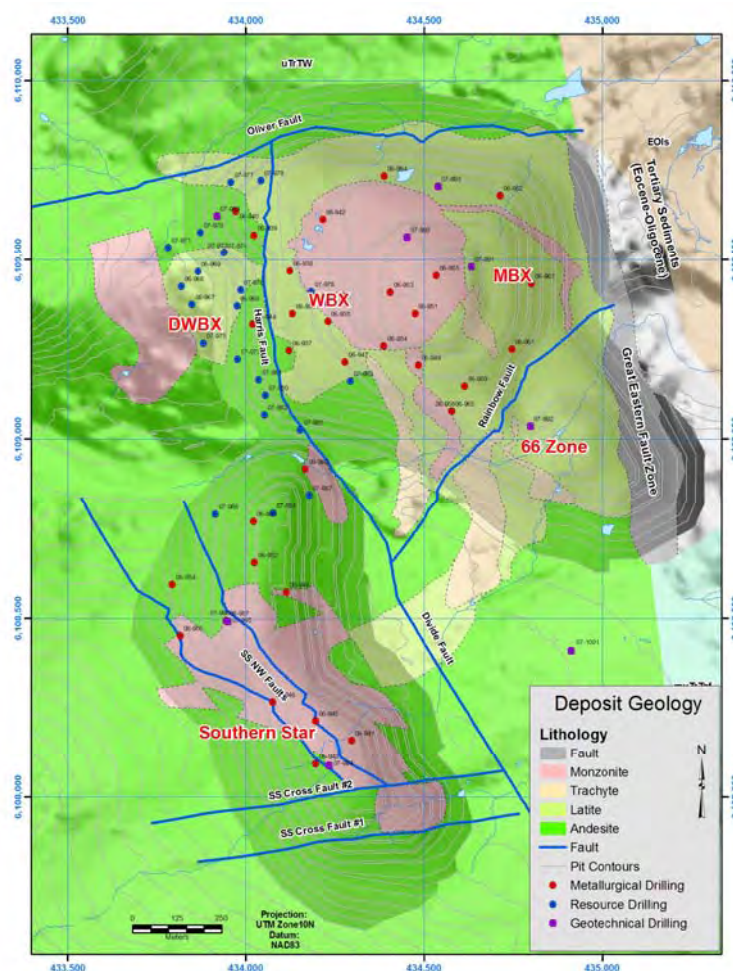


Figure 4: Mt Milligan Geology and Mineralized Zones (Ref. Terrane Metals Corp., 2008)

Mt. Milligan is a tabular, near-surface, alkalic copper-gold porphyry deposit that measures some 2500 metres (m) north-south, 1500 m east-west and is 400 m thick (Terrane Minerals Corp., 2008). It consists of two principal zones, the Main Zone and Southern Star (SS) Zone. The Main Zone

includes four contiguous sub-zones: MBX, WBX, DWBX and 66, all of which are spatially associated with the MBX monzonite stock and Rainbow Dyke (Figures 4-5). The SS Zone is centred on a monzonite stock of the same name and is some 500 m south of the Main Zone.

Main Zone mineralization and associated alteration are primarily hosted in volcanic rocks, whereas in the SS Zone, mineralization is hosted equally in monzonite stock and volcanic rocks. Mineralization in both zones consists of pyrite, chalcopyrite and magnetite with bornite localized along intrusive-volcanic contacts. The pyritic 66 sub-zone is notable in that it is comparatively gold-rich and copper-poor.

Copper-gold mineralization is primarily associated with potassic alteration with both copper grade and alteration intensity decreasing outwards from the monzonite stocks. Pyrite content increases dramatically outward from the stocks where it occurs in association with propylitic alteration, which forms a halo around the potassic-altered rocks. In terms of alteration, Mt Milligan features a poorly developed supergene blanket over the deposit with limited supergene enrichment. Potassic alteration is widespread and occurs principally as massive K-feldspar and biotite replacement of fine-grained matrix in porphyritic tuffs and flows. A phase of propylitic alteration consisting of epidote- calcite+/-pyrite-albite-chlorite in part overprints the potassic alteration.

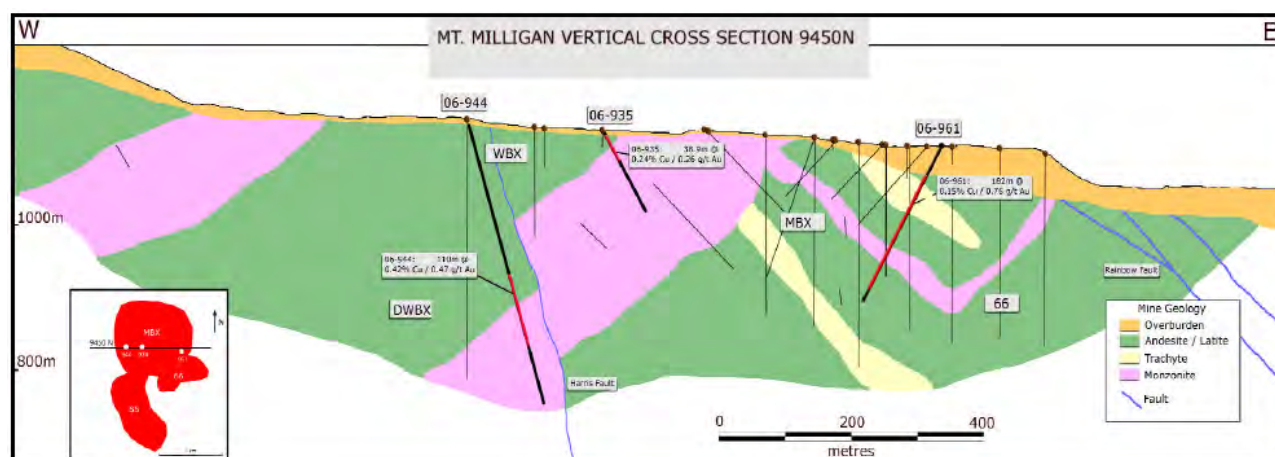


Figure 5: Cross-Section Across MBX Stock at Mt Milligan (Ref. Terrane Metals Corp., 2008)

In terms of structure, At least four episodes of faulting have effected the area, the earliest being the shallow east-dipping Rainbow Fault. Important east-northeasterly trending cross-faults and northwesterly trending, steeply easterly dipping faults separate the MBX stock from the Southern Star stock. The regional Great Eastern Fault truncates mineralization to the east and juxtaposes Takla Group volcanic rocks against Early Tertiary rocks (see Figure 4).

The Main Zone at Mt. Milligan consists of a number of zones partly within and adjacent to the west-dipping MBX stock (Figure 4). The MBX Zone is the most important Cu-Au zone and is situated along the footwall of the stock and along the Rainbow Dyke (Figure 4). The WBX Zone is a

Cu-Au deposit situated along the western hanging wall of the MBX stock. A down-faulted extension to this zone, the DWBX has been displaced vertically along the Harris Fault. To the south, the 66 Zone is essentially gold-only, with a boundary marked by Cu-Au zonation. Mineralization in the Southern Star deposit is hosted in the Southern Star stock. Mineralization extends from the eastern contact of the MBX stock to the Great Eastern Fault.

Mineralization consists of chalcopyrite and lesser bornite and magnetite in areas of potassic alteration, and pyrite in areas of propylitic alteration. Mineralization is best developed in areas of potassic alteration in the footwall. The highest copper-gold grades are related to chalcopyrite adjacent to the MBX and Southern Star stocks. The highest gold grades are in the 66 Zone and are associated with abundant pyrite. Pyrite occurs as disseminations and veinlets, up to 10 to 20%.

1.3 Previous Geophysics

Previous geophysics on the property has included IP surveys which outline primarily the pyritic haloes surrounding the intrusions and mineralized zones. Ground magnetic surveys indicate that the MBX and Southern Star stocks are positive magnetic anomalies, although the MBX stock is within an area strongly influenced by the highly magnetic Mt. Milligan Intrusive Complex to the north. Previously, airborne survey covering the area north and west of the deposit area have included magnetics and VLF-EM. The EM data exhibited a pattern very similar to the IP ground surveys (Terrane Metals Corp., 2008). More recently, VTEM survey were completed in 2007 by Geotech for Geoscience BC as part of the QUEST project

2 Data Presentation

The nature of the AFMAG fields is such that, as with VLF, buried, tabular conductors and resistors produce cross-over responses (see Fig. 3). As such, although the field results are shown as cross-over profiles, additional post-processing is applied to convert these cross-over's into peak responses, to make them more useful as mapping tools. These include 2 types: the 90-degree Phase Rotation (Lo, et. al, 2008) which is a Geosoft-based FFT process applied to the grid data, and the Total Divergence (DT) which is a summative, horizontal derivative process method (Kuzmin, et al., 2005) - both of these have been used in this test case.

The ZTEM field results are presented as plan-view profiles of:

- a) In-Phase Z/X component, multi-frequency (30-360Hz) profiles over the mid-frequency (90Hz) Phase Rotated (PR) In-Phase Z/X component grid (see Fig. 6a)
- b) In-Phase Z/Y component, multi-frequency (30-360Hz) profiles over the mid-frequency (90Hz) Phase Rotated In-Phase Z/Y component grid (see Fig. 6b).
- c) Quadrature Z/X component, multi-frequency (30-360Hz) profiles over the mid-frequency (90Hz) Phase Rotated Quadrature Z/X component grid
- d) Quadrature Z/Y component, multi-frequency (30-360Hz) profiles over the mid-frequency (90Hz) Phase Rotated Quadrature Z/Y component grid

The ZTEM processed results are presented as plan-view grids of:

- a) In-Phase DT (see Fig. 8) and Quadrature DT grid contour at 90Hz
- b) In-Phase Resulting Phase-Rotated (RPR) grid (Fig. 7) and Quadrature PR contour at 90Hz
- c) 3D View of the multi-frequency In-Phase DT (45-90-180-360Hz) grid contours, plotted at equivalent skin depth (600 to 2000m depth – assuming 1k ohm-m half-space) with DEM model at surface (Fig. 10).
- d) 3D View of the multi-frequency In-Phase Resulting Phase-Rotated (RPR) Grid (45-90-180-360Hz) grid contours, plotted at equivalent skin depth (~600 to ~1700m depth – assuming 1k ohm-m half-space) with DEM model at surface.

In addition to the ZTEM results, the following Magnetic maps are presented as plan-view grids:

- e) Total Magnetic Intensity (TMI) grid contour.
- f) First Vertical Derivative (Gradient) grid contour (Fig. 9b).

3 Data Analysis

The Mt Milligan area ZTEM results, in particular, showcase the generally high level of data quality, in terms of signal/noise and well defined anomaly resolution. Particularly given the fact that a) the data were obtained in mid-late October, and therefore not at the peak season of sferic activity – hence at best moderate natural field levels expected; and b) the data were obtained using aircraft flying at ~100km/hr, approximately 100m above ground level – hence without significant stacking or additional processing applied.

3.1 Plan view Results

The two In-Phase Tipper profile data (Z/X = In-line – Z/Y = Cross-line) with corresponding 90-degree Phase-Rotated (PR) grids are presented for the 90 Hz frequency, in Figure 6, for comparison purposes. The outline of the Mount Milligan MBX, 66 and SS porphyry deposits are also shown.

There are distinctive differences observed between the Z/X (In-Line) component profile results (Figure 6a), which are most sensitive to structures orientated perpendicular to the In-Line direction- notably the 1-2 major NS structures defined east of the Mt-Milligan porphyry copper deposits, which appear correspond to the known Great Eastern Fault Zone that marks the Tertiary-Quesnel contact. This image contrasts the Z/Y (Cross-line) component profiles (Figure 6b), which are sensitive to structures oriented oblique/parallel to the In-Line flight direction – notably: 1) a probable NW-SE fault structure southwest of Mt Milligan; 2) a possible NE-SW fault structure east of Mt Milligan, and 3) a possible east-westerly structure that bounds the northern edge of the MBX Zone. When the 2 Tippers are combined, using either the PR or DT grid methods, as shown in Figures 7 and 8, the imaging of geoelectric structures becomes omni-directional, with all orientations being highlighted.

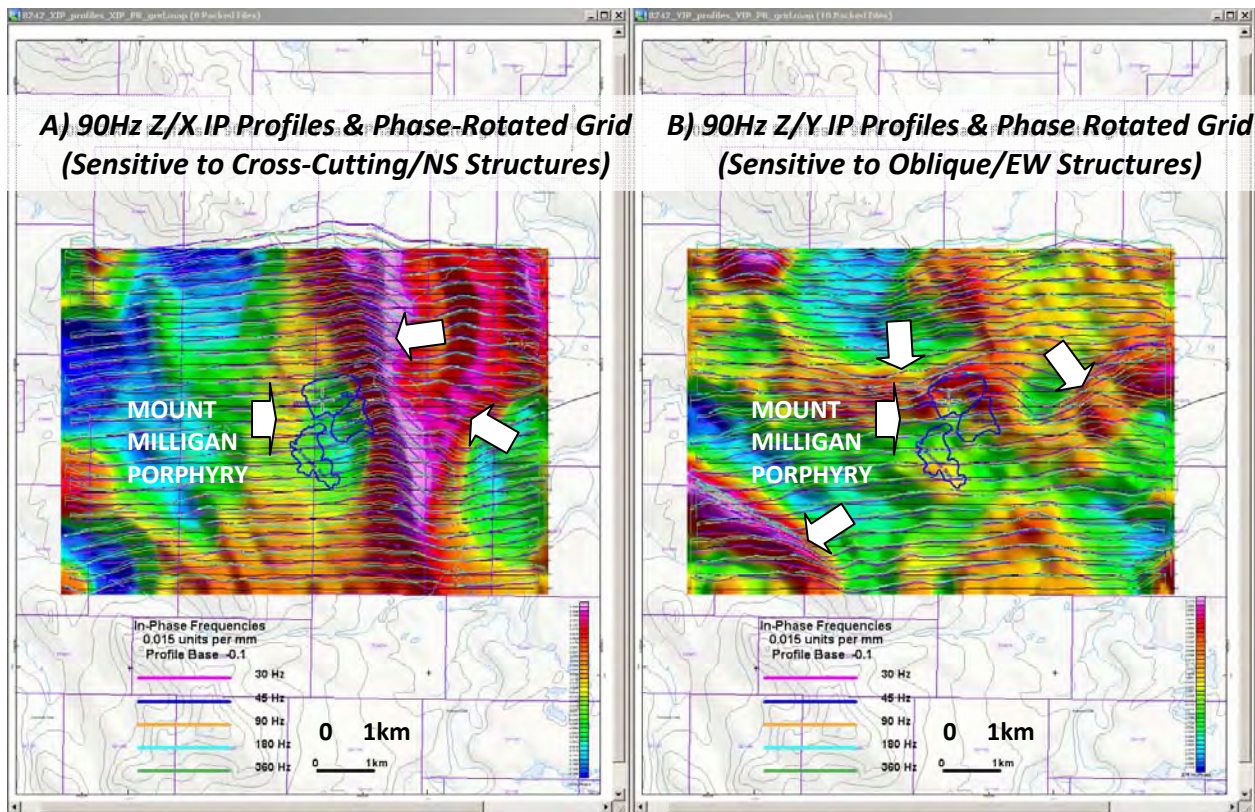


Figure 6: Mt Milligan ZTEM Test Block: In-Phase Z/X Component Profiles over 90Hz Phase-Rotated (PR) Grid (left) versus Corresponding 90Hz In-Phase Z/Y Profiles and PR Grid (right).

The Resulting PR and the DT images shown in Figures 7 and 8 each also demonstrate the notable differences in the frequency-dependence of the responses, that imply resolved differences in the vertical depth of the defined structures– including a) the main NNW-SSE Great Eastern Fault zone contact response, occurring east of Mt Milligan, that progressively weakens from low to high frequency (Fig. 7b & Fig 8b). This might reflect the fact that this is a major geologic/geoelectric contact that more strongly fault-fractured/alterd with greater depth penetration. In contrast, the conductive lineament, which appears to be structurally related and that borders the Mt Milligan porphyries to the north (the Oliver Fault – Fig. 4), progressively weakens in strength with decreasing frequency and increasing depth-penetration. This suggests that it relates more to the near-surface geology and not the deep geologic structure below the Mt. Milligan zones. Also highlighted in these images, particularly the RPR grids in Figure 7, is the subtle circular-like high resistivity anomaly that directly coincides with the Mt. Milligan porphyry and might therefore reflect the potassic alteration halo.

Figure 9 shows the 90 Hz In-Phase DT results (Fig 9a), as well as the corresponding calculated 1ST vertical magnetic gradient (CVG) results (Fig. 9b) and compares them both directly with the structural interpretation, taken from Figure 7-8 and shown as an overlay. Clearly, both the DT and the CVG results both map similar inferred fault-fracture structures, including the main NNW-SSE Great Eastern Fault Zone (GEFZ); however there locus of the ZTEM resistivity lows appears to provide stronger evidence of these structures relative to the magnetic results in Figure 9b. The

results showcase the complementary nature of the ZTEM and Magnetic evidence. They also highlight the geologic mapping capability using resistivity contrasts that ZTEM provides.

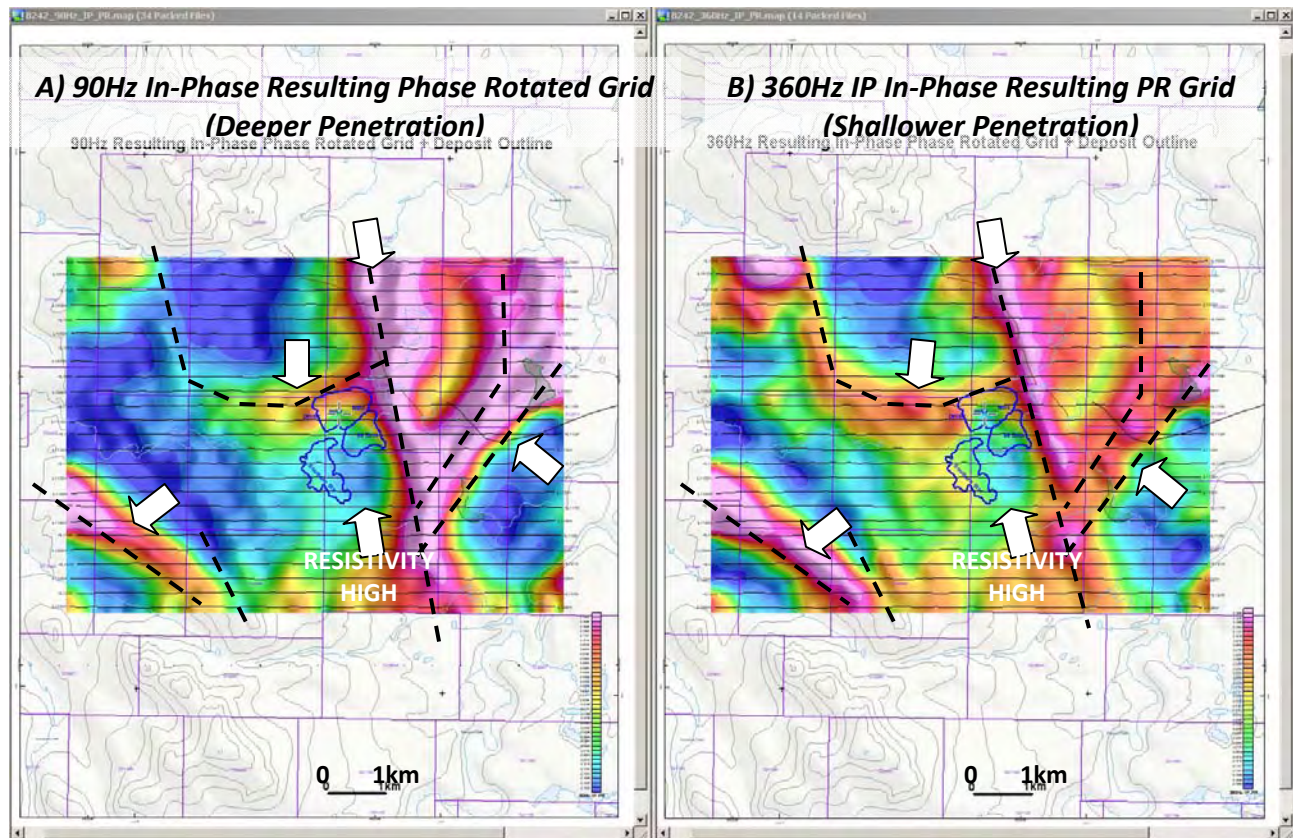


Figure 7: Mt Milligan Test Block: In-Phase Z/Y Component Profiles over 360Hz Total Divergence (DT) Grid (left) versus Corresponding 90Hz In-Phase DT Grid (right) and structural interpretation.

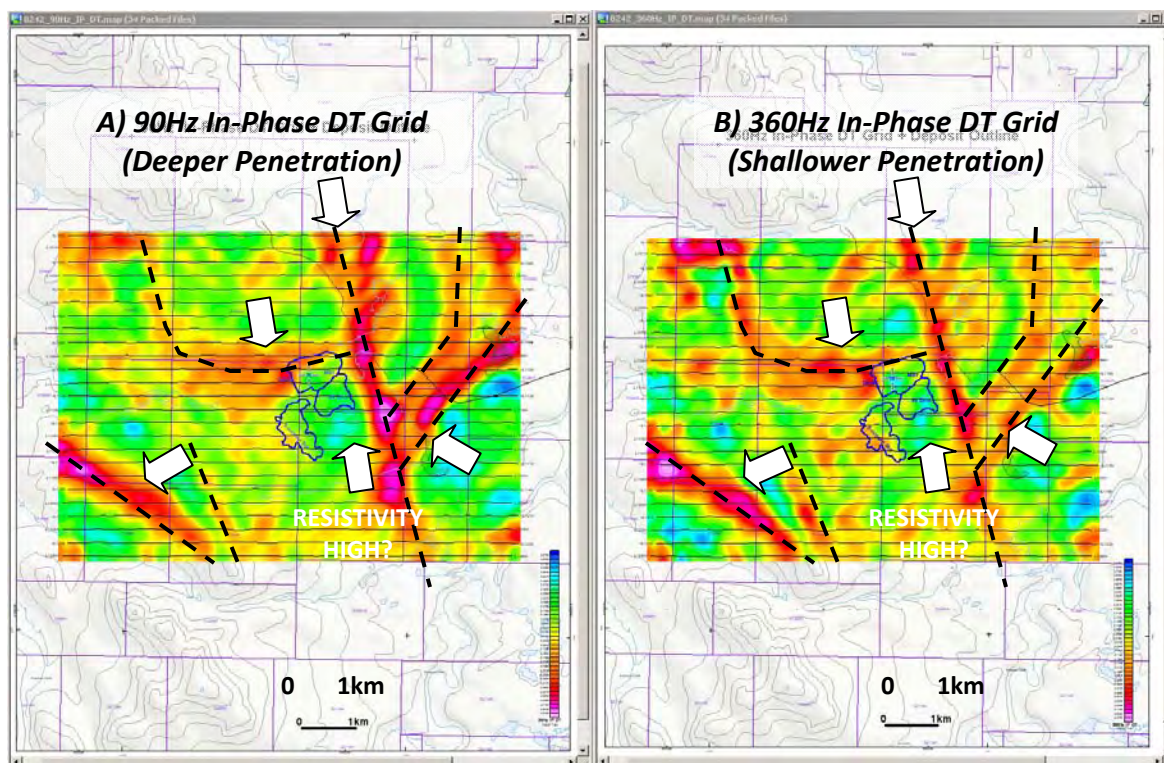


Figure 8: Mt Milligan Test Block: In-Phase Z/Y Component Profiles over 360Hz Total Divergence (DT) Grid (left) versus Corresponding 90Hz In-Phase DT Grid (right).

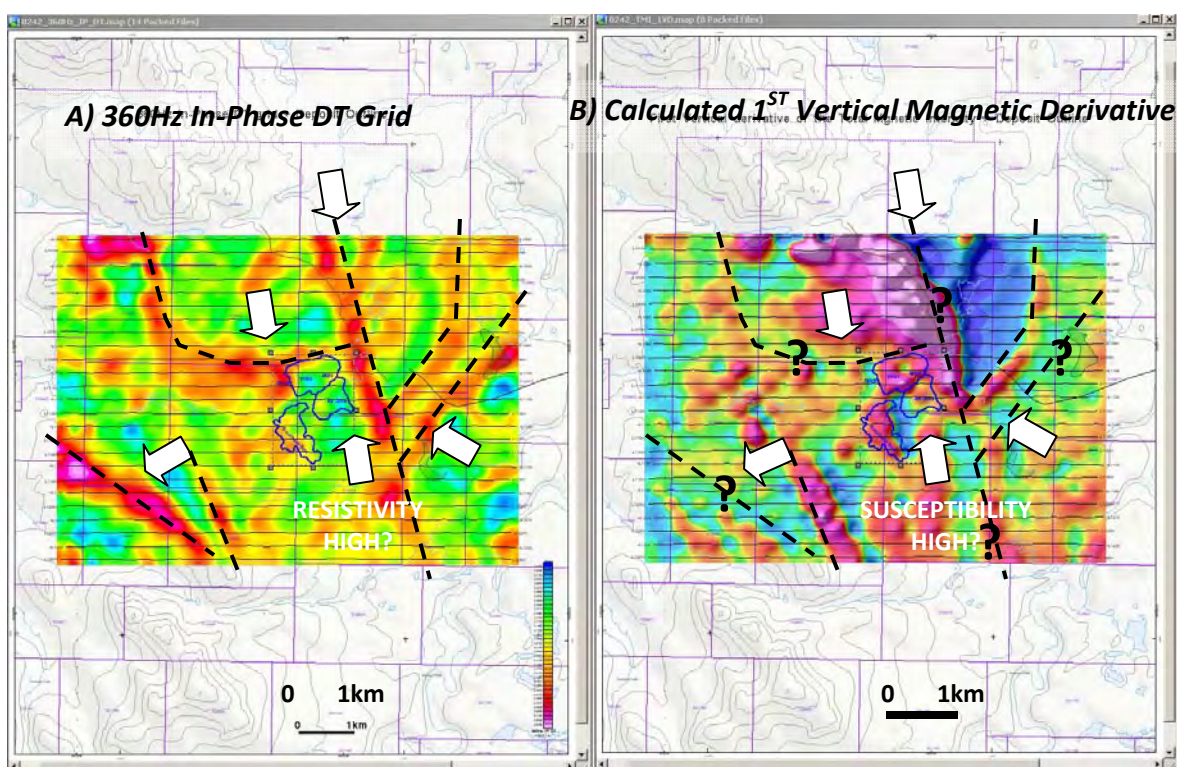


Figure 9: Mt Milligan Test Block: 360Hz In-Phase DT Grid and Interpreted Structures (left) versus Corresponding Calculated 1ST Vertical Magnetic Grid (right).

Figure 10, presents a 3D composite image of the multi-frequency DT's from Mt Milligan plotted at the equivalent MT skin depth, assuming a 1,000 ohm-m average resistivity. As shown, the depth of the DT slices increases with decreasing frequency (360Hz-30Hz) from ~600m to ~1700m.

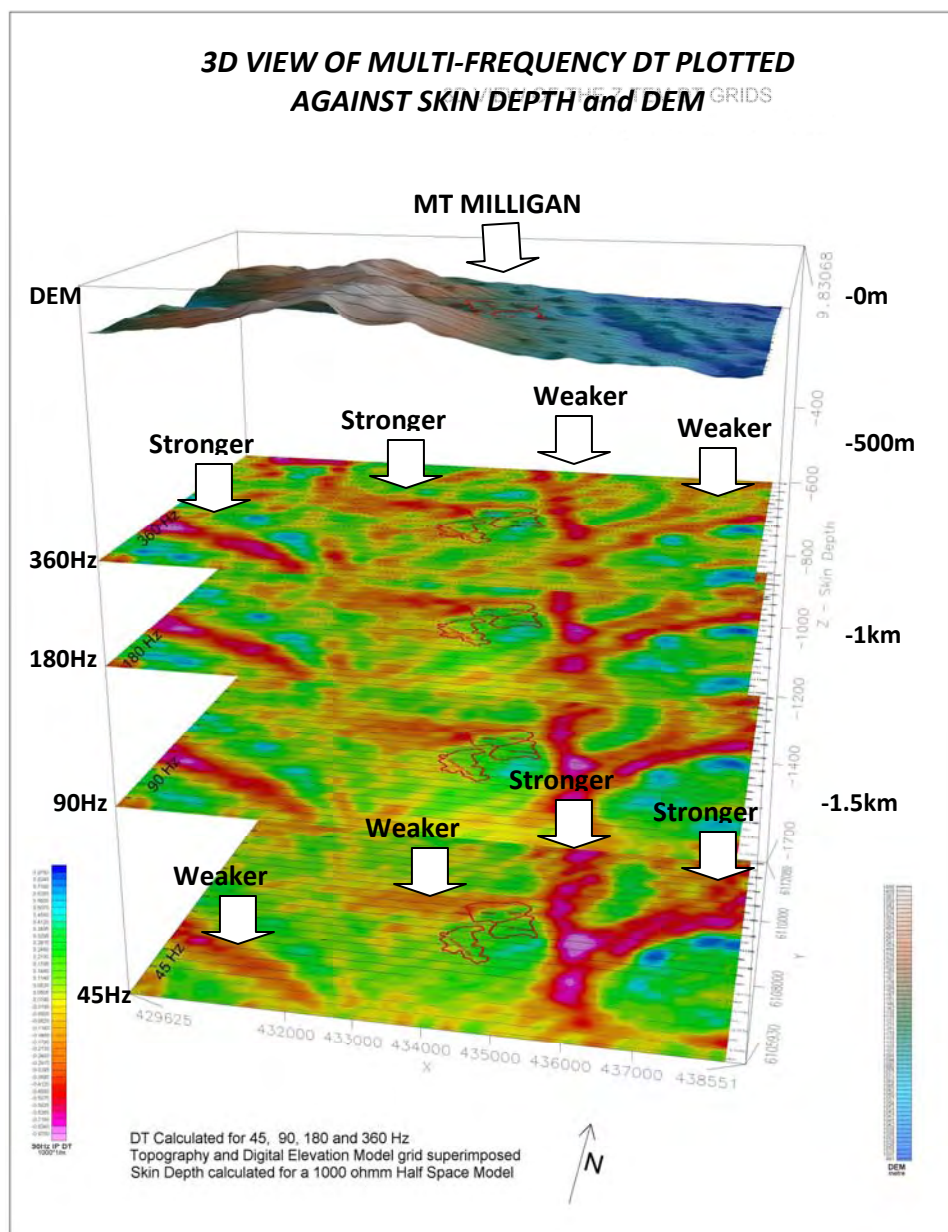


Figure 10: 3D Perspective view of Multi-frequency In-Phase DT's plotted according to MT skin depth (using 1k ohm-m half-space Earth) and DEM model at ground level.

As shown, this image highlights the frequency dependency of the ZTEM responses obtained, hence possible differences in the depth-range – notably the 2 signatures to the west, that include Mt-Milligan, that weaken with progressive depth and therefore suggests that these are structures are closer to the surface; and the 2 easternmost highlighted features that strengthen with depth which therefore suggests that these are major bedrock fault-fracture zones or contacts.

3.2 2D Inversion Analysis

Cross-sectional images of the ZTEM results have been generated using 2D inversion algorithm, in the manner proposed by Perrson et al. (2008) for airborne VLF data. The Zvert2d™ code developed for Geotech Ltd. is based on the Gauss-Newton algorithm of deLugao and Wannamaker (1996) by Prof. Phil Wannamaker at University of Utah. It was specifically modified to take into account the “air” layer between the ZTEM aircoil sensor and the ground level. It is designed to run on a desktop Pentium with 3GHz processor, requiring approximately 20 minutes to execute for a typical ZTEM profile.

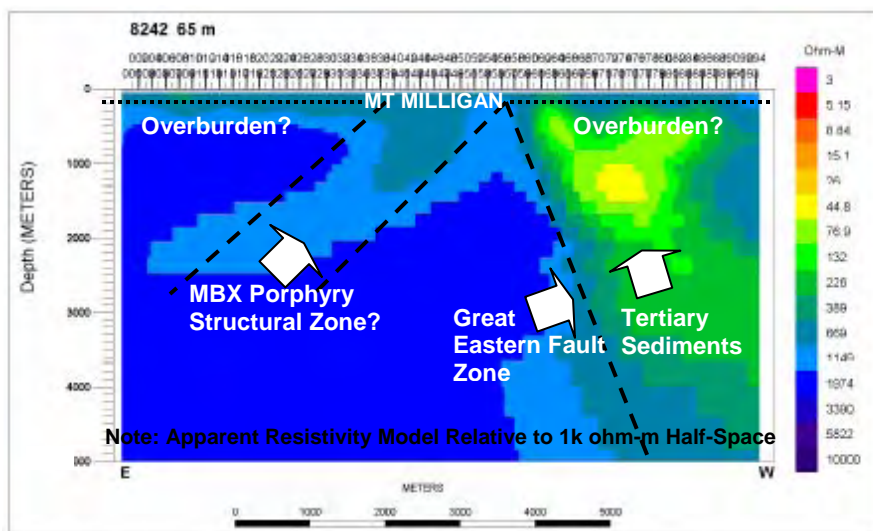


Figure 11 Above: Inversion image for line 8242 with the flight line 65 m above the ground. Below: Observed and computed inversion model responses for line 8242-65m.

Figure 11: 2D Inversion image with Interpreted Structures and Calculated vs. Observed Z/X profile at 360Hz s for flight line directly over Mt Milligan Deposit, 65m above ground level.

The In-line (Z/X) data for a single line profile, taken directly over the center of the Mt Milligan Main Zone Porphyry (MBX), were used to create the 2D inversion image presented in Figure 11. The input data utilized both the In-Phase and Quadrature Phase data from all five measured frequencies. Due to the impractical nature of the >1000 data points from the ZTEM profile, these were undersampled to 90 points in order to perform the calculation and proved effective. An error of 2% was assigned to the data for inversion. A host of 1000 ohm-metres was assumed for the starting model. Despite non-ideality of the data error, a value of nRMS of close to unity (1.0) was achieved in 4-6 iterations, with starting nRMS values of 5-6.

Figure 11 presents the 2D resistivity cross-section obtained from the Mt Milligan line-profile and the corresponding In-Phase and Quadrature profiles showing the measured vs. 2D forward model data fits at 360Hz, for comparison (note that the Quadrature profile is reversed for convention purposes; ref. Wannamaker, 2008). As shown, the data variation is relatively complex with an initial high-frequency minimum in the In-Phase Z/X profile appearing near $x = 5.5$ km, and then generally positive values of IP (Z/X) developing over the rightmost portion of the line. This results in a crudely Y-shaped conductive anomaly in the eastern third of the inversion section with the initial high-frequency anomaly responsible for the upper left limb of the Y (Wannamaker, 2008).

This corresponds to the known Tertiary Sediments that lie east of the older Quesnel-Takla rocks that host the Mt Milligan porphyry, whose boundary is marked by the Great Eastern Fault Zone (GEFZ), which appears to be east-dipping. Based on the ZTEM inversion results, the Tertiary sediments extend quite deeply – to below several km depths. Below a thick conductive overburden cover, a moderate resistivity low feature that is centered on the Mt Milligan MBX porphyry copper zone, in the middle of the profile, appears to dip westward and extends to below several km depths – suggesting a structural zone that resembles the geologic cross-section shown in Figure 4. It appears therefore that the 2D inversion image bears a reasonable resemblance to the known geology.

4 Conclusion and Recommendations

The ZTEM test results performed over a known copper-gold porphyry deposit in the north-central BC has highlighted the high quality and high resolution structural and alteration mapping, as well as deep penetration capability of the AFMAG data obtained.

The ZTEM results appear to correlate very well with the known geology, in particular the presence of both major and secondary fault structures and geologic contacts. In addition, the ZTEM results appear to indicate differences in the relative source depth and vertical depth-extent of the defined structures that are geologically plausible. In particular, the ZTEM results point to the presence of a major NNW-SSE-trending conductive fault or contact structure that cross-cuts the survey area and relates the Great Eastern Fault Zone, east of the Mt Milligan deposits, marking the boundary between the Quesnel Takla group rocks to the west and the younger, down-faulted Tertiary sediments to the east. The Mt. Milligan deposit area itself is marked by a subtle but well-defined circular resistivity high feature, that possibly relates to the potassic alteration halo centred over the porphyry copper zones. As well a weaker, east-westerly low resistivity zone that appears to border the Mt. Milligan porphyries to the north, might relate to the Oliver structural fault zone

or possibly the potassic-propylitic alteration boundary which appears to weaken with depth – suggesting that it relates to the near-surface outcropping geology, rather than a deep feature.

The 2D inversion using the Zvert2d algorithm appears to have been able to compute accurate ZTEM responses in the air and to invert them for reasonable earth resistivity cross section directly over the Main MBX Zone at Mt Milligan. Provided approximate constraints on the host resistivity are available, inversion anomaly positions are more accurate. With poor constraints, trials with a variety of host resistivities are required to judge their dependency. Overall, the Great Eastern Fault Zone and Tertiary sediments are clearly defined, and a possible west-dipping structural zone relating to Mt Milligan porphyry is also suggested that extends to great depth.

We recommend that these ZTEM results be compared with the available geoscientific data, in order to better explain the observed correlations with the known geology. This might include comparisons with any geophysical survey data, in particular, ground EM and possibly also ground magnetotelluric and tipper MT results. We also recommend that additional interpretation of the ZTEM data be attempted, using 2D inversions with geologically-referenced starting models.

Respectfully submitted

Jean M. Legault, M.Sc., P.Eng. P.Geo.
Manager, Data Processing & Interpretation
Geotech Ltd., Aurora ON

Biljana Milicevic, M.Sc.
Geophysical Consultant
Geotech Ltd., Aurora, ON

5. References

- De Lugao, P.P., and Wannamaker (1996). Calculating the two-dimensional magnetotelluric Jacobian in finite elements using reciprocity, *Geophys. J. Int.*, Vol. 127, pp. 806-810.
- Kuzmin, P., Lo, B., and Morrison, E. (2005). Final Report on Modeling, interpretation methods and field trials of an existing prototype AFMAG system, Misc Data Release 167, Ontario Geol. Survey.
- Labson, V. F., Becker A., Morrison, H. F., and Conti, U. (1985). Geophysical exploration with audiofrequency natural magnetic fields, *Geophysics*, Vol. 50, pp. 656-664.
- Lo, B., Legault, J.M., Kuzmin, P. (2008). Z-TEM (Airborne AFMAG) tests over unconformity uranium deposits, extended abstract submitted to 20TH ASEG International Geophysical Conference & Exhibition, Adelaide, AU.
- Persson, L., Erlström, M., Bastani, M., and Pederson, L. (2008). Airborne VLF measurements over the Island of Gotland, Sweden, paper presented at AEM2008 – 5th International Conference on Airborne Electromagnetics Haikko Manor, Finland, May 2008.
- Terrane Metals Corp. (2008), Technical Report – Feasibility Mt. Milligan Property, Northern BC, prepared by Wardrop (Vancouver, BC), Document No. 0652590200-REP-R0015-01, 384 pp.
- Wannamaker, P.E. (2008). Two-dimensional inversion of ZTEM data: Synthetic model study & test profile images, technical report by Emblem Geophysical Inc. for Geotech Ltd., Dec-2008, 25 pp.
- Ward, S. H. (1959). AFMAG - Airborne and Ground: *Geophysics*, Vol. 24, pp. 761-787.

**PRELIMINARY REPORT ON HELICOPTER-BORNE ZTEM TIPPER AFMAG SURVEY RESULTS
over SHEA CREEK TEST BLOCK, on behalf of AREVA RESOURCES CANADA LTD.
April 2009**

Introduction

In April 2009, ZTEM (Z-Axis Tipper Electromagnetic) surveys were conducted, on behalf of AREVA Resources Canada Ltd. (Saskatoon, SK), over the Shea Creek Test Block that is situated in the Cluff Lake region of the western Athabasca Basin. The ZTEM survey consists of airborne Tipper AFMAG (audio frequency magnetic) measurements, as well as aeromagnetics using a caesium magnetometer. The survey consisted of twenty four (24) 18km long, NE-SW oriented (N-060°E) flight lines, totaling 432 line-km, that were obtained at 400m nominal line spacings over an approximately 9 x 18km area. The area was chosen because it hosts the well known Shea Creek uranium deposits (Figure 1), it is overlain by a significant thicknesses of Athabasca sandstone (650+ metres) cover, it hosts a major graphitic horizon and sandstone alteration zones at depth, and has been the focus of extensive airborne and ground geophysical coverage (Figure 2).

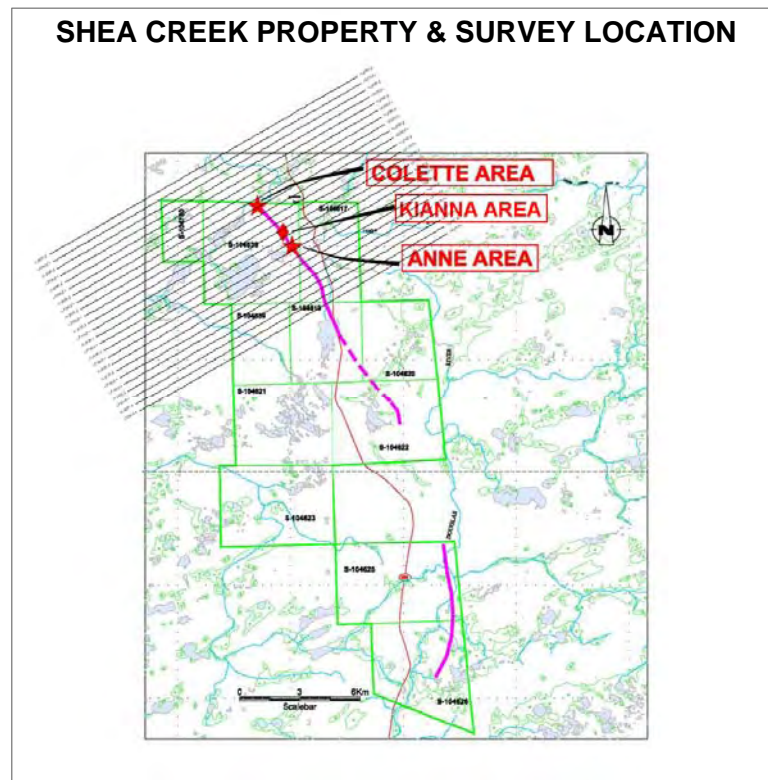


Figure 1: Location map showing uranium deposits and ZTEM flight lines (courtesy AREVA Res. Can. Ltd.)

The Z-axis tipper measurements of the vertical (Z) component were obtained using Geotech's patented ZTEM aircoil system, suspended at approximately 70m elevation above ground level. The vertical component data (H_z) were then ratio'd to fixed horizontal field measurements (H_x - H_y) obtained using identical reference coils, that were oriented in the in-line (X) and cross-line (Y) directions, in order to obtain the tipper functions Z/X and Z/Y. The In-Phase and Quadrature components of the tipper ratio data were extracted using Fourier-based, digital signal processing analyses, at 5 frequencies, between 30Hz and 360Hz.

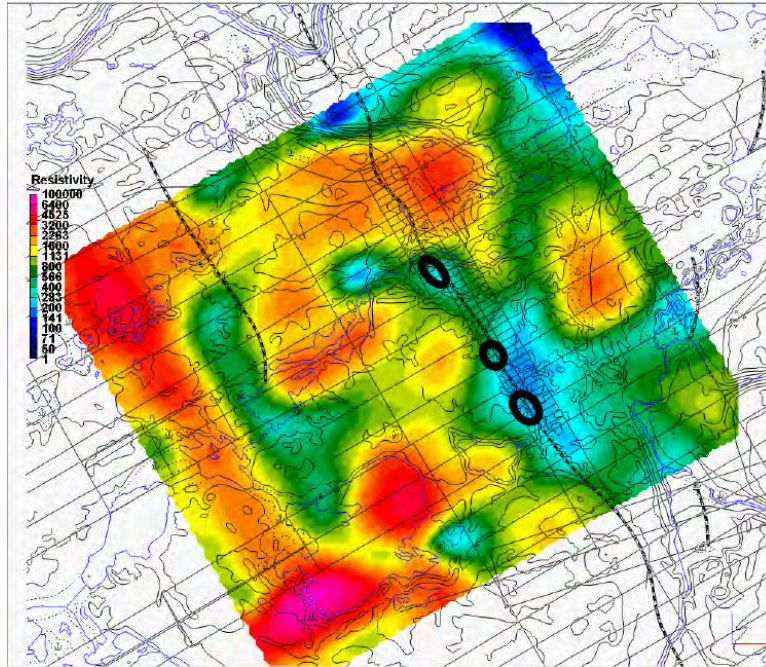


Figure 2: Ground resistivity survey results showing conductive sandstone alteration zones (blue) above graphitic EM conductors (striped lines) and deposits (circles) at Shea Creek (courtesy AREVA Res. Can. Ltd.)

General Theory

The ZTEM airborne AFMAG system measures the anomalous vertical secondary magnetic fields that are created by the interaction between naturally occurring, plane wave audio frequency EM fields and electrical heterogeneities in the earth. Because the primary fields are naturally occurring, ZTEM requires no transmitter. The fields resemble those from VLF except that they are lower frequency (tens & hundreds of Hz versus tens of kHz), hence provide significantly deeper penetration (approx. 7x-25x) and are not strongly directionally polarized. These AFMAG EM fields, derived from world wide atmospheric thunderstorm activity, have the unique characteristic of being uniform, planar and horizontal, and also propagate vertically into the earth – to great depth, up to several km, as determined by the EM skin depth, which is directly proportional to the ratio of the bedrock resistivity to the frequency. At the frequencies used for ZTEM, the EM skin depths likely range between <1km to >3km in this region of the Athabasca Basin, according to the following equation for skin depth (Vozoff, 1972):

$$\delta_s = 503 * \sqrt{(\rho_A / f)} \text{ metres}$$

if $\rho_A = 1\text{ k ohm-m}$, $\delta_s \approx 800\text{m at } 360\text{Hz}$ and $\sim 3.0\text{km at } 30\text{Hz}$

The other unique aspect of AFMAG fields is that they react to relative contrasts in the resistivity, and therefore do not depend on the absolute conductance, as measured using inductive EM systems, such as VTEM – hence poorly conductive targets, such as alteration zones and fault zones, can be mapped, as well as higher conductance features, like graphitic units. Conversely, resistive targets can also be mapped using AFMAG – provided they are of a sufficient size and contrast to produce a vertical field anomaly. Hence AFMAG can be effective as an all-round resistivity mapping tool, making it unique among airborne EM methods.

The nature of the AFMAG fields is such that, as with VLF, buried, tabular conductors and resistors produce cross-over responses. As such, although the field results are shown as cross-over profiles, additional post-processing is applied to convert these cross-overs into peak responses, to make them more useful as mapping tools. These include 2 types: the Total Divergence (DT), which is a summative horizontal derivative process method that combines both the Z/X and Z/Y results (Kuzmin et al., 2005), and the 90-degree Phase-Rotation (Lo and Zang, 2008), shown here, which is a Geosoft-based FFT process applied to grids of the individual Z/X and Z/Y component data - only the In-Phase Z/X In-line preliminary results are presented in the current study (Figures 3).

The In-line (Z/X) component of the In-Phase Tipper data are shown as 90-degree Phase-Rotated grids in Figures 3, with the high (360Hz) and low-frequency (30Hz) spectrum shown together, for depth-comparison purposes. The Z/X (In-Line) component results shown in Figure 3 are most sensitive to structures orientated perpendicular to the In-Line direction. Geologic and geophysical features of interest from Figure 2 are also shown as overlays.

There are notable differences in the frequency-dependence of the responses that implies a difference in the vertical source depth. Specifically, the higher frequency Z/X results (Fig. 3 left) appear to be more strongly influenced by north-south drainage patterns, which reflects their shallower penetration (<1km); whereas the lower frequency Z/X results (Fig. 3 right) appear to most influenced by more NW-SE trending basement stratigraphies that occur at >650-700m depths. In particular, the strongest ZTEM response

corresponds to the Shea Creek graphitic horizon that occurs in the center of the block, which agrees with the known geology. As well, to the northeast, a V-shaped low resistivity zone that is also observed in the high frequency data corresponds to an inlier of Douglas Formation mudstones, that lie at relatively shallow depth (<500m); the weakening response in the lower frequency ZTEM results appears to confirm that these Douglas mudstones are depth-limited, in comparison to the Shea Creek graphitic response.

Conclusion and Recommendations

The ZTEM test results performed over an unconformity-type uranium target in the western Athabasca basin has highlighted the deep penetration and resolution capability of the technology as well as the high quality and high accuracy of the AFMAG data obtained.

The ZTEM results appear to agree very well with the inferred/known geology, in particular the presence of a major NW-SE trending conductive zone that likely corresponds to main Shea Creek graphitic horizon that is known to occur at depths exceeding 600-700m, and had previously proved to be a challenge in terms of depth-penetration for airborne and ground geophysical techniques.

In addition, the ZTEM results appear to easily differentiate between shallow and deep seated target geology – notably overburden drainage patterns and Douglas Formation mudstones that are more strongly felt in the high frequency/shallow penetration data; versus the Shea Creek basement graphites that are easily detected in the low frequency/deep penetration data, below 650m-700m depths.

We recommend that these ZTEM results be compared with the available geoscientific data, in order to better explain the observed correlations with the known geology. This might include comparisons with any geophysical survey data, in particular, ground EM and possibly also magnetotelluric and tipper MT results. We also recommend that additional interpretation of the ZTEM data be attempted, including 2D-3D inversions.

Respectfully submitted

Jean M. Legault, M.Sc., P.Geo.
Manager, Data Processing & Interpretation

Harish Kumar, M.Sc., P.Geo.
Senior Geophysicist

Geotech Ltd., Aurora ON

April, 2009

References

Kuzmin, P., Lo, B., and Morrison, E. (2005): Final report on modeling, interpretation methods and field trials of an existing prototype AFMAG system, Miscellaneous Data Release 167, Ontario Geological Survey.

Lo, B., and Zang, M. (2008): Numerical modeling of ZTEM (airborne AFMAG) response to guide exploration strategies, SEG Expanded Abstracts, **27**, 1098-1101.

Vozoff, K. (1972): The magnetotelluric method in the exploration of sedimentary basins, *Geophysics*, **37**, 98-141.

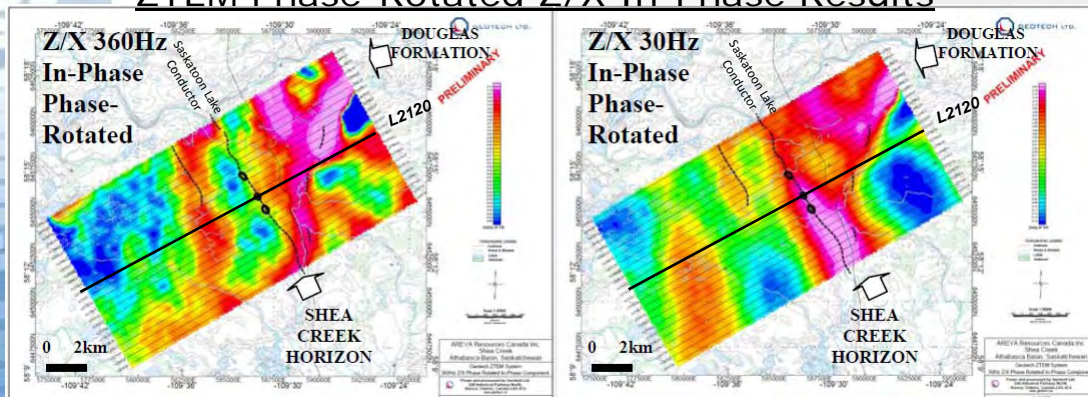


GEOTECH LTD.

AIRBORNE
GEOPHYSICAL
SURVEYS

ZTEM Features: Deep Penetration Example at Shea Creek, NW Sask.

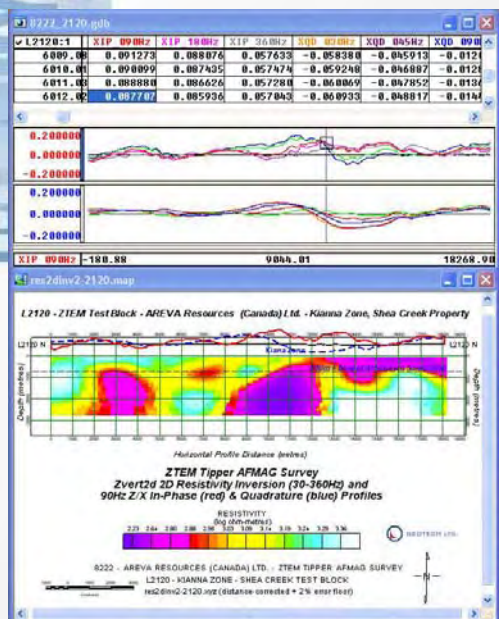
ZTEM Phase-Rotated Z/X In-Phase Results



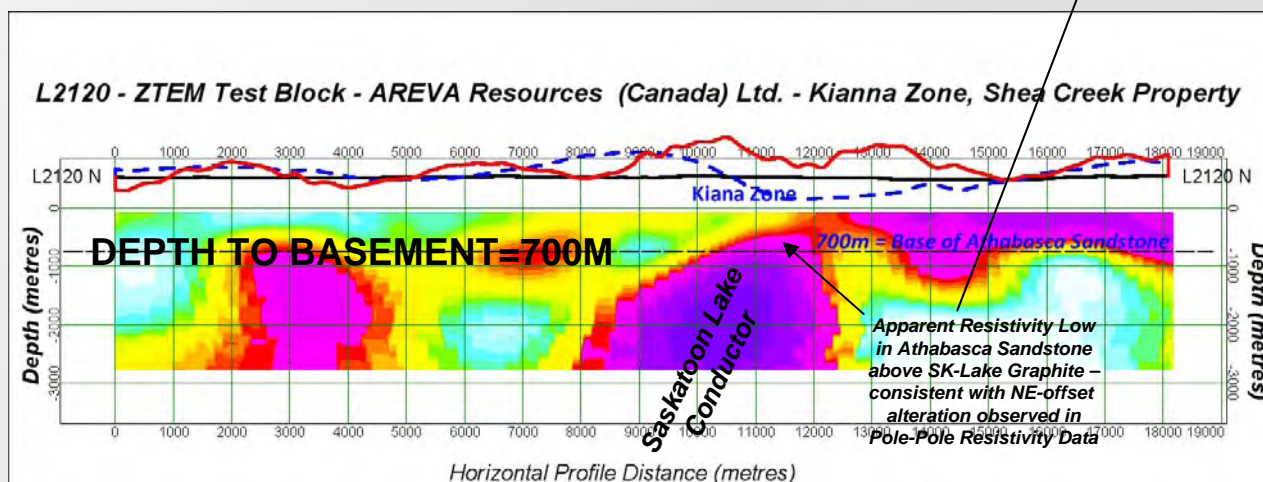
Shallower Penetration

Deeper Penetration

ZTEM In-Line IP & QD Results



2D ZTEM Resistivity Inversion



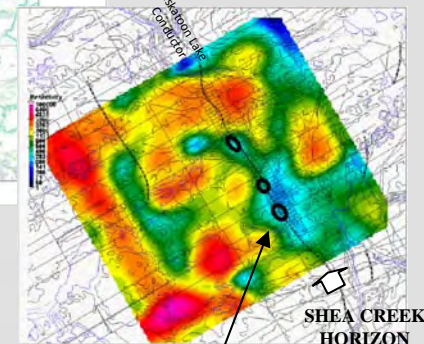
(Courtesy AREVA Resources (Canada) and UEX Corporation)

Showing ZTEM Results over Kianna Zone, at Shea Creek NW Saskatchewan Canada

SHEA CREEK PROPERTY & SURVEY LOCATION



3D Pole-Pole DC Inversion



(modified after Bingham et al., 2006)
Note Reverse colour scale (Blue=Low Resistivity) relative to all other figures

ZTEM Tipper AFMAG Results over the Lalor Lake VMS deposit

In November, 2009, Geotech Ltd. carried out a helicopter-borne geophysical survey for Hudbay Minerals Ltd. over the **Lalor Lake** polymetallic copper-zinc-gold volcanogenic massive sulphide deposit situated near Snow Lake, central Manitoba (Figure 1b), approximately 3km northwest of the Chisel North Mine. Principal geophysical sensors included the **Z-axis Tipper Electromagnetic (ZTEM)** system and caesium magnetometer (Figure 1a). A total of 370 km were flown at a nominal line-spacing of 100-200m over a 66 km² area. The objective of the ZTEM survey was test its ability to map the Lalor Lake VMS deposit, lying below 550m of volcanic cover, which has escaped detection in previous airborne geophysical surveys.

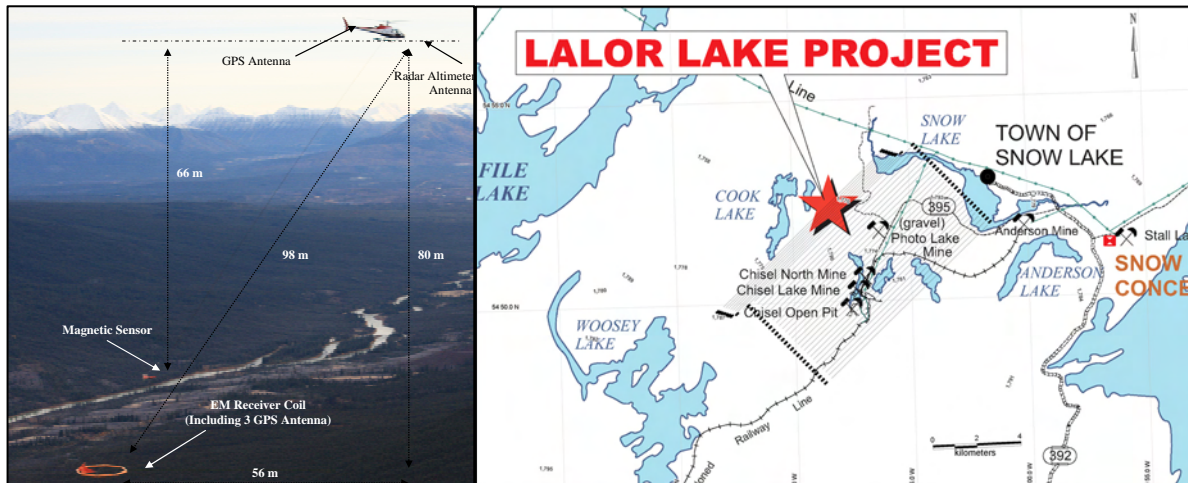


Figure 1: a) ZTEM helicopter receiver system (left) and b) Lalor Lake location with ZTEM flight lines (right - modified after Blakley, 2008).

Deposit Geology

The Lalor Lake deposit is situated in the Flin Flon Greenstone Belt and is a classic volcanogenic massive sulphide (VMS) deposit similar to other massive sulphide bodies in the Chisel sequence (Chisel Lake, Ghost-Lost Lake, Chisel North, and Photo Lake). Lalor Lake lies along the same stratigraphic horizon as the Chisel Lake and Chisel North ore bodies (Figure 1b). The Lalor Deposit was discovered in March 2007 by drill hole testing a ground fixed loop Time Domain electromagnetic anomaly that intersected high grade zinc mineralization at a depth of approximately 800 m below surface, approx. 3 km northwest of the Chisel North Mine. Mineralization occurs as massive to disseminated sulphides consisting of mainly of sphalerite, pyrite and chalcopyrite, with lesser galena and arsenopyrite. Rock units in the hanging wall include mafic and felsic volcanic rocks that have been overturned and are in unconformable possibly fault contact with the footwall rocks. The mineralization is immediately underlain by a thick zone of intense metamorphosed, hydrothermally altered rocks. The deposit dips shallowly to the northeast and occurs at depths between 550 m and 1200 m (Figure 2a). It has a lateral extent of about 900 metres in the north-south direction, and 700 metres in the east-west direction (Figure 2b). The zinc-rich base metal indicated resource of 12.3 Mt 1.6 g/t Au, 24.2 g/t Ag, 0.66% Cu, 8.70% Zn (Inferred resource 13.2 Mt 2.9 g/t Au, 34.1 g/t Ag, 0.70% Cu, 8.19% Zn) is geologically interpreted as six stacked lenses (Figure 2a). In addition, potential gold zones of 10.6-12.0 Mt 4.3-5.2 g/t Au, 30.0-33.0 g/t Ag, 0.40-0.60% Cu, 0.30-0.40% Zn occur in five other separate, disseminated mineralized zones (Ref. Gilmore et al., HBMS, from PDAC 2010 abstracts and Hudbay Minerals, from PDAC 2010 core shack notes).

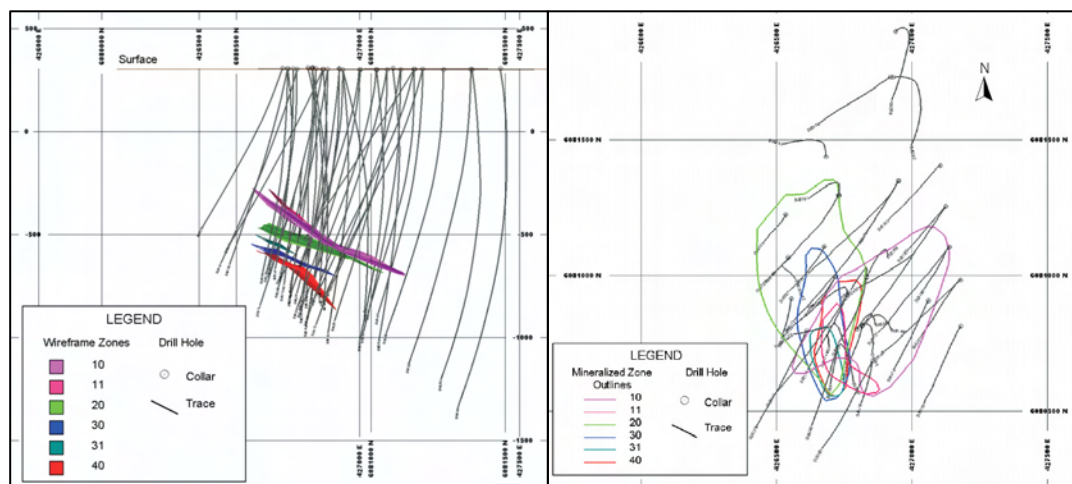


Figure 2: Lalor Lake Deposit drill holes and mineralized zone outlines in a) long section (left) and b) plan (right – after Blakley, NI 43-101, 2008).

ZTEM System

The ZTEM survey instrumentation consists of a single vertical-dipole receiver coil (7.4m dia.) that is towed roughly 80m below the helicopter (Figure 1a), at a 100m nominal flight height, and is flown over the survey area in a grid pattern, similar to other regional airborne surveys. Two orthogonal air-core horizontal axis coils (3.5m dia.) are placed close to the survey site to measure the horizontal EM reference fields. Data from the three coils are used to obtain the Z/X (In-line) and Z/Y (cross-line) AFMAG tippers, whose transfer functions (In-Phase & Quadrature) are derived at six frequencies in the 30 to 720 Hz band. ZTEM tipper AFMAG is recognized for its unique ability to map resistivity contrasts associated with lithology, structure and alteration that are typically associated with VMS and other similar deposits to great depths, exceeding 1-2km.

ZTEM Tipper AFMAG Results

Figure 3 presents the ZTEM tipper results in plan shown as Phase Rotated (PR) images (that convert the tipper cross-overs into peaks) of the In-line (Z/X) tipper In-Phase component, comparing the 360Hz (shallower penetration) and 30Hz (deepest) responses, with the outline of the Lalor Lake deposit and drill holes overlain. In the PR image, warm colours represent conductive structures and contacts; cool colours represent more resistive units. The Lalor Lake deposit is not well defined in the 360Hz high frequency data likely due to the limited skin depth penetration and poor relative contrasts in this depth range; whereas in the deeper, lowest frequency 30Hz image, the Lalor Lake deposit and alteration are better contrasted with the surrounding rocks. The effect of the NE-SW powerline to the Chisel mine is strongest in the 360Hz image, but the Chisel Lake horizon (center), a graphitic horizon (west) and mineralized horizon to the northeast (east) are easily resolved from high to low frequencies. Figure 4 presents the 2D cross-sectional resistivity data results obtained from the 2D inversion of the In-Line (Z/X) ZTEM tipper data from the L1020 profile directly over Lalor Lake deposit (see Fig. 3) using Geotech's proprietary Zvert2d code. The 2D inversion image defines a buried, north-east dipping conductive body from 500-1000m depth, which is consistent with the known position and geometry of the Lalor Lake VMS deposit, as shown in Figure 4.

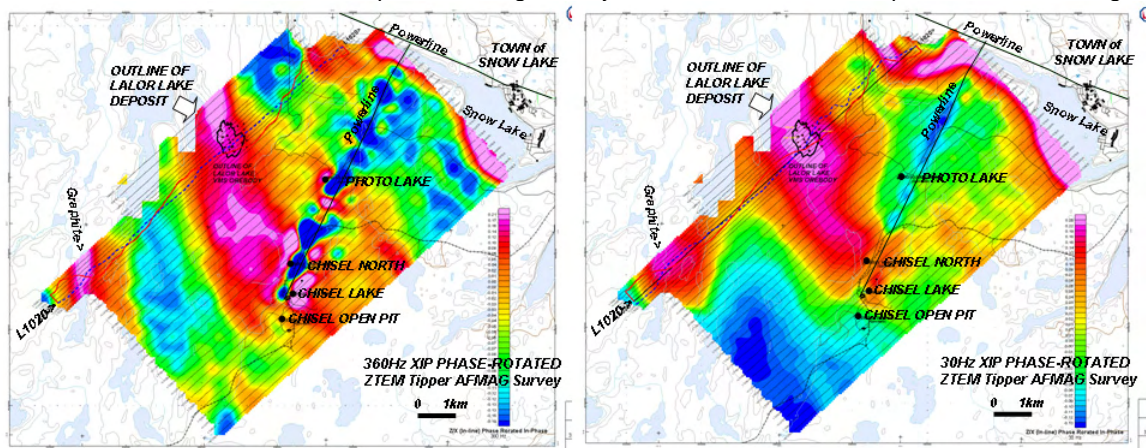
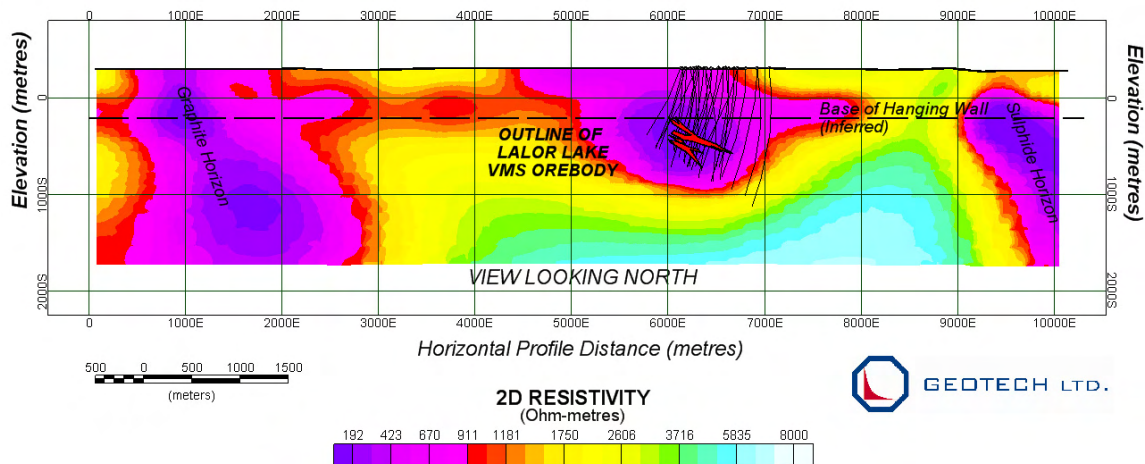


Figure 3: ZTEM Tipper AFMAG field results shown in plan as grid contours of 90-degree Phase-Rotated (PR) In-line (Z/X) In-Phase component at: a) 360Hz high frequency showing shallower penetration (left) and b) 30Hz low frequency showing deeper penetration (right) and Lalor Lake deposit outline.

L1020 - ZTEM Airborne Tipper Survey - Hudbay Minerals Inc. - Lalor Lake Block



ZTEM Tipper AFMAG Survey Zvert2d 2D Resistivity Inversion (30-720Hz)

Figure 4: 2D Resistivity cross-section for L1020 over centre of Lalor Lake deposit from Zvert2d inversion of ZTEM In-line (Z/X) tipper data.

ZTEM Tipper AFMAG Results over the Morrison Copper/Gold Porphyry deposit

Introduction

As part of a larger geophysical survey program, Geotech Ltd. carried out a helicopter-borne **ZTEM (Z-axis Tipper Electromagnetic)** survey test over the **Morrison Copper/Gold Property**, belonging to Pacific Booker Minerals Inc. (Vancouver, BC), in May, 2010. The Morrison Property and adjoining Hearne Hill Property (Figure 1b), are situated in the Babine Lake Region of central BC, approximately 65 km northeast of the town of Smithers and 35 km north of Granisle village, and lie within 30km of the former Granisle and Bell porphyry copper/gold mines (Figure 1a). Principal geophysical sensors included the ZTEM AFMAG (audio frequency magnetics) system and caesium magnetometer. A total of 163 km were flown along 15 x 10.9km long profiles at a nominal line-spacing of 250m over a 38 km² area (Figure 1c). The objective of the ZTEM survey was to determine its ability to detect and map the Morrison and Hearne Hill porphyry copper deposits, based on resistivity contrasts derived from airborne tipper measurements.

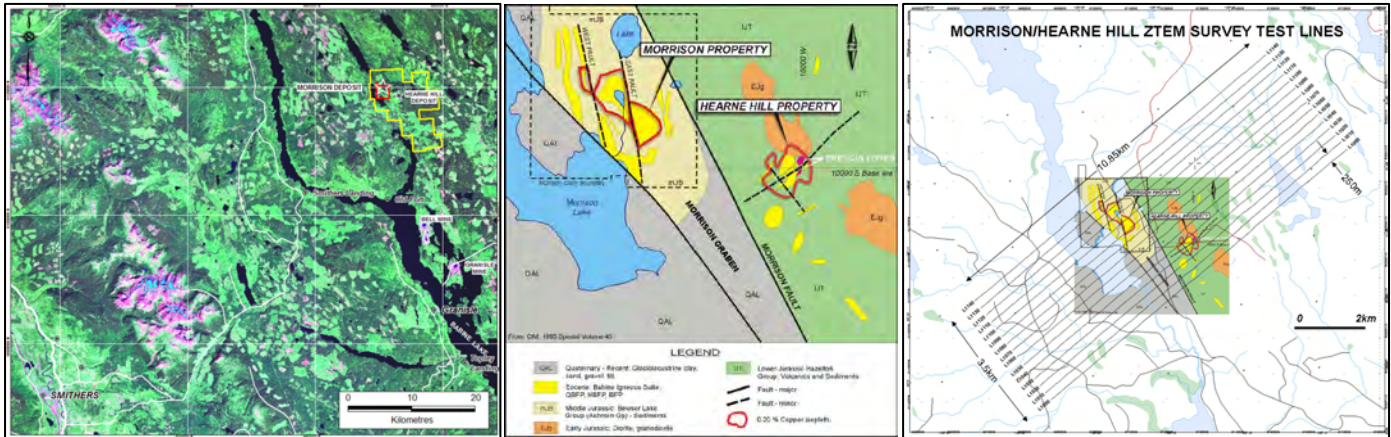
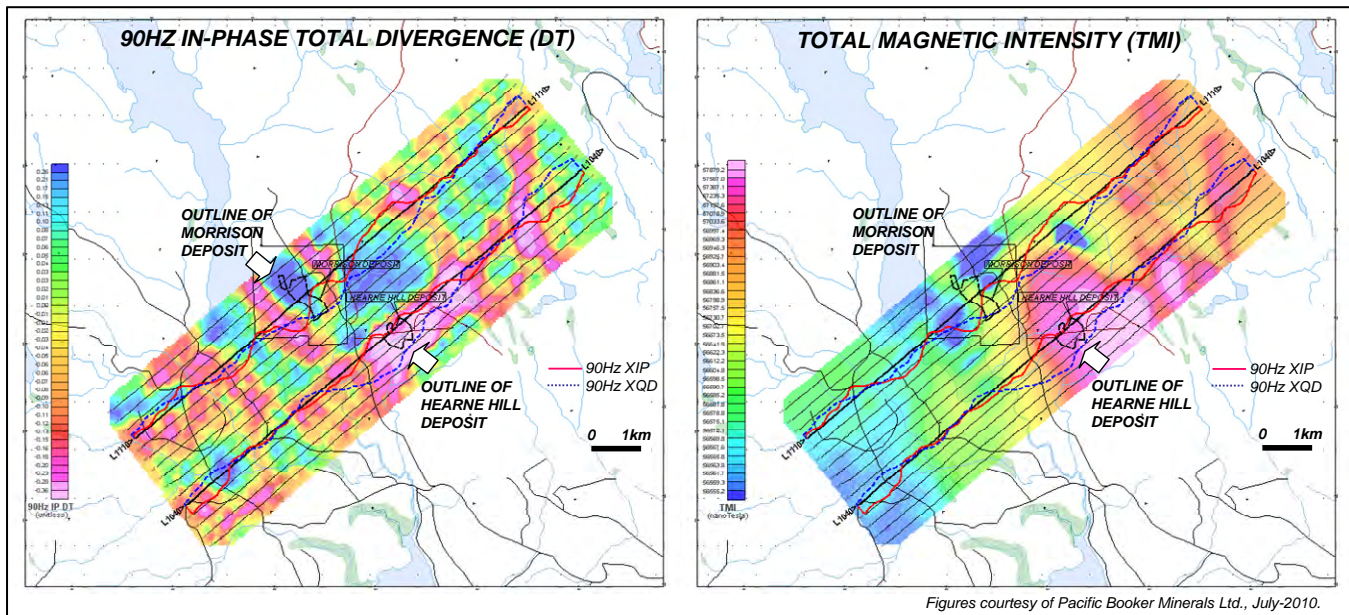


Figure 1: a) Morrison/Hearne Hill property location (left), b) general geology (center), c) ZTEM flight lines (right; modified after Robertson, 2009).

Deposit Geology

The Morrison deposit is classified as a calc-alkaline copper-gold porphyry, whose geologic settings and general style of hydrothermal alteration and mineralization are similar to other porphyry deposits in the northern Babine Lake area. Babine Lake is a well known and historically significant porphyry copper district that hosts dozens of deposits and occurrences, all spatially related to the Eocene Babine Intrusions, that include most notably the past-producing Granisle (152.7 Mt @ 0.47% Cu, 0.20 g/t Au) and Bell (77.2 Mt @ 0.47% Cu, 0.26 g/t Au) mines. The Hearne Hill deposit, which lies 2.0km southeast of Morrison, is a comparatively small but high grade copper-gold resource in two breccia pipes defined within a larger porphyry system and hosting an indicated resource (non 43-101 compliant) of 2.9 Mt @ 0.72% Cu and 0.23 g/t Au. The Morrison deposit contains a measured and indicated resource of 208.2 Mt averaging 0.39% Cu, 0.19 g/t Au and 0.005% Mo. It is currently at the advanced mine feasibility stage (Ref. J. Robertson, NI 43-101 report, Mar-2009).



Figures courtesy of Pacific Booker Minerals Ltd., July-2010.

Figure 2: ZTEM Tipper AFMAG field results shown in plan as grid contours of In-Phase Total Divergence (DT): a) 90Hz mid frequency IP DT showing resistivity contrasts (left) and b) Magnetic TMI image showing distributions of ferromagnetic minerals (right) and Morrison + Hearne Hill deposit outlines.

The Morrison property is situated on the northern edge of the Skeena Arch in a region underlain by volcanic, clastic, and epiclastic rocks ranging in age from the Lower Jurassic to Lower Cretaceous. The property geology is dominated by the 1.5-2km wide Morrison Graben that is NW-SE trending (Figure 1b) and hosts Mid Jurassic Ashman Formation siltstone, sandstone and greywacke sediments that are locally intruded by Eocene Babine Intrusions of biotite feldspar porphyry (BFP), quartz diorite and granodiorite. These rocks are down-faulted relative to older Lower Jurassic Hazleton volcanics and sediments to the east and west of the graben (Figure 1b). The copper-gold porphyry mineralization at Morrison is developed in a BFP plug and related dykes. The hydrothermal alteration at Morrison is concentrically zoned with a central potassic altered core surrounded by chlorite-carbonate zone. No well developed phyllic alteration has been identified at Morrison. Sulphides show strong relationships with underlying BFP plug, with the abundance of pyrite decreasing towards the center of the Morrison deposit along with 0.2% Cu associated with chalcopyrite. The deposit has been defined to below 400m depths (Figure 2) but remains open at depth, with the deepest mineralized drillhole depth of 700m below surface. A pyrite halo developed in the chlorite-carbonate altered wall rocks surrounds the copper zone and contains 5-15% pyrite down to 1-2% at the edges. The Morrison Fault is believed to dextrally disrupt the Morrison/Hearne Hill copper-gold porphyry system into two displaced bodies, 2.0 km apart, with the Morrison deposit representing the downward extension of the higher level Hearne Hill deposit. The Morrison deposit is also displaced by the East and West dextral on echelon faults (Ref. J. Robertson, NI 43-101 report, Mar-2009).

ZTEM System

The ZTEM survey instrumentation consists of a single vertical-dipole receiver coil (7.4m dia.) that is towed roughly 80m below the helicopter, at a 100m nominal flight height, and is flown over the survey area in a grid pattern, similar to other regional airborne surveys. Two orthogonal air-core horizontal axis coils (3.5m dia.) are placed close to the survey site to measure the horizontal EM reference fields. Data from the three coils are used to obtain the Z/X (In-line) and Z/Y (cross-line) AFMAG tipplers, whose transfer functions (In-Phase & Quadrature) are derived at five to six frequencies in the 30 to 720 Hz band. ZTEM tipper AFMAG is recognized for its unique ability to map resistivity contrasts associated with lithology, structure and particularly the alteration zones that are typically associated with porphyry copper and other similar deposits to great depths, exceeding 1-2km.

ZTEM Tipper AFMAG Results

Figure 2 presents the ZTEM survey results in plan, comparing the Total Divergence (DT) images (that convert the tipper cross-overs into peaks) of the In-Phase tipper data at 90Hz (left) and the Total Magnetic Intensity (TMI) responses (right), with the outline of the Morrison and Hearne Hill deposits overlain, as well as selected tipper profile data. In the DT image, warm colours represent conductive structures and contacts; cool colours represent more resistive units. The Morrison deposit is well defined in the 90Hz mid frequency DT data as a higher resistivity anomaly that is consistent with its potassic altered core. The DT resistivity high is in turn surrounded by a U-shaped lower resistivity border, which is normally consistent with the more conductive pyrite-rich alteration halo, but could otherwise also be due to fault-fracture structure associated with the Morrison Graben. The TMI image shows that the Morrison deposit is weakly magnetic, which is also consistent with the expected alteration in the core; the surrounding low magnetism matches the DT conductive zone and suggests magnetite-depletion associated with the pyrite halo. The Hearne Hill deposit occurs above a larger magnetic high, likely associated with an intrusive, and lies with a broad band of more conductive NE-trending rocks – possibly due to the breccia zones or a discordant fault/clay-alteration zone. Figure 3 presents the 2D cross-sectional resistivity data results obtained from the 2D inversion of the In-Line (Tx) ZTEM tipper data from the L1110 profile directly over Morrison deposit (Fig 2) using Geotech's proprietary Zvert2d code. The 2D inversion image defines a subcropping resistive body, consistent with the known potassic altered core, which gradually pinches below 500-750m depth that seems consistent with the known deposit geology. The Morrison high is flanked by 2 steeply conductive features that either possibly represent the pyritic alteration halos or more likely the faulted edges of the Morrison Graben.

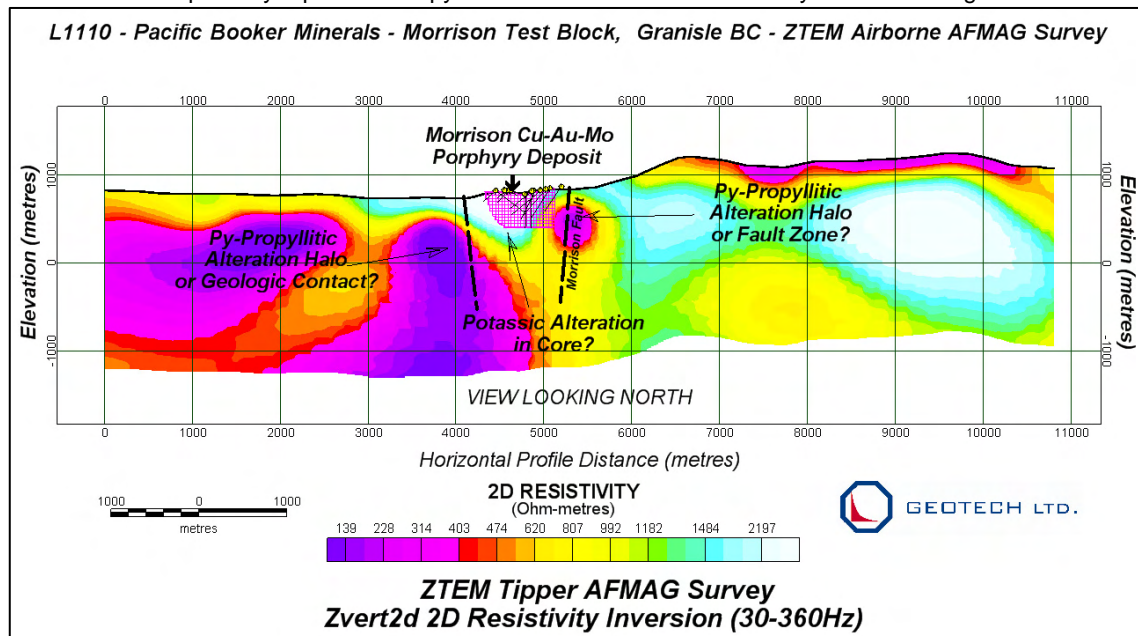


Figure 3: 2D Resistivity cross-section for L1110 over centre of Morrison Lake deposit from Zvert2d inversion of ZTEM In-line (Z/X) tipper data.

TRIBUTE MINERALS INC

&

THE RING OF FIRE

TBM IS AIRBORNE

Alexander Prikhodko-Geotech Ltd
March 2010

Tribute Minerals Inc

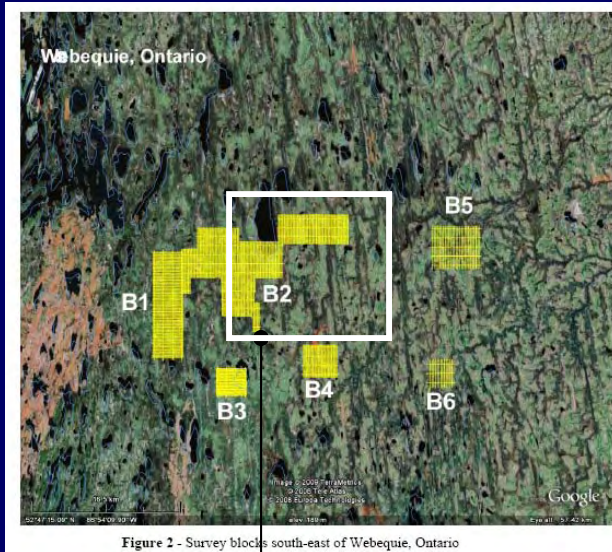
- 11 Z-TEM Surveys Covering Approx 68,000 Acres
- First Results over previously flown V-TEM on Block 2
- Excellent targets on best results from combined V & Z-TEM
- Sunday Anomaly to be Drilled early September
- Defining future targets on remaining 10 blocks – on going

Tribute Minerals Inc

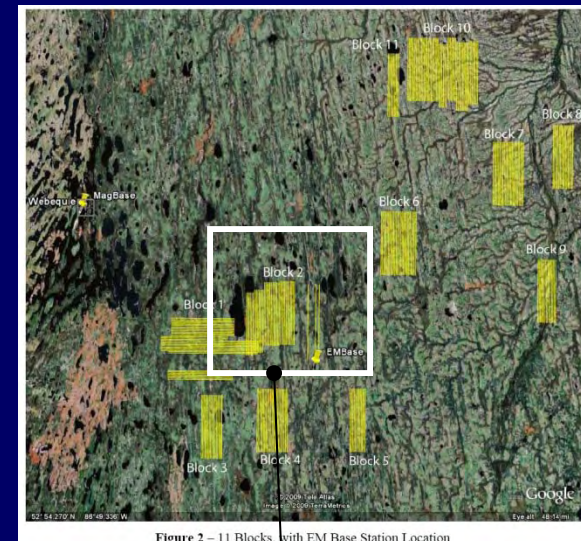
Target # 1 -Primary Selection
VTEM and ZTEM Results Over
Block 2 in the Ring of Fire

Current Focus on Block 2

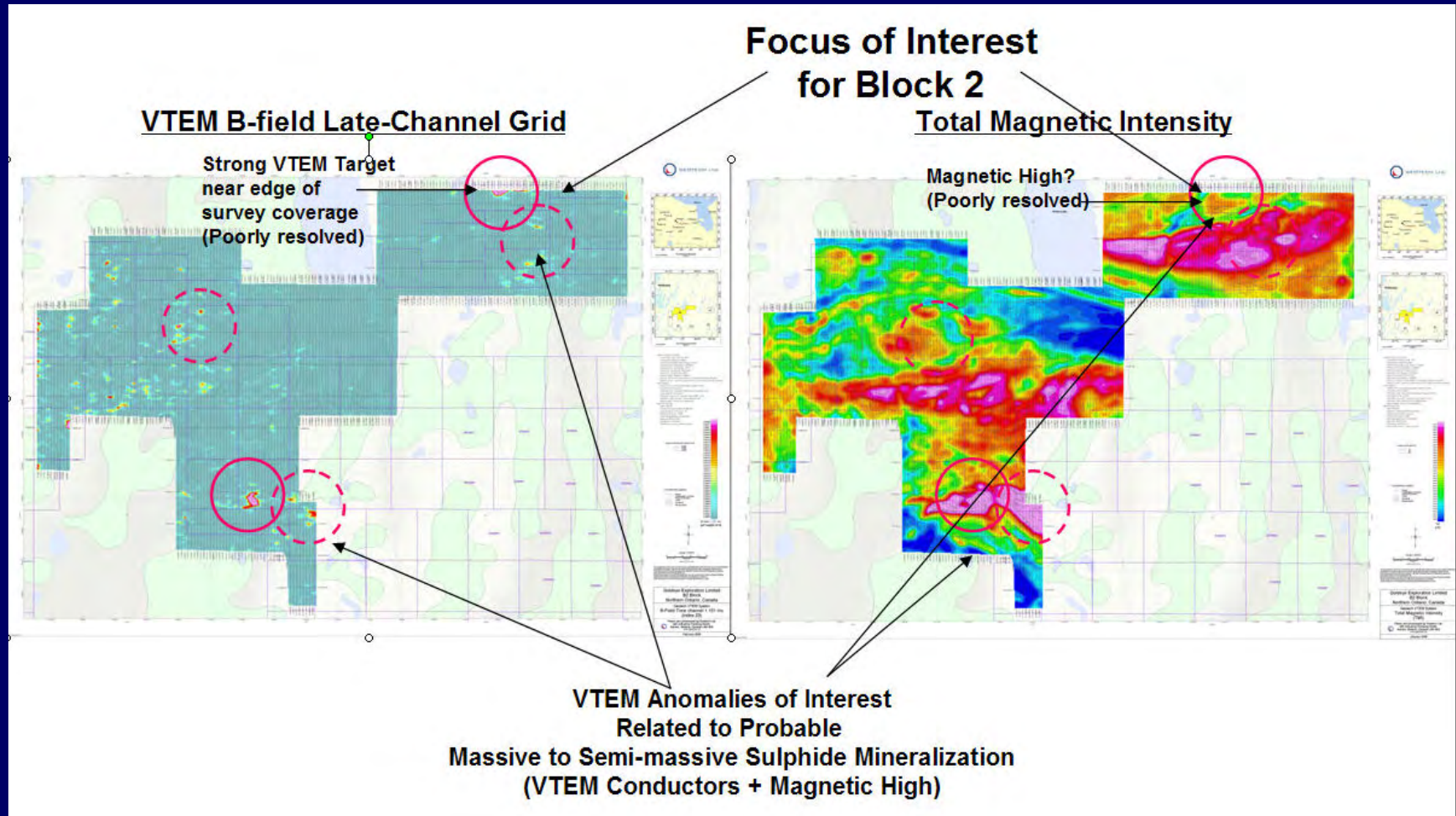
VTEM Survey March 2008
6 Blocks - 1860km flown



ZTEM Survey May-June 2009
11 Blocks - 2393km flown

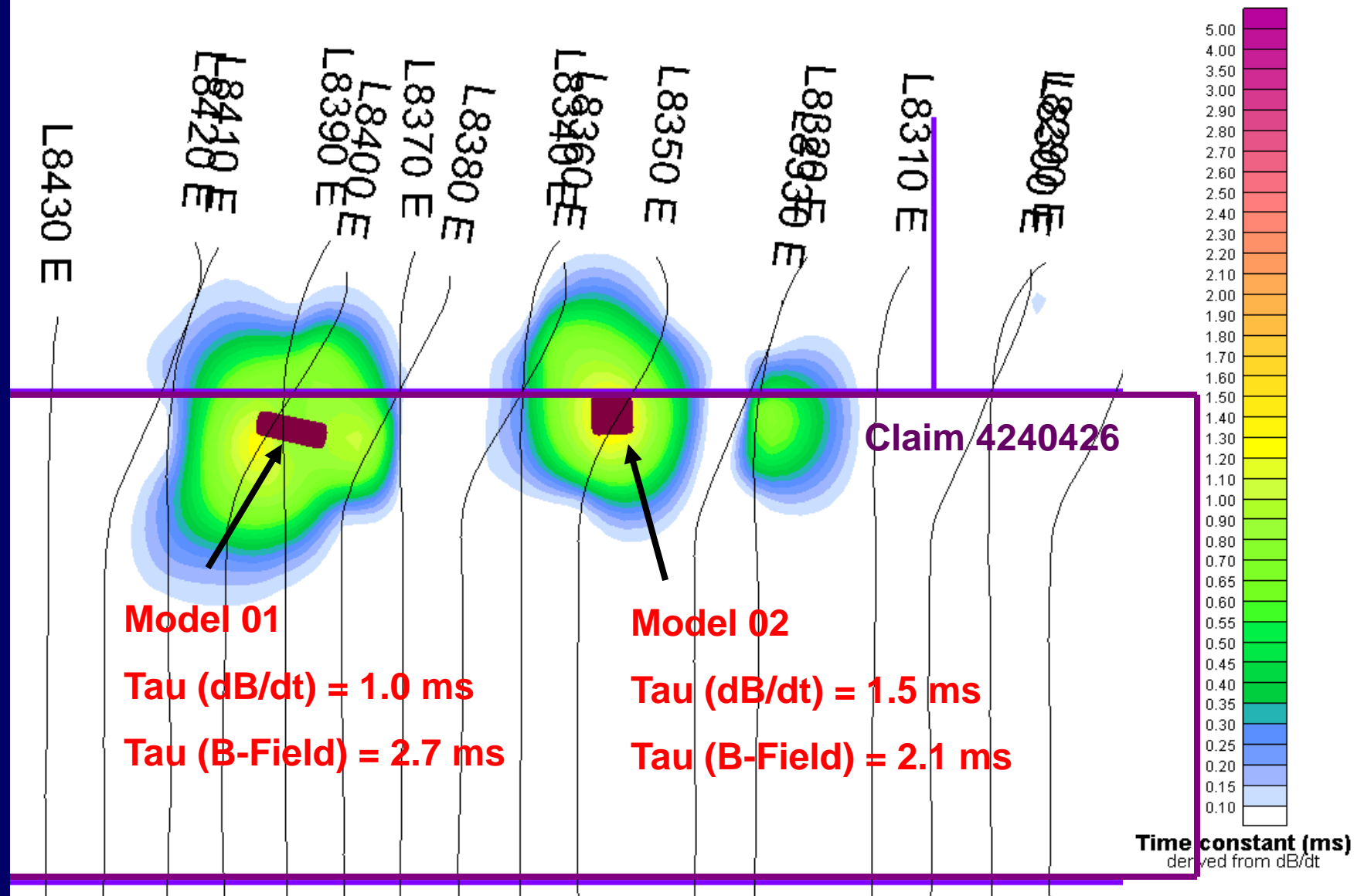


Zone of Interest in Block 2

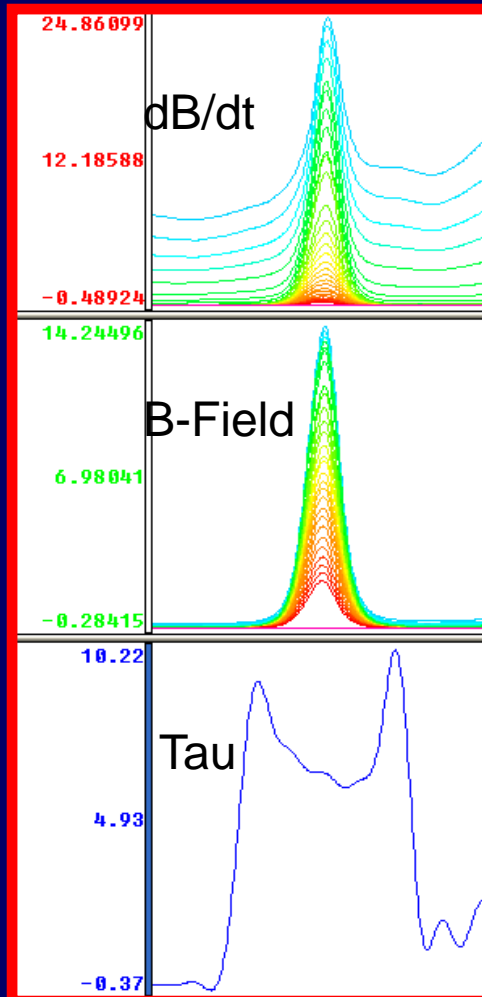


Extended VTEM survey lines

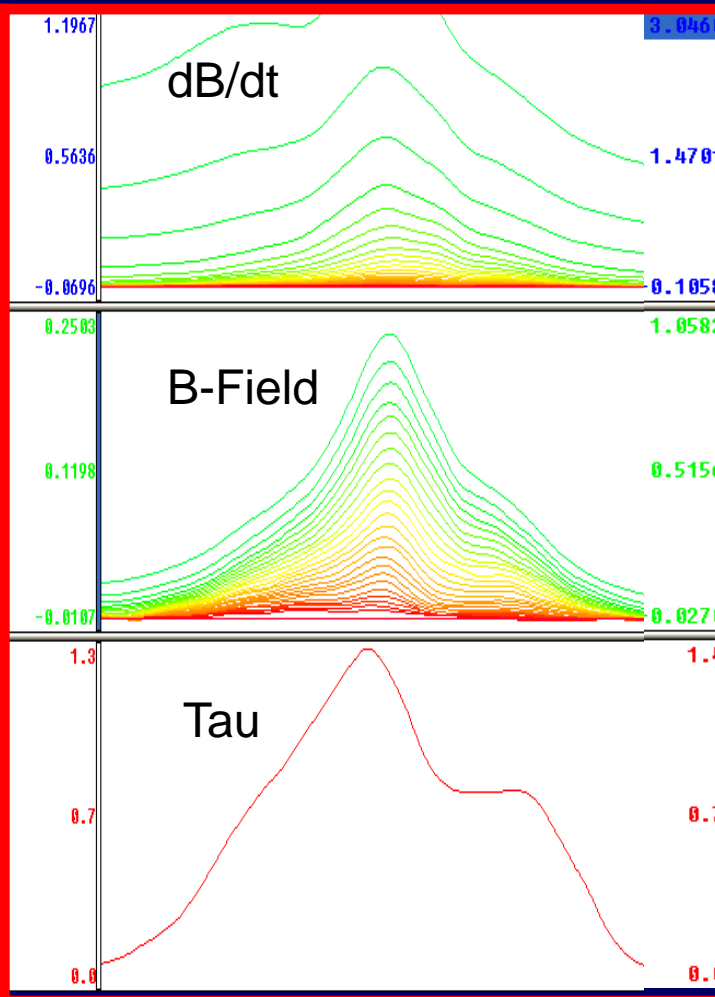
(Job 8045, block 2)



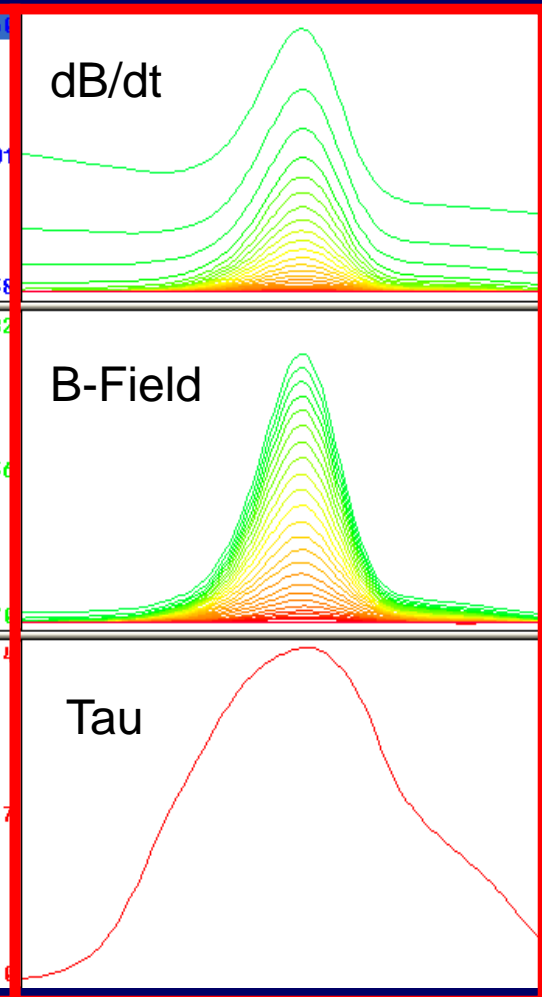
Eagle One



Anomaly 1



Anomaly 2

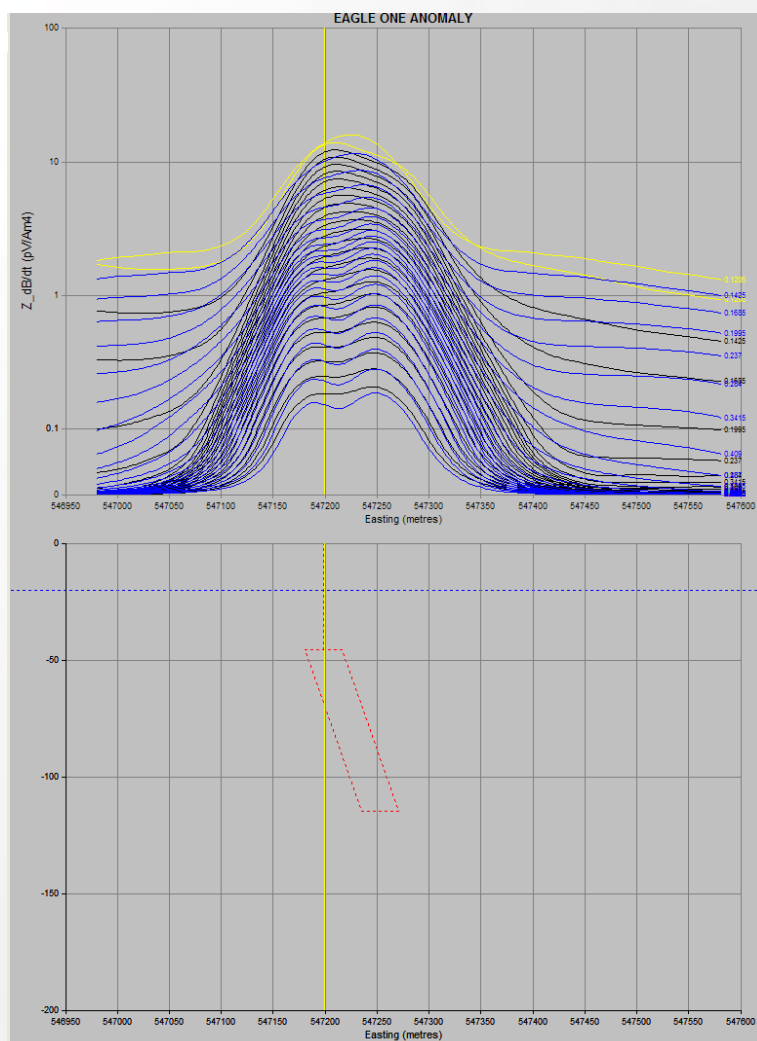




GEOTECH LTD.

AIRBORNE
GEOPHYSICAL
SURVEYS

GEOPHYSICAL SURVEYS



Noront's Maxwell Model Of Eagle One

Parameter	Maxwell Plates
Plate	Thick
Dip	50°
Depth	45.3
Location	$x=547198.5$ $y=5843595$
Conductance	452.9 S
Depth extent	90 m
Strike length	100 m
Half space res.	α
Overburden	Depth= 20 m Cond.= 1.5 S

Model 01, Flight Line 8400

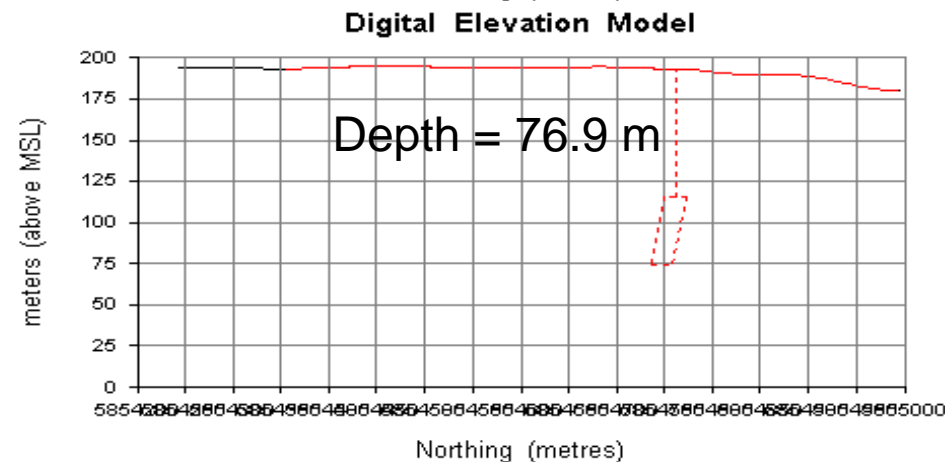
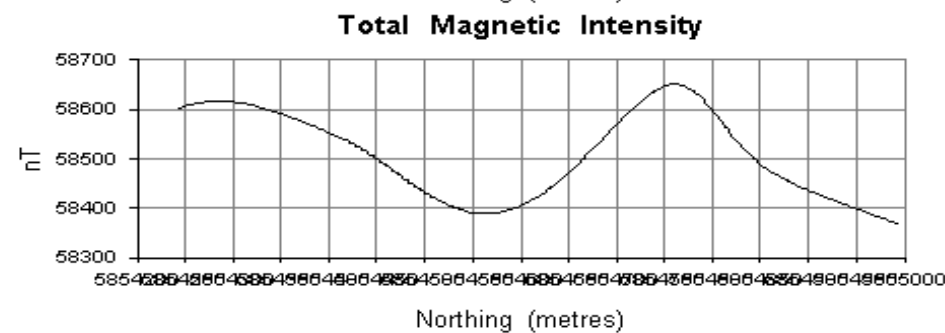
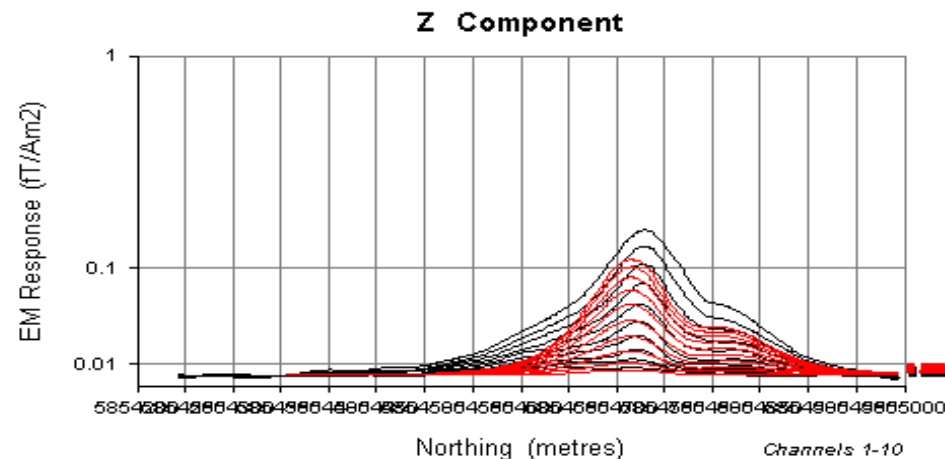


PLATE PARAMETERS

Name	Model01
X	506115
Y	5854750
Z	115.836
Length	100
Depth Extent	44.8679
Dip	69
Dip Dir.	192.1496
Plunge	0
Cond-Th.	585

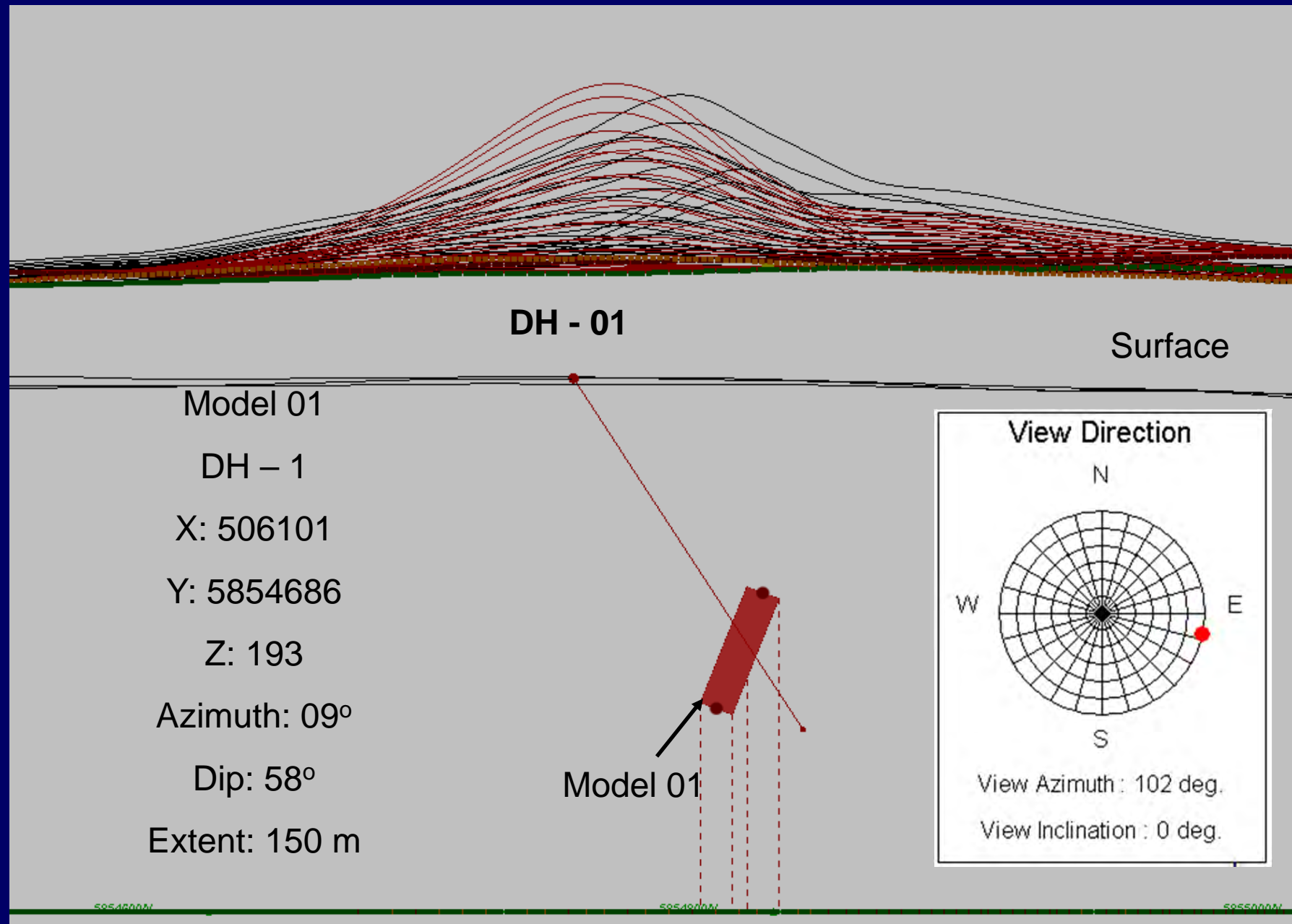
Electromagnetic Imaging Technology

James Bay Prospect
VTEM Survey
PROFILES OF
B-Field RESPONSE
Line L8400:14

Drawn : Geotech, Ltd

Job No. : 8045

Model 01 Suggested Drilling Parameters



Model 02, Flight Line 8400

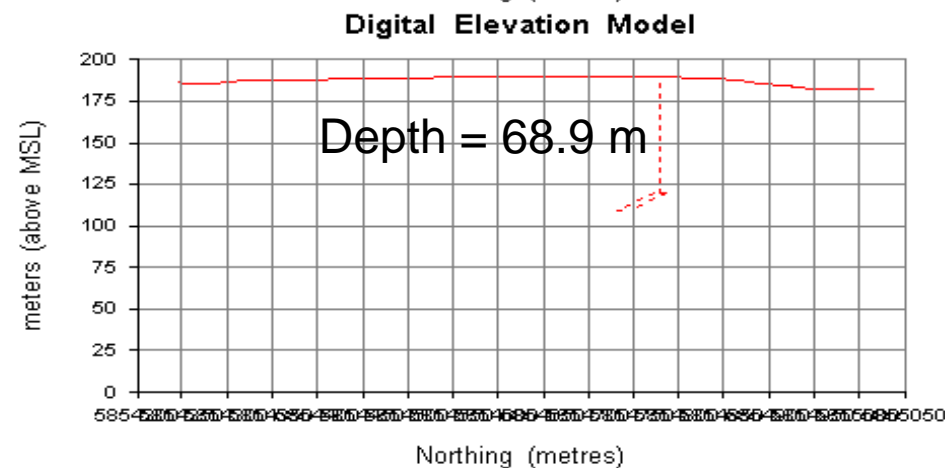
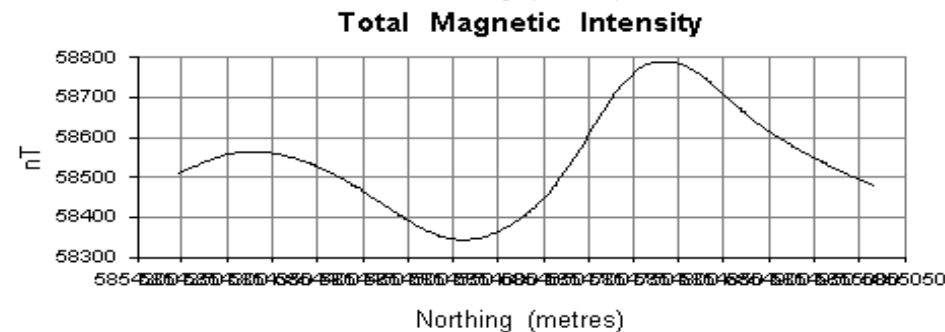
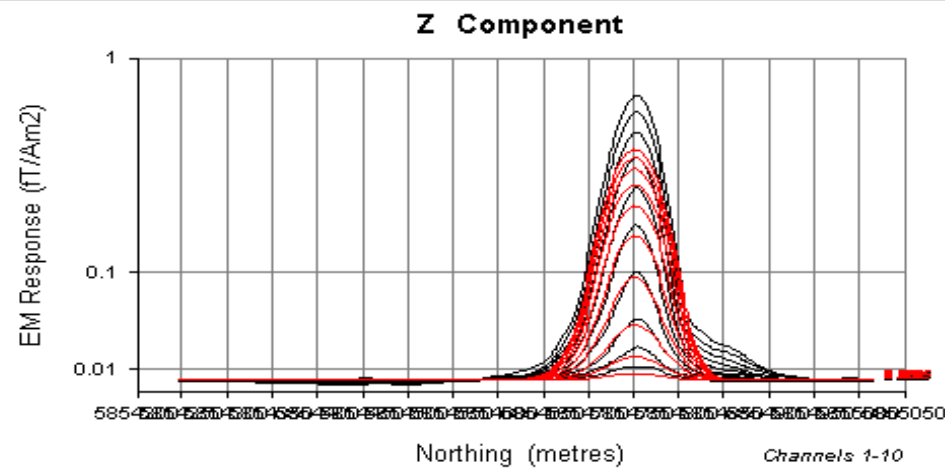


PLATE PARAMETERS

Name	Model02
X	506655
Y	5854785
Z	120
Length	50
Depth Extent	45.1036
Dip	14.7463
Dip Dir.	177.5
Plunge	0
Cond-Th.	400

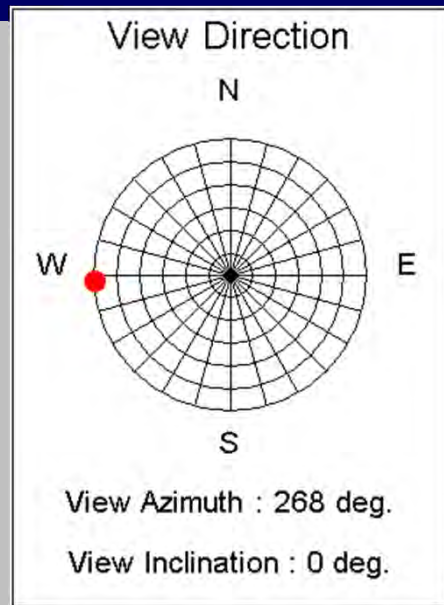
Electromagnetic Imaging Technology

James Bay Prospect
VTEM Survey
PROFILES OF
B-Field RESPONSE
Line L8350:14

Drawn : Geotech, Ltd

Job No. : 8045

Model 02 Suggested Drilling Parameters



Model 02

DH - 2

X: 506658

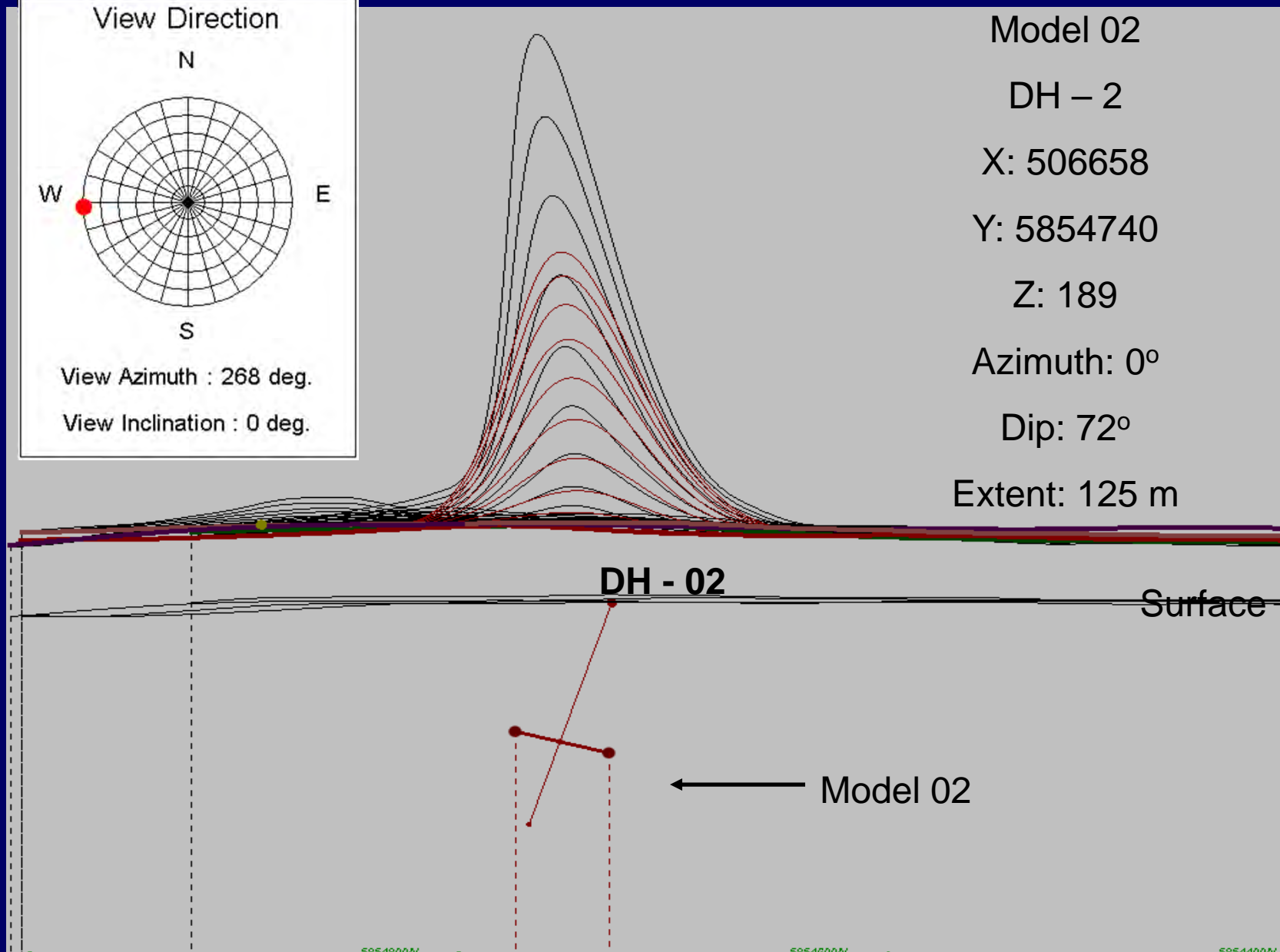
Y: 5854740

Z: 189

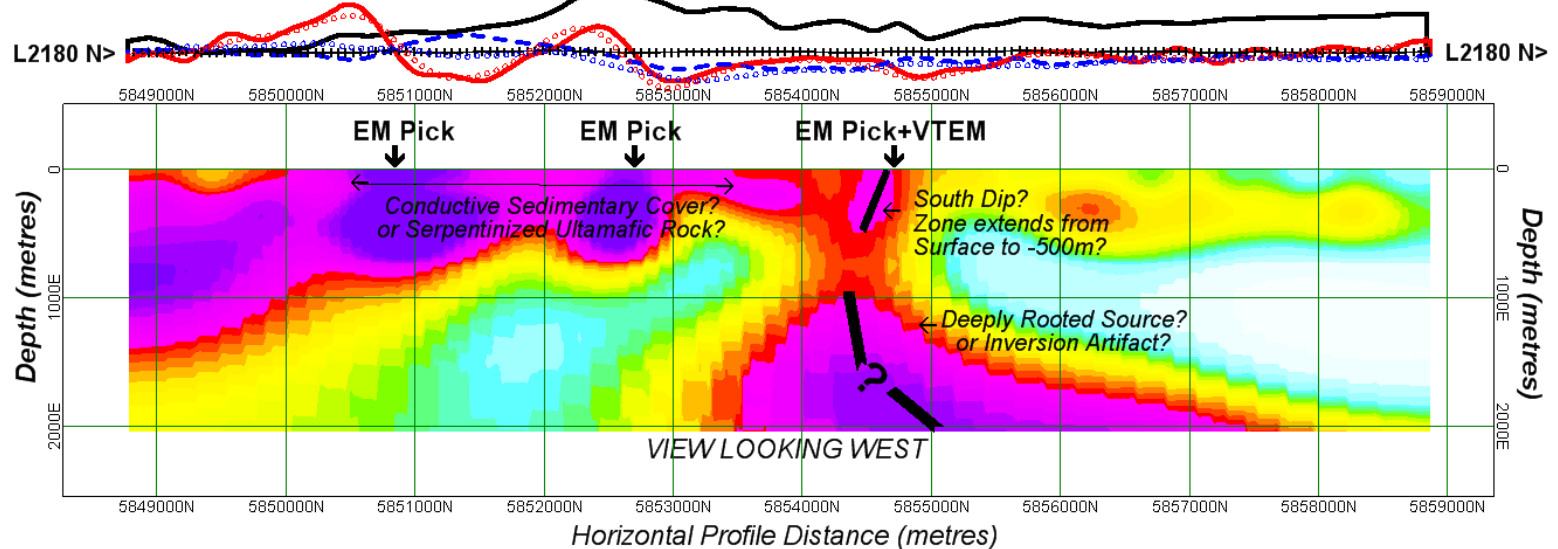
Azimuth: 0°

Dip: 72°

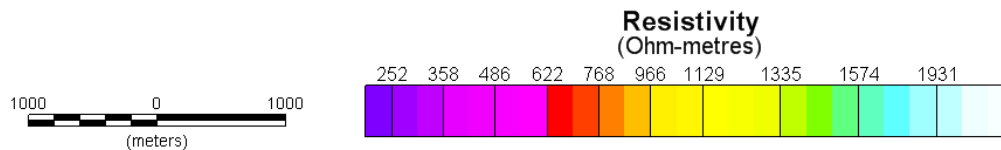
Extent: 125 m



L2180 - Tribute Minerals Inc. - Block 1, McFauld's Lake, ON - ZTEM Airborne AFMAG Survey



ZTEM Tipper AFMAG Survey
Zvert2d 2D Resistivity Inversion (30-720Hz)
over 360Hz Z/X In-Phase (red) Quadrature (blue) & Magnetic (black) Profiles
Observed Data = Curves / Calculated Data = Circles



9054 - TRIBUTE MINERALS INC. - BLOCK 1, McFAULD'S LAKE, ON - ZTEM TIPPER AFMAG SURVEY

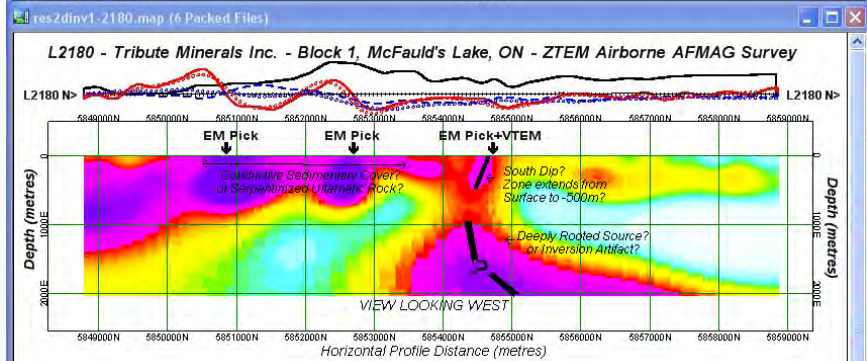
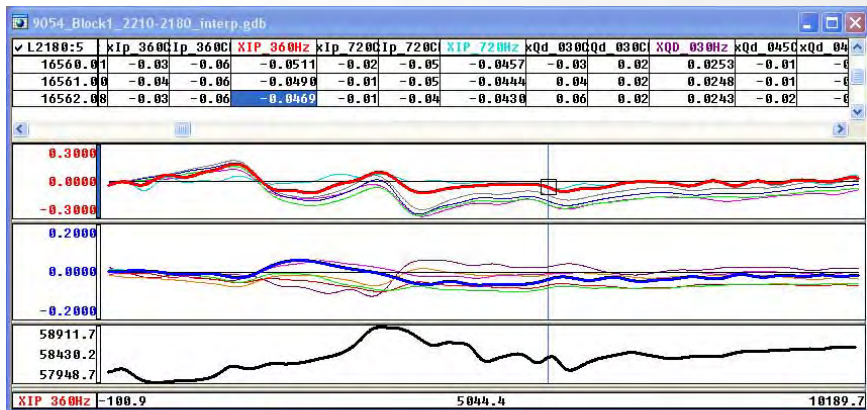
L2180 - Block 1 - 30-720Hz - Date: May-June, 2009

res2dinv1-2180.xyz (Distance-corrected + 2.5% IP&QD error; 0.91% RMS in 4 iters.)

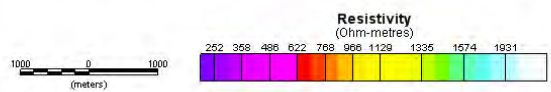


GEOTECH LTD. AIRBORNE GEOPHYSICAL SURVEYS

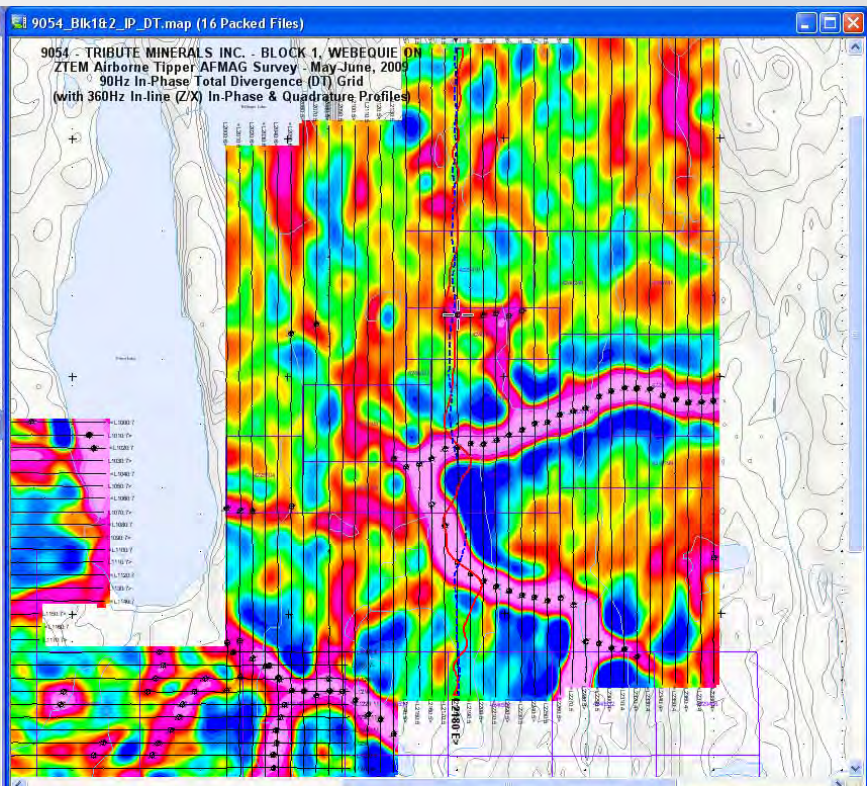
GEOPHYSICAL SURVEYS



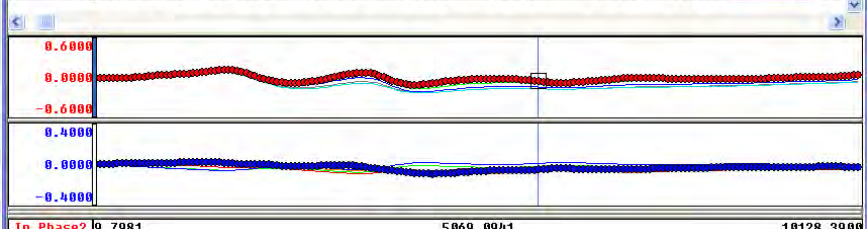
ZTEM Tipper AFMAG Survey
Zvert2d 2D Resistivity Inversion (30-720Hz)
over 360Hz Z/X In-Phase (red) Quadrature (blue) & Magnetic (black) Profiles
Observed Data = Curves / Calculated Data = Circles



9054 - TRIBUTE MINERALS INC. - BLOCK 1, McFAULD'S LAKE, ON - ZTEM TIPPER AFMAG SURVEY
L2180 - Block 1 - 30-720Hz - Date: May-June, 2009
res2dinv1-2180.xyz (Distance-corrected + 2.5% IP&QD error, 0.91% RMS in 4 iters.)



97.0	5854506.81	81.5000	151.50	720.0000	-0.0288	-0.0366	360.0000	-0.0444
98.0	5854565.48	83.3000	153.30	720.0000	-0.0372	-0.0357	360.0000	-0.0519
99.0	5854624.14	84.6000	154.60	720.0000	-0.0464	-0.0342	360.0000	-0.0599

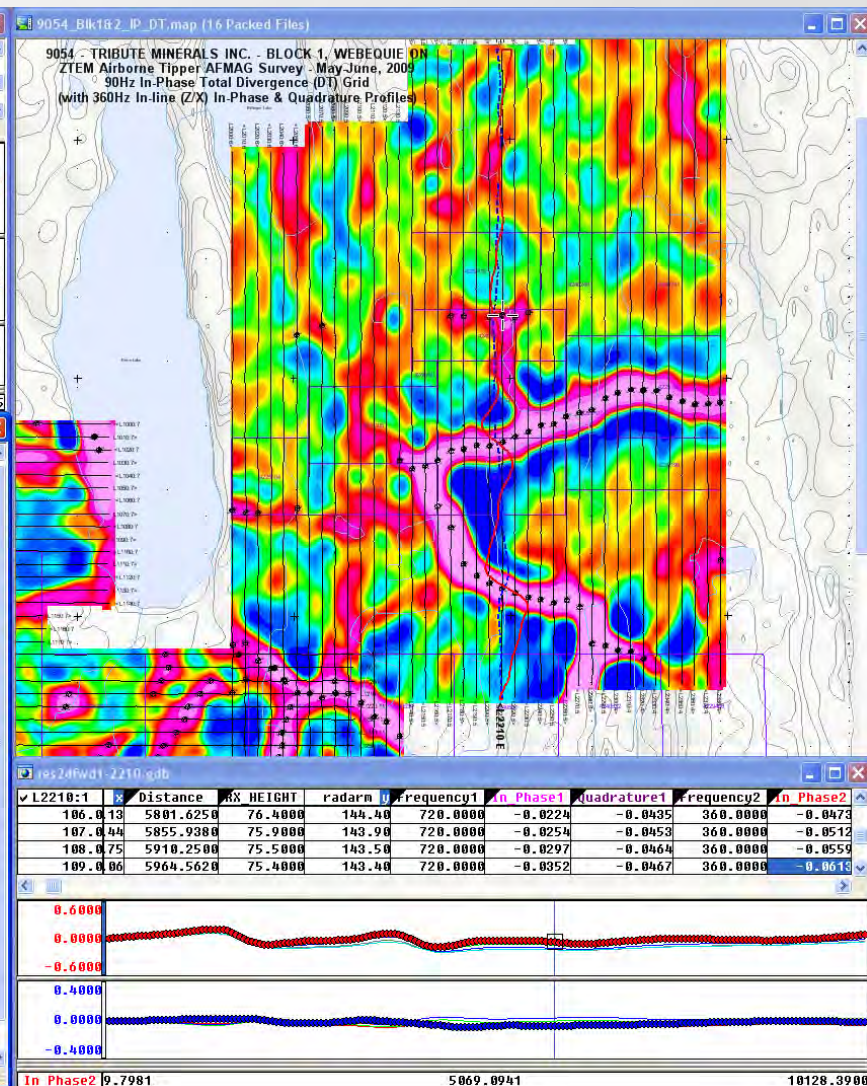
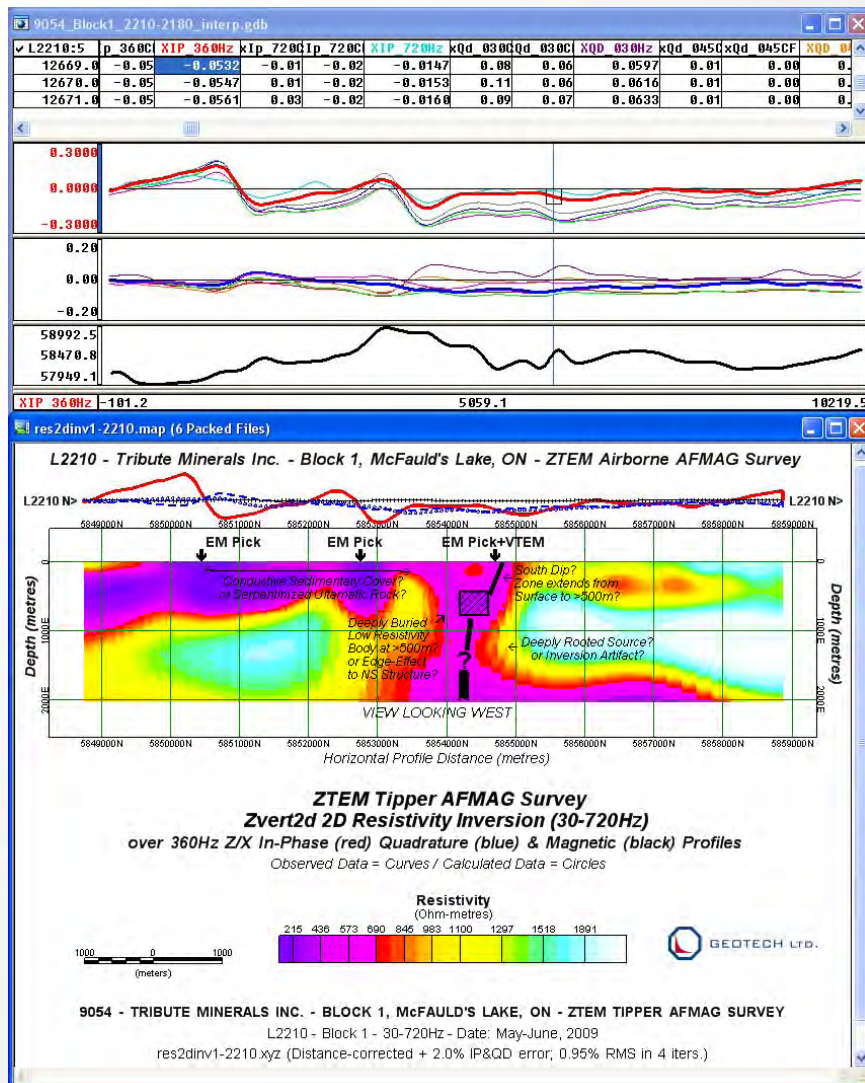




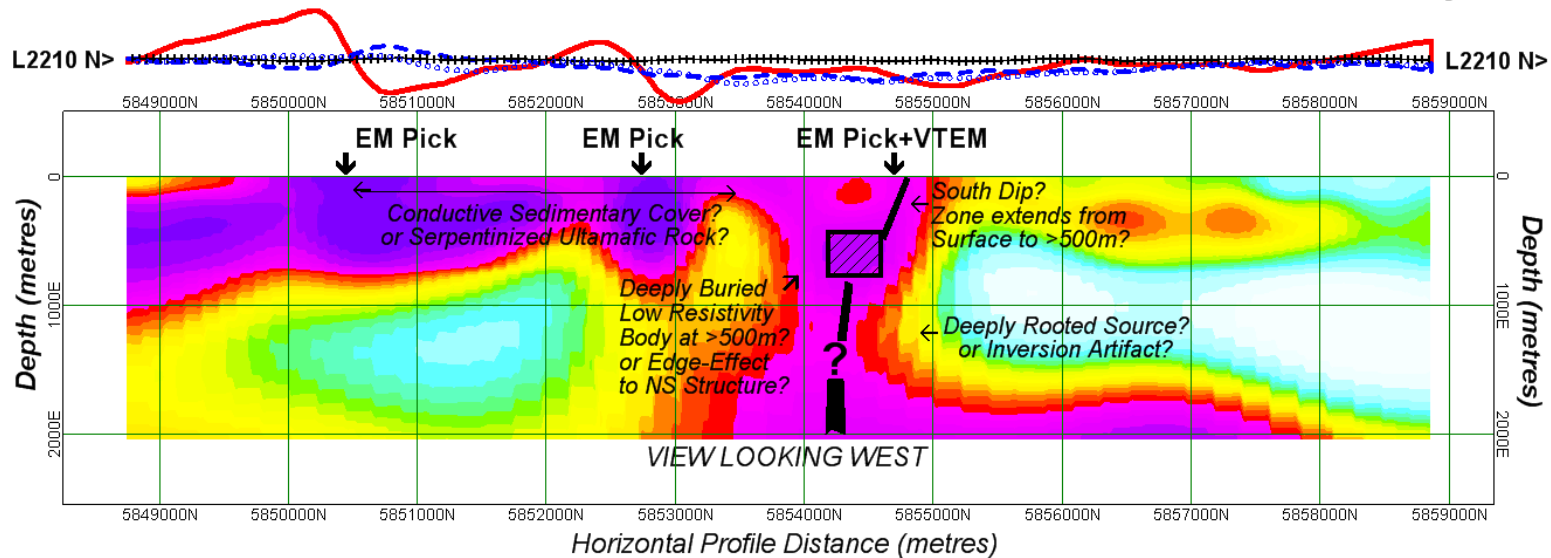
GEOTECH LTD.

AIRBORNE GEOPHYSICAL SURVEYS

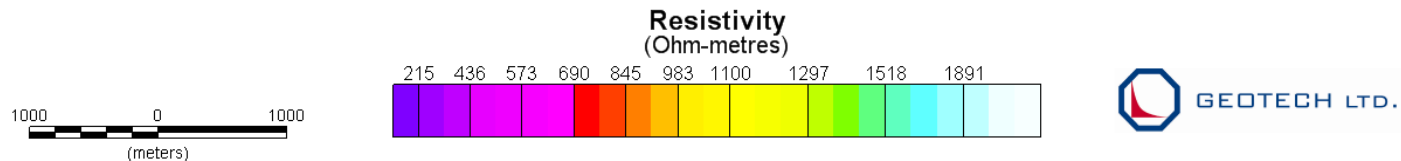
GEOPHYSICAL SURVEYS



L2210 - Tribute Minerals Inc. - Block 1, McFauld's Lake, ON - ZTEM Airborne AFMAG Survey



ZTEM Tipper AFMAG Survey
Zvert2d 2D Resistivity Inversion (30-720Hz)
over 360Hz Z/X In-Phase (red) Quadrature (blue) & Magnetic (black) Profiles
Observed Data = Curves / Calculated Data = Circles



9054 - TRIBUTE MINERALS INC. - BLOCK 1, McFAULD'S LAKE, ON - ZTEM TIPPER AFMAG SURVEY

L2210 - Block 1 - 30-720Hz - Date: May-June, 2009

res2dinv1-2210.xyz (Distance-corrected + 2.0% IP&QD error; 0.95% RMS in 4 iters.)

AN ASSESSMENT OF VTEM AND ZTEM DATA OVER THE POZO SECO SKARN-CRD MOLYBDENUM-GOLD DEPOSIT, MEXICO

Ken Witherly
 Condor Consulting, Inc.
 Lakewood, CO, USA
ken@condorconsult.com

SUMMARY

In the present study the results from two airborne EM surveys over the two CRD deposits. Both EM provide information about the conductive and resistive zones associated with the mineralization. In the case of the economically significant Pozo Seco deposit, both EM systems produced a strong conductive response directly below the actual zone of mineralization, which appears to lie along a major fault zone. Results over the associated José Manto zone were less clear in either EM system but showed a strong IP anomaly.

Key words: airborne EM, VTEM, ZTEM, Skarn-CRD, inversion

INTRODUCTION

Airborne EM (AEM) techniques have been used to search for a variety of mineral deposit styles since the inception of the technology in the late 1940s. However, the application of AEM technology to the search for Carbonate Replacement Deposits (CRD) is relatively new. CRD style occurrences are an important class of economic deposit commonly found in northern Mexico and AEM technology is now being applied to assist in the location and definition of these deposits. In this study, the initial results of application of two AEM techniques to the Pozo Seco CRD deposit located on the Cinco de Mayo property owned by MAG Silver Corp. in northern Chihuahua State, Mexico will be examined.

POZO SECO DEPOSIT

The Pozo Seco deposit was located by MAG Silver in their Cinco de Mayo project area in 2009. Earlier exploration in the area (Robertson and Megaw 2009) had located significant silver, lead and zinc mineralization at the José Manto property approximately 5 km to the NNE. A geological map of the Pozo Seco area is shown in Figure 1¹ and a conceptual cross-section in Figure 2. This section shows the observed variety of different mineralization styles associated with the intrusive system. MAG Silver is continuing to drill off the Pozo Seco discovery and a significant resource of molybdenum and gold has been defined.

AIRBORNE EM SURVEYS

Two AEM systems provided by Geotech Ltd were flown over the Pozo Seco area; VTEM and ZTEM. VTEM is a helicopter borne time domain EM technology (Witherly et al 2004) and ZTEM is as well a helicopter based system that is relatively new adaptation (Kuzmin et al) of Afmag technology first applied to airborne surveying in the 1950s.

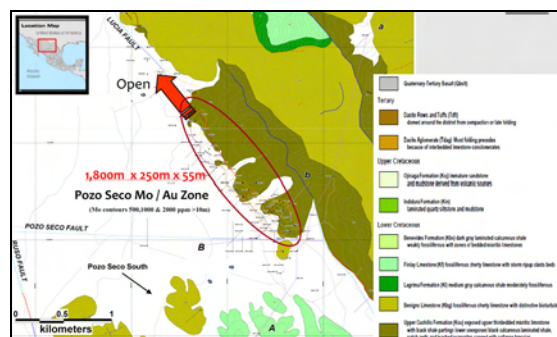


Figure 1: Local geology at Pozo Seco deposit (from MAG Silver).

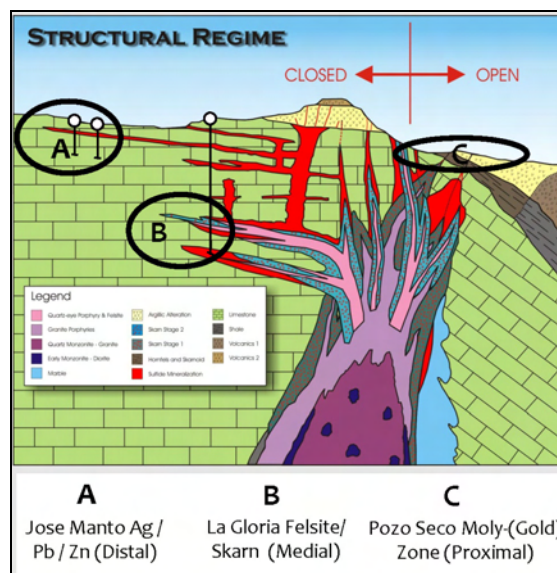


Figure 2: Cross-section (looking south) showing styles of mineralization found in Cinco de Mayo area (from MAG Silver).

Figure 3 shows the location of the two surveys with respect to Pozo Seco deposit and José Manto zone. Over the José Manto zone, the client had acquired IP-resistivity data which were also used in this assessment.

DATA PROCESSING

The two EM data sets were processed using proprietary codes; a layered earth inversion code LEI-1 on the VTEM data and a 2D Occam on the ZTEM (Sattel et al 2010). These codes provide a depth conductance section from the line data. In addition, grid based products were generated for both surveys. Contractor provided products were as well assessed and some of these outcomes are provided in this assessment.

¹ Derived from the MAG Silver web site: www.magsilver.com

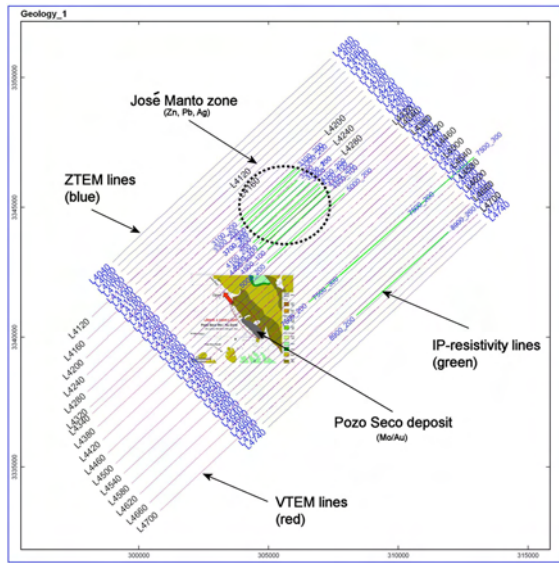


Figure 3: Flight path of VTEM and ZTEM over Pozo Seco deposit.

OUTCOMES

VTEM: Figure 4 shows the basic magnetic and EM outcomes. The locations of the Pozo Seco deposit and José Manto zone are shown as well.

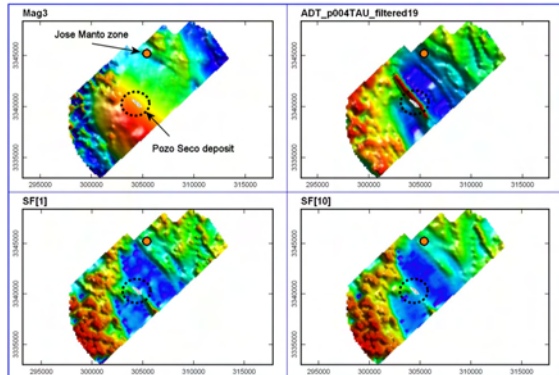


Figure 4: VTEM magnetic and EM outcomes.

The magnetic results show the Pozo Seco deposit to lie along the eastern flank of a large NW-trending high. This feature is believed to be a deep-seated intrusive body. The José Manto zone appears to lie along a fault contact. The EM outcomes are derived from the dB/dT results and show channels 1 and 10 as well as AdTau (time constant) outcomes. These results are all fairly similar and show alternating bands of high and low conductivity that are believed to likely represent different lithologies. The conductive zones are thought likely to be altered sediments. The Pozo Seco deposit lies along a distinctive narrow conductive feature that separates two zones of low conductivity that reflect silicified breccias as well as unaltered limestone and shales. There is some complexity in this linear feature that could be a reflection of secondary structure which is related to the occurrence of the deposit.

Figure 5 shows the depth slices from the EM inversion model from basically at surface to ~200 m depth along with the client-provided geology map for the Pozo Seco area.

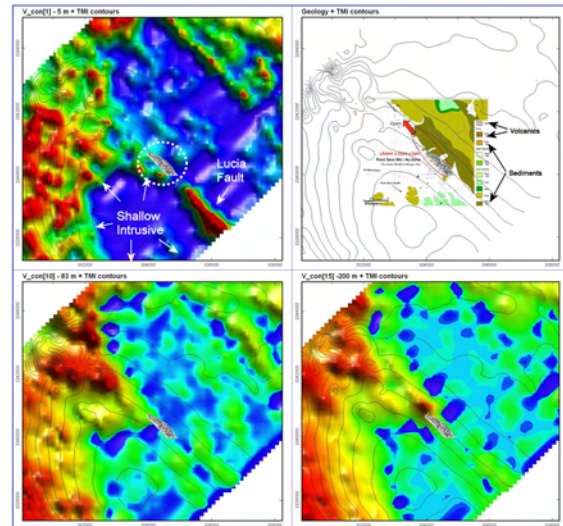


Figure 5: LEI depth slices with TMI (contours) around Pozo Seco deposit.

Referring first to the shallowest depth slice, the deposit is located along the Santa Lucia fault structure that the EM shows to be a complex feature. Just south of the deposit there is a gap in the EM expression of the fault and then further to the SE, the fault appears with a much stronger response than noted elsewhere. However, in the deeper depth slices, this strong SE extension of the fault zone is not apparent. Referring again to the shallowest depth slice, to the west of the deposit, there is an embayment of low conductivity that closely matches the contours of the magnetic high (suspect intrusive). Mapping in the area only shows limestone to be present but this is deemed to be a fairly thin veneer overtop of the intrusive.

Figure 6 shows the VTEM conductivity depth response in section along with an outline of the deposit and the geological section “B-b”.

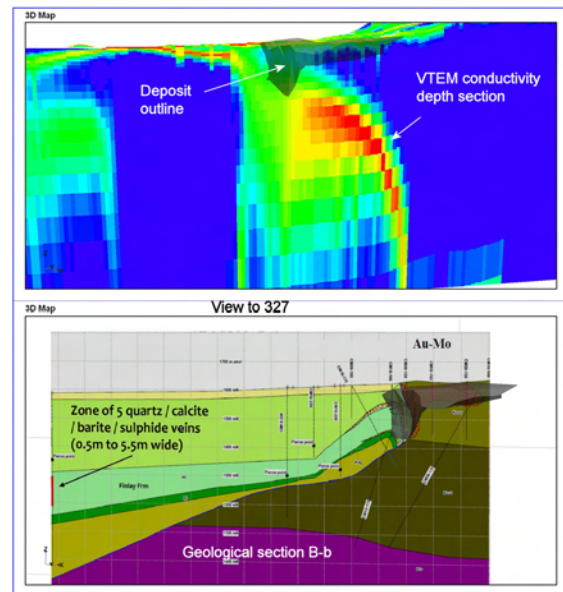


Figure 6: VTEM conductivity depth section, ore deposit and geological section “B-b”.

This shows the deposit to be shallower than the EM response. The deposit itself appears to be located at the overturned fold-nose of a thrust fault dipping to the west. The source of the EM response is unclear but the correlation with a mapped fault suggests that mineralization hosted along the fault structure is causing the VTEM response. An assessment of the VTEM by the survey company showed there to be a very long, single axis conductor associated with the fault. While this shows considerable lateral consistency, the depth slices through the conductivity model show that there is considerable variability of conductivity with depth.

ZTEM: As shown in Figure 3, the ZTEM coverage was slightly off-set from the VTEM. Figure 7 shows the apparent conductance or AppCon (Sattel et al 2010) for the five frequencies the ZTEM operated at. Figure 8 is the same themes but enlarged around the area of the Pozo Seco deposit. This product provides an image of the conductance with the geometric effects of the system removed (cross-over's become peaks).

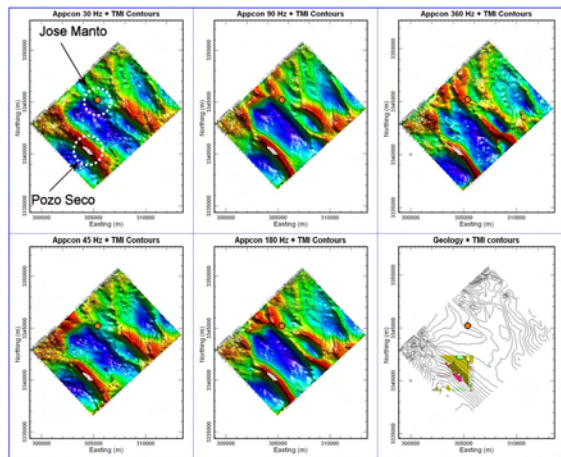


Figure 7: ZTEM AppCon outcomes.

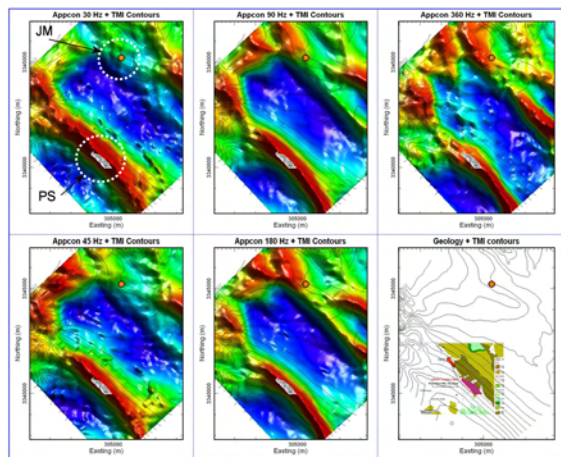


Figure 8: AppCon outcomes focused around Pozo Seco.

These outcomes look similar to the VTEM but with some differences. The two large areas of low conductivity appear in both outcomes. However, the conductivity structure Pozo Seco is hosted along appears more continuous in the ZTEM than the VTEM results, which indicated where there was a gap in the structure just south of the deposit.

Another means to compare the two surveys is through the depth inversion models shown in Figure 9. Here three conductivity slices of roughly equivalent depth are shown for the two surveys.

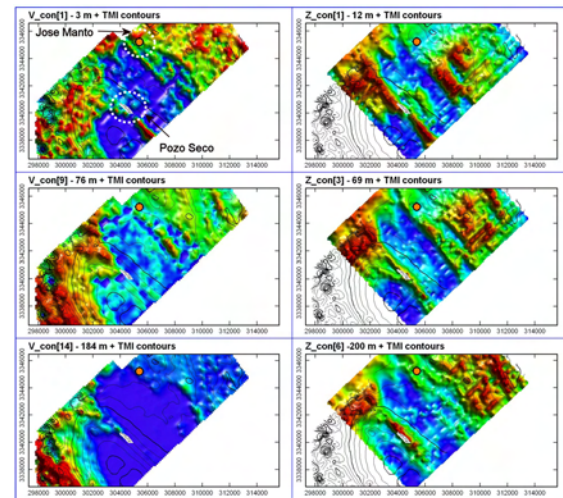


Figure 9: VTEM and ZTEM conductivity depth slices.

In this result, the two shallowest slices both show a gap in the linear conductor, interpreted fault that the deposit lies on. In deeper slices, on the VTEM the structure disappears whereas in the ZTEM the linear persists but without the gap. The significance of the gap regards the formation or location of the deposit is unclear but for this style of deposit, structure is deemed important in providing conduits for mineralizing fluids and barriers that result in solutions being trapped.

Figure 10 shows the ZTEM depth section in perspective that is closest to the geological section B-b; the deposit is shown as well. As with the VTEM results shown in Figure 6, the bulk of the conductivity response is located below the actual deposit, suggesting the ZTEM as well is responding to some aspect of the mineral system and not the economic mineralization directly.

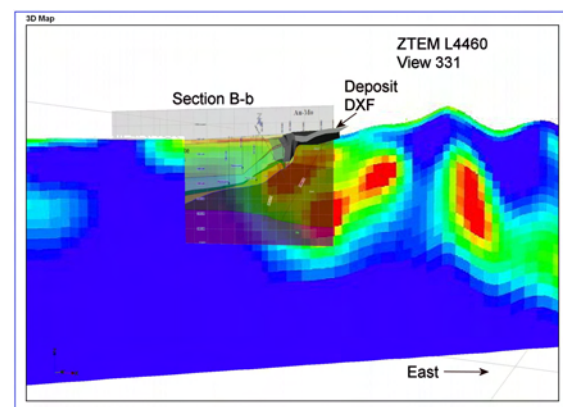


Figure 10: ZTEM L4460 depth section with geological section B-b and deposit outline.

Figure 11 shows a comparison between the VTEM and ZTEM depth sections. Both outcomes show a strong response directly under the deposit but the ZTEM also shows a major conductive zone dipping to the east. Given the

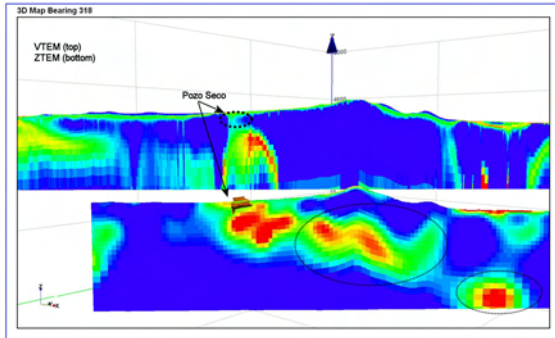


Figure 11: VTEM and ZTEM depth section over Pozo Seco (for L4500).

resistive nature of the geology for the most part, the VTEM would be expected to detect a significant conductor where the ZTEM is responding. The inference then is that the ZTEM is more likely responding to a geological contact where there is enough of a resistivity gradient to promote a strong currently channelling effect.

Over the José Manto zone, IP-resistivity was run to try and better define the mineralization. Figure 12 shows the results of the IP-DC resistivity, ZTEM and VTEM in the vicinity of the deposit. Given the processing formats available for the IP results, the ZTEM conductivity has been inverted to conform to the convention of the DC-resistivity where the more resistive parts of the model was warm colors. The VTEM has been left as normally displayed (more conductive zones warmer colors).

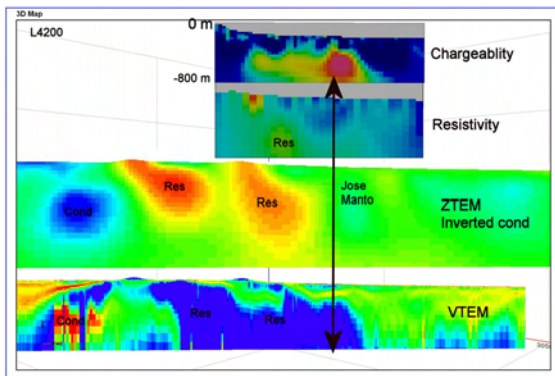


Figure 12: Results over José Manto; IP chargeability, DC-resistivity, ZTEM and VTEM.

These results indicate that the style of mineralization at the José Manto zone is more amenable to being detected as a chargeability feature rather than resistivity. On the VTEM and ZTEM results, they show a reasonable coincidence of both resistive and conductive zones across the section. The ZTEM appears to give a somewhat enhanced response to the resistive zones whereas the VTEM outcome appears more diagnostic with respect to the conductive zones. The DC resistivity and ZTEM show a reasonable agreement as well. The VTEM shows considerably more thin horizontal conductivity than the ZTEM; this could be a function of the higher frequency content of the VTEM mapping the near surface with more detail. Also, the Afmag technique is inherently insensitive to horizontal conductivity; hence less information about layered conductors is expected.

Figure 13 shows a composite of four themes over the José Manto deposit area. As noted earlier this style of mineralization is different than Pozo Seco. The area of mineralization is close to a small magnetic high, deemed likely to be a shallow intrusive. The VTEM and ZTEM first depth slice is shown and suggests the deposit is near (just east) of a contact and possible fault. Some possible levelling issues are noted in the ZTEM data with an apparent resistive zone trending parallel to the flight lines noted.

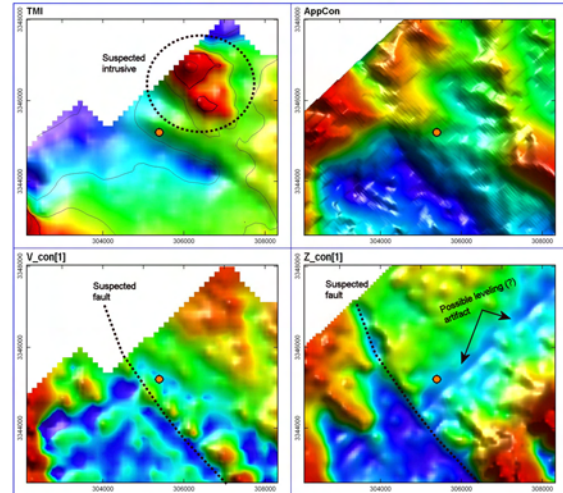


Figure 13: Geophysical responses in vicinity of José Manto.

CONCLUSIONS

In the present study, VTEM and ZTEM data over two major zones of mineralization; one a classic CRD and the other an intrusive related Mo/Au deposit have been examined. The ZTEM outcomes appear to provide superior results at mapping resistive zones in terms of spatial resolution. Also, the ZTEM appears to be defining conductive zones deeper than VTEM (Figure 11); this outcome is surprising and forward modeling of the ZTEM defined conductivity model for the VTEM system is planned to validate this result. Good agreement was observed between the DC resistivity results and ZTEM. Again, forward modeling of the ZTEM conductivity model for the DC resistivity solution would be a useful means to validate these results.

ACKNOWLEDGMENTS

Condor Consulting, Inc. wishes to express thanks to MAG Silver Corporation and Mr. Ken Robertson for the opportunity to present the outcomes shown here.

REFERENCES

- Kuzmin, P., Lo, B., and Morrison, E. 2005, Final Report on modeling, interpretation methods and field trials of an existing prototype AFMAG system, Misc Data Release 167, Ontario Geol. Survey.
- Robertson, K. and Megaw, P., 2009 Cinco de Mayo: A new silver, lead, and zinc discovery in northern Mexico; Leading Edge June 2009 p. 730-734
- Sattel, D., Witherly, K., and Becken, M., 2010, A brief analysis of ZTEM data from the Forrestania test site, WA; Preview Number 147; 2010 Conference Handbook

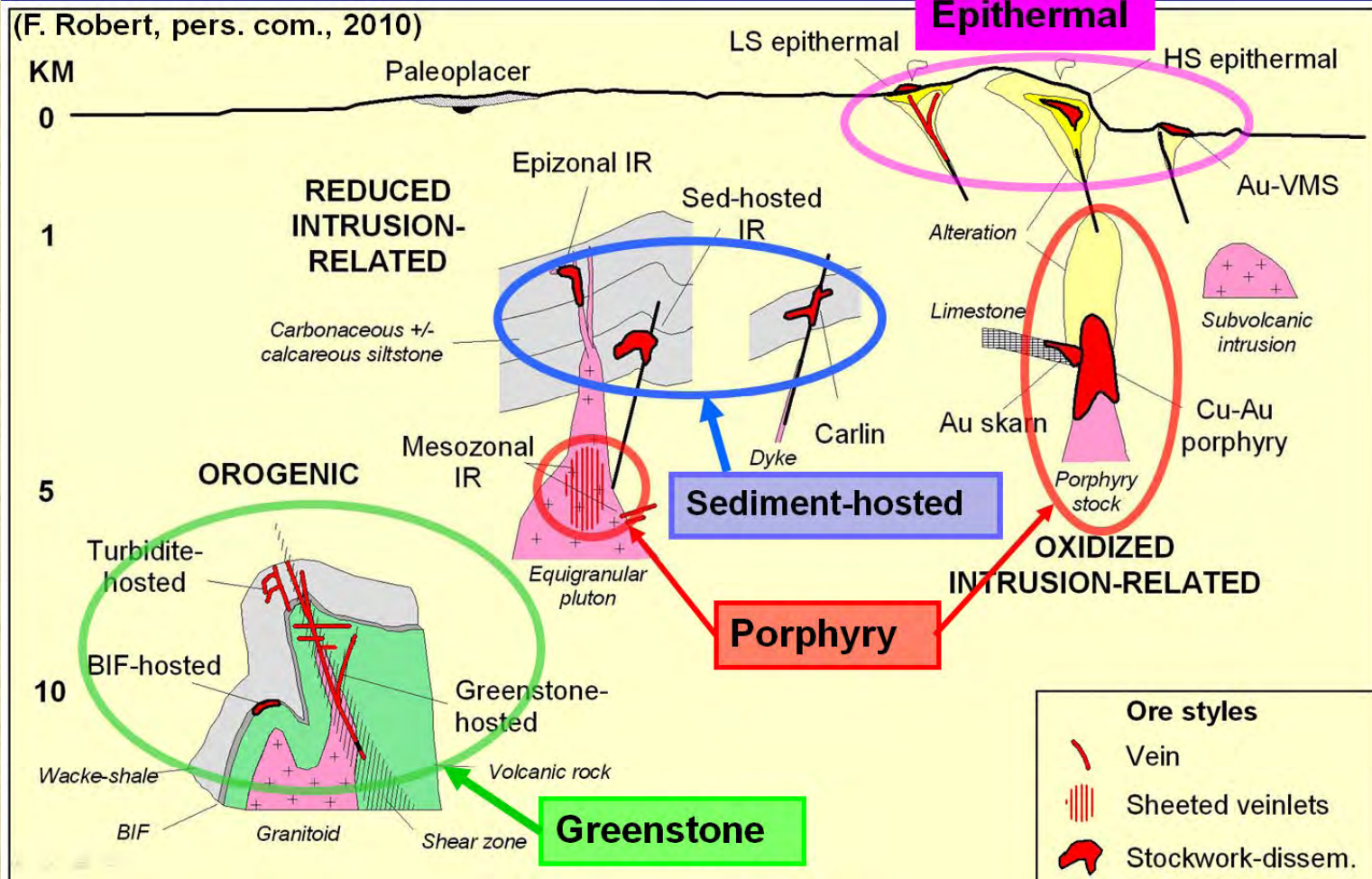
ZTEM For Precious Metals Exploration; Extending the Envelope



Ken Witherly Condor Consulting, Inc.

Precious Metals

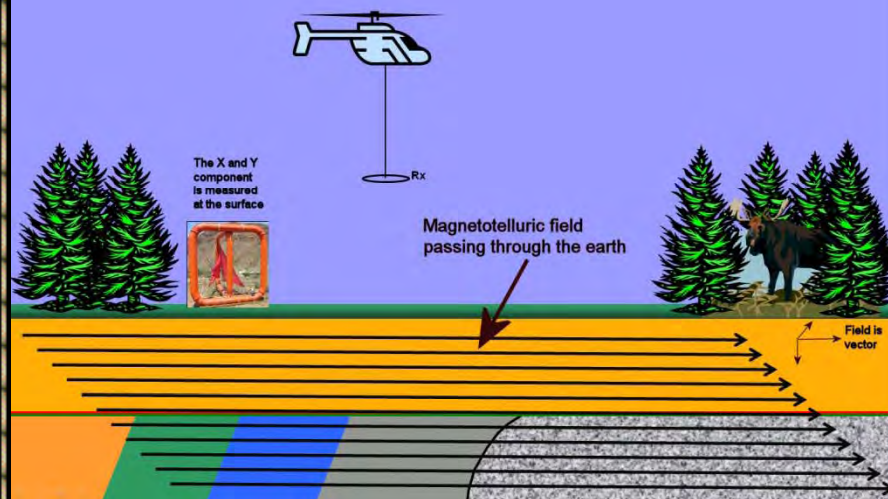
Main Geological Types of Gold Deposits



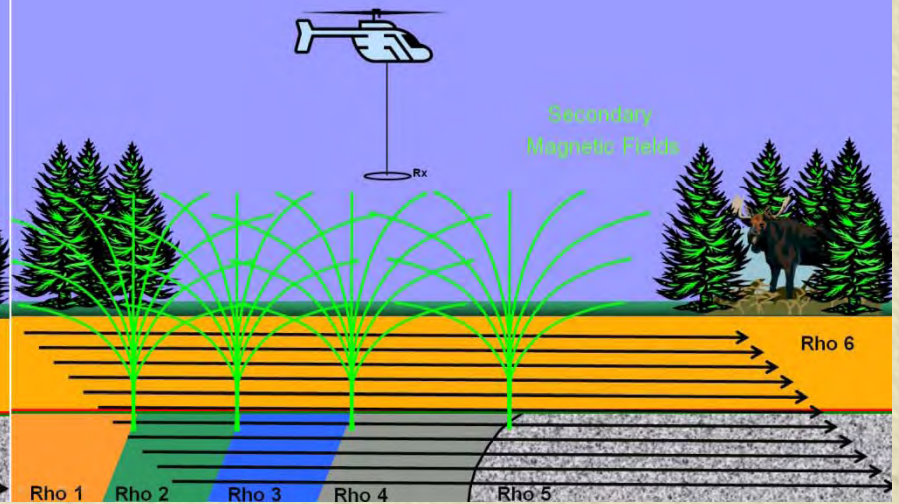
Precious Metals



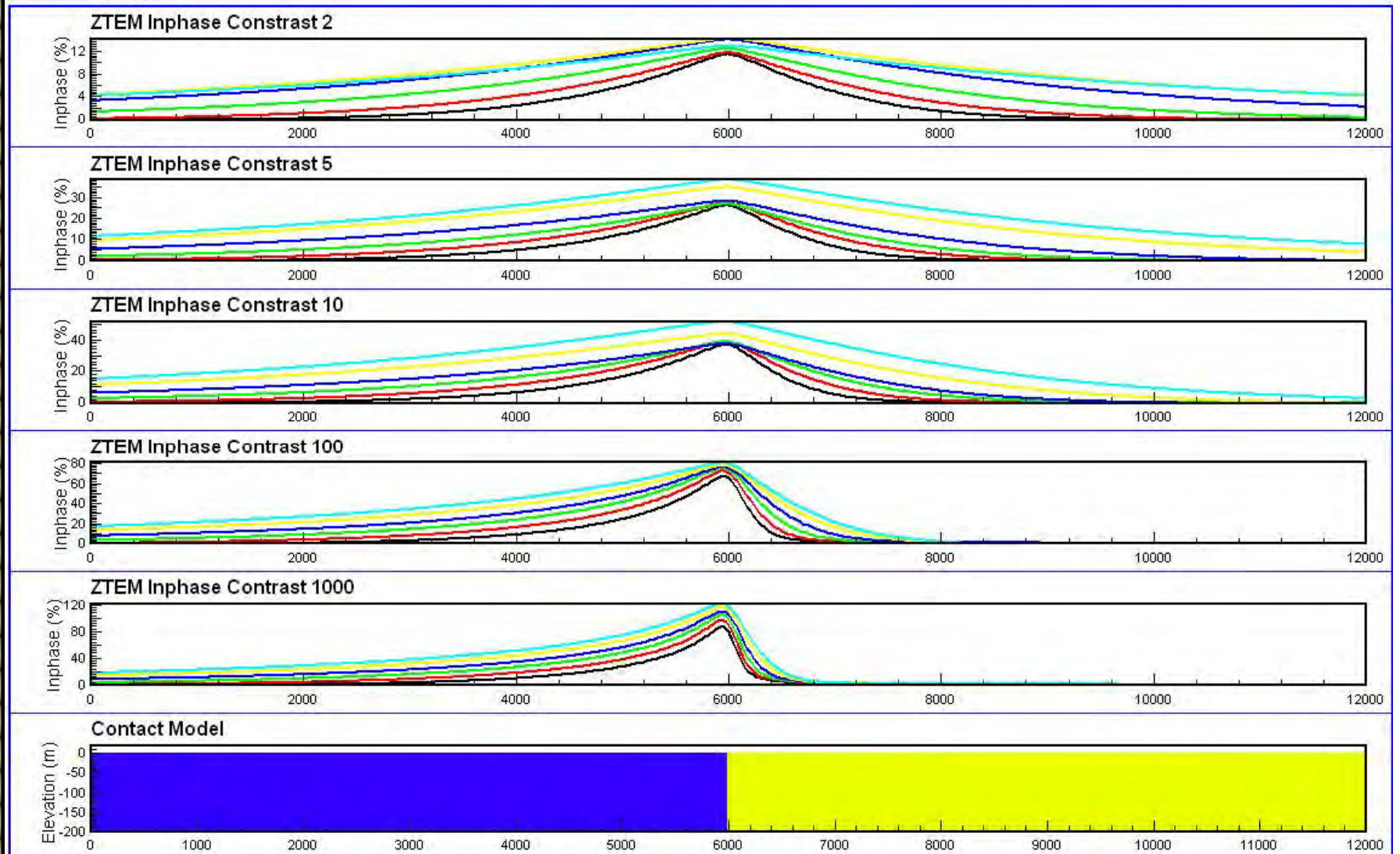
Principle of ZTEM: EM Induction



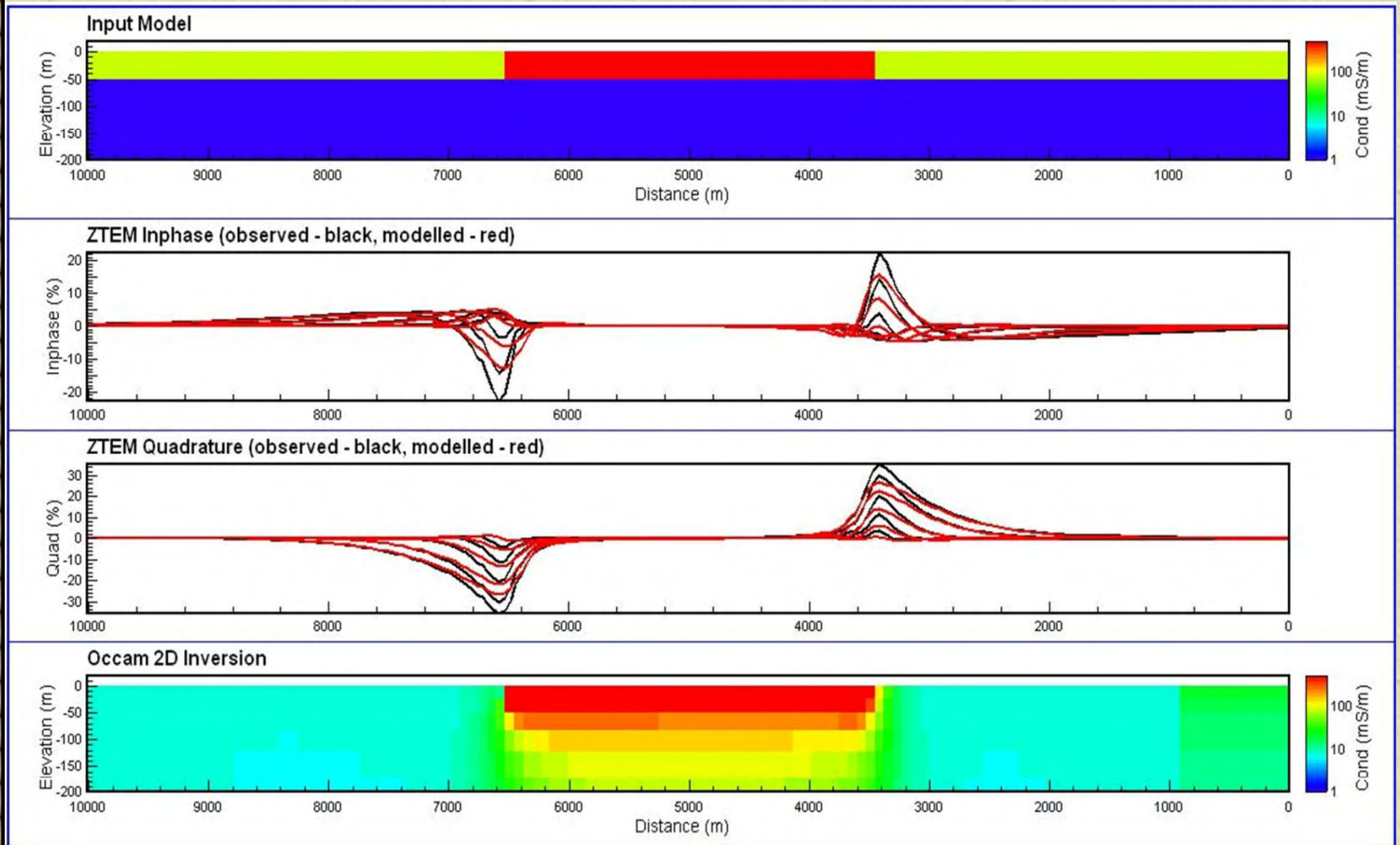
Principle of ZTEM: EM Induction



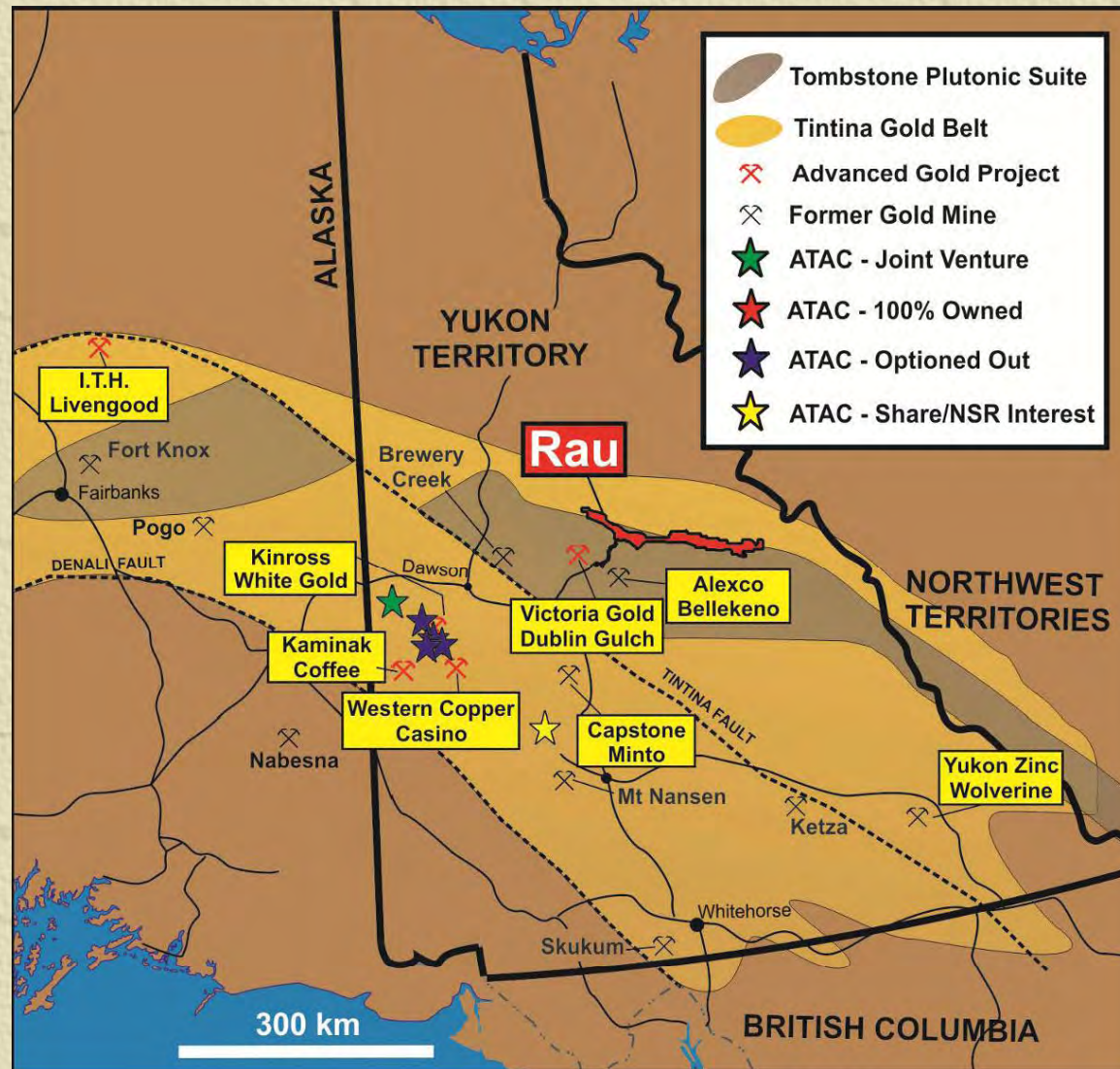
Precious Metals



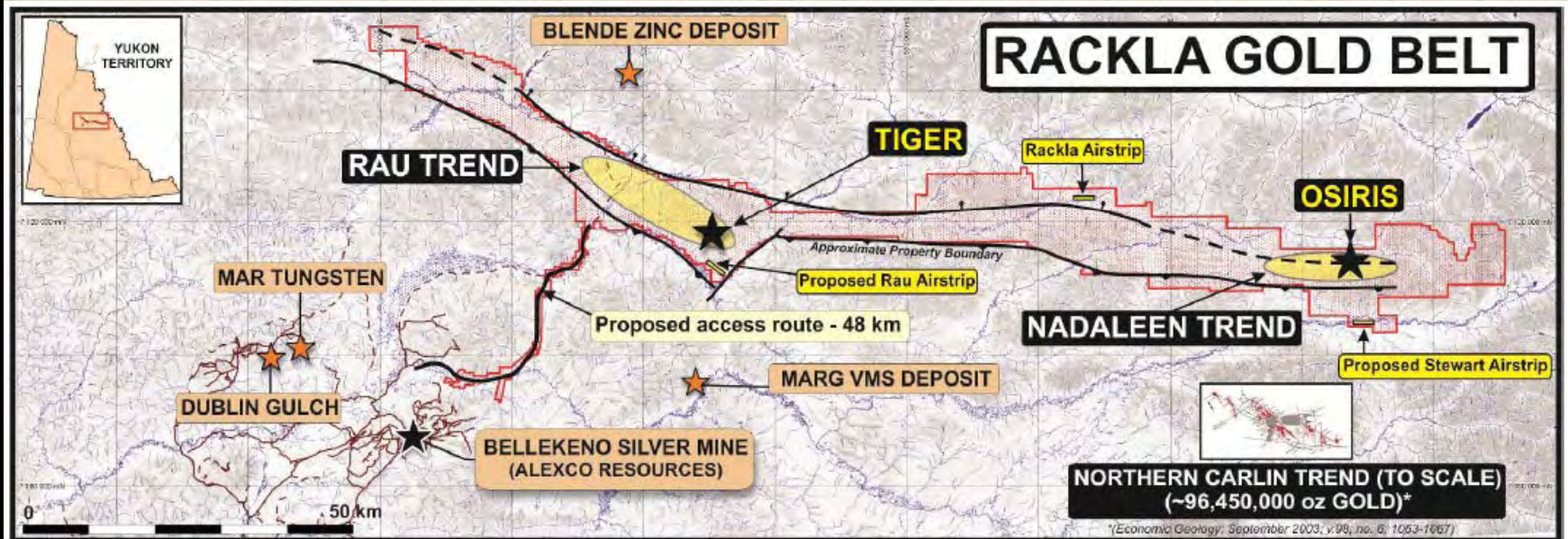
Precious Metals



Precious Metals-Tiger Zone

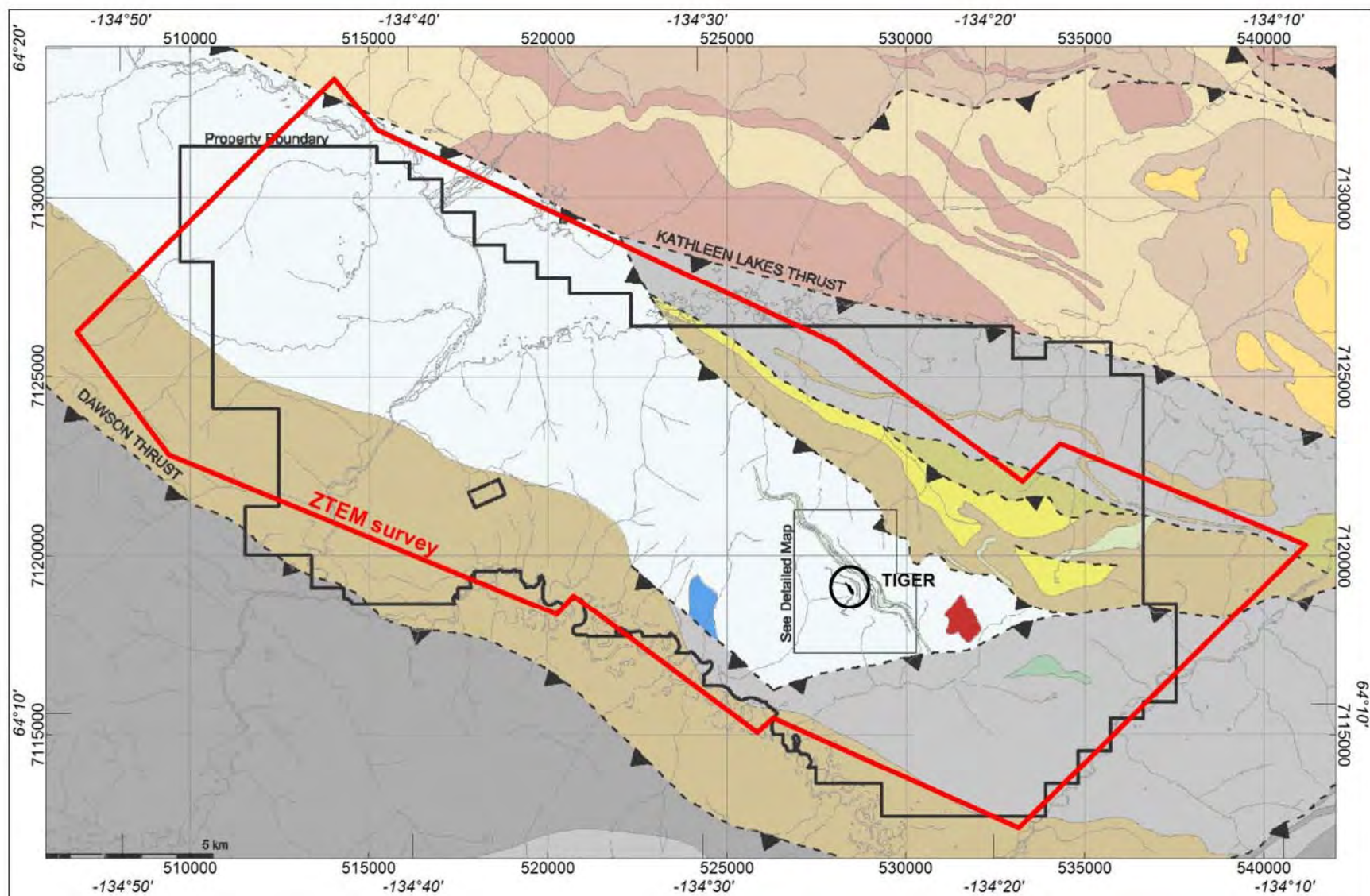


Precious Metals-Tiger Zone

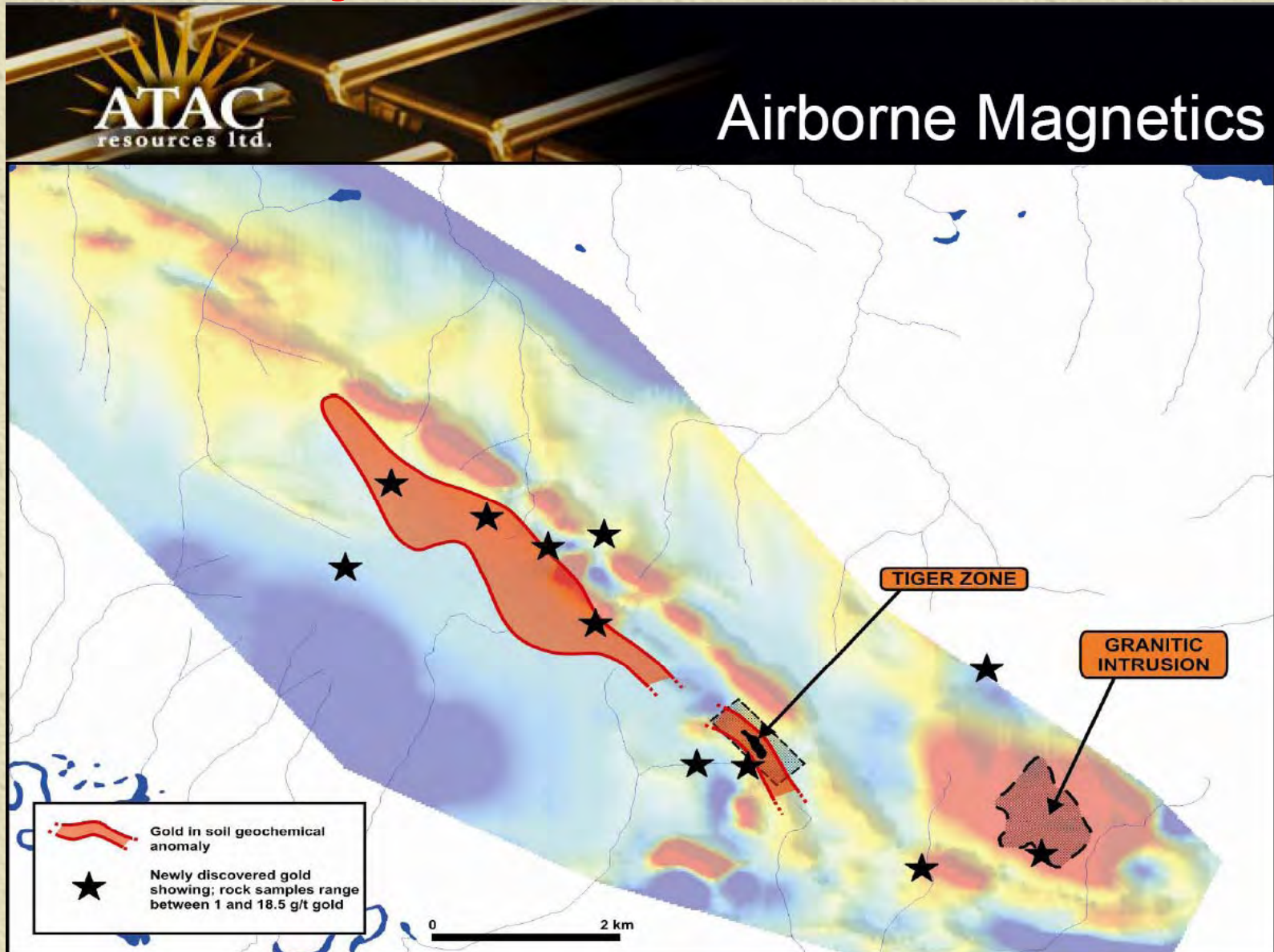


Length of Long Island, NY – (185 km/115 miles)
Driving distance between Toronto and London, ON – (185 km/115 miles) 8

Precious Metals-Tiger Zone



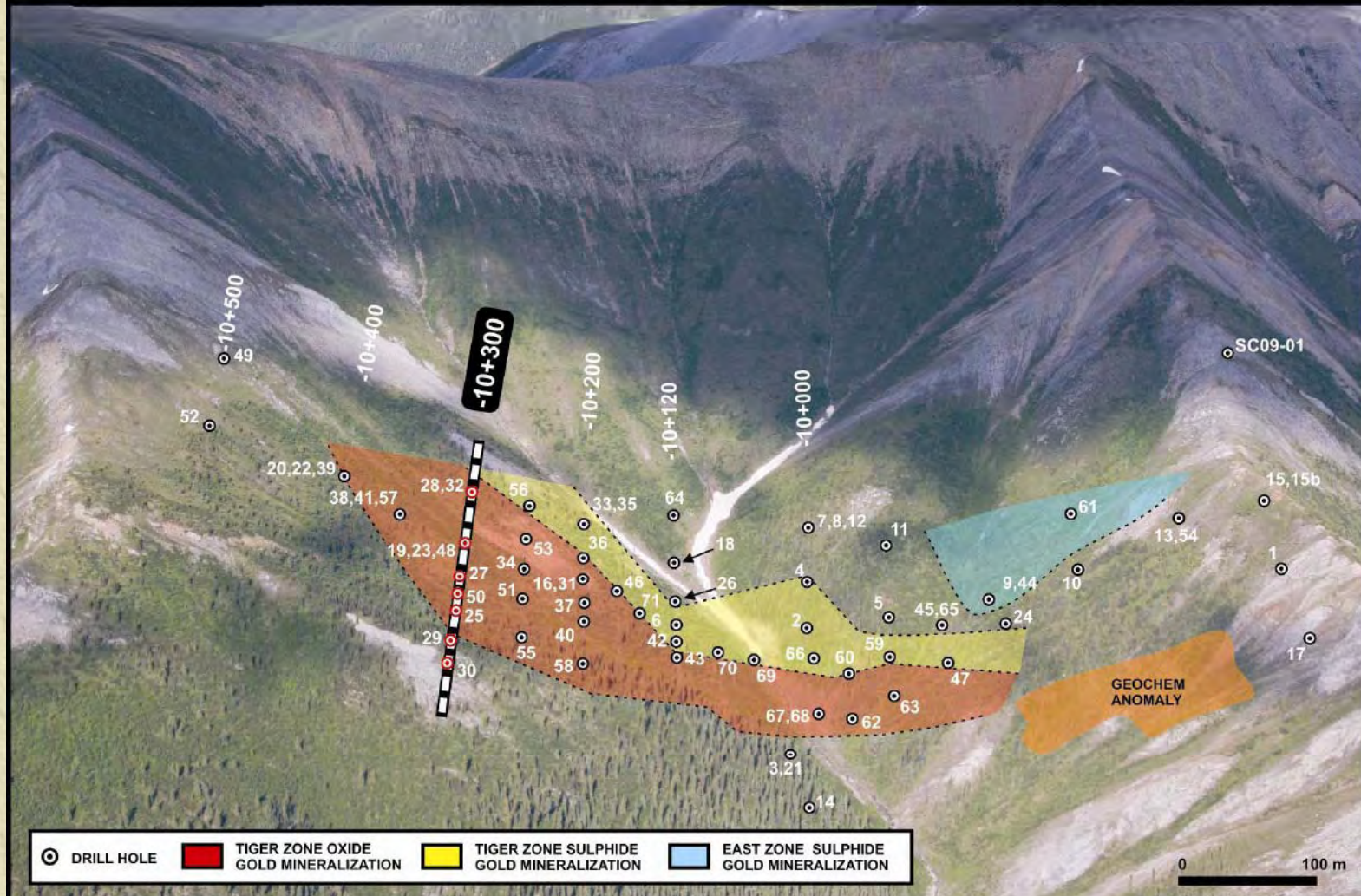
Precious Metals-Tiger Zone



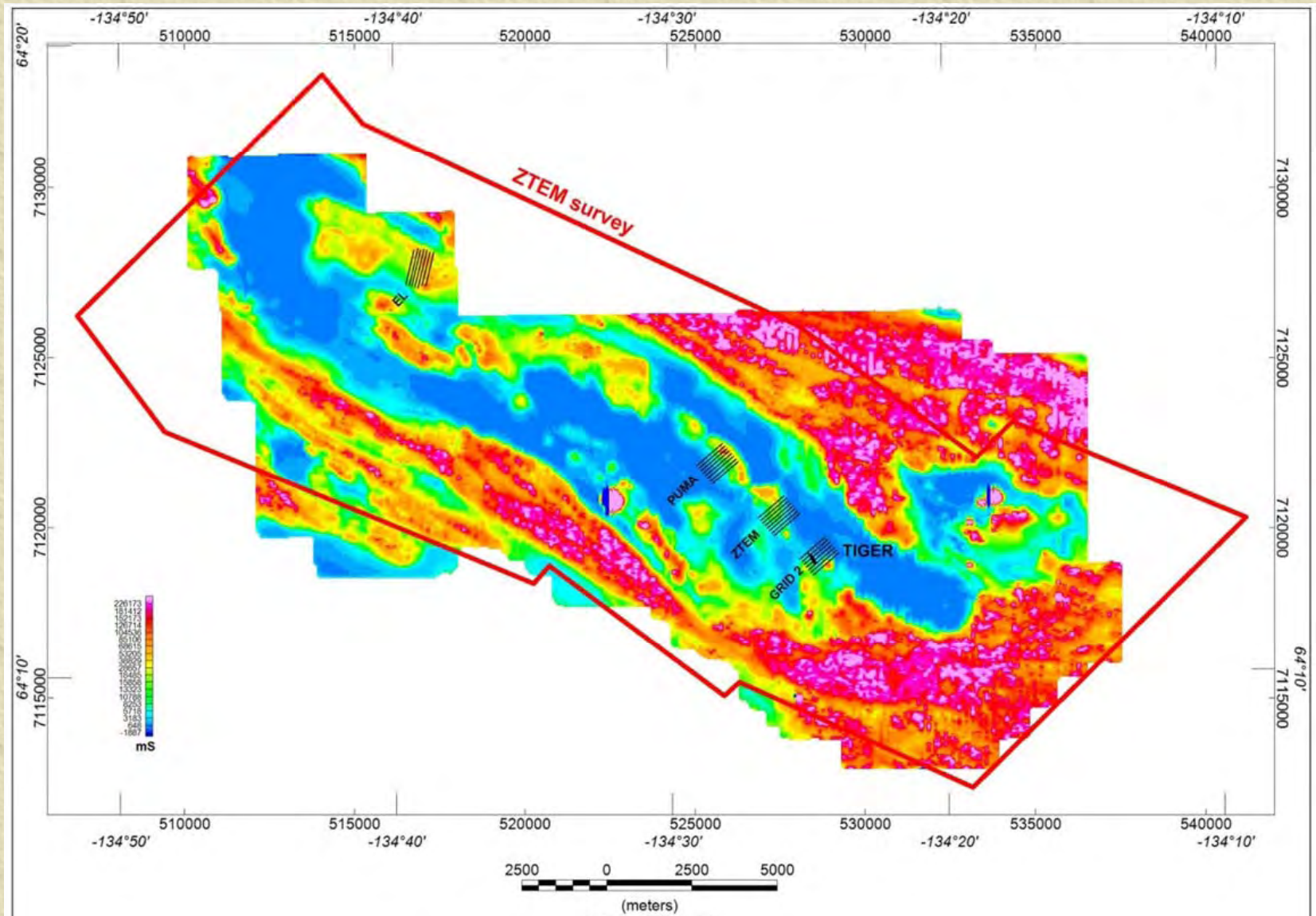
Precious Metals-Tiger Zone



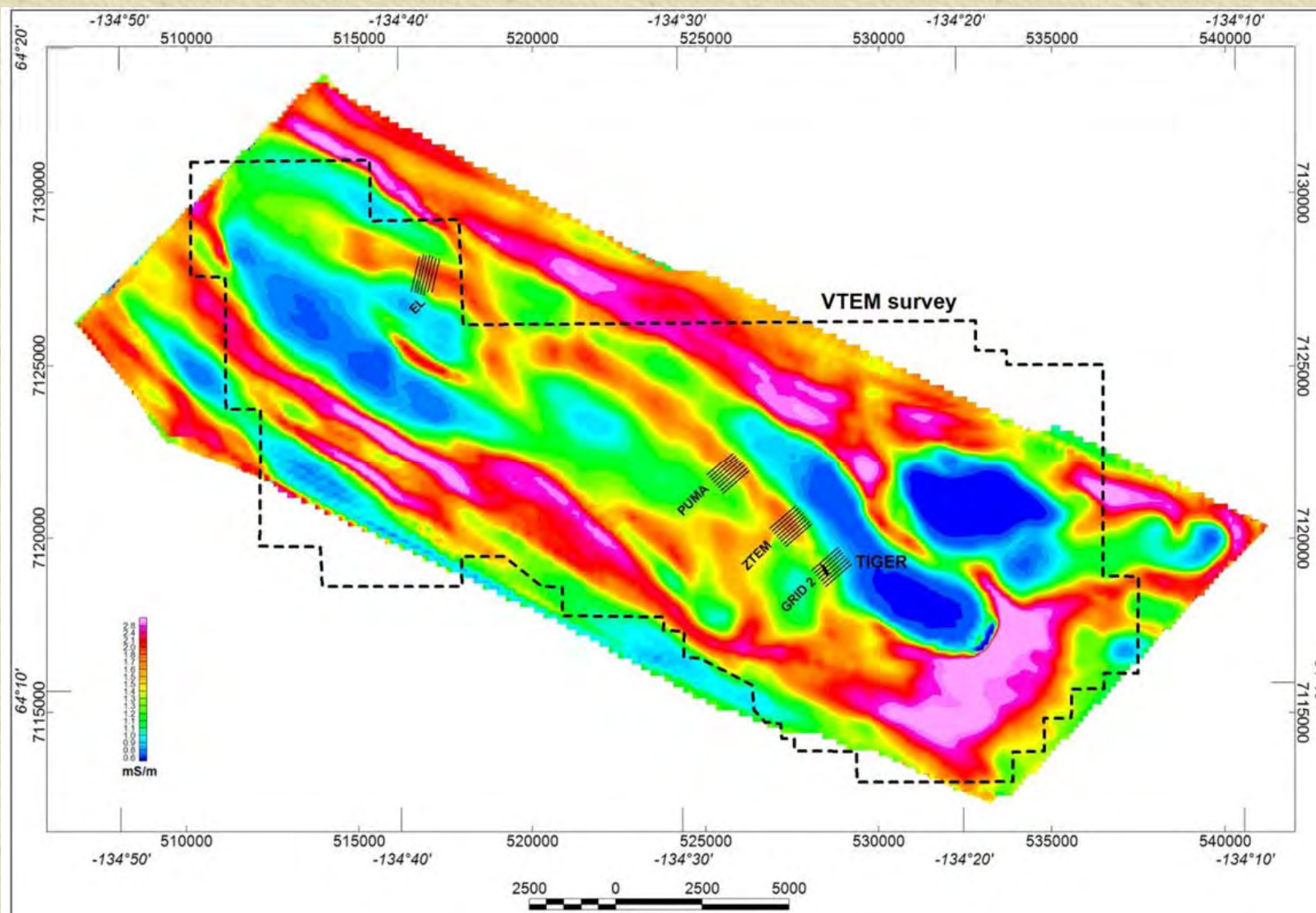
CROSS-SECTION LOCATION KEY SECTION -10+300



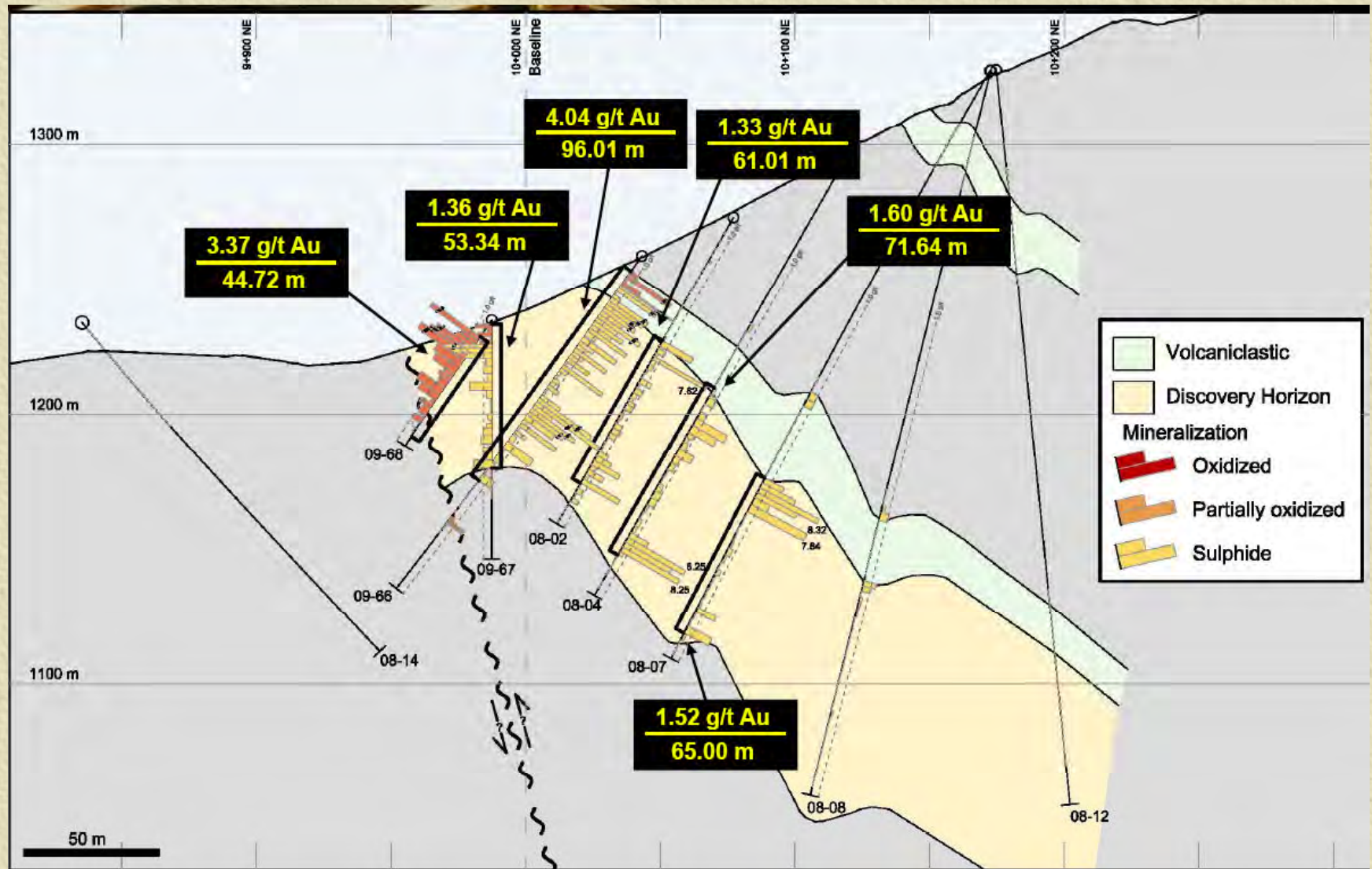
Precious Metals-Tiger Zone



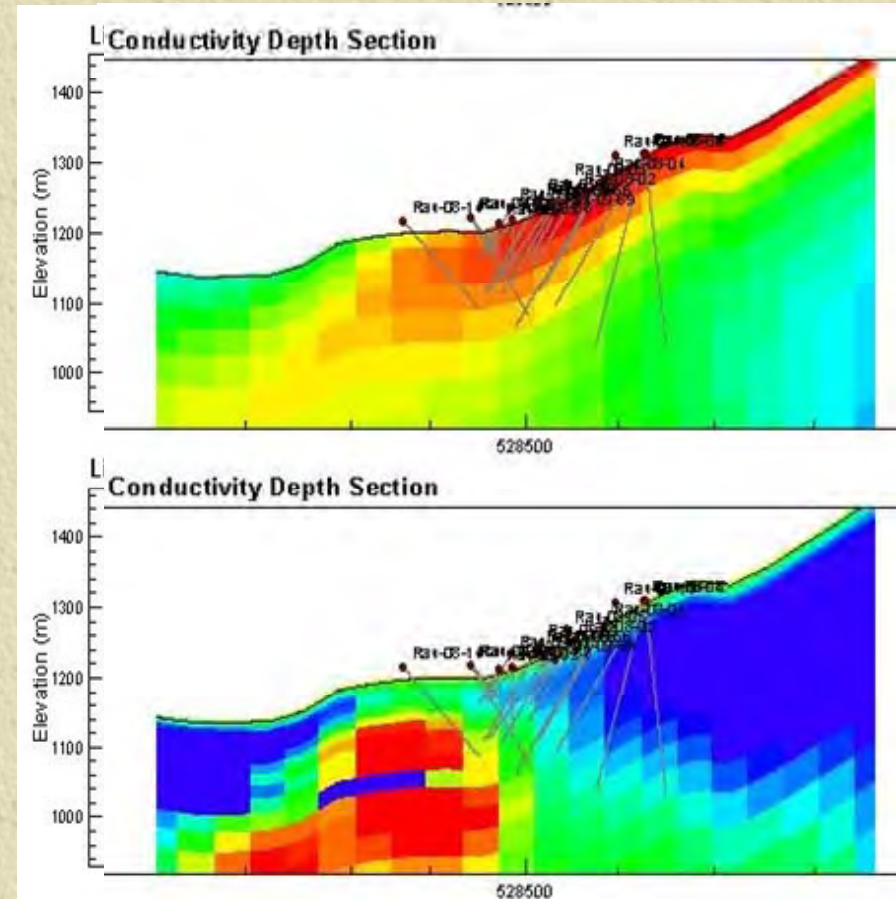
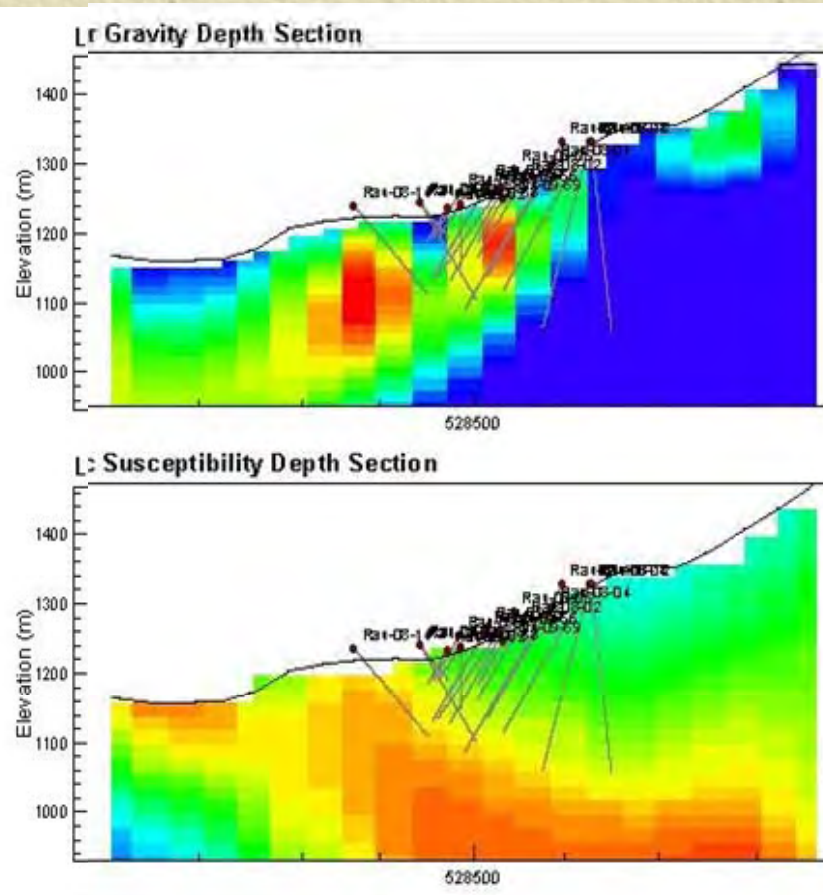
Precious Metals-Tiger Zone



Precious Metals-Tiger Zone



Precious Metals-Tiger Zone



Precious Metals-Pozo Seco



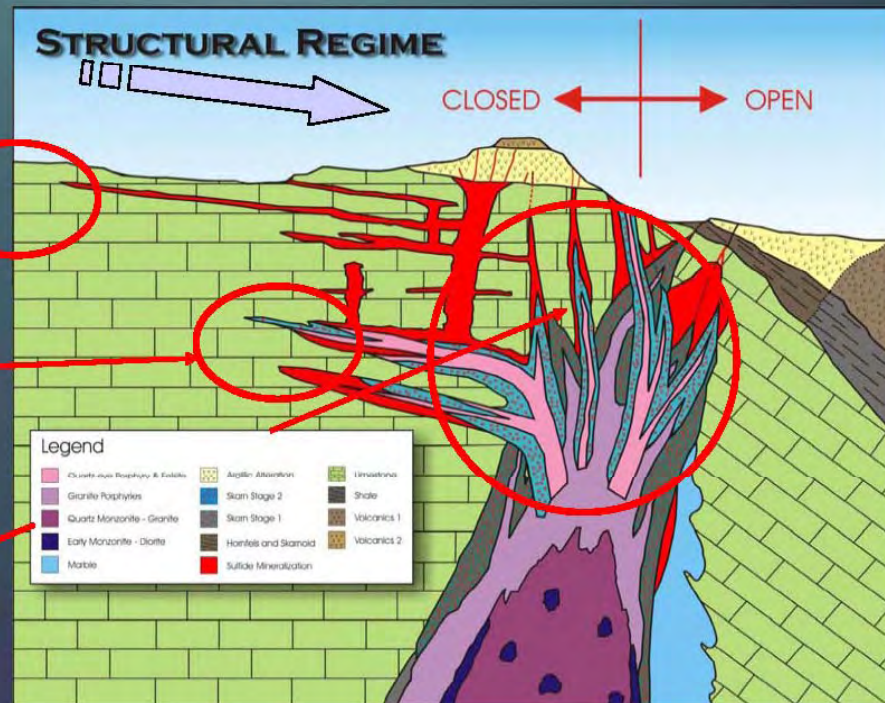
Cinco de Mayo - Model

M
A
G

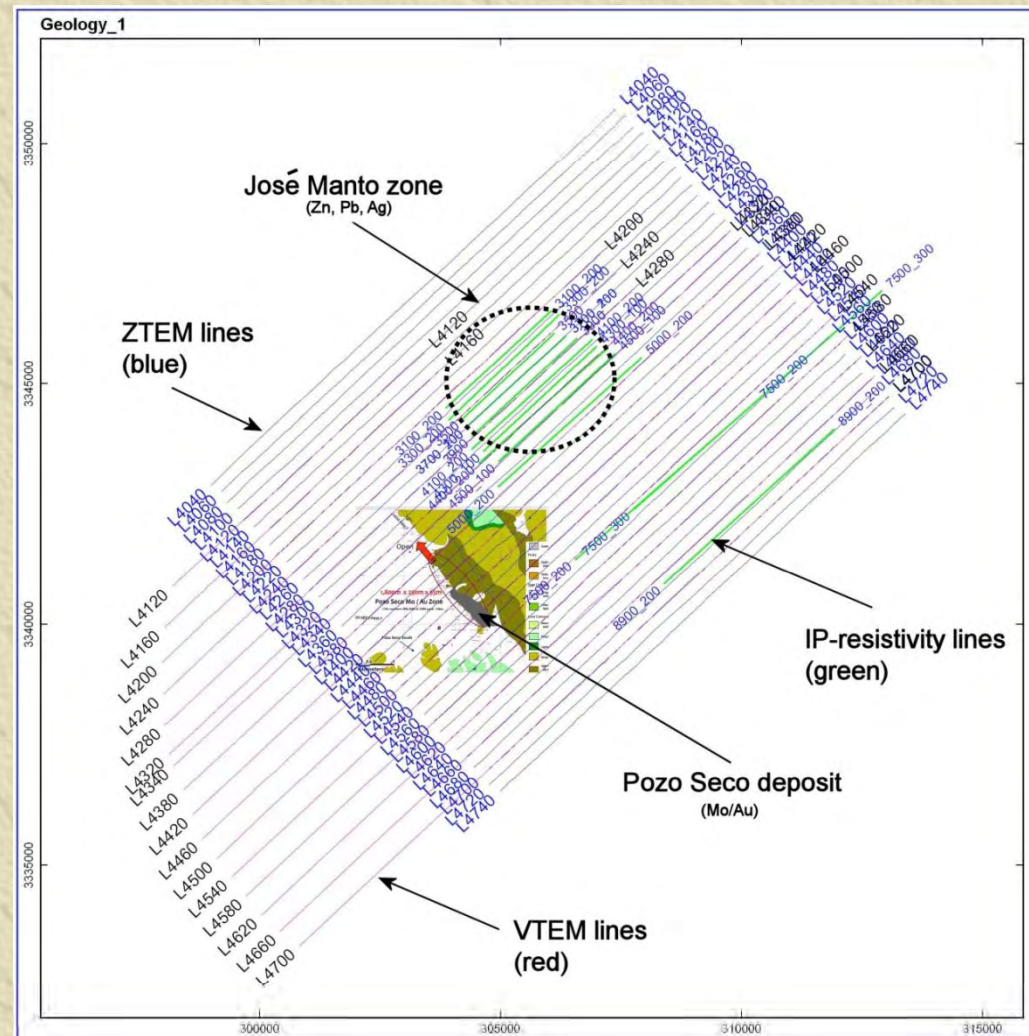
Jose Manto Ag /
Pb / Zn (Distal)

La Gloria felsite
and skarn
(Medial?)

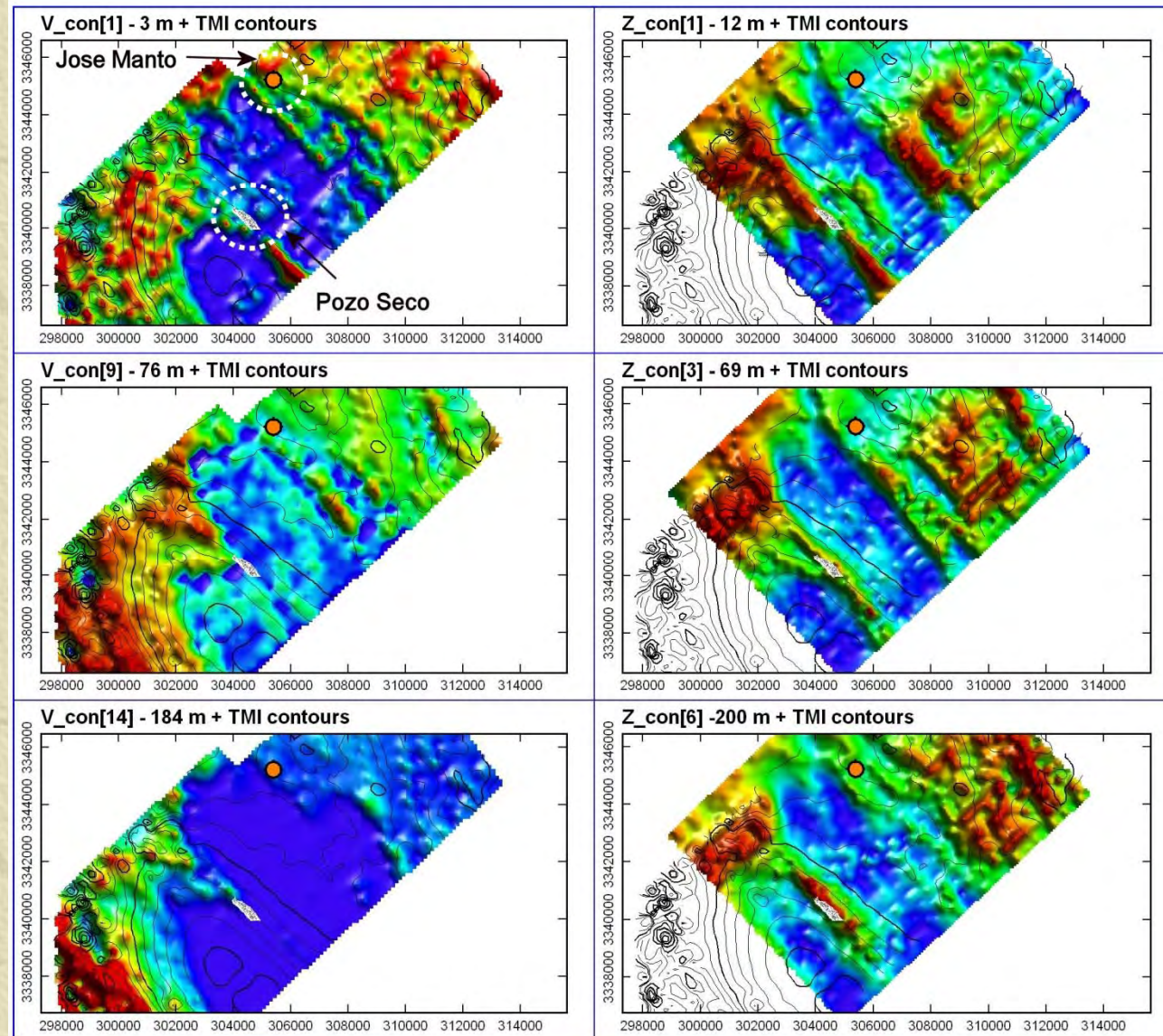
Pozo Seco Moly-
(Gold) Zone
(Proximal?)



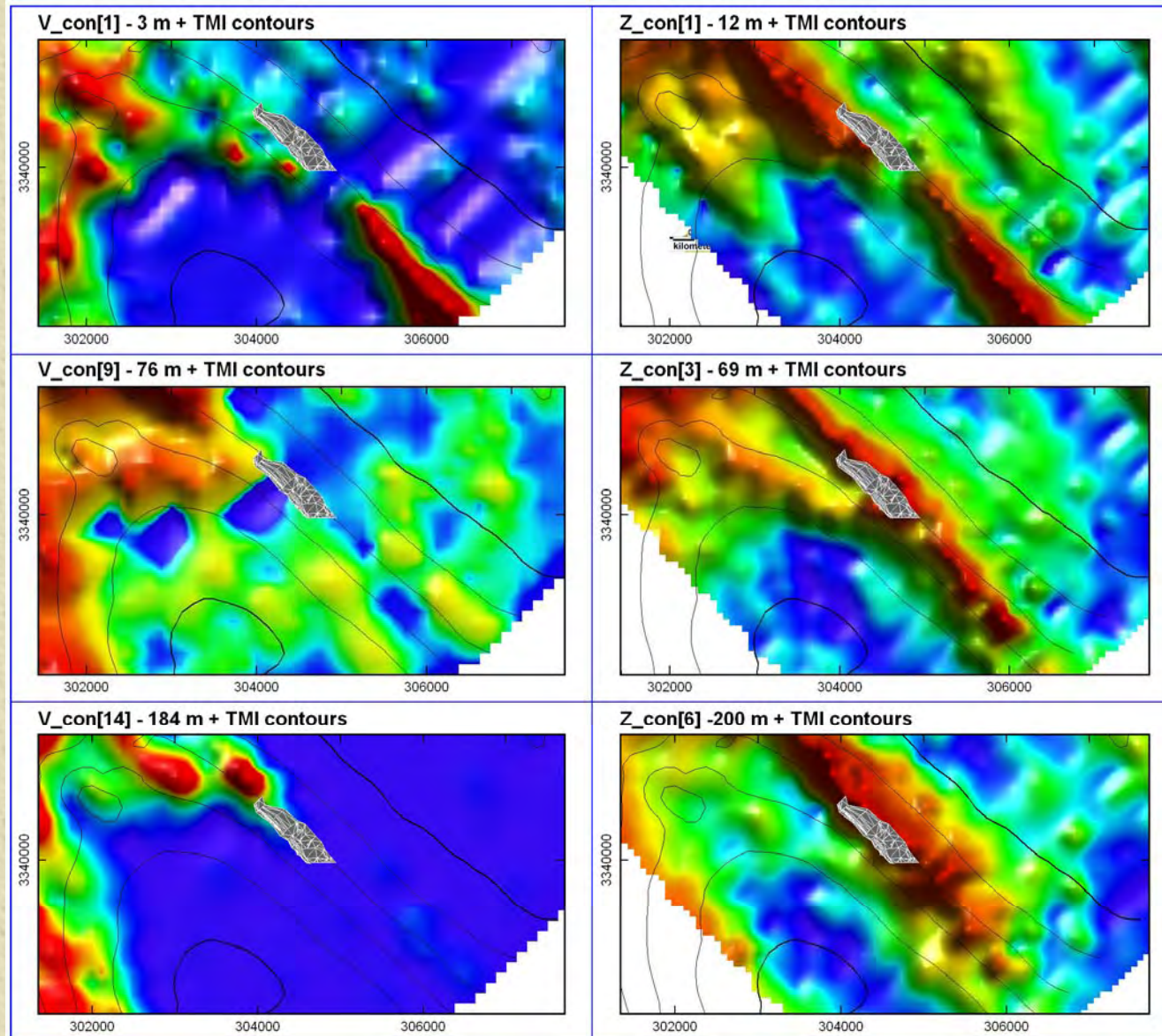
Precious Metals-Pozo Seco



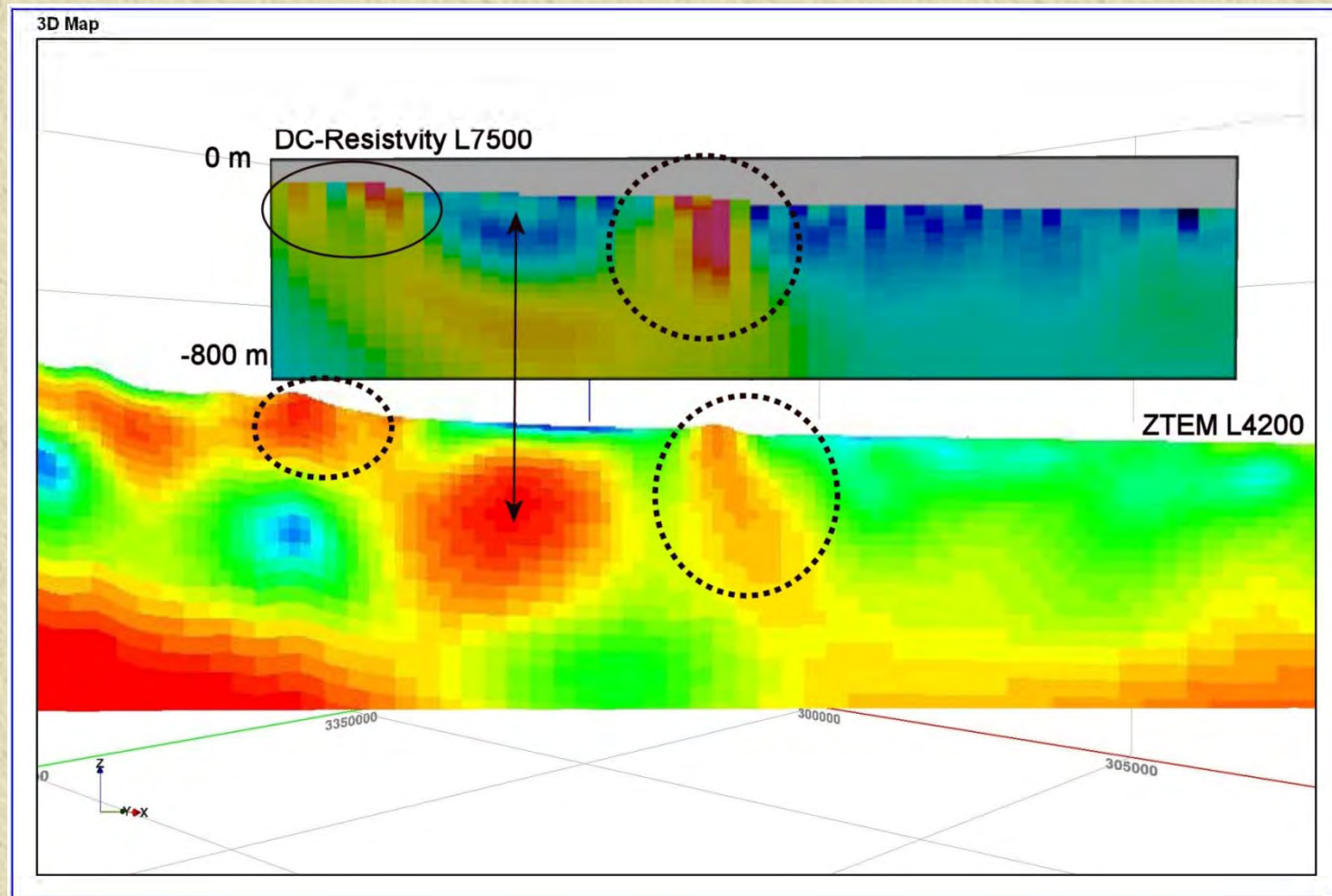
Precious Metals-Pozo Seco



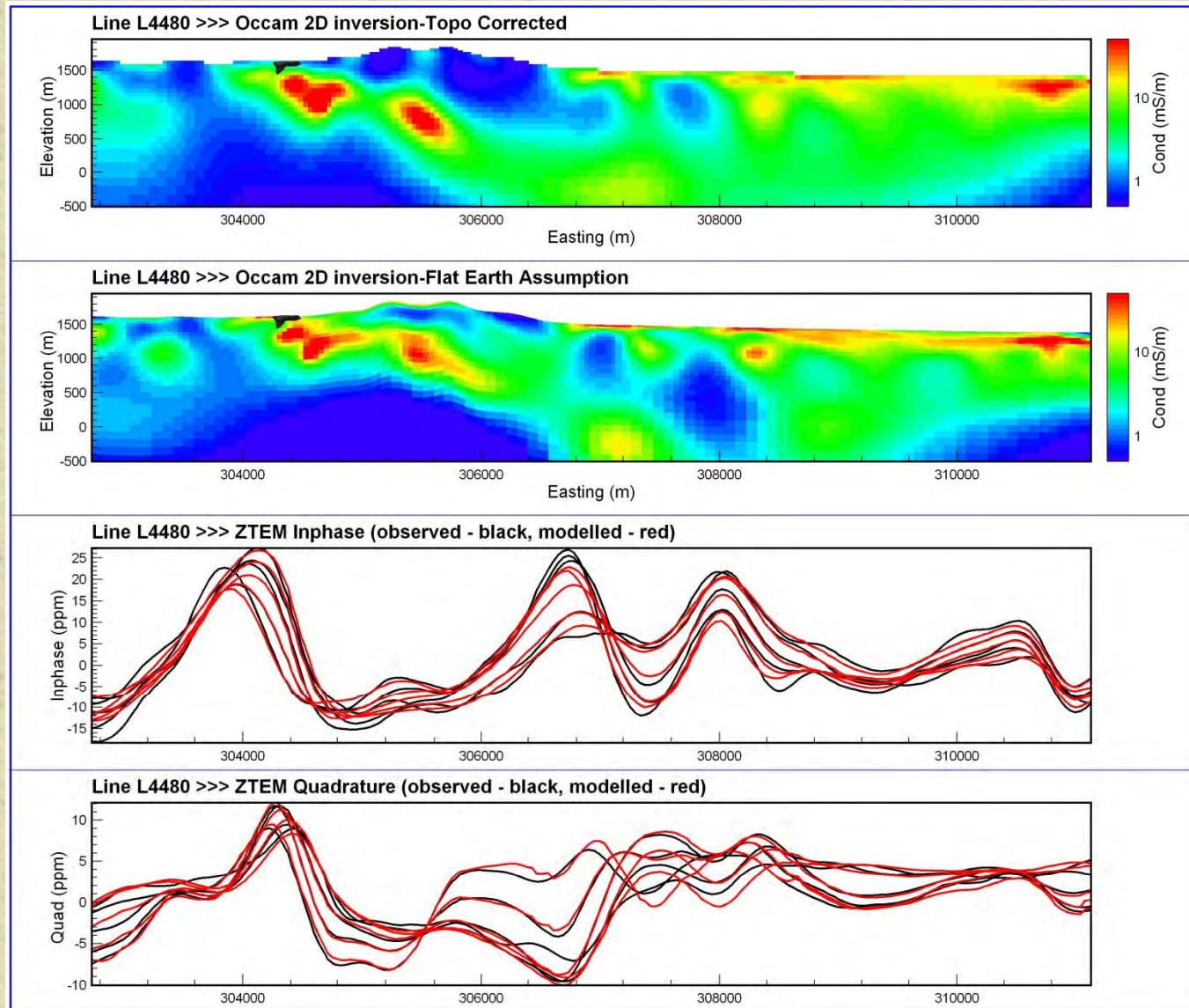
Precious Metals-Pozo Seco



Precious Metals-Pozo Seco



Precious Metals-Pozo Seco



Precious Metals-Pebble



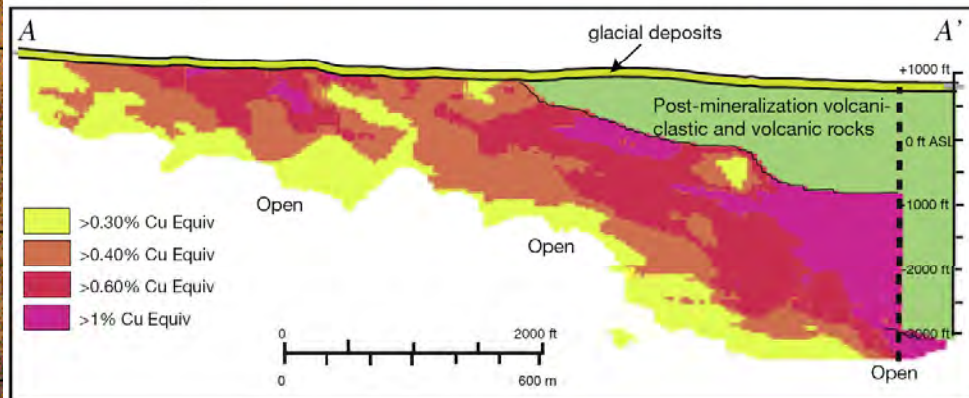
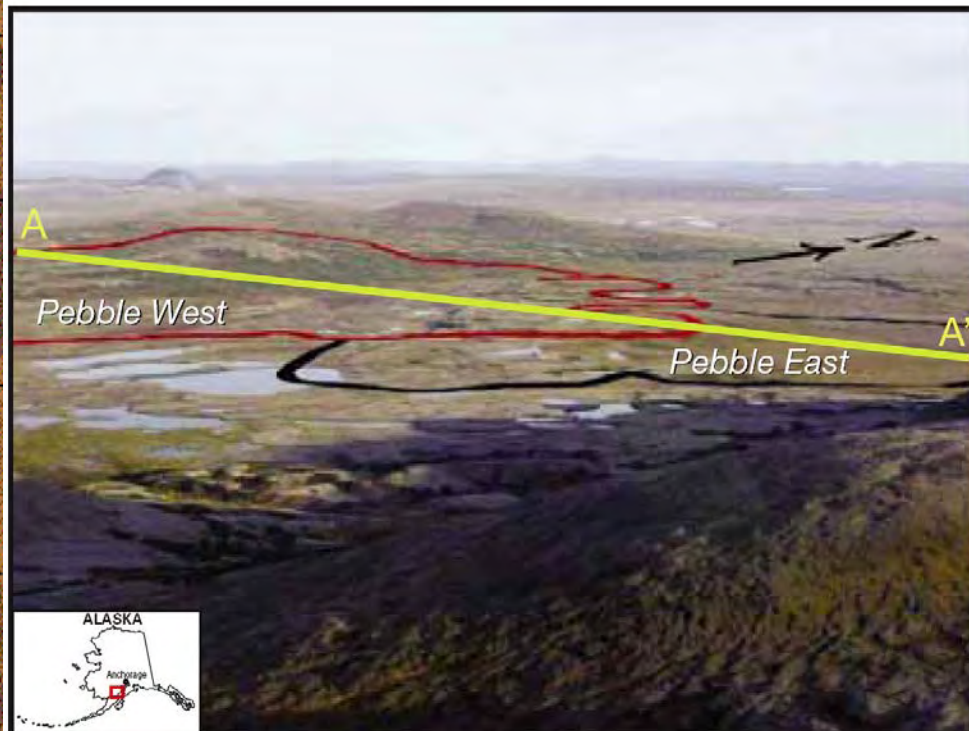
5,942 million tonnes (Mt) at 0.42% Cu,
0.35 g/t Au, and 250 ppm Mo (0.30%
CuEQ cutoff)

Measured and Indicated Mineral Resources

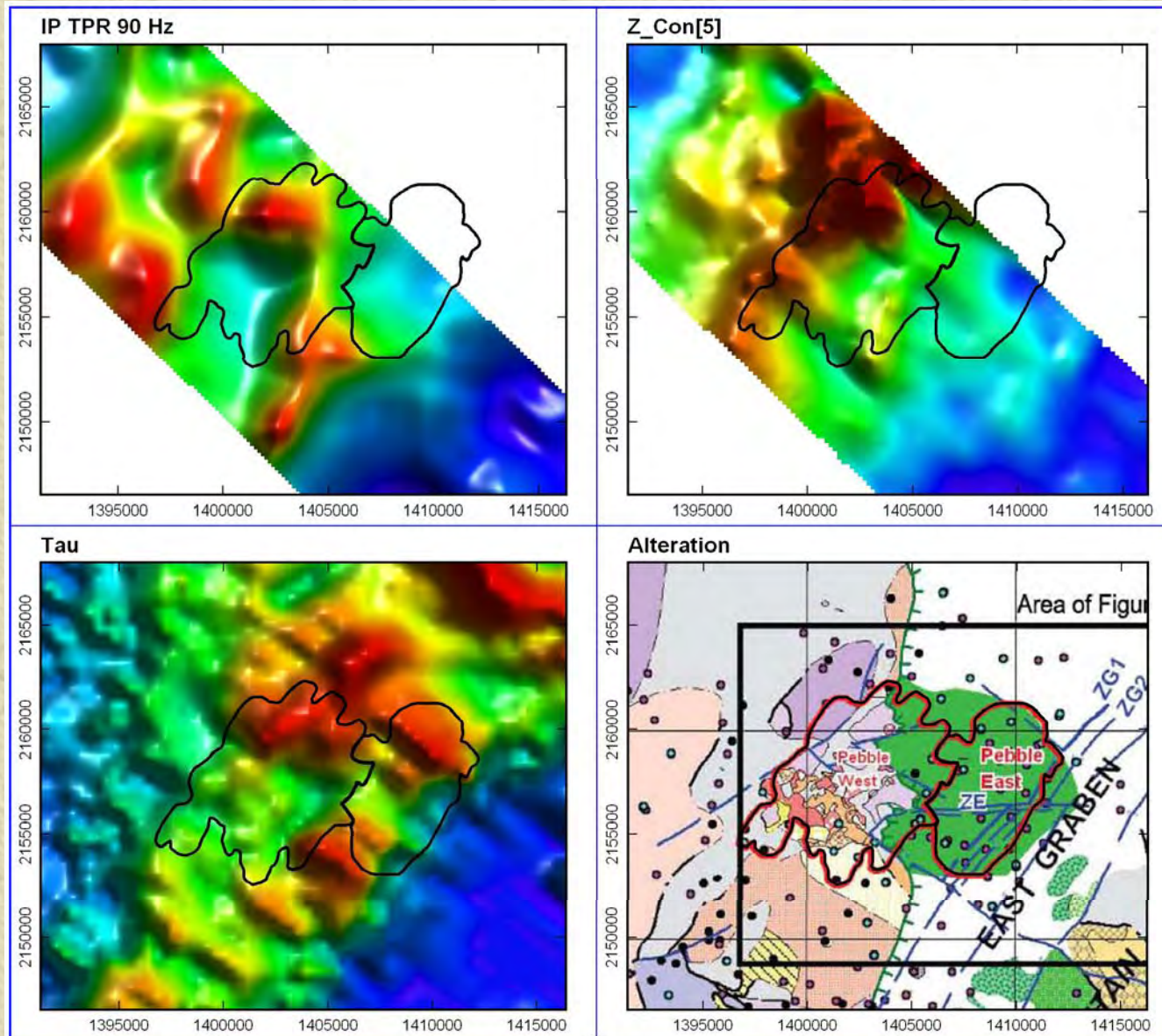
Cut-Off	Size	Grade				Contained Metal		
		Copper %	Gold g/t	Moly ppm	CuEQ %	Copper B lbs	Gold M oz	Moly B lbs
.30	5,942	.42	.35	250	0.78	55.0	66.9	3.28
.40	5,399	.45	.36	260	0.83	53.6	62.5	3.09
.60	3,668	.55	.41	293	0.98	44.5	48.3	2.37
1.00	1,449	.76	.52	341	1.29	24.3	24.2	1.09

Inferred Mineral Resources

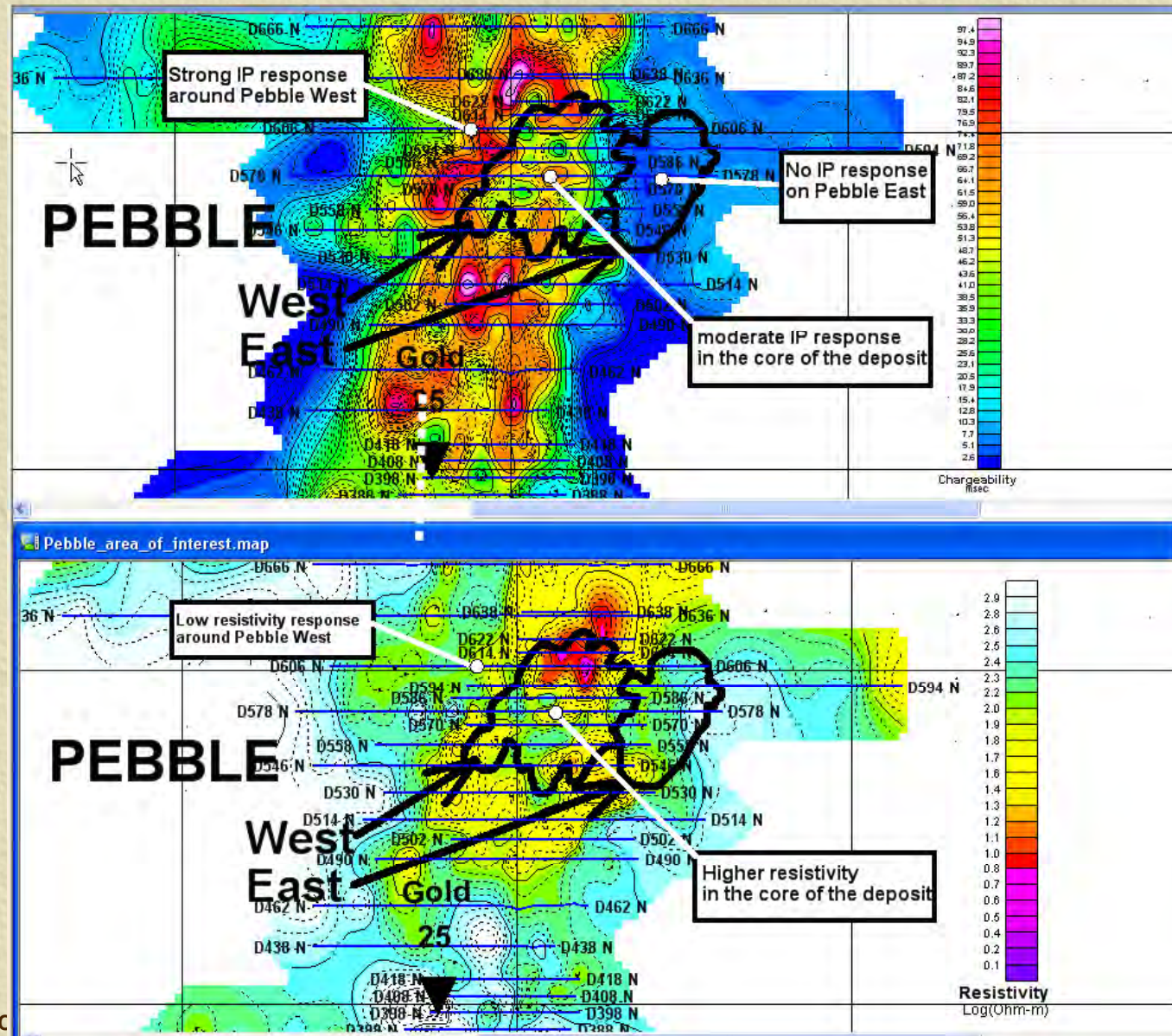
Cut-Off	Size	Grade				Contained Metal		
		Copper %	Gold g/t	Moly ppm	CuEQ %	Copper B lbs	Gold M oz	Moly B lbs
.30	4,835	.24	.26	215	0.53	25.6	40.4	2.29
.40	2,845	.32	.30	259	0.66	20.1	27.4	1.62
.60	1,322	.48	.37	289	0.89	14.0	15.7	0.84
1.00	353	.69	.45	379	1.2	5.4	5.1	0.29



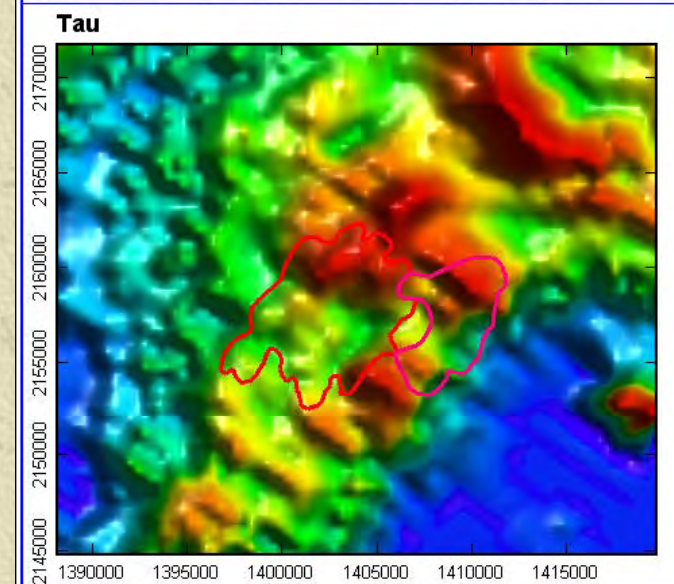
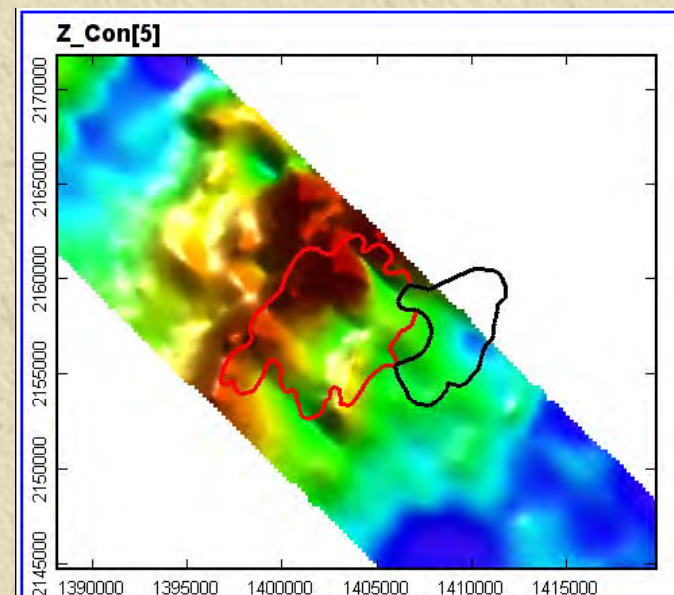
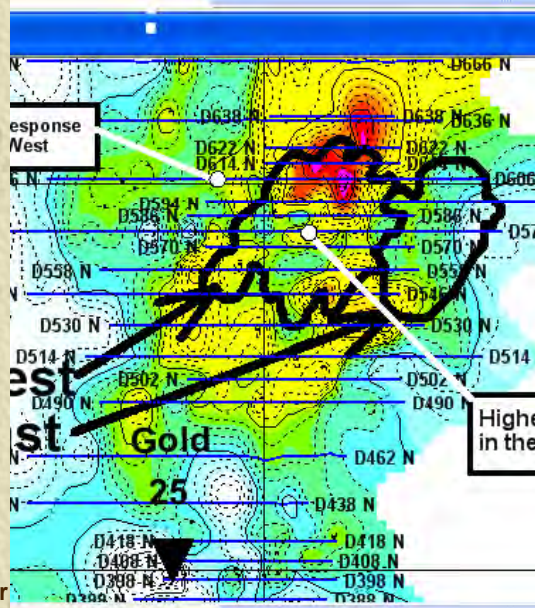
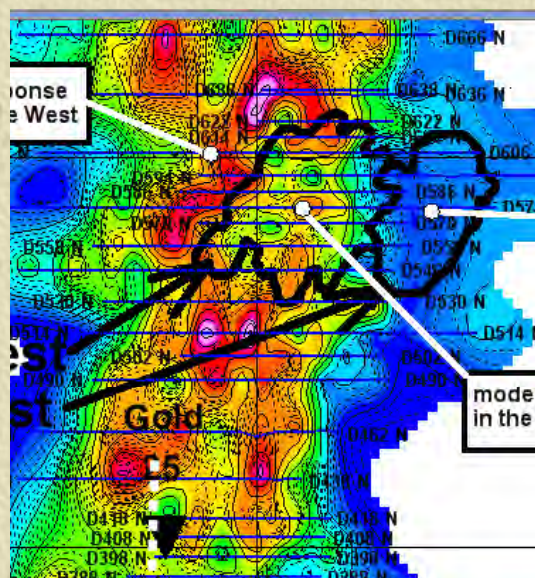
Precious Metals-Pebble



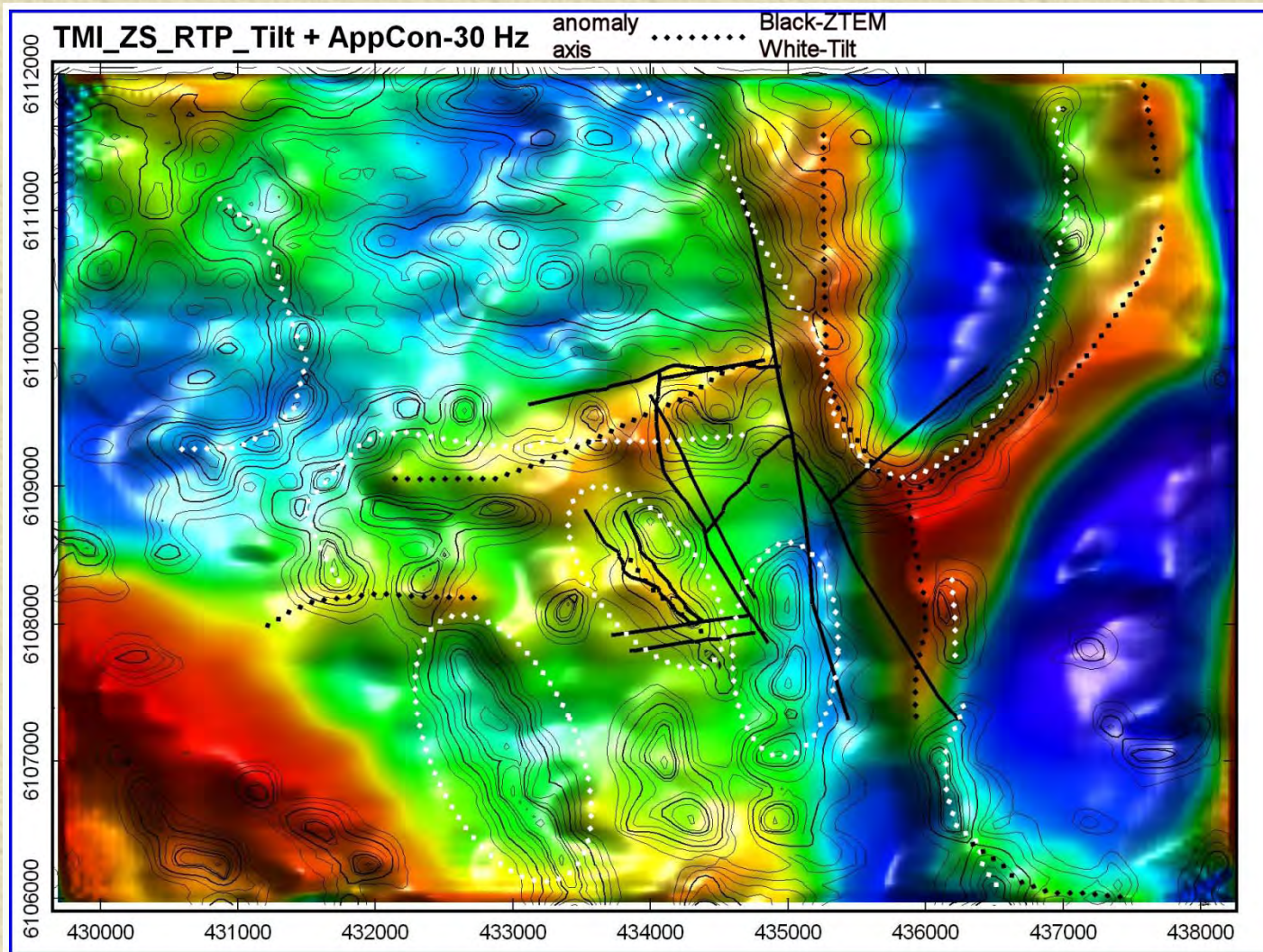
Precious Metals-Pebble



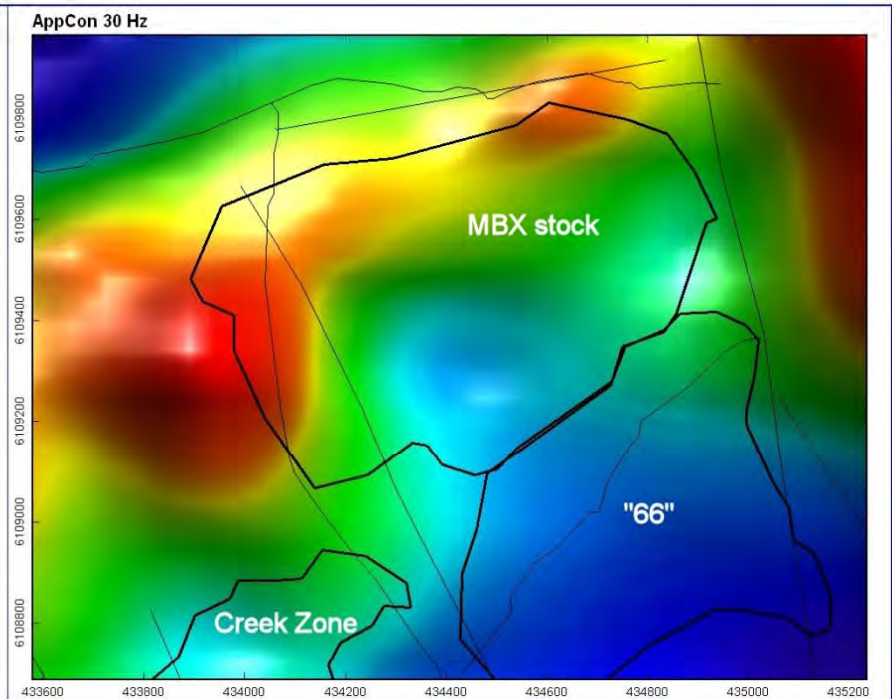
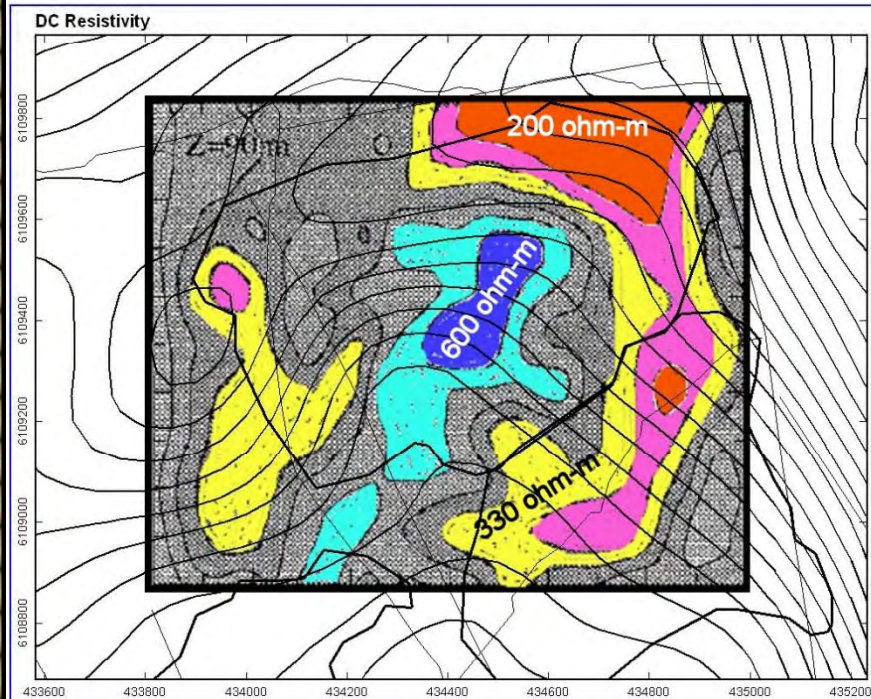
Precious Metals-Pebble



Precious Metals-Mt Milligan



Precious Metals-Mt Milligan



Acknowledgements



✦ Daniel Sattel-EM Solutions

✦ ATAC Resources Ltd.

- ◆ Rob Carne

- ◆ Bill Wengzynowski

✦ MAGSilver

- ◆ Ken Robertson

✦ Anglo American Exploration (Canada) Ltd.

- ◆ Pascal Pare

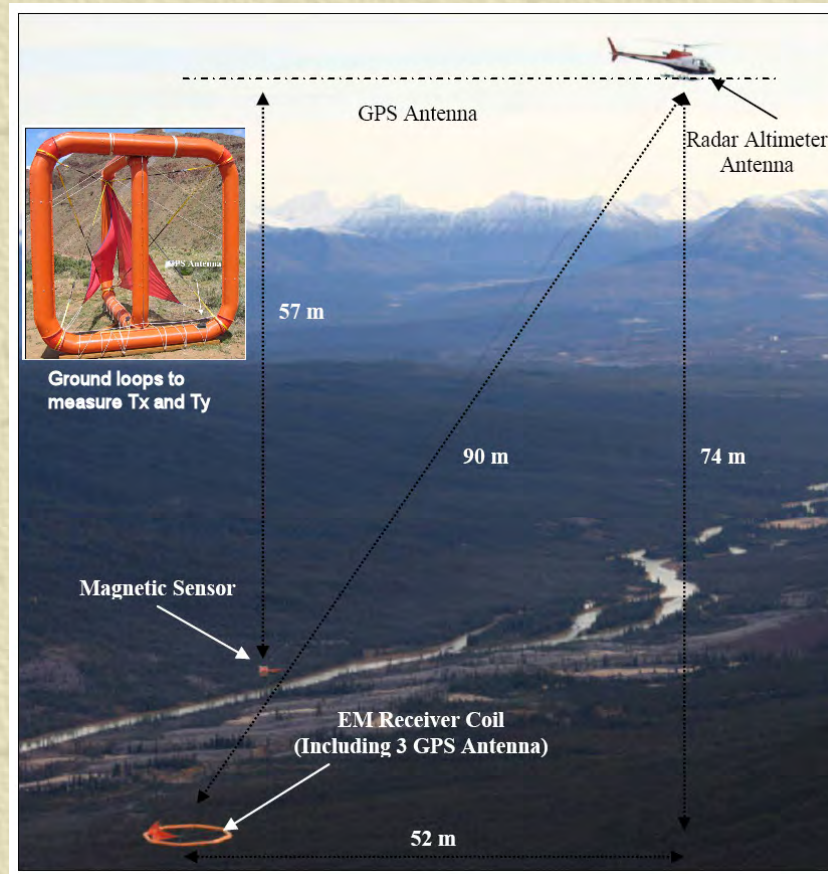
✦ Geotech Ltd.

- ◆ Paolo Berardelli

- ◆ Jean Legault

ZTEM

A New Paradigm in Airborne EM

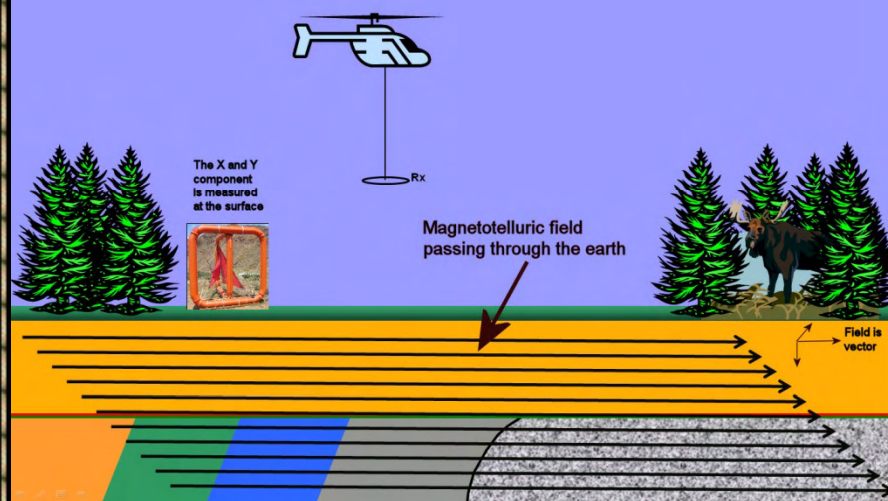


Ken Witherly-Condor Consulting, Inc.
CAMESE Seminar March 2011

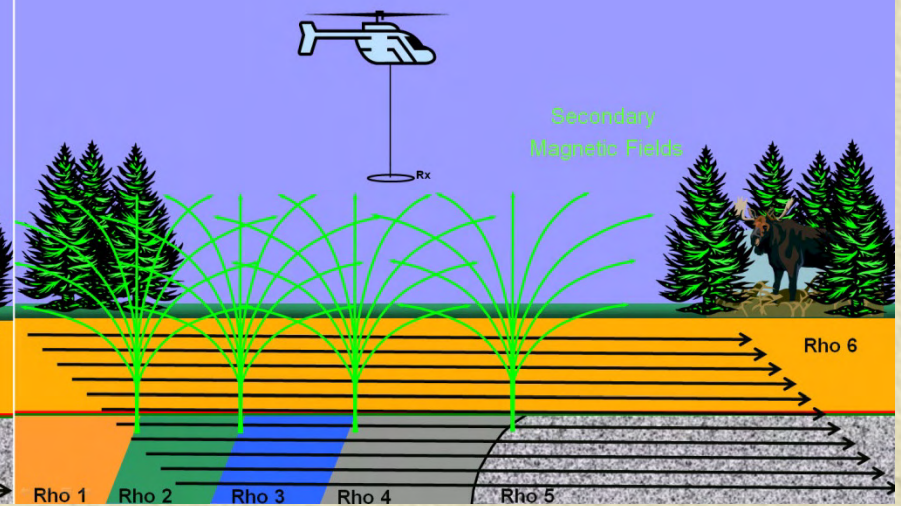
ZTEM



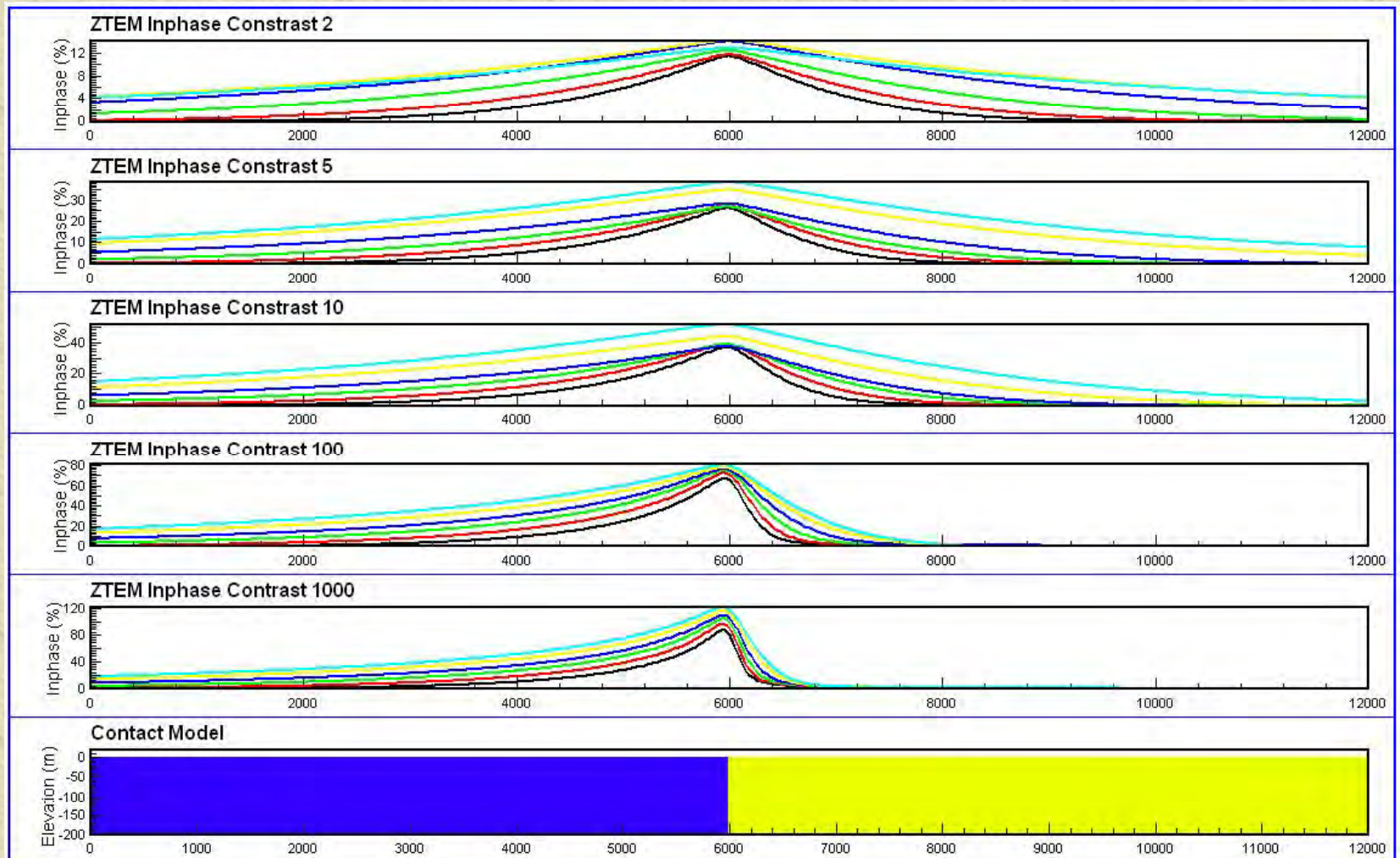
Principle of ZTEM: EM Induction



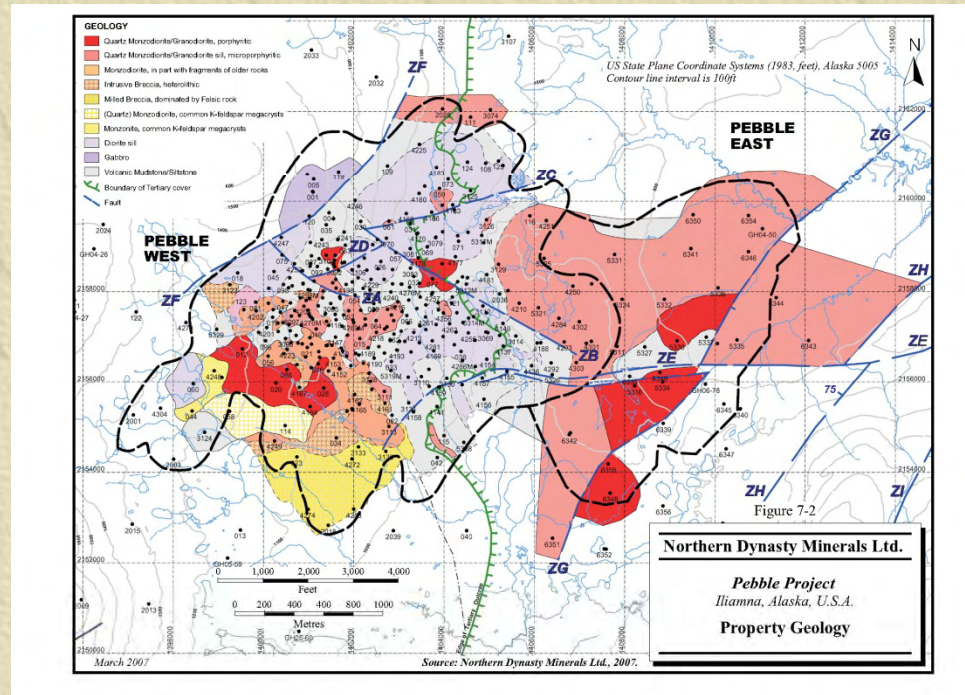
Principle of ZTEM: EM Induction



ZTEM



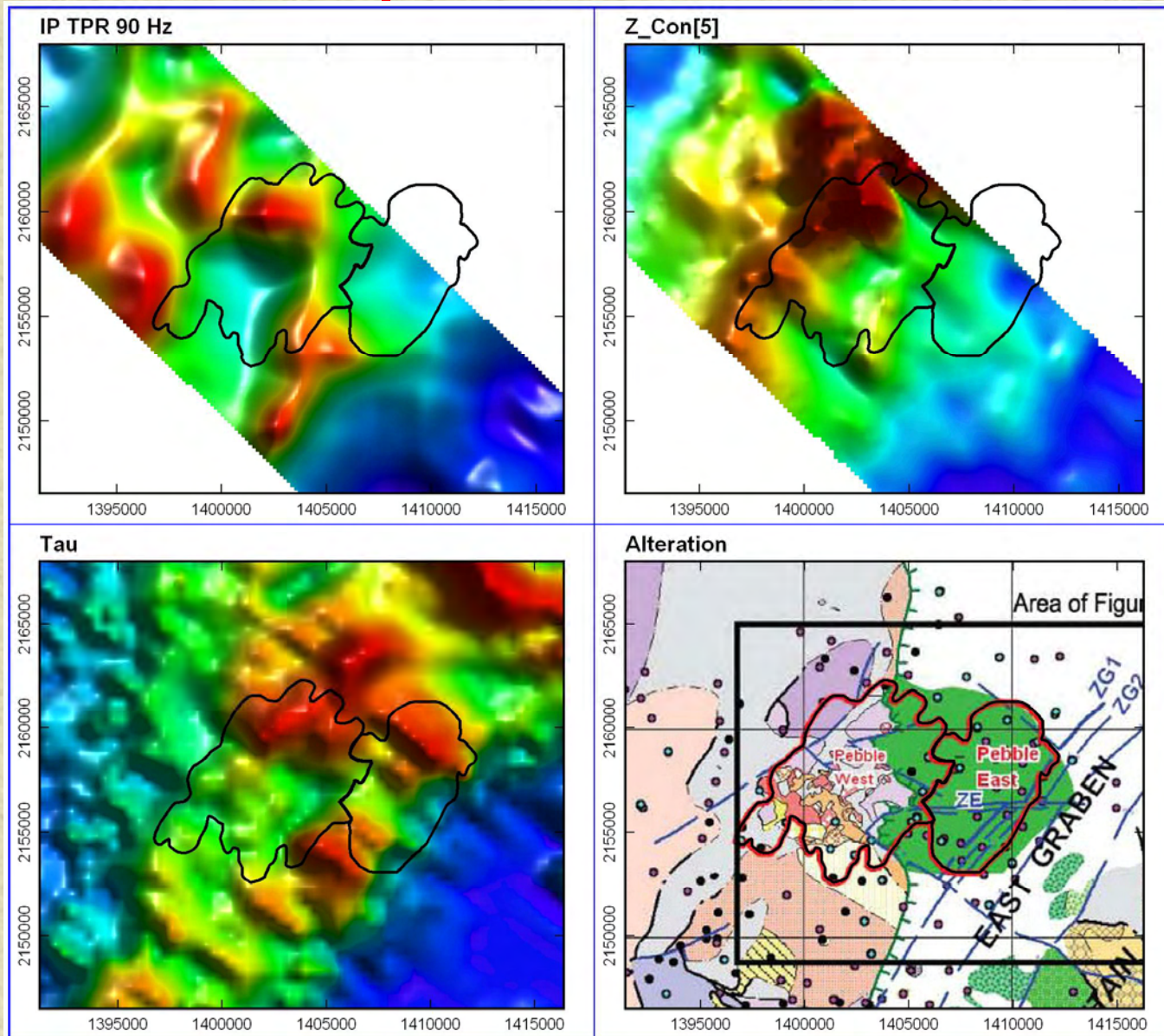
ZTEM-Pebble Deposit



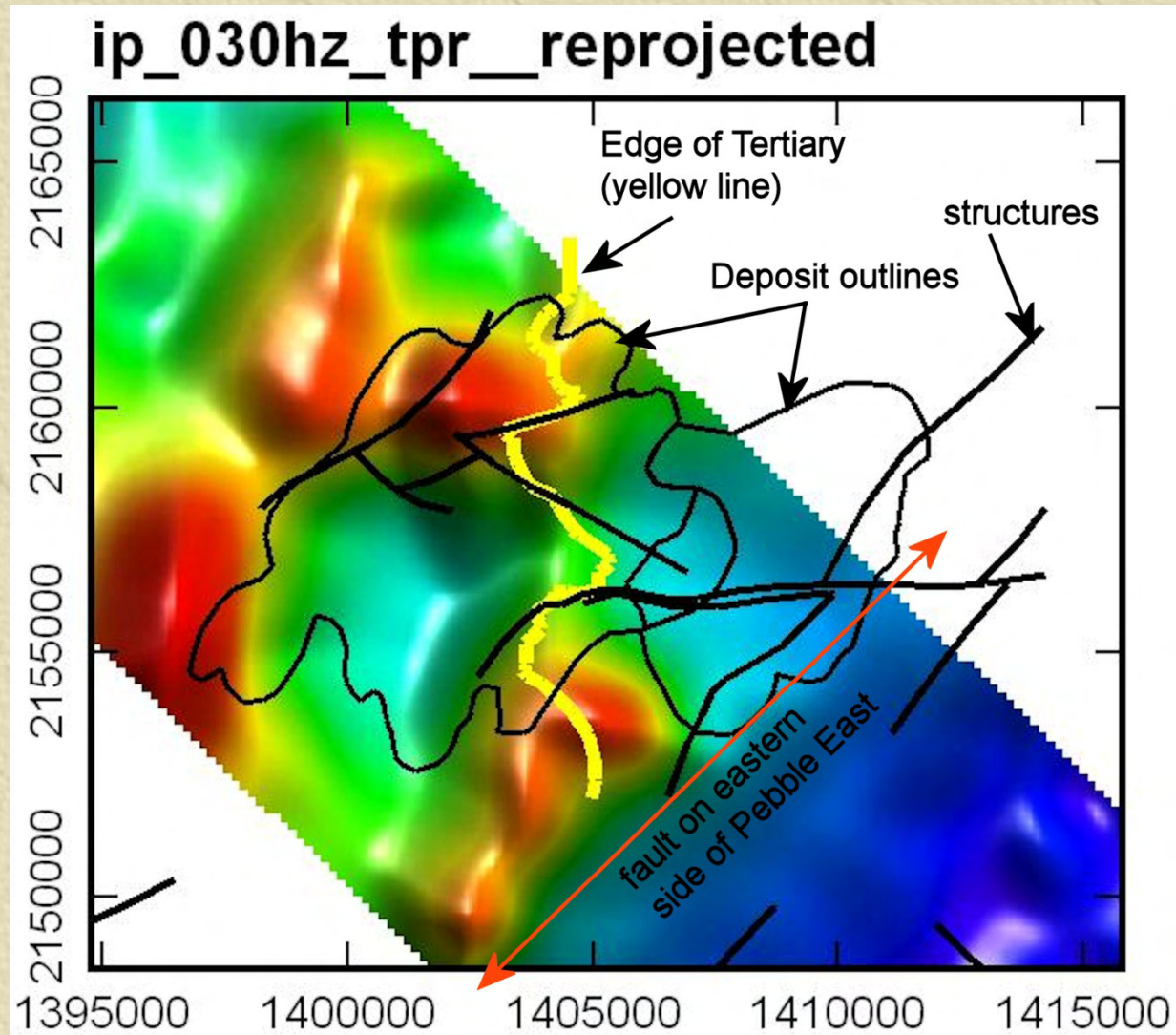
Measured and Indicated Mineral Resources

Cut-Off	Size	Grade			Contained Metal		
		Copper %	Gold g/t	Moly ppm	Copper B lbs	Gold M oz	Moly B lbs
.30	5,942	.42	.35	250	0.78	55.0	3.28
.40	5,399	.45	.36	260	0.83	53.6	3.09
.60	3,668	.55	.41	293	0.98	44.5	2.37
1.00	1,449	.76	.52	341	1.29	24.3	1.09

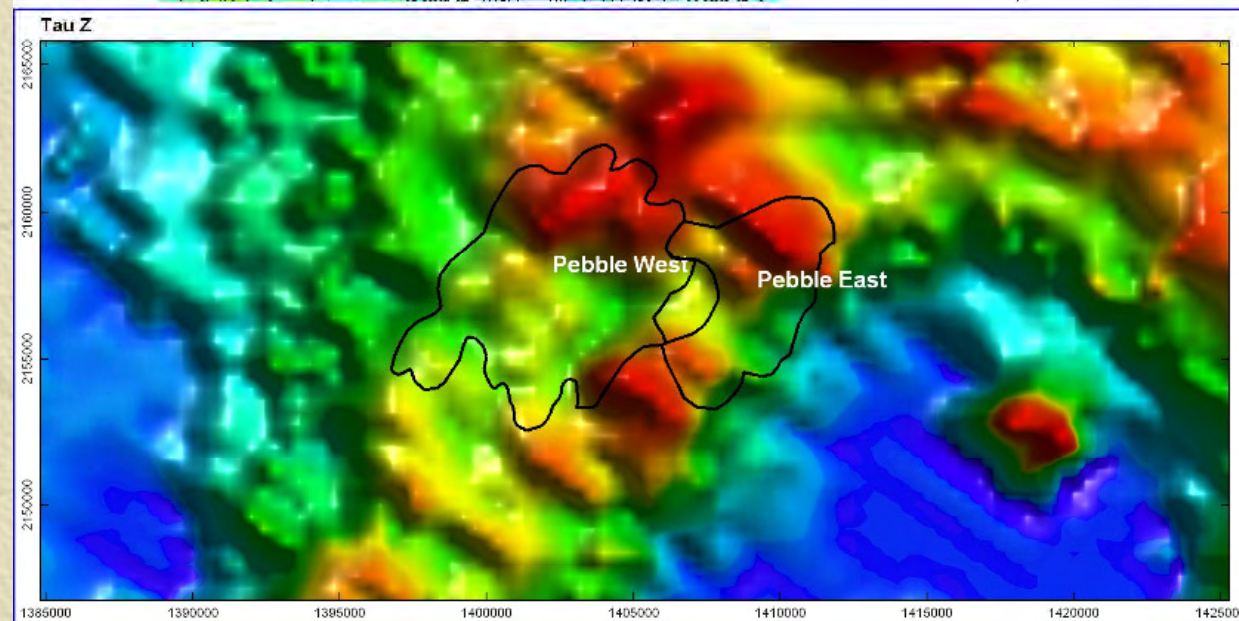
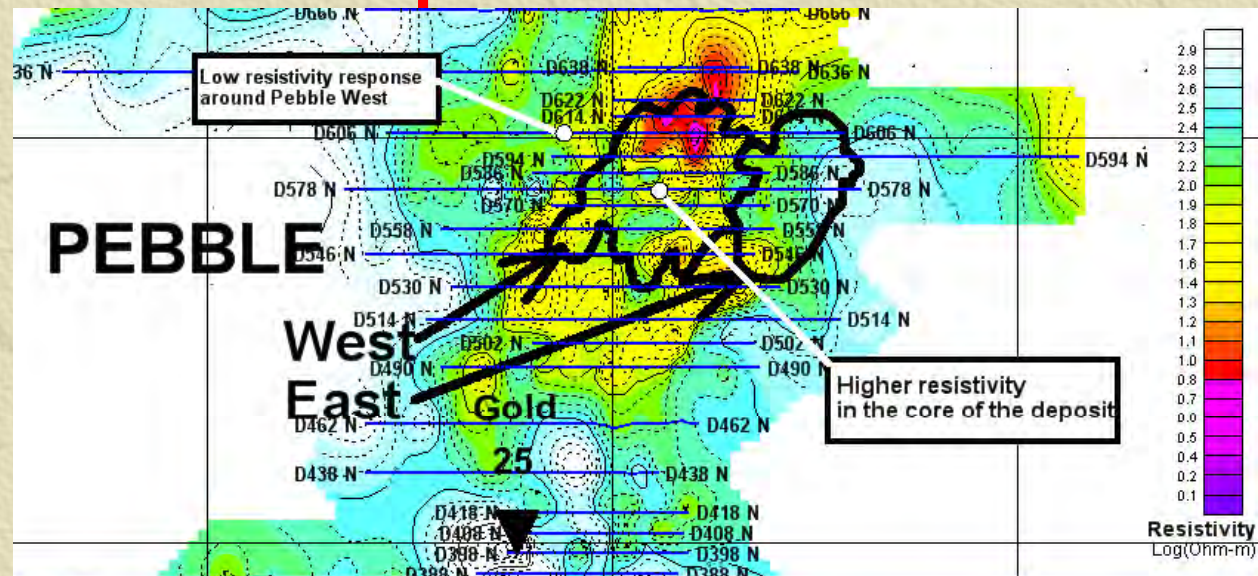
ZTEM-Pebble Deposit



ZTEM-Pebble Deposit



ZTEM-Pebble Deposit



ZTEM-Pozo Seco



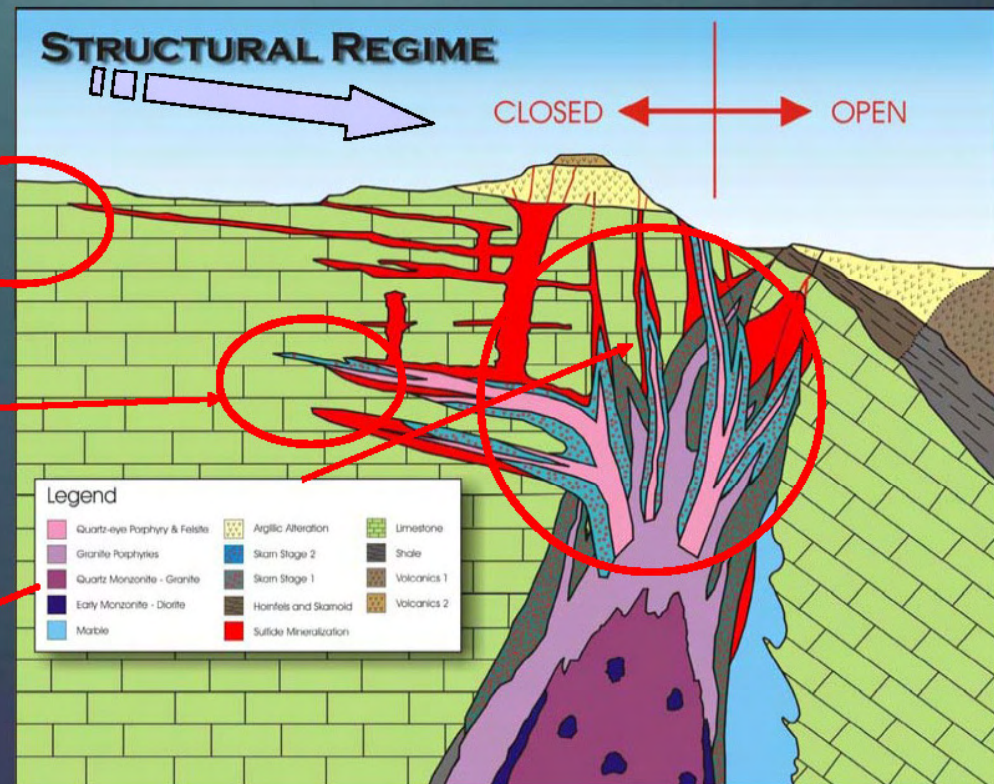
Cinco de Mayo - Model

M
A
G

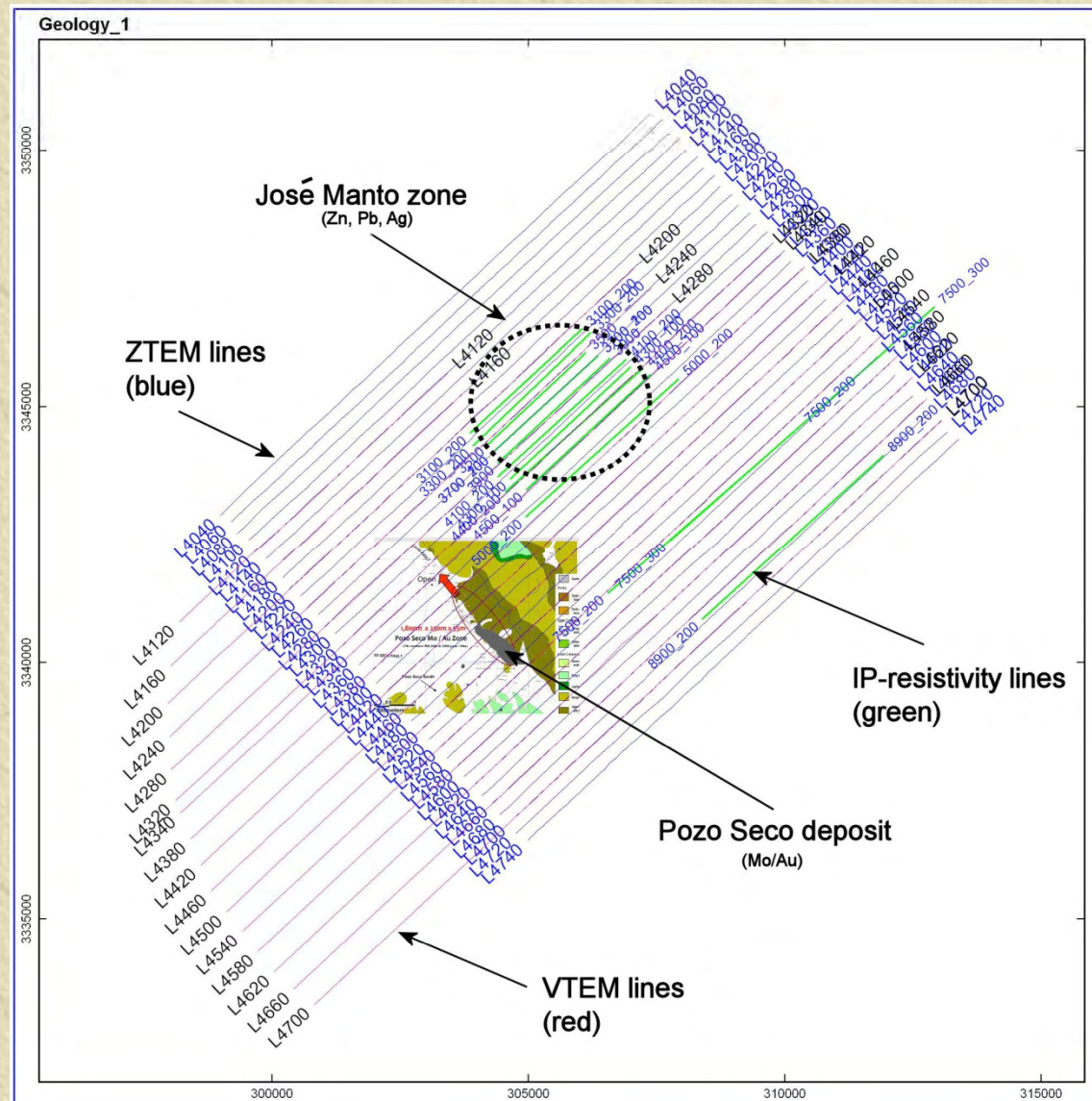
Jose Manto Ag /
Pb / Zn (Distal)

La Gloria felsite
and skarn
(Medial?)

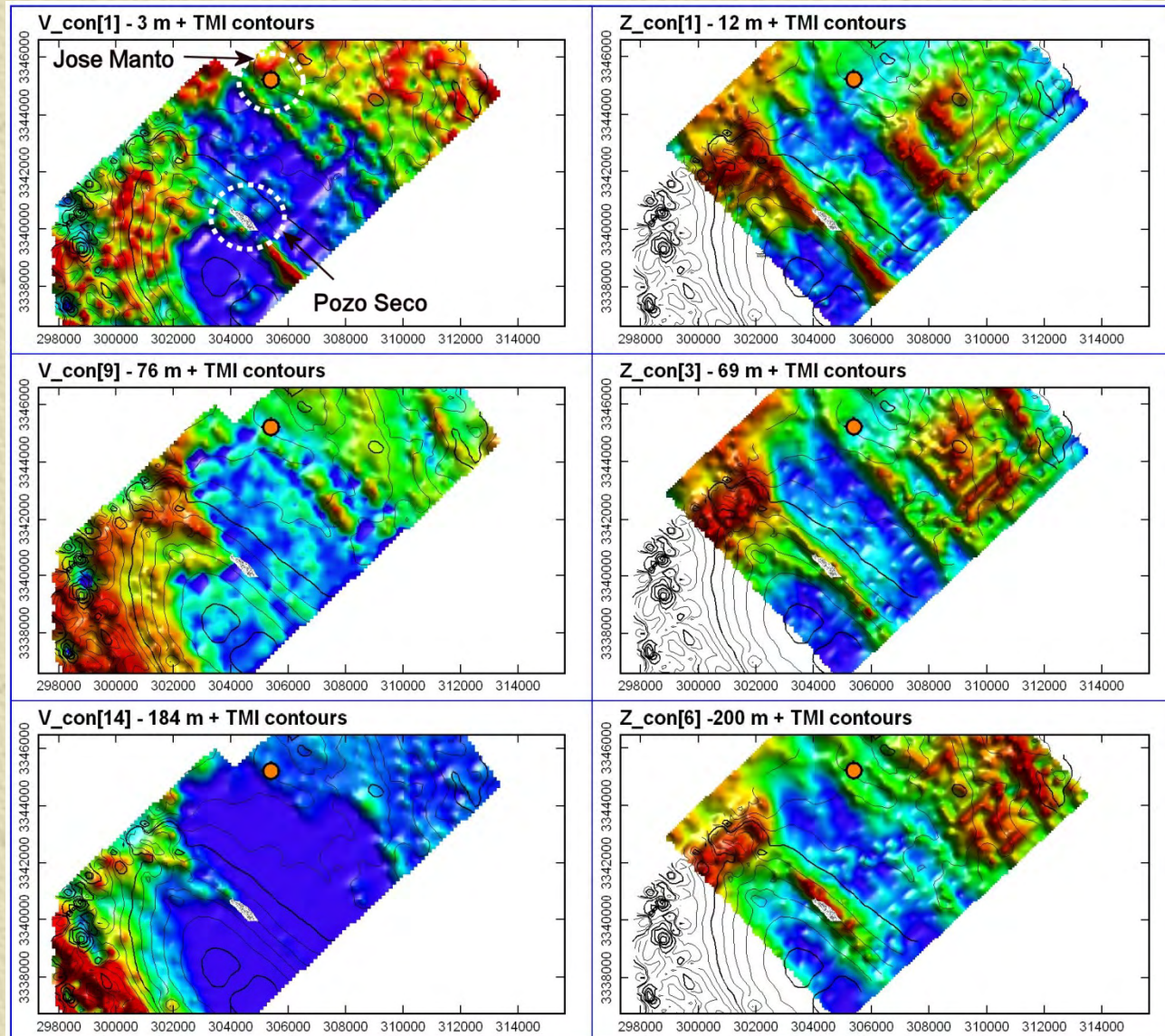
Pozo Seco Moly-
(Gold) Zone
(Proximal?)



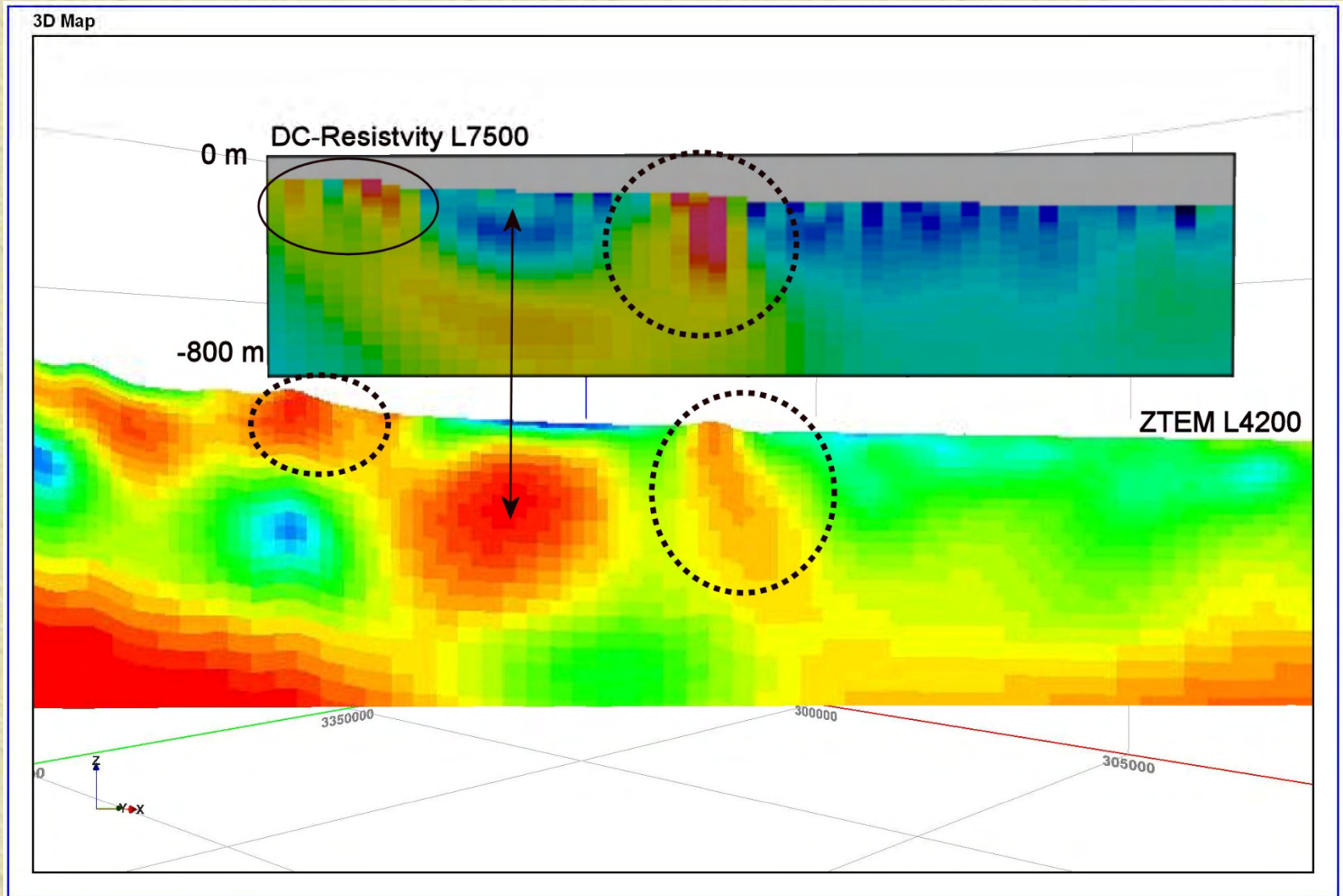
ZTEM-Pozo Seco



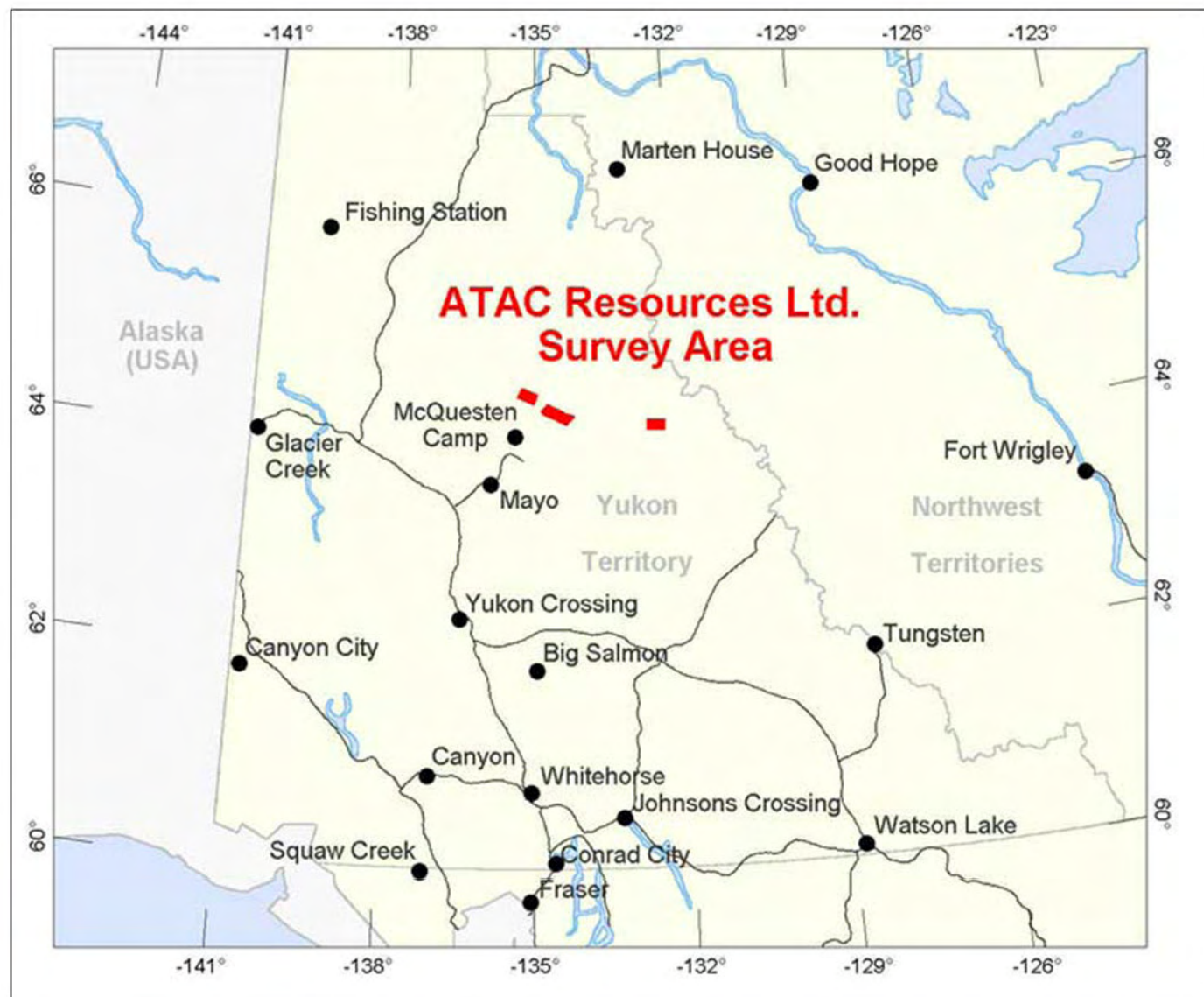
ZTEM-Pozo Seco



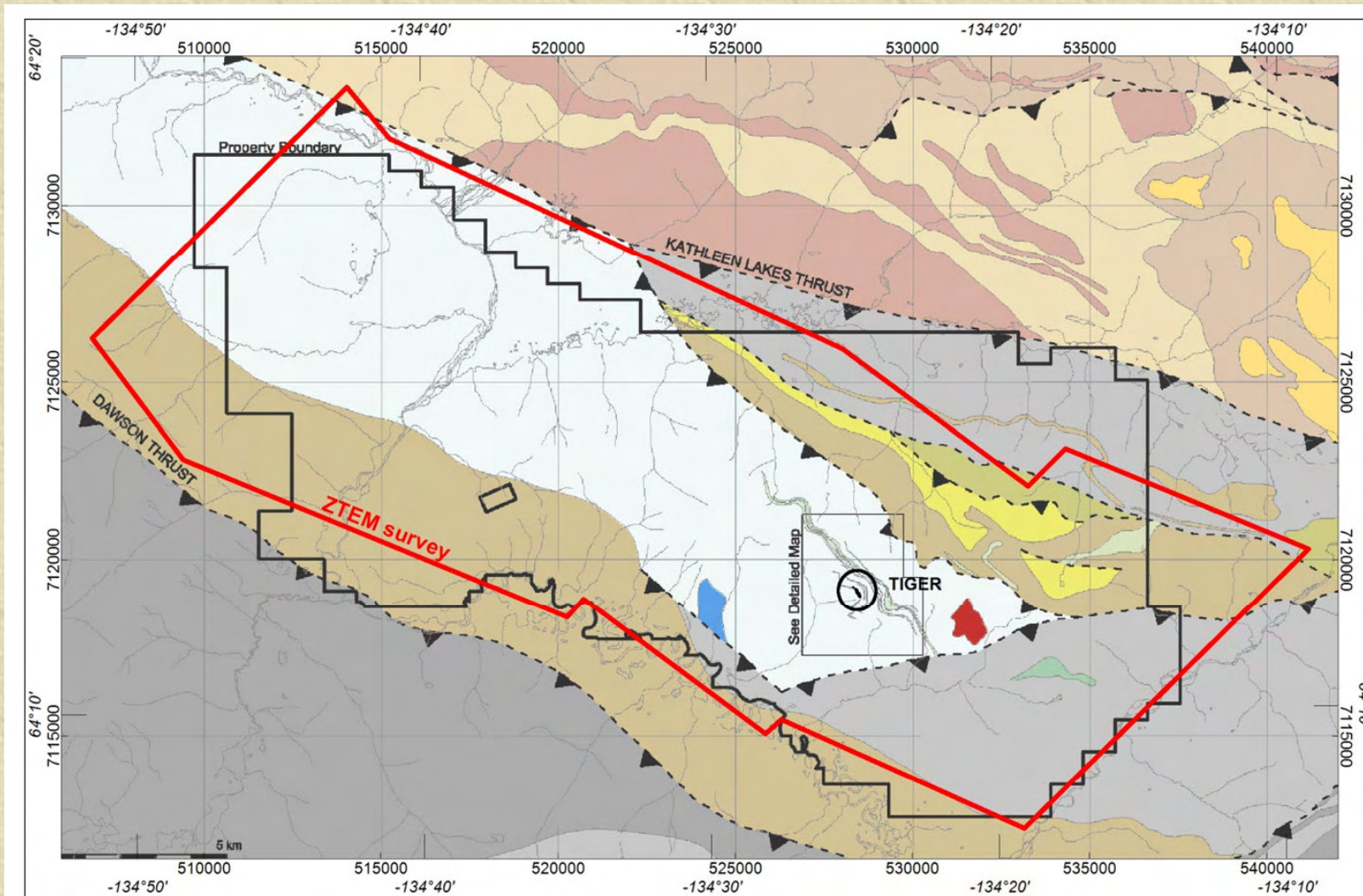
ZTEM-Pozo Seco



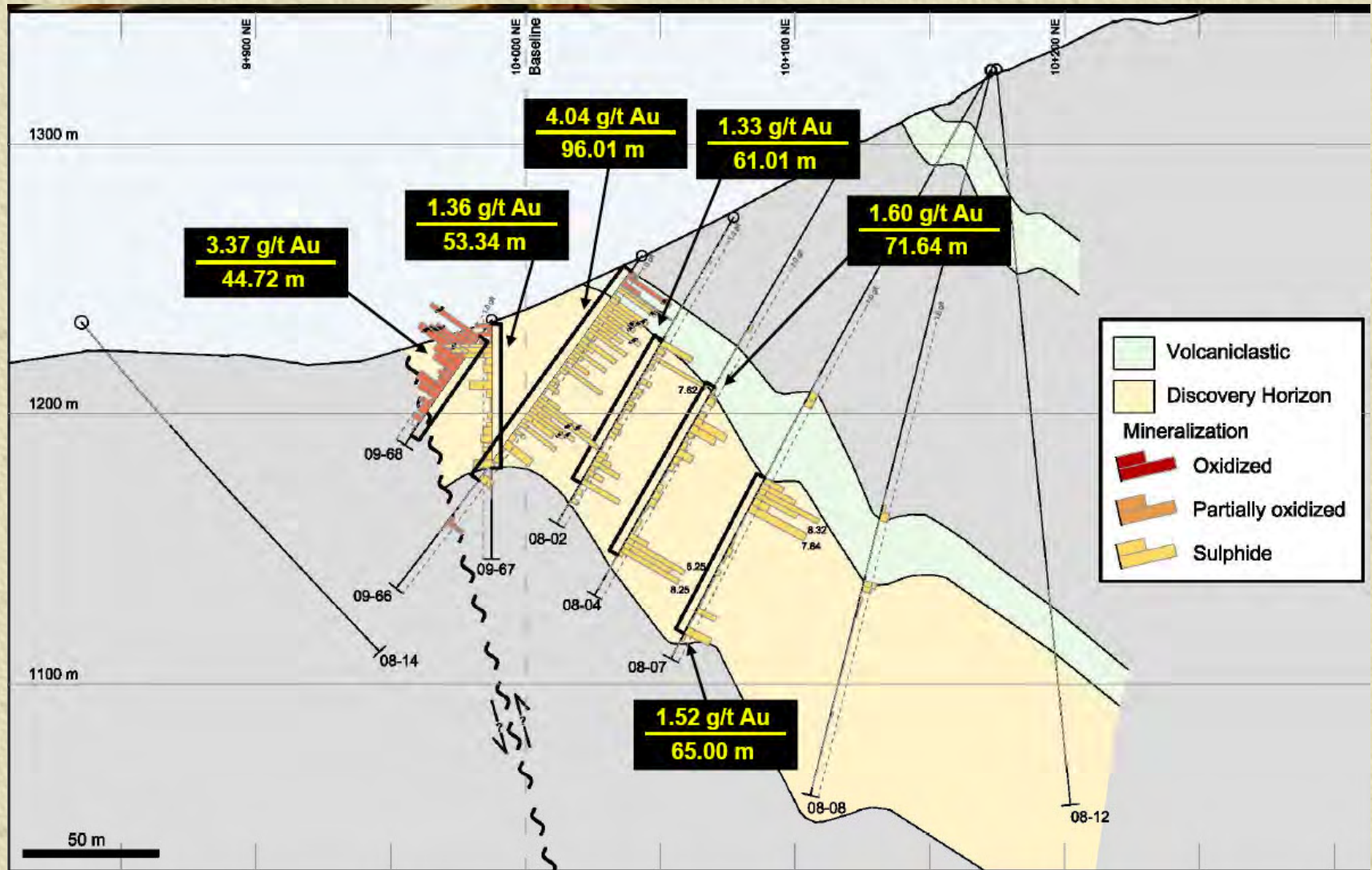
ZTEM-Tiger Zone



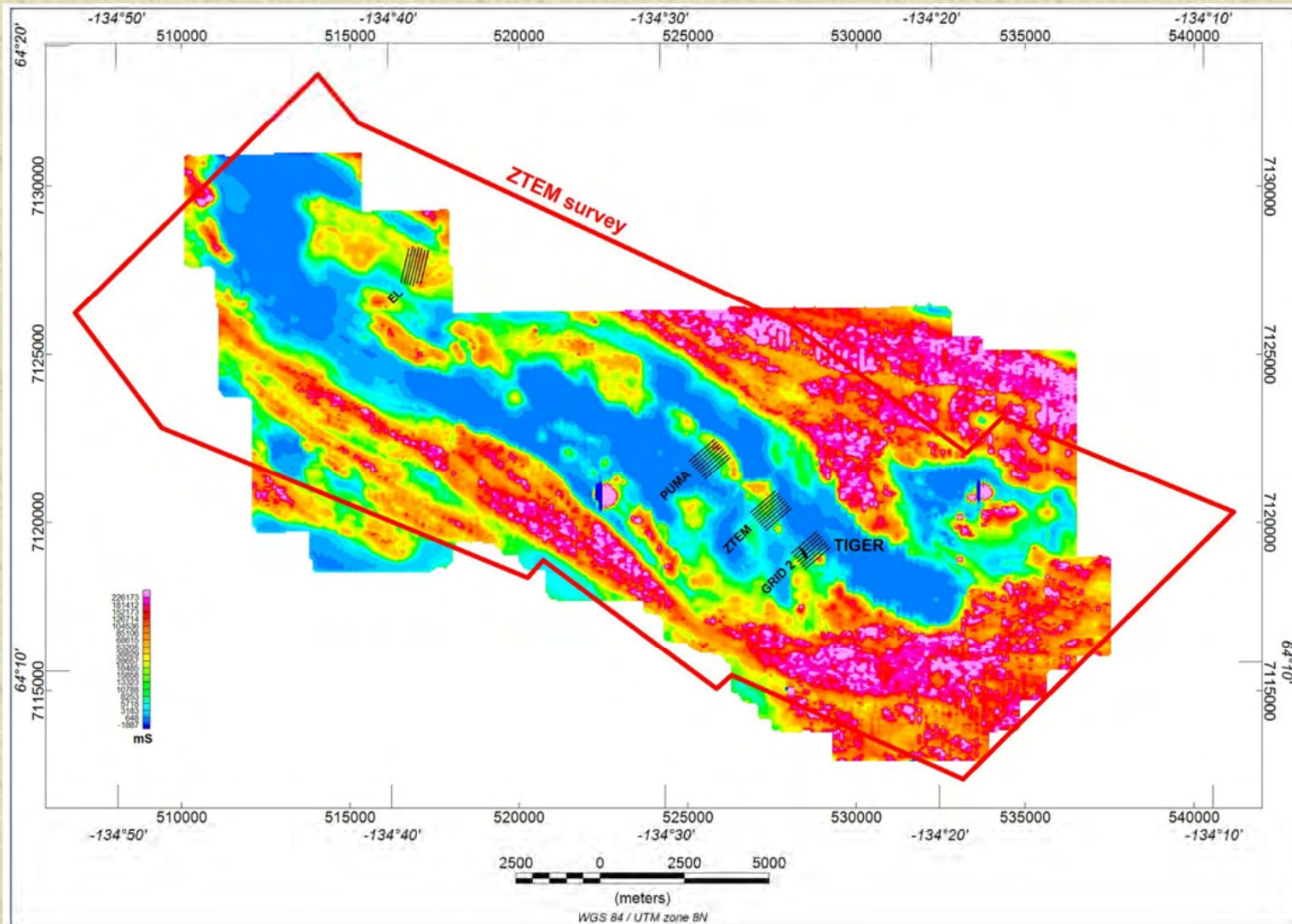
ZTEM-Tiger Zone



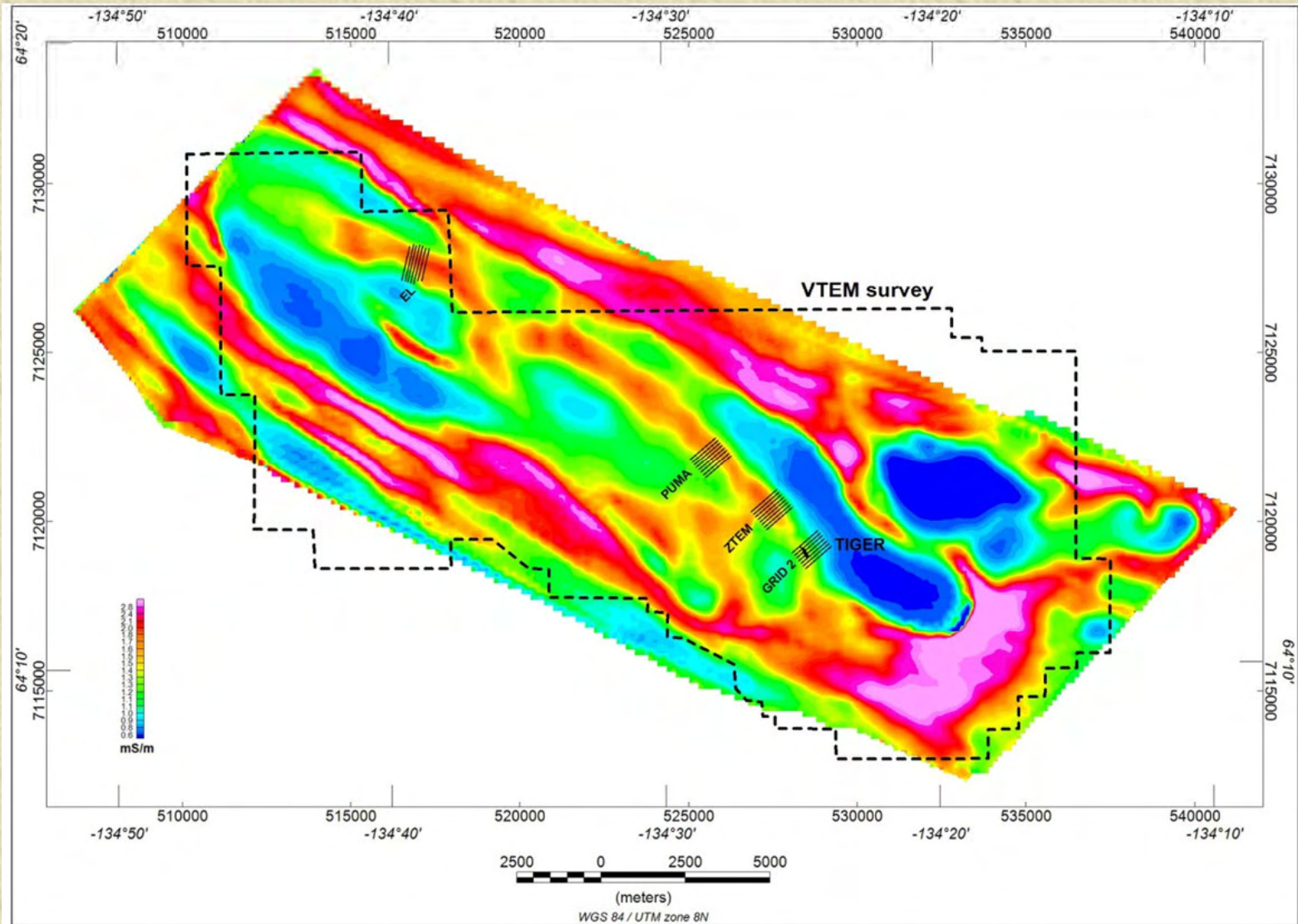
ZTEM-Tiger Zone



ZTEM-Tiger Zone



ZTEM-Tiger Zone



Acknowledgements



✧ ATAC Resources Ltd.

- ◆ Rob Carne
- ◆ Bill Wengzynowski

✧ Geotech Ltd.

- ◆ Paolo Berardelli
- ◆ Jean Legault

AN ASSESSMENT OF SPECTREM AND ZTEM DATA OVER THE PEBBLE COPPER-GOLD PORPHYRY COPPER DEPOSIT, ALASKA

Ken Witherly

Condor Consulting, Inc.
Lakewood, CO, USA
ken@condorconsult.com

SUMMARY

In the present study the results from two airborne EM surveys over the Pebble copper-gold porphyry deposit have been assessed; a Spectrem time domain and a ZTEM Afmag survey. Both systems produce strong conductivity responses over the known mineralization and appear to show evidence of faulting of the deposit to depths of >0.5 km. The exact origins of the EM response are not clear but a pyrite-rich alteration product termed QSP is believed to be likely a major source of the observed EM response. This alteration is noted to extend well outside the zone of economic mineralization as do the EM responses. The ZTEM system produces depth conductivity results similar to the Spectrem but smoother. Finally, there is evidence that the ZTEM responds to resistivity gradients more than absolute conductivity.

Key words: airborne EM, Spectrem, ZTEM, porphyry copper, inversion

INTRODUCTION

Airborne EM (AEM) techniques have been used to search for a variety of mineral deposit styles since the inception of the technology in the late 1940s. The use AEM to aid in the search for porphyry copper deposits however, is not well documented although there is some evidence Barringer applied an early version of INPUT to attempt to locate porphyry coppers in the mid-1960s. In more recent efforts (Harrison 2004, King and LaRoux 2007) there is evidence that the supergene blanket of weathered porphyry systems can be detected with an AEM system. In other situations, the extensive primary and secondary alteration appears to produce conductivity responses that an AEM system can detect (Schaefer, et al 1998). The present assessment presents the results of two AEM systems over the Pebble porphyry copper-gold deposit, Alaska. One system was the Spectrem technology, a modern time domain system and the other was ZTEM, a relatively new adaptation of Afmag technology first applied to airborne surveying in the 1950s. The two surveys have been processed in a similar fashion and compared with existing ground geophysical results and geological information.

PEBBLE DEPOSIT

The Pebble porphyry copper-gold deposit is located 320 km southwest of Anchorage, Alaska. Including both the Pebble West and East zones, the deposit has a measured and indicated resource of ~6 billion tonnes at 0.42% Cu, 0.35 g/t Au, and 250 ppm Mo (0.30% Copper Equivalent CuEQ cutoff). The deposit is basically buried and remains open in several directions. The Pebble is currently operated by the Pebble Limited Partnership (PLP), an equal rights venture

between Northern Dynasty Minerals Ltd. and Anglo American.

The following geological description of the deposit is drawn from Kelley et al 2010. The oldest rocks in the Pebble district are upright, gently folded, Jura-Cretaceous andesitic mudstone, siltstone, and sandstone with lesser interbedded basalt and associated gabbroic intrusions. Alkaline biotite pyroxenite, monzodiorite to monzosyenite/monzonite and diorite intrusions and related intrusion and/or diatreme breccias were emplaced between 99 and 96 Ma. Subalkalic, porphyritic hornblende granodiorite of the Kaskanak batholith was emplaced at ~90 Ma, along with smaller, petrographically nearly identical granodiorite stocks and sills that have a spatial and genetic relationship to at least some stages of Cu-Au-Mo mineralization. The Pebble deposit comprises the contiguous East and West zones (Figure 1), which may be separate centers of a single, large magmatic-hydrothermal system.

The West zone extends from surface to about 500 m depth and encloses four small porphyritic hornblende granodiorite plugs emplaced into andesitic siltstones, diorite and granodiorite sills, and alkaline monzonite intrusions and related breccias. The higher-grade East zone extends to depths of up to 1 650 m within granodiorite of the East zone stock and surrounding andesitic siltstones that are cut by granodiorite sills. The East zone was partially eroded and is now concealed by an east-thickening wedge of Late Cretaceous to Paleocene volcanic and sedimentary rocks. On the eastern side of the East zone, high-grade mineralization has been truncated and dropped 600 to 900 m by normal faults which form the northwest boundary of the northeast-trending East Graben. This is illustrated in Figure 2, a section through A-A' (Figure 1) showing both the geology and distribution of mineralization through the deposit.

AIRBORNE EM SURVEYS

As part of PLP's efforts to better understand the signature of a major buried porphyry deposit, Anglo American flew their proprietary airborne EM system, Spectrem over the deposit. In addition Geotech Ltd. was contracted to fly an orientation ZTEM survey over the immediate deposit area. The outlines of these surveys are shown in Figure 3¹.

Condor Consulting, Inc. undertook to process the EM data acquired by the Spectrem and ZTEM surveys. These outcomes are presented in this summary along with other geoscience data acquired by the PLP over the deposit.

DATA PROCESSING

The two EM data sets were processed using proprietary codes; a layered earth inversion code LEI-1 on the Spectrem

¹ Note: The reader is advised that PLP uses the imperial units system at Pebble to adhere to legacy standards; this review observes that standard but also uses metric in some instances.

data and a 2D Occam on the ZTEM (Sattel et al 2010). These codes provide a depth conductance section from the line data. In addition, grid based products were generated for both surveys. Contractor provided products were as well assessed and some of these outcomes are provided in this assessment.

OUTCOMES

Spectrem: While the Spectrem survey covered a large area around the deposit, the results have been windowed down to facilitate the comparison with the ZTEM results. Figure 4 shows the Spectrem-derived TMI and time constant (Tau) results over the deposit area.

The deposit can be seen to lie on the eastern flank of a NE-trending zone of higher magnetic response. An intrusive appears as an intense magnetic high to south of the deposit but is not believed to be related to the Pebble. The Tau image shows that the deposit is situated regionally on a platform of higher conductivity and locally is flanked by highs to the north and east. There is an extensive zone of higher conductivity to the north of the deposit the origins of which is not well understood at this time but are believed to be a combination of primary lithologic and potential alteration responses. A synthesis of earlier IP results is shown in the figure and this outline (25 mrad contour) correlates with the elevated Tau response that hosts the deposit.

Figure 5 shows the four depth slices from the conductivity model for depths 25 m, 83 m, 200 m and 500 m. This set of images shows that the conductivity changes significantly with depth.

Figure 6 shows the DC resistivity and Tau results over the deposit. There appears to be a reasonable correlation between the two surveys. Both show a conductive zone to the north of the deposit as well as a resistive core associated with Pebble West. Figure 7 shows an extract of the conductivity depth inversion from L21370. Shown as well are the CuEq grades and major structures.

The EM depth section shows an extensive lateral zone of conductivity at a shallow depth across most of the line. The Anglo plate models all report in a quite shallow depths. The section over Pebble West shows an elevated conductivity; this also extends to the west past the defined limits of the deposit. Where the Pebble East zone is down-dropped by faulting there appears to be a down-thrown segment of the conductivity depth section, although a thin shallow segment of conductivity also continues to the east. The conductivity response at depth appears to be terminated at the location of the fault-off set on the eastern side of Pebble East.

ZTEM: As shown in Figure 3, the ZTEM coverage was focused over the Pebble deposit. The ZTEM results are presented in two formats; conductivity depth sections similar to conductivity inversions performed to the Spectrem data and processed grids of the various frequency components². Figures 8 and 9 show examples of the grid products generated from the ZTEM outcomes. Figure 8 shows the DT (total divergence) product for the In-phase component at all

frequencies. Figure 9 shows the full suite of processing for the 45 Hz signal.

The color bar for Figure 8 has been left as initially derived such that the warm colors represent more resistive areas. Frequencies 30, 45, 90 and 180 Hz all show a resistive zone centered within Pebble West; this correlates with what is observed with the Spectrem and DC resistivity outcomes. Other features such as the Tertiary contact (yellow line) and several of the mapped faults also appear to be reflected in the ZTEM outcomes.

In Figure 9, the complexity of the ZTEM outcomes is apparent given the marked changes in patterns for the different products. The geological veracity of these images is difficult to establish in the present study due to the lack of well defined geological information away from the deposit area.

Figure 10 shows again the Spectrem conductivity depth section for L21370 as well as the corresponding ZTEM-derived conductivity depth section for L10120 (locations of the two lines are shown in Figure 11). In terms of broad conductivity mapping, the Spectrem and ZTEM outcomes are similar but the ZTEM outcome is much smoother. Figure 12 shows an enlargement of the resistivity high defined in the In-Phase DT response (Figure 8) along with the depth conductivity section and a plot of the AppCon (Apparent Conductivity).

While the grid image shows the resistive feature to be quite distinct, the depth conductivity and conductivity results show the response to be somewhat modest. The strength of the response in the grid display is attributed to partially caused by the presence of conductive zones on either side enhancing the current channelling response that is dominate mode of excitation for ZTEM.

CONCLUSIONS

The results of a Spectrem and ZTEM surveys over the Pebble deposit have been examined. The processed outcomes appear similar, especially the depth conductivity sections. Both systems appear to be responding to changes in the geology at depths > 0.5 km depth. The ZTEM grid products show character that is only partially understood due to in part limitations of the geological knowledge away from the immediate area of the deposit. The source of the conductivity observed around the deposit is attributed to be largely caused by QSP (quartz-sericite-pyrite) alteration. Physical property measurements, either on core or in drill holes would help to better establish the exact relationship between the observed conductivity and geology. The ZTEM system appears less sensitive to absolute conductivity and more to gradients between zones of low and high conductivity.

ACKNOWLEDGMENTS

Condor Consulting, Inc. wishes to express thanks to Anglo American and PLP for permission to release these outcomes.

REFERENCES

Acorn, W, Coyoli, R., and Legault, J. 2009 Report on a Helicopter-Borne Z-Axis Tipper Electromagnetic (ZTEM) and Aeromagnetic Geophysical Survey Pebble Property Lliamna, Alaska; report for Pebble Limited Partnership; Geotech Ltd. November 2009

² Geotech has outlined the derivation of their ZTEM products in a series of their commercial reports; i.e. Steffler et al 2009 and Acorn et al 2009.

Harrison, M., 2004 Airborne EM in the Search for Chilean Porphyry Copper Deposits; BHP Billiton Internal Report. 2004

Kelley, K, Lang, J. and Eppinger, G., 2010 Exploration Geochemistry at the Giant Pebble Porphyry Cu-Au-Mo Deposit, Alaska; Society of Economic Geologists Newsletter No 80 (January 2010)

King, A., and LaRoux, T., 2007, Spectrem as a Mapping and Discovery Tool; Preview Issue 131 December 2007

Sattel, D., Witherly, K., Becken, M., 2010 A brief analysis of ZTEM data from the Forrestania test site, WA; for presentation at ASEG 2010, Sydney, Australia, August 22-26, 2010

Schaefer, M. J., Gingerich, J., and Lemieux, J., 1998, Case study: The evolution of airborne time domain electromagnetic applications for geologic mapping; a Noranda perspective Exploration Geophysics, 29, no. 2, 204-210, (1998)

Steffler, E., Milicevic, B. and Legault, J., 2009 Report on a Helicopter-Borne Z-Axis Tipper Electromagnetic (ZTEM) and Aeromagnetic Geophysical Survey, Mt. Milligan Test Block Mackenzie Region, British Columbia; Project 8242 for Geoscience BC & Terrane Metals Corp; Geotech Ltd. January 2009

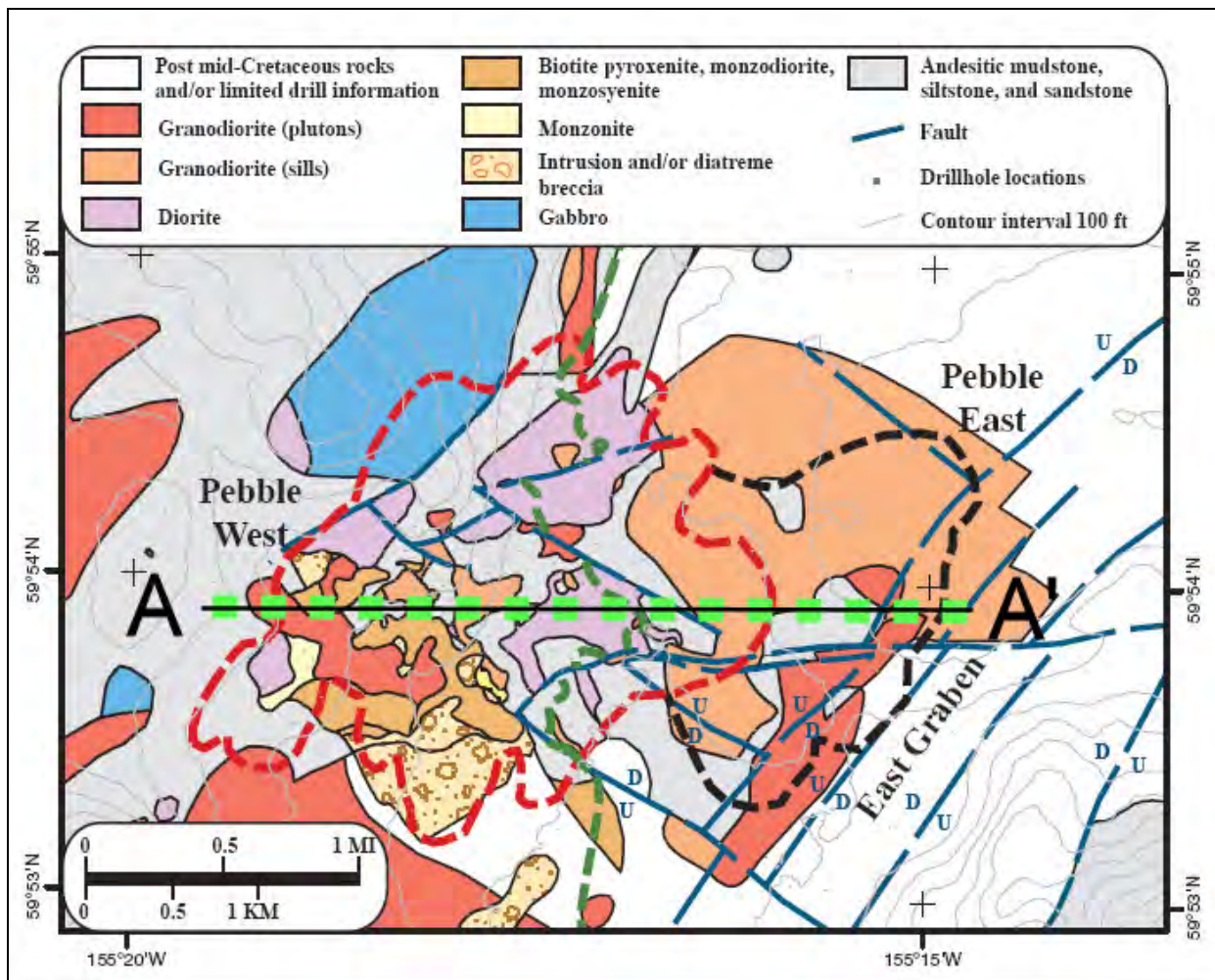


Figure 1: Geology of the Pebble deposit showing West and East Zones (from Kelley et al 2010).

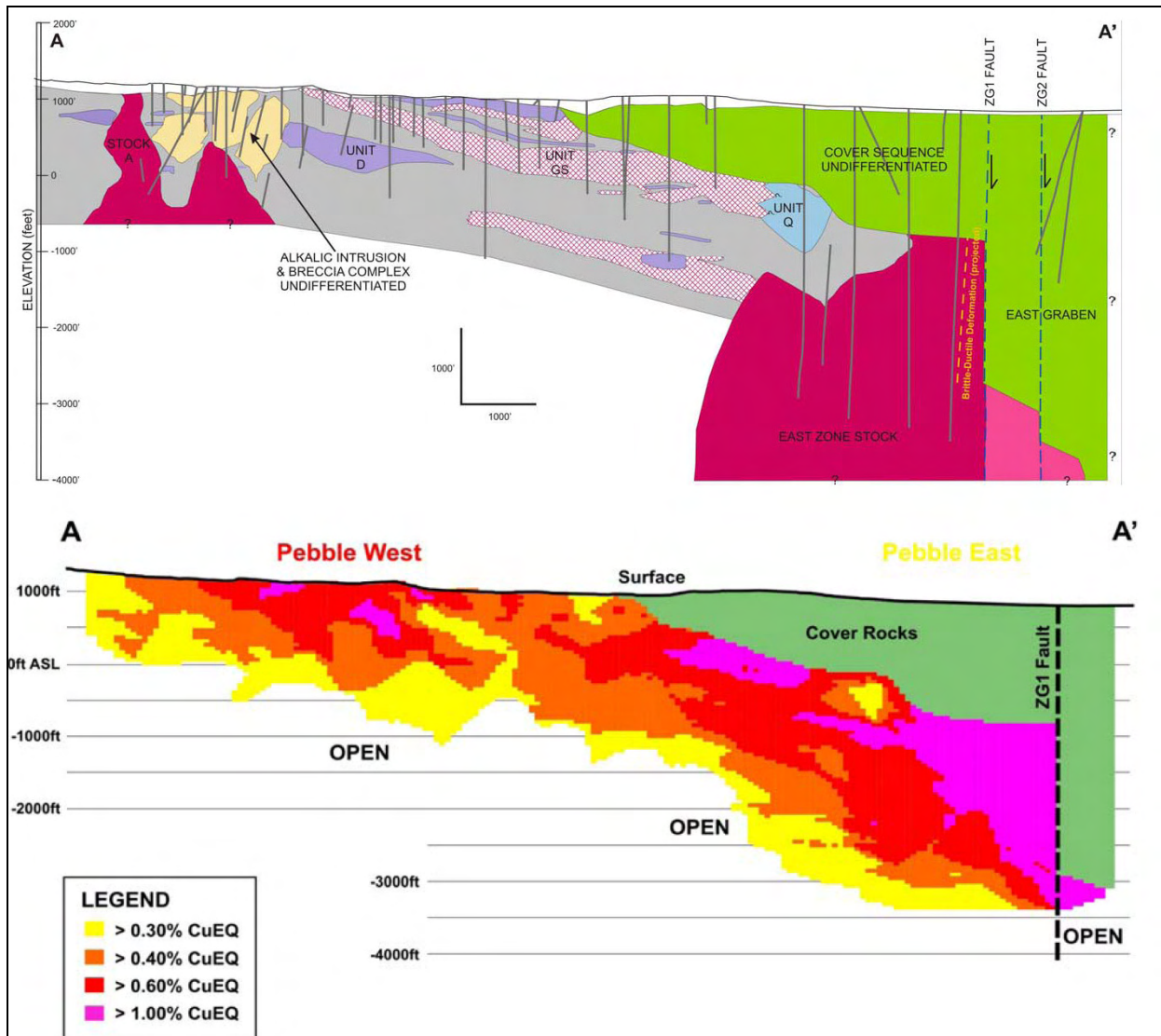


Figure 2: Geology and mineralization along W-E section A-A' (see Figure 1) through the Pebble deposit.

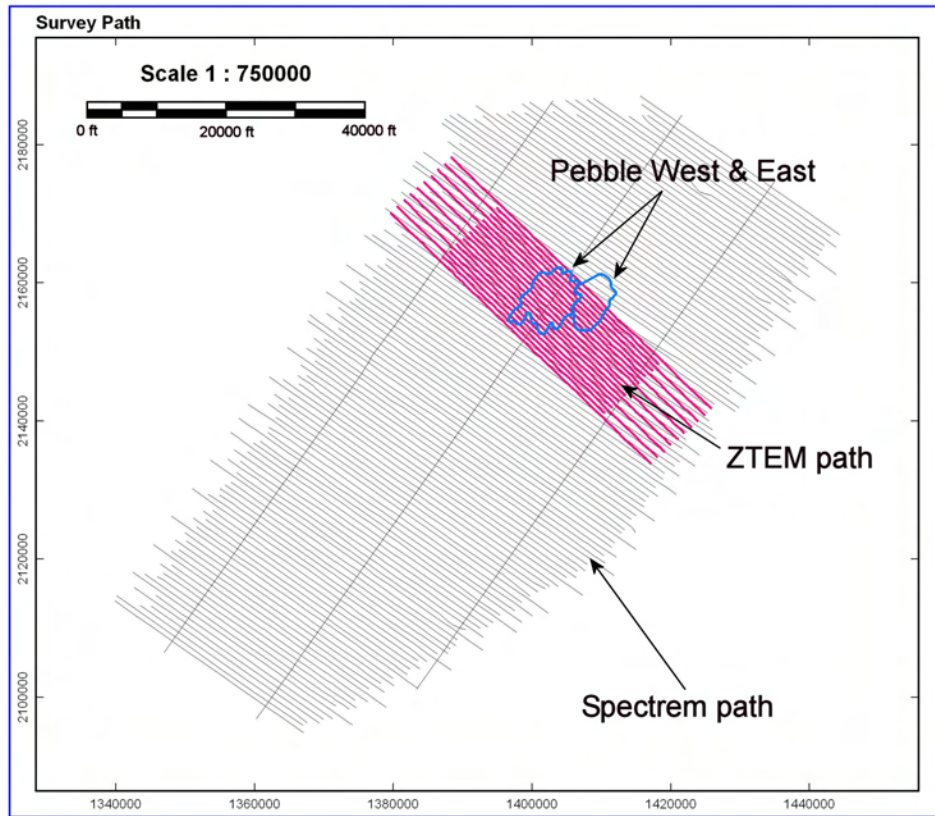


Figure 3: Flight path of Spectrem and ZTEM surveys over the Pebble deposit.

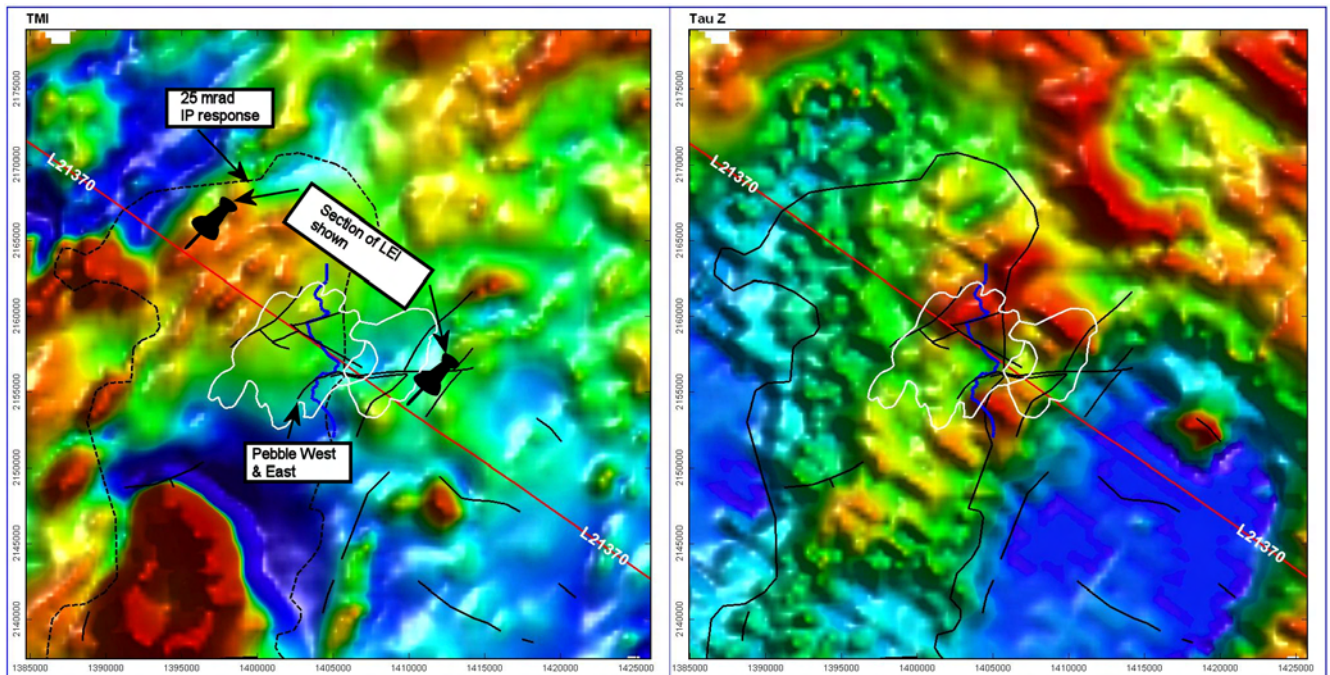
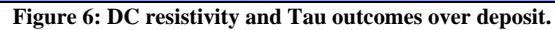
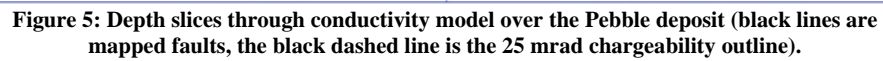


Figure 4: TMI and Time constant (Tau) from Spectrem survey over deposit.



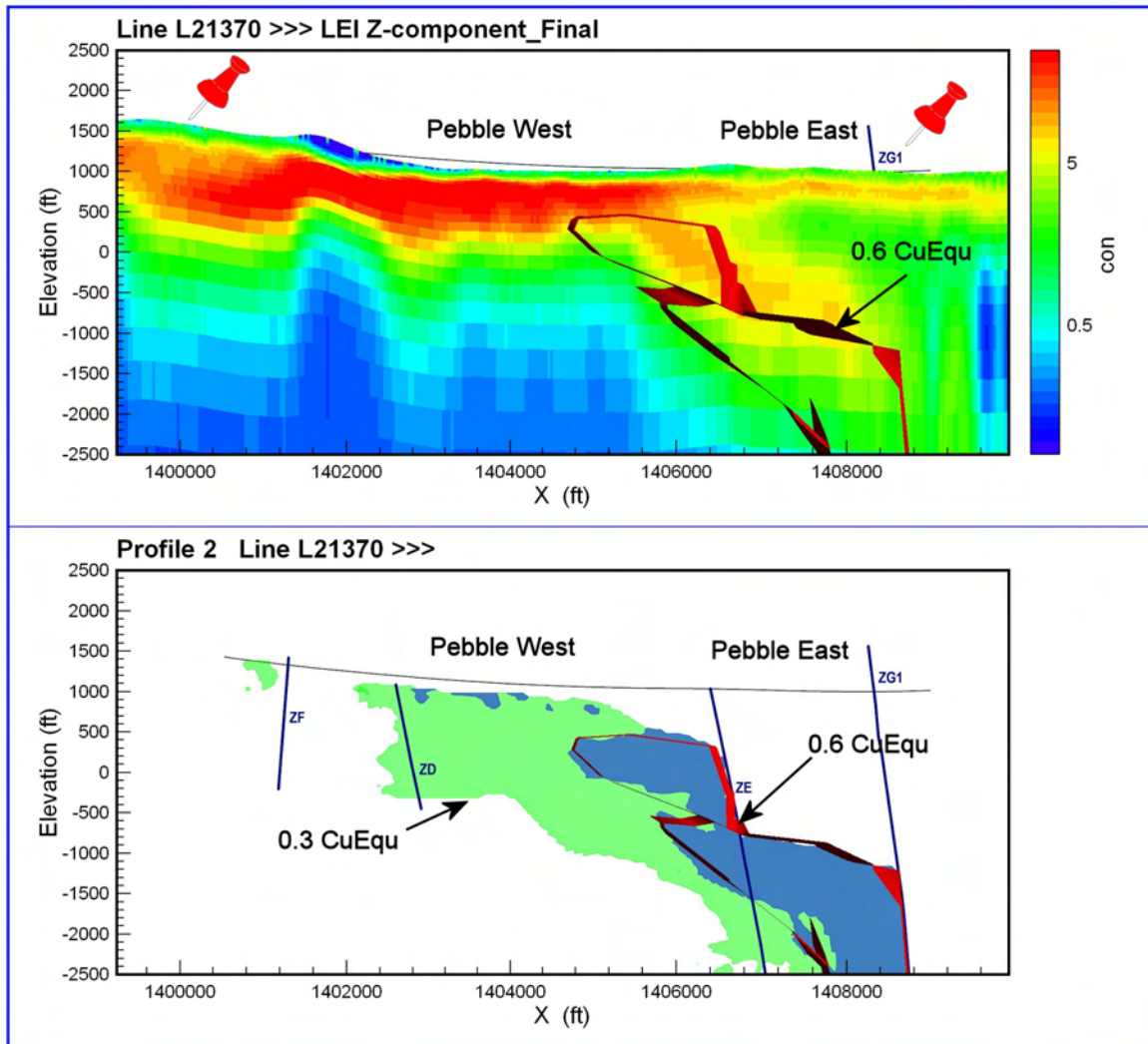


Figure 7: Section for L21370 over Pebble deposit showing Spectrem conductivity depth inversion and CuEq results (location of section shown in Figure 5 upper left image)

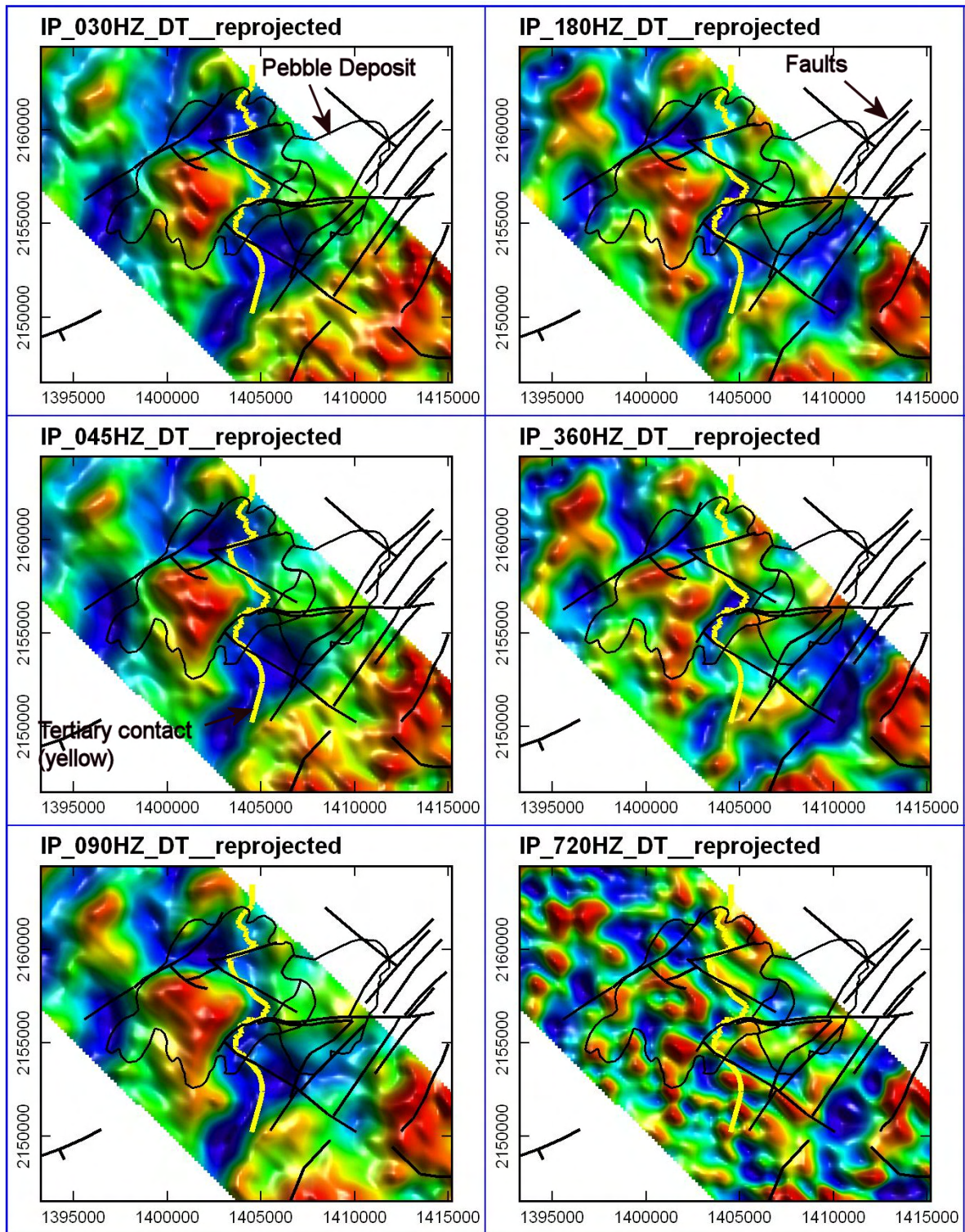


Figure 8: Full suite of ZTEM frequencies processed with total divergence (DT).

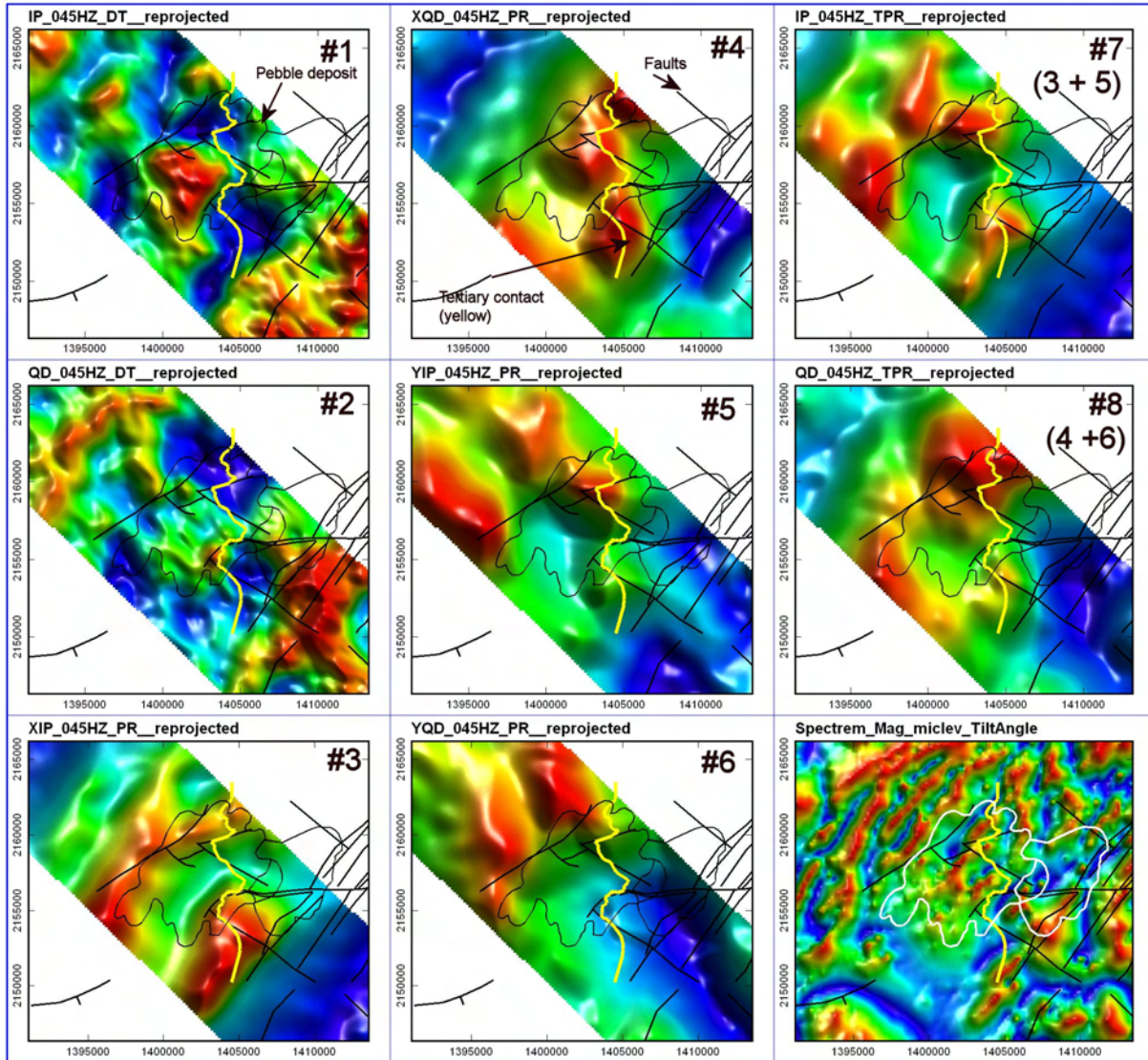


Figure 9: Full suite of ZTEM processing for 45 Hz.

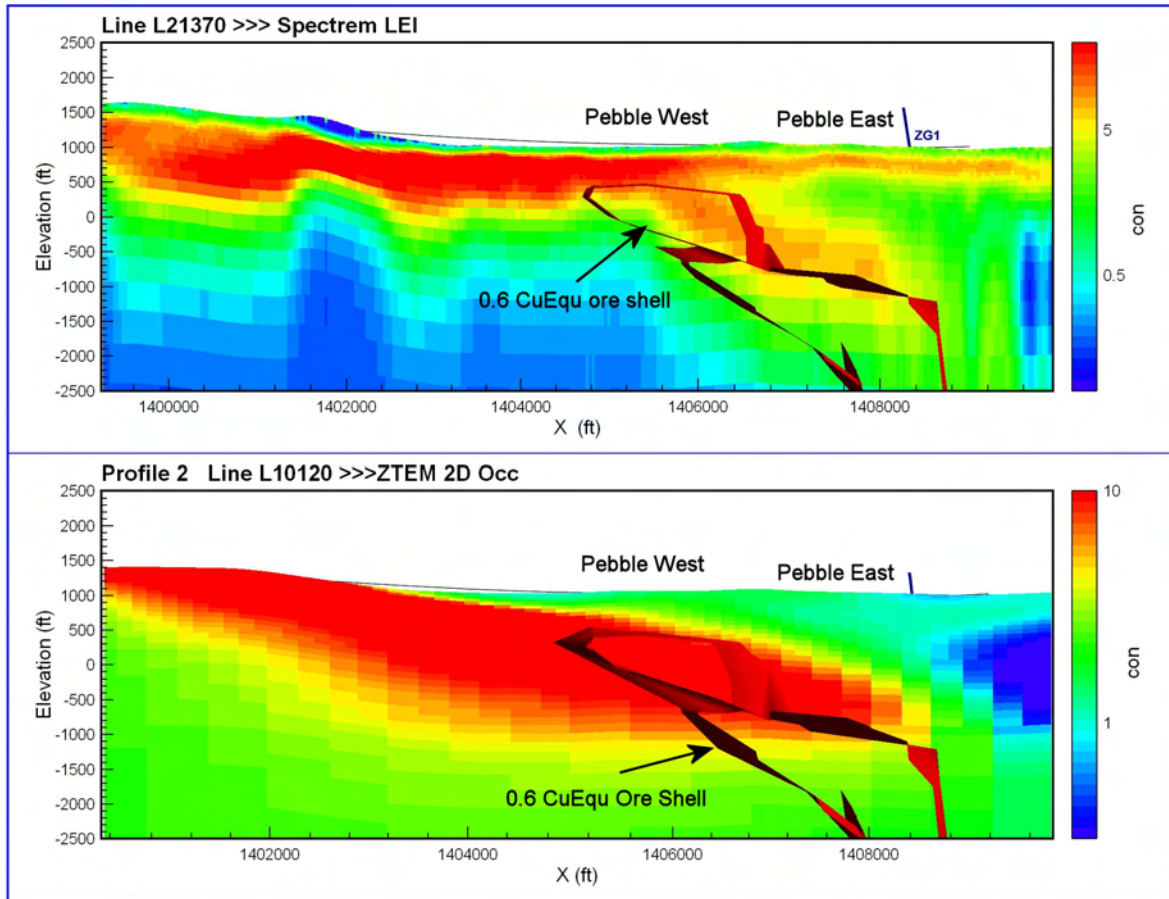


Figure 10: Spectrem L21370 and ZTEM L10120 conductivity depth sections CuEq outcomes.

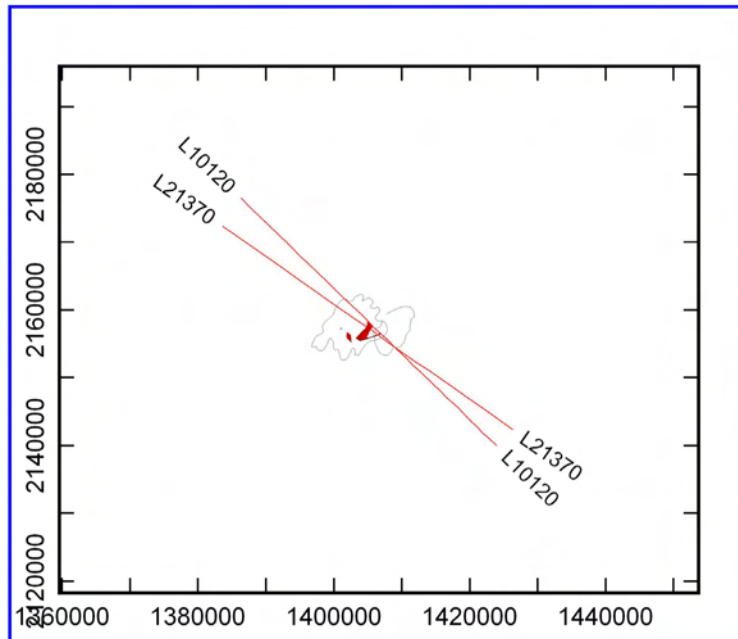


Figure 11: Location of Spectrem L21370 and ZTEM L10120 over Pebble deposit.

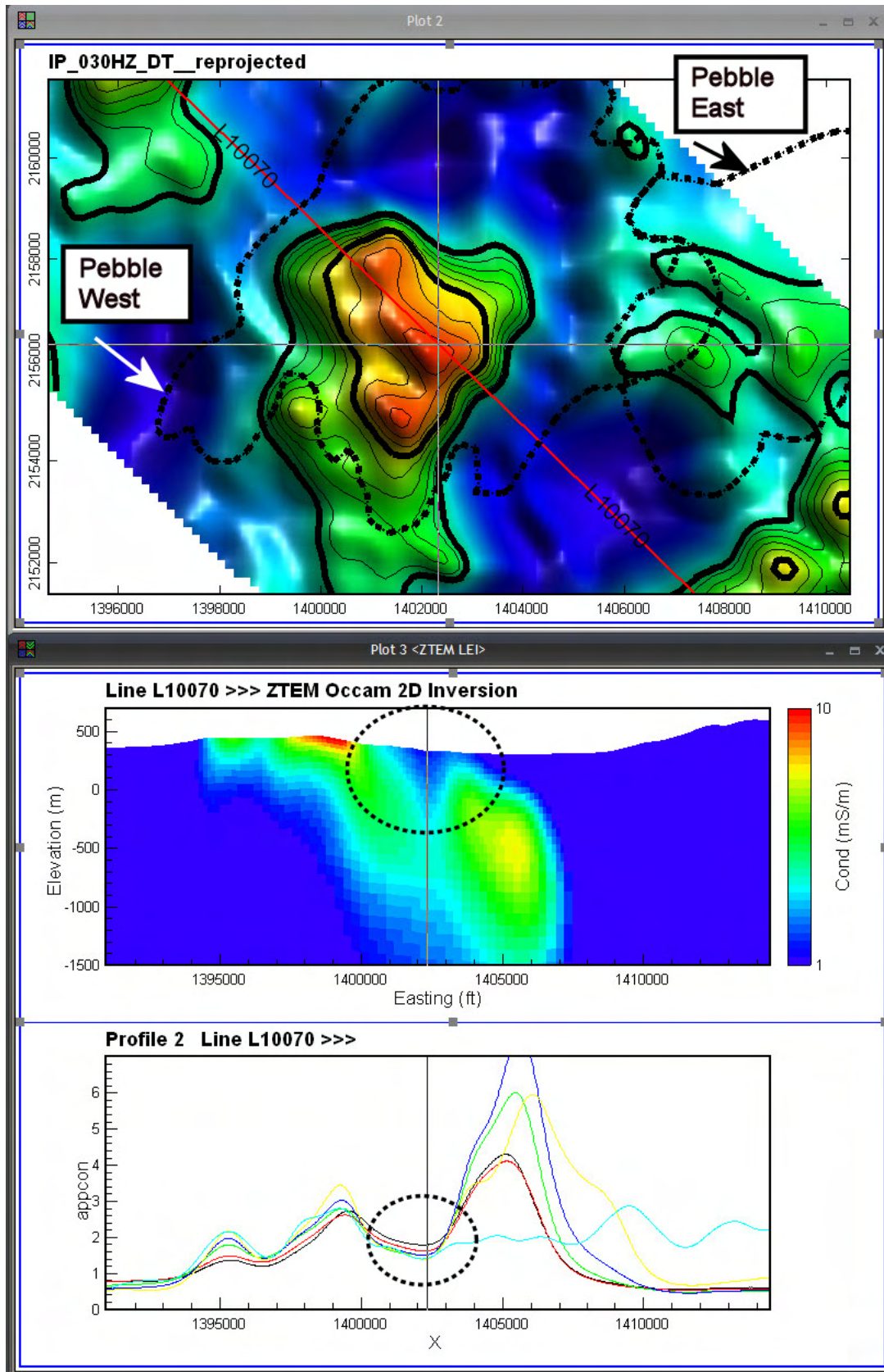


Figure 12: ZTEM In-Phase 30 Hz DT grid with depth conductivity section and AppCon profiles over Pebble West.